THERMAL AND CHEMICAL BEHAVIOUR *of an* ENERGETIC MATERIAL *and a* HEAT RELEASE RATE ISSUE

HUBERT BITEAU

DOCTOR *of* PHILOSOPHY

THE UNIVERSITY *of* EDINBURGH

2009

DECLARATION

This thesis and the research described and reported herein has been completed solely by Hubert Biteau under the supervision of Professor Jose L. Torero and Professor Dougal D. Drysdale. Where other sources are quoted, full references are given.

Hubert Biteau

Abstract

Energetic materials encompass a wide range of chemical compounds all associated with a significant risk of fire and explosion. They include explosives, fireworks, pyrotechnics, powders, propellants and other unsteady chemicals. These materials store a high level of chemical energy and are able to release it rapidly without external contribution of oxygen or any other oxidizer. The behaviour of these materials in case of explosive detonations is relatively well-known from empirical and practical points of view. However, fundamental scientific questions remain unanswered related to the mechanisms of heat release. The current understanding of these mechanisms lacks appropriate thermochemical characterisation. The aim of the study is the analysis of thermal and chemical characteristics of energetic materials under conditions that exclude detonations. Detonation is excluded in order to better isolate the thermal and chemical mechanisms involved in the burning process. The experimental work has been conducted using the FM Global Fire Propagation Apparatus (FPA) [ASTM E2058-03]. One of the benefits of using this experimental apparatus rather than the Cone Calorimeter is that it allows controlling the feed of heat and oxidizer to the reaction zone.

The material chosen to conduct experiments on is a ternary smoke powder based on a mixture of starch and lactose as fuel components and potassium nitrate as oxidizer. This product is currently used by fire brigades to assess smoke venting systems efficiency of buildings. The kinetics associated with the combustion of the material was assessed slow enough to allow measuring instruments to capture the thermal and chemical evolution during combustion reaction. Thermal analysis has first been carried out by means of DSC, TGA, DTA, MS and FTIR data in order to understand the decomposition of the material and its energetic evolution when undergoing heating. However, if the latter methods help defining the decomposing path of the material, they do not provide an integral view of its combustion behaviour, in particular, the emissions of toxics which are kinetic path dependent. Subsequently, combustion tests have been carried out using the FPA. Its ability to capture the evolution of gases emissions formed during the reaction has been proved. The influence of two configuration parameters on the combustion behaviour and on the gaseous emissions of the material has been investigated. The proportion fuel/oxidizer has been varied as well as the composition of the reacting atmosphere. Results shows that the quantity of oxidizer in the material affects the

kinetics of the reactions taking place in the condense phase. Increasing the concentration of potassium nitrate in the mixture enhanced the reaction rate of the smouldering combustion. Higher quantity of volatiles is released which favoured the initiation of a diffusion flame regime in the gaseous phase, above the sample. While the kinetics of the condense phase is governed by the oxidizer concentration, experiments show that the flaming regime is influenced by the concentration of oxygen (O_2) in the reacting atmosphere. A transition from diffusion to premixed flame is found when the concentration of O_2 surrounding the sample is reduced below 18%. An analytical model has been used to explain the existence of a transition for a critical O_2 concentration. Finally, thermal and combustion analyses have allowed to characterise the behaviour of the material under critical conditions, in terms of decomposition taking place in the condense phase but also potential toxic emissions that can be released.

Toxicity, kinetics, temperature evolution do not provide a complete view of the combustion phenomenon. Beside these elements that characterise the behaviour of a material for given conditions as well as also the degree of fire hazard encountered, the energetic issue holds as an essential feature that cannot be neglected. The heat release rate (HRR) is a critical parameter that defines a fire. It does not constitute an intrinsic material property but it describes the energetic response of the couple formed by the material and its environment. Oxygen Consumption calorimetry (OC) and Carbon Dioxide Generation calorimetry (CDG) are widespread methods to calculate the HRR resulting from a combustion reaction. Apparatuses such as the FPA or the cone calorimeter have already proved their potential to qualify the burning behaviour of common fuels in addition to polymers when their data are combined with an adapted calorimetric procedure.

The same approach has been applied to energetic materials. However, prior to using these techniques, it is fundamental to have identified their restrictions. These techniques provide approximate estimations of the HRR. Results are affected by the propagation of uncertainties. Several sources of uncertainties can be found. One can cite:

1. Uncertainties associated with the sample material;
2. Uncertainties associated with the test conditions;
3. Uncertainties associated with the measurements;
4. Uncertainties associated with calculation assumptions.

If uncertainties cannot always be estimated, the three first sources cited have received attention in the past from the scientific community, alike the last one. The restrictions associated with the assumptions developed for using the OC and CDG principles have to be clarified. The limits of validity of the hypotheses have to be clearly defined. In particular, the present dissertation questions the relevance of the energy constants that have been specified for OC and CDG as well as their related uncertainties. One of the purposes of the research deals with the ability to estimate accurate error bars for the calculation of the HRR. Once uncertainties related to the calorimetric methods are assessed, a method adapted from the basic OC and CDG principles is introduced that allows estimating the HRR of energetic materials. The approach is based on considering the chemical decomposition of the burning compound and defining a fictitious molecule for which energy coefficients can be calculated. Nevertheless, it requires the material to be known. Finally, the question of the advantage brought by these techniques over others, in terms of accuracy, is discussed within the framework of unconventional products, such as energetic materials or compounds whose composition is ignored. The results from this work will contribute to the development of fire-analysis methodologies and validate their use with energetic materials.

Acknowledgements

I believe one the principal lessons when doing this PhD was to learn the balance between when focus and when escape from something. For that, I think it as a great experience. It is often when it is time to leave that one remembers the whole story. A twelve years step back is necessary to find the square one of this work. At this time, I would have never guessed that my future would be so much related to this summer month of I spent in the U.S.A. I have to confess, I was reluctant to go. Like many of my fellowmen, I did not inherit of the gene embedding the skill of foreign languages ability. My family encouraged me to go. They knew they were right long before me. I am grateful for all the sacrifices they did and still do for me. I also have to thank them for having always supported me to follow my own choices whether they agreed or not. I am also very thankful to Annie and Jean-Jacques Beloeil who are like second mother and father to me and my grand-parents who have been an infinite source of caring encouragements over the years.

Back to my memories of summer 1997, I should thank Pierre Joulain who introduces me to my future supervisor, José L. Torero and his family. I did not catch any fire yet. Six years after, in engineering school, I was going to attend a lecture about fire supposed to be delivered by a “Mexican firefighter”. I do not think this person ever showed up. Instead, an introduction to Fire Safety Engineering was given by one of the most expert in the field, José. That was the first time I heard about this topic and paradoxically it was really “cool”. It happened to also coincide with the first moment I got an idea about what I would like to do. In the end, it is always about meeting the right person at the right times. José has the skill to always appear at these spells. I am grateful to him for offering me the opportunity to do a PhD at the University of Edinburgh. I am also very grateful for his constant support, his precious advice and the patience he had for dealing with me during the last four years. Reading my silences is not always easy.

The other decisive element for the completion of the present study holds in the amazing environment formed by the firegroup, here in Edinburgh. I cannot see any better place to learn about fire, but also cultures, history or life styles from everywhere. Every day is being part of a live National Geographic channel. In the last four years, my mind visited South America, Europe, North America or Asia. I am thankful to all the people in the firegroup who brought me

new perspectives on life, and all the paradoxes. I learn from the Chilean philosophy. I like the German discipline. I am impressed by the English efficiency. I acknowledge the Italian wisdom. I wish I could have Portuguese communication intelligence. I esteem the Corsican spirit and the dynamism of the Auvergne. I would like to thank my two “old” friends, Pedro Reszka and Thomas Steinhaus for all the attention they gave me, for their support and all the things they taught me about fire but not only. They know their company and talks have been an important factor for enjoying these last four years. I am very grateful to Adam Cowlard and Cecilia Empis Abecassis for their support, the motivation they gave me and specially for making these last few months so good. Paradoxically, they are responsible if I keep nice memories from the longest period I spent on writing this thesis. I cannot forget my two other companions, Francesco Colella, Nicolas Bal, as well as Wolfram Jahn. I owe them for their support and all the interesting talks and laughs we had over the last three years.

Another important person for me is Andres Fuentes. He highly stimulated the initial impulses of this work and contributed greatly in moving forward over the last three years. I would like to thank Albert Simeoni for his precious help and also for giving me the opportunity to get a few times out of the energetic materials to discover the complex but interesting domain of wildland fires. I thank Guillermo Rein for his valuable advice for the completion of this study, as well as Jean-Pierre Vantelon for his judicious comments and observations during the defence of the present PhD.

I thank the Institut National de l’Environnement Industriel et des Risques (INERIS) for funding this work and for its technical support. I am particularly grateful to Guy Marlair for supervising the research in France and for his helpful advice. I am also thankful to Jean-Pierre Bertrand for his priceless contribution to carry out most of the experiments presented in the study. I would like to thank Richard Turcotte for his contribution and the data provided, Sylvain Brohez for his assistance and Jerzy Respondek from the Swiss Institute of Safety and Security in Neufchatel who provided the smoke powders. Finally, I am

In the end, this work is simply what I understood. But given the great help I had, all the blame is mine if I missed the point and got it wrong.

Table of Contents

List of Tables

Chapter 7.

List of Figures

1. Aims and Prospects from a Material Issue

Energetic materials encompass a wide range of chemical compounds associated with significant risks of fire and explosion. Formerly mainly dedicated to explosives, their singular features have later influenced the rise of a wide variety of new applications. Besides explosives, energetic materials also include propellants, pyrotechnics such as fireworks, smoke powders or flares as well as other unsteady chemicals [1]. Their characteristic profile comprehends very fast reactions upon initiation and large quantities of energy release [2]. Such behaviour emanates from the composition of the material itself. Their composition comprises an internal oxidizer that releases oxygen (O_2) during thermal decomposition. The pair fuel and oxidizer are both directly embedded in the matrix. As the material decomposes, a homogeneous gaseous combustible mixture is formed where O_2 and the volatiles are intimately connected favouring fast reaction rates. The occurring reactions can be self-sustained independently of the supporting atmosphere. Furthermore, their source of energy comes from the fact that most of their components contain large positive heats of formation.

The advantages that could bring this aspect of the energetic materials have been early applied, probably prior to be really understood.

Historians and researchers agree to report that the first recognised energetic material was black powder. It typically consists in a potassium nitrate (~75%), charcoal (~15%) and sulphur (~10%) mixture. It was discovered by the Chinese around 200 A.D. The earliest mention of it is found in a Chinese military manual dated from 1044 A.D. It reveals that Chinese used this powder for warfare [3]. Bamboo tubes of gun powder were fixed on arrows to contrive “rocket arrows”. Later, in the 13th century, the material composition got exported to Europe and by the year 1327 A.D., wars went under fire. The formula of the black powder composition got published by Sir Francis Bacon [3]. He was so impressed by the quantity of energy release that he predicted the end of wars by fear of the black powder power (Few centuries later, a significantly more powerful destructive tool would suggest an identical thought.). Davis [3] cites black powder has one of the three inventions accountable for ending the Middle Ages, the two others being the printing and the discovery of the New World. From this time to the

First World War, the use of black powder became more and more intense. Over the years, man began to find other intentions than war for the use of such compounds. To witness the first non-military usage of black powder, one needs to wait until the beginning of the 17th century. Black powder got used in Hungary for mining [3]. The first commercial production in the United States was by DuPont in the early 19th century [4]. By the mid to late 19th century, the development of high explosives was achieved based on the newly formalised modern chemistry. Nowadays, commercial purposes have overtaken the development of war tools and the manufacture of explosives has become more oriented towards industrial applications rather than military ones. They are optimized according to their particular usages. Besides providing large and rapid releases of energy, controlling the reaction rate as well as the chemical emissions presents interests for developing tools that would require a high force or the generation of particular compounds for a given duration. Propulsion and pyrotechnic devices entail such characteristics. Explosives, propellants and pyrotechnics share common traits. They are liquids or solids and undergo combustion very fast but their distinctions condition their intended applications [1].

The major aim of explosives is to maximize their performance in terms of gaseous expansion and heat release. In order to achieve this specific design, several requirements need to be satisfied,

1. Molecules decompose into lighter compounds with low formation energy so that the reaction is exothermic;
2. In the general case, the oxidizer has to supply enough O_2 to the volatiles to quickly oxidize most of the C-H base compounds into CO_2 and H_2O. however, various types of oxidizers (some containing no O atom) and fuels (exhibiting different structures than the usual C-H base) can be encountered;
3. The oxidation reaction has to occur rapidly enough to support the shock wave reaction.

Nowadays, military high explosives still follow requirements (1) and (2), even if high level of O_2 content is not necessary for all materials. They are usually designed to detonate (i.e. a combustion wave propagating at a velocity greater than the speed of sound [1]). While they can be seen as a research of high energy for maximum damage where the control of the reactions taking place does not always appear as a crucial aim, other applications have arisen

in the last decades where thermal and energetic stability is a critical characteristic. Such compounds are sometimes referred as low explosives. They burn slower than high explosives and generally undergo deflagration (i.e. flame propagation at a subsonic velocity [5]).

As previously noted, energetic materials are characterised by expansion of gases and heat release. The first cited property is of great interest for applications requiring a pressure build-up for a short spell. This represents one of the features characterizing propellants. Propellants are designed for propulsion purposes. They require releasing large quantities of gases at a defined production rate. Thus, the rate of reaction has to be controlled [1]. Moreover, the pressure build-up exhibited by propellants is significantly lower than by explosives (Rocket propellants burn bellow 20 MPa while the burning pressure in guns rises above 100 MPa) [6]. Their physical state is usually solid even if liquid propellants can operate as rocket propulsion [7]. Solid propellants composition is generally based on three complementary components: fuel, oxidizer and binder compounds. Binder and fuel are often incorporated in the same substance [1].

The four elements, light, sound, smoke and motion constitute some of the features that define explosives [8]. Lowering the effects of a fast energetic reaction by modifying the composition of the material reduces the magnitude of the explosives properties which brings then a possibility for other utilisations. This class of materials is defined as pyrotechnics. Babrauskas described them as devices relying on a chemical reaction to produce light, smoke, gases, sound and/or motion [1]. They receive military and civilian applications. Fireworks stand for a patent category of pyrotechnics. They could apply for the oldest tradition based on the most complex and advanced chemistry. Fireworks have built a unique relation with people based on the cultural heritage of many countries [9]. Then, it looks legitimate that they represent the showcase of the pyrotechnic field. Nevertheless, they are not the only one. Devices requiring gases expansion with a fast response such as airbag inflators [10] and actuators (airplane, ejection seats, satellites or other military applications) [11] [12] are also included. Beside entertainment and safety device contexts, signalling is the third major aim of the use of pyrotechnics. Production of flares accounts as an important area of pyrotechnics manufacture. Pyrotechnics mainly consist of solid fuel/oxidizer mixtures, often powders. The main difference with explosives is a slower rate of reaction which avoids detonating scenarios. Babrauskas explains that the performance of energetic materials is influenced by the Oxygen Balance

(%OB) of the mixture. It defines the difference between the oxygen contained in the compound and the amount required to reach stoichiometric conditions, expressed as a mass percentage of the initial substance considered [13]. The closer to zero, the closer is the mixture to stoichiometric conditions, correlating to the highest potential of energy release. In the case of pyrotechnics, to prevent reactions runaway, each of the constituents usually presents a substantial positive or negative %OB, so the reaction rate is driven by the slower intermolecular interactions between fuel and oxidizer rather than a fast intramolecular reactivity where the main reacting elements can be found within the same component [1].

One shortly introduced the three main classes of energetic materials that can be encountered. For each category, the material is designed to provide an optimized performance. Distinctive gases emissions and reaction rates characterize the attributes of each group. Because the evolution of the material through the reactions is a very complex process implying manifold factors, the optimization is mainly directed on key reactions mechanisms and quantification of the amount of energy released [14]. Research has been focused on developing and assessing methodologies which allow manipulating and controlling the energy release. Significant attention has been given to study the performance design of energetic materials [9] [15]. Evolution of the energy emissions depending on the mixture composition or the presence of additives, the conditions of initiations affecting the reaction rates are different characteristics that have been investigated [16][17].

However, the emergence of environmental questions highlighted a lack of understanding regarding side but critical aspects related to the use of energetic materials. Environmental and safety issues have received significantly less attention than the optimisation of performance design [18]. Although, by definition, conditions exist for which energetic materials can evolve to unstable conditions. Three major risks can be identified: explosion [19], fire [21] [22] and toxicity [23]. Evaluating thermal stability of such compounds within intended boundaries [14] is necessary in not sufficient in terms of safety. Characterisation of the material behaviour outside normal limits where unstable behaviour can be encountered has to be evaluated [24] [25] [26]. Given the peculiarity of energetic materials, critical questions remain to be inquired in order to evaluate the level of safety and environmental barriers required during their life process, from the manufacture, storage, [27] [28]transport [29] and use to final disposal or recycling [30] [31].

It is essential to identify the potential weaknesses encountered during synthesis, processing, handling, storage and destruction or recycling of these compounds. In the last few years, various accidents have been reported (cf. Table 1.1). They highlight potential risks in every step of the life cycle of energetic materials. As a consequence, a severe trouble pertaining to the use of these compounds stems in the difficulty to identify the numerous vulnerabilities susceptible to lead to a catastrophic event. In order to challenge these hazards, classifications such as the SEVESO II directive have been developed [38]. Explosives, propellants and pyrotechnics are regrouped within Categories 4 and 5. The latter corresponds to the most hazardous substances hazardous characteristics are described through the Risk Phrase R3, “a substance or preparation which creates extreme risk of an explosion by shock, friction, fire or other sources of ignition...”. Category 4 refers to substances which properties can be associated with the Risk Phrase R2, “a substance that creates the risk of an explosion by shock, friction, fire or other sources of ignition...”. It includes pyrotechnics that are defined as, “a substance (or mixture of substances) designed to produce heat, light, sound, gas or smoke or a combination of such effects through non-detonating, self-sustained exothermal reactions, or ... an explosive or pyrotechnic substance or preparation contained in objects ...”.

In a near future, Seveso will be replaced by a new legislation [39] based on the Globally Harmonised System (GHS) [40] developed through the United Nations for classification and labelling of dangerous compounds. Nevertheless, both classifications are based on a generic criteria approach to identify the dangerous properties of chemical substances [41]. Prior to any classification, the potential risks need to be carefully ascertained. As a consequence, apart from an optimized efficiency for the application they are devoted to, the safety aspects of the energetic imply to be understood. The evolution to a detonation regime, the behaviour of the material when submitted to unusual temperatures (i.e. initiation of decomposition) and when undergoing combustion, the level of toxicity and the generated combustion emissions, the contamination by spread of emissions and residues to the soil or the surrounding environment, vulnerability to external factors are as many points where new emphases need to be addressed

Table 1.1. Series of accidents having involved energetic materials in the last 25 years.

Date (Location)	EM* Class	Description	\Type of Accident \Process \Fatalities
June 1985 (USA, Oklahoma)	Pyrotechnics	Chain detonations in a fireworks factory initiated during unloading of pyrotechnics [27]	\ Chain Explosions \ Transport & manufacture \ 21 fatalities 5 injuries
August 1997 (Greece)	Explosives	Explosion in an ammunition plant during the disposal of a composition containing an excess of KNO_3 [29]	\ Unintended explosion \ Disposal \ 1 fatality 5 injuries
October 1997 (UK)	Explosives	Fire initiated on a truck carrying 100 kg of explosives [29]	\ Fire, no explosion \ Transport \ 1 injury
2000 (Netherlands)	Pyrotechnics	Fire started in the warehouse at the SE Fireworks depot in Enschede and spread to the storage area and extended to the ammonium refrigeration system of the adjacent brewery [27]	\ Explosion \ Storage \ 22 fatalities > 950 injuries
Sept. 2001 (France)	AN Fertilizers**	Explosion in warehouse where chemicals were stored within a chemical plant [32]	\ Explosion \ Storage \ 30 fatalities
October 2003 (France)	AN Fertilizers**	Delayed explosion about 1 hour after a fire started in a warehouse where fertilizers were stored [33]	\ Delayed explosion \ Storage \ 3 injuries
March 2003 (France)	Pyrotechnics	Explosion in a manufacture factory of civilian explosives [34]	\ Explosion \ Manufacture \ 4 fatalities
2006 (China)	Pyrotechnics	Air Pollution during the Lantern Festival in Beijing [35]	\ Emission of toxics \ Use \ None
Sept. 2009 (Serbia)	Explosives	Explosion in an ammunition plant. Preliminary investigation highlighted a “human factor” [36]	\ Explosion \ Manufacture, handling \ 7 fatalities, 14 Injuries

* EM: Energetic Material

** Fertilizers are not considered as energetic materials. However, Thermal runaways are possible if fertilizers undergo thermal decomposition, releasing oxidizing agents. Thus, a combustion reaction can initiate with the organic matter [37].

Integral characterisation of energetic materials is a fundamental requirement. Time and cost issues related to the formulation, synthesis and testing of systems do not allow carrying out extensive experiments on every new release. Consequently, a demand for predictive models has emerged. Prior to the development and spread of utilization of new mixtures, these tools must provide accurate insights of properties and behaviour for assessing the performance design but also for evaluating their stability in a maximum of configurations beyond normal usage boundaries where risks are potentially identified. Nevertheless, the development of these models still entails accurate and actual data that only experimentation can provide. In the end, critical assessment for validation, correction and improvement of models rely on the availability of increasingly detailed analyses.

A major issue associated with these types of compounds lies in their ability to undergo combustion The burning behaviour of these materials in case of detonations has been particularly studied since it usually represents the purpose they have been designed for [6] [42]. However, fundamental scientific questions remain unanswered related to the mechanisms of heat release and the emissions of generated gases when no transition to a detonation arises. Unlike for “conventional” fuels [43], a methodology susceptible to allow the estimation of the heat release rate (HRR) from a fire involving energetic materials has not been defined yet. The current understanding of the reaction mechanisms lacks appropriate characterization. More accurate descriptions of the physical and chemical phenomena undergoing during the burning of such compounds become essential. Potential risks can be identified from the manufacture to the disposal of energetic materials (cf. **Table 1.1**). Hazards pertaining to the thermal decomposition and the transition to a combustion regime are acknowledged [18] [27]. The production of toxic species and the fast reaction rates associated with sudden energy releases have been highlighted [23]. Nevertheless, the chemical pathways allowing the understanding of the physical and chemical mechanisms such as the ones associated with the generation of toxics or the heat release still remain to be investigated.

For “conventional” fuels, characterisation of the burning behaviour usually relies on two types of analyses:

- A thermal and chemical analysis is performed in order to explore the thermal degradation of the tested material and identify the different processes taking place during the reaction. Differential Scanning Calorimetry (DSC), and Thermogravimetry (TGA – DTA) constitute the

acknowledged tools used to describe the thermal degradation of materials. Coupling these techniques with Mass Spectrometry (MS) and Fourier Transform Infrared spectroscopy (FTIR) allows the detection and estimation of the concentration of the major chemical species generated during the process. Thermal analysis is generally associated with heating rates significantly lower than heating rates that would be encountered in the case of a fire. However, it offers a better glance of the evolution of the material chemistry during combustion as it potentially facilitates the separation of the different reaction mechanisms. It enables to develop a reaction scheme of the decomposition and improve the description of the phenomena taking place. Such approach is also interesting to characterise the emissions of toxic species and correlate them with reaction factors such as the temperature.

- A calorimetric analysis completes the characterisation. Knowledge of the HRR is a key indicator of the intensity of a fire [44]. It can be related to the evolution of heat and the rate of toxic gases emissions within a confined space. Because fire safety regulations and material classifications rely on the HRR, it has to be accurately estimated as well as its associated uncertainty. Furthermore, this variable also becomes highly valuable for the development and the validation of fire models. Various methods have been developed, principally based on the measurement of the burning rate [45], the evolution of chemical species during the combustion reaction [43] or the rise of enthalpy [46].

The chemical and calorimetric characterisations of a compound are usually carried out through small scale fire experiments. They are performed using apparatuses such as the Cone Calorimeter [47] [48] or the FM Global Fire Propagation Apparatus [49] [50]. They have been specially designed to provide estimations of the emissions of combustion gases as well as the HRR resulting of a combustion reaction.

The present study intends to assess the ability of the aforementioned techniques to characterise the chemical and thermal behaviour of a pyrotechnic material consisting of two ternary powders based on starch/lactose (fuels) and potassium nitrate (oxidizer) mixtures. These compositions are mostly used to create buoyant smoke for military purpose (Screening effect) or to assess the efficiency of venting systems in buildings [23]. The first aim will be to describe the main reactional mechanisms taking place during the combustion of the sample material based on the qualitative results derived from the thermal and chemical analysis.

Afterwards, the ability to accurately estimate the HRR associated with the reaction involving the sample pyrotechnic powders for different experimental conditions will be ascertained. In particular, one will investigate if classical HRR approaches can still be applied with such materials and for atypical combustion conditions like an inert atmosphere.

This chapter introduces the problematic and objectives of the present research. Subsequently, chapter 2 consists of the thermal and chemical analysis of two compositions of the starch, lactose, potassium nitrate ternary mixture. Given the complexity of the material, each component is first considered separately. In a second part, from the conclusions derived from the study of the thermal decomposition of each constituent, one aspires to describe the main reactional processes taking place during the degradation of the ternary powders. Species emissions are measured in order to identify a potential toxicity pertaining to the burning of the sample material. Combustion tests are also performed in order to evaluate the influence of the oxidizer as well as the role of the reacting atmosphere. Conclusions from chapter 2 should answer the questions relative to the ability of small scale testing such as the FPA to capture the reaction dynamics of energetic materials when undergoing combustion. Moreover, outcomes should allow a qualitative description of the decomposition reactions taking place in the material and the oxidation processes competing during the combustion.

Once the chemical behaviour of the sample material is better understood, the energetic problematic of the sample ternary powders is investigated. Chapter 3 intends to explain the importance of the estimation of an accurate HRR. It presents different techniques that have developed in order to calculate the HRR from a combustion reaction. Two particular methods are highlighted, based on the measurement of the evolution of the species concentrations during the burning process. Their main interest is that information about the sample material is not required to process an HRR approximation. This characteristic relies on the hypothesis of empirical constants of energy that can be applied to most of the materials.

Chapter 4 proposes to assess the validity of the assumption of energy constants by extended it to a large panel of components. In order to evaluate the robustness of the energy constants postulate, data have been compiled from the literature and calculations have been performed to investigate this questioning. An objective is to determine the possibility of limitations associated with the use of energy constants. The critical question that arises is to know if consistent uncertainties can be defined on the energy values used to approximate a HRR.

Instead of energy constants, one can wonder if the real critical need would rather not be the ability to define accurate error bars for the HRR calculations. Consequently, approaches are developed in order to define a confidence range confining the most potential values for the energy coefficients of a material.

After having reviewed the assumption of energy constants, one suggests to ascertain in chapter 5 the different sources of error that are encountered in the calculation of the HRR. Several sources of uncertainties can be defined. The test conditions, the sample material are sometimes difficult to estimate. The repeatability of combustion tests allows minimizing them. Finally, one stresses two main sources of errors in the HRR approximations: the ones related to the measurements and the ones associated with calculation hypotheses. Sensitivity analyses are carried out in order to estimate the contribution of the different variables and assumptions to the overall uncertainty of the HRR results.

After the restrictions related to the use of HRR estimation procedures become well defined, chapter 6 introduces an approach to estimate the HRR resulting from the combustion of the ternary powders. Furthermore, the methods previously described to approximate a relevant error (or confidence) range of a HRR calculation are also processed. At last, the accuracy and the limitations of the newly defined procedures are discussed.

Chapter 7 ends the present study with the conclusions that arise from the different investigations carried out to attempt a description of the principal mechanisms activated during the combustion of the sample ternary powders. One intends to stress the influence of the oxidizer and the reacting medium on the reactional process. Regarding the heat release issue, prior to present a method allowing the estimation of the HRR from the combustion of an energetic material, a review of three HRR calculation procedures is presented. The existence of limitations associated with the different techniques is argued. According to the experimental conditions and the knowledge about the material, preference could be directed to some methods rather than others. The essential question that needs to be discussed is related to a pursuit of precision. Should the HRR methods characterised in the present study be considered as accurate tools or just approximation tools to get an order of magnitude? Depending on the answer, the present study will show that the methodology can be conceived differently.

References

[1] Babrauskas, V., Explosives, propellants, pyrotechnics and reactive substances, in: Ignition Handbook, Fire Science Publishers, Issaquah, 2003, pp. 444 – 496;

[2] Rice, B., M., Overview of Research in Energetic Materials, in: Energetic Materials, Part 2: Detonation, Combustion, Editors: Politzer, P., A., Murray, J., S., Theoretical and Computational Chemistry, Vol. 13, Elsevier B.V., Amsterdam, 2003;

[3] Davis, T., L., The Chemistry of Powder and Explosives, Angriff Press, reprint of two volumes: 1941, 1943;

[4] Hopler, E., ISEE Blaster's Handbook, 17th Edition, International Society of Explosive Engineers, Cleveland, OH, (1998);

[5] Zalosh, R., Explosion Protection, in: SFPE Handbook of Fire Protection Engineering, 3rd Edition, Section 3, Chapter 10, The National Fire Protection Association Press, 2002, pp. 3-402 – 3-421;

[6] Kubota, N., Propellants and Explosives, Thermochemical Aspects of Combustion, Wiley – VCH, Germany, 2002;

[7] Summerfield, M., The Liquid Propellant Rocket Engine, Princeton University Press, New Jersey, pp. 439 – 520, 1959;

[8] Shimizu, T., Fireworks – The Art Science and Technique, Pyrotechnica Publications, Austin, 1981;

[9] Conkling, J., A., Chemistry of Pyrotechnics, Basic Principles and Theory, Marcel Dekker, New York, 1985;

[10] Deppert, T.,M., Barnes, M., W, Mendenhall ,I., V., Taylor ,R., D., Development of Gas Generants for Passive Automobile Restraint Systems, proceedings of the 2nd international symposium on sophisticated car occupant safety systems: AirBag 2000 Conference, Karlsruhe, Germany, November 1994. p. 10 – 17;[11] Rossi, C.,

Estève, D., Mingués, D., Pyrotechnic Actuator : A New Generation of SI Integrated Actuators, Sensors and Actuators A: Physical, 74 (1 – 3), pp. 211 – 215 (1999);

[12] Rossi, C., Estève, D., Fabre, N., Do Conto, T., Conédéra, V., Dilhan, D., Guélou, Y., A new MEMS based microthrusters for microspacecraft applications, in: Proceedings of the Micro/Nanotechnology for Space Applications (MNT'99), Pasadena (USA), 10–15 April, 1999;

[13] Shanley, E., S., Mehlem, G., A., The Oxygen Balance Criterion for Thermal Hazards Assessement, Process Safety Progress, 14 (1), pp. 29 – 31 (1995);

[14] Politzer, P., A., Murray, J., S., Energetic Materials – Part 2: Detonation, Combustion, Theoriticla and Computational Chemistry, Vol. 13, Elsevier B.V., Amsterdam, 2003;

[15] Badgujar, D., M., Talawar, M., B., Asthana, S., N., Mahulikar, P., P., Advances in Science and Technology of Modern Energetic Materials: An Overview, Journal of Hazardous Materials, 151, pp. 289 – 305 (2005);

[16] Krause, H., H., New Energetic Materials, in: Energetic Materials – Particle Processing and Characterization, Chapter 1, Editors: Teipel, U., Wiley – VCH, Weinheim, 2005; pp. 1 – 26;

[17] Berger, B., Parameters Influencing the Pyrotechnic Reaction, Propellants, Explosives, Pyrotechnics, 30 (1), pp. 27 – 35 (2005);

[18] Marlair, G., Kordec, M – A., Branka, R., Energetic materials and the fire problem, Proceedings from Poster the 8th International Symposium for Fire Safety Science (Poster), Beijing, September 2005, p. 1639;

[19] De Yong, L., V., Campanella, G., A Study of Blast Characteristics of Several Primary Explosives and Pyrotechnics Compositions, Journal of Hazardous Materials, 21, pp. 125 – 133 (1989);

[20] Wild, R., Propagation of blast waves produced by a pyrotechnic mixture, Journal of Hazardous Materials, 7, pp. 75 – 79 (1982);

[21] Hall Jr., J., R., Fireworks Related Injuries, Deaths and Fires, NFPA Report, Quincy (MA), USA, May 2003;

[22] Marlair, G., Branka, R., The Fireworks Explosion and Fire in Kolding, Denmark, November 2004, Communication at the OECDIGUS EPP Meeting at HSL (Buxton), 13 - 14 June, 2005;

[23] Marlair, G., Turcotte. R., Qwok, Q., S., Branka, R., Toxicity Issues Pertaining to Burning Pyrotechnics, Proceedings of the 33rd International Pyrotechnic Seminar, 16 – 21 July, Fort Collins, USA, 2006, pp. 467 – 484;

[24] Hosseini, S., G., Pourmortazavi, S., M., Hajimirsadeghi, S., S., Thermal decomposition of pyrotechnic mixtures containing sucrose with either potassium chlorate or potassium perchlorate, Combustion and Flames, 141 (3), pp. 322 – 326 (2005);

[25] Brown, M., E., Thermal Analysis of Energetic Materials, Thermochimica Acta, 148, pp. 521 – 531 (1989);

[26] Scanes, F., S., Thermal Analysis of Pyrotechnic Compositions containing Potassium Chlorate and Lactose, Combustion and Flame, 23, pp. 363 – 371 (1974);

[27] Carson, P., Mumford, C., Pyrotechnics and Loss Prevention, Loss Prevention Bulletin, 173, pp. 3 – 15 (2003);

[28] Sivapirakasam, S., P., Surianarayanan, M., Swaminathan, G., Hazard Assessment for the Safe Storage, Manufacturing and Handling of Flash Compositions, Journal of Loss Prevention in the Process Industries, 22, pp. 254 – 256 (2009);

[29] Duijm, N., J., Hazard Analysis of Technologies for Disposing Explosive Waste, Journal of Hazardous Materials, A90, pp. 123 – 135 (2002);

[30] Akhavan, J., Grose, I., Rabin, S., Modification of Pyrotechnic Formulations to Aid Recovery, Recycling and Demilitarization, Propellants, Explosives and Pyrotechnics, 22 (2), pp. 81 – 86 (1997);

[31] Mitchell, A., R., Chemical Conversion of Energetic Materials to Higher Value Products, Proceedings of the 24th International Annual Conference of ICT, Karlsruhe (1993);

[32] Dechy, N., Bourdeaux, T., Ayrault, N., Kordek, M-A., Le Coze, J-C., First lessons of the Toulouse ammonium nitrate disaster, 21st September 2001, AZF plant, France, Journal of Hazardous Materials, 111, pp. 131 – 138 (2004);

[33] Marlair, G., Kordek, M., A., Safety and Security Issues Relating to Low Capacity Storage of AN-based fertilizers, Journal of Hazardous Materials, A123, pp. 13 – 28 (2005);

[34] Le Coze, J., C., Accident in a Dynamite French Factory: An Example of an Organisational Investigation, Safety Science, 48 (1), pp. 80 – 90 (2010);

[35] Wang, Y., Zhuang, G., Xu, C., An, Z., The air pollution caused by the burning of fireworks during the lantern festival in Beijing, Atmospheric Environment, 41, pp. 417 – 431 (2007);

[36] BBC, Serb arms plant blasts kill seven, 4th of September 2009, BBC Article;

[37] Babrauskas, V., Information on specific materials and devices, in: Ignition Handbook, Chapter 14, Fire Science Publishers, Issaquah, 2003, pp. 675 – 1021;

[38] Council Directive 96/82/EC of 9 December 1996 on the control of major-accident hazards involving dangerous substances , Official Journal, L 010 , 14/01/1997, pp. 0013 – 0033;

[39] Regulation (EC) No 1272/2008 of the European Parliament and of the Council of 16 December 2008 on classification, labelling and packaging of substances and mixtures, amending and repealing Directives 67/548/EEC and 1999/45/EC, and amending Regulation (EC) No 1907/2006, Official Journal of the European Union, L 353/1–1355, Brussels, 31/12/2008;
http://eur-lex.europa.eu/LexUriServ/LexUriServ.do?uri=OJ:L:2008:353:0001:1355:EN:PDF.

[40] UNECE, Globally Harmonized System of Classification and Labelling of Chemicals (GHS), First published in 2003; http://www.unece.org/trans/danger/publi/ghs/ghs_welcome_e.html.

[41] Wood, M., H., The Seveso II experience in the application of generic substance criteria to identify major hazard sites, Journal of Hazardous Materials, 171, pp. 16 – 28 (2009);

[42] Badgujar, D., M., Talawar, M., B., Asthana, S., N., Mahulikar, P., P., Advances in science and technology of modern energetic materials: An overview, Journal of Hazardous Materials, 151, pp. 289 – 305 (2008);

[43] Janssens, M., Parker, W., J., Oxygen Consumption Calorimetry, in: Heat Release in Fires, Chapter 3, Editors: Babrauskas, V., and Grayson, S., J., Elsevier Applied Science, New York, 1992, pp., 31 – 59;

[44] Babrauskas, V., Peacock, R., D., Heat Release Rate: The Single Most Important Variable in Fire Hazard, Fire Safety Journal, 18, pp. 255 – 272 (1992);

[45] Drysdale, D., An Introduction to Fire Dynamics, 2nd Edition, Chapter 1, Wiley, Chichester, pp. 1 – 30 (2002);

[46] Smith, E., E., Heat Release Rate Calorimetry, Fire Technology, 32 (4), pp. 333 – 347 (1996);

[47] ISO 5660, "Fire Tests – Reaction to Fire – Part 1: Rate of Heat Release from Building Products (Cone Calorimeter)", International Standards Organisation, Geneva, 1993;

[48] ASTM 1354-905, "Standard Test Method for Heat and Visible Smoke Release Rates for Materials and Products Using an Oxygen Consumption Calorimeter", American Society for Testing Materials, Philadelphia, 1995;

[49] ASTM E2058-03, "Standard Test Method for Measurement of Synthetic Polymer Material Flammability Using a Fire Propagation Apparatus", ASTM International, West Conshohocken, 2003;

[50] NFPA 287, Standard Test Methods for Measurement of Flammability of Materials in Cleanrooms Using a Fire Propagation Apparatus (FPA). National Fire Protection Association, Quincy, MA, USA, 2007;

2. Thermal Analysis of Starch, Lactose and Potassium Nitrate Based Ternary Mixtures

2.1. Introduction

The present chapter proposes to investigate the thermal and chemical behaviour of two pyrotechnic compounds. The question of how much they are representative of energetic materials can be argued on an energy release point of view. Nevertheless, they are recognised as pyrotechnics with military, signalling or entertainment applications [1]. The considered compositions consist in two ternary smoke powders based on lactose ($(C_{12}H_{22}O_{11}\cdot H_2O)_n$), starch ($(C_6H_{10}O_5)_n$) and potassium nitrate (KNO_3) mixtures. The main feature of these pyrotechnics is the emission of smoke. Rather than a consequent energy release, a controlled reaction rate to achieve the requested concentration and density of smoke is more required. However, the smoke powder contains fuel components, lactose and starch embedded with an oxidizer, KNO_3. It complies with the class of pyrotechnics. According to the general definition of this group of compounds, smoke powder can be considered as an energetic material. The heats of combustion of the two fuel compounds, starch and lactose, are respectively 16.2 and 15.08 $kJ.g^{-1}$ [2]. The values are relatively low compared to hydrocarbons or polymers heats of combustion. The limited reaction rate of the “smoke” compositions restricts the rate of energy release. Furthermore, they usually undergo thermal decomposition at low temperatures (200 – 400°C) [3] which can potentially promote the production of toxic species. The interest of such mixtures holds in the strength of the reaction. Sustained combustion can be obtained without transition to deflagration or detonation regime. The pressure and temperature rises are low enough to avoid the measuring instruments such as thermal analysis devices or calorimeters to be compromised. The reaction rates are low enough for the mass, gases and heat evolutions to be captured by standard apparatuses. Furthermore, the constituent, KNO_3, present in the ternary mixture is an extensively used oxidizer, notably found in the composition of the black powder. The potency of the oxidizer to modify the behaviour of the material in terms of emissions and energy release is a critical trait [4].

The combustion behaviour of a solid is strongly related to its thermal decomposition. The capacity to identify the endothermic and exothermic processes taking place as well as the gaseous emissions is essential to assess the reaction pathways. An accurate description of the chemistry occurring during the thermal decomposition provides valuable insights for understanding the physical and chemical mechanisms involved during the combustion reaction. Consequently, thermal and chemical analysis techniques are highly valuable to examine the thermal behaviour of solid compounds. Regarding the pyrotechnic powders,, the presence of the oxidizer within the material promotes oxidation reactions and so the amount and rate of energy release during the thermal decomposition.. Furthermore, it also affects the nature of the gaseous products. Understanding the influence of such a parameter during thermal degradation will help improving models and designing effective safety barriers preventing from hazardous conditions. The reactivity of the fuel components and the energy required for their decomposition as well as for the oxidizer decomposition are other strong factors that determine the evolution to a combustion reaction. Another key variable, independent of the structure of the material, is the nature of the supporting or reacting atmosphere (i.e. the atmosphere in which the reaction takes place). These parameters are the ones that limit the stability of the mixture in extreme configurations the causes of potential toxic emissions.

The aim of this chapter is to provide thermal and chemical views for the characterisation of the two ternary powders based on a lactose, starch and KNO_3 mixtures. Firstly, the thermal analysis of each component is studied separately on order to clearly identify thermal and chemical transitions occurring during their thermal decomposition. Subsequently, the thermal analysis of lactose/starch/KNO_3 ternary mixtures is performed. Results are interpreted according to the information collected from the study of the single components. From the different conclusions dressed, a recombination is attempted in order to propose a chemical pathway for the decomposition of the ternary mixture when exposed to increasing temperatures. In particular, it allows assessing the temperatures at which the decomposition initiates and also providing energetic characteristics of the reaction (i.e. exothermic or endothermic). Identification of the decomposition gases provides an insight of the potential toxicity of the powder. In addition, it will provide a valuable description of the chemical reactions and thermal processes taking place during the combustion reaction.

2.2. Sample Material and Experimental Setup

2.2.1. Sample material

As previously mentioned, the energetic material used during the different experiments carried out within the framework of the present study belongs to the class of pyrotechnics materials. It is a ternary powder based on a mixture of starch ($(C_6H_{10}O_5)_n$) , lactose ($(C_{12}H_{22}O_{11})_n$) as fuel components and potassium nitrate (KNO_3) as oxidizer. This product is used by fire brigades in Switzerland and in France to control the efficiency of building smoke venting systems [4]. It is assumed to generate a “clean” buoyant smoke. However, the question of the potential toxicity of such material has only been addressed lately [5]. The two compositions tested are indicated on Table 2.1. Contents in each component are given in mass percentage. For each composition, both fuels compounds are present in equal quantities. For a given mass m of ternary mixture,

$$m_{lactose} = m_{starch} \quad (1)$$

Discussion about the influence of the composition on the combustion behaviour will be proposed in Chapter 3.. However, it can already be noticed that, in terms of stoichiometry, both sample powders exhibit fuel rich conditions. Elemental analysis highlights that the smoke powder 2 highlights burning conditions closer to the stoichiometry than the smoke powder 1.

Table 2.1. Composition in mass percentage of tested smoke powders.

Components	Smoke Powder 1	Smoke Powder 2
Starch ($C_6H_{10}O_5$)	30%	25%
Lactose ($C_{12}H_{22}O_{11}$)	30%	25%
Potassium nitrate (KNO_3)	40%	50%

2.2.2. Experimental setup

The experimental method of the thermal analysis relies on the application of Differential Scanning Calorimetry (DSC), Thermogravimetric (TGA) and Differential Thermal (DTA) analyses [6]. The experimental results describing the thermal behaviour of each single component have been gathered from various studies collected in the literature. The data related to the ternary mixtures and handled in the latter study originate from tests campaign carried out at the Canadian Explosives Research Laboratory within the Explosives Branch of the Minerals and Metals Sector at Natural Resources Canada [7].

In order to investigate the thermal behaviour and the mode of energetic process (i.e. exothermic or endothermic) during decomposition, a DSC study has been conducted. Tests were realised on samples weighing between 1 and 2 mg placed in aluminium pans sealed with pin-hole lids. They were heated from 40 to 550°C and the heating mode was controlled by a constant ramp of 5°C.min^{-1}. The DSC analyser was calibrated for heat flow [8] and temperature [9]. Experiments have been conducted under air and N_2 atmosphere in order to identify and examine the thermal mechanisms induced by the presence of the internal oxidizer within the material. Thermal characterisation based on mass and species evolutions was also performed using a TGA/DTA technique coupled with Fast Fourier Transform Infrared Spectrometry (FTIR) and Mass Spectrometry (MS). This will allow identifying the major species generated, the temperatures related to the emissions and in which thermal regions the main transformations take place. 5 mg samples and the reference material (Platinum foil) were disposed in alumina pans. The temperature ramp was set constant to 10°C.min^{-1}, up to 1200°C. Calibrations were operated prior to the tests [9].

2.3. Thermal Analysis of the Mixture Single Components

In order to apprehend the complexity of the thermal and chemical behaviour of the 40% and 50% KNO_3 ternary mixtures, characteristics of each component of the compositions have been first studied separately.

2.3.1. Oxidizer thermal decomposition

The peculiarity of the sample material comes from the presence of an oxidizer in its composition. KNO_3 is supposed to decompose and release O_2 in the medium. As the sparking plug is activated, the surface temperature of the material increases. Heat is conducted inside the solid beyond the critical decomposition temperature of KNO_3 in the mixture. Several studies have been carried out on KNO_3. They highlighted that it may decompose following several paths.

Freeman studied the decomposition of KNO_3 and concluded that two reactions occurred depending on the temperature [14]. For temperature between 500 and 700°C, potassium nitrite (KNO_2) was the major species formed. Above 700°C, potassium nitrite decomposes into potassium oxide (K_2O), N_2 and O_2. The two reactions are expressed as,

1st decomposition reaction, T>500°C:

$$KNO_3 \longrightarrow KNO_2 + \frac{1}{2}\, O_2 \quad (\Delta H_{r1} = 124.8\ \mathrm{kJ.mol^{-1}}) \tag{2}$$

2nd decomposition reaction, T>700°C:

$$2\, KNO_2 \longrightarrow K_2O + N_2 + \frac{3}{2}\, O_2 \quad (\Delta H_{r2} = 189\ \mathrm{kJ.mol^{-1}}) \tag{3}$$

From the heats of reaction ΔH_{r1} and ΔH_{r2}, it clearly appears that the thermal decomposition of KNO_3 is endothermic. Oza and Szper also observed the generation of NO and NO_2 compounds from the decomposition of potassium nitrite [15] [16].They assumed the reaction:

$$2\, KNO_2 \longrightarrow K_2O + NO_2 + NO \quad (\Delta H_{r3} = 127.8\ \mathrm{kJ.mol^{-1}}) \tag{4}$$

According to Oza and Szper, reaction (4) occurs above 683 K (410 °C) [15] [16].

In parallel to the decomposition to nitrite, for temperatures beyond 810 ±10 K (537 ±10°C), potassium nitrate can also decompose directly into potassium oxide according to reactions [17] [18],

$$2\, KNO_3 \longrightarrow K_2O + 2NO_2 + \frac{1}{2}O_2 \quad (\Delta H_{r4} = 278.8\ \mathrm{kJ.mol^{-1}}) \tag{5}$$

$$2\,KNO_3 \longrightarrow K_2O + N_2 + \frac{5}{2}O_2 \qquad (\Delta H_{r5} = 311.9\ \mathrm{kJ.\,mol^{-1}}) \tag{6}$$

Reactions (2) to (6) evolve potassium oxide, oxygen, nitrogen but also nitrogen oxides. These reactions can occur simultaneously, consecutively or they can overlap. Thermal analysis allows assessing the temperature at which these reactions start to take place.

Between 10 and 20% of grade potassium nitrate is consumed for the production of explosives or pyrotechnics [19]. Given the strategic condition of being able to understand the behaviour of such oxidizer, several studies have been carried out, allowing access to important data. Kramer et al performed Differential Scanning Calorimetry (DSC) experiments on KNO_3 over the temperature range 280 – 650°C [20]. Samples were heated at a constant rate of 10°C per minute. Such scan rate was assumed to be appropriate to capture the phase transitions of the component [21]. The DSC was calibrated to within 0.05°C of the melting point of indium (156.63°C). Samples were dried and encapsulated in high-pressure stainless steel pan, sealed by crimping [20]. Figure 2.1 illustrates the trace of KNO_3 from a DSC experiment.

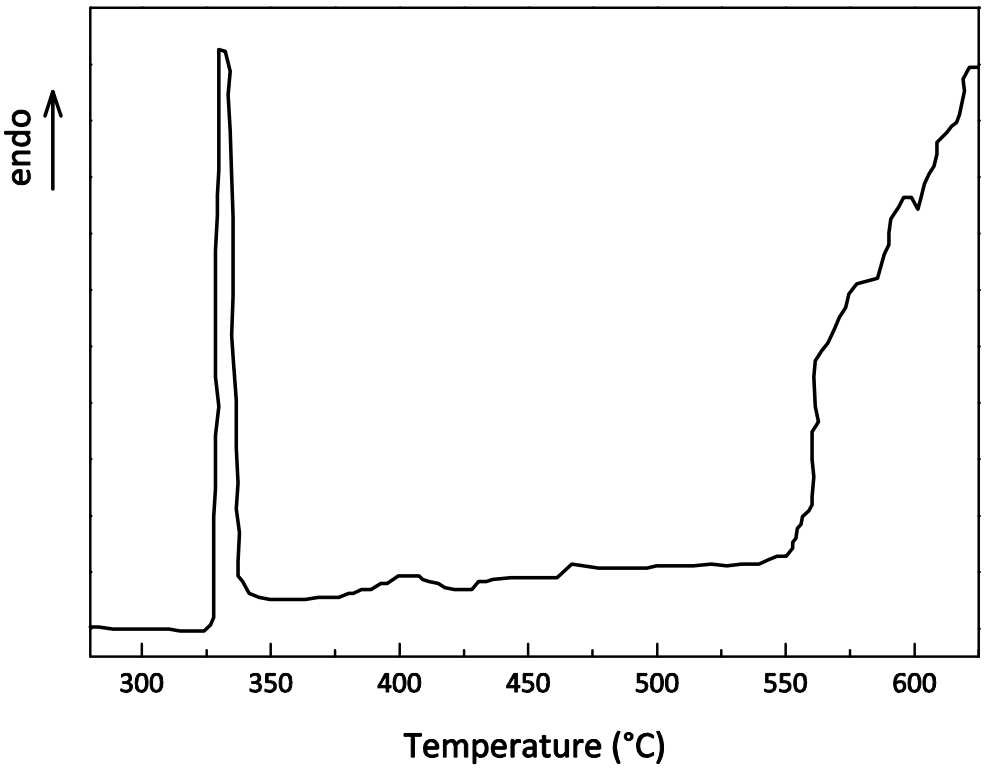

Figure 2.1. DSC experiment carried out on KNO_3 under air atmosphere (heating rate: 10°C.min^{-1}) [20].

A large endothermic peak is observed around 330°C which corresponds to the melting point of KNO_3 (onset temperature: ~ 325°C [21]). The second increase appearing around 550°C. This temperature is higher than the one reported by Freeman. However, the technique he had used may have been more sensitive than the DSC measurements.

Kramer also highlighted that the average KNO_2 decomposition temperature observed by means of DSC was about 530°C, thus, slightly lower than the DSC decomposition temperature of KNO_3. Considering reactions (2), (3) and (4), KNO_3 decomposes into KNO_2 which also subsequently decomposes. He made the assumption that the DSC decomposition temperature for KNO_3 depends on the stability of KNO_2. Therefore, he estimated that reactions (2), (3) and (4) are a plausible reason of the endothermic increase rather than reactions (5) and (6).

DSC results are often compared to Differential Thermal Analysis (DTA) ones in order to verify that the behaviour observed is representative of the material and is not affected by the technique used. Gordon and Campbell carried out a large investigation on the thermal behaviour of inorganic compounds using DTA [22]. Their results are presented on Figure 2.2. The heating rate used during the experiments was kept constant at about 15°C per minute.

A first endothermic peak is observed at 128°C. It corresponds to a crystalline transition. This transformation has not been observed in the DSC experiment. The range of studied temperatures was too high and the transformation had already occurred. The DTA experiment locates the melting of KNO_3 at 330°C. Using DSC, a similar temperature was obtained. The decomposition transition of melted KNO_3 and/or KNO_2 to oxide occurs around 700°C which is higher than the temperature reported using DSC.

The experimental configurations differ for DTA and DSC methods. DTA samples were apparently positioned on an open block while the DSC samples were located inside capsules creating different atmospheres above them when decomposing. The supporting atmosphere influences the reaction that take place [17]. Freeman [14] carried out his experiments in closed reaction vessels. His sample setup was closer to the one used for the DSC analysis. On the other hand, Sirotkin mentions that KNO_3 in contact with air decomposes at 550 - 700°C into KNO_2 and O_2 [23]. Precisely, he observed that important amounts of KNO_2 were generated above 650°C for heating longer than 2 hours. He also measured the total combined nitrogen

and noted that KNO_2 highly predominated in the reaction products. The latter tends to confirm that reactions (2), (3) and (4) are dominant in terms of occurrence.

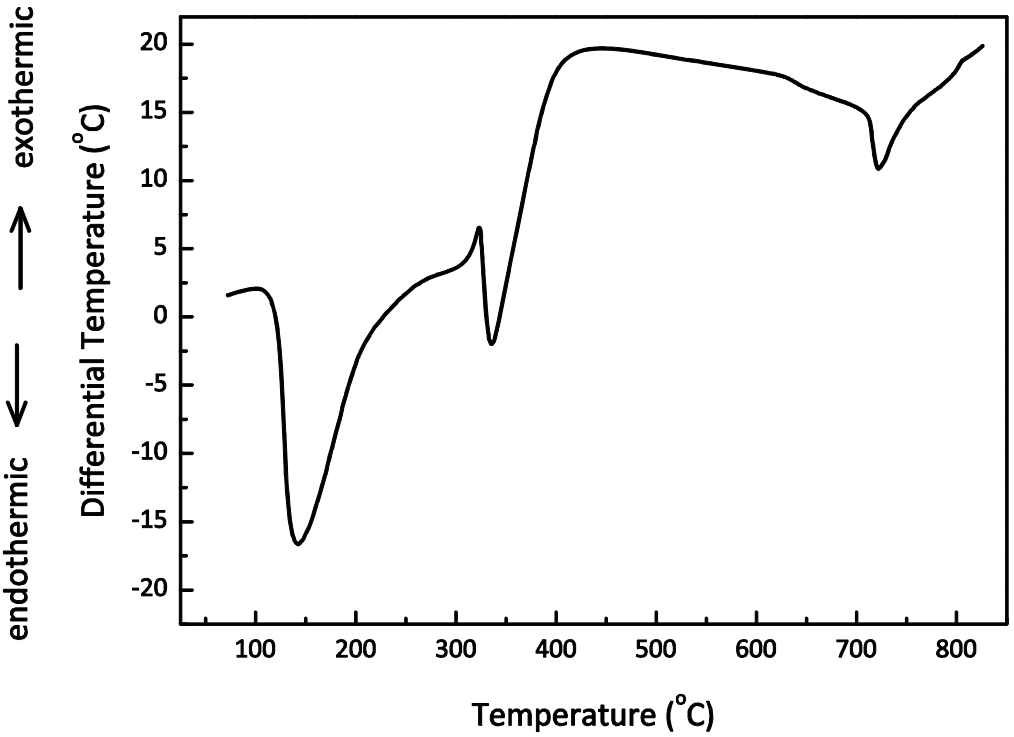

Figure 2.2. DTA curve of KNO_3 performed under air atmosphere for a heating rate of about 15°C per minute [22].

2.3.2. Fuel components thermal decomposition

Another interesting point is the ability to predict how the fuel components of the mixture will decompose. The two fuel components of the tested powders are lactose ($(C_{12}H_{22}O_{11}\cdot H_2O)_n$) and starch ($(C_6H_{10}O_5)_n$). They are two common materials and thermal analyses related to them can be found in the literature.

2.3.2.1. Lactose, $(C_{12}H_{22}O_{11}\cdot H_2O)_n$

Figure 2.3 presents DSC results obtained for α-lactose monohydrate by Itoh et al [24]. Samples were 5 mg and the heating rate was set at 15°C/min. They observed a first endothermic peak around 150°C corresponding to the dehydration. The water of crystallisation is eliminated from the compound. The second endothermic peak around 220°C coincides with the melting transition accompanying the thermal decomposition of lactose.

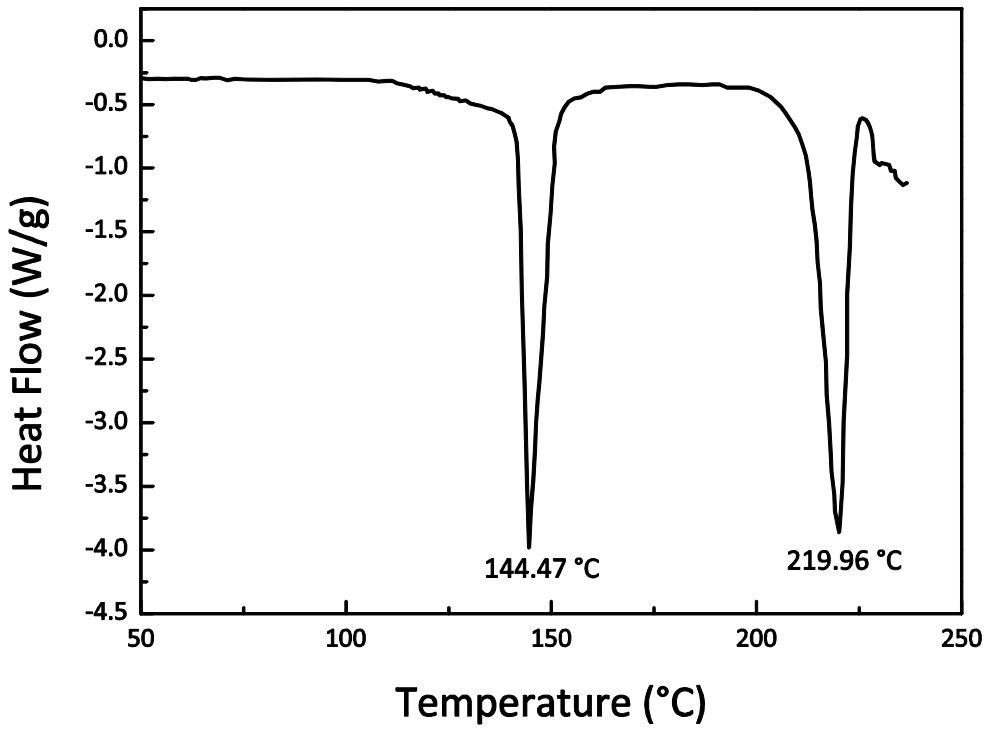

Figure 2.3. DSC Curve for α-Lactose Monohydrate under N_2 atmosphere [24].

2.3.2.2. Starch, $(C_6H_{10}O_5)_n$

The second fuel component of the powder is starch. It is a compound offering a wide range of industrial applications [25]. Starch is a polysaccharide carbohydrate combining amylopectin and amylose. The thermal behaviour of starch has been studied on the base of techniques such as DSC and TGA-DTA [26] [27]. O'Connell [28] studied the thermal decomposition of corn starch using DTA under N_2 atmosphere. Figure 2.4.a. presents the DTA curve obtained with a heating rate of 10°C/min. Samples were analyzed in a platinum crucible under dry N_2. Decomposition is clearly endothermic. Three endothermic peaks are visible. The first peak occurs around 60°C. It corresponds to the gelatinization of starch [29]. This process occurs when heat is applied to starch. It describes the order-disorder transition in the crystalline structure of the compound. Starch shows a tendency to diffuse and absorb water vapour until equilibrium. The phenomenon comes with the formation of hydrogen bonds between the granules (i.e. amylose and amylopectin) and water molecules. The diffusion and absorption are accompanied by swelling of granules due to the penetration of water inside the crystalline structure and coating on the surface [30]. The swelling is reversible if starch is dried. However,

at elevated temperatures, the changes in the crystalline structure become irreversible. Rupture of the hydrogen bonds constituting the crystalline network is enhanced allowing further hydration on new sites and the structural order tends to disappear. At this time, the process is characterised by heat absorption which explains the first peak observed on the DTA curve. Figure 2.4.a. stresses two other peaks, one around 280°C and the other around 310°C. The same two peaks also appear on the DTG curve on Figure 2.4.b. The first peak is simultaneous with the initiation of mass loss. Aggarwal [27] explains that the initial peak is overtaken by the main degradation. Further study allows supposing that the first peak is due to modifications on the surface of the compound which would apparently end up with the generation of more reactive surface components. As the temperature is increased, the main decomposition takes place, leading to a large production of CO, CO_2. About 20% of carbonaceous residue remains at the end of the decomposition. The data measured under N_2 have also been compared to the ones obtained under flowing air [26]. Aggarwal noted that under air atmosphere, two regimes of combustion can be observed: A gaseous combustion, where the gaseous degradation products ignite and sustained flaming is achieved, then, a glowing combustion, where surface oxidation of char is observed with production of CO, CO_2 and water [31] [32]. The two stages clearly emerge on the DTA curve of Figure 2.5.

A first endothermic peak appears simultaneously with the initiation of mass loss. The same behaviour was noticed under N_2 atmosphere which highlights a non-oxidative process. It corresponds to the degradation of starch. The endotherm takes place under the gaseous combustion of the produced volatiles. This large exothermic event overtakes the endothermic reaction. This explains the important exothermic peak observed around 33 minutes. The peak coincides with a change in slope of the mass loss. The second phase of mass loss is still related to an exothermic process. However, the reaction occurring corresponds to the combustion of the carbonaceous residue. The reaction is self-sustain and defines a phenomenon usually called “glowing combustion”.

In the present study, experiments will be carried out on a ternary mixture base on potassium nitrate, lactose and starch. A state of the art of the thermal decomposition of each of the components has been accomplished. Given the understanding of their thermal behaviour, the present work will now focus on the thermal analysis of the ternary mixture.

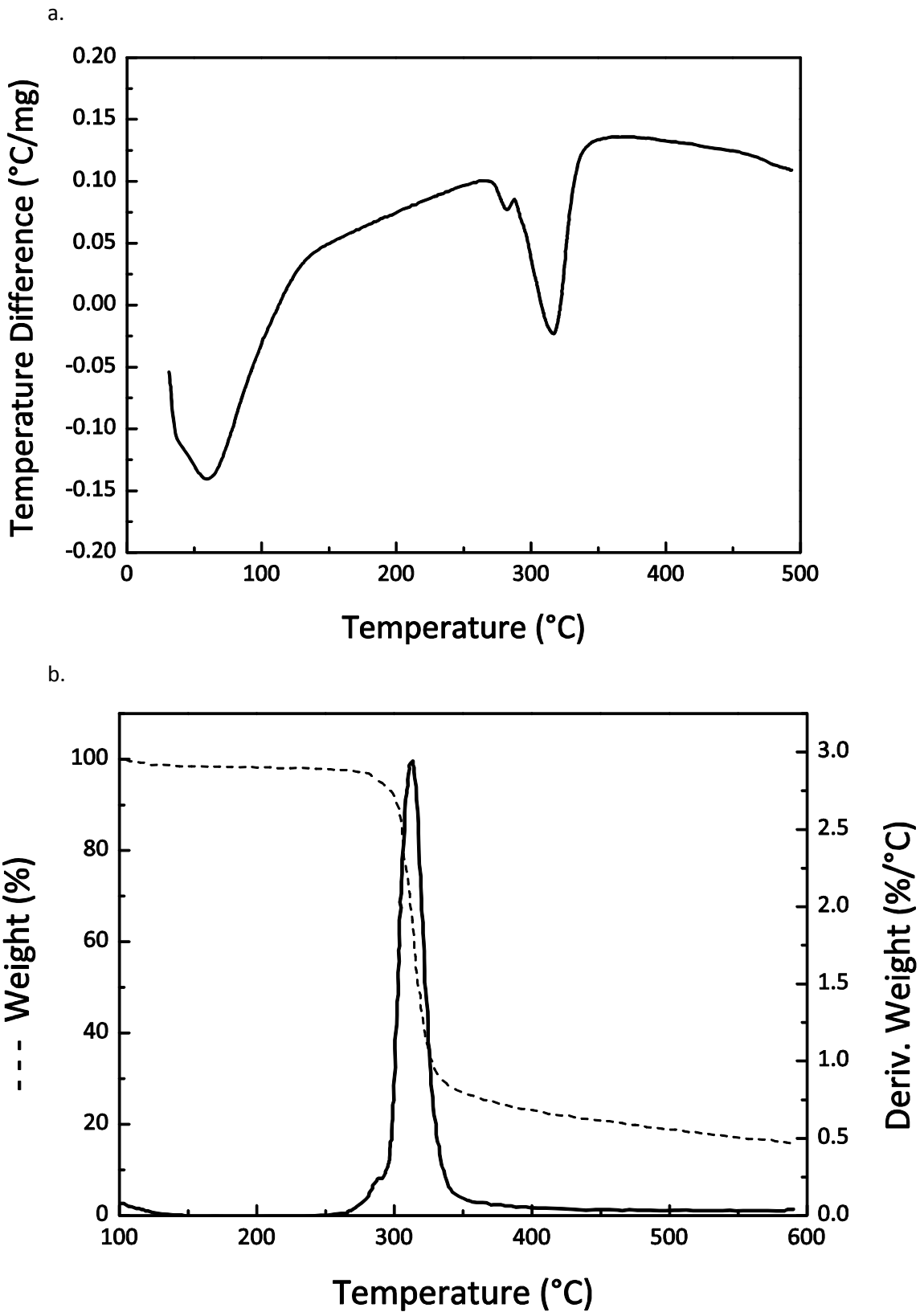

Figure 2.4. DTA (a.) and TG-DTG (b.) curves for corn starch at a heating rate of 10°C/min under N_2 atmosphere [27] [28].

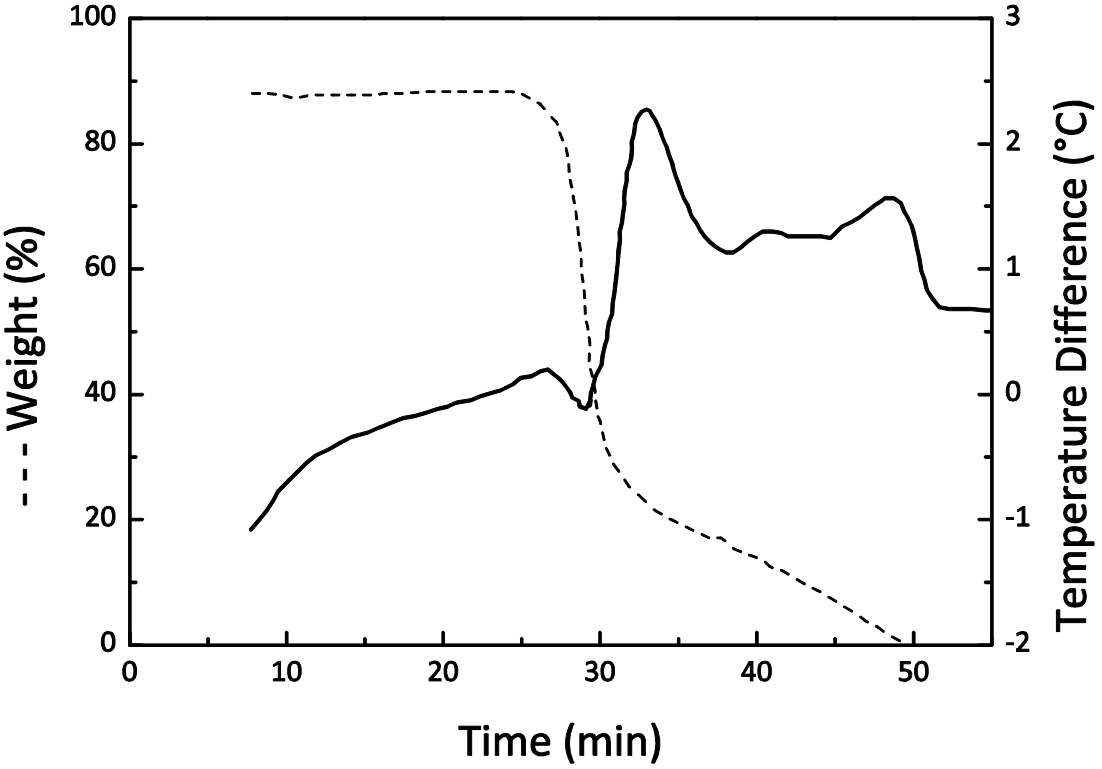

Figure 2.5. TG-DTA curves of corn starch at a heating rate of 10°C/min under air atmosphere [29].

2.3.3. Ternary mixture thermal decomposition

From the observations and conclusions arisen for the different compounds, a reconstruction of the thermal and chemical evolution of the ternary mixture is attempted. Finally, a chemical pathway is proposed describing the decomposition of the material when submitted to relatively low temperature rises.

Figure 2.6 illustrates the DSC curve obtained for a sample of 40% KNO_3 powder under air atmosphere. A first endothermic peak is observed around 140°C. Given Figure 2.2, a hypothesis is the crystalline transition of KNO_3. Thermal analysis allowed the evaluation of a transformation temperature which was relatively close to the present measured one. A second endotherm appears around 150°C. According to Figure 2.3, it apparently corresponds to the loss of the water of crystallization. Figure 2.6 exhibits a third endotherm around 200°C. It coincides with the decomposition temperature of lactose that was previously noticed (cf. Figure 2.3). As the temperature goes higher, the DSC curve reveals exothermic processes. Four slope changes can be identified between 250 and 350°C. A shoulder appears around 280°C and

is followed by a first exotherm peak at about 300°C. According to the previous thermal analyses carried out on the different components of the sample material, these temperatures correspond, respectively, to a surface reaction and the start of degradation of starch. One considers that the main process taking place is the oxidation of lactose by O_2 from the air. A second exotherm exhibits around 325°C and is rapidly overwhelmed by a third one, larger, around 340°C. An assumption is to consider that the first peak is correlated to the oxidation of starch and lactose with O_2 from the air; the second peak coincides with the decomposition of KNO_3. KNO_3 releases O_2 which enhances the oxidation reactions occuring and lead to a higher exothermic flow.

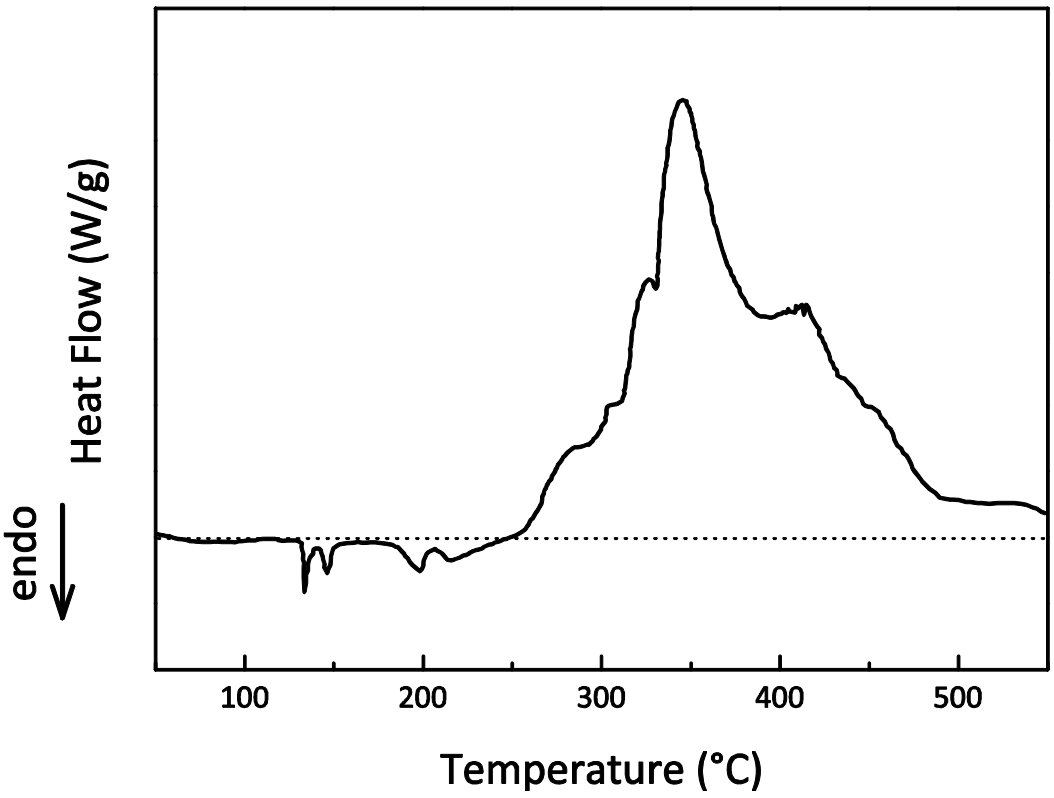

Figure 2.6. DSC curve of 40% KNO_3 powder at a heating rate of 5°C/min under air [33].

In order to verify these hypotheses, DSC experiments have been carried out under N_2 atmosphere. The curve obtained is presented on Figure 2.7. Compared to the one under air, only a light shoulder appears around 300°C. The two peaks previously observed on Figure 2.6 at 300 and 325°C are not present. It tends to confirm the hypothesis based on the surface oxidation by the O_2 from air. The large exothermic peak observed under air still emerges under

N_2 but is narrower and emerges around 330°C, a slightly lower temperature then the one noticed under air. It corresponds to the melting point of KNO_3. This phenomenon is probably the reason of the initiation of the exothermic reaction. This tends to confirm the assumption that, in the situation of the present ternary mixture, KNO_3 decomposes at a significantly lower temperature than the one obtained by Freeman [14], Kramer [20] or Gordon and Campbell [22]. The O_2 released from KNO_3 will oxidize the thermally degraded fuel compounds, inducing the exothermic peak.

The exotherm temperature corresponds to the melting of KNO_3. In the case of the ternary mixture, it seems that KNO_3 undergoes decomposition as it melts. Another exothermic peak or shoulder is identified around 420°C. The same phenomenon was observed in the temperature region for the starch thermal analysis. It appears for both DSC curves, under air and N_2 atmosphere conditions.

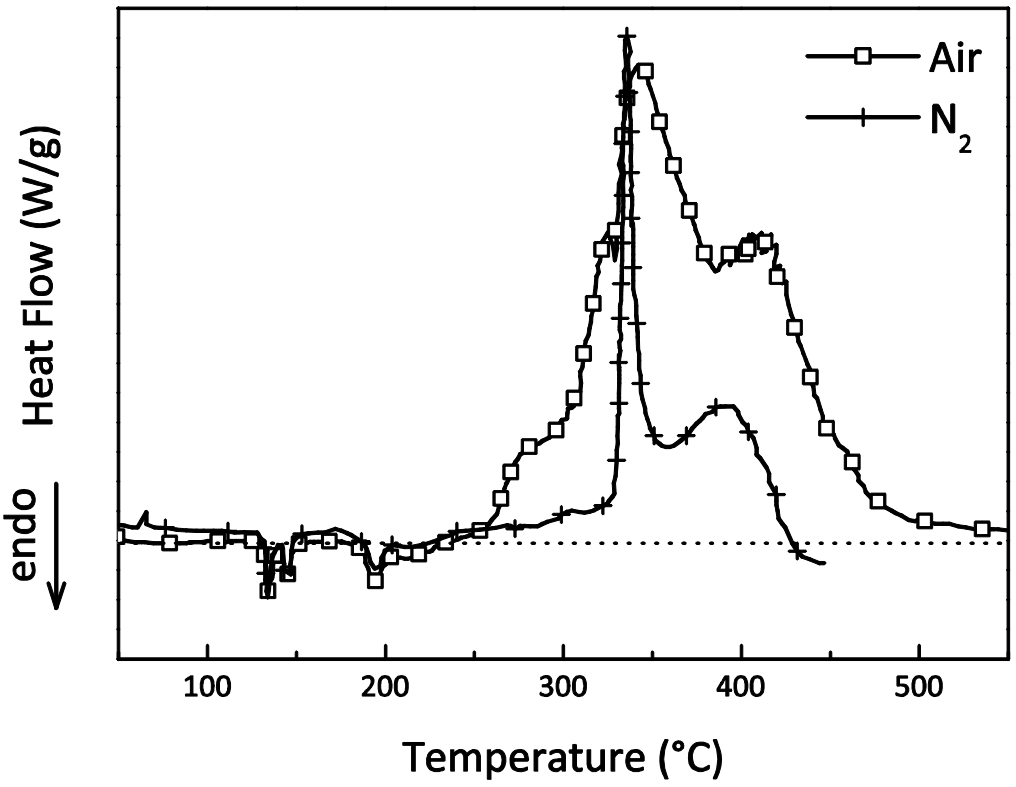

Figure 2.7. DSC curves of 45% KNO_3 powder at a heating rate of 5°C/min under air and N_2 atmospheres [33].

According to the previous study conducted on starch, one can assume that char oxidation and glowing combustion occur in the region. So, carbonaceous residues are oxidized by O_2 from the air as well as from KNO_3. It has to be noticed that char oxidation and glowing combustion

are achieved for slightly lower temperature (i.e. 390°C) in the case of experiments carried out under N_2 atmosphere. The conjecture developed in the present study is that, in a first time, oxidation of the fuel compounds undergoing thermal degradation and glowing combustion (surface oxidation of carbonaceous char, which consists in an intense smouldering phenomenon where the material has been heated so much that it radiates in the visible spectrum [34]) take place in the condensed phase and the gaseous phase if volatiles give rise to a flammable atmosphere.. In a second time, char oxidation is also initiated and the different processes overlap themselves. In the end, the production of carbonaceous residue remains, allowing the sustaining of glowing combustion and char oxidation.

Finally, three different regimes manifest themselves. First lactose and starch degrade and low temperature oxidations begin. In a second time, KNO_3 degrades to form O_2 and further oxidation of the fuel compounds take place (with an extra supply of O_2 for the experiments ran under air atmosphere) as well as carbonaceous residues evolve into glowing combustion and char oxidation (smouldering processes). In a third time, once the mixture has fully decomposed and only residue is left, glowing combustion and char oxidation due to residual O_2 remain the last active modes.

DSC experiments have also been performed on 50% KNO_3 powder under air atmosphere. The curve is displayed on Figure 2.8.

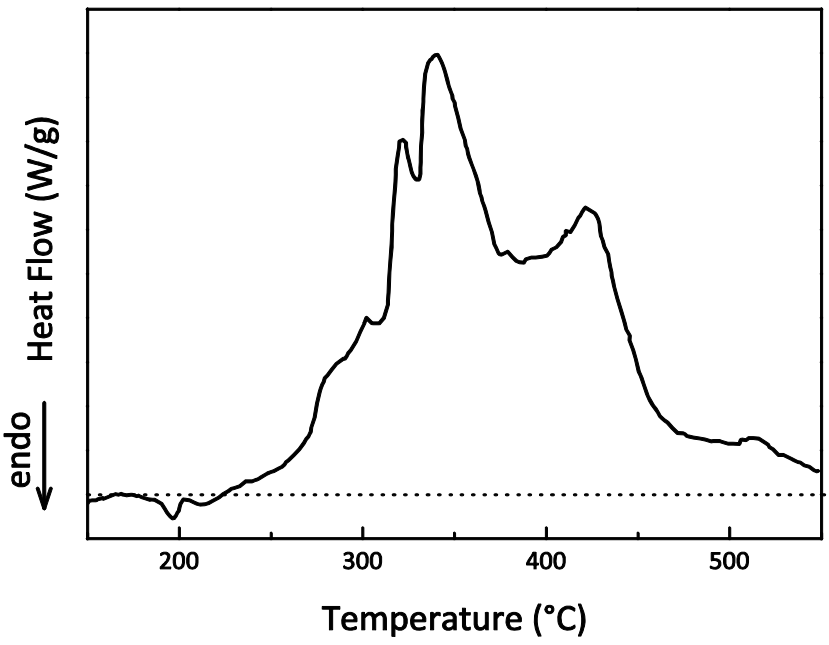

Figure 2.8. DSC curve of 50% KNO_3 powder at a heating rate of 5°C/min under air [33].

The thermal behaviour of the sample is very similar to the response of the 40% KNO_3 powder. Endothermic and exothermic peaks are located for identical temperatures. Nevertheless, Peaks are more pronounced and present higher magnitude than the ones observed with the 40% KNO_3 powder. It clearly indicates that the enthalpy of reaction was higher with this mixture.

The previous results can be compared to TG-DTA plots presented on Figure 2.9. The DTA curve is relatively similar to the DSC one. The three endothermic peaks appear at the same temperature than the ones measured by DSC. The large exothermic peak around 350°C is comparable to the one illustrated on Figure 2.6. However, the shoulder and the two preceding exothermic peaks are less distinct than during the DSC analysis. Furthermore, the glowing region is identified for the same temperatures but, again, less explicit. In the end, results obtained by DSC and TG-DTA correlate well. The hypotheses exposed previously comply with the shape observed on the DTA curve.

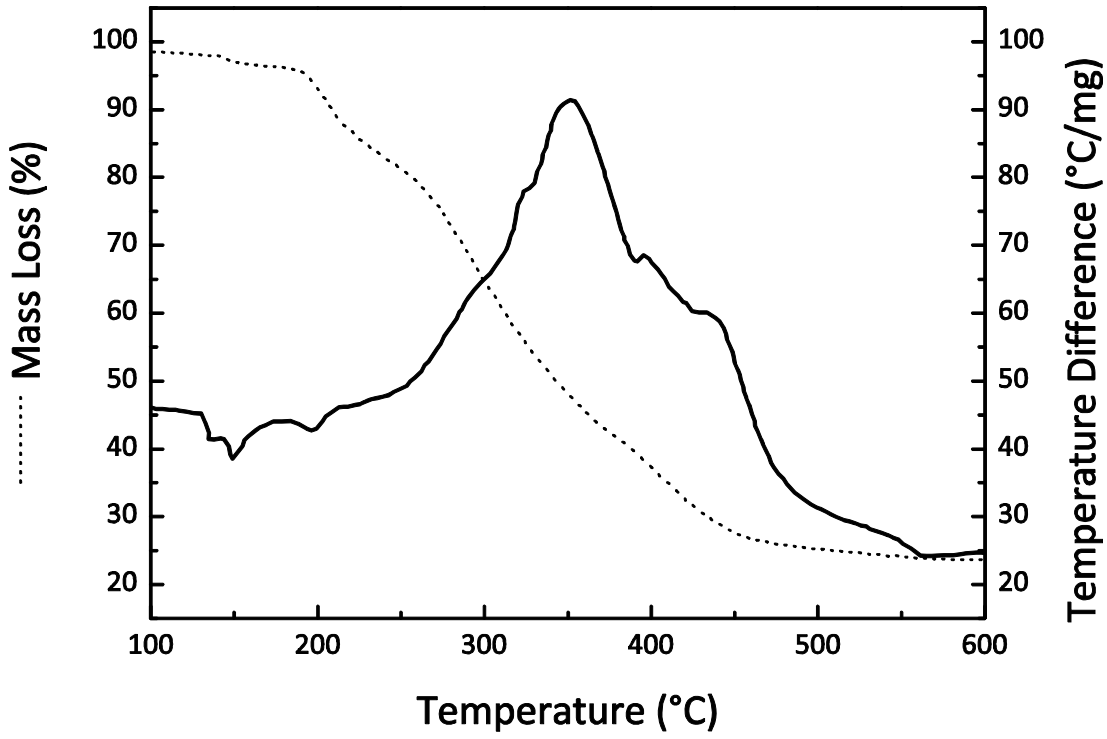

Figure 2.9. TG-DTA curves of 40% KNO3 powder at a heating rate of 5°C/min under air [33].

The mass loss presents a slight variation between 140 and 200°C. It is in agreement with the assumption of a release of water vapour. The apparent mass loss initiation would coincide with

the assumed degradation of lactose. A change in slope is observed around 230°C and could be interpreted as the beginning of the starch and KNO_3 decompositions. The lower slope can be explained by the two endothermic processes. Energy is required to initiate the reactions. Then, between 250 and 360°C, the mass loss slope is the stiffest. This region would correspond to the oxidation of the decomposing fuel compounds coupled to a glowing combustion and char oxidation. Above 400°C, the slope decreases. This would strengthen the assumption that only glowing combustion and char oxidation remain at this time, active. Sample residue is about 24% of the initial mass.

In order to further investigate the validity of previous hypotheses, gases emissions need to be analysed. DSC technique has been coupled to a Fourier Transform Infrared (FTIR) spectrometer. Results are presented on Figure 2.10. It has to be noticed that the FTIR was not calibrated for quantitative measurements and only qualitative observations are outlined. Nevertheless, approximate relative concentrations can be estimated using the scaling factors of Brill et al [35]. It can be used to convert the absorbance intensity of equal partial pressures of gases concentrations relative to CO_2.

The first identified gas to be formed is water vapour. The loss of water of crystallization starts around 150°C and confirms the assumption about the origin of the DSC and DTA endothermic peak in this region. At about 200°C, fusion of lactose is supposed to begin. For this temperature, the FTIR data show initiation of the formation of CO_2, CO, aldehydes (CH_2O, $C_2H_4O_2$), formic acid (CH_2O_2) and at a very low level, NO_2. Between 210 and 400°C, the major gaseous species produced are CO_2, H_2O, CO, aldehydes and formic acid. The two last compounds are only formed inside the present temperature range. Previous studies highlighted that the temperature level affect their generation. They are formed for low temperatures [36] which hold within the operating temperature range of smoke powders (200 - 400°C, [4]). Transitions occur at 240°C and 320°C. Peaks or shoulders are observed for all the major species. If peaks appear clearly for H_2O, aldehydes and formic acid, the shoulders observed, respectively, at 240°C for CO and 320°C for CO_2 are slighter. Main peaks for CO and CO_2 emerge, respectively, at 320°C and 370°C. These observations agree with the hypotheses previously put forward. The first peaks at 240°C probably correspond to the degradation of lactose which gets oxidized by O_2 from the air. The second peaks around 320°C result from the decomposition of starch and the melting of KNO_3. O_2 released by KNO_3 and O_2 from the air

coupled with the thermal degradation of lactose and starch enhance the oxidation reactions. The behaviour noticed between 320 and 370°C could originate from a combination of two regimes, flaming combustion and smouldering combustion. In this region, generations of CO and H_2O decrease which indicates that the reaction rate of the oxidation reaction is reduced.

Above 400°C, the hypothesis is that glowing combustion is predominant. The carbonaceous residue is oxidized. Figure 2.7 previously showed that glowing combustion was achieved under air and also N_2 atmosphere. Thus, the large production of N_2O in this temperature zone also allows the assumption that another reaction occurs, involving KNO_3 and the carbonaceous residue. Turcotte et al. explain the production of N_2O by a contribution from the following reaction [37]:

$$2\,KNO_3 + 2C \longrightarrow 2\,CO_2 + K_2O + N_2O \quad (7)$$

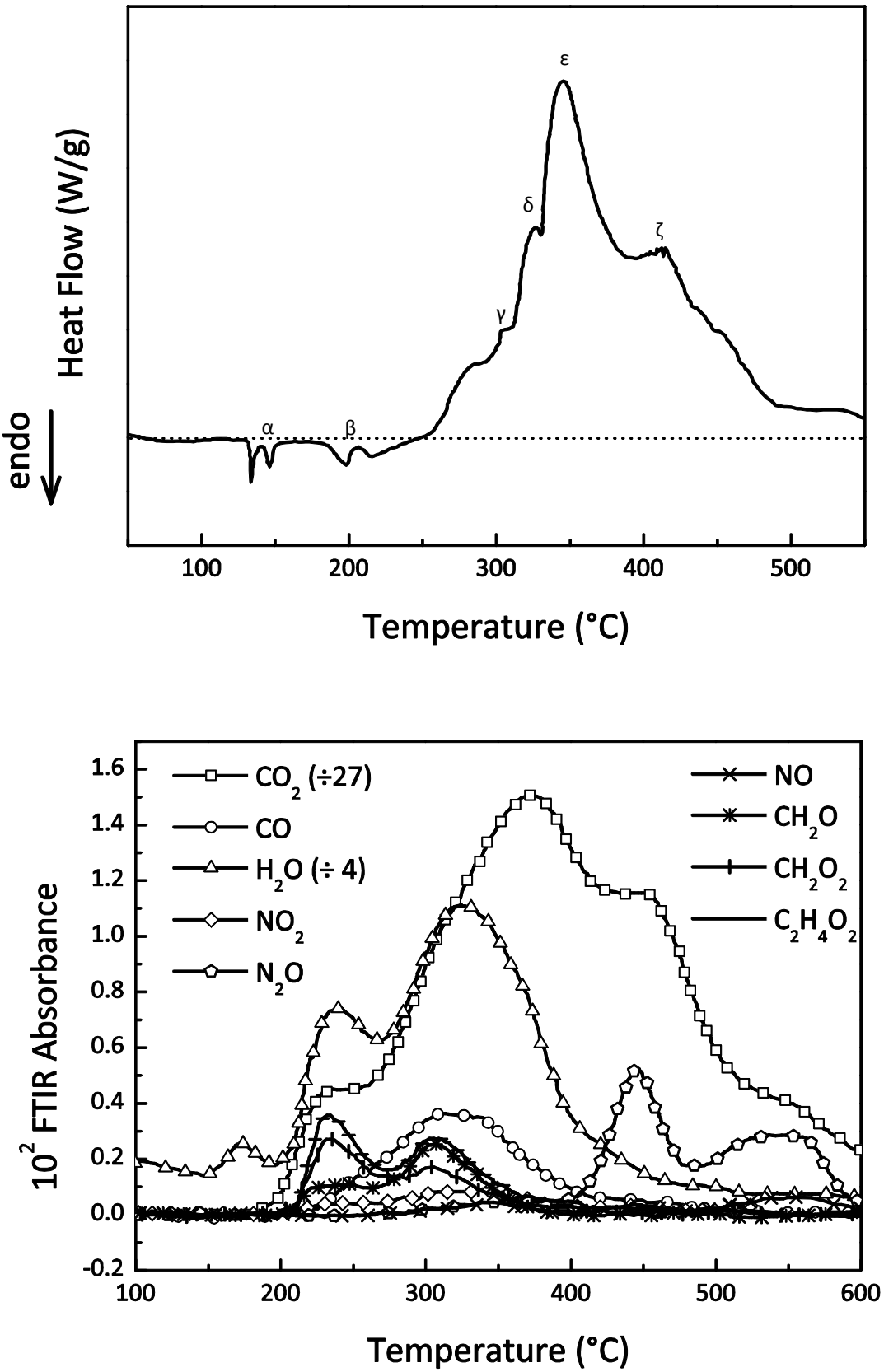

Figure 2.10. DSC – FTIR curves of 40% KNO_3 powder at a heating rate of 5°C/min under air.

2.3.4. Discussion

Based on the hypotheses developed, a potential scheme of the powder decomposition can be sketched. The DTA and DSC methods might be criticized due to the slow heating rates applied during the experiments. The temperature increase once the combustion reaction starts can be relatively fast. Although the heating rate might appear as a serious drawback, it allows to exhibit two different regimes: a flaming combustion and a smouldering combustion evolving to glowing at the surface of the material. These two stages must also be effective during the combustion reaction. The second regime probably occurs very rapidly after the first one due to the fast rate of temperature increase. The reactions may eventually overlap each other. Furthermore, DSC and DTA allow the study of species emissions in a range of temperature corresponding to the one encountered during the use of KNO_3 ternary powders (200 - 400°C, [4]). Results have highlighted the production of toxic compounds such as aldehydes, formic acid and nitrous oxides. They stress the potential toxic behaviour of the material when used within these temperatures. Nevertheless, in case of combustion, higher temperatures are reached and FTIR analyses have shown that the generation of toxic elements, apart from CO, tended to decrease to relatively low levels. A suggested explanation is that, for aldehydes and formic acid, the flame, acting as an incinerator, induces further oxidation of these compounds which are not released anymore in the atmosphere.

Regarding Figure 2.10, endothermic and exothermic peaks and shoulders have been denoted α to ζ. The two endotherms α are respectively explained by a rhombic to trigonal KNO_3 phase transition (around 130°C) and the loss of water of crystallization from lactose (around 150°C) [37].

A third endothermic peak is located around 200°C (β). It corresponds to the melting point of lactose. At this temperature, only two reaction products clearly evolve, H_2O and CO_2. This observation could be explained by the following reaction:

$$C_{12}H_{22}O_{11} \cdot H_2O + \frac{48}{5}\, KNO_3 \longrightarrow 12\, CO_2 + 12\, H_2O + \frac{24}{5}\, K_2O + \frac{24}{5}\, N_2 \qquad (8)$$

KNO_3 is soluble in solvents containing hydroxyl groups like lactose. Reaction (8) may have been activated by a partial solution of KNO_3 in liquid lactose. In the same temperature region, traces

of NO_2 are detected. According to Blackwood and Bowden [38], at these temperatures, KNO_3 reacts with organic compounds to form NO_2, confirming the previous hypothesis. Vaporisation of the liquid lactose compound starting around 220°C, the reaction ceases given that liquid lactose will not remain in the mixture.

Between peak β and shoulder γ, the reaction becomes noticeably exothermic under air and lightly under N_2. The major species generated are H_2O, CO_2, aldehydes and acetic acid, the two last being characteristic of low temperature reactions. It indicates that the previous reaction (8) may still occur at a low reaction rate. Furthermore, the generation of aldehydes and acetic acid suggests that the degradation of lactose operates. A large number of studies can be found in the literature dealing with the thermal degradation of polysaccharide carbohydrate such as lactose and starch [39] [40] [41]. Many carbohydrates, including lactose and starch [40] [42], evolve to the same volatile products during the pyrolysis. It can be assumed that they all degrade into similar intermediate compounds, the major one being Levoglucosan. The latter undergoes two competing reactions [39]:

- Degradation to volatiles of low molecular weight and tar;
- Polymerization and aromatization ending to form char;

Although this mechanism has been observed for various carbohydrates including lactose and starch, it cannot be affirmed with certitude that identical intermediate compounds are formed when reaction involves not only lactose and starch but also KNO_3. However, low molecular weights products, such as aldehydes and acetic acid have been identified. They have been shown to be formed in small quantities during the pyrolysis of polysaccharide carbohydrates. It is probable that lactose and starch decompose following a similar process.
Under air, the exothermic region observed between β and γ is mainly due to the aerial oxidation of the decomposing lactose. The reaction can be defined by,

$$C_{12}H_{22}O_{11} \cdot H_2O + 12\ (O_2 + \ 3.76\ N_2) \longrightarrow \ 12\ CO_2 + 12\ H_2O + 45.12\ N_2 \qquad (9)$$

Furthermore, under N_2, the major species produced is water. The dehydration can be described by the following reaction,

$$C_{12}H_{22}O_{11} \cdot H_2O \longrightarrow 12\,C + 12\,H_2O \quad (10)$$

Simultaneously to the release of water vapour, reaction (10) outlines the formation of char. Finally, reactions (9) and (10) define the two principal overall reactions used to describe the process taking place on the interval β to γ.

The exotherm δ rises around 320°C, close to the decomposition temperature of starch as well as the melting point of KNO_3. The main exotherm observed under N_2 atmosphere begins to evolve at the same temperature. This latter phenomenon is probably initiating the flaming combustion. Furthermore, the decomposition temperature of starch is about 320°C. Similarly to the shoulder γ, peaks of H_2O, aldehydes and acetic acids occur within the exotherm δ, indicating that the degradation of starch into volatiles operates. NO_2 continues to be generated from the decomposition of KNO_3. CO becomes one of the major species formed, after H_2O and CO_2. Peaks of H_2O, CO, aldehydes and acetic acids coincide as the formation of CO_2 increases. It suggests that the oxidation process of lactose and starch undergoing decomposition is sustained by O_2 from air as well as from the KNO_3 decomposition following, for lactose, reactions (8) and (9) and for starch,

$$C_6H_{10}O_5 \cdot H_2O + \frac{24}{5}\,KNO_3 \longrightarrow 6\,CO_2 + 6\,H_2O + \frac{12}{5}\,K_2O + \frac{12}{5}\,N_2 \quad (11)$$

$$C_6H_{10}O_5 \cdot H_2O + 6\,(O_2 + 3.76\,N_2) \longrightarrow 6\,CO_2 + 6\,H_2O + 22.56\,N_2 \quad (12)$$

The ventilation conditions allow complete oxidation of a fraction of the fuel compounds. Nevertheless, formation of incomplete species is identified, the main compound being CO. One assumes these productions to originate from the incomplete oxidation of the fuel volatiles by the O_2produced by the KNO_3 decomposition. The incomplete oxidations of lactose and starch can be illustrated, respectively, by the two following reactions,

$$C_{12}H_{22}O_{11} \cdot H_2O + \frac{24}{5}\,KNO_3 \longrightarrow 12\,CO + 12\,H_2O + \frac{12}{5}\,K_2O + \frac{12}{5}\,N_2 \quad (13)$$

$$C_6H_{10}O_5 \cdot H_2O + \frac{12}{5}\,KNO_3 \longrightarrow 6\,CO + 6\,H_2O + \frac{6}{5}\,K_2O + \frac{6}{5}\,N_2 \quad (14)$$

δ closely precedes the large exotherm ε. In contrast to the previous exothermic peak, apart from CO_2, the concentration of the major gases (H_2O, CO, aldehydes, acetic acid) starts to decrease. It could suggest that rate of decomposition of the fuel compounds declines and so the associated oxidation processes.. Nevertheless, although little H_2O and CO are generated, CO_2 continues to rise. Another reaction occurs, different from the oxidation of the degrading fuels. Alike lactose, a portion of starch has pyrolysed following the reaction,

$$C_6H_{10}O_5 \cdot H_2O \longrightarrow 6\,C + 6\,H_2O \tag{15}$$

Then, the second reaction occurring in ε is the oxidation of the carbonaceous residue mainly by potassium nitrate but probably also by O_2 from the air at the surface of the solid. The main gaseous product is CO_2 with small amounts of H_2O and CO.

As the temperature continues rising, the only process remaining is the glowing combustion. It was observed under air and N_2 atmospheres. Moreover, at this stage, very little H_2O and CO evolve. CO_2 is the main reaction product. A significant production of N_2O emerges. It has been described by equation (7). The shoulder ζ corresponds to the oxidation of the char from lactose and starch by the remainder of KNO_3.

A conjecture has been developed about the thermal decomposition of an energetic powder based on a ternary mixture of starch, lactose and potassium nitrate as an oxidizer. As previously underlined, the behaviour described in the analysis may diverge from the reality of the combustion reaction. DSC and DTA techniques rely on constant low heating rates. On the contrary, combustion is characterised by rapid increases in temperature and one reaction regime may be overwhelmed by another one. Nevertheless, the present analysis gives an essential insight in later understanding of the behaviour of the material under combustion.

In the second part of this chapter, interest will be directed to the physical and chemical response of the material when combustion takes place. Particularly, the influence of the oxidizer on the reaction will be investigated.

2.4. Concluding Remarks

Thermal analysis is a critical method in order to understand the physical and chemical mechanisms taking place during the thermal degradation of a material. With the aim to characterise the thermal behaviour of two ternary smoke powders based on a starch, lactose and potassium nitrate mixtures, a thermal analysis has been carried out. Such product belongs to the category of pyrotechnics. The two compositions differ by their concentration in KNO_3 which varies, in mass, from 40% to 50%. In a first part, because each compound exhibits a different thermal behaviour, they have been studied separately. In a second, to interpret DSC, TG – DTA and MS experimental results, one decided to use a composite method. After having extracted from the literature DSC, TG – DTA and MS data providing information on their thermal decomposition, combination of the previous results have been compared to results derived from DSC, TG-DTA and MS for the 40% and 50% KNO_3 ternary mixtures. Similarities enabled to draw up hypotheses on the thermal decomposition taking place.

Thermal decomposition of both ternary mixtures exhibits exothermic and endothermic peaks for identical temperatures. Results only differ by the magnitude of the peaks; reaction is more energetic for the 50% KNO_3 ternary mixture as exotherms rise higher. From the thermal analysis, two main exothermic processes are observed:

1. Oxidation of the degrading fuel compounds by O_2 from the air and/or (if test carried out under inert atmosphere) O_2 resulting from the thermal decomposition of KNO_3;
2. Oxidation of the carbonaceous residue materialised by glowing combustion at the surface of the sample.

The global chemical pathways is postulated as follow:

- The crystalline transition of KNO_3 (endotherm, ~140°C). Few degrees above (endotherm, ~150°C), dehydration takes place;

- Under air, a large exothermic peak arises between, 250°C and 350°C. It consists in several exothermic reactions overlapping. One assumes that they are mainly engendered by oxidation processes. Between 250°C and 320°C, the major reaction is the oxidation of the decomposing lactose by O_2 from the air (reaction (9)).Around 325°C, as lactose oxidation

still proceeds, starch starts decomposing undergoes oxidation by O_2 from air (reaction (12). A higher exothermic peak is then observed, corresponding to a release of energy initiated by oxidation of both fuel compounds. A steep exotherm exhibits around 340°C which coincides with the fusion of KNO_3. It appears for experiments performed under air and under N_2 atmosphere. This indicates that KNO_3 has initiated its thermal decomposition. At the sight of the thermal analysis results, it appears that KNO_3 un_dergoes decomposition at lower temperatures than the ones stated by Freeman [14]. KNO_3 is soluble in lactose and this could be the reason of the decomposition activation at lower temperatures than the ones observed by Freeman. Fuel volatiles from lactose and starch are oxidized by O_2 resulting from the KNO_3 decomposition (cf. reactions (8) and (11)) causing the 340°C exothermic peak.; Under N_2 atmosphere, the exotherm is significantly narrower. This indicates that under air, both oxidation modes, based on O_2 resulting from the KNO_3 decomposition and from air, take place simultaneously;

- Char oxidation and glowing combustion are encountered around 420°C. As the smouldering front propagates, the structure of the residual material is altered and a char layer is formed. The process can be described, respectively for lactose and starch, by the reactions (10) and (15). Chelliah modelled carbon graphic oxidation [43]. He showed that the major oxidation reactions taking place were:

$$C_{solid} + H_2O \longrightarrow CO + H_2 \quad (16)$$

$$C_{solid} + CO_2 \longrightarrow 2CO \quad (17)$$

$$2C_{solid} + O_2 \longrightarrow 2CO \quad (18)$$

Given the interpretations arisen from the thermal analyses of the two ternary powders, the bulk of the heat released is generated at the fusion of KNO_3. However, under air, exothermic processes begin to occur as lactose starts to decompose. The lower temperature is the one that defines the stability of the composition.

Regarding the gaseous emissions, the FTIR analysis showed that, under air, the major species emitted are H_2O, CO_2, CO. For temperature between 210 and 400°C, noticeable amount of toxic species (mainly aldehydes and formic acids) are also generated. Traces of NO_2 are also

highlighted over this temperature range. This indicates that a fraction of KNO_3 has already started to decompose. Two acknowledged mechanisms related to the thermal evolution of KNO_3 have been suggested through reactions (4) and (5). The generation of nitrous oxides tends to consolidate the assumption of soluble KNO_3 that would decompose at temperatures below its melting point in a lactose solution. One assumes that these emissions were associated with the thermal decomposition of KNO_3. Beyond 400°C, the generation of NO_2 nearly ceases. The production of N_2O coincides with the oxidation of the carbonaceous residue when the latter becomes the main exothermic process taking place. The N_2O generation implies that KNO_3 has not entirely reacted and still decomposes. The production of N_2O can be explained by reaction (7) between the carbonaceous residue and KNO_3.

Finally, the analysis of the combustion residue suggests the formation of K_2CO_3. Such compound has also been identified during the combustion of black powder. Regarding the temperature range encountered during the combustion experiments, different reactions can explain its emergence. KNO_3 can have reacted with residual C. Another hypothesis relies on a reaction involving products of the oxidizer decomposition such as K_2O and CO_2.

The thermal decomposition that has been drawn up relies only on the analysis of results obtained through DSC, DT-TGA, MS and FTIR experiments. The thermal study that has been conducted was only qualitative. Hypotheses have been developed that would have to be verified. In order to assess them, the best method would be to integrate them in a kinetic model. However, this has not been carried out in the present analysis.

Given the previous results, thermal analysis describes slow processes in terms of temperature rises. It allows characterising the response of the samples when undergoing thermal decomposition. Such description helps understanding the combustion behaviour of a material. Nevertheless, it does not provide an integral description of the reaction. During combustion, the decomposition and reacting processes are faster. The rates of temperature rise can be several orders higher (from 5°C.min^{-1} for a DSC experiment, to more than 200°C.s^{-1} achieved during combustion of the 50% KNO_3 ternary mixture under air atmosphere). In this configuration, decomposition reactions overlap with oxidations and capturing the different reactions becomes too much complex or even impossible.

A critical unknown in terms of safety issues of a material such as the ternary mixtures considered in the present study is its behaviour when it becomes involved in a fire. Thermal analysis provides insights about the initiation mechanisms and the evolution of the combustion reaction involving the material. Because of the different heating rates, a combustion analysis remains necessary in order to improve the description of the physical and chemical processes and acquire a better understanding of the material behaviour when undergoing combustion. Several interrogations arise regarding the ignition, the burning behaviour and the potential toxic emissions induced.

2.5. References

[1] Bailey, A., Murray, S., G., Explosives, Propellants and Pyrotechnics, Brassey's, London, 1989;

[2] Babrauskas, V., Heat of Combustion and Potential Heat, in Heat Release in Fires, Edited by Babrauskas, V., and Grayson, S., J., 1st Edition, Elsevier Applied Science, London, 1992;

[3] Hemmilä,M., Hihkiö, M., Pasanen, A., L., Kasanen,J., P., Turunen M., Linnainmaa, K., Evaluation of Toxicity and Irritation Potency of a White Buoy Smoke for Marine Use, Proceedings of the 31st International Pyrotechnic Seminar, July 11-16, 2004, Fort Collins, CO (USA), pp. 609-624;[4] Marlair, G., Turcotte, R., Qwok, Q., S., M., Branka, R., Toxicity issues pertaining to burning pyrotechnics, Proceedings of the 33rd International Pyrotechnics Seminar, 16 – 21 July, Fort Collins, USA, 2006, pp. 467 – 484;

[5] Marlair, G., Kordek, M-A., Branka, R., Energetic Materials and the fire problem, Proceedings of the 8th International Symposium for Fire Safety Science, Beijing, China, 2005, p1639;

[6] Principles and Applications of Thermal Analysis, Editor: Gabbott, P., Blackwell Publishing, Oxford, 2008;

[7] The Canadian Explosives Research Laboratory, http://www.nrcan.gc.ca/smm-mms/expl-expl/sci-sci-eng.htm;

[8] ASTM E968-02, Standard Practice for Heat Flow Calibration of Differential Scanning Calorimeters, American Society for Testing and Materials, West Conshohocken, PA, USA, 2008;

[9] ASTM E967-03, Standard Practice for Temperature Calibration of Differential Scanning Calorimeters and Differential Thermal Analyzers, American Society for Testing and Materials, West Conshohocken, PA. USA, 2003;

[10] ASTM E2058-03, Standard Test Methods for Measurements of Synthetic Polymer Material Flammability Using a Fire Propagation Apparatus (FPA), West Conshohocken, PA: The American Society for Testing and Materials, 2001;

[11] Tewarson, A., Pion, R., F., Flammability of Plastics – I. Burning Intensity, Combustion and Flame, 26, pp. 85 – 103 (1976);

[12] Kovacich, R., P., Martin, N., A., Clift, M., G., Stocks, C., Gaskin, I., Hobby, J., Highly Accurate Measurement of Oxygen using a Paramagnetic Gas Sensor, Measurement Science and Technology, 17, pp.1579 – 1585 (2006);

[13] Holm, T., Aspects of the Mechanism of the Flame Ionization Detector, Journal of Chromatography A, 842, pp. 221 -227 (1999);

[14] Freeman, E., S., The Kinetics of Thermal Decomposition of Potassium Nitrate and of the Reaction between Potassium Nitrite and Oxygen, Journal of the American Chemical Society, 79, pp. 838 – 842 (1957);

[15] Oza, T., M., Journal of Indian Chemical Society, 22, p. 173 (1945);

[16] Szper, V. J., Fiszman, K., Anorg, Z., Allg. Chem., 206, p. 257 (1932);

[17] Stern, K.,H., Journal of Physical Chemistry, Ref Data, 1, p. 747 (1972);

[18] Freeman, E., S., Journal of Physical Chemistry, 60 , p. 1487 (1956);

[19] Ullman's Encyclopedia of Industrial Chemistry, 6th Edition, Wiley, 2002;

[20] Kramer, C., M., Munir, Z., A., Volponi, J., V., Differential Scanning Calorimetry of Sodium and Potassium Nitrates and Nitrites, Thermochimica Acta, 55, pp. 11 – 17 (1982);

[21] Paul Gabbott, Principles and Application of Thermal Analysis, Blackwell Publishing, Oxford, 2008;

[22] Gordon, S., Campbell, C., Differential Thermal Analysis of Inorganic Compounds, Analytical Chemistry, 27, pp. 1102 – 1109 (1955);

[23] Sirotkin, G., D., Equilibrium in Melts of the Nitrates and Nitrites of Sodium and Potassium, Russian Journal of Inorganic Chemistry, Vol. 4, 11, pp 1180 – 1182 (1959);

[24] Itoh, T., Satoh, M., Adachi, S., Differential Thermal Analysis of α- Lactose Hydrate, Journal of Dairy Science, Vol. 60, No. 8, pp. 1230 – 1235. (1977);

[25] Whistler, R., L., Bemiller, J., N., Paschall, E., F.m Starch: chemistry and technology, 2nd Ed. Orlando: Academic Press, 1984;

[26] Aggarwal, P., Dollimore, D., The Effect of Chemical Modification on Starch Studied Using Thermal Analysis, Thermochimica Acta, 324, pp. 1 – 8 (1998);

[27] Aggarwal, P., Dollimore, D., The Combustion of Starch, Cellulose and Cationically Modified Products of These Compounds Investigated Using Thermal Analysis, Thermochimica Acta, 291, pp. 65 – 72 (1997);

[28] O'Connell, C., The Effects of Methylparaben on the Gelatinization and Thermal Decomposition of Corn Starch, Thermochimica Acta, 340 – 341, pp. 183 – 194 (1999);

[29] Aggarwal, P., Dollimore, D., A Thermal Analysis Investigation of Partially Hydrolyzed Starch, Thermochimica Acta, 319, pp. 17 – 25 (1998);

[30] Shiotsubo, T., Takahashi, K., Changes in Enthalpy and Heat Capacity Associated with the Gelatinization of Potato Starch, as Evaluated from Isothermal Calorimetry, Carbohydrate Research, 158, pp 1 – 6 (1986);[31] Tsuchiya, Y., Sumi, K., Thermal Decomposition Products of Cellulose, Journal of Applied Polymer Science, Vol. 14, Iss. 8, pp. 2003 – 2013 (1970);

[32] Wodley, F., Pyrolysis Products of Untreated and Flame Retardant Treated α-cellulose and Levoglucosan, Journal of Applied Polymer Science, Vol. 15, Iss. 4, pp 835 – 851 (1971);

[33] Kwok, Q., S., M., Acheson, B., Rahman, M., Turcotte, R., Marlair, G., Thermal Decomposition of Smoke Powders, Presented at NATAS'06, Bowling Green, USA, 2006;

[34] Rein, G., Smouldering Combustion Phenomena in Science and Technology, International Review of Chemical Engineering, 1, pp. 3 – 18 (2009);

[35] Brill, T., B., Arisawa, H., Brush, P., J., Congwer, P. E., Williams, G., K., Surface Chemistry of Burning Explosives and Propellants, Journal of Physical Chemistry, 99, pp 1384 – 1392 (1995);

[36] Morikawa, T., Toxic Hazards of Acrolein and Carbon Monoxide during Combustion, Journal of Fire Sciences, 2, pp. 142 – 152 (1984);

[37] Turcotte, R., Fouchard, R., C., Turcotte, A.-M., Jones, D., E., G., Thermal Analysis of Black Powder, Journal of Thermal Analysis and Calorimetry, 73, pp 105 – 188. (2003);

[38] Blackwood, J., D., Bowden, F., P., The Initiation, Burning and Thermal Decomposition of Gunpowder, Proceedings of the Royal Society of London, Series A, Mathematical and Physical Sciences, 213, 1114 (1952), pp 285 – 306;

[39] Glassner, S., Pierce III, A., R., Gas Chromatographic Analysis of Products from Controlled Application of Heat to Paper and Levoglucosan, Analytical Chemistry, 37, pp. 525 – 527 (1965);

[40] Gardiner, D., The Pyrolysis of Some Hexoses and Derived Di-, Tri-, and Poly-saccharides, Journal of the Chemical Society C: Organic Chemistry, pp 1473 – 1476 (1966);

[41] Kato, K., Pyrolysis of Cellulose, Part III: Comparative Studies of the Volatile Compounds from Pyrolysates of Cellulose and its Related Compounds, Agricultural and Biological Chemistry, Vol. 31, 6, pp 657 – 663 (1967);

[42] Lakshmanan, C., Hoelscher, H., E., Production of Levoglucosan by Pyrolysis of Carbohydrate: Pyrolysis in Hot Inert Gas Stream, Industrial and Engineering Chemistry Product Research and Development, 9 (1), pp 57 – 59 (1970);

[43] Chelliah, H., K., Makino, A., Kato, I., Araki, N., Modeling of Graphite Oxidation in a Stagnation-Point Flow Flied using Detailed Homogeneous and Semiglobal Heterogeneous Mechanisms with Comparisons to Experiments, Combustion and Flame, 104, pp. 469 – 480 (1996);

3. Combustion Analysis of Starch, Lactose and Potassium Nitrate Based Ternary Mixtures

3.1. Introduction

Sustained combustion of energetic materials has received significantly less attention than the transition to detonation although recent accidents have stressed that the scenarios related to fire risk were probable and not isolated cases. Several fires involving pyrotechnics or explosives have been reported (c.f. Chapter 1, Table 1.1). Enclosure fires involving energetic materials are realistic scenarios. It is critical to be able to predict how the mixture will chemically evolve when the reacting atmosphere varies in terms of emissions of combustion gases and to, in the end, be able to identify the factors susceptible to compromise the stability of energetic materials. It then allows defining safety barriers that prevent or reduce to a minimum the risks to have the system reaching hazardous configurations. Consequently, the characterisation of an energetic material when undergoing combustion is essential regarding the gaseous emissions and the level of energy release.

Following the conclusions of the thermal analysis conducted in Chapter 2, the aim of this section is to achieve a qualitative description of the combustion behaviour of the two ternary powders based on starch/lactose and KNO_3 mixtures. The ability to characterise the evolution of the material when submitted to a temperature rise is fundamental to determine its thermal stability. A definition of the chemical pathways is also necessary for predicting the gaseous emissions. Finally, a detailed description of the thermal decomposition process of such samples allows the identification of the physical and chemical mechanisms that will take place during combustion. Nevertheless, unlike decomposition reactions achieved at a controlled heating rate, combustion implies fast temperature rise (More than 200°C.s^{-1} achieved during the combustion of 50% KNO_3 ternary powder under air atmosphere). Rapid chemistry takes place. As a consequence, different chemical processes overlap each other. Therefore, if the thermal analysis stresses the major phenomena encountered during combustion, the fast kinetics creates a different chemistry different from the one observed during the thermal

degradation. Several interrogations arise regarding the ignition and the burning behaviour (propagation mechanisms of the combustion, energy release and potential toxic emissions). While ignition is highly correlated to the thermal decomposition of the different constituents of the ternary powder, the characterisation of the burning behaviour is affected by the limits of the thermal analysis techniques. The description of a combustion phenomenon requires the measurement of critical parameters such as the gaseous emissions, the burning rate and the Heat Release Rate (HRR). Estimation of the HRR will be later developed in chapters 4, 5 and 7.

Chemical species production gives information on the level of toxicity and the efficiency of the combustion that are affected by different factors. The burning rate helps highlighting the different reaction processes as well as the reaction dynamics. Therefore, conducting combustion tests can enlighten essential information. Tools have been developed to carry out bench scale fire experiments and provide measurements such as gaseous emissions, mass loss rate and HRR. The present study intends to assess their capacity to provide pertinent and accurate data for the characterisation of energetic materials.

The peculiarity of the 40% and 50% KNO_3 ternary mixtures to carry an oxidizer confers intrinsic combustion properties to the material. One can assume that the physical behaviour of the ternary powders is affected by the proportion of fuel and oxidizer in the mixture. Moreover, the ability to sustain combustion under an inert atmosphere holds as another consequence inherent in the presence of an internal oxidizer in the composition. Finally, the influence on the burning process of two critical factors (that is to say the proportion of the different compounds in composition of the powders and the nature of the reacting atmosphere) needs to be investigated.

In a first part, one will attempt to define parameters pertinent to stress the intrinsic combustion properties of the ternary powders. Such indicators should allow predicting the degree of contribution of the oxidizer to the combustion behaviour. They will help to analyse the influence of the proportion of oxidizer as well as the influence of the reacting atmosphere on the combustion of the two ternary mixtures. In a second part, after having described the experimental setup, results from the combustion of the two ternary mixtures undergone under ambient air will be compared to determine the influence of the inter oxidizer on the burning process. In a third part, combustion experiments will first be carried out under inert atmosphere (N_2). The differences observed from the tests performed under ambient air on the

burning behaviour and the gaseous emissions will be examined. Then, another set of combustions tests will be conducted under various compositions of reacting atmosphere. The mole fraction of O_2 will be decreased from 20.95 % (ambient air) to 0 % (inert atmosphere) in order to observe and analyse potential variations on the combustion behaviour of the sample materials. The outcomes will be focused on ascertaining the role of the reacting atmosphere to support the combustion reaction. Nature and evolution of the chemical emissions can be correlated to these parameters. The following analysis will bring valuable data on the burning behaviour of the ternary powder.

The characterisation of the combustion behaviour of the ternary mixture based on lactose, starch and KNO_3 is a milestone offering an overall view of his responses to strong factors governing its stability. This analysis enables minimizing safety issues related to the process, the storage, the transportation or the disposal of such products. Furthermore, all the results obtained provide detailed data for assessing the validity of predictive models that are developed.

3.2. Intrinsic Combustion Properties

The peculiarity of energetic materials stems from the presence of the oxidizer directly inside the material. The rate of energy release is highly dependent on the concentrations of fuel and oxidizer. In order to assess performances, key reaction mechanisms need to be understood. One of the main traits of this type of materials is to react very rapidly, releasing consequent amounts of energy.

Among the parameters characterising a combustion reaction, the energy release, the emission of gases and the flame temperature achieved are critical ones. In case of standard materials, the equivalence ratio is a pertinent variable to have an insight of the previously defined parameters. It allows estimating the overall interaction of the oxidizer and the fuel on the system's performance. The equivalence ratio is defined as,

$$\Phi = \frac{\frac{m_{fuel}}{m_{air}}}{\left(\frac{m_{fuel}}{m_{air}}\right)_{stoic.}} = \frac{\frac{n_{fuel}}{n_{air}}}{\left(\frac{n_{fuel}}{n_{air}}\right)_{stoic.}} \quad (1)$$

Fuel rich mixtures are characterised by $\Phi > 1$ while fuel lean mixtures exhibit $\Phi < 1$. For a stoichiometric mixture, the equivalence ratio equals unity. Usually, the major species of lean combustion are CO_2, H_2O, O_2 and N_2, while for fuel rich mixture, they are H_2O, CO_2, CO, unburned hydrocarbons, H_2 and N_2 [1]. Maximums of heat release and adiabatic flame temperature are achieved are considered to be achieved at the stoichiometry. It has been noted that peak values of adiabatic flame temperature were usually measured slightly on the rich side for hydrocarbons. This is due to the decrease in heat release in the presence of product dissociation [2]. For hydrocarbon/air mixtures, Law showed that there was more dissociation on the lead side with the consequence of a heat release peak on the rich side. Nevertheless, it has been largely acknowledged that the adiabatic flame temperature is obtained around the stoichiometry ($\Phi \sim 1$).

If the equivalence ratio gives a right indication of the fuel richness or leanness of a mixture, it does not consider the intra-molecular fuel / oxidizer interaction within a compound. For instance, an oxidizing element can be contained in a fuel compound, or mixtures can enclose fuel and oxidizer compounds in a condensed phase like for many energetic materials. Bakhman drew attention to the fact that for a given value equivalence ratio, different mixtures could substantially differ in terms of inside contribution of fuel and oxidizer [3]. In order to account of the oxidizing potential of a mixture, an Oxygen Balance (%OB) has been defined [4]. It indicates the level of oxygen present in the mixture to achieve complete combustion. If %OB is negative, it means that the amount of O_2 present in the composition is not sufficient to induce a complete combustion. If %OB is positive, there is more O_2 in the composition than the amount needed to undergo complete combustion. Considering a compound $C_xH_yO_z$, an expression of %OB is given by,

$$\%\mathrm{OB} = -100 \times \frac{16}{M_{material}}\left(2x + \frac{y}{2} - z\right) \quad (2)$$

This method is often used for explosives where mixtures tend to approach a zero %OB. However, one of the downsides of this expression is that it only considers the oxidation of C, H or metal atoms. For example, the presence of N atom in the molecule could allow the formation of NOx with the consequence that %OB would be overestimated.

Another method has been developed by Jain et al [5]. They defined an elemental stoichiometric coefficient also applicable to multi-component systems. They started with the

assumption that during combustion, all the chemical bonds present in the reacting molecules break, resulting in the formation of monoatomic elements that recombine to constitute stable products. Given that complete combustion products are irrespective of the composition of the hydrocarbons participating in the reaction, the recombination mainly depends on the combining ability for the fuel and oxidizer elements. This aptitude can be characterised by the valence of the fuel and oxidizer elements.

The elemental stoichiometric coefficient, ϕ_e, expresses the ratio of oxidizing to reducing (i.e. fuel) elemental composition. The calculation is irrespective of whether the reducing or oxidizing atoms are present in the oxidizer or the fuel compounds. ϕ_e is defined as,

$$\phi_e = \frac{Total\ number\ of\ oxidizing\ elements\ in\ the\ mixture}{Total\ number\ of\ reducing\ elements\ in\ the\ mixture} \tag{3}$$

$$\iff \phi_e = \frac{\sum_o n_o v_o}{(-1)\sum_r n_r v_r} \tag{4}$$

Where, *n* is the number of an element in the mixture and *v* is its valence. The subscript o and r refer respectively to the oxidizing and reducing elements. With a view of clarity, the valence of a fuel compound is assumed negative and that of an oxidizer, positive.

The calculation for the 50% KNO_3 ternary powder is presented. Table 3.1 indicates the valence relative to every element present in the composition.

Table 3.1. Valence of several elements.

Element	C	H	O	N	K
Valence	-4	-1	2	0 (*)	-1

(*) In the present calculation.

In terms of moles, the mixture composition is given in Table 3.2,

Table 3.2. Mass and Mole percentage of the ternary mixture Lactose/starch/KNO_3.

Compound	Mass %	Mole %
Lactose ($C_{12}H_{22}O_{11}$)	25	10.1
Starch ($C_6H_{10}O_5$)	25	21.4
KNO_3	50	68.5

The total oxidizing and reducing valences are, respectively,

$$\sum_o n_o v_o = \left(\frac{68.5}{100} \times 3 + \frac{21.4}{100} \times 5 + \frac{10.1}{100} \times 11\right) v_{o_2} \tag{5}$$

$$\sum_r n_r v_r = \frac{68.5}{100} \times (1 \times v_K + 1 \times v_N) + \frac{21.4}{100} \times (6 \times v_C + 10 \times v_H) + \frac{10.1}{100} \times (12 \times v_C + 22 \times v_H) \tag{6}$$

The elemental stoichiometric coefficient, ϕ_e, can be calculated and for the present mixture equals 0.564.

A value of $\phi_e < 1$ indicates that the mixture is fuel rich. It clearly shows that, following the KNO_3 decomposition assumed on Figure 3.1, complete combustion will not be achieve if only the fuels and oxidizer contained in the composition participate in the combustion.

This method is of certain interest for compounds having both fuel and oxidizer elements. Their contribution would not be obvious when using the equivalence ratio. On the other hand, Jain showed that for different mixtures having equal heats of combustion, the isoenergetic aspect would not be underlined with the equivalence ratio while ϕ_e for all the mixtures was the same [6]. Furthermore, he also noted another important aspect related to this variable. While studying the ignition characteristics of mixtures of ammonium perchlorate with various methyl-ammonium perchlorates, it appeared that although the critical concentration for each composition varied depending on the number of methyl groups, ϕ_e remained the same. This variable might be an essential parameter to characterise the combustion behaviour of the ternary mixtures KNO_3/Lactose/Starch. Considering the later remark, ϕ_e has been calculated for both compositions as well as the %OB. Results are presented in Table 3.3.

Table 3.3. Oxygen balance and elemental stoichiometric coefficient for the different compositions of ternary mixture.

Sample Composition	Oxygen Balance (%)	ϕ_e
40% KNO_3	-35.2	0.480
50% KNO_3	-27.1	0.564

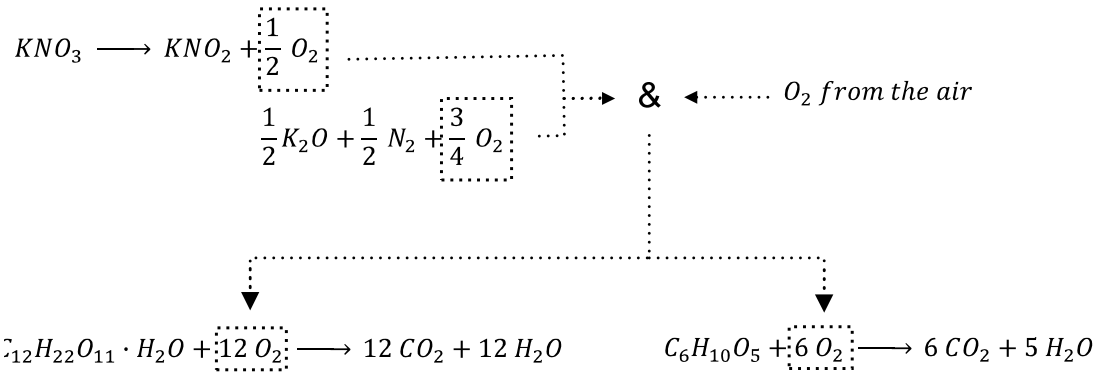

Figure 3.1. Assumed reaction scheme for complete combustion of the ternary mixture KNO_3/Lactose/Starch.

Parameters able to assess the "a priori" contribution of the oxidizer factor have been defined. Calculations of oxygen balance and elemental stoichiometric coefficient relative to the ternary mixture reveal negative values. These values indicate that the only oxidizer present inside the material will not be able to sustain a complete combustion of the fuel components. In order to characterise the combustion of the mixture, several aspects need to be studied. It is essential to understand the influence of the oxidizer on the reaction, regarding the burning rate, the amount of energy release or the emissions of gaseous products. The interaction between KNO_3 and air has to be investigated bringing the questioning about the ability of the material to burn in an inert atmosphere and the possible issues induced by this aptitude. Fundamental answers will stand in the analysis of the results of the combustion tests carried out.

3.3. Experimental setup and repeatability

All the combustion experiments have been carried out using the same two compositions of the ternary powders than the ones presented in chapter 2 (cf. Table 2.1).

3.3.1. Experimental setup

The analysis of their combustion behaviour has been performed using a fire calorimeter. The benefit of such equipment is that it allows thermal, chemical emissions, mass transfer and energy release measurements. The combustion experiments have been carried out using the FM-Global Fire Propagation Apparatus (FPA) [7]. Two different models have participated in the tests campaigns, a standard model located at the University of Edinburgh and a customized

version developed at INERIS in the 90's and based on an evolution of the original design defined by Tewarson who was the initiator of the device [8]. A scheme of the FPA is presented in Figure 3.2. Table 3.4 specifies the model of FPA used according to the experimental conditions. Material was positioned in a glass or aluminium sample holder on a load cell providing mass loss information during the experiments. The combustion chamber is confined within a quartz tube. Decomposition and combustion gases are collected in the exhaust duct and dispatch through series of filters to on-line species analysers (CO/CO_2, O_2, Total hydrocarbons (THC)) to finally be extracted by a hood. The O_2 analyzer uses a paramagnetic technology. By use of a paramagnetic sensor, the partial pressure of O_2 is obtained from the measurement of the magnetic sensibility of the gas [9]. Paramagnetic gases such as O_2 are attracted to a magnetic field while, conversely, diamagnetic gases will be repelled. The advantage of a paramagnetic sensor is its high selectivity to O_2. The only major other paramagnetic gases are NO and NO_2. However, the error they introduce in the measurement is usually not significant as their concentration remains generally low during fire experiments. The CO_2/CO measurements rely on an infrared technology. Their concentration is estimated according to the emission absorbed by the particles at a given wavelength. The THC analyser is based on a Flame Ionization Detection [10]. Holm explains that hydrocarbons degrade into CH_4 in the precombustion zone of the hydrogen flame. Then, the ion formation in the flame has been acknowledged to be mainly a chemi-ionization of CHO* resulting from the reaction of O with CH:

$$CH + O \longrightarrow CHO^* \longrightarrow CHO^+ + e^- \quad (7)$$

Ions are detected by two electrodes. The movement induced by the ions induces a current between the electrodes. The response of the detector roughly depends on the number of ions hitting the plate. The FID is defined as a "methane detector". The concentration response is proportional to the number of C atoms, the simplest hydrocarbon being CH_4.

The exhaust duct is fitted with thermocouple and a Pitot tube for estimation of the exhaust flow rate. Laser extinction is applied to evaluate the extinction coefficient across the exhaust duct and the soot molar fraction. Infrared heaters surround and target the sample to provide an external heat flux. Nevertheless, in the present work, choice was taken to carry out combustion tests without applying any external heat flux to the sample. The material being reactive, homogeneous heating of its surface could potentially initiate the decomposition and

combustion reaction over the entire area. The reaction rate might be too high to allow the measuring instruments to capture the kinetics. Furthermore, rapid activation of the combustion reaction over the entire surface of the material can favour the transition to an explosion mode.

Table 3.4. FPA Models used to conduct the combustion tests given the experimental conditions.

FPA Model	Conducted Experiments
University of Edinburgh	Combustion tests under air
INERIS	Combustion tests under: – Air; – Various O_2 concentrations [0 % ⟶ 20.95 %]; – Inert atmosphere (N_2).

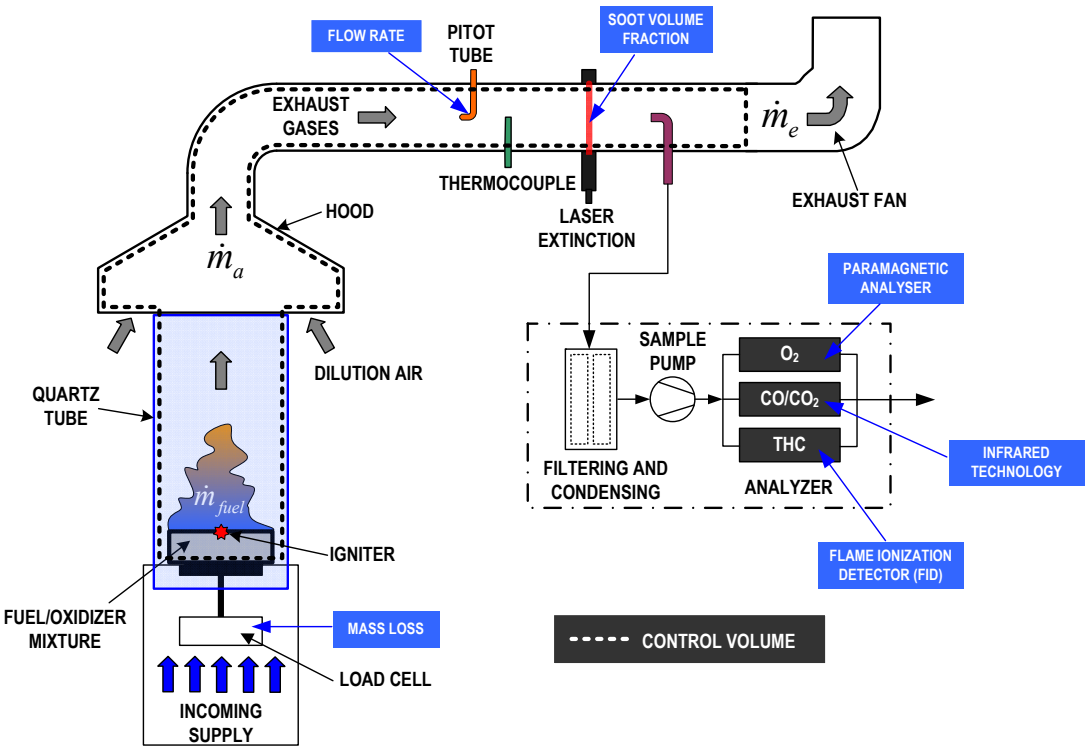

Figure 3.2. Scheme of the FM-Global Fire Propagation Apparatus in the present study configuration.

In order to launch the reaction, a hot spot needs to be created on the surface of the material. As a consequence, the standard configuration of the FPA has been slightly modified for the experiments carried out under low O_2 concentration in the reacting atmosphere. For the tests where the ethylene/air pilot flame usually used for piloted ignition could not be sustained, the system was replaced by a glow-plug. It was supplied by a 12V generator and requires about 30 seconds to reach a temperature of 500°C.

3.3.2. Repeatability of the experiments

Each experiment was repeated 4 times in order to investigate the ability to reproduce identical results. Ignition of the 40% KNO_3 mixture was sometimes more difficult to achieve and the time to ignition showed little variations. However, the duration of the tests was relatively identical. The reactions involving a 40% KNO_3 mixture lasts about 105s ± 4s while the ones involving the 50% KNO_3 composition holds for about 38s, ± 3s. The reaction durations are untypical to the ones from experiments usually carried out in a calorimeter. Combustion tests conducted with KNO_3 ternary powders will allow the assessment of the ability of the FPA to capture the evolution of the kinetics of such compounds.

Table 3.5 presents the standard deviations relative to the peaks and integrals of CO_2, CO and O_2 molar fractions obtained for the different experiments carried under air for the 40% and 50% KNO_3 mixtures. For the three species considered, standard deviation never exceeds 20%. Given the experimental setup, discrepancies highlighted between the different experiments are acceptable to assume the repeatability of the procedure for identical test conditions.

It appears that the greatest variations are measured for CO. Furthermore, standard deviation decreases as the concentration of oxidizer is increased within the material. The main element able to explain this difference between the 40 and 50% KNO_3 compositions stems in the time to attain ignition. As noticed during the experiments, the 50% KNO_3 composition reaches flaming regime faster than the 40% one. Furthermore, the observation of the propagation of the reaction front can only be observed for the material with the lowest oxidizer concentration.

Powders were randomly arranged in the sample holder. Nevertheless, care was taken to place the igniter (pilot flame or glow-plug) at the same position for the different tests. As previously noticed, regarding the 40% KNO_3 mixture, the time between the start of the experiment and

the transition to flaming may vary from one test to another. It seems to mainly depend on how the reaction front spreads inside the material. Then, the disposal of the powder can influence the propagation. The distribution of the glowing spots expelled from the initial hot spot will also be different for each experiment and may affect the time when flaming will occur. The latter could explain the origin of the discrepancies stressed by the repeatability analysis. The 50% KNO_3 mixture, presenting a faster reaction rate and transition to flaming, is less influenced by the powder distribution or glowing spots. In this experimental condition, it can be assumed that one of the critical parameters will be the mass burning rate. As the flaming period and the mass of residue remain relatively constant for the different tests, it is likely that the 50% KNO_3 powder samples present similar mass loss rate. The ventilation condition being identical, the gas emissions should not significantly differ. Figure 3.3 shows the mass loss and mass loss rates obtained from several experiments carried out with 50% KNO_3 material under air. As expected, no large discrepancies are observed between the different tests.

Repeatability of the experiments is a requirement in order to be confident in the thermal and chemical analysis of the parameters (gases emissions, Heat Release Rate...) describing the material behaviour. In the present work, repeatability has been achieved.

Table 3.5. Standard Deviations of CO_2, CO and O_2 molar fraction peaks and integrals for the different tests carried under air.

	Standard Deviation (%)					
	CO_2		CO		O_2	
Mixture	*Peak*	*Integral*	*Peak*	*Integral*	*Peak*	*Integral*
40% KNO_3	13.5	10.3	18.4	9.5	0.4	15.2
50% KNO_3	4.5	2.7	12.8	14.7	0.14	2.9

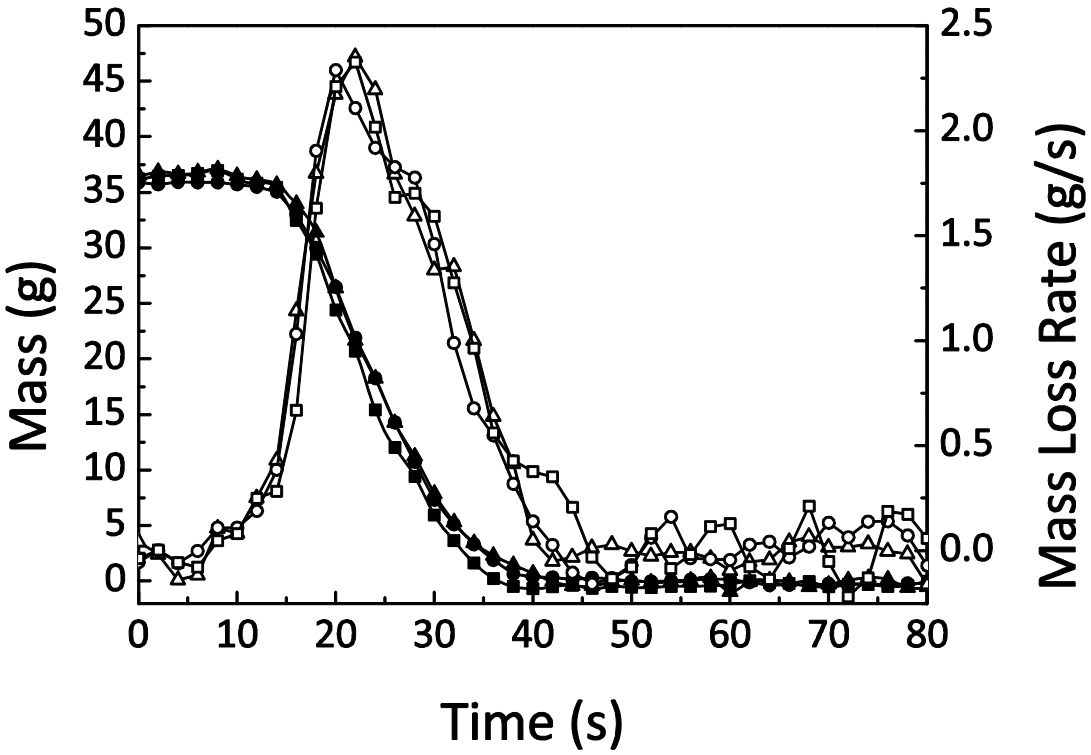

Figure 3.3. Mass Loss and Mass Loss Rate for 50% KNO_3 experiments under air atmosphere.

3.4. Analysis of the contribution of the oxidizer to the combustion

Energetic materials present the singularity to embed an oxidizer in their structure. When decomposition of the material is initiated, volatiles evolved from the fuel compounds pyrolysis react with the O_2 liberated from the oxidizer decomposition undergoing oxidation. Consequently, combustion can take place without the need of O_2 from the ambient air as a primary reaction partner. Sustained combustion reaction can develop without consuming O_2 from the air or using it only for secondary oxidation reaction [4]. The influence of the concentration of oxidizer in the ternary mixture based on starch, lactose and KNO_3 is studied in the following. Attention has been dedicated to the qualitative analysis of the initiation of the reaction, the intensity of the reaction (i.e. the reaction rate, flame height, spread through the material), the gaseous emissions, the flaming mode observed and the evolution of the ternary powder structure. Experiments have been carried out on 50g samples of 40% and 50% KNO_3 ternary mixture. The combustion tests were conducted using the FPA. The reacting chamber

(i.e. volume inside the quartz tube) was traversed by a flow of air. Initiation of the reaction was realised using the pilot flame or a glow-plug to create a local hot-spot at the surface of the sample. However, prior to begin any dissection of the results, it is fundamental to verify that every experiment carried out can be repeated with a minimum variation within the data of the different trials. Repeatability of the measurements is a necessary and sufficient condition for being able to draw any statement on the combustion behaviour of the two ternary mixtures.

3.4.1. Analysis of experiments carried out under air atmosphere

Combustion tests on 40% and 50% KNO_3 ternary mixtures have been conducted using the FPA. The steps from the initiation of the reaction, the propagation of a smouldering process through the material to a transition to flaming are described. An analysis of the combustion gases emitted is proposed.

3.4.1.1. 40% KNO_3 ternary mixture

3.4.1.1.1. Experimental observations

Sample

The ternary mixture was composed of 30% lactose, 30% starch and 40% KNO_3. Test was carried out under air atmosphere at a 0.1 $m.s^{-1}$ (200 $l.min^{-1}$) flow. In the current setup, ignition was achieved using an ethylene/air pilot flame. No external heat flux was applied. This was done to avoid a homogeneous heating of the sample which would increase the rate of reaction. The combustion area was delimited by a quartz tube. Each sample weighed 50g, randomly arranged in a glass or aluminium small dish.

	Time	
Initiation of the reaction		
1. Hot-spot	*0 s*	
		A hot-spot is created by the pilot flame heating the material locally. Glowing occurs on the surface. A smouldering front propagates through the material. Glowing spots flare from the reaction zone to the virgin material inducing local reactions and possibly enhancing the decomposition. Short flames are observed at the limit between the reaction front and the virgin material.
2. Propagation of the reaction front		
		Important swelling of the residue is observed as the reaction front continues to propagate. Glowing still occurs on the surface as well as important release of smoke. White smoke is first produced but as the reaction involves, smoke becomes darker.
3. Transition to Flaming	*54s*	
		Instantaneous transition to flaming takes place 54s after initiation of the reaction. Flames originate from the base of the sample and engulf the reacting material. They first arise with a blue colour and then become brighter as the flame height grows. The flaming regime lasts for about 50 s.

Extinction 	*104 s*	Extinction comes about 104 s after ignition. The residue has significantly swollen. Glowing is still observed on the surface.
Residue 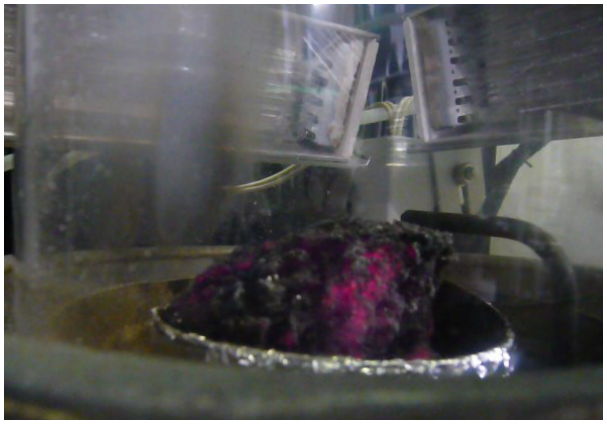		Residue corresponds to about 26% of the initial mass. At the surface, glowing process remains active after flaming extinction. The inside of the material is characterised by high temperatures and in contact with air, glowing occurs.

3.4.1.1.2. Experimental Results

Figure 3.4 illustrates the emissions of CO_2, CO, Total Hydrocarbons (THC) and the O_2 depletion from the combustion of 40% KNO_3 powder. The total productions of CO_2, CO and THC are indicated on Table 3.6. The major gases produced are CO_2, H_2O and CO. From Figure 3.4, first emissions are measured in the time region α. This period corresponds to the beginning of the emission of smoke observed during the experiment. During α_1, slight productions of CO, THC and CO_2 are measured with an order of magnitude of few ppm. This part of time seems to coincide with the observed white smoke emission. During α_2, a change of slope of the gases molar fractions emerges. This interval concurs with a release of dark smoke from the sample. The transition from α_2 to β coincides to the evolution of the reaction to flaming. A change of

slope is then observed on Figure 3.4 for the CO_2 molar fraction and the depletion of O_2. Reaction rate is increased. Variations are also noticed on CO and THC molar fractions and are illustrated by shoulders at the transition time. Maximum emissions for CO_2, CO and THC are detected at the same time. The flame decay and extinction take place during the interval γ and occurs simultaneously with the reduction of combustion gases emissions. After extinction, glowing is observed at the surface of the sample during about 20 seconds (interval δ). A smouldering combustion process persists at the transition γ to δ, shoulders are visible on the CO_2, CO and THC curves of Figure 3.4.

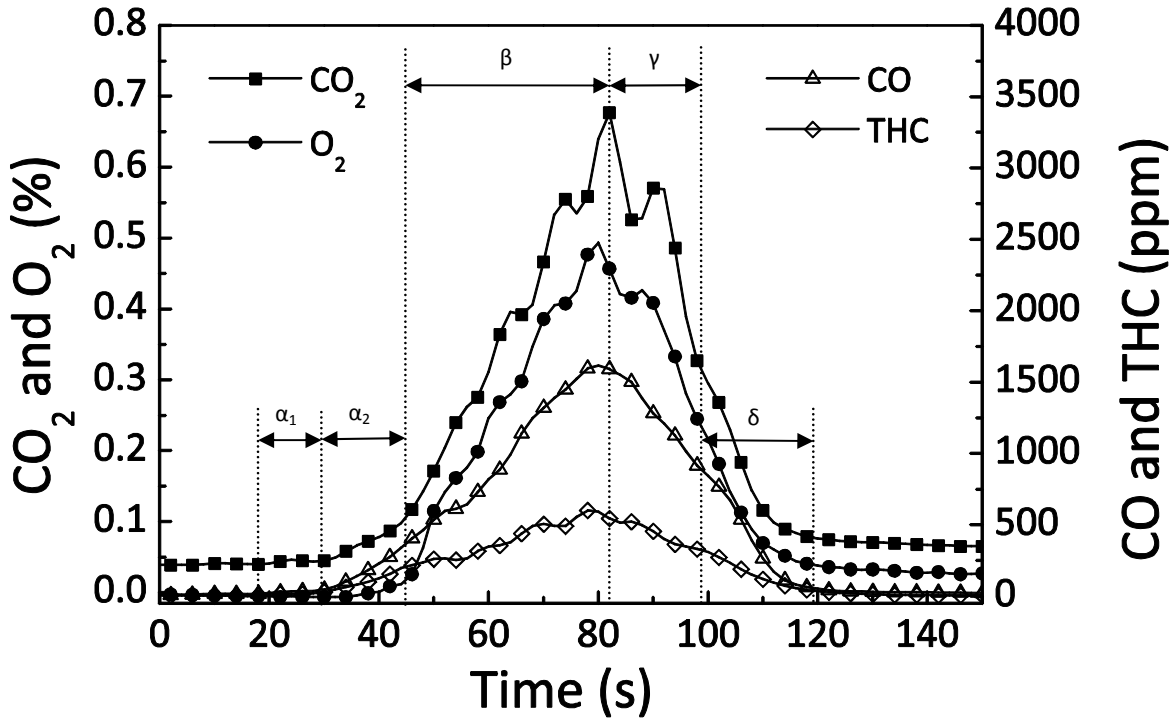

Figure 3.4. Gas emissions from the combustion of 40% KNO_3 ternary powder under air atmosphere (200 $l.min^{-1}$).

Regarding the intensity of the gases molar fractions, CO_2 reaches a maximum molar fraction of 0.67% while the maximum O_2 depletion is 0.5%. CO and THC attain, respectively, maximums of 1600 ppm and 600 ppm. In order to investigate the completeness of the combustion, the CO/CO_2 ratio has been calculated. It was given by the following expression,

$$\frac{X_{CO}^{A}(t)}{X_{CO_2}^{A}(t)} = \frac{\dot{n}_{CO}(t)}{\dot{n}_{CO_2}(t)} \quad (8)$$

The CO/CO_2 ratio is indicated on Figure 3.5. Characterisation of the curve has been conducted according to the time regions defined previously. During α_1, an increase of the CO/CO_2 ratio is evaluated. It stresses a small CO emission probably engendered be the early initiation of the reaction. α_2 reveals a significantly steeper rise in the $CO\backslash CO_2$ ratio. The formation of combustion gases is enhanced. This period corresponds to the transition to darker smoke. During this first stage of the reaction, the CO generation appears to be promoted compared to the one of CO_2. The decomposition of the material is initiated. It engenders volatiles from the fuels degradation and O_2 from the oxidizer. The oxidation of the volatiles to CO is apparently favoured rather than the generation of CO_2. Pitts has underlined that in case of enclosure fires, the oxidation of hydrocarbons to CO was favoured compared to the oxidation of CO to CO_2 if the available amount of O_2 was noticeably below stoichiometry [11]. One can assume that, at initiation of the reaction, the quantity of O_2 released from the oxidizer decomposition is limited. Its temperature of decomposition is higher than the ones of the fuel components. Larger amount of volatiles start being generated while not enough O_2 is present inside the material to reach stoichiometry. Consequently, the oxidation process leading to the formation of CO is eased in relation to the oxidation of leading to CO_2. The maximum ratio for the 40% KNO_3 ternary mixture is 0.35. One needs to point out that in parallel to the oxidations of the volatiles, the process of char oxidation also takes place. The maximum of the CO/CO_2 ratio corresponds to the transition to flaming, attained between α_2 and β. During approximately the first 10 seconds of β, the CO/CO_2 ratio decreases. The gaseous mixture exiting the material reach flammable conditions and a regime of diffusion flame gets established. O_2 from ambient air also supports the combustion reaction. The amount is sufficient to assure both oxidation processes: oxidation to CO and oxidation to CO_2. Subsequently, the CO/CO_2 ratio remains relatively constant around 0.27. It can be interpreted as the oxidation rate of CO into CO_2 having attained a steady state. Furthermore, the order of magnitude of the CO/CO_2 ratio over still exhibits an incomplete combustion. As the flame regime begins to decay (γ), the CO/CO_2 ratio stays constant. It seems to suggest that the amount of volatiles and O_2 formed from the oxidizer decomposition decreases at an identical rate. After the flame extinguishes (δ), glowing combustion prevails for few seconds. Only char oxidation occurs. This phenomenon is stressed by an enhancement of the CO/CO_2 ratio. The reaction that seems to prevail can be expressed as,

$$C + \frac{1}{2}O_2 \longrightarrow CO \quad (9)$$

Consequent traces of CO are measured which allows to think that reaction conditions were below the stoichiometry. Oxygen Balance and Elemental Equivalence Ratio have previously underlined the lack in oxygen in the mixture to sustain complete combustion of the fuel components. The current tests have been carried out while air was introduced into the combustion zone at a constant flow rate of 0.1 $m.s^{-1}$ (200 $l.min^{-1}$). It is of interest to calculate the equivalence ratio, ϕ. Assuming the decomposition of KNO_3 into K_2O and accounting for the O_2 released by the oxidizer, considering the mass of fuel elements in the mixture, ϕ has been estimated to about 0.6. The reaction takes place under fuel lean conditions.

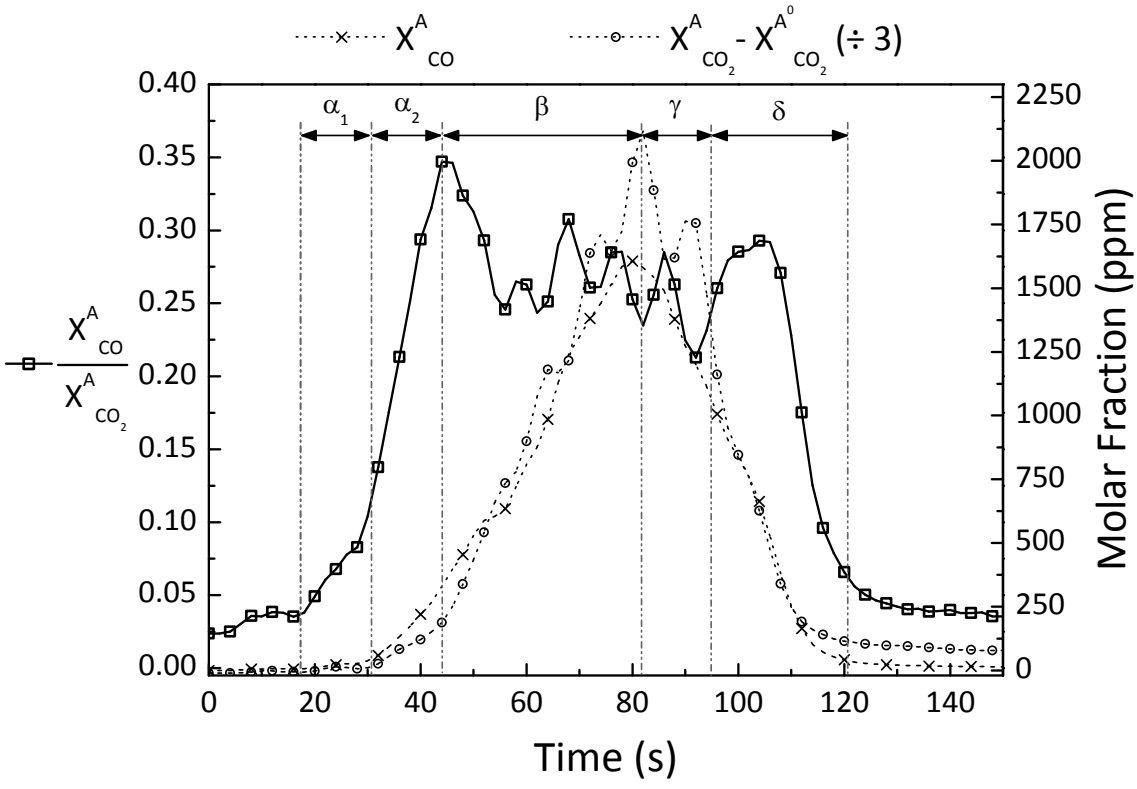

Figure 3.5. CO/CO2 ratio from the combustion of 40% KNO3 ternary powder under ambient air (200 $l.min^{-1}$).

3.4.1.1.3. Discussion

Reaction is induced by the generation of hot spots at the material surface. An identical behaviour has been widely commented for the combustion of black powder [12]. The heat propagates inside the material allowing the start of the decomposition. A smouldering combustion is initiated. The spread of the reaction front can be discerned. The surface is reacting with O_2 from air or the oxidizer. Glowing points appear at the frontier of virgin material and reaction front. Some are expelled, creating hot spots in different locations. However heating elements being relatively small, they heat up the material very locally but will not contain enough energy to start a sustained decomposition reaction in another region.

Smouldering occurs inside the material. Important swelling of the sample is noticed (cf. Figure 3.6). One first assumes that starch is plausibly responsible of the phenomenon. The assumption that can be hold is the initiation of the process of gelatinization of starch. Starch gelatinization has been widely studied over the last decades. Gelatinization is seen as additive irreversible modifications occurring in the starch granule in the presence of moisture and heat [13]. Swelling due to absorption of moisture by the amorphous region of the granule is one of the different changes taking place. It also includes leaching of amylase and loss of the crystalline order. However, one can wonder about the fact that the phenomenon of gelatinization still occurs during flaming when temperatures are much higher than the usual acknowledged gelatinization temperature range 45°C - 110°C [14]. Furthermore, the combustion in the solid phase also rises to temperatures much higher than 110°C. Water gets vaporized so an inverse process would be expected beyond the characteristic temperature range. In the end, the assumption of a gelatinization is arguable. As a conclusion, one believes that swelling is likely to be initiated by another phenomenon that has not been identified in the present work.

As the reaction front spreads downward, white smoke is generated. This corresponds to the time period α_1. Very low productions of THC, CO and CO_2 are measured. The hypothesis to explain the colouring of the smoke is that, at this time, water vapour is mainly released. At the transition to α_2, the rate of reaction is increased as shows the rise in THC, CO and CO_2 generations. At this moment, the smoke becomes darker, probably due to a higher concentration in C atoms and soot. Regarding the CO/CO_2 ratio, prior to transition to a diffusion flaming regime, the oxidation to CO appears to be favoured compared to the process

leading to the generation of CO_2 (β_1). One assumes that the combustion reaction mainly takes place in the slid phase where O_2 is provided by the decomposition of KNO_3. Considering the negative %OB, the amount of O_2 is limited at the smouldering front. Similarly to the results found by Pitts, it appears that the reaction leading to CO is promoted. When flaming occurs (β_2), the production of CO_2 is enhanced, the reaction rate increases. Figure 3.5 shows that the CO/CO_2 ratio tends to stabilize. As O_2 from ambient air gets involved in the combustion, the quantity of oxidizing agent is large enough to allow processing both oxidation reactions.

During the decomposition of the material, O_2 is released from KNO_3; volatiles are also formed from the decomposition of the fuel components. Furthermore, air is injected in the combustion zone. Gases will mix and flaming will begin once the fuel concentration is enough to support combustion [15]. This assumption will be developed more in details when studying the influence of the O_2 concentration on the combustion of the ternary mixture.

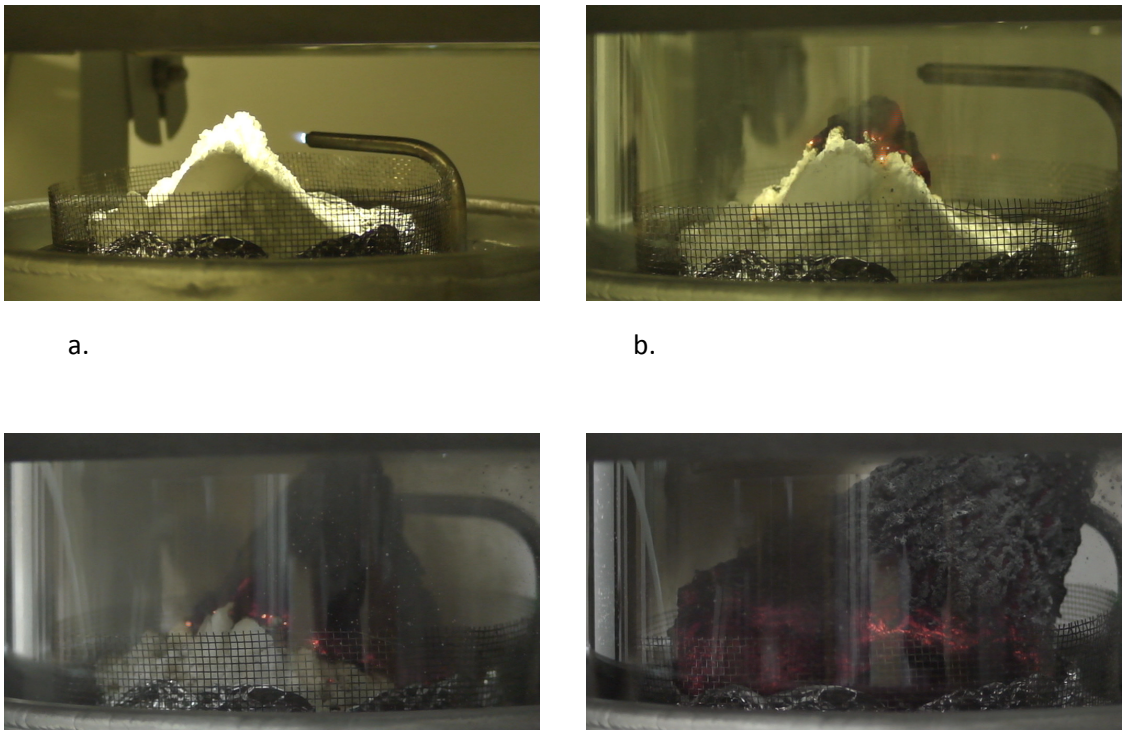

a. b.

c. d.

Figure 3.6. Observation of the swelling of 40% KNO_3 ternary mixture during combustion test under air atmosphere at various moments: a. Prior ignition, b. Start of decomposition reaction, c. Propagation of the reaction front, c. After extinction.

As shown on Figure 3.7, flaming is observed at the side of material and originates from the base of the sample. The same behaviour seemed to emerge when only smoke was released. However, the flow of air induced a movement of the smoke all over the sample which could not allow clearly distinguishing the demeanour. The surface of the sample gives the impression of acting as a shield preventing the combustion gases to be released through the surface. A hypothetic explanation can be developed based on the swelling behaviour. Experimental observations for the 50% KNO_3 mixture differ from the ones described for the present mixture. Its behaviour will be discussed in more details in the next section. Nevertheless, it needs to be underlined that no swelling took place during the combustion reaction of 50% KNO_3 ternary powder. Furthermore, during the combustion of the latter material flames rose all over the material surface while less fuel was present in the material.

Figure 3.7. Flame Position with regard to the sample.

One can assume that the swelling slows down the diffusion of the volatiles and decomposition products through the medium. A first hypothesis is that the mixture, volatiles and O_2 from oxidizer, is not homogeneous to initiate a flame. But it can be also expected that the combustible gas – air mixture will not be rich enough in fuel to initiate and sustain a flame. Given Figure 3.7, it turns out that flammability is only reached on the side of the sample. Most

of the combustible gases are released from the base of the material. Mixing with air is eased by the flow; flaming starts where flammable conditions exist.

Observation of the flame colours gives an insight of the completeness of the combustion. Considering Figure 3.8, the base of the flame is dominated by a blue – violet emission. According to Glassman [16], a blue radiation is emitted in fuel lean mixture and is due to the excited, CH*, radicals. In hydrocarbon flames, CO_2* and OH* radicals can also play a role in the blue emission [17]. The presence of potassium in the material may explain the violet coloration of the flame, as lilac is peculiar to the combustion of this element. The transition to orange and yellow radiation informs on the flame structure and the elements present. Yellow bright emission is characteristic of soot radiation while a reddish glow is induced by radiation of CO_2 and water vapour [16] [18].

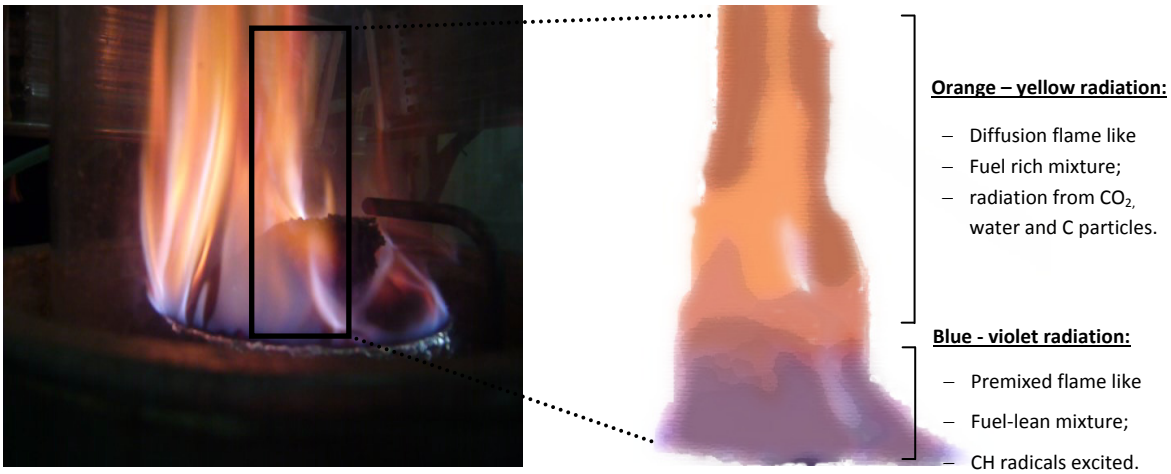

Figure 3.8. Picture of flames observed and scheme of the different flame regions.

Knowing these features, one can try to draw an arguable explanation. The temperature rise is high enough to allow initiation of the material decomposition into combustible gases, O_2 originated from the oxidizer, and inert degradation products. Once the volatiles – air mixture reached flammable conditions, flames develop. Then, the particles are heated by the flame front and pyrolysed. By mixing with air, combustible mixture in which the combustion occurs continues to be formed. On the other hand, the colour of the flame suggests lower temperature at its base and a rise in the flame front. While the base of the flame presents similarities with a premixed flame, the upper region and the tip are rather identified to a

diffusion flame. As the material pyrolysed, mixing occurs between volatiles and O_2 released from the oxidizer decomposition. The combustible gases – O_2 from KNO_3 mixture is homogeneous when entering the combustion zone. It has been previously exhibited that the Oxygen Balance as well as the elemental equivalent ration of the mixture highlighted a lack of O_2 to assure complete combustion. Nevertheless, the contribution of the flow of ambient air moves the mixture into fuel lean conditions which could explain the blue radiation of the base of the flame. As the ternary composition is richer in fuel, it has to be expected that the O_2 supplied by the oxidizer is not sufficient to react all the volatiles. Remaining combustible gases mix with air but if the diffusion characteristic time through the flame front is smaller than the mixing characteristic time, it has to be expected that the gas air mixture will not be homogeneous and would result in a sooty fire even for reactions with an equivalence ratio below 1. An incomplete combustion would take place as it has been observed given the CO and THC emissions. This could explain their generation under the present experimental conditions.

The material keeps decomposing after extinction. Glowing occurs at the surface of the sample which contributes to the production of CO and CO_2 through char oxidation. The CO/CO_2 ratio shows an increase in the production rate of CO compared to CO_2. This suggests that char oxidation inside the material is limited by the low amount of O_2 available in the structure. The phenomenon lasts about 20 seconds after extinction, as long as the material releases enough heat. The materials still degrades on the inside. A significant gradient of temperature exists in the material. It clearly emerges if the top of the residue is removed. Glowing starts again at the revealed surface of the sample when it gets in contact with O_2 from the air. The outer residue plays the role of a thermal shield while decomposition reaction is still active inside.

Table 3.6. Average total production of CO_2, CO and THC and related standard deviation for burning of 40% and 50% KNO_3 ternary mixture under air.

	CO_2	
Mixture	Total Production (g)	Standard Deviation (g)
40% KNO_3	21.94	0.78 (3.6%)
50% KNO_3	26.62	1.11 (4.2%)

	CO	
Mixture	Total Production (g)	Standard Deviation (g)
40% KNO_3	3.96	0.05 (1.3%)
50% KNO_3	1.17	0.35 (30.2%)

	THC	
Mixture	Total Production (g)	Standard Deviation (g)
40% KNO_3	0.86	0.05 (5.7%)
50% KNO_3	0.14	0.05 (31.9%)

3.4.1.2. 50% KNO_3 ternary mixture

3.4.1.2.1. Experimental observation

Sample

The ternary mixture was composed of 25% lactose, 25% starch and 50% KNO_3. Tests have been carried out under air atmosphere at a 200 l/min flow. The setup presented 2 different systems for ignition. It could be achieved using an ethylene/air pilot flame or a glow-plug. No external heat flux was applied. The combustion area was delimited by a quartz tube. Each sample weighed 50g.

Time

Initiation of the reaction

1. *Hot-spot* — *0 s*

A hot-spot is engendered by contact with the pilot flame or the glow-plug. The reaction is faster than for the 40% KNO_3 mixture. Glowing spots flare from the ignition point heating up the material in different locations. Little flames are observed.

2. *Fast Transition to Flaming* — *5 s*

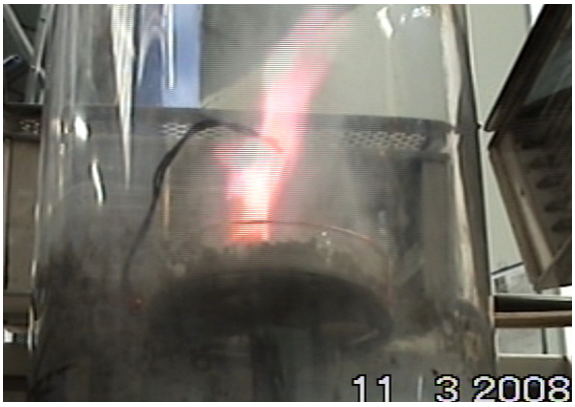

About 5 s after ignition, larger flames appear at the surface of the sample. About 2 seconds later, flaming occurs on all the surface of the material.

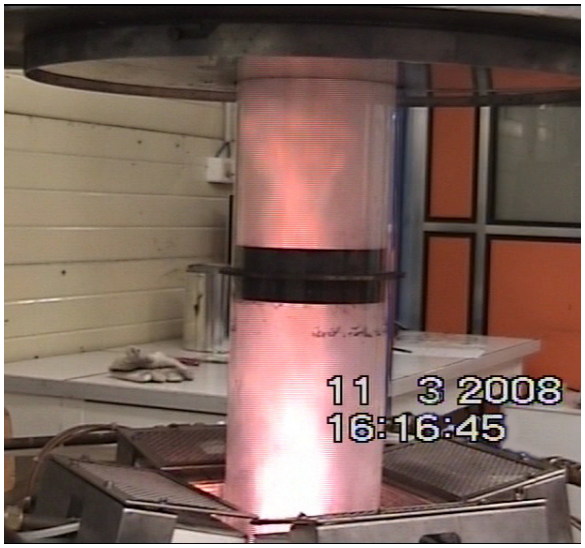

Flaming regime is established and presents large bright flames. It lasts for about 30 s. The tip of the flame reaches the hood located about 60 cm above the sample.

Extinction *35 s*

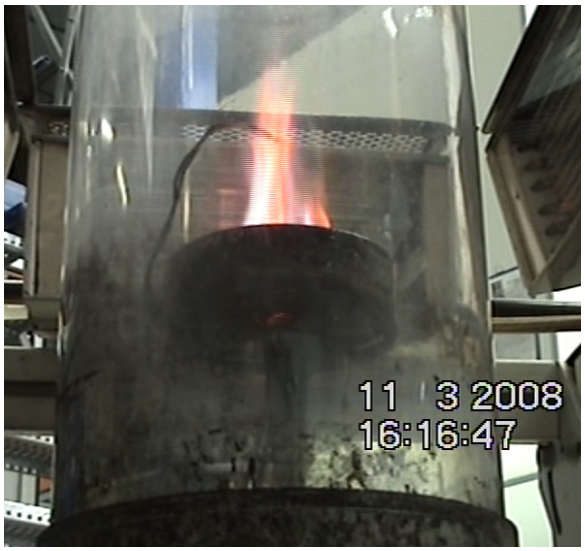

35 s after ignition, the material reaches extinction. Glowing is observed on the surface of the residue. No swelling phenomenon was noticed.

Residue

Glowing combustion lasts for few seconds after extinction. Residue represents about 27% of the initial mass of the sample.

3.4.1.2.2. Experimental Results

Figure 3.9 displays the gas emissions from the combustion of 50% KNO_3 ternary mixture. CO_2 is largely produced. The CO_2 molar fraction rises up to 2.33%. CO and THC are also generated with respective molar fraction peaks of 740 and 200 ppm. Combustion is not complete as indicated by the presence of CO and THC. Nevertheless, the ratio $\frac{(X_{CO}^A)_{max}}{\left(X_{CO_2}^A\right)_{max}} \approx 0.1$, denotes that the CO_2 emission is the predominant species emitted. The maximum O_2 depletion is 1.63%. Regarding the reaction stoichiometric conditions, the equivalence ratio, ϕ , has been estimated and, given the KNO_3 decomposition assumptions, was found to be about 0.7. With the air flow rate applied, the mixture should then be fuel lean. Table 3.6 gives the total production of CO_2, CO and THC. The ratio $\frac{CO}{CO_2}$ is equal to about 0.04. It strengthens the previous statement that CO_2 is the major gas produced and although the reaction is not complete, few CO and THC are produced. The CO/CO_2 ratio is indicated on Figure 3.10. One observes that it remains inferior to 0.1 for the duration of the combustion reaction which is characteristic of well ventilated conditions.

Figure 3.9 exhibits two different behaviours. While the CO_2 and the O_2 depletion curves show kinetics with one peak, two peaks are present on the THC and CO molar fractions measurements. According to Figure 3.9 and Table 3.7, first gases identified are THC. They start being produced before ignition. CO generation begins just after THC. Then, in α_1, ignition occurs and large bright flames arise all over the material. This coincides with the initiation of CO_2 generation. Practically at the same instant, THC reaches a first peak value (~ 204 ppm) followed about 4 seconds later by the first CO peak (~744 ppm) in α_2. CO remains relatively constant for few seconds while THC decreases. In α_3, CO_2 attains a maximum molar fraction value (2.33%) 4 seconds after the first CO maximum and then start decreasing. The fall of CO_2 tallies with lower flames until extinction was reached. Nevertheless, prior to extinction, side reactions take place. Glowing is observed during flaming (cf. Figure 3.11). THC and CO exhibit an inflexion point respectively in β_1 and β_2 followed by new increases. At this time, flames heights are lower. Second peaks of THC and CO come respectively in γ_1 (78 ppm) and γ_2 (497 ppm). Extinction results about 35 seconds after ignition. Glowing is observed at the surface of the sample for few seconds. All molar fractions come back to their initial values about 70 seconds after flaming started.

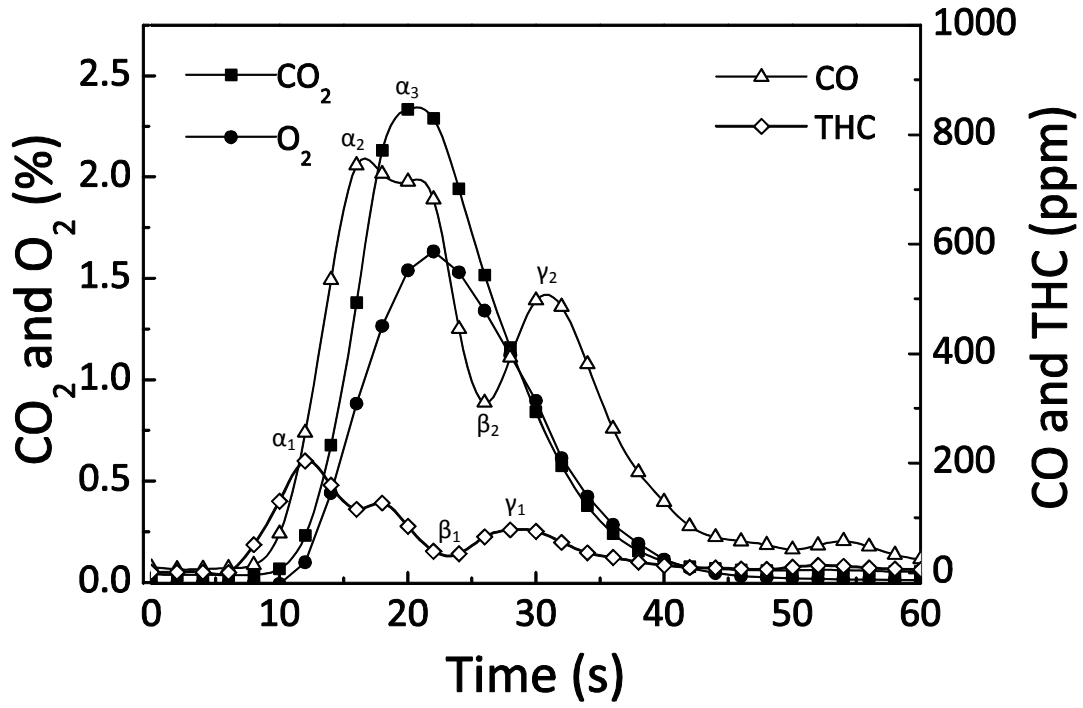

Figure 3.9. Gas emissions from the combustion of 50% KNO_3 ternary powder under air atmosphere (0.1 $m.s^{-1}$).

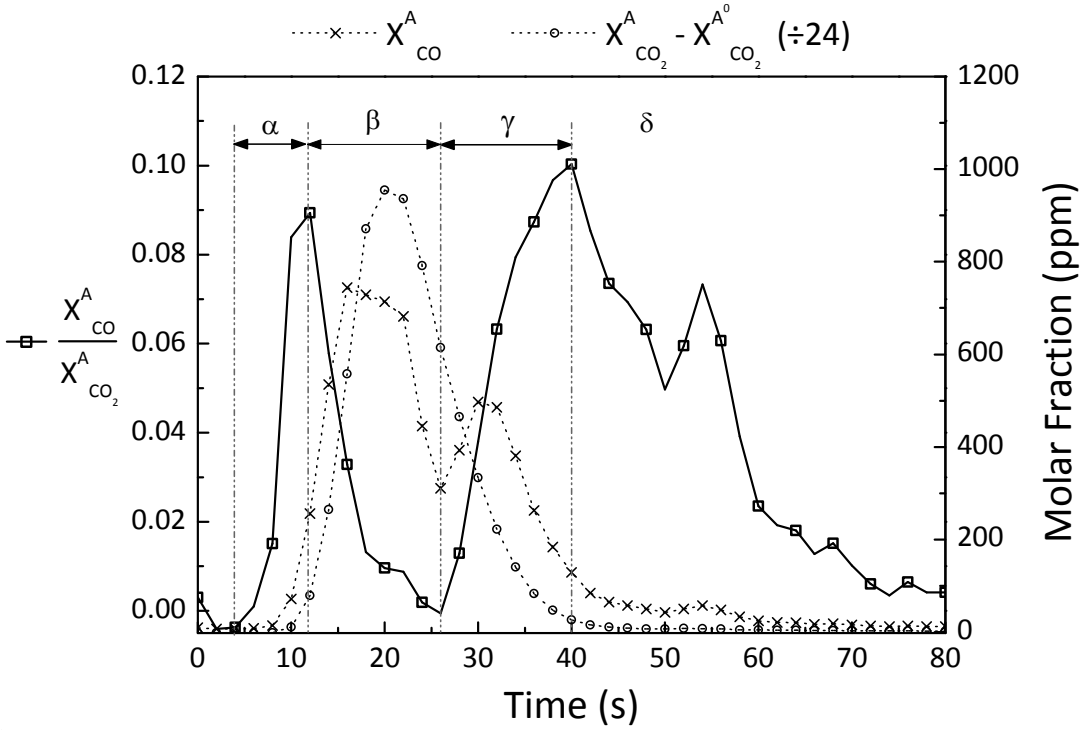

Figure 3.10. CO/CO_2 ratio from the combustion of 50% KNO3 ternary powder under ambient air (0.1 $m.s^{-1}$).

Table 3.7. Time Description of THC, CO and CO_2 emissions.

Time	7 s	8 s	11s	12 s	16 s	20 s	22 s	24 s	26 s	28 s	30 s	...	70 s
THC	↗	⇢	↗	Λ 1st peak (204 ppm)	↘	⇢	↘	V inflexion (35 ppm)	↗	Λ 2nd peak (78 ppm)	↘		→ (0 ppm)
CO	→ (0 ppm)	↗	⇢	↗	Λ 1st peak (744 ppm)	↘	⇢	↘	V inflexion (310 ppm)	↗	Λ 2nd peak (497 ppm)		→ (0 ppm)
CO_2	→ (0.04%)	→	↗	⇢	↗	Λ 1st peak (2.33 %)	↘	⇢			↘		→ (0.04%)
			Ignition		Combustion			Combustion + Side Reactions (glowing)					

It is interesting to compare the generation of CO to the one of CO_2. Considering Figure 3.10, the period α corresponding to the time following the initiation of the reaction highlights an increase in CO production while no CO_2 generation is measured. Similarly to the interpretation developed for the 40% KNO_3 ternary powder, one assumes that volatiles formed by thermal decomposition of the fuel components are first oxidized into CO. This oxidation process appears to be first favoured compared with the oxidation reaction leading to CO_2. Only a limited amount of O_2 is available in the material at this time. According to Pitts [11] and Gottuk et al. [19], the concentration of free radicals (i.e. $OH\cdot$, $HO_2\cdot$) needed for the conversion of CO to CO_2 remains low when significant amounts of unburnt hydrocarbons are present. The free radicals are more reactive with the latter. If the concentration of hydrocarbons reduces or if the quantity of free radicals rises, the radical "buffer" increases and promote the oxidation to CO_2. Regarding Figure 3.10, the transition α to β is characterized by an inflexion in the CO/CO_2 ratio. The amount of CO produced by the reaction compared to the one of CO_2 decreases to a very low level ($CO/CO_2 < 0.1$). This behaviour tends to suggest that CO gets oxidized into CO_2 once the release of O_2 from KNO_3 is established but also from the moment the diffusion flame initiates. In a matter of fact, the flame promotes the oxidation process leading to the formation of CO_2. During this period, the processes of smouldering and flaming are coupled. The transition from β to γ corresponds to the extinction of the diffusion flame regime. Only the char oxidation persists for few seconds. One observes that the formation of CO increases compared to the one of CO_2. Char oxidation mainly occurs inside the material where the amount of O_2 is very poor. Glowing combustion takes place on the surface but only locally and the temperature gradient above the surface might be too high to allow complete oxidation of the char. The period δ coincides with the end of the char oxidation process.

Figure 3.11. Observation of glowing inside the flaming region during combustion of 50% KNO_3 ternary mixture (Coupling of smouldering and flaming combustions).

3.4.1.2.3. Discussion

Ignition appears to be initiated by hot spots. By applying the glow-plug up to a temperature of about 400°C at the surface of the sample, a hot spot is created. Surface of the material becomes incandescent. Droplets are expelled from the initial heating zone, creating localized ignition. This phenomenon looks similar to the one reported by Blackwood and Bowden for the initiation of the burning of black powder [12]. They suggest that the propagation of burning may be caused by fine sprays of residue, probably potassium carbonate droplets, in the molten state (at a temperature between 550°C and 700°C). Hot spots can be formed from adiabatic compression of entrapped air distributed through the powder. By impinging unburnt material, they create localized ignition points. Given their small sizes, they cool and solidify quickly but considering a temperature of about 500°C, it can be expected to they can spread decomposition reaction in the material in several places. As heat propagates, volatiles mix with O_2 generated by the decomposition of KNO_3. The mixture is probably homogeneous and this explains the small discontinuous flames observed at the surface of the material. Concurrently, white smoke starts being emitted. As assumed previously, most of the emission is expected to be water vapour. On the other hand, THC and CO were measured in little quantity before ignition so they will be also present in the smoke particles. Then, gases diffuse into the O_2 from ambient air and once flammability conditions are attained, flaming is activated over the reacting components. Considering Figure 3.10, it appears that volatiles are first formed, the temperature of decomposition of lactose being lower than the one of KNO_3. Once KNO_3 releases O_2, the limited quantity does not allow complete oxidation of the volatiles. They are first oxidized into CO. As flaming initiates, CO gets further oxidized to CO_2.

Large and bright orange – white flames are observed rising up to 0.6 m above the sample (cf. Figure 3.12). As it emerges on Figure 3.13.a, a blue – violet envelop is discerned surrounding the outer part of the flame. The latter colour might be related to the combustion of KNO_3, typical of the potassium emission.

Figure 3.12. Flames from the combustion of 50% KNO_3 ternary mixture under air atmosphere (V_{air} = 0.1 $m.s^{-1}$).

Different regions of emission exhibit from the structure of the flame as it is described on Figure 3.13.b. and Figure 3.14. At the really base, the radiation tends to blue and dark violet above. Fuel vapours and O_2 generated from the decomposition of the lactose, starch and KNO_3 are mixed when they enter this zone. According to Gaydon and Wolfhard [20], OH, CH and C_2

radicals are formed in this region and oxidation occurs. Fuel and vapours are in intimate contact. The present behaviour shows similarities with flames resulting from premixed conditions. In this zone CO reaches a peak and then falls as CO_2 is being produced. However, the %OB and the elemental equivalence ratio, previously estimated (cf. section 3.2, Table 3.3), allowed stressing the lack in O_2 inside the material to attain stoichiometric conditions. Thus, it has to be expected that combustible gases and particles are still present in the flame. Beyond the base, orange radiations are observed. It is typical from the formation of carbon particles. Based on the assumption that CO is first produced from the oxidation of light hydrocarbons and then oxidize into CO_2, Gordon and Wolfhard developed a criterion to estimate when carbon particles would start to be produced. They simply considered the ratio of carbon atoms to oxygen atoms, $\frac{n_C}{n_O}$, and assumed that as long as the ratio is less than unity, all the carbon evolve into CO and then consider gaseous equilibriums between CO_2, CO, H_2, H_2O. However, when $\frac{n_C}{n_O} > 1$, production of carbon particles should be expected. Considering these conditions, taking into account that oxidation of HC occurs at the base of the flame, where O_2 and the volatiles are mixed, one can assume that above this region, n_O is very low and $\frac{n_C}{n_O}$ significantly high. The presence of carbon is very likely in the inner zone and would explain the orange radiation. As the carbon particles rises, they penetrate deeper into a region of burnt gases containing CO_2, H_2O and CO. Moreover, as the gases diffuse into ambient air, n_O becomes higher. $\frac{n_C}{n_O}$ is lower and a preference to generate CO is observed. The region above the inner zone can be seen as an envelope where diffusion occurs. CO, H_2 and remaining hydrocarbons vapour are oxidised into H_2O and CO_2. CH and OH radicals are expected to be found. If the carbon particles are not entirely consumed, smoke and soot particles are released. The inner zone and the outer envelope manifest a structure similar to those noticed for diffusion flames.

The study of the structure of the flame is of great interest to get an insight of the combustion gases emissions. The blue and violet radiations tend to suggest that if the reaction is not complete, the emissions of incomplete elements are not tremendously significant. On the other hand, the amount of soot observed is relatively low. Figure 3.9 and Table 3.6 tend to justify the previous assumption.

a.

b.

Figure 3.13. (a.) Flame from the combustion of 50% KNO_3 ternary mixture submitted to a flow of air of 200 $L.min^{1}$; (b.) different zones of the flames highlighted.

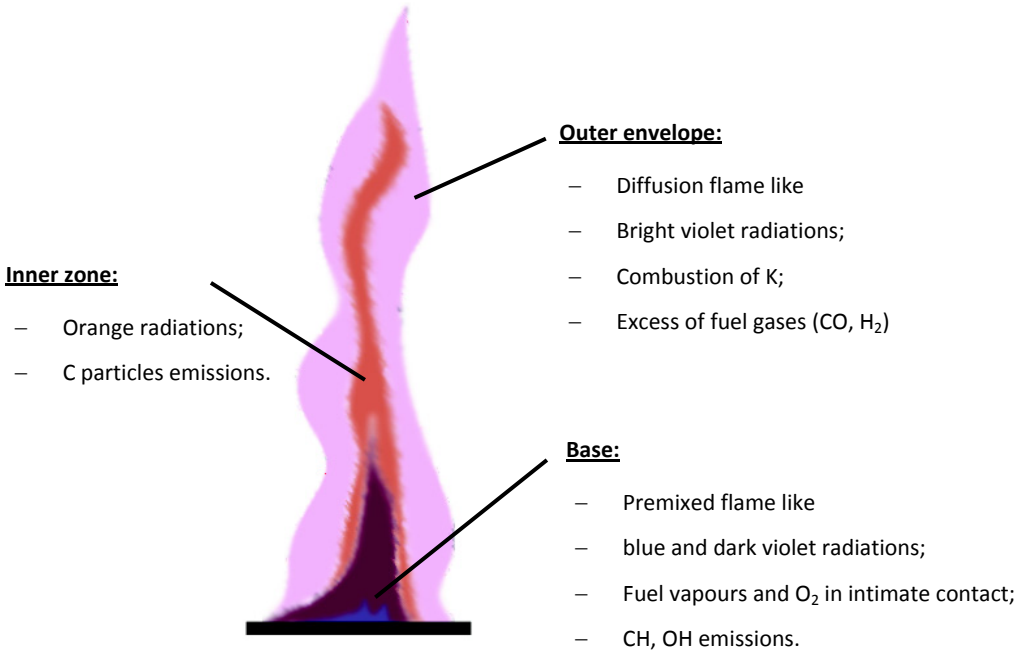

Figure 3.14. Structure of the flame obtained from the combustion of 50% KNO_3 ternary mixture submitted to a flow of air of 200 L.min^{1}.

First, HC are identified. In the previous section of the thermal analysis, it was noticed that lactose and starch started to decompose prior to KNO_3. The two fuels components are heavy carbohydrates that degrade under lighter elements. One can assume that the detection of HC is related to the beginning of the fuel components decomposition around 300°C. Nevertheless, as mentioned previously, the different between the thermal analysis experiments and combustion tests carried out with a calorimeter is that the temperature rise is significantly faster with the latter. Then, reactions that would occur at different times during DSC or TGA analysis are likely to become superimposed during combustion. CO starts indeed being emitted almost simultaneously, followed few seconds after by CO_2. First, fuels volatize into lighter HC. According to Freeman [22], the decomposition of KNO_3 leads to the formation of O_2 elements, following,

1st decomposition reaction: $KNO_3 \longrightarrow KNO_2 + \frac{1}{2}\, O_2$ (10)

2nd decomposition reaction:

$2\, KNO_2 \longrightarrow K_2O + N_2 + \frac{3}{2}\, O_2 KNO_2 \rightarrow K_2O + N_2 + \frac{3}{2} O_2$ (11)

A homogeneous mixture of fuel vapours and O_2 and the rising temperature will favour the formation of CO. Pitts [11] explains that competing reactions occur for the oxidation of fuel vapours to CO and CO to CO_2. He describes a trend where free radicals, such as OH, react faster with fuel than CO. According to the flame structure, one can define a hypothesis where most of CO is produced at the base of the flame from the oxidation of light HC and gets oxidized into CO_2 in the envelope region where diffusion with ambient air is important.

It has to be pointed out that the generation of the combustion gases depends on several parameters. The temperature and the residence time in the reactive zone as well as the diffusion and chemical times are critical quantities. If the temperature is too low, if the residence time is small compared to the chemical time or if the diffusion time is relatively long, the combustion zone can be considered unreactive. The production of CO_2 allows asserting that the chemical and residence times are small enough compared to the residence time in the reactive zone so oxidation reaction can occur. However, concentrations of HC and CO are measured. According to the equivalence ratio, ϕ, the material vapours – air mixture is supposed to be fuel lean. Several hypotheses can be drawn. It is possible that O_2 was locally depleted in combustion zone preventing all HC and CO to be oxidized; the residence time becoming too short for the diffusion of O_2 close to the gases at a medium temperature high enough for reaction.

Experimental observations emphasize that the combustion of the 50% KNO_3 ternary mixture was characterized by two processes: flaming combustion and glowing combustion. Emission of light and heat, from surface oxidation of the carbonaceous residue, was observed during the experiments (cf. Figure 3.11). In terms of emissions, Figure 3.9 exhibits rising productions of THC and CO (peaks γ_1 and γ_2) at flameout. Inside the residue, the temperature remains high enough to allow oxidation at the surface generating glowing and heat. This phenomenon could have an influence on the evaluation of the amount of energy release by the material during combustion. The two phenomena, flaming and glowing, overlap each other preventing to estimate their own exact contribution. However, the CO peak located in γ_2 emerges while flameout has already occurred. The generation of CO relating to the latter peak entirely originates from glowing combustion. An estimate of the CO formed by glowing can be done. During experiments under air, the average production of CO from the combustion of a 50g sample of ternary mixture with 50% KNO_3 was 0.56 g. A calculation of the CO generation after

flameout gives about 0.25g. Moreover, it has been observed that during flaming, glowing was also active. In case CO was released at the surface of the sample, it is likely that it gets oxidized in the flame. In any case, the production of CO by glowing appears to be very limited.

3.4.2. Influence of the oxidizer concentration

Two different mixtures have been studied. Their distinction stems from the concentration of oxidizer in the material. It allows evaluating the influence of KNO_3 on the combustion behaviour of coupling fuel/oxidizer.

3.4.2.1. Initial Composition

Different behaviours have been observed depending on the composition of the ternary mixture. The flame structure, the aspect of the char, the gases emissions as well as the burning rates present discrepancies.

First consider the variations of compositions in terms of elements present in the material. Table 3.8 and Table 3.9 indicate, respectively, the mass and mole percentage of each elements present in the ternary mixtures. In terms of mass, the main noticeable changes are related to the carbon (C) and potassium (K) atoms. The molecular weight of potassium is 39.1 $g.mol^{-1}$ [21]. It is more than two times heavier than any other element of the material. A variation of K moles is emphasized when considered as mass. Lactose and starch belongs to carbohydrate compounds. They consist of long chains of monosacharride units, which often correspond to ($C{\cdot}H_2O$) groups. The molecular weight is 342.3 $g.mol^{-1}$ for lactose and 162.1 $g.mol^{-1}$ for starch. Each monomer of starch and lactose respectively contain 6 and 12 C atoms. Contrary to light hydrogen (H) atoms, a 10 % change of the quantity of fuel in the mixture is apparent when considering the mass of C element. A shift of about 4.3 % is observed. Regarding the mass of oxygen (O), it only varies of 0.3 % when the amount of KNO_3 is raised or reduced by 10 %. During the reaction of combustion, oxidation of the volatiles is mainly provided by the O_2 released by the oxidizer's decomposition. Nevertheless, O atoms are also present in the fuel components, lactose and starch. Finally, Figure 3.15 shows that the mass of O2 will only vary between 47.7 % and 50.3 % of the total mass of the sample when changing the ratios of the different components.

Table 3.8. Mass percentage of elements present in the mixture.

Mixture	$C_{\%\ mass}$	$H_{\%\ mass}$	$O_{\%\ mass}$	$N_{\%\ mass}$	$K_{\%\ mass}$
40% KNO_3	26	3.8	49.3	5.5	15.4
50% KNO_3	21.6	3.2	49	6.9	19.3

Table 3.9. Mole percentage of elements present in the mixture.

Mixture	$C_{\%\ mole}$	$H_{\%\ mole}$	$O_{\%\ mole}$	$N_{\%\ mole}$	$K_{\%\ mole}$
40% KNO_3	22	38.5	31.4	4	4
50% KNO_3	20	35	34	5.5	5.5

Finally, one notices that if a rise of the quantity of fuel induces a rise of the mass of C, paradoxically, for the tested ternary mixture, an increase of the amount of oxidizer is accompanied by a decrease of the mass of oxygen present in the material. However, it has to be highlighted that the calculation considered all the oxygen present in the material. The assumed decomposition of KNO_3 has been previously described [22]. It emerged that a part of the oxygen contained in the oxidizer would not take part in the oxidation of the gases evolved from the fuels decomposition. Figure 3.15 shows the evolution of the mass percentage of effective O when the fuel/oxidizer ratio of the mixture is varied. As expected, the amount of mass of oxygen available in the material to participate in the oxidation process is less than previous. A part of the O atoms are used for the generation of K_2O. A change of 10% of the amount of fuel is associated to a 1.1% variation of the mass of O_2 that can take part to the oxidation process. The similar paradoxical tendency regarding the level of oxygen able to react is pointed out. For identical sample masses, increasing the amount of oxidizer goes with a decrease of the overall oxygen available for the combustion reaction. More oxygen is provided by the oxidizer but, considering that both fuels contain O atoms, as the mass of fuel is reduced, the mass of oxygen originated from lactose and starch becomes also less. However, following the last statement, the number of C and H atoms is lowered at the same time. Finally, given the decreasing rates of C, H and O, the material combustion behaviour will differ. If the number of moles of C and H declines faster than the moles of O, the reaction, only considering the material, will tend to approach the stoichiometry.

Table 3.10. Mass percentage of O and effective O present in the mixture.

Mixture	$O_{\%\ mass}$	$O_{\%\ mass\ effective}$
40% KNO_3	49.3	46
50% KNO_3	49	45

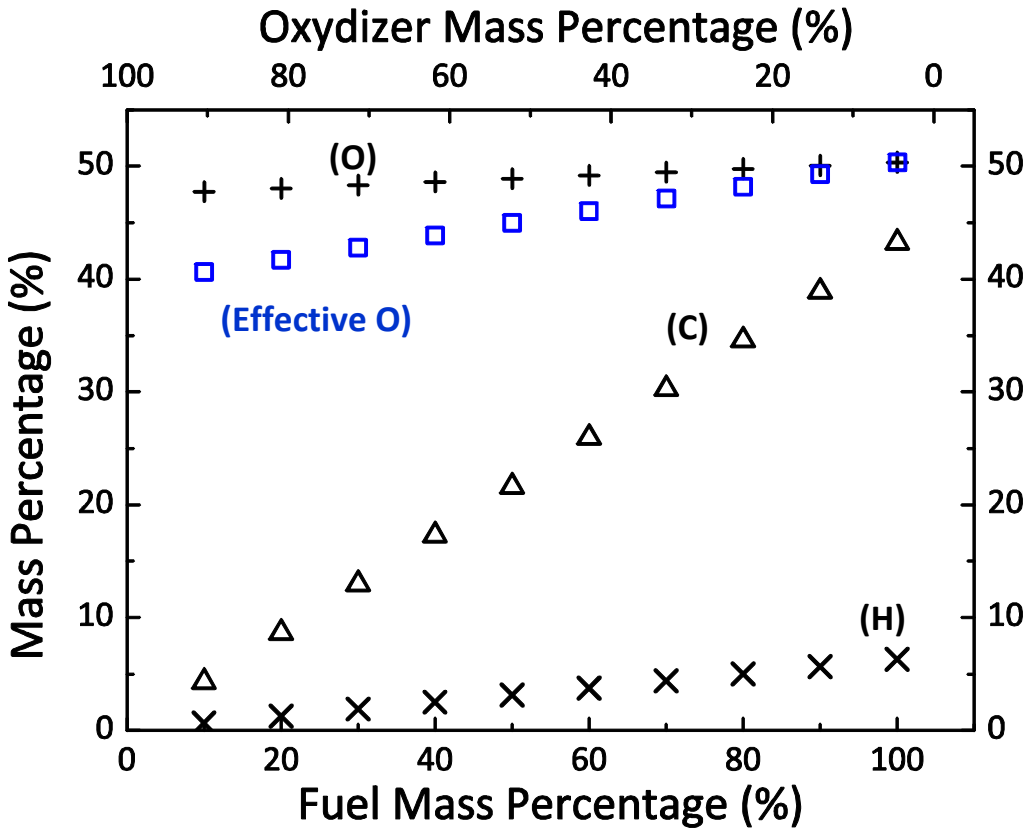

Figure 3.15. Mass percentage of C, H, O in the mixture according to the fuel and oxidizer ratios.

Based on the principle of oxygen balance, one can define a parameter to estimate the portion of oxygen present in the material according to what would be required to draw a stoichiometric reaction. The oxygen ratio, φ_{O_2}, is expressed as follow,

$$\varphi_{O_2} = 100\ \frac{z}{2x + \frac{y}{2}} \tag{12}$$

Where, assuming, $m\%_{fuel\,1} = m\%_{fuel\,2} = \frac{m\%_{fuel}}{2}$,

$$x = \left(\frac{\psi_{C_{fuel\,1}}}{M_{fuel\,1}} + \frac{\psi_{C_{fuel\,2}}}{M_{fuel\,2}}\right)\frac{m\%_{fuel}}{2} \tag{13}$$

$$y = \left(\frac{\psi_{H_{fuel\,1}}}{M_{fuel\,1}} + \frac{\psi_{H_{fuel\,2}}}{M_{fuel\,2}}\right)\frac{m\%_{fuel}}{2} \tag{14}$$

$$z = \left(\frac{\psi_{O_{fuel\,1}}}{M_{fuel\,1}} + \frac{\psi_{O_{fuel\,2}}}{M_{fuel\,2}}\right)\frac{m\%_{fuel}}{2} + \frac{\psi_{O_{oxidizer}}\,(1 - m\%)}{M_{oxidizer}} \tag{15}$$

The oxygen ratio φ_{O_2} is plotted on Figure 3.16 as a function of the fuel and oxidizer mass percentage.

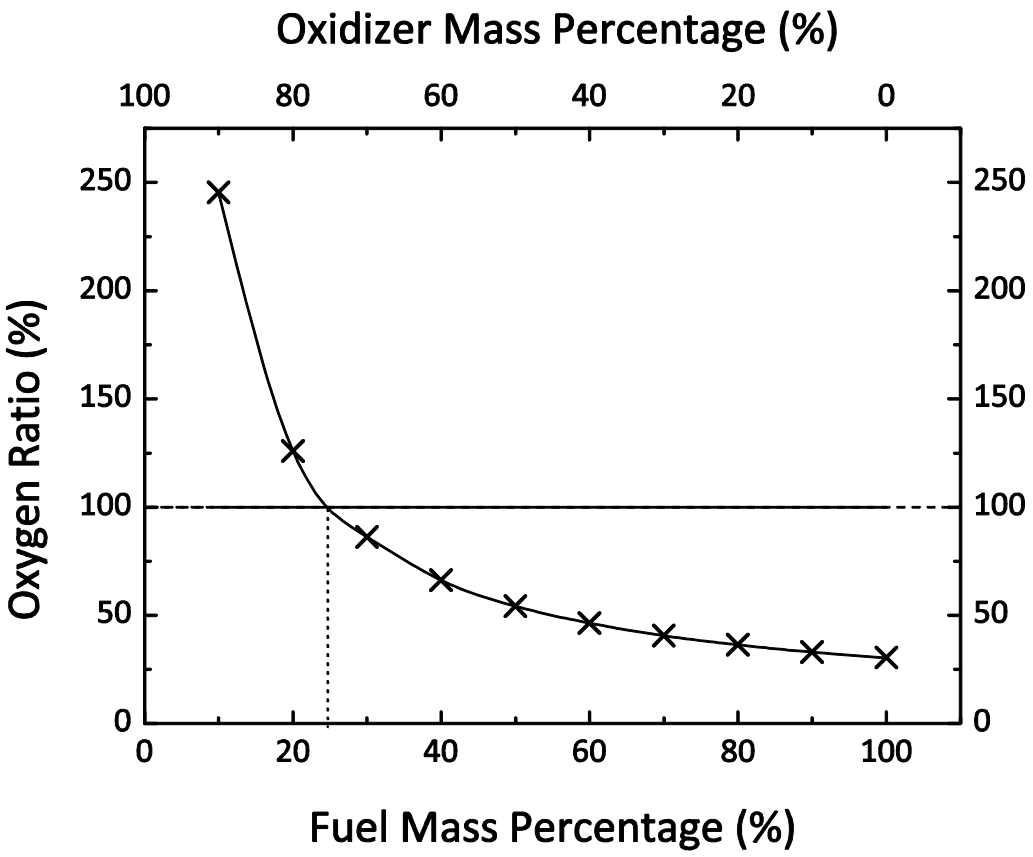

Figure 3.16. O_2 ratio as a function of the fuel and oxidizer mass percentages.

The graph exhibits a $\frac{1}{x}$ shape. It reveals that below 25.5 % of fuel, enough O would be present in the material to assume a stoichiometric reaction. The two tested compositions, ternary mixtures containing 40 % and 50 % KNO_3 (i.e. respectively 60 % and 50% of fuel) show an

oxygen ratio of, respectively, 46.3 % and 54.3 %. It clearly underlines that the mixture moves closer to the stoichiometry when the proportion of oxidizer is increased but a lack of O_2 reveals the need of a secondary oxidation partner to achieve a more complete reaction. It is in agreement with the measurements of CO_2, CO and THC obtained for the two compositions during the experiments carried out under air atmosphere. The CO/CO_2 ratio for the 50 % KNO_3 ternary mixture was lower than the one estimated for the 40 % KNO_3 composition (cf. Figure 3.5 and Figure 3.10).

3.4.2.2. Initiation and transition to flaming

Transition to flaming is observed for the different experiments under air. Although a complete explanation of the physical phenomenon was beyond the scope of the present work, a qualitative analysis is developed based on observations and experimental data. However, most conclusions drawn will remain at a state of postulate.

The combustion reaction occurs in two stages. First, the surface of the material is locally submitted to a pilot flame for few seconds. A hot spot is created and the decomposition of the mixture components is initiated. The first step of the process is the solid heating. The temperature of the material at the reaction front rises up to a pyrolysis temperature, T_{py}, where pyrolysis vapours start to be released. As discussed earlier, respective pyrolysis temperatures for lactose and starch are about 220°C and 320°C, while the thermal decomposition of KNO_3 occurs around 500°C (Melting starting at about 330°C). Nevertheless, thermal analysis has shown that KNO_3 mainly reacts with the fuel compounds from the moment it reaches its fusion temperature (cf. Chapter 2, Figure 2.7. Lactose and starch will start decomposing prior to KNO_3. The temperature rise inside the material has been measured using a type K thermocouple. Figure 3.17 and Figure 3.18 present the results obtained for both ternary mixtures. They highlight a fast temperature increase with a steepest for the latter composition, the combustion being more vigorous. Regarding the 40% KNO_3, the time required to ascend from 200°C to 400°C is about 6 seconds, while it takes about 2 seconds during the combustion of the 50% KNO_3 mixture. Pyrolysis of the fuel components is activated only a few seconds prior the decomposition of the oxidizer. This has been previously confirmed by the measured emissions of the combustion products and the CO/CO_2 ratio curves (cf. Figure 3.4, Figure 3.5, Figure 3.9 and Figure 3.10). It was noticed that the first gases released prior to the

transition to flaming were CO and THC, characteristics of pyrolysis gases. As KNO_3 decomposes and generates O_2, a heterogeneous mixture is formed with the fuel vapours. At this stage, reactions are endothermic and have been induced by the heat generated by the hot spot. Decomposition gases spread into the medium by diffusion and convection at high temperatures. The presence of O_2 produced from KNO_3 allows initiation of exothermic oxidation. Part of the heat released is transferred to the virgin material by conduction and radiation providing the necessary condition to allow downward propagation of the degradation front as shown on Figure 3.19 [23]. A self sustained smouldering reaction is induced, consisting in a surface combustion reaction that propagates through a porous medium. The propagation is controlled by a balance between the heat generated, the heat transferred ahead of the reaction front and the heat lost to the surrounding [24]. The main difference with common fuels developing smouldering is the presence of oxidizer directly inside the material. Oxidizer availability is usually a limiting parameter for smouldering propagation [25]. In the case of the sample ternary mixture, a large amount of O_2 is directly present in the reaction zone mixed with combustible gases. It induces a stronger reaction that would be if the oxidizer had to reach the degradation front by diffusion and convection. Furthermore, residual char is formed behind the reaction front. Glowing combustion corresponds to an intense smouldering process occurring at the surface of the residual char that releases enough heat to the point that it radiates in the visible spectrum and can then be observed [26] [27]. It is observed at the surface of the char region but also at the side of the degradation front. It ceases once reacting surface is cooled. This phenomenon highlights char oxidation. It leaves behind a more porous medium which allows an increase of O_2 originated from the decomposition of KNO_3 as well as from air to flow in.

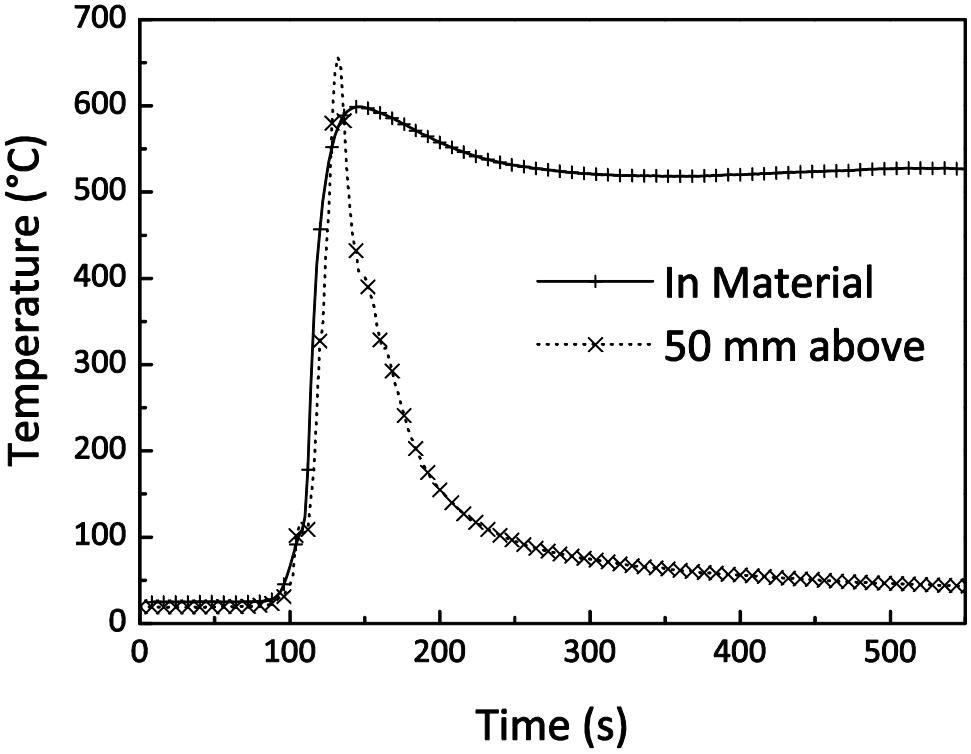

Figure 3.17. Evolution of the temperature inside and 50 mm above the surface of the material. Combustion reaction of a 40% KNO_3 ternary mixture under air atmosphere.

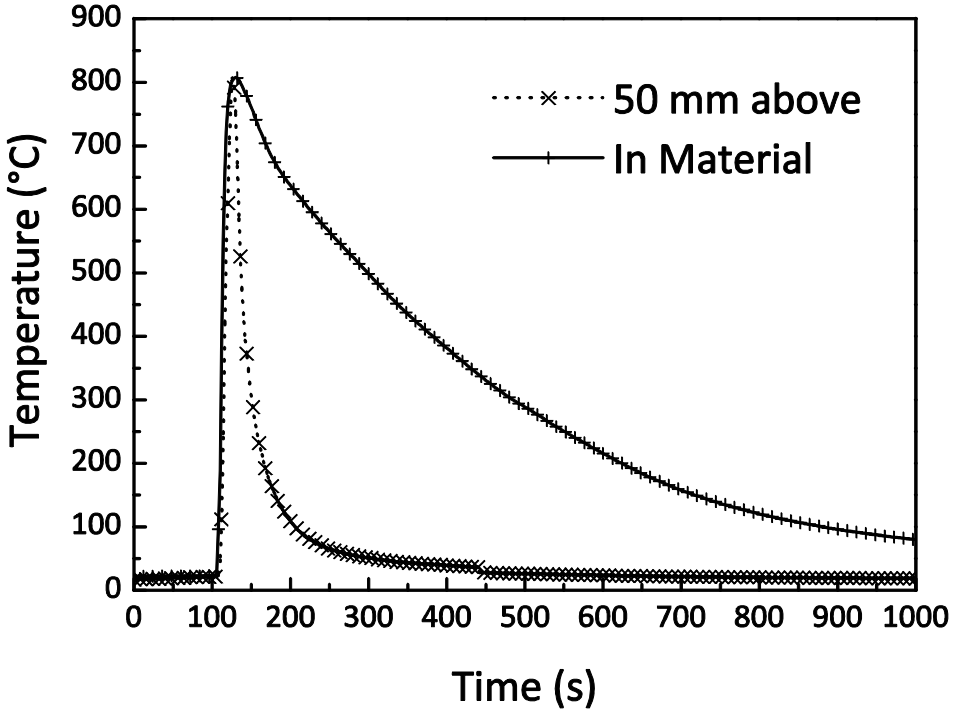

Figure 3.18. Evolution of the temperature inside and 50 mm above the surface of the material. Combustion reaction of a 50% KNO_3 ternary mixture under air atmosphere.

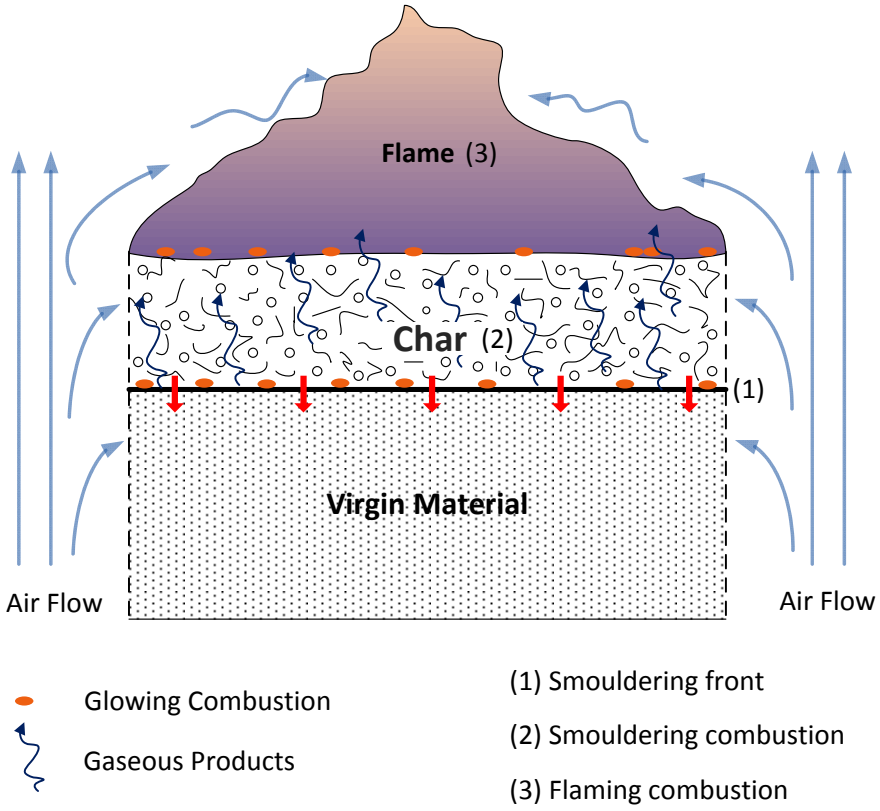

Figure 3.19. Schematic of one dimensional smouldering reaction in a ternary mixture Starch/Lactose/KNO3 leading to a flaming reaction above the surface.

Finally, two distinctive oxidation processes occur: oxidation of the pyrolysis gases characterizing the flaming combustion and oxidation of the char characterizing the smouldering phenomenon. These exothermic reactions transfer heat to the virgin material and propagation is preserved as long as,

$$\dot{Q}_{gases\ ox} + \dot{Q}_{char\ ox} > \dot{Q}_{pyr\ fuels} + \dot{Q}_{dcp\ Ox} + \dot{Q}_{loss\ surroundings} \quad (16)$$

As the front propagates downward, gaseous products are released and char is formed. The hot gases produced by the fuels decomposition and the char engendered behind the smoulder reaction meets with the internal supply of oxidizer and can undergo exothermic oxidation reactions, possibly leading to a transition to flaming.

For the latter phenomenon to be established, the fuel vapours/oxidizer mixture needs to reach flammable conditions. Buoyancy induced flows occur in the char and above. A combustible

mixture can be formed and would just need a local hot spot or high enough temperature resulting from char oxidation to supply the energy necessary for ignition. According to this assumption, a premixed flame can be initiated. On the other hand, the forced flow induced in the tube also diffuses inside the powder and participates in the combustion reaction by intensifying the oxidation process. A sustained diffusion flame is obtained above the surface of the sample if gaseous products can elevate by buoyancy and mix with the ambient air. The required energy for ignition can be transferred to the gas phase by radiation of local glowing points or by a premixed flame that would arise from the inside of the material.

The emergence of a buoyant flow and, as a consequence, the emergence of flaming combustion is highly dependent on the permeability of the char [25]. The char region is more porous than the virgin material and the temperature inside the component high enough to induce convection. The permeability of the powder is assumed to be low. For the 40% KNO_3 mixture, smoke clearly exits from the side of the sample, precisely at the interface between the degraded powder and the virgin powder as shown on Figure 3.20. The effect of permeability is stressed from the experiments carried out. Completely different behaviours emerge during transition to flaming between the 40% and the 50% KNO_3 ternary mixtures.

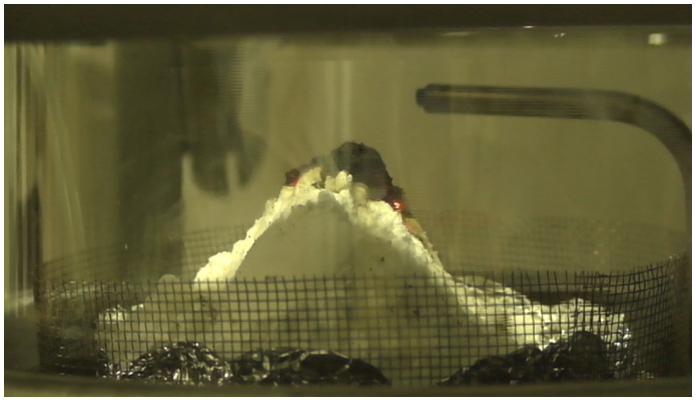

Figure 3.20. Release of smoke at the interface between the reacting front and the virgin material.

3.4.2.2.1. Initiation of the reaction

For the experiments performed with the 40% KNO_3 ternary mixture, the propagation of the degradation front was observed before the transition to flaming. A significant swelling of the char region is observed as gases are released as exhibited on Figure 3.22.a. Between the

beginning and the end of the experiment, the volume of the sample has increased by approximately a factor of 3. This phenomenon seems to be instigated by a pressure rise inside the structure, created by the generation of gases. Gaseous products are mainly expelled at the char/virgin material interface. The degradation front spreads until the end of the sample. Then, the combustion gases largely exit from the back of the sample in contact with the sample holder. Once the combustible mixture released reach flammable conditions, flaming combustion is activated. Flames originate from the interspaced region between the reacting material and the sample holder. The order of magnitude of the flames height is about 20 centimetres.

The experiments carried out with the 50% KNO_3 ternary mixture present a faster transition to flaming after initiation of the reaction than the 40% KNO_3 composition. The propagation of the degradation front is simultaneous with the flaming reaction as it appears on Figure 3.21. For the present mixture, only a slight swelling is noticed (cf. Figure 3.22.b.). Gaseous products emerge through the overall surface of the material and flame covers the sample. The reaction is more intense than with the 40% KNO_3 composition. The order of magnitude of flames height is about 1 meter.

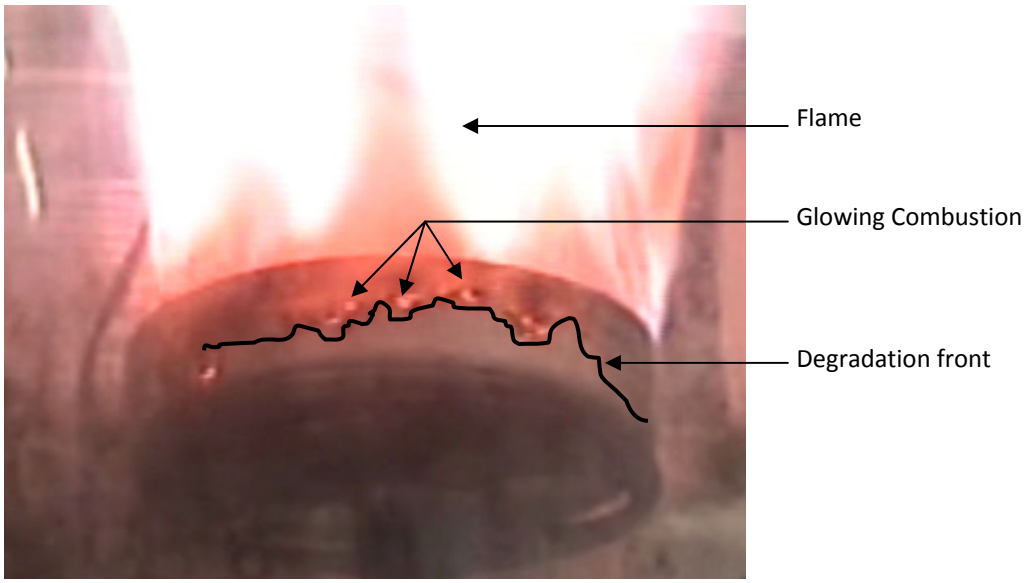

Figure 3.21. Combustion of 50% KNO_3 ternary mixture at an air flow rate of 200 $l.min^{-1}$ (≡ air velocity of 0.1 $m.s^{-1}$) : propagation front and flame.

(a.) 40% KNO_3 ternary mixture

Virgin Material

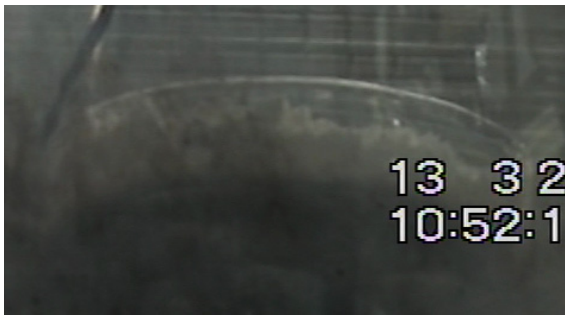

Residue

(b.) 50% KNO_3 ternary mixture

Virgin Material

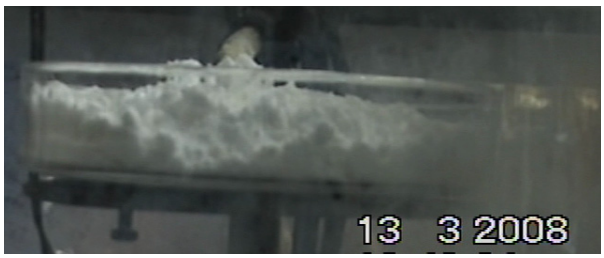

Residue

Figure 3.22. Evolution of the material volume during the combustion reaction.

In order to investigate the possible reasons for the two sample materials explaining the distinction between the combustion behaviour, mass losses, residues composition and species yields have been estimated. Figure 3.23 indicates average adimensioned mass losses obtained from the experiments carried out under air atmosphere with 40% and 50% KNO_3 ternary mixtures. Error bars representing the standard deviation of the measured variable have been added. Discrepancies are larger with the 40% KNO_3 ternary powder than with the 50% KNO_3 one. Ignition takes longer to occur with the first mixture and is more dependent of the propagation of the smouldering front. The total mass loss for the 40% KNO_3 composition represents about 71.63% of the initial mass and the decrease occurred in about 78 seconds while for the 50% KNO_3 composition, about 72.68% of the initial mass has been released into the gas phase and the soot in about 30 seconds (cf. Table 3.11). A steepest decrease results

from the combustion of the 50% KNO_3 composition. As the inflexion appearing on the mass loss curve for the 50% KNO_3 ternary mixture remains relatively constants, a change of slope is visible for the 40% KNO_3 composition and corresponds to the transition to flaming. Linear fittings have been performed and are shown on Figure 3.23. The slopes of the fitted curve can be seen, given experimental conditions, as a mass loss rate characteristic of a reaction or a combination of reactions occurring. The slope obtained for the 50% KNO_3 ternary mixture gives a maximum mass loss rate of about 2.6 $g.s^{-1}$. Two phenomena are competing, oxidation of the pyrolysis gases and the char inside the material and flaming above the surface. Two curves are stressed from the mass loss measured from the burning of the 40% KNO_3 ternary mixture. The first fitted line coincides with the outlined smouldering phenomenon, the second with the flaming combustion, considering that char oxidation probably still befalls. The characteristic mass loss rates estimated are, respectively, 0.8 and 1.3 $g.s^{-1}$. One notices that the reaction rate relative to flaming combustion is higher than the one of smouldering.

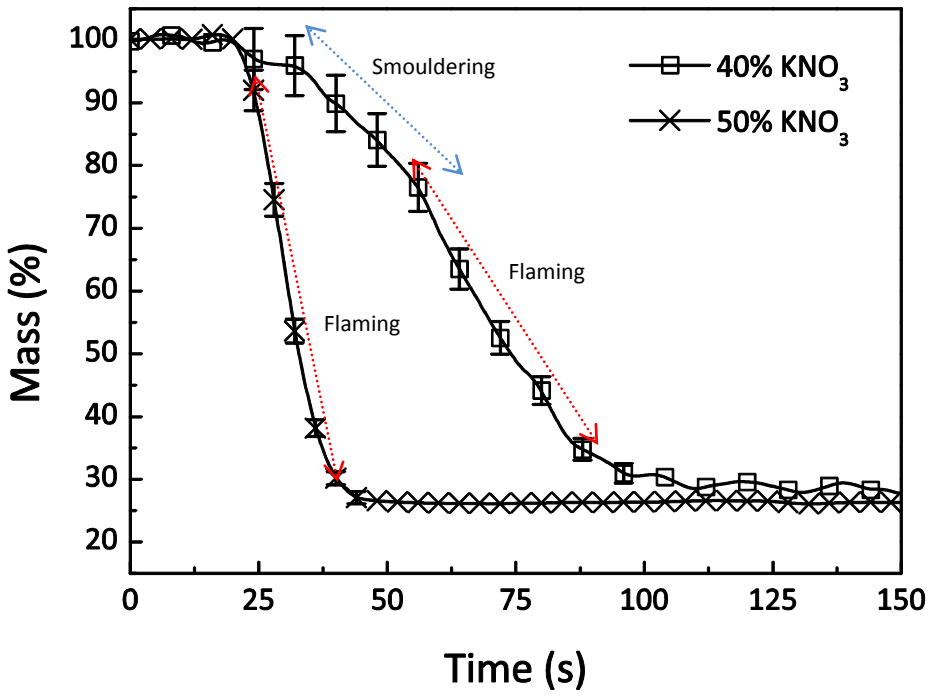

Figure 3.23. Percentage of mass loss from initial sample during the combustion of 40% and 50% KNO3 ternary mixture and dominant combustion modes.

Table 3.11. Average mass loss and residue percentages from sample combustion and residue content.

Sample	Mass Loss (%)	Residue (%)	$\%C_{total}$ in Residue	%K in Residue
40% KNO_3	71.63	28.55	13.00	48.33
50% KNO_3	72.68	27.32	12.20	47.33

Regarding the two different compositions, it comes that the reaction is more vigorous with the 50% KNO_3 ternary mixture. It is interesting to analyse the completeness of the combustion reactions through the emissions and the composition of the residues. Table 3.12 presents the main species yields from the gases released during the combustion for both mixtures. In the given experimental conditions, the 50% KNO_3 composition highlights a nearly stoichiometric behaviour. CO_2 is the main species generated and very few CO or THC are released. If CO_2 is still largely the major gas produced, CO_2 yield from the burning of the 40% KNO_3 composition is lower. Furthermore, Table 3.12 reveals emissions of CO and THC. In the prescribed experimental conditions, the combustion reaction of the 40% KNO_3 ternary mixture depicts a fuel rich configuration, further from the stoichiometry. According to Table 3.8, there is more fuel available in the 40% KNO_3 mixture than in the 50% KNO_3 mixture. Moreover, assuming the oxidizer decomposition, the flow of air is supposed to supply enough O_2 to the material to reach stoichiometric conditions. Nevertheless, emissions of CO and THC indicate that a fraction of the flammable gases released are not fully oxidized. The mass percentage of residue is about 1% higher for the powder composition containing the larger quantity of fuel. A deeper analysis of the species embedded in the residues reveals that the main elements are potassium (K), oxygen (O).and carbon (C). The amount of total C and K remaining in the residue are higher for the composition with the richer fuel content (cf. Table 3.11). The percentage of elements recovery compared to the initial mass in the material is introduced in Table 3.13.

Table 3.12. Species yields from the combustion of 40% and 50% KNO3 ternary mixture at an air velocity flow of 0.1 $m.s^{-1}$ (200 $l.min^{-1}$).

Species Yield (Standard Deviation)	40% KNO_3 composition	50% KNO_3 composition
$y_{CO_2}\left[\frac{g}{g}\right]$	0.608 (0.029)	0.715(0.012)
$y_{CO}\left[\frac{g}{g}\right]$	0.110 (0.002)	0.034(0.010)
$y_{THC}\left[\frac{g}{g}\right]$	0.024 (0.001)	0.004(0.001)
$y_{O_2}\left[\frac{g}{g}\right]$	0.316 (0.025)	0.383(0.005)

Table 3.13. C and K percentage recovery, in the gaseous products and residue, from the initial mass of the element in the material; $\%C_{unidentified}$ represents the percentage of C from the initial mass which did not evolved in the gaseous products or the residue.

Sample	% $C_{products}$	% $C_{Residue}$	% $C_{unidentified}$	% $K_{Residue}$
40 % KNO_3	63.02	14.29	22.69	89.33
50 % KNO_3	72.97	15.41	11.62	66.99

Regarding the K element, almost 90% of the potassium originated from the 40% KNO_3 composition remains in the residue. However, the 50% KNO_3 ternary mixture only exhibits a 67% recovery. A third of the potassium initially carried by the material has been driven out of the solid phase. K based compounds have high vaporization temperatures$\left(T_{vap} > 1000\ K\right)$. Such temperatures can be reached in the flame but potassium is a relatively heavy element $(M_K = 39\ g.mol^{-1})$. Such hypothesis would require having an insight on how K raised up to the flame. Another assumption to explain the low amount of K in the residue is based on the observation of the experiments. During initiation of the decomposition reaction of the 50% KNO_3 ternary mixture, due to local pressure rise, incandescent particles were expulsed from the reacting region to the virgin material creating local hot spots. Similar phenomenon was mentioned by Blackwood and Bowden [12] during the initiation of black powder thermal decomposition. According to the authors, incandescent particles in a molten state are expelled. Their temperature is estimated to be around 500°C. Once a particle lands on the virgin material, it spreads the reaction in adjacent zone creating other sprays of

incandescent particles. The behaviour observed during initiation with the ternary mixture conjures up analogies. One can assume that KNO_3 is encompassed in some of the incandescent particles and sprays away from the sample holder. To argue this hypothesis, it needs to be noticed that melted particles were identified on the quartz tube used to delimit the combustion region. Finally, depending on the strength of the reaction, an incomplete recovery of potassium in the residue occurs due to spray of particles, probably KNO_3, K_2O and K_2CO_3 (product of the decomposition reaction of KNO_3 with residual char [40] or CO_2 [41]) outside the sample holder. As the reaction is more violent, the rate of particles spray increases and more potassium get expelled.

In regard to the C element, following Table 3.11, the mass percentage in the residue is higher for the 40% KNO_3 ternary mixture. It suggests that, taking as reference the initial amount of C in the material, the latter is more depleted of this element for the burning of the 50% KNO_3 composition. This assumption is verified on Table 3.13 which gives an estimation of C recovery, in the gaseous products, 10% higher for the 50% KNO_3 than for the 40% KNO_3 ternary mixture. It also indicates that most of the C evolves in the gaseous products. The percentage of C in the residue only varies from about 1% between the two different compositions. Finally, the main discrepancy appears for the "unidentified" C, defined as follow,

$$\%C_{unidentified} = 100 - \%C_{products} - \%C_{residue} \quad (17)$$

$\%C_{unidentified}$ reports the amount of C neither in the gaseous products nor the residue. This value increases as the concentration of oxidizer is decreased from 50% to 40%. For C and K alike, one can assume a fraction of C contained in the material is expelled during the reaction initiation. Nevertheless, $\%C_{unidentified}$ and reaction rate should present the same tendency when the latter is increased. It is possible that this behaviour happened however, if C is present in the sprays, it will get oxidized given the temperature and be identified in the gaseous products. A more robust hypothesis to draw the course of $\%C_{unidentified}$ is to relate this quantity to the generation of soot. No accurate measurement of soot concentration has been performed; nevertheless, video observations of the experiments as well as the state of the quartz tube at the end of the tests provide an insight. More soot is generated as the concentration of oxidizer in the material is lowered. Similarly, the layer of soot covering the quartz tube after burning is thicker for the 40% KNO_3 ternary mixture than with the 50% KNO_3

one. The soot generation is enhanced when the material embeds a lower concentration of oxidizer.

From the analysis of the mass loss rates, the species yields and the composition of the residue resulting from the burning experiments, it arises that the composition with the lowest oxidizer concentration exhibits a slower reaction rate and generates incomplete combustion gaseous products while experimental conditions should allow to reach a stoichiometric behaviour.

In order to draw hypotheses about the distinctions observed on the burning behaviour of the 40% and 50% KNO_3 ternary mixtures, an overall view of the reacting processes taking place is attempted. As the powder decomposes, combustible vapour gases and O_2 are released. As they mix, exothermic reactions and flammable conditions can be established. Decomposition of the components corresponds to endothermic operations while oxidation of the fuel vapours is an exothermic mechanism. Enough energy has to be released by the exothermic reactions to sustain the decomposition of the powder. The propagation of the degradation front relies on the balance between the heat generated by the oxidation reactions and the energy transferred by conduction and radiation to the virgin material ahead of the reaction zone. The limiting parameters are the temperature and the O_2 availability in the medium. The variations among the two powder compositions have been studied in the previous section. For the same mass of material, the amount of O_2 available does not differ significantly between the compositions unlike the amount of fuel available. The 40% KNO_3 ternary mixture presents a fuel-rich configuration while the 50% KNO_3 composition is closer to stoichiometric conditions mainly due to a reduced amount of fuel in the material.

Reactions are initiated by hot spots. Local temperature exceeds 500°C allowing the powder to decompose. Heat transfer provides the path to propagate the reaction. The level of energy evolved controls the rate of spread and can be related to the O_2 – fuel vapours ratio of the mixture. The mass loss curves presented on Figure 3.23 clearly shows a higher reaction rate for the composition with a higher concentration of oxidizer. The O_2 available – fuel vapours ratio is closer to stoichiometric conditions and it supposes a higher rate of heat release. Increasing the amount of fuel or decreasing the quantity of oxidizer impoverished the energetic balance of the reaction. When less energy is released, the heat transfer is lowered as well as the temperature in the reaction zone and causes a longer time to reach decomposition temperature, slowing down the reaction rate. The oxidation of the fuel vapours gets more

intense as more O_2 is generated by the oxidizer decomposition. Formation of char ensues from the propagation of the degradation front altering the structure of the material.

Torero [25], Ohlemiller [28] and Rogers [29] have emphasized that the permeability of a porous material such as polyurethane foam depends on the strength of the reaction and of the char structure. Pictures (Figure 3.22.a and Figure 3.22.b) and videos of the experiments underline different char behaviour depending on the mixture composition. Based on the results obtained and the analyses produced by the previous authors, hypotheses are developed in order to interpret the discrepancies observed. Given the complexity of the reactional mechanisms, a complete understanding of the decomposition of the tested powder was not considered as a critical objective of the present work. Nevertheless, the following reasoning is based on insights and interpretations from studies presenting similarities with the actual study. Deeper investigations would have to be performed in the future in order to verify the formulated postulates.

Temperature remains relatively constant inside the char when burning samples of 40% KNO_3 ternary mixture. The flux of air penetrating the medium is very limited and reveals a low char permeability. The assumption of low char permeability for the 40% KNO_3 composition is consistent for explaining the observed swelling phenomenon. Most of the O_2 generated from the oxidizer decomposition is consumed by the oxidation of the fuel volatiles. Char oxidation is limited; the chemical structure is not altered. Flow of air from the outside to the inside of the char region is restricted by its low permeability. Nevertheless, the degradation front keeps spreading, releasing gaseous products. Buoyancy induces gas flows that are contained in the material interior because of low permeability. Inside pressure increases and gases induce forces on the char structure resulting in its swelling. Finally, Gases exit at the interface between the material and the sample holder where openings emerge.

For the 50% KNO_3 ternary mixture, the inside material temperature curve, illustrated on Figure 3.18, indicates a marked decrease compared to the 40% KNO_3 composition once the flaming ceased. Oxidation reaction is more intense and leaves a rather porous material allowing air to flow in. The char microstructure has been altered and presents numerous voids. The material is cooled by air flowing through the structure and suggests that the permeability of char is significantly higher when the reaction is more vigorous. Intensive work carried on smouldering combustion of polyurethane foam stressed similar behaviour [24] [25] [29]. Studies have

shown that the permeability of the char region left behind the reaction front, increases according to the intensity of the reaction. Nevertheless, the raise is not linear as it has been shown by Torero (cf. Figure 3.24). He conducted experiments of forward and downward smoulder of polyurethane foam. Air was used as oxidizer and was forced in the direction and in the opposite direction of the reaction propagation. He noticed that at small air flow rates through the sample, the structure of the char is not altered while as the smouldering reaction becomes stronger, filaments that form the microstructure of the foam tear down ensuing in a permeability increase. The assumption developed to explain the divergence in the burning behaviour of 40% and 50% KNO_3 ternary mixtures is based on the analysis of Torero et al. Variations observed during initiation and combustion reaction emanates from the change in permeability of the char. The char permeability depends on the intensity of the reaction and the degree of char oxidation. From the energetic powder perspective, the restrictive parameter for permeability is the concentration of oxidizer. The diffusion of O_2 evolved from the oxidizer decomposition drives char oxidation and controls the modification of the structure which results in modification of the permeability.

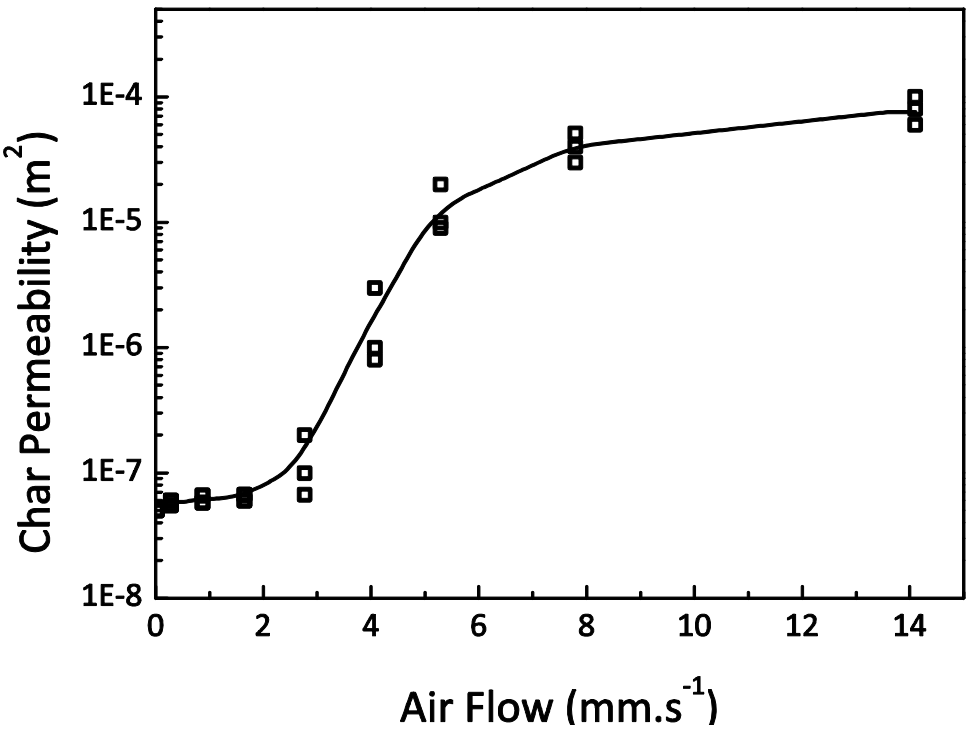

Figure 3.24. Variation of the average char permeability depending on the air flow velocity during downward forward smouldering of polyurethane foam [30].

3.4.2.2.2. Transition to flaming

Transition to flaming is also affected by the char permeability. Different flame structures and heights have been described from the combustion of 40% and 50% KNO_3 ternary mixtures. Decomposition and oxidation reactions provide gaseous products and heat required to trigger combustion reaction. Although combustible gases, oxidizer and heat were present, for the mixture to ignite, flammable conditions have to be attained. The fluid flow through the porous media plays a critical role. Volatiles and O_2 evolved from the powder decomposition rises driven by a buoyant flow. Oxidation of the volatiles and oxidation of the char occur as the gases travel through the material structure. Finally, the mixture exiting the sample structure is composed of gaseous vapours and O_2 originated from the virgin material decomposition as well as oxidation products. Two flaming modes are engaged during the combustion reaction. The fuel/oxidizer mixture allows the emergence of premixed flaming. From the products released out of the structure, incomplete combustion gases such as CO can undergo further oxidation when diffusing into atmospheric air. As the flammable mixture diffuses into air, if it reaches flammability conditions and a high enough temperature, spontaneous ignition can proceed and a regime of sustained diffusion flame gets activated.

Like the initiation of the reaction, the transition to flaming reveals an influence of the material composition. The analysis of the video footage for the carried experiments brings insights of the evolution of the gas phase resulting from the burning of 40% and 50% KNO_3 ternary mixtures. Figure 3.25 shows small premixed flames observed on the side of the sample few seconds prior to establishment of bright diffusion flames. They remain close to the sample surface. Flaming combustion initiates in a region where flammable conditions are encountered. The phenomenon is balanced by heat transfer and diffusion of species [31].

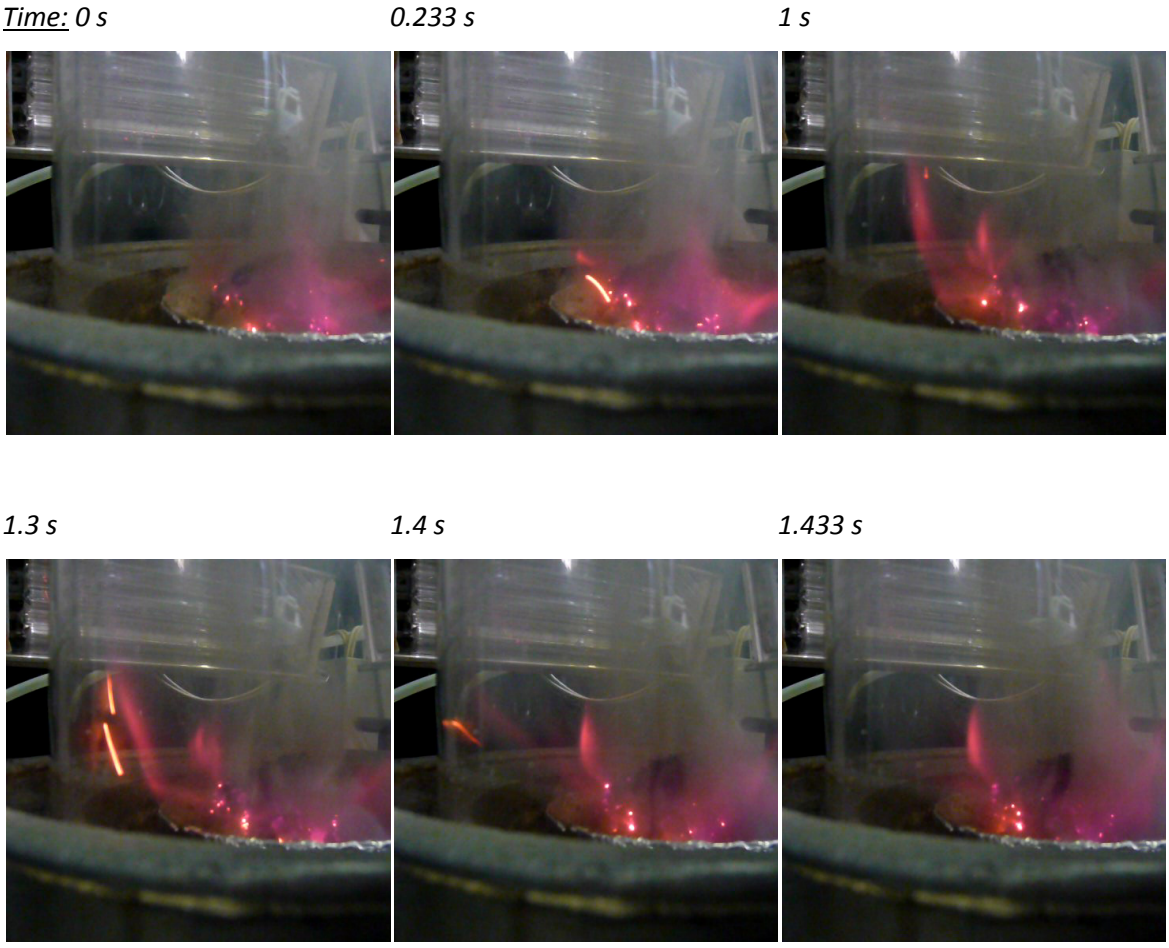

Figure 3.25. 40% KNO_3 ternary mixture premixed flame prior establishment of sustained diffusion flame.

Hot combustible gases compressed in the low permeability char structure are expelled at the interface of the char and virgin material. Gases exiting the char with a velocity u_0 also diffuse into the air, bringing a second mixing process between fuel and oxidizer. The mixing of flammable gases with air can potentially lead to the rise of a diffusion flame regime. If ignition is initiated, at the location of the flame, the fuel and oxidant mixture are assumed to react at the stoichiometry. One of the conditions for ignition and sustained flaming is the necessity of having local zones close to a stoichiometric mixture. The ignition concept is based on the thermal theory developed by Semenov. Sustained combustion is initiated when the rate of energy release overwhelms the rate of thermal energy dissipation. A critical state is met when the two quantities become equal. Considering a control volume of flammable mixture where temperature and density would be uniform, the heat accumulated inside can be described using the following equation,

$$\rho\, V C_v \left(\frac{dT}{dt}\right) = \dot{q}_r - \dot{q}_{loss} \tag{18}$$

With $\dot{q}_r$ the heat generated by the chemical reaction and can be represented by the simplified form,

$$\dot{q}_r = \Delta H\, V \dot{\omega}_A''' = \Delta H\, V\, Z'(\rho^n Y_A^n) e^{-\frac{E}{RT}} \tag{19}$$

And $\dot{q}_{loss}$ represents the heat losses at the interface of the control volume and can be expressed as follow,

$$\dot{q}_{loss} = hS(T - T_0) \tag{20}$$

Where T_0 is the initial temperature of the gaseous mixture in the control volume. The temperature of the system rises from T_0 to a temperature of ignition, T_i. Semenov stated that critical conditions for spontaneous ignition exist at T_i when $\dot{q}_r = \dot{q}_{loss}$ and $\left.\frac{d\dot{q}_r}{dT}\right|_{T_i} = \left.\frac{d\dot{q}_{loss}}{dT}\right|_{T_i}$. Semenov solved equation (18) and obtained an approximation for T_i [32],

$$T_i \sim T_0 + \frac{RT_o^2}{E} \tag{21}$$

For many cases, specially hydrocarbons, T_i is close to T_0. The difference has an order of few tens of degrees Kelvin. Estimation of T_i allows to calculate the rate of chemical reaction at critical ignition,

$$\dot{\omega}_A'''(T_i) \sim \dot{\omega}_A'''(T_0)e \tag{22}$$

If the reaction operates at a constant corresponding to T_0, a chemical characteristic can be defined by,

$$\tau_{ch} = \frac{\rho}{\rho^n Y_A^n Z' \, e^{-\frac{E}{RT}}} \tag{23}$$

The cooling rate of the gases when reaction has stopped is given,

$$\rho V \, C_v \left(\frac{dT}{dt}\right) = -hS(T - T_0) \tag{24}$$

A heat loss characteristic time, τ_{loss}, is defined by Glassman [33] as,

$$\tau_{loss} = \frac{\rho V \, C_v}{hS} \tag{25}$$

A Damköhler number can be defined based on the ratio of the two previous characteristic times,

$$D_a = \frac{\tau_{loss}}{\tau_{ch}} = \frac{C_v}{eQ} \frac{RT_0{}^2}{E} \tag{26}$$

D_a constitutes an indicating parameter for ignition. If the heat loss characteristic time is very small compared to the chemical reaction time then, $D_a \ll \frac{C_v}{eQ} \frac{RT_0{}^2}{E}$, and the process will not take place.

A similar criterion can be developed for flame propagation based on the ratio of the characteristic chemical reaction time to a characteristic gases diffusion time (or flow time) [34],

$$D_a = \frac{\tau_{diff}}{\tau_{ch}} \tag{27}$$

A characteristic diffusion time, τ_{diff}, can be interpreted as the time need for the flammable mixture to flow through the reaction zone [35]. It can be defined as,

$$\tau_{diff} = \frac{l}{u_0} \tag{28}$$

Where u_0 is the flow velocity of the gases exiting the sample and l is the characteristic length of the reaction zone. Based on equations (21) and (22), τ_{ch} can be rewritten for T_0,

$$\tau_{ch} = \frac{\rho Q l}{h} \frac{E}{R T_0^2} e \tag{29}$$

Assuming $l \sim \frac{V}{S}$.

Finally, the criterion parameter is given by,

$$D_a = \frac{h R T_0^2}{\rho Q E e \, u_0} \tag{30}$$

When $D_a \gg 1$, the reaction rates are faster than the diffusion of the gas flow. If the mixing time for the combustible gases expelled from the sample with the ambient air is too long, then extinction occurs and no sustained flaming subsists. The two driving parameters are the temperature, T_0, and the velocity of the gas flow, u_0. Given equation (30), one can assume that, below a critical flow velocity, D_a becomes too large for flaming to be sustained.

An estimation of the buoyant flow of gases expelled from the material residue would be necessary to define the conditions of a sustained flaming. One assumes that premixed flames first initiate prior diffusion ones. Flame propagation is considered stationary when the velocity of the supply gases is equal to the flame speed. In the present work, the supply velocity can be regarded as the gaseous products of the smouldering combustion taking place in the condensed phase. By evaluating the flame speed, u_0, one could assess the velocity of the buoyant flow of combustible gases released through the residual char. From Zeldovich, Frank-Kamenetskii and Semenov theories, one can determine an approximation of u_0 [31] [32] [33],

$$u_0 = \left(\frac{2 \, k \, \Delta H}{\rho^2 {C_p}^2 (T_i - T_0)} \int_{T_i}^{T_f} \dot{\omega}_f''' \, dT \right)^{\frac{1}{2}} \tag{31}$$

Where, T_f is the flame temperature (K), T_i the ignition temperature (K), ρ the density of the gaseous smouldering products (kg.m^{-3}), C_p the specific heat (J.kg^{-1}.K^{-1}), k the thermal conductivity (W.m^{-1}.K^{-1}), ΔH the heat of reaction (J) and $\dot{\omega}_f'''$ the reaction rate (s^{-1}.m^{-3}). The reaction rate, $\dot{\omega}_f'''$, depends on the temperature and can be expressed as,

$$\dot{\omega}_f''' = Z'(\rho^n Y_A^n)e^{-\frac{E}{RT}} \quad (32)$$

The complete calculation is presented in Appendix D.

The gases velocity is function of the reaction rate and also of the temperature at which they flow through the char structure. Increase of the reaction rate induces rise of flame speed. An estimation of u_0 allows having an approximation of the magnitude of the flow velocity of the gaseous products rising from the burning sample. u_0 has not been estimated in the present work, the estimation of the reaction rate being to intricate. Nevertheless, the calculation of u_0 represent one of the perspective works that will need to be carry. The knowledge of an order of magnitude for u_0 will allow the comparison with the velocities of the gaseous flows induced by buoyancy usually observed for conventional fires.

3.4.2.2.3. Flaming behaviour for 40% and 50% KNO3 mixtures

Flaming has been achieved for both ternary mixtures. The transition is described on Figure 3.26 and Figure 3.27, respectively, for the 40% and the 50% KNO_3 compositions. It has been noted previously that the diffusion flame initiated while burning the 40% KNO_3 ternary mixture was preceded by a premixed flame regime (cf. Figure 3.25). According to Figure 3.26, an amount of flammable gas is released from the sample and ignites (flamelet at 0 s). Gas temperature and flow velocity attained critical values to initiate the process. The reaction propagates around the sample where released gases have diffused in air forming a flammable mixture. Sustained diffusion flame is activated about in 0.266 second after the initial flamelet.

It has previously been noticed that the 50% KNO3 ternary mixture ignites only few seconds after initiation of the reaction. The behaviour is different to the 40% KNO_3 composition. The degradation of the powder is more vigorous. The ratio fuel vapours\O_2 released is closer to the stoichiometry. Oxidation of the gaseous products and of the char is more complete, generating a higher level of energy. As the char is oxidized, the material structure is altered allowing the produced gases to create a buoyant flow. They rise through the char structure and are released above the sample surface where diffusion with air can occur. A part of O_2 from the oxidizer decomposition is still available to react. It is mixed with the fuel vapours and products generated during the smouldering combustion of the material. It forms a premixed mixture. Small premixed flames appear above the sample as it is shown on Figure 3.27. Diffusion

flamelets arise simultaneously but are not sustained. A transition of about 4 seconds is observed during which premixed flaming develops along with intermittent diffusion flames. Finally, a sustained diffusion flame regime takes place about 6 seconds after the start of the reaction.

The oxidation occurring during the decomposition of the material is stronger with the 50% KNO_3 ternary mixture. Temperatures inside the material are higher than for the 40% KNO_3 composition. The reaction rates are higher which, according to equation (31), will induce a higher velocity of the gas flow exiting the sample. Diffusion of the gases in the ambient air is increased. The mixing is enhanced which induces higher flame lengths and in the case of the present study a more complete reaction.

3.4.2.3. Discussion

The composition of the material has a critical impact on its combustion behaviour. The concentration of the oxidizer influences the decomposition as well as the transition to a flaming regime. The decomposition of the virgin material requires energy that needs to be supplied by exothermic oxidation reactions. Their strength drives the reaction rate. Furthermore, the concentration of oxidizer also plays a role on the evolution of the char structure. The permeability of the char is enlarged as the smouldering reaction gets more vigorous. It allows, above a certain oxidizer concentration, the produced gases to be released through the surface and not only at the interface between the virgin material and the char. With the 50% KNO_3 ternary mixture, gaseous products are released over a larger area and at a higher flow, increasing the diffusion in the air. As a consequence, when ignition occurs, larger diffusion flames are observed with the highest oxidizer concentration. On the other hand, parallel to the initiation of a diffusion regime, premixed flame were observed at the surface of the sample where gaseous products emerged. This informs that a fraction of the O_2 generated by the oxidizer decomposition is still available and has not reacted during the degradation of the material. It mixes with the combustible gases resulting from the smouldering combustion and creates a premixed mixture. In order to verify the last assumption, tests have been carried out under an inert atmosphere of nitrogen (N_2). This allows studying the weight of the oxidizer in the combustion reaction.

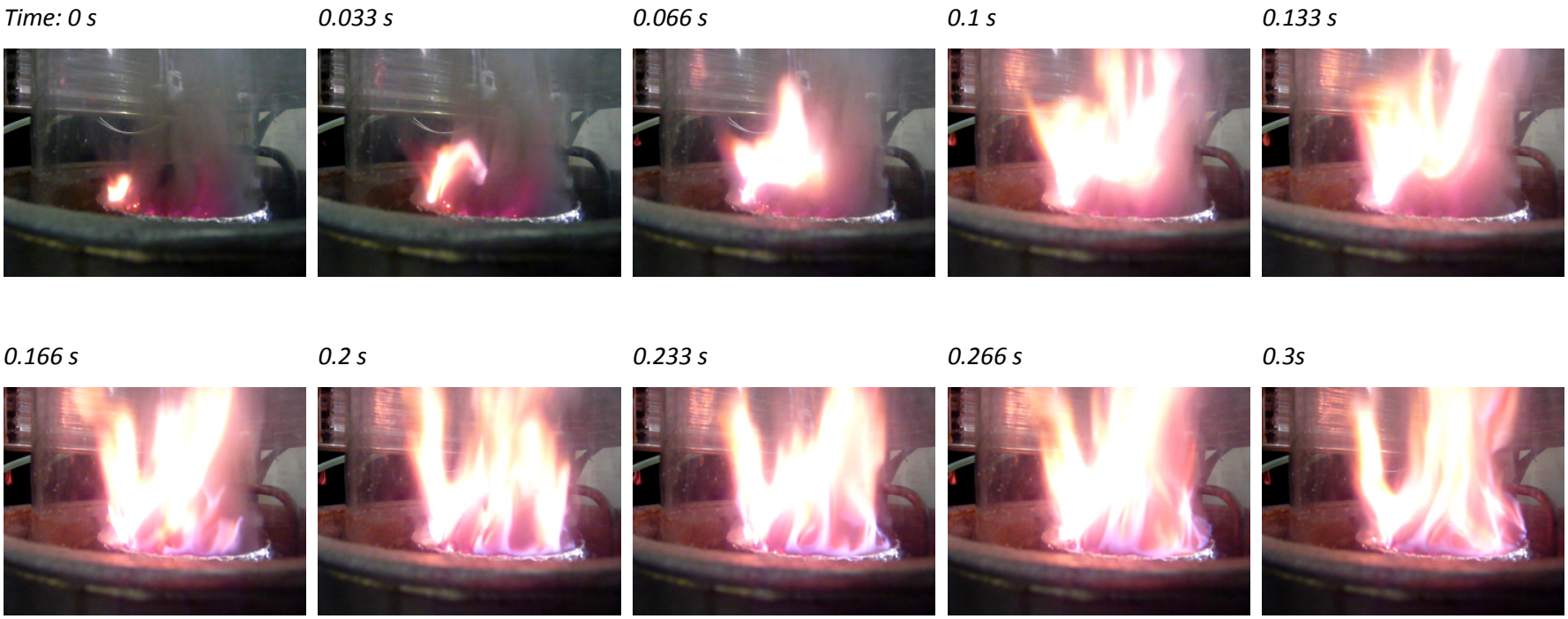

Figure 3.26. Transition to flaming: 40% KNO_3 ternary mixture at a 200 $l.min^{-1}$ flow of air.

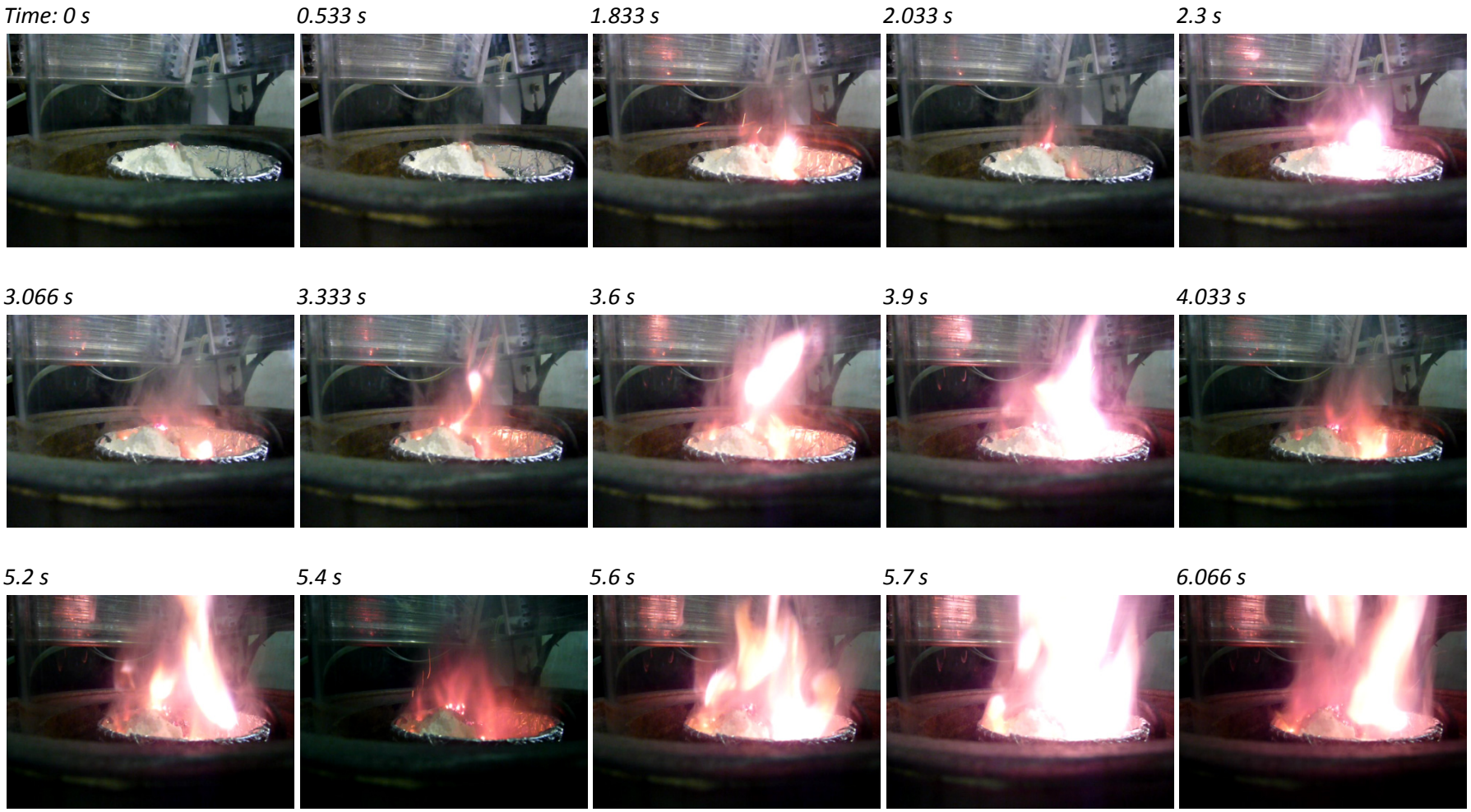

Figure 3.27. Transition to flaming: 50% KNO_3 ternary mixture at a 200 $l.min^{-1}$ flow of air.

3.5. Contribution of the Reacting Atmosphere to the Combustion

After having investigated the influence of the oxidizer concentration on the combustion behaviour of the ternary powder, concern is brought to a second factor susceptible to affect it. One can assume that such materials are most of their lifetime stored in a warehouse. Consequently, enclosure fire appears as a severe potential risk. The main characteristic of enclosure fires is the confinement effect [36]. Combustion gases and soot rise by buoyancy creating a smoke layer principally constituted by reaction products and residuals of air. As the fire develops, the buoyant smoke accumulates and the layer lower boundary descends. Smoke continues to be injected through the plume. If no sizable openings or vents are present, the smoke layer height progresses further down, up to the fire source or the floor of the facility. In conventional fires, the smoke layer may act as a suppressant given the O_2 depletion within. However, for fires involving energetic materials, the scenario can be different. There is a strong probability that the presence of the oxidizer in the composition allows the material to burn without support of O_2 from air. Consequently, even a vitiated fire can still develop. Another underlying problem holds in the formation of toxic compounds. Energetic material can undergo thermal degradation at low temperatures. It has been stressed that within such temperature ranges toxic emissions were susceptible to be engendered [37]. In order to characterise this behaviour, experiments have been carried out under N_2 atmosphere. This allows investigating if the combustion can initiate and reach a sustainable level. Also, the gaseous emissions will be analysed and compared to the ones measured during the tests conducted under air atmosphere. Variations highlight different kinetics taking place and the potential favouritism in toxic emissions according to the composition of the reacting atmosphere. Furthermore, to investigate the existence of a transition in the powder behaviour, experiments have realised under various concentration of O_2 in the reacting medium.

3.5.1. Modification of the experimental setup

The experimental setup has been modified in order to carry out experiments under an inert atmosphere. A nitrogen (N_2) flow of 0.1 $m.s^{-1}$ (200 $l.min^{-1}$) is supplied within the quartz tube.

The combustion zone has been insulated from ambient air and the N_2 flow is large enough to avoid recirculation from ambient air. Furthermore, an obstructer has been positioned at the top of the quartz tube to create a pressure increase [38]. The time required to feel the quartz tube with N_2 has been estimated to be approximately 10 seconds but in order to be sure an inert atmosphere was well established, one minute was always left so that the O_2 analyzer of the supply line gave a concentration of less than 0.5%. The usual ethylene/air pilot flame is inadequate for the present setup being blown off in the inert atmosphere. Instead, a glow-plug is used It was supplied by a 12V generator and requires about 30 seconds to reach a temperature of 500°C.

3.5.2. Experimental observations

3.5.2.1. Combustion of 40% KNO_3 ternary mixture

	Time	
Setup and Sample	*0s*	
		Experiments were carried out with 50g samples of 40% and 50% KNO_3 ternary mixture. Material was randomly disposed on a glass sample holder. The glow-plug was located above the sample and set in a way to generate a single point contact for heat transfer with the material.
1. Initiation of the Reaction	*28s*	
		First smoke emissions are observed Smoke colour tends to white. At this time, main gas released is assumed to be water vapour.

2. Swelling and glowing

31s

Smoke becomes denser. Glowing spots are initiated at the surface of the material. It indicates that O_2 is released from the oxidizer decomposition. Degradation of the material is engendered. The reacted material evolves as char. Swelling phenomenon of the carbonaceous residue takes place simultaneously.

39s

The reaction propagates. Glowing and swelling become more intense. Intermittent premixed flamelets emerge from the material surface but no sustained flaming regime develops.

48s

As the decomposition reaction becomes stronger, glowing particles are expelled from the reaction front, impacting the virgin material and creating local hot spots susceptible to initiate the decomposition reaction.

55s

As the decomposition front spreads, the reaction rate is enhanced. Smoke emitted becomes darker, stressing the presence of carbon particles and other incomplete products generated by the smouldering. Short intermittent premixed flames still arise. Glowing is emphasized at the surface.

59s

Glowing increases with the decomposition rate. Radiation from the different spots is noticed. Swelling and dark smoke of incomplete products persist.

78s

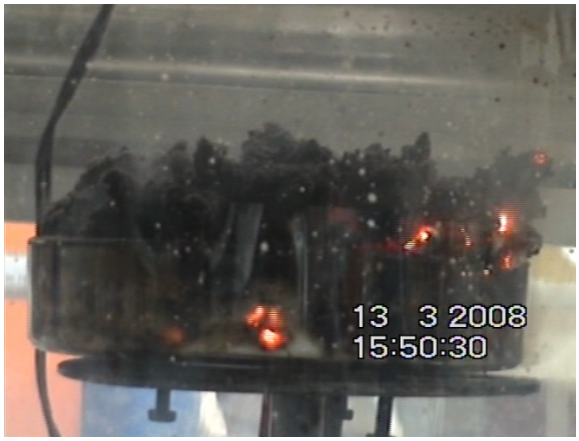

Reaction rates start to decline. Smoke emitted emanates less dense. The rate of glowing spots on the surface decreases.

3. End of reaction and residue 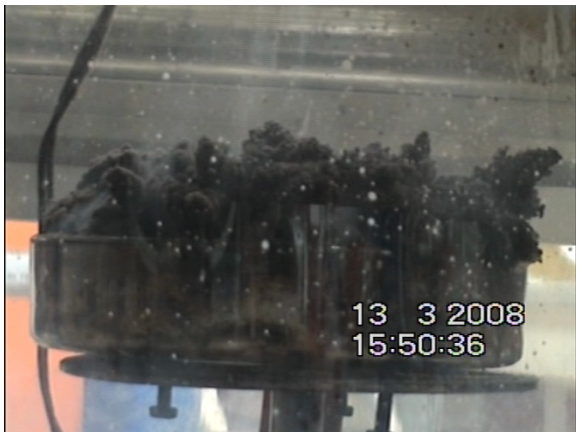	*84s*	The reaction ceases. The decomposition front reached the end of the sample. No virgin material remains left. Swelling stops and glowing extinguishes. Few seconds after, no more smoke is generated.

3.5.2.2. Observations Combustion of 50% KNO_3 ternary mixture

	Time	
Setup and Sample	*0s*	
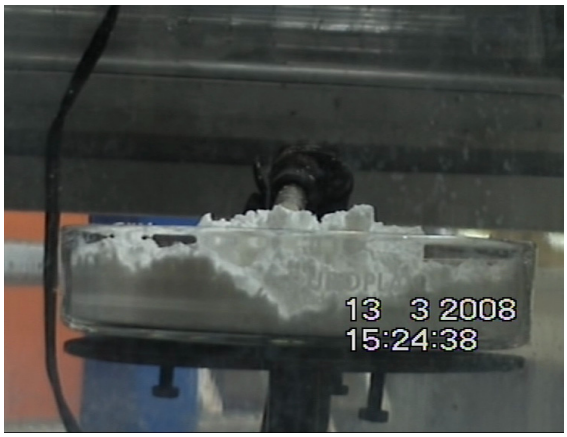		The experimental setup is identical to the one described previously.
1. Initiation of the Reaction	*~25s*	
		Light smoke is first released. Given the appearance of the smoke, it is assumed to be mainly water vapour. Then, this stage corresponds to the dehydration process of chemical bond water in lactose. A hot spot is created by the glow-plug. Particle glowing occurs contributing to the heat transfer through the virgin material.
2. Glowing and flamelets	*26s*	
		Surface oxidation releases energy allowing heat transfer through the material by conduction and radiation. Fuel vapours resulting from lactose and starch decomposition mix with O_2 generated by the KNO_3 decomposition. A premixed mixture is obtained. If the temperature of the gases is high enough, spontaneous ignition can occur. Intermittent premixed flamelets arise from the sample surface.

27s

Glowing particles are expelled from the reaction front, impacting virgin material and creating local hotspots. If the heat transferred to the material overwhelms the losses, another initiation of the reaction can spread from these locations. Several intermittent premixed flames emerge.

3. Transition to premixed flaming *29s*

Sustained premixed flames start to propagate above the sample surface. Flame length lies between 1 and 2 cm. No noticeable swelling of the char layer is encountered. The emission of smoke becomes darker and denser. The reaction rate is increasing and products from incomplete combustion commence being released.

31s

Flame length increases up to about 3 cm. The flaming regime is accompanied by surface glowing. Particles including soot are emitted. The reaction rate is enhanced as flames become higher, brighter and as more glowing spots appear on the sample surface.

33s

Reaction is more vigorous, flames rise higher (up to about 5 cm) and radiate brighter. Emission of soot is increased. Glowing particles merge to form incandescent aggregates. Furthermore, glowing is also initiated in depth of the material as it is revealed by the picture beside ( ). Radiation inside the structure might be an important contributor for augmenting the reaction rate.

38s

Orange premixed flames rise up to 6 cm. Pictures highlight a relatively homogeneous flame structure. Glowing spots are largely present along the sample surface

4. Decline and extinction

41s

After a 10s periods of relatively large sustained premixed flames, the reaction rate begins to reduce. Glowing is still observed at the sample surface. Soot is less generated and the smoke emission gets lower.

46s

Premixed flames become very short (<1cm) and localized. Glowing is still active at the surface of the material.

49s

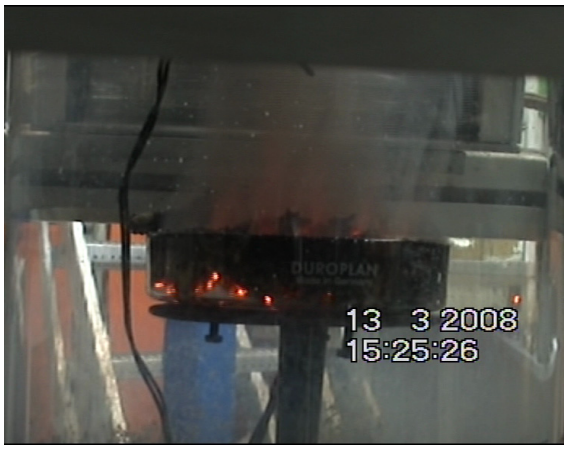

Flameout occurs. Light emission above the sample surface is due to glowing spots radiation.

62s

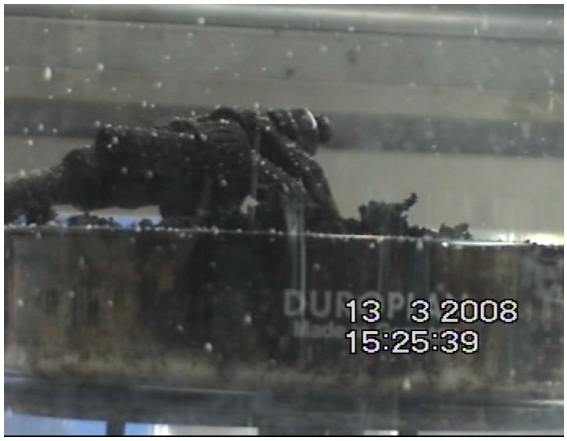

Reaction has ended. No more glowing is observed along the sample. Smoke emission has ceased. The residue on the tube is constituted by white particles expelled during the reaction. One can assume that the latter particles are potassium compounds which were expelled from the sample in a melting state and cooled down on the quartz tube face.

3.5.3. Initiation of the reaction

The reaction involving the 40% KNO_3 ternary mixture is instigated by a hot spot engendered at the surface of the materials by the glow-plug. The heat is transferred by conduction and radiation inside the material initiating the decomposition of the components. The first observed phenomenon is the emission of a light smoke, corresponding to the release of water molecules embedded as moisture in the powder. The decomposition front spread deeper inside the material. Locally, particles start glowing on the surface. Residue from the decomposition front reveals the formation of a char layer. Similarly to experiments carried under air, swelling of the char takes place during the reaction (cf. Figure 3.28). The volume of the sample was roughly estimated to have increased approximately 2.5 times during the reaction. Previously, a factor of 3 has been roughly evaluated from the expansion of the 40% KNO_3 ternary mixture under ambient air. The nearness of the results tends to suggest that the swelling phenomenon only depends on the reaction taking place in the solid phase and is independent of the composition of the reacting atmosphere. Observation of the char residue reveals a branching of particles clusters. This characteristic is more emphasized compared to the experiments carried under air atmosphere. Furthermore, smoke is emitted at the interface of the virgin material and the reaction front. No visible gaseous products appear to exit the sample through the surface of the char region. As the decomposition spreads, more material gets engaged in the reaction and the emission of smoke is enhanced. It becomes denser and darker, so gaseous products different from water vapour are generated. The colour suggests that they are soot and incomplete combustion products.

Like previously, a hot spot induced the initiation of the burning of the 50% KNO_3 ternary mixture. Light smoke is first released and is assumed to be water vapour. At the same time, glowing particles develop at the surface of the sample at the hot spot position. Projection of glowing spots enhances the propagation of the decomposition reaction. Virgin material is impacted by incandescent particles. Contact allows heat to be transferred in depth by conduction and radiation. Several hot spots arise. If the energy they generate allows the activation of the decomposition of the material, the reaction starts to propagate from several positions, which increases the reaction rate. Glowing spots become more intense and manifold. Intermittent premixed flames result from the gaseous products generated inside the

material and rising by buoyancy. Black particles, supposedly carbon, progress in the smoke. Incomplete combustion gases are expected to be released.

a.

b.

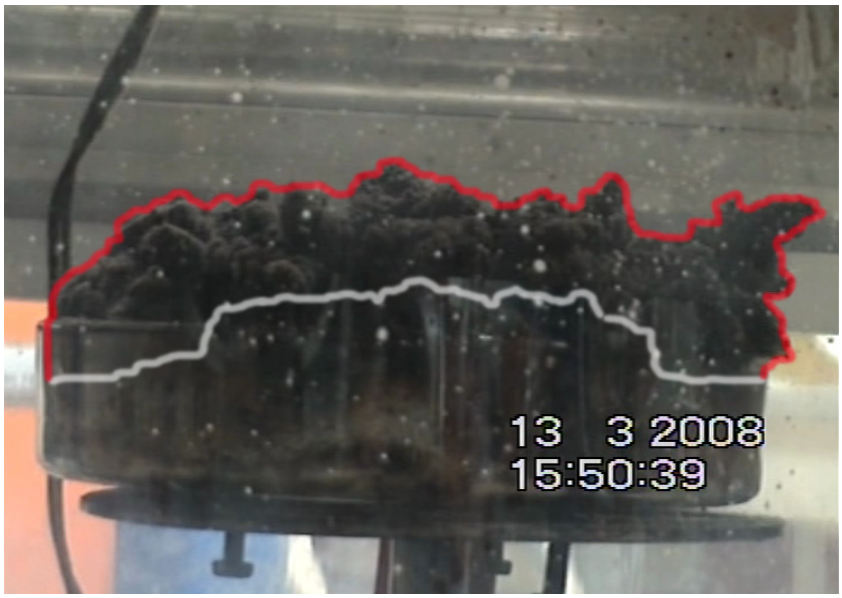

Figure 3.28. Swelling of the 40% KNO_3 ternary mixture during decomposition reaction; initial state (a.) and carbonaceous residue (b.), the white line representing the contour of surface of the initial sample, the red one the contour of the residue.

3.5.4. Transition to flaming

No sustained flame regime has been attained during the experiments carried with the 40% KNO_3 composition under N_2. Few short discontinuous premixed flames develop from the inside of the material. However, the major luminous emissions are the radiation from the glowing particles. The overall reaction from the initiation to the glowing extinction and the end of smoke emission lasted for about 1 minute.

Unlike the 40% KNO_3 ternary mixture, for the 50% KNO_3 composition, a sustained premixed flame regime becomes established about 30 seconds after the start of the experiment and about 4 seconds after the initiation of the decomposition reaction. It requires less than 2 seconds for the flame to spread all over the sample surface. The mixture of fuel vapours generated by the lactose and starch decompositions and O_2 produced under heating by the oxidizer. Increase of the flame length up to 6 centimetres occurs simultaneously with an increase of the rate of glowing spots visible at the surface of the sample. These two phenomena result from the rise of the reaction rate. However, from a simple observation, the increase of the reaction rate does not result from a higher level of energy supplied to the reaction front but rather by the spread of the reaction over the sample area. The reaction front is extended and more material participates in the reaction, inducing a higher concentration of gaseous products release. According to Figure 3.29, the premixed flame structure is relatively homogeneous. Bright orange radiation emanates from it. Glassman [33] explains the orange glow indicates gases at high temperature and is mainly initiated by the radiation of CO_2 and water vapour. The large emission of soot suggests that parts of the gases released are incomplete combustion products. Analysis of the video footage reveals that a light swelling of the char happens during flaming. Figure 3.29 highlights the phenomenon. The maximum expansion is of the order of 3 mm. It is significantly less marked than the swelling observed for the experiments carried out with the 40% KNO_3 composition. Similarly, at the end of the reaction, the carbonaceous residue exhibits finer particles clusters and no branching arises from the char structure.

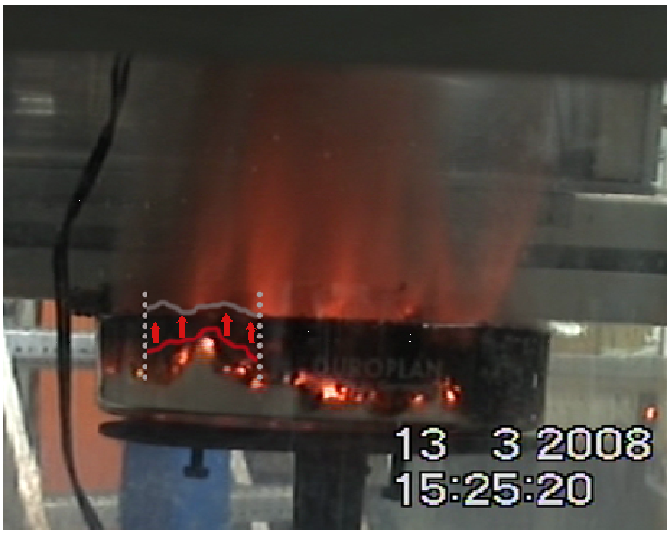

Figure 3.29. Flame structure and swelling phenomenon during the combustion of 50% KNO_3 ternary mixture under N_2 atmosphere; red line: initial sample surface, grey line: char surface.

3.5.5. Gaseous emissions

3.5.5.1. Results

Combustion experiments have been carried out on 40% and 50% KNO_3 ternary mixtures within a N_2 atmosphere. Species emissions have been measured after collection in the FPA exhaust duct. Major gases produced are CO_2, water vapour, CO and THC. Figure 3.30 and Figure 3.32 represent the species production rates during the reaction, respectively, for the 40% and the 50% KNO_3 ternary mixture.

For the 40% KNO_3 composition, the major product generated is CO_2. The production rate rises up to 0.32 $g.s^{-1}$. On a molar basis, the main fundamental element of lactose ($C_{12}H_{22}O_{11}$) and starch ($C_6H_{10}O_5$) is H. A consequent production of water vapour is expected. Figure 3.30 confirms the latter statement. According to the analyser measurements, water vapour generation increases up to 0.21 $g.s^{-1}$ and remains relatively constant for about 10 seconds. CO and THC rates reveal a production peak of, respectively, 0.13 and 0.04 $g.s^{-1}$. The ratio of CO_2 compared to CO generation, when production rates reach their maximum value, is about 2.5. The combustion reaction is incomplete. Another important information resulting from the analysers measurements is the beginnings of emission for each species. According to Figure 3.30, gaseous products start to be released at the same time. However, the data acquisition sampling rate needs to be considered. It is 0.5 Hz, which implies a 2 seconds lag between each

measurement. Water evaporation probably appears prior to other species as it is released, between 120 and 150°C according to the previous DSC analyses [cf. Chapter 2, Section 2.3.3.]. Nevertheless, recalling the temperature rise for the experiment carried out under air, the time, from 100°C to reach the decomposition temperature of the powder components was less than 2 seconds (cf. Figure 3.17 and Figure 3.18). One can assume the temperature increase between 100°C and 300°C for the experiments carried out under N_2 atmosphere to be relatively similar to the one under air. No flaming was occurring at this stage and the role of O_2 from the air is considered to be limited. The accuracy on the measurements of the gases emission is related to the data acquisition. In the end, Figure 3.30 indicates that the time delay between CO_2, CO, THC and H_2O production rates lies within 2 seconds. The first stage α corresponds to the initiation of the reaction. Heat is transferred by conduction and radiation to the material which starts to decompose. Reaction spread takes place along two directions, one vertical and one horizontal. Gases are formed at the decomposition front but also at the glowing spots and inside the few intermittent premixed flames. The transition between α and β emphasizes an increase in the species production rates. At this moment, most of the surface of the sample initiated decomposition, so the reaction front only propagates downward. One can assume that downward spread rate is enhanced as more energy becomes available. A peak is attained at the transition between β and χ. After most of the material has undergone decomposition, the reaction rate decreases as it is shown by the species production rates. One can notice that, while CO_2, H_2O and THC production rates achieved a maximum "supposedly" at the same moment (i.e. considering the 0.5 Hz sampling frequency), the CO maximum rate is measured 2 seconds later. A tentative explanation is to consider that most of the material has reacted. Less O_2 starts being generated by KNO_3. Recalling that the composition is fuel rich, the decline of O_2 concentration within the material favours the generation of incomplete combustion products such as CO [11]. Figure 3.31 illustrates the CO/CO_2 ratio. It rises up to 0.58, which clearly stresses the incomplete characteristic of the reaction. The period ε (α and β on Figure 3.30) coincides with the increase in gaseous emissions. One notices that the CO/CO_2 ratio rises over this interval. It illustrates the lack in O_2 in the mixture. The oxidation process leading to CO is favoured. ζ describes the beginning of the decay of the reaction. One observes that, despite the CO and CO_2 reaction rates drop, the CO/CO_2 ratio remains relatively constant over this period. Finally, one underlines a growth of the CO/CO_2 ratio at the transition between

ζ and η. This corresponds to the oxidation of char with a production of CO promoted due to the lack of O_2 in the reacting medium.

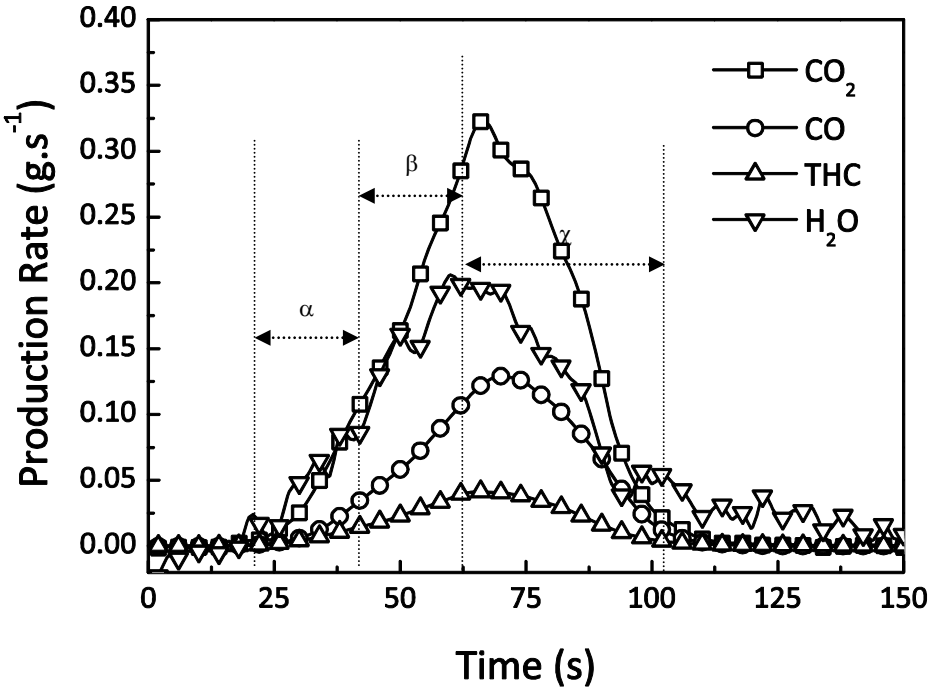

Figure 3.30. Production Rates of major species generated during the combustion of 40% KNO_3 ternary mixture under N_2 atmosphere (N_2 flow of 0.1 $m.s^{-1}$).

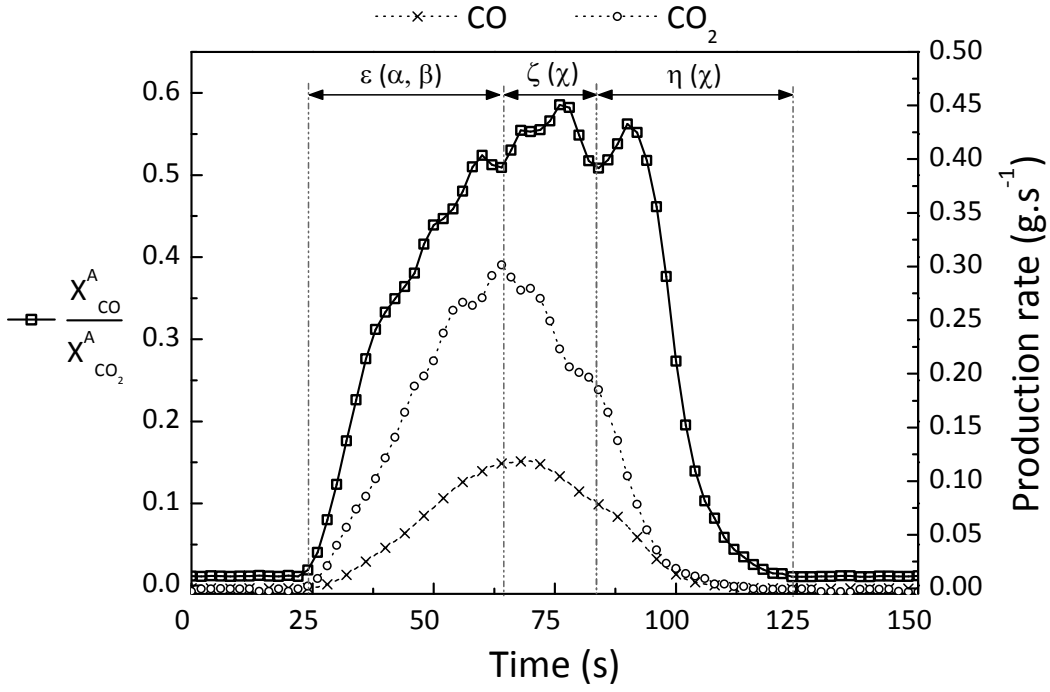

Figure 3.31. CO/CO_2 ratio from the combustion of 40% KNO3 ternary powder under N_2 (N_2 flow of 0.1 $m.s^{-1}$).

Production rates from the combustion of 50% KNO_3 ternary mixture samples under N_2 are shown on Figure 3.32. The major species generated is CO_2. The production rate augments up to 0.66 $g.s^{-1}$. Water vapour, CO and THC reach a maximum emission of, respectively, 0.33 $g.s^{-1}$, 0.32 $g.s^{-1}$ and 0.06 $g.s^{-1}$. According to Figure 3.33, the CO/CO_2 ratio rises up to about 0.96. The combustion reaction is incomplete. This was expected as the mixture is fuel-rich. The stage δ represents the initiation of the reaction. First water vapour is emitted which is in accordance with the light smoke release observed in the videos of the experiments. Glowing and intermittent premixed flames were also noticed during this period. This is enlightened by a slight increase of the CO_2 emission. However, an uncertainty on the starting time of water and CO_2 productions persists given the sampling frequency of 0.5 Hz. Reaction spread takes place along two directions, horizontally and downward. However, contrary to the evolution of the reaction when experiments under inert atmosphere were realised with 40% KNO_3 ternary mixture, the horizontal propagation is much faster. Most of the surface of the sample undergoes decomposition in a very short time which magnifies the rate of reaction. The transition to ε corresponds to the institution of the sustained premixed flame regime. Large increases of CO_2, CO and THC are measured. During δ and ε, the CO/CO_2 ratio increases, stressing the preference of the oxidation process leading to the formation of CO. Once the major fraction of the material has undergone char formation, the reaction rate begins to reduce and the species emissions decrease. This process is depicted by the transition between ε and ϕ. Firstly, the CO/CO_2 ratio continues to rise. This phenomenon stresses that the CO_2 emission reduces faster than the CO one. The oxidation mechanism leading to CO_2 is first affected by the completion of the reaction.

It is important to notice that, taking into account the uncertainty on the maximum location due to the low sampling frequency, the peak of CO emission is recorded during the ϕ stage. The assumed explanation is similar to the one drawn previously for the experiment carried out with the 40% KNO_3 composition under N_2. The rarefaction of O_2 in the material favours the formation of CO instead of CO_2. The release of water vapour is the first to end, about 6 seconds before the CO_2, CO and THC. One can assume that during this spell, only glowing and char oxidation occurs resulting in generation of CO and CO_2. The change in slope noticed on Figure 3.33 during the interval μ (representing the end of the interval ϕ on Figure 3.32) is representative of the oxidation of char still occurring in

the residue of the material. Correct understanding of the contribution to the combustion process of the oxidizer concentration within the composition and the role of the supporting atmosphere requires the knowledge of quantitative parameters such as species production rates. Because pertinent interpretations and conclusions depend on the confidence allotted to calculated variables, the measured data allowing their access have to be accurate.

One defines an experiment as the approach whose aim is to analyse one or several characteristics of a considered material, using given measuring instruments and procedures and following a given experimental setup. Disregarding the possibility of a bias in the experimental setup, the degree of repeatability of the experiments constitutes an indicator of the uncertainty associated with measured data. In the present study, each experiment has been repeated four times. Consequently, any variable (species production (or consumption) rates, total productions (or consumptions)) can be calculated four times. In order to minimize the error associated with the experiment, the average of the four values is considered as the final result. To assess the degree of confidence that can be assigned to it, error bars are evaluated as the standard deviation of the distribution formed by the four values.

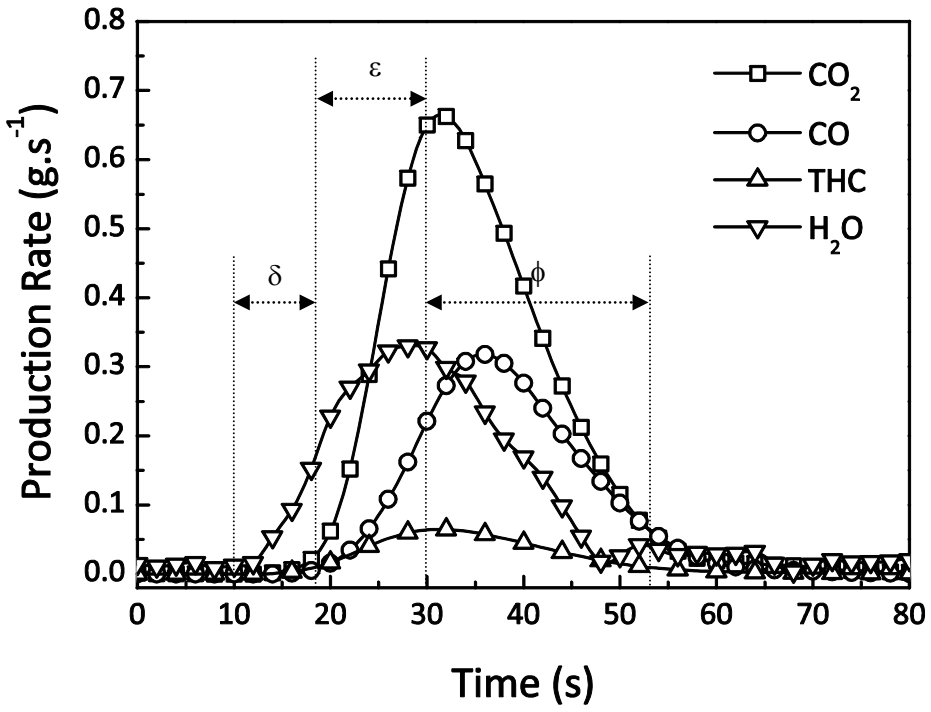

Figure 3.32. Production rates of major species generated during the combustion of 50% KNO_3 ternary mixture under N_2 atmosphere (N_2 flow of 0.1 $m.s^{-1}$).

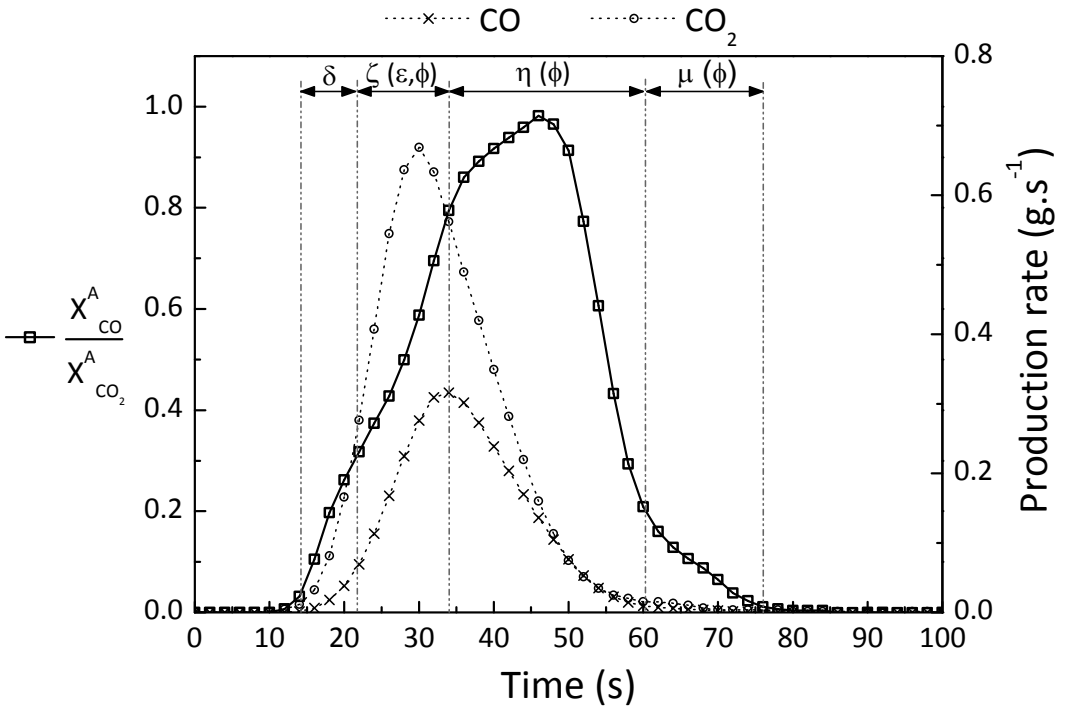

Figure 3.33. CO/CO_2 ratio from the combustion of 50% KNO3 ternary powder under N_2 (N_2 flow of 0.1 $m.s^{-1}$).

Figure 3.34 to Figure 3.37 represent the production rates of CO_2, CO, THC and water vapour for the 40% and 50% KNO_3 ternary mixtures under inert atmosphere (N_2). The plotted production rates consist in averages as exposed in the previous paragraph. of the results obtained for each experiment Error bars are added in order to underline the repeatability of the tests carried out. The differences between the species emission rates for the two powders highlight the influence of the oxidizer to promote the combustion.

Figure 3.34 represents the CO_2 production rates measured under N_2 atmosphere for both tested ternary mixtures. The error bars estimated for the 40% KNO_3 composition are larger than for the 50% KNO_3 one. In a general way, repeatability of the experiments carried out with the larger concentration of oxidizer exhibits better results with smaller standard deviations. An assumption to explain this outcome can be related to the rate of reaction. Given that the ratio fuel/O_2 in the material is closer to stoichiometric conditions for the 50% KNO_3 mixture, oxidation of the decomposition gases and oxidation of the char are more vigorous which increases the heat released to the virgin material and promote the propagation of the reaction and thus the rate of reaction. The spread over the surface

occurs significantly faster. Within few seconds, the only direction for the decomposition reaction to propagate becomes downward. As the sample preparation, the mass of powder and the experimental conditions do not differ from one test to another, the downward spread is expected to be repeatable once the entire surface undergoes decomposition homogeneously. Moreover, the flame acts as a filter for the species emissions favouring CO_2 and CO generations in proportions determined by the amount of O_2 available. Finally, discrepancies between experiments mostly derived from the propagation path of the decomposition reaction. Several variables are susceptible to alter the reacting process: the configuration of the material (i.e. the arrangement on the sample holder), the projection of glowing particles or the presence of a flaming regime. The progress of the decomposition front for experiments carried out with 40% KNO_3 ternary mixture is more influenced by the arrangement of the material and the position of glowing particles ejected.

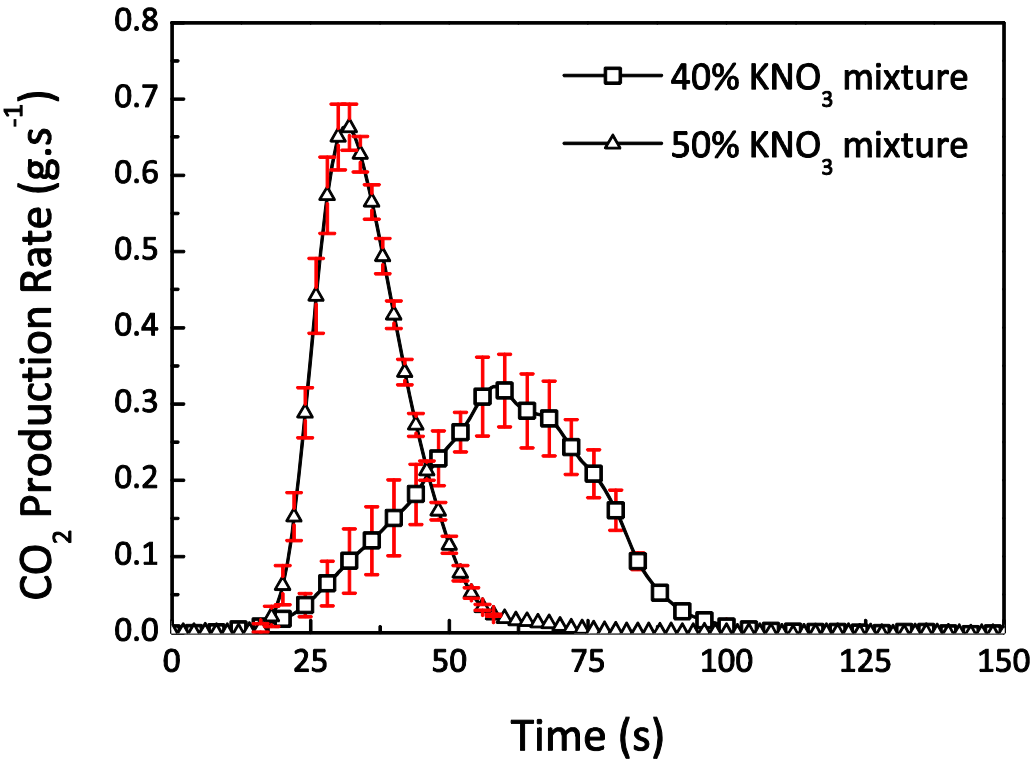

Figure 3.34. CO_2 production rates from the combustion of 40% and 50% KNO_3 ternary mixtures under N_2 atmosphere (N_2 flow of 0.1 $m.s^{-1}$).

The potential of the latter to create hot spots able to initiate the decomposition from different points affects the evolution of the spread. The effects of these interfering

variables grow as the reaction rate becomes slow leading to a more random behaviour which makes it more complicated to reproduce experimental results obtained. Given the experimental setup, a lower repeatability of the experiments realised with the 40% KNO_3 composition is rational.

The emission rates for the 50% KNO_3 ternary mixture reach higher values than for the 40% KNO_3 ones. Respective maximum rates are 0.66 $g.s^{-1}$ and 0.32 $g.s^{-1}$ (corresponding to CO_2). In the same way, reaction rate is faster for the composition with the highest concentration of oxidizer. The comparison of CO, THC and water vapour emission rates leads to similar comments (cf. Figure 3.35 to Figure 3.37). Emissions attain higher rates on a shorter time for the composition containing the highest concentration of oxidizer.

In terms of total emissions, Table 3.14 indicates the percentage of mass burnt as well as the CO_2, CO, THC and water vapour yields. For the same amount of powder, the rise of the concentration of KNO_3 from 40% to 50% induces a 2% increase in the total mass burnt. Less residue remains from the combustion of the 50% KNO_3 ternary mixture. Taking into account that more O_2 is available inside the material, one can assume that char oxidation is more important with the latter composition. This statement stands in accordance with a higher number of glowing spots observed over the surface of the powder enclosing 50% of KNO_3. Furthermore, an analysis of the composition of residues formed from the combustion of 40% and 50% KNO_3 ternary mixtures reveals a higher proportion of organic C for the lowest concentration of oxidizer (cf. Table 3.15). C that cannot be oxidized because of the lack of O_2 available remains in the carbonaceous char.

Table 3.14. Percentage of mass burnt and species yields of experiments carried out under N_2 atmosphere (Std Dev : Standard Deviation).

Sample	% Mass Burnt	CO_2 (Std Dev) [$g.g^{-1}$]	$CO_{(Std\ Dev)}$ [$g.g^{-1}$]	$THC_{(Std\ Dev)}$ [$g.g^{-1}$]	$H_2O_{(Std\ Dev)}$ [$g.g^{-1}$]
40% KNO_3	$69.2_{(0.85)}$	$0.37_{(0.009)}$	$0.145_{(0.003)}$	$0.05_{(0.002)}$	$0.276_{(0.043)}$
50% KNO_3	$71.4_{(0.33)}$	$0.357_{(0.002)}$	$0.178_{(0.004)}$	$0.041_{(0.0003)}$	$0.226_{(0.028)}$

Table 3.15. Carbon total, carbon inorganic and potassium total percentages in the residues resulting from the combustion of 40% and 50% KNO_3 ternary mixtures.

Sample	$\%C_{total\ (Std\ Deviation)}$	$\%C_{inorganic\ (Std\ Deviation)}$	$\%K_{total\ (Std\ Deviation)}$
40% KNO_3	$25_{(0.6)}$	$7_{(1)}$	$39.2_{(Na^*)}$
50% KNO_3	$13.4_{(0.6)}$	$8_{(2)}$	$50_{(Na)}$

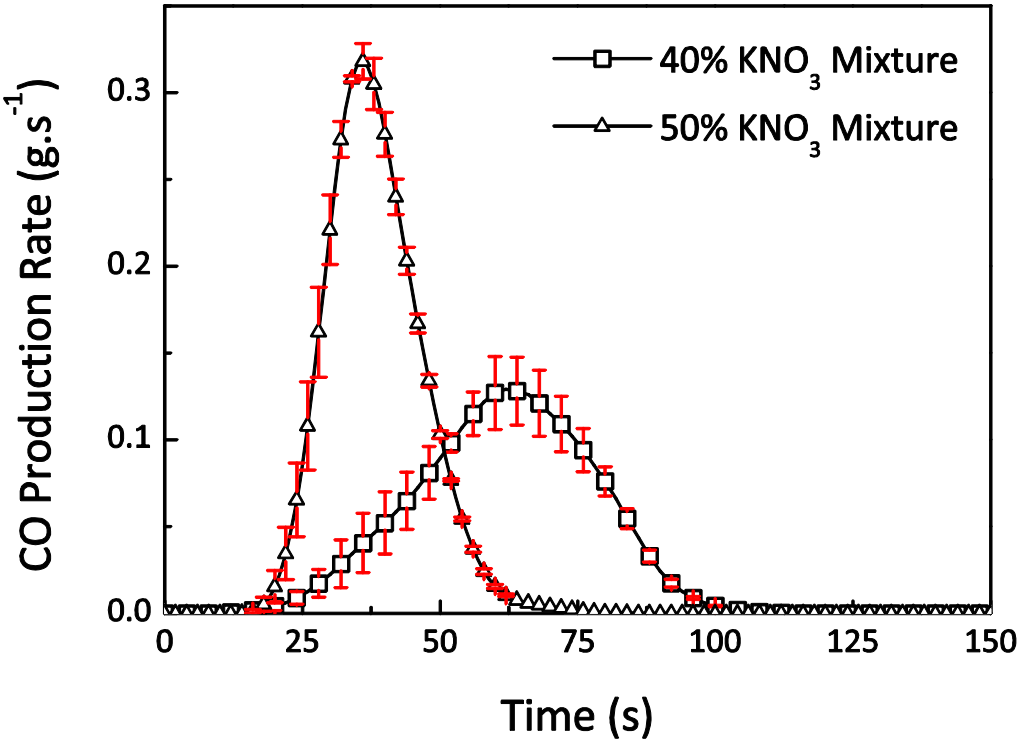

Figure 3.35. CO production rates from the combustion of 40% and 50% KNO_3 ternary mixtures under N_2 atmosphere (N_2 flow of 0.1 $m.s^{-1}$).

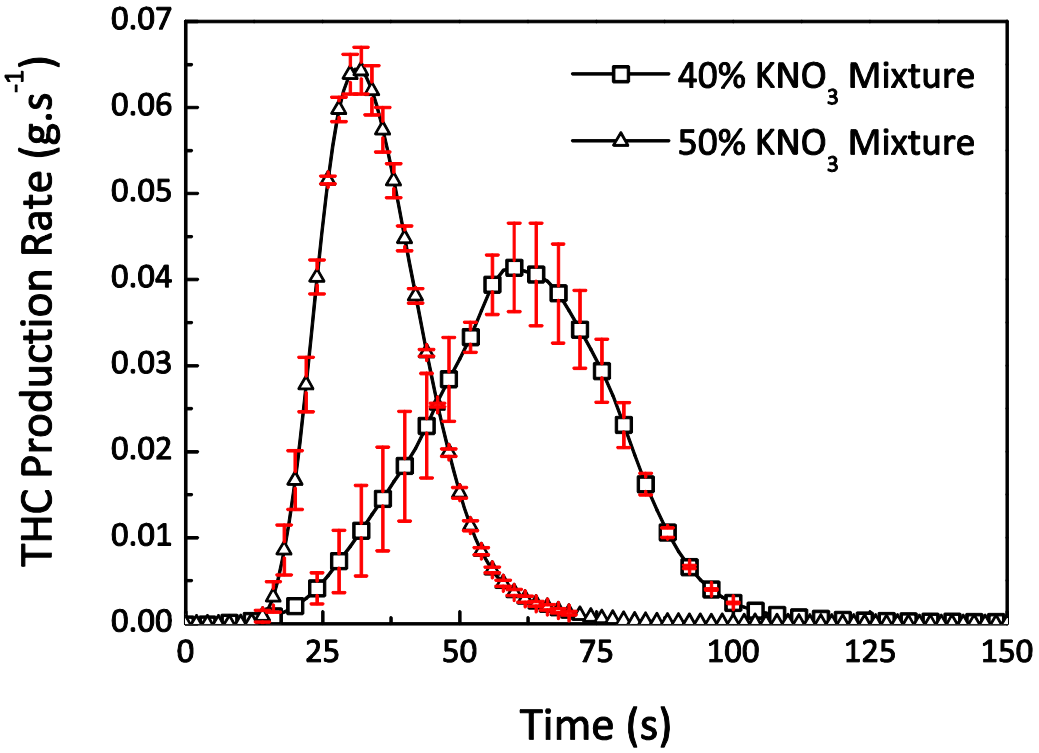

Figure 3.36. THC production rates from the combustion of 40% and 50% KNO_3 ternary mixtures under N_2 atmosphere (N_2 flow of 0.1 $m.s^{-1}$).

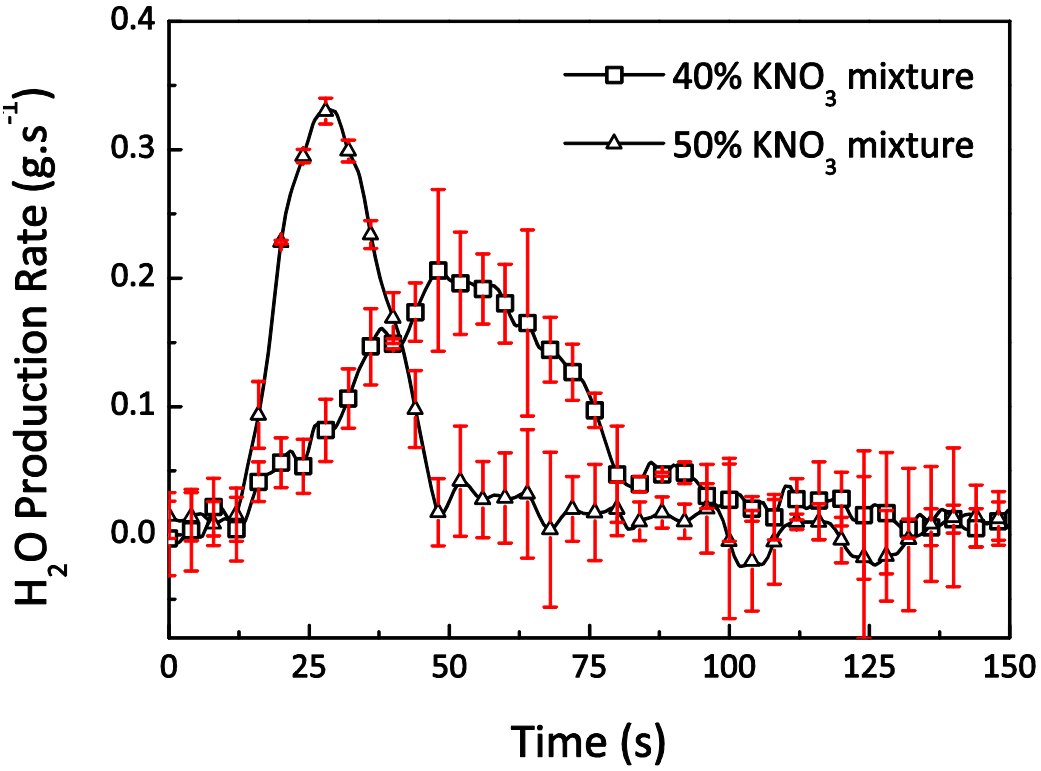

Figure 3.37. THC production rates from the combustion of 40% and 50% KNO_3 ternary mixtures under N_2 atmosphere (N_2 flow of 0.1 $m.s^{-1}$).

The recovery percentage of the K element is about 50% in the char residue of the 50% ternary mixture while it is about 39% for the 40% one. More K is contained in the sample with the highest concentration of oxidizer. On the other hand, according to the previous remark, increasing the quantity of oxidizer leads to more efficient oxidation with more C evolving in the combustion gases and less remaining in the char while potassium stays in the solid phase. The evolution of C from char to gaseous products increases the amount of material burnt as well as the proportion of K in the residue. At the same time, the fraction of inorganic C in the residue does not significantly differ between the experiments carried out with the 40% and the 50% KNO_3 composition. This strengthens the assumption that a part of the solid phase evolved into K_2CO_3 as observed during the combustion of black powder [40]. The temperature range assessed for the formation of K_2CO_3 goes from 350°C (~620 K) to 550°C (820 K) [39]. Such temperatures have been measured in the material during the combustion reaction (cf. Figure 3.17 and Figure 3.18). Several origins can explain the formation of K_2CO_3 [40]. The exact source(s) of this production have not been investigated in the present study. According to Urbanski [41], the formation of K_2CO_3 could originate from the following reaction,

$$4\,KNO_3 + 5\,C \longrightarrow 2\,K_2CO_3 + 3\,CO_2 + 2\,N_2 \quad (33)$$

Another assumption would be to consider that the generation of K_2CO_3 arises from the reaction between CO_2 and products of the KNO_3 decomposition (for instance K_2O) [40],

$$K_2O + CO_2 \longrightarrow K_2CO_3 \quad (34)$$

The generation of K_2CO_3 is limited by the quantity of C and K available to react. A change in the oxidizer concentration has opposite effects on the quantity of C and K in the solid phase. This can be the reason why only a slight variation of the fraction of inorganic C is observed in the residue content although the composition of the material has been modified.

Comparison of the species yields, from the combustion under N_2 of 40% and 50% KNO_3 ternary mixture, estimated on Table 3.14does not exhibit considerable differences. The 50% KNO_3 composition undergoes combustion with a higher reaction rate. Nevertheless, the average total production of CO_2 for 50g samples of 40% and 50% KNO_3 ternary mixtures is, respectively, 12.73 g and 12.81 g. Also, surprisingly, the CO yield is higher

with the material sample containing the highest concentration of oxidizer. Consider a Fuel/O_2 ratio defined as follow,

$$r_{Fuel/O_2} = \frac{\frac{\%C + \%H}{\%O}}{r_{st}} \tag{35}$$

$\%C$, $\%H$ and $\%O$ correspond to the respective percentages of C, H and O in the material and r_{st} being the Fuel/O_2 ratio when enough O is present in the composition to allow a "theoretical" stoichiometric reaction leading to the only formation of CO_2 and H_2O. r_{Fuel/O_2} values for 40% and 50% ternary mixtures are, respectively, 2.02 and 1.69. As $r_{Fuel/O_2} > 1$, products of incomplete combustion are generated. Considering that oxidation of fuel vapours is the dominant process and referring to the global equivalence ratio defined by Pitts [11], one can assume that the production of CO is supposed to increase as r_{Fuel/O_2} rises. Analysing THC and H2O yields, it comes that their generation is more important during the experiments carried out with the 40% KNO_3 composition. This indicates that water vapour is preferably formed from the lactose and starch decomposition. Considering hydrocarbons combustion, Glassman [33] explains that OH· radicals react fast with fuel volatiles resulting from fuels decomposition to form H_2O. Furthermore, the higher concentration of C present in the residue formed from the combustion of 40% KNO_3 ternary mixture, suggests that a lack of O_2 is the cause of the end of the reaction. A higher THC yield has also been calculated with this composition compared to the 50% KNO_3 one. The latter evidence is in agreement with the previous hypothesis of the reaction stopping because O_2 limited. The assumed chemical pathway is based on the decomposition of the fuel components into lighter hydrocarbon groups which become oxidized by O_2 evolved from KNO_3 to form CO. Once all the fuel has reacted, the remaining O_2 interacts with CO to form CO_2. This reasoning is based on Pitts's investigation on the combustion products generated in fires [11] [42]. In case of fuel rich conditions, not enough O_2 is available to oxidize CO into CO_2. The generation of CO is favoured, OH· radicals reacting faster with fuel volatiles than with CO. Nevertheless, although r_{Fuel/O_2} rises when decreasing the concentration of KNO_3, the CO yield decreases while the CO_2 yield remains relatively constant. Emissions of CO and CO_2 originate from two different modes: by oxidation of the fuel vapours in the gas phase and by oxidation of the char. In the gas phase, the CO/CO_2 production rates are driven by the rate of decomposition of the fuel components

and the oxidizer. The initial mixture is assumed to be homogeneous. When decomposition starts, a premixed system of volatiles and O_2 is generated. Exothermic oxidation takes place. Heat is released allowing the reaction front to propagate. The energetic efficiency of the oxidation reaction depends on the fuel vapours/O_2 ratio. The 40% KNO_3 ternary mixture contains more fuel than the 50% KNO_3 composition but both contain about the same amount of O_2. The quantity of heat evolved from the oxidation reactions decreases as r_{Fuel/O_2} rises. Compared to the powder embedding 50% KNO_3, less energy is released at the decomposition front of the 40% KNO_3 ternary mixture given that fuel vapours is in large excess compared to O_2. The time to achieve the decomposition temperature of the components is extended; the spread of the reaction is slower and consequently, species emission rates are lower. On the other hand, the carbonaceous residue resulting from the burning of the 40% KNO_3 composition undergoes an important swelling and the permeability of this system is assumed low as no gaseous products appear to be released through the surface of the char. Gases flow away from the sample at the interface between the char and the decomposition front. Considering the swelling induced by the pressure rise of the gaseous products and the limited area for them to be released, one can assume that their residence time is more important during the burning of the 40% KNO_3 composition. A hypothesis is that the residence time is long enough to allow the evolution of CO into CO_2. The temperature inside the structure remains between 750 K and 900 K during the mean time when gas emissions are measured. According to Pitts, if gases are trapped inside the char structure, the temperature allows oxidative reactions to occur. However, this supposes that most of the hydrocarbon volatiles have been oxidized and are no longer present in the mixture to allow the formation of CO_2.from CO. If THC yield remains relatively low, it needs to be recalled that it is nevertheless higher for the reaction involving the 40% KNO_3 ternary mixture. This can suggest that almost all O_2 was depleted in the gaseous medium preventing further formation of CO and CO_2. Further investigations would be required to clear this point, for example by repeating similar experiments with the ternary powder embedding a lower concentration of oxidizer. The production of CO and CO_2 does not only proceed from fuel vapours oxidation. Char is also an actor of CO and CO_2 emissions. CO formation is favoured at high temperatures but CO_2 may be a product of both char and CO oxidation. Di Blasi explains that the reactivity of the char can be influenced by several parameters, the release rate of volatiles being a

critical one [43]. Considering the longer residence time for the gases emitted from the decomposition of the 40% KNO_3 composition, CO_2 might be favoured by surface oxidation of the char. As the carbonaceous medium swells, the surface is enhanced and allows nascent carbon sites to develop, which can react with O_2. In the case of the 50% ternary mixture, a slight swelling is observed and the permeability of the char is larger as indicated by the spread of the flame over the whole surface of the sample. The diffusion of the gaseous products away from the sample is achieved faster than with the 40% KNO_3 composition. Higher temperature inside the material combined with a shorter residence time promotes the generation of CO. The gaseous mixture resulting from the decomposition of the 40% KNO_3 powder reveals about the same level of CO_2 and a lower level of CO than the one generated by the 50% KNO_3 composition. The hypotheses developed previously to explain the occurring process have not been verified and represent only insights that would require in-depth analysis that has not been carried in the present work.

3.5.5.2. Emissions Comparison of 40% and 50% KNO_3 ternary mixtures

For experiments carried under N_2 atmosphere, the fuel/oxidizer ratio influences the propagation of the decomposition reaction and ergo the reaction rate. It has been underlined earlier that, for the two compositions tested, the main difference stems from the fuel content. The 40% KNO_3 composition exhibits enhanced fuel-rich conditions compared to the 50% KNO_3 one. Once the decomposition initiated, the fuel vapours and O_2 mixture is closer to stoichiometric conditions for the material embedding the highest oxidizer concentration. More energy released allows stronger propagation of the combustion at an increased reaction rate. Major species generated are CO_2, H_2O, CO and THC. Estimated species emission rates reach higher levels for a shorter reaction time with the 50% KNO_3 ternary mixture. More energetic combustion allows more material to decompose and burn. As the composition becomes richer in fuel, reaction in the gas phase should promote production of higher concentrations of incomplete combustion products. Compared to the 50% KNO_3 powder, total emissions from the burning of 40% KNO_3 composition would be expected to disclose more CO formation while CO_2 generation would be limited. Estimations of the species yields between the experiments carried out with the 40% and 50% KNO_3 ternary mixtures, reveal that the CO_2 generation

remains almost constant while more CO is produced from the combustion of the 50% KNO_3 composition. The residence time might be a cause of the phenomenon. CO gases trapped in the 40% KNO_3 sample at temperatures above 800 K can undergo oxidation to form CO_2 [11]. Also, long time residence can favour char oxidation and CO_2 generation. Reactivity of the char depends on the rate of decomposition of the material. Analysis of the carbonaceous residue indicates a higher C content for the experiments realised with the 40% KNO_3 ternary mixture. Less energy is involved in the volatilization of the fuel/oxidizer mixture. As a consequence, less C elements evolve into the product gases and remain in the char. Coalescence of char particles is observed. The phenomenon is more characterised with the 40% KNO_3 powder; more residual C is present. Important swelling of the char appears for low reaction rate. Gaseous products are trapped in the carbonaceous residue which denotes a low permeability of the structure. Swelling is engendered by the pressure induced by the generated gases. For the 50% KNO_3 ternary mixture, the char structure exhibits a higher permeability allowing the product gases to flow through the surface. The spread of the decomposition and oxidation reactions influence the permeability and structure of the carbonaceous residue.

3.5.5.3. Comparison of gaseous emissions under air and N_2 atmospheres

In order to analyse the contributions of the internal (i.e. KNO_3) and external (i.e. O_2 from the air) O_2 supplies for two different compositions of the starch/lactose/potassium nitrate ternary powder, combustion experiments have been carried out using the FPA under air and N_2 atmosphere. .CO_2, CO, THC and H_2O production rates have been estimated and illustrated on Figure 3.38 to Figure 3.41. They correspond to average values obtained from several repetitions of a same experiment. Error bars are included in order to that a good repeatability was achieved over the different experiments. Divergences never exceeded 20% between two similar experiments which, according to the experimental set-up, is considered as an acceptable criterion.

Figure 3.38 shows the CO_2 emissions rates for both ternary mixtures under air and inert atmospheres. Considering the 40% ternary mixture, for the first 25 seconds after initiation, both CO_2 production rate curves rise following an identical slope. This could suggest that square one of CO_2 emissions only relies on the oxidation of fuel vapours by O_2 resulting from the oxidizer decomposition. Afterwards, the CO_2 production rate estimated for experiments carried out under air rises above the one obtained during experiments operated under N_2. It comes clearly that O_2 from the air participates in the reaction as demonstrated by the gap between the two curves. Recalling that no sustained flaming regime was attained during the experiments carried out with the 40% KNO_3 ternary mixture under N_2 atmosphere, one can assume that the difference corresponds to the contribution of the flame. Table 3.16 gives information about the ratios for both compositions of the CO_2 production rates (maximum (1) and total (2) production rates) under N_2 atmosphere over the one under air. For the 40% KNO_3 composition, $|CO_2|_{N_2/Air} \approx 0.61$. About $\frac{2}{5}$ of the CO_2 emitted apparently emanates from the flame. The reacting atmosphere influences species emissions. It can be noticed that the overall reaction period remains constant whether the reaction medium is air or N_2. The burning behaviour is controlled by the decomposition rate of the solid phase.

Figure 3.39.a. illustrates the CO production rates under air and N_2 of the 40% KNO_3 composition. Emissions measured under air seem to rise earlier than under N_2. This can

originate from surface oxidation at the primary hot spot as glowing is prematurely observed. Next, the increase of CO emission is more intense under N_2 than under air. The magnitude of emission is higher under inert atmosphere. The same behaviour is encountered with the THC generation. The two species are characteristic of incomplete combustion products. The ratios, $|CO|_{N_2/Air}$ and $|THC|_{N_2/Air}$, confirm that more emissions of these gases are measured during the tests carried under N_2 atmosphere. For rich conditions, CO and THC are produced in preference to CO_2 [11]. The reactivity of free radicals, like OH· and HO_2·, is much faster with THC (forming CO) than with CO (to form CO_2). Figure 3.41.a. displays the water vapour emission rates. The trend is similar to the one noticed for the CO_2 production rates. The first seconds following initiation exhibit the same slope for the two water vapour production rates. Like CO_2, the initial formation of H_2O seems to result from reactions only involving elements of material. H_2O generation is independent on the reacting medium since it only relies on the material composition.

Regarding the 50% KNO_3 ternary mixture, Figure 3.38.b, Figure 3.39.b, Figure 3.40.b and Figure 3.41.b present, respectively, the CO_2, CO, THC and H_2O production rates. Identical trends between experiments realised under air and N_2 appears to take place on a really short period of about 4 seconds. Then, the generations of CO_2 and H_2O resulting from the combustion under air remain more intense than the ones under N_2. Unlike CO_2 and H_2O, opposite behaviour is underlined for CO and THC. The rise of incomplete products emissions for experiments under N_2 highlights the role of O_2 from air as reaction partner in the gas phase. The total amount of CO_2 and H_2O produced are about two times higher for experiments carried out under air than for the ones operated under inert atmosphere.

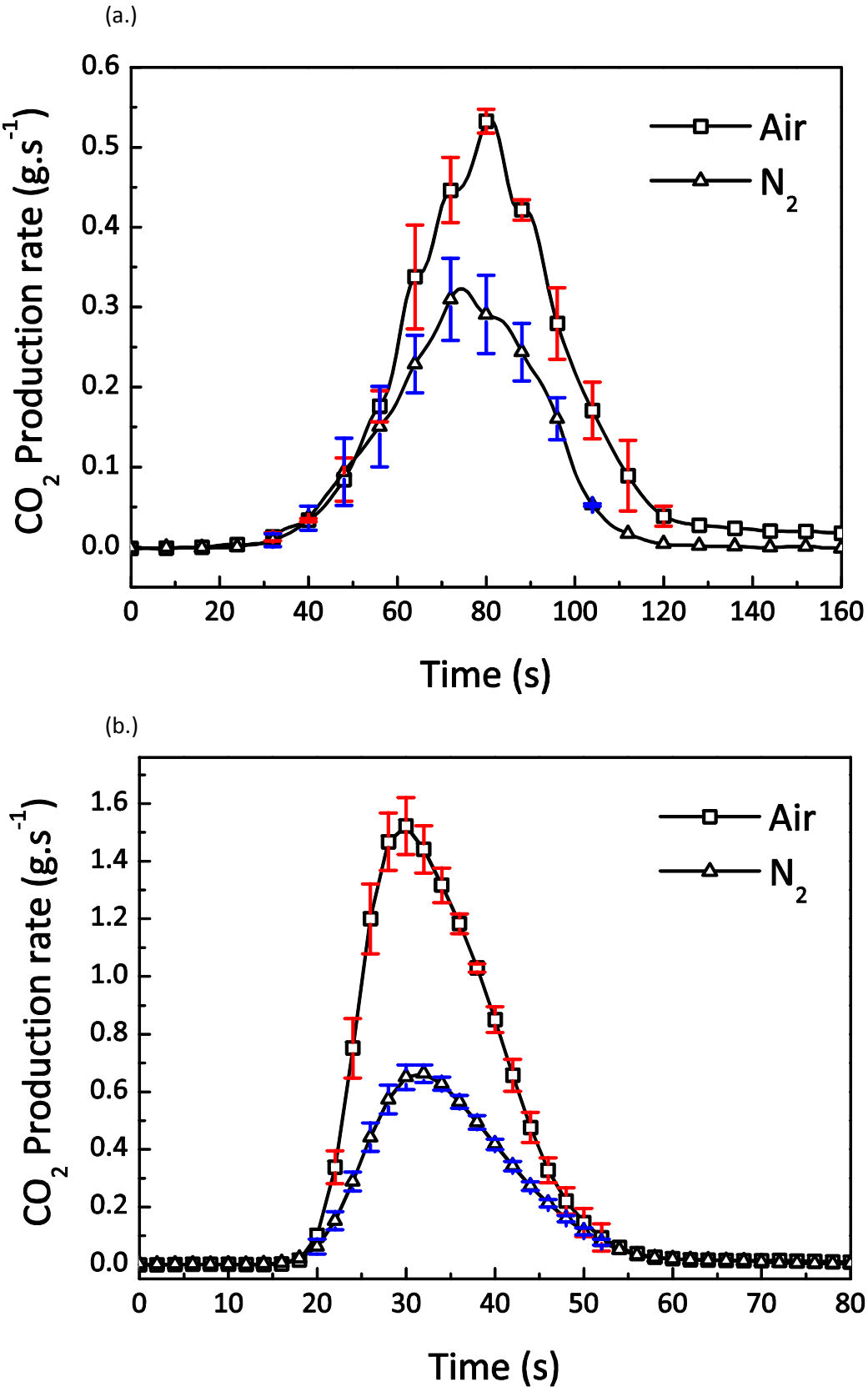

Figure 3.38. CO_2 production rates resulting from the burning of 40% (a.) and 50% (b.) KNO_3 ternary mixture under air and N_2 atmosphere.

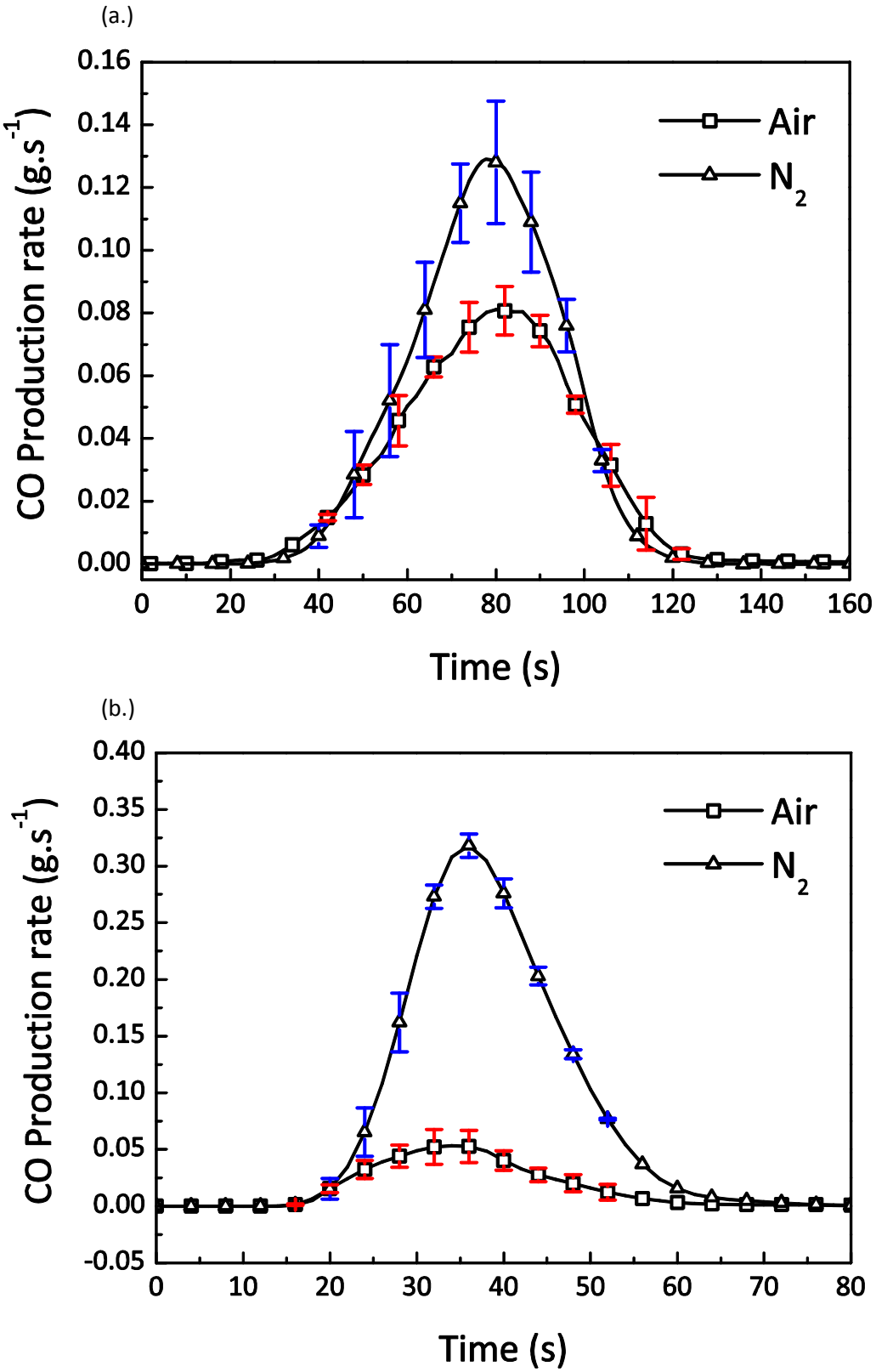

Figure 3.39. CO production rates resulting from the burning of 40% (a.) and 50% (b.) KNO_3 ternary mixture under air and N_2 atmosphere.

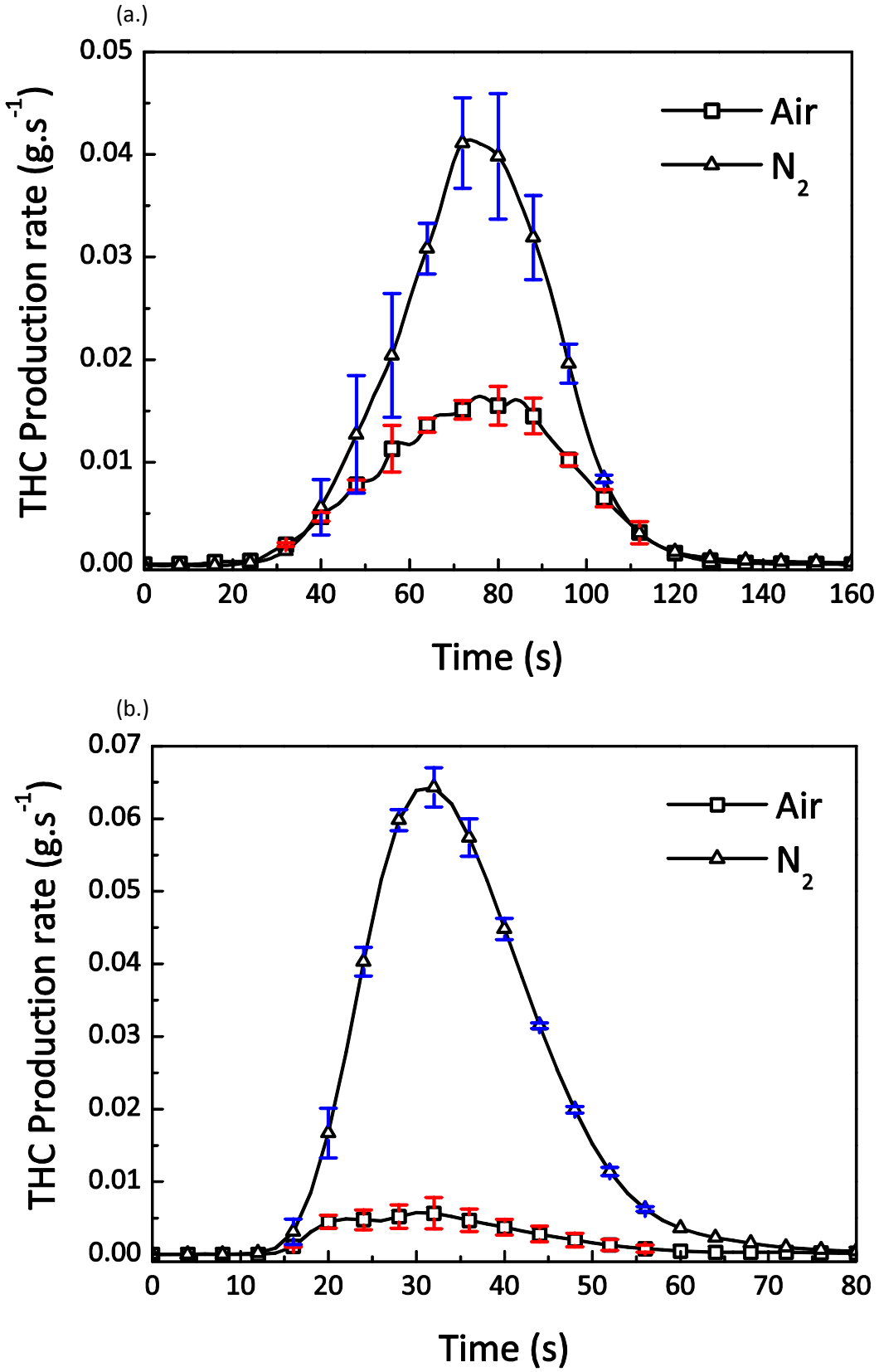

Figure 3.40. THC production rates resulting from the burning of 40% (a.) and 50% (b.) KNO_3 ternary mixture under air and N_2 atmosphere.

(a.)

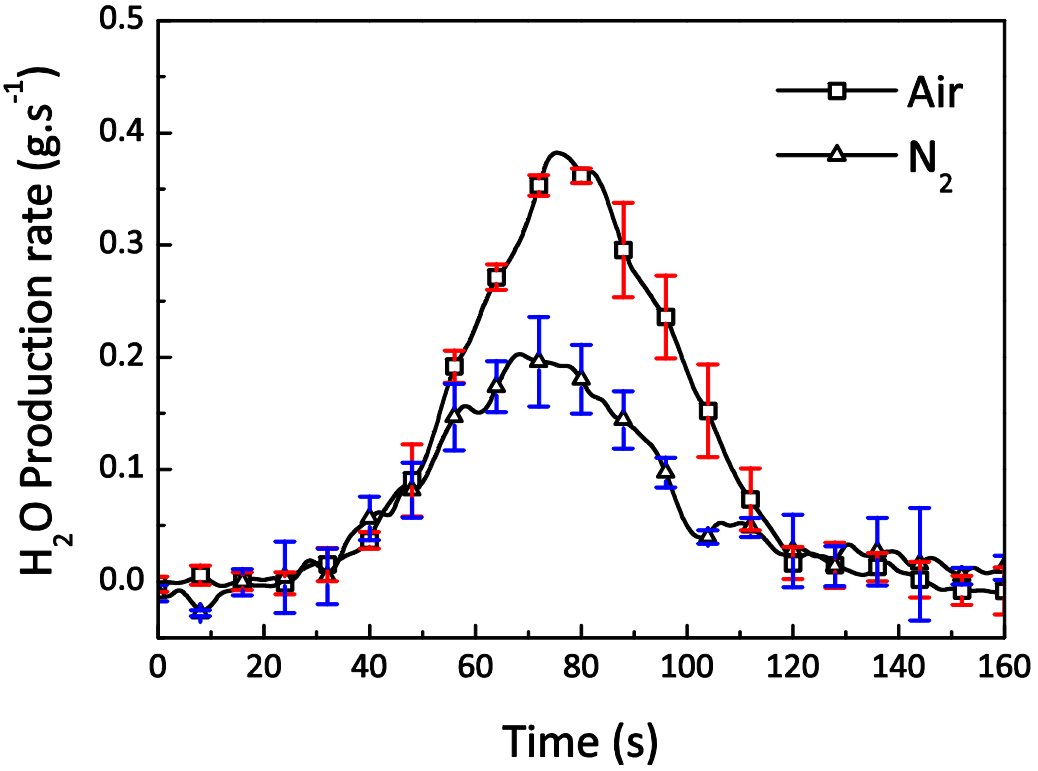

(b.)

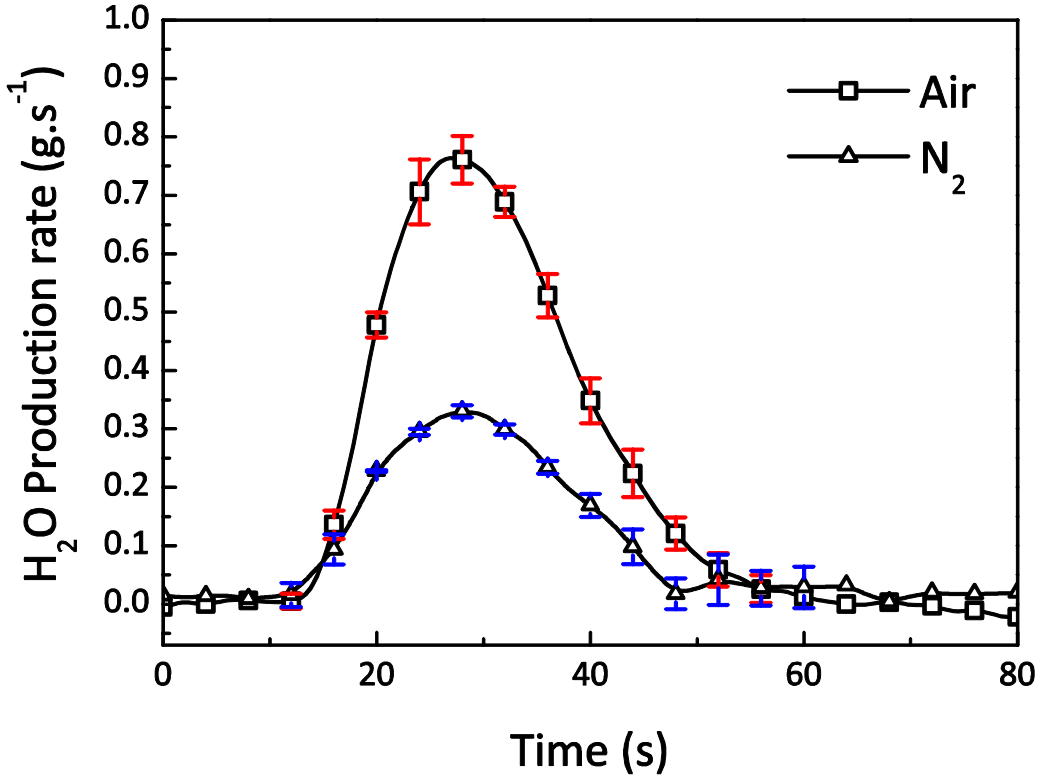

Figure 3.41. H_2O production rates resulting from the burning of 40% (a.) and 50% (b.) KNO_3 ternary mixture under air and N_2 atmosphere.

Table 3.16 also stresses the consequent variations in CO and THC total productions. The low CO and THC concentrations measured for the experiments operated under air, indicates that in the latter configuration, the mixture of fuel vapours and O_2 released from the material, diffusing into the air and undergoing combustion reaction is close to stoichiometric conditions. When the reaction atmosphere is changed into an inert medium, CO and THC concentrations increase which signifies the oxidizer concentration is too low supply enough O_2 to the system so that it reaches a more complete burning mode. The lack of O_2 causes oxidation of THC to be favoured over CO oxidation. Nevertheless, analogously to the experiments carried out with the 40% KNO_3 ternary powder, the reaction period is not influenced by the reacting atmosphere. One can assume that the decomposition of the solid phase is only controlled by the material configuration. Variations in the emissions, between tests carried out under air and under N_2 with the 50% KNO_3 ternary mixture, can be interpreted as the contribution of the diffusion flame regime only established during the experiments realised under air. The gases generated from the decomposition of the material diffuse through the material and engender a flammable mixture of fuel vapours and O_2. The premixed mixture evolves to flaming as gases are expelled from the sample. Under N_2, a short premixed flame (cf. Figure 3.42.b) is sustained as long as the concentration of O_2 allows the mixture to be within flammable limits. The flame length can be related to the flow of the gaseous products. The latter depends on the strength of the smouldering reaction occurring inside the material and the permeability of the char layer. Under air, a premixed flame is assumed to develop above the sample surface. It releases a combustible mixture, rising by buoyancy and composed, in particular, of CO and THC. The fuel mixture in contact with air induces a diffusion flame regime (cf. Figure 3.56.a). Furthermore, it has been noticed that the difference in O_2 content (mass considered) in the gaseous compounds generated under air and in the ones generated under N_2 corresponds to the amount of O_2 consumed during the experiments carried out under air,

$$\Delta m_{O_2}^{air} = m_{O_2\ in\ products}^{air} - m_{O_2\ in\ products}^{N_2} \quad (36)$$

Where $\Delta m_{O_2}^{air}$ is the mass of O_2 consumed during the experiments carried out under air, $m_{O_2\ in\ products}^{air}$ and $m_{O_2\ in\ products}^{N_2}$ are, respectively, the mass of O_2 in the gaseous products generated during the experiments carried out under air and under N_2

atmosphere. More than half of CO_2 generated stems from the oxidation of CO by O_2 from ambient air.

Table 3.16. Ratios of production rates under N_2 atmosphere over the one under air: (1) the variable considered is the maximum production rate; (2) the variable considered is the total production rate.

Sample	$\|CO_2\|_{N_2/Air}$		$\|CO\|_{N_2/Air}$		$\|THC\|_{N_2/Air}$		$\|H_2O\|_{N_2/Air}$	
	(1)	(2)	(1)	(2)	(1)	(2)	(1)	(2)
40% KNO_3	0.61	0.61	1.58	1.24	2.52	1.77	0.54	0.57
50% KNO_3	0.44	0.49	5.97	5.15	11.22	9.8	0.43	0.45

It has been previously argued that the composition of the ternary mixture, specially the oxidizer content, influences its combustion behaviour. The analysis of the gases emissions under air and N_2 stresses, for a same composition, two different behaviours. For the 40% KNO_3 ternary mixture, a sustained flame regime cannot be attained under inert atmosphere. Smouldering and surface oxidation are the main reactions taking place. Oxidation reactions encounter an important deficiency of O_2 which results in favoured formation of CO and THC rather than CO_2. The composition of the 50% KNO_3 powder carries enough oxidizer to allow a sustained premixed flame regime to develop even if the reaction is initiated under inert atmosphere. Emissions under N_2 reveal an increase in THC and CO emissions while CO_2 and H_2O are reduced compared to the ones measured under air. The concentration of oxidizer in the material remains too low to allow a complete reaction relying only on the supply of this internal reaction partner. Air brings an important contribution on oxidizing the fuel vapours and for surface oxidation as highlighted by the production rates ratios from Table 3.16. Apart from CO_2 and H_2O, emissions from the premixed flame form a fuel mixture that can be oxidized. A diffusion flame arises from the combustion of these combustible compounds with O_2 from air.

Both powder compositions exhibit a transition regime. Intuition suggests the transition to be related to the concentration of O_2 in the reacting medium. In order to investigate the insight, further experiments have been carried out. The reacting medium is the element that will be modified. Starting at 0% of O_2 (N_2 atmosphere), O_2 concentration will be raised between each different experiment. This will allow understanding how the transition from one regime to another operates.

3.5.6. Influence of the O_2 concentration on the combustion behaviour

The next analysis will be only focused on the 50% KNO_3 ternary mixture. A similar phenomenon has been underlined with the 40% KNO_3. Nevertheless in order to avoid redundancy in the ongoing reflection, only the results achieved with the composition embedding the highest concentration of oxidizer are discussed.

3.5.6.1. Combustion behaviour transition

The experimental setup is almost similar to the one defined for the previous experiments. The difference stems in the inlet supply to the reaction chamber. Tests have been carried out under supporting atmospheres of different compositions, consisting in O_2/N_2 mixtures. The latter were kept constant for the duration of the tests, starting with 20.95 % of O_2 (ambient air). Then, the O_2 concentration was decreased after each set of experiments until 0% (inert atmosphere, N_2). The aim was to investigate the transition from short premixed flame to large diffusion flame (cf. Figure 3.42.a. and 2.52.b.). In particular, tests allow verifying if the evolution of dynamics is driven by the O_2 concentration in the reacting zone.

Experiments reveal that the transition of dynamics from short premixed to large diffusion flame occurs for a critical O_2 concentration. Large bright flames, similar to the one observed on Figure 3.42.a, develop for $X_{O_2}^A \geq 18\%$. Under this critical concentration, only short premixed flames arise above the sample surface. A similar outcome is obtained when repeating the experiment with the 40 % KNO_3 mixture. The diffusion flame regime is achieved for $X_{O_2}^A \geq 18\%$. Below this critical value, only smouldering combustion is sustained.

a. Air atmosphere

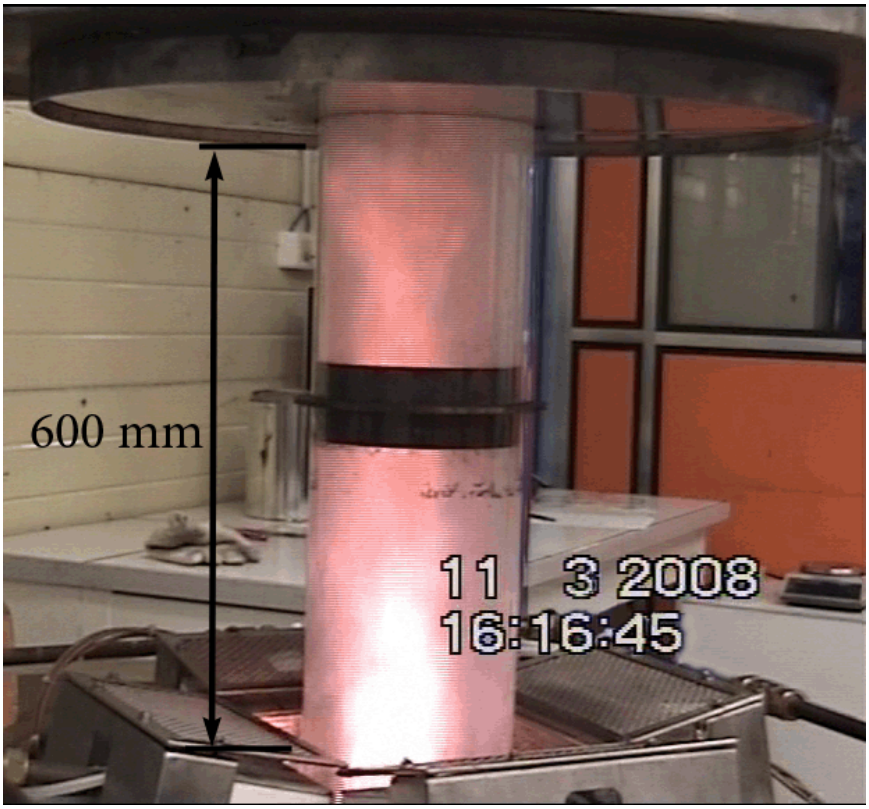

b. N_2 atmosphere

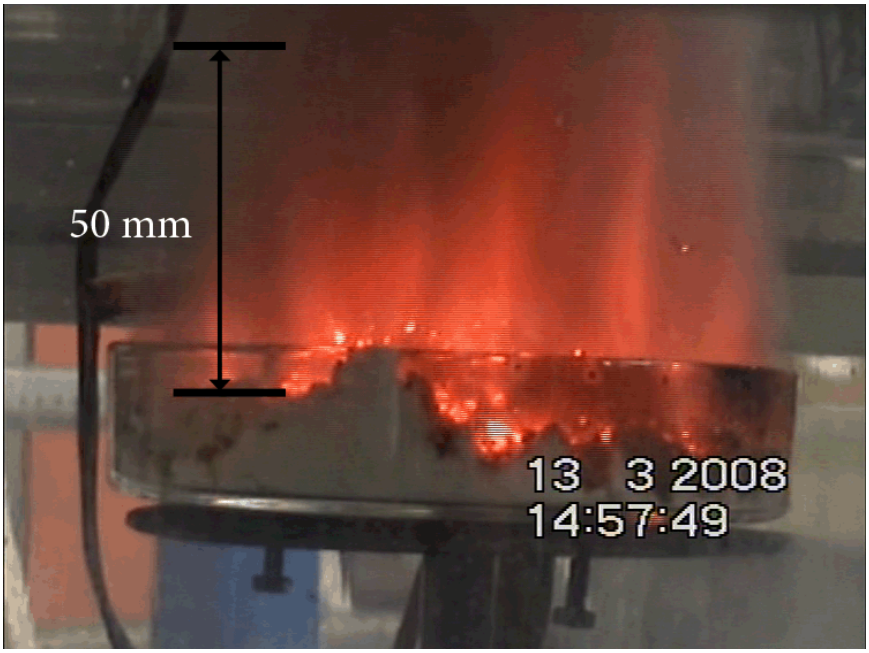

Figure 3.42. Flame length from the combustion of 50% KNO_3 ternary mixture under air (a.) and N_2 atmosphere (b.).

Figure 3.43, Figure 3.44 and Figure 3.45, respectively, represent the evolution of CO_2, CO molar fractions and O_2 depletion from combustion tests of 50% KNO_3 ternary mixture run under different reacting atmospheres. Experiments have been started under an inert atmosphere (N_2) and then the O_2 concentration was raised for every following experiment from 0 to 17%. For each of the tests carried out, the measured CO_2, CO molar fractions and O_2 depletions exhibit similar dynamics. Increasing the level of O_2 of the reacting atmosphere within the quartz tube does not promote further oxidation of CO into CO_2. Emission levels of chemical species remain unchanged for O_2 concentrations between 0 % and 17 %. When O_2 molar fraction is elevated beyond 18 % and up to 20.95% (ambient air), generation of CO_2 as well as the depletion of O_2 are enhanced. It coincides with a decrease of the CO production. One can assume that diffusion of the fuel gases rising from the sample through the reacting atmosphere gives rise to a medium that becomes reactive above a critical O_2 concentration, around 18%. Below the critical value, chemical emissions follow an asymptotic behaviour.

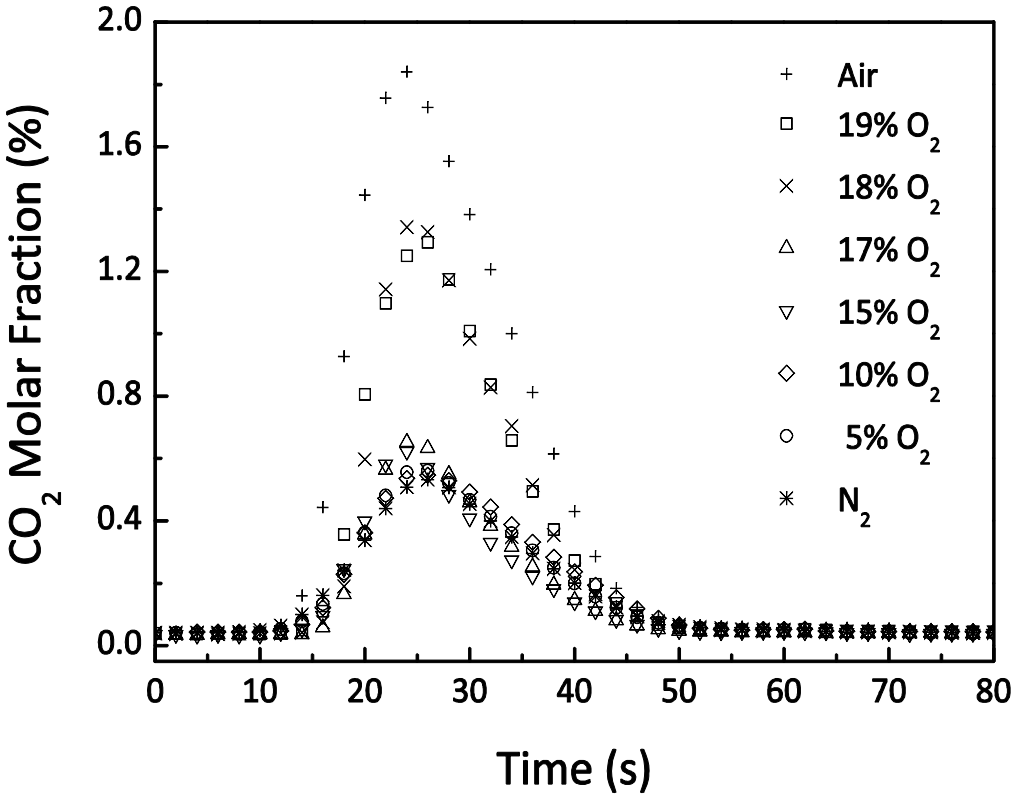

Figure 3.43. Evolution of the CO_2 molar fractions from combustion tests of 50% KNO_3 ternary powder carried out under different O_2 concentrations and N_2 atmospheres.

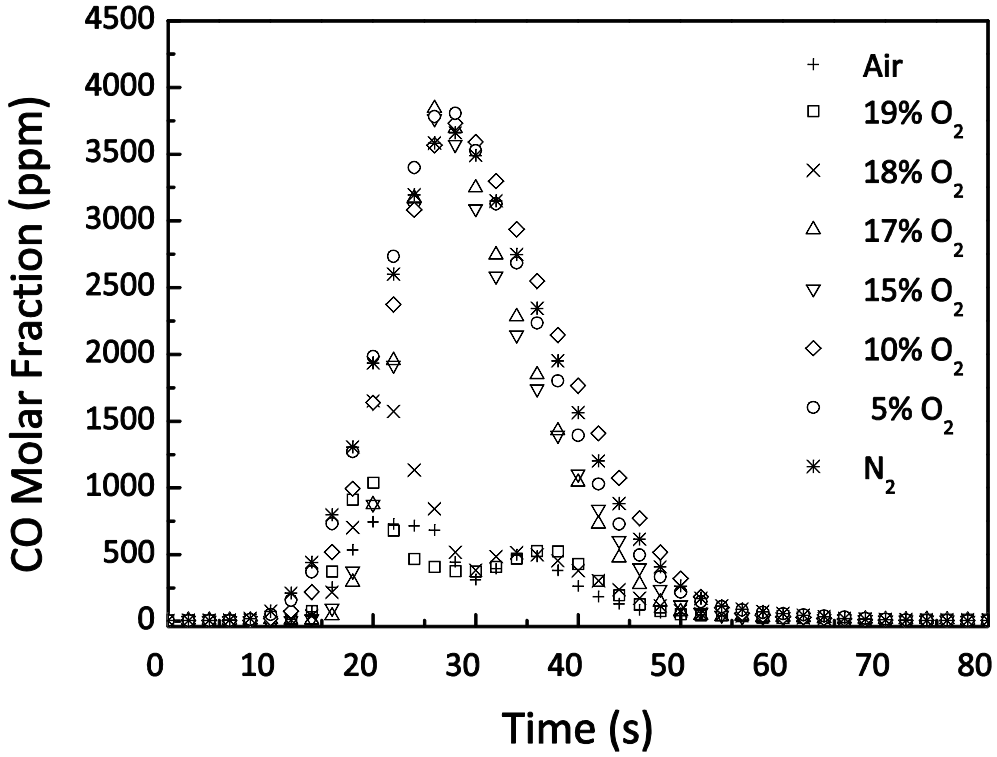

Figure 3.44. Evolution of the CO molar fractions from combustion tests of 50% KNO_3 ternary powder carried out under different O_2 concentrations and N_2 atmospheres.

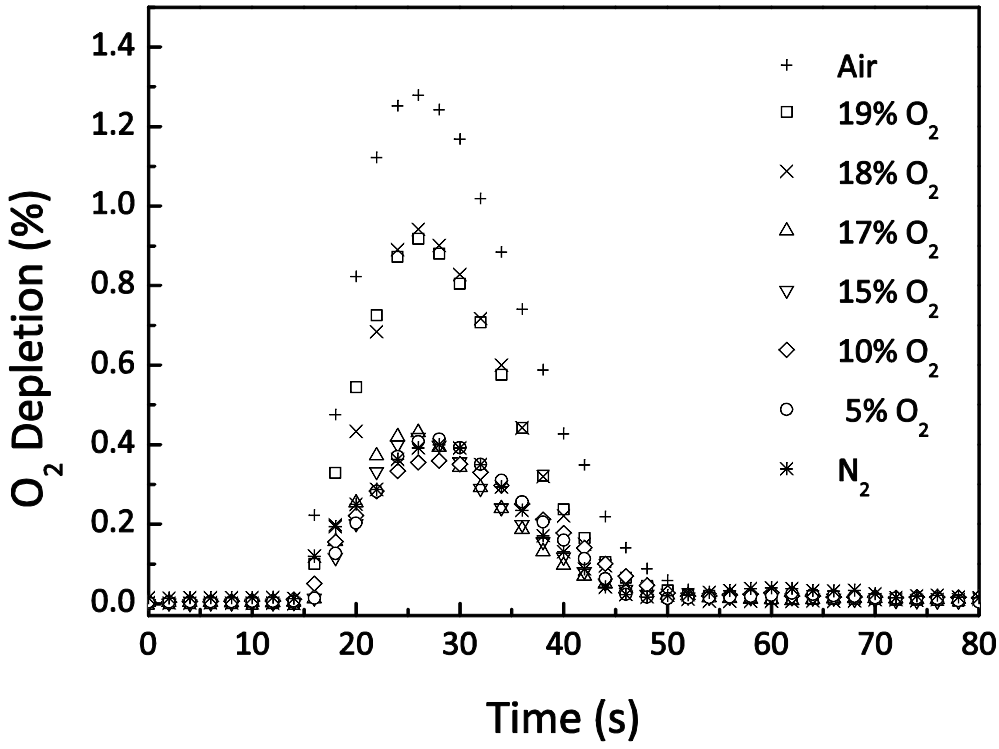

Figure 3.45. Evolution of the O_2 depletion from combustion tests of 50% KNO_3 ternary powder carried out under different O_2 concentrations and N_2 atmospheres.

Experiments have underlined the existence of a critical O_2 concentration that drives the flaming transition from premixed to diffusion dynamics. Chemical emissions differ according to the flame regime. Below this critical O_2 concentration, asymptotic behaviours are measured. For a given species, chemical emission remains unchanged for tests carried out under N_2 (i.e. 0% O_2) up to 17% O_2. This indicates that the only oxidizing agent of the fuel vapours evolved from the material decomposition is KNO_3 contained in the material itself. Reactions taking place within the powder, at its surface or within the premixed flame are self sustained and the reacting medium does not participate in their propagation. Smouldering and flaming combustions only rely on the material composition. Although part of the gases generated from smouldering combustion, surface oxidation or premixed flaming combustion and rising from the sample are not completely oxidized, O_2 from the reacting medium does not promote further oxidation. The system formed by the gaseous products and the supporting atmosphere is unreactive. The transition of flaming dynamics takes place at an O_2 concentration of 18%. The system product gases/O_2 from air is reactive beyond this molar fraction. Oxidation of the volatiles originated from the material by O_2 from air takes place within a diffusion flame. Secondary combustion reaction initiates and leads to generation of more complete combustion products as it was when only a premixed flame developed. CO_2 emission and O_2 depletion are increased while CO is oxidized into CO_2 and sees its concentration being reduced.

Figure 3.46 illustrates the total production of CO and CO_2 from the combustion of 50% KNO_3 ternary mixture under different concentration of O_2 in the reacting atmosphere. The mode transition clearly appears around 18% of O_2. Below the critical concentration, CO_2 and CO productions remain constant and are not influenced by the composition of the reacting atmosphere. Above the critical value, CO_2 is significantly enhanced while CO is reduced. Combustion occurs with O_2 from the reacting medium as a secondary partner promoting the completeness of the reaction.

Another indicator of the transition from a diffusion flame dominated regime to a smouldering one coupled with premixed flaming can be defined by estimating the CO/CO_2 production ratio as a function of the O_2 concentration in the reacting atmosphere. The CO/CO_2 production signature of the 50% ternary powder is presented in Figure 3.47. The ratio remains relatively

low ($CO/CO_2 < 0.1$) for O_2 concentration in the supporting atmosphere above 18%. Below the critical O_2 concentration the CO/CO_2 ratio increases suddenly and reaches a plateau between 0.45 and 0.5. Like the estimations of CO and CO_2 total productions, this indicator clearly emphasizes the decrease of CO_2 and increase of CO emissions when the smouldering process becomes the dominant one. On the other hand, when the diffusion flame regime establishes, the concentration of CO_2 grows while the CO generation is reduced. The evolutions underlined on the CO/CO_2 ratio tend to consolidate the hypothesis of CO produced by the smouldering and getting oxidized in the diffusion flame to form CO_2. CO/CO_2 ratios of various solid compounds susceptible to undergo smouldering and flaming should be evaluated in order to investigate the possibility of a characteristic value describing the flaming/smouldering transition.

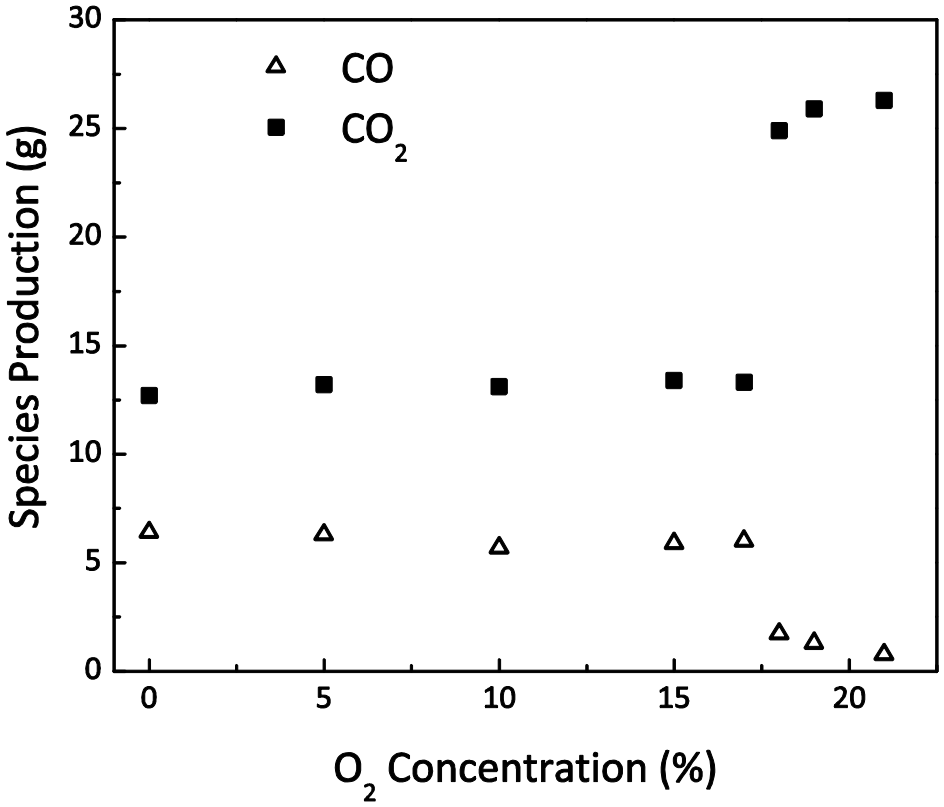

Figure 3.46. CO_2 and CO total productions from the combustion of 50% KNO_3 ternary mixture as a function of the O_2 concentration in the supporting atmosphere.

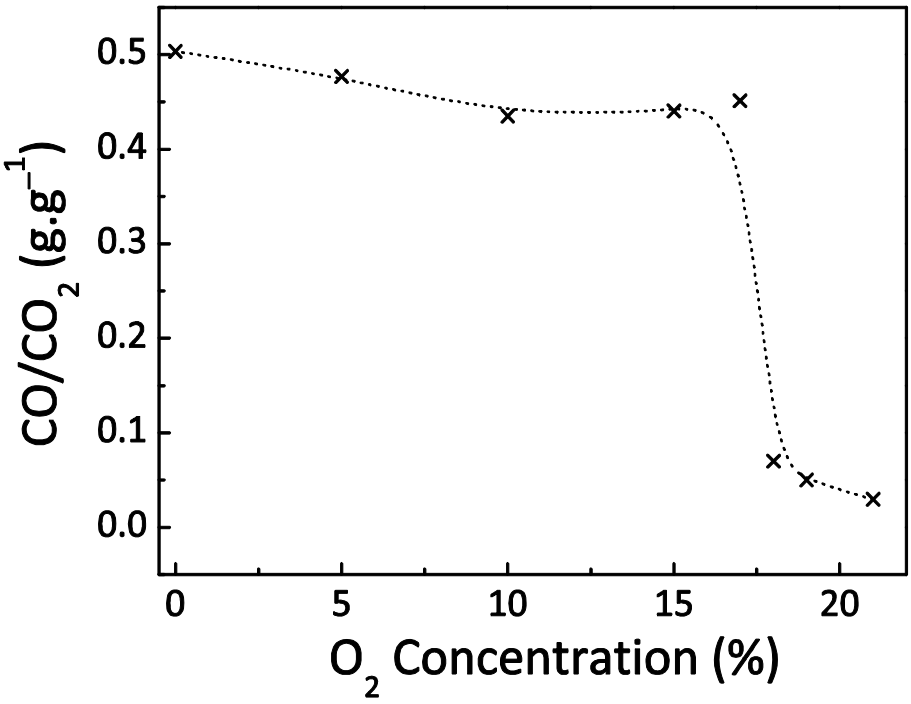

Figure 3.47. CO/CO_2 production ratio from the combustion of 50% KNO_3 ternary powder as a function of the O_2 concentration of the reacting atmosphere.

3.5.6.2. Critical O_2 concentration: Analytical model

A critical O_2 concentration value has been stressed during the experiments described previously. A transition was observed from short premixed flame to large diffusion flame when O_2 concentration in the reacting chamber exceeds 18%. Based on a flammability criterion, a simple analytical model has been developed to estimate the minimum O_2 concentration required to engender a sustained diffusion flame when reacting with the combustible gases released from the smouldering combustion and char oxidation of the material.

First recall the kinetics assumed to take place during the combustion of the ternary mixture. Allowance is made for two different dynamics. Smouldering combustion develops in the condensed phase. Flaming combustion initiates in the gas phase. A hot spot is created on the surface. Heat is transferred through the powder rising its temperature. Referring to the thermal analysis carried out previously (cf. Chapter 2), decomposition temperatures for lactose and starch stand, respectively, around 493 K (220°C) and 593 K (320°C). KNO_3 starts melting around 603 K (330°C). First dehydration of the fuel compounds occurs. Water vapour is the

first gas released. Decomposition temperature of lactose is the lowest one of the powder compounds. Volatiles originated from lactose are first assumed to be released. However, monitored temperatures inside the material highlight a steep increase. Less than 2 seconds are required for the temperature to ascend from 200 to 400°C. Combustion of the 50% KNO_3 ternary mixture lasts for more than 30 seconds. Considering this characteristic time scale, from its magnitude, and the mixture being homogeneous, one can assume that volatilization of the powder components initiates almost simultaneously. Fuel compounds evolve into lighter hydrocarbons (HC). KNO_3 is supposed to follow the decomposition phases stated by Freeman [22]. The two reactions are expressed as follow,

For T>500°C: $$KNO_3 \longrightarrow KNO_2 + \frac{1}{2}\, O_2 \tag{37}$$

For T>700°C: $$2\, KNO_2 \longrightarrow K_2O + N_2 + \frac{3}{2}\, O_2 KNO_2 \rightarrow K_2O + N_2 + \frac{3}{2} O_2 \tag{38}$$

Analyses of the gaseous emissions and the residue through a mass balance of their constituting elements suggests the assumption that the decomposition reactions are initiated in the ternary mixture at lower temperatures than the ones defined by Freeman. Fuel vapours mix with the O_2 released as KNO_3 decomposes. The temperature is sufficiently high for the gaseous mixture to be reactive [11]. Light HC gets oxidized into CO. CO formation is favoured due to higher reactivity of the free radicals with unburned HC than with CO. The oxidation of HC into CO is controlled by the O_2 produced from the decomposition of the KNO_3. Residual O_2 participates in the oxidation process leading to the formation of CO_2. Calculation of the %OB and the elemental stoichiometric coefficient denotes a lack of O_2 that can be formed from the KNO_3 decomposition to promote complete combustion of the fuel. A gas phase is formed and products rise by buoyancy through the structure. Carbonaceous residue remains from the smouldering combustion and can be described by coalescence of C particles resulting from the recalled pyrolysis reactions,

Lactose: $$C_{12}H_{22}O_{11} \cdot H_2O \longrightarrow 12\, C + 12\, H_2O \tag{39}$$

Starch: $$C_6H_{10}O_5 \cdot H_2O \longrightarrow 6\, C + 6\, H_2O \tag{40}$$

As KNO_3 decomposes, some emitted compounds react with the residual char to form K_2CO_3 [40] [41]. As the gaseous products ascend through the carbonaceous layer, char is oxidized by the residual O_2. Glowing also occurs on the surface and within the material. Major constituents

of the gas phase are CO_2, CO, THC, H_2O and N_2 and residual O_2 from the oxidizer. As the smouldering reaction was incomplete, the gaseous mixture carries fuel compounds (mainly CO and THC) that can undergo a secondary combustion. When the gaseous mixture gets released through the surface of the sample, if the concentrations of residual O_2 (originated from oxidizer) and fuel vapours meet flammable conditions, a premixed flame can develop. Combustible compounds are still present and diffuse in the reacting medium. The kinetics is governed by the diffusion. A diffusion flame arises if flammable conditions are encountered between fuel vapours (mainly CO and THC) and O_2 from the reacting atmosphere. The atmosphere inside the reacting chamber provides O_2 required for the oxidation of CO into CO_2.following the kinetic mechanism [44],

$$CO + OH \rightleftharpoons CO_2 + H \quad (41)$$

Hottel and Williams explain that the forward step governs the generation rate, the reverse step being negligible. Abam studied the CO oxidation in laminar diffusion flames [45]. He showed that the flame structure was characterized by interactive diffusive and chemically reactive flow. He correlated the CO concentrations with a parameter defined as mixture fraction. However, the concentration dependence for values corresponding to the reactive zone is modified by the Damköhler number introduced as the ratio of the diffusion time over a chemical reaction time. Assuming constant reaction rates, variations of diffusion times between the different compositions of ternary mixture is a possible cause of the different flame heights observed. Abam noticed that species spent longer diffusing and reacting when the flames are small. The chemical character of the flame is influenced by the local species concentrations (mixture fraction) and Damköhler numbers [46]. Assuming a low O_2 level in the reacting chamber, when the concentration of O_2 in the reacting medium is increased, mass and heat diffusivities are raised through elevation of flame temperatures. Consequently, both diffusion and reaction times are enhanced. One can assume a temperature dependence of the combustible mixture. If a critical temperature condition exists within the reactive zone, transition to diffusion flame may be initiated. Warnatz showed that the conversion of CO into CO_2 occurs via a reaction with temperature dependence [47]. Considering the combustible mixture initiated from the smouldering combustion and char oxidation taking place in the condensed phase, by increasing the O_2 concentration (i.e. decreasing the level of N_2) in the reacting atmosphere, the specific heat capacity of the gaseous mixture, formed from the combustion products evolved from the condensed phase and the O_2/N_2 composition of the

reacting medium, decreases as $C_{p_{N_2}} > C_{p_{O_2}}$. It has been suggested that a critical temperature for the reactive zone exists below which diffusion flame cannot develop. The presence of inert species such as N_2 can be comprehended as a suppressant by its contribution to the heat capacity of the gas mixture. As the concentration of inert species gets reduced, the flame temperature increases. For a critical O_2/N_2 composition, the critical temperature is reached and transition from premixed to diffusive combustion is initiated. The rise of the temperature elevates the reaction rates sufficiently to induce a change of dynamics. The transition criterion relies on the assumption of a thermal limit [48].

Analysis of the influence of the O_2 concentration on the transition of flame dynamics requires taking into account all the constituents of the gaseous products evolved from the condensed phase and the ones of the reacting atmosphere. The simple criterion that has been developed is based on several assumptions,

1. The reaction occurs in the gas phase.
2. Species considered are N_2, CO_2, CO, THC, H_2O and O_2. Diffusion flame arises in complement of the premixed flame. Concentration of the fuel compounds corresponds to the one measured when only a premixed flame develops, i.e. the gases released from the premixed flame undergo combustion in the diffusion flame;
3. The Burke-Schumann model for a diffusion flame is applicable;
4. The chemical kinetics in premixed and diffusion flames are identical;
5. Transition from premixed to diffusion flame is a thermal limit: a critical temperature exists under which diffusion flame cannot be achieved;
6. Heat losses are neglected;
7. There is no chemical interaction between the inert species and the other constituents.

According to assumption (3), the flame envelop is located where fuel and oxidizer meet stoichiometric proportions. Following this hypothesis and considering an element of the reaction zone complying with the latter, the heat of combustion released within this element increases the enthalpy of the combustion products as well as the inert species (N_2). The temperature of the reactive zone elevates. An expression is given by,

$$\Delta H_c \, X_{fuel} = \left(\sum_i n_i C_p(i) + n_{N_2} C_p(N_2) \right) \left(T_f - T_0 \right) \tag{42}$$

Where, ΔH_c is the heat of combustion of the fuel compounds (i.e. CO and THC); X_{fuel} corresponds to the fuel molar fraction when the fuel is mixed stoichiometrically with the oxidant stream; n_i is the number of moles of the product i of complete combustion per mole of reactants (stoichiometric mixture of fuel and oxidant streams); $C_p(i)$ represents the heat capacity of the combustion product i, T_f is the critical flame temperature and T_0 is the temperature of the stoichiometric mixture prior reaction.

Given assumption (7), the amount of energy that can potentially be released is independent of the concentration of inert species. However, assuming that the initial concentration in the reacting atmosphere is only N_2, as the concentration of O_2 is increased the heat term $n_{N_2} C_p(N_2)$ gets reduced (as the level of N_2 is lowered), the temperature difference term, $\left(T_f - T_0 \right)$, decreases. As T_0 is supposed constant, when the flame temperature exceeds the critical value T_{fl}, transition to diffusion flame initiates. The basis of the simplified chemical model used in the present study results from a former work carried by Beyler [15]. Introducing the equivalence ratio to estimate the fuel mass fraction, it gives,

$$X_{fuel} = \phi \; X_{O_2} \, r_{st} \tag{43}$$

Where,

$$r_{st} = \left(\frac{n_{fuel}}{n_{react\ atm}} \right)_{stoichiometry} \tag{44}$$

Which corresponds to the stoichiometric ratio of the moles of fuel (n_{fuel}) over the moles of the reacting atmosphere ($n_{react\ atm}$).

Defining the two parameters, K_i and K_{N_2} as follow, to reduce the energy equation,

$$K_i = \sum_i n_i C_p(i) \tag{45}$$

And

$$K_{N_2} = n_{N_2} C_p(N_2) \tag{46}$$

Expression (42) can be rewritten,

$$\Delta H_c \, \phi \; X_{O_2} \, r_{st} = \left(K_i + K_{N_2}\right)\left(T_f - T_0\right) \tag{47}$$

The equivalence ratio, ϕ_{cr}, encountered when equation (47) is verified is given by,

$$\phi_{cr} = \left(\frac{K_i + K_{N_2}}{\Delta H_c \; X_{O_2} \, r_{st}}\right)\left(T_f - T_0\right) \tag{48}$$

The flame transition criterion is defined as $\frac{\phi}{\phi_{cr}}$, the fraction of the actual equivalence ratio of the fuel/reacting atmosphere mixture over the critical equivalence ratio, ϕ_{cr}. The flame transition criterion is addressed function of the concentration of O_2 in the reacting atmosphere. Transition occurs at $\frac{\phi}{\phi_{cr}} = 1$.

$\frac{\phi}{\phi_{cr}} < 1$, corresponds to a premixed flame mode.

$\frac{\phi}{\phi_{cr}} \geq 1$, corresponds to a diffusion flame mode.

The fuel gases of the mixture are CO and THC. ΔH_c is estimated from the proportion of the two fuel compounds. The stoichiometric ratio r_{st} is calculated based on the quantity of fuel in the mixture. Regarding the temperatures, T_f is estimated from the adiabatic temperatures of CO (1450 K) and THC (1700 K) [15] according to the proportion of each of the fuels. In the present study, T_f was assumed to be about 1500 K. The temperature of the mixture prior to the flame transition is estimated to lie between 1000 and 1300 K according to measurements from thermocouples located above the surface of the material.

Figure 3.48 indicates the results obtained for the flame transition criterion, function of the O_2 concentration in the reacting atmosphere. $\frac{\phi}{\phi_{cr}}$ equals unity for an O_2 concentration between 17 and 18%. The simple chemical model has been able to predict the critical O_2 concentration governing the transition from a premixed flame to a diffusion flame dominated regime.

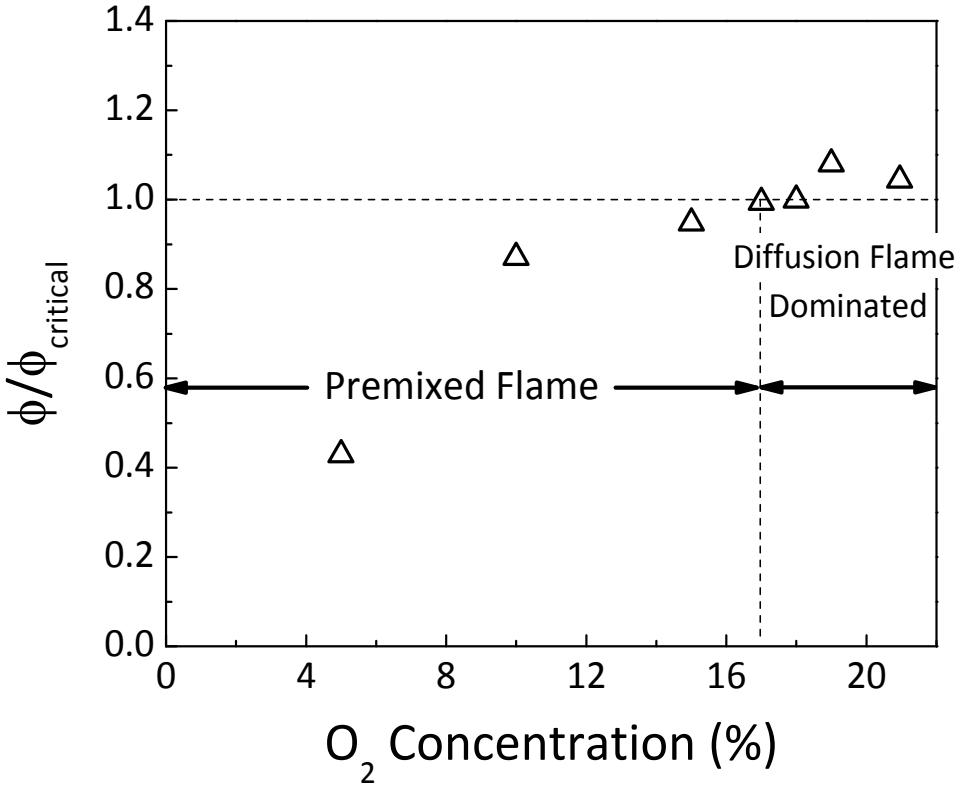

Figure 3.48. Transition criterion from premixed to diffusion flame dynamics.

3.5.6.3. Evolution of the mass loss

The chemical emissions are affected by the combustion behaviour transition. Another important variable used to characterise combustion is the mass loss of the burning sample. A change in the kinetics should result in a modification of the burning rate. Figure 3.49 represents the mass losses measured during experiments with the 50% KNO_3 ternary mixture carried out under different O_2 concentrations (i.e. from 20.95% (air) to 0% (N_2) O_2). Surprisingly, mass loss profiles are all similar. Little variations are within the uncertainty of the measure and do not suggest a change in kinetic paths above a certain critical value of O_2 concentration. One could presume that the transition from a short premixed flame to a large diffusion one would affect the mass loss rate. Drysdale describes, for solids, the mass loss as the amount of volatiles produced by a chemical decomposition that can escape from the surface and burn in the flame [27]. According to this definition, the mass loss of a solid is an expression of the evolution of the condensed phase.

Chemical decomposition, oxidation of the pyrolysis gases and char oxidation account for the main reactions taking place in the condensed phase as smouldering combustion. Flaming combustion occurs in the gas phase. If the flame dynamics influences reactions happening in the condensed phase, then the mass loss is also affected. The feedback from the flame is expected to contribute by conduction and radiation through the material to increase the temperature of the charred region. One can assume that the rate of production of volatiles will be enhanced and so the mass loss [49] [50]. Nevertheless, this is inconsistent with the mass losses illustrated on Figure 3.49.

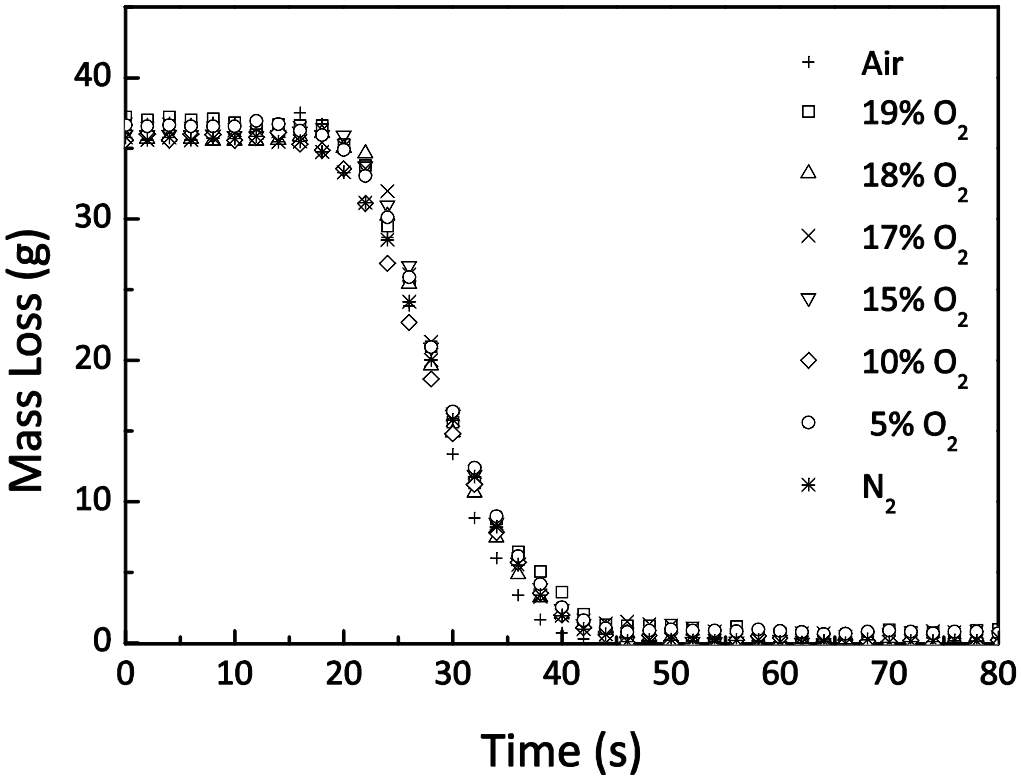

Figure 3.49. Evolution of mass loss measurements from combustion tests of 50% KNO_3 ternary powder carried out under different O_2 concentrations and N_2 atmospheres.

With regard to Figure 3.49, no variations arise from the mass losses. Heat transfer from the flame does not intensify processes undergone in the condensed phase (smouldering front and char layer). Heat transfer in a porous media is driven by convection, conduction and radiation.

Smouldering combustion induces the formation of a carbonaceous char. Observation of the residue underlines coalescence of carbon particles and indicates a rise of the porosity of the char structure. Conduction in highly porous chars is a poor mode of heat transfer [51]. Bar-Ziv explains that thermal conductivity decreases as oxidation of char occurs [52]. Variation of thermal conductivity depends on three factors: the total porosity, the dimensions of the microstructures and the connectivity between the microstructures. The increase in porosity due to char formation and oxidation lowers the conduction inside the material. The char layer acts as an insulating layer. As the flame strengthens, the surface temperature grows but the temperature gradient below the surface remains low.

During smouldering combustion, the char is saturated with volatiles, O_2 and inert gases which carry heat creating convective flows. Convective flows can be engendered by pressure differences or temperature gradients. Their intensity depends on the permeability of the medium and can be related to it through Darcy's Law [53]. The contribution of the flame to the convective flows hangs on the gradient of temperature induced inside the char layer. Recalling the insulating property of the charring region, one can assume that the temperature gradient is maintained sufficiently low, so the support from the flame on convection is limited.

Despite the relatively low temperature inside the char region (between 300 and 600°C), the radiation heat transfer can constitute an important propagation mode [54]. However, intensive works carried on charring materials [55] [56] and propellants [57] [58] highlighted that for a wide range of carbonaceous residues, the radiation contribution can be neglected at temperatures below 1000 K. Ibiricu and Williams [59] estimated the effects of a radiant heat flux on the burning rate of solid propellants. They highlighted two distinct cases, whether the gas phase or the condensed phase reaction controls the mass loss. When the gas phase governs the mass loss, the influence of the radiation is induced by the flame temperature. When the condensed phase drives the mass loss, an expression of the latter could be defined embedding an effective non dimensional gas phase feedback heat flux term. The authors showed that the influence of the radiation arises according to where it is absorbed and how the heat feedback term is modified. They estimated that for temperature under 1000 K, the sway of the radiation on the heat feedback term can be neglected. Finally they draw the qualitative principle that considering a reaction zone source of the mass loss, radiations absorbed in layers deeper that this region, engender an increase of the mass loss rate but,

radiations absorbed above are ineffective. This suggests that radiation emitted by the smouldering combustion prevails at the reaction zone but the low temperature measured inside the material tends to assume that the radiation feedback from the flame is negligible. Besides, the reaction front propagates downwards leaving char behind. As the char thickness grows, the distance between the flame and the reaction front increases. Insulation of the char layer thickness becomes important. If the sizes of the radiation and conduction characteristic lengths are significantly shorter than the smouldering length, the feedback from the flame will not contribute to the mass loss.

It needs to be noticed that the thermal insulation of the char coating causes an elevation of the surface temperature. This supposedly enhances glowing combustion and char oxidation throughout a thin layer below the sample surface. Nevertheless, the contribution of these reactions appears minor as no variation is underlined when the feedback of the flame intensified.

The char layer develops a thermal insulating coat that limits conduction and radiation deeper in the material. Convection contribution instigated from the flame feedback is also restrained by the buoyancy effect driving the volatiles released through the char. Furthermore, the smouldering propagates downward. The char layer thickness increases in time enhancing the insulating behaviour [60] and lowering the impact of heat transfer feedback from the flame. Finally, the mass loss results from the smouldering combustion. The condensed phase controls the mass loss and the feedback from the flame has a minimal influence on it.

3.5.7. Pyrolysis gases evolved from the condensed phase

Experiments have highlighted two different processes taking place during the combustion of the powder: one in the solid phase, the second in the gas phase. Smouldering combustion occurs at the reaction front. Gaseous products released are driven by buoyancy through the char layer of the material where they exit the sample. If the fuel/oxidizer mixture reaches flammable conditions, flaming combustion develops in the gas phase. The burning gases result from the propagating reaction occurring within the material. Emissions measured correspond to the gaseous products released from the flaming combustion. This physical occurrence varies according to different parameters, such as the nature of the fuel mixture rising from the

sample and the reacting medium. The flaming behaviour appears to be highly affected by the reacting medium. Knowing the nature of the gaseous mixture engendered by the smouldering combustion allows better understanding of the kinetics taking place in the gas phase and the resulting emissions of the flame. Pyrolysis experiments have been carried out on 40% and 50% KNO_3 ternary mixtures using the FPA. The reacting chamber (i.e. volume inside the quartz tube) has been insulated from the outside and the atmosphere inside is assumed to be inert (filled with 100% N_2). The sample material has been submitted to an external and constant heat flux of 10 $kW.m^{-2}$. Results presented are relative to the 40% KNO_3 composition. This mixture was preferred since it embeds a lower concentration of oxidizer. A lower decomposition rate is induced during heating. Slower process allows measurement devices to better capture the reaction taking place. External heating radiates homogeneously over the entire surface of the sample. With the 50% KNO_3 ternary mixture, uniform surface heat-up could potentially lead to violent reaction if autoignition occurs.

At the initial stage of the experiment, radiant heaters rise the temperatures inside the material. Swelling of the structure initiates. The surface of the sample melts and forms a black insulating coating with low permeability. Apart from water vapour, no noticeable emission is recorded from the analyzers during swelling of the material. Decomposition reactions slowly take place in the solid, the protective layer restraining the release of reaction gases while the low thermal conductivity prevents from important temperature rise. Type K thermocouples have been positioned inside the material. In the first 3 minutes, the temperature in the material elevates from 300 K to about 430 K. During the next 23 minutes, the temperature increase does not exceed 60 K. The period coincides with the initiation of the decomposition of the material. The main reactions taking place are endothermic. This explains the slow temperature rise. Given the low temperature inside the material ($T<500K$), one can assume that the gases generated from the decomposition of the powder components are unreactive. About 28 minutes after starting the experiment, the swollen structure breaks due to the overpressure applied on the inside surface by the gaseous products. Within few seconds the temperature elevates up to 800 K. Afterwards, gases are expelled from the sample for about 45 seconds. Major species concentrations are shown on Figure 3.50. The fast and strong increase of species concentrations corresponds to the blow out of the swollen structure. Referring to Pitts findings, the gas temperature is high enough to assume that pyrolysis gases are reactive. First species to be detected are HC. The peak of HC is simultaneous to the start of

CO production. One can assume that HC gets oxidized by O_2 generated from the KNO_3 decomposition to form CO. Pitts explains, in the case of enclosure fires, that oxidation of the fuel to CO requires sufficient concentration of free radicals to initiate the reaction [61]. This explains the first HC increase in Figure 3.50. As the oxidizer decomposes, free radicals get generated. The production of CO starts once enough free radicals are present in the reacting medium. Pitts indicates that the reaction between free radicals with fuel is fast and HC is rapidly oxidized into CO. This explains the decrease of the level of HC once the generation of CO begins [62]. He also stresses that free radicals manifest a preference to react with fuel rather than with CO [11]. As a consequence, in the case of fuel rich mixtures, as long as a significant concentration of HC remains in the mixture, the production of CO is favoured over the generation of CO_2. This assumption is confirmed by the CO/CO_2 ratio curves (cf. Figure 3.31 and Figure 3.33). A consequent amount of incomplete combustion products is present in the gaseous mixture emitted. A comparable behaviour arises on Figure 3.50. CO_2 and CO show similar dynamics and both ascend up to about 5000 ppm. In terms of moles, about as much CO as CO_2 is produced.

Pyrolysis gives information about the nature of the gases released from the decomposition of the powder components. The strength of the reaction indicates that exothermic processes take place. Oxidation of the pyrolysis gases by the O_2 resulting from the oxidizer decomposition occurs. The large concentration of CO reveals that despite the oxidizer, the material clearly highlights a lack of O_2. Because free radicals (e.g. $HO\cdot$, $HO_2\cdot$) react faster with HC than with CO, the condition of a fuel rich mixture promote the formation of CO. Further oxidation of CO into CO_2 supposes residual O_2 to be available.

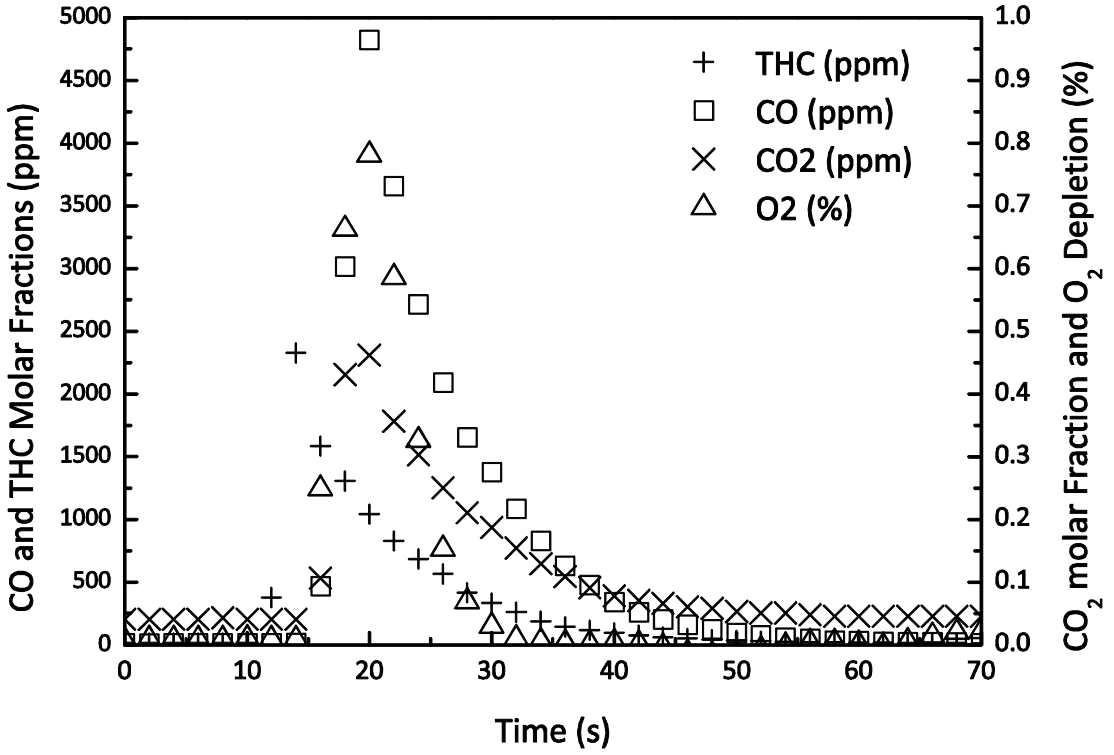

Figure 3.50. Gases Emissions from the pyrolysis of 50% KNO_3 powder under an external heat flux of 10 kW/m^2.

3.6. Concluding Remarks

Thermal analysis gives a fundamental insight on how the chemistry of the powder operates and evolves when the material is submitted to low heating rates ($\Delta T \leq 10\ °C.min^{-1}$). In the context of combustion, the rates of temperature rise achieved exhibit significantly higher order of magnitude (cf. Figure 3.17 and Figure 3.18). Consequently, the different steps of the thermal decomposition of the material overlap each other and can be assumed simultaneous. During combustion, compared to slower thermal decomposition, the reaction rates are enhanced and the energy release can allow the initiations of other reactions and then lead to different kinetics. In order to characterise the combustion, temperature and chemical species evolution, flame and carbonaceous residue structure have been studied. The aim was to investigate the influence of the oxidizer and the reacting atmosphere on the burning performance.

The presence of an internal oxidizer within the composition induces a different combustion behaviour than the one that would be usually observed if only fuel constituents were present

in the mixture. The internal O_2 supply provides intrinsic flaming and smouldering properties to the ternary powders based on lactose, starch and KNO_3 mixtures studied in the present work. Alike conventional fires with the equivalence ratio, the contribution of the oxidizer on the combustion reaction can be "a-priori" assessed by defining various intrinsic parameters. The O_2 balance (%OB), the elemental equivalence ratio based on the elements valance (ϕ_e) or the O_2 ratio (φ_{O_2}) defined by equation (12) constitute valuable indicators to ascertain the degree of completion of the combustion processes taking place. A fuel – oxidizer composition characterised by a fuel concentration in excess is likely to release incomplete combustion products and, potentially, toxic gases or pollutants such as aldehydes or nitrous oxides. Consequently, the information delivered by these intrinsic parameters is essential to be able to predict, prior to any experiment, some critical characteristics of the burning process. They allow an assessment of the potential risks that could be encountered. Furthermore, their calculation constitutes a precious assistance in order to define safely and appropriately experimental setup.

Combustion tests have been carried out using two different models of the FM-Global Fire Propagation Apparatus. In a first stage, temperatures and species emissions were investigated. Experimental tools, such as fire calorimeters, have been developed in order to characterise the physical and chemical evolutions of material undergoing combustion. Their use to provide a detailed description of the burning behaviour of an energetic material had not been attempted yet. Consequently, the first aim of the study was to enquire the ability of the FPA to capture the dynamics of the chemistry resulting from the combustion of the sample powders. It appeared that the reaction times were long enough to allow the measuring instruments to provide accurate responses in terms of temperature, pressure difference, mass loss and species evolution. From the interpretation of the results, a simplified portrait of the overall combustion reaction can be drawn.

The series of experiments that have been performed stressed that the reactions occurring during the combustion process originated from two phases. A smouldering combustion takes place in the condensed phase while gas phase promotes flaming combustion. Reactions were initiated by local hot-spots; heat was transferred inside the material by conduction. As the temperature increases, thermal decomposition activates. Volatiles are generated from the fuels pyrolysis and O_2 is produced by the KNO_3 decomposition. Oxidation in the condensed

phase releases energy and heat gets transfer by conduction and radiation to the virgin material. It allows the smouldering combustion to spread and propagate downward. The propagation of the smouldering front gives rise to the formation of a carbonaceous residue while gaseous products generated elevates by buoyancy. According to the permeability of the char, gases emitted will flow through it and escape or accumulates in the char structure causing the residue to swell. Char oxidation is activated by the buoyant gases produced by the smouldering combustion. If they get released within the reacting atmosphere and if as they diffuse through it, the gaseous mixture reaches flammable condition, flaming combustion is initiated in the gas phase. According to the level of O_2 in the reacting medium, a diffusion or premixed flaming mode takes place. Simultaneously, at the sample surface, smouldering evolved to glowing combustion was heated up to radiating in the visible spectrum.. The latter process is maintained after flameout, as long as the surface temperature of the sample allows the reaction. This indicates that smouldering combustion spreads longer than the flaming ragime. The major gaseous species emitted are CO_2, CO, H_2O and THC. In terms of toxicity, significant amounts of CO are measured when the amount of oxidizer (from air or KNO_3) available was limited. At low temperatures (between 210 and 400°C), traces of aldehydes and formic acids are detected [64]. Nevertheless, species concentrations vary according to "configuration" factors, the proportion of oxidizer in the ternary mixture and the composition of the reacting medium.

3.6.1. The influence of the internal oxidizer concentration

The two different ternary powder compositions allowed the assessment of the contribution of the oxidizer to the combustion process and how the latter is altered by varying the concentration of KNO_3 in the mixture. Considering the same quantity of 40% and 50% KNO_3 ternary powder, the variation in the mass composition in terms of elements lies principally in the C amount rather than in the O element. Then, increasing the concentration of oxidizer reduces the fuel richness of the mixture. This characteristic is easily stressed by evaluating the %OB, ϕ_e or φ_{O_2} intrinsic parameters.

The present analysis has stressed that varying the oxidizer concentration induces several modifications in the overall combustion phenomenon:

– The reaction kinetics increases with the oxidizer concentration. The combustion of 50% KNO_3 ternary mixture engenders higher reaction rates than the 40% KNO_3. Smouldering propagates faster in the reacting medium and transition to flaming occurs earlier with the compositions embedding the highest fraction of KNO_3. Furthermore, higher temperatures are measured in the residual char structure generated by the combustion of the 50% KNO_3 ternary mixture. It indicates an intensity of reaction growing with the proportion of oxidizer.

– The dominating phenomenon is dependent of the oxidizer concentration in the mixture. Experiments conducted under inert atmosphere with the 40% KNO_3 ternary powder showed that the dominant combustion process was smouldering. Furthermore, experiments carried out under air with the same material, smouldering also prevailed from the initiation of the reaction to the transition to flaming. The current analysis underlines that the initiation of flaming is controlled by the kinetics of the smouldering. When increasing the KNO_3 mass fraction up to 50%, a diffusion flame dominated regime prevails.

– The different combustion regimes encountered are characterised by different species emissions. The major products are CO_2, H_2O, CO and HC. Traces of aldehydes and formic acids have been detected. This indicates that the low temperature reactions take place in the solid and that a fraction of smouldering products are only partially oxidized. The production of fully oxidized species (CO_2 and H_2O) rises with the oxidizer concentration. Species are first generated in the condensed phase (smouldering). Gases elevate by buoyancy through the char layer and above, in the supporting atmosphere. A diffusion flame regime develops if flammable conditions are encountered when gases elevates from the structure of the material residue. Results of the tests conducted under N_2 atmosphere stressed that noticeable amounts of CO and THC were produced in the condensed phase. When these species diffuse into the reacting medium, O_2 from ambient air is in large excess to support complete oxidization of most CO and THC. Nevertheless, some quantity of CO and THC do not fully react with O_2 through the established diffusion flame. This feature is enhanced as the concentration of oxidizer is reduced. One suggests two hypotheses to interpret this phenomenon.

- A Damköhler number can be defined as the ratio of a residence time to a chemical reaction time. Reaction rates are lower during the combustion of the 40% KNO_3 ternary mixture than for the 50% KNO_3. Smouldering in the solid phase is less intense for the mixture embedding the lowest concentration of KNO_3. The Damköhler number

might fall beyond a critical value due to a too long chemical reaction, limiting the flame height. Combustible gases such as CO and THC and particles like soot, cannot achieve complete oxidation even if the concentration of O_2 is sufficient to theoretically obtain a complete combustion. As a consequence, noticeable amounts of incomplete combustion products, such as CO and THC, pass through the flame without being oxidized. For the 50% KNO_3 ternary mixture, less incomplete products are engendered. Temperatures in the structure are above 800 K. Gaseous mixture is reactive; in particular, CO oxidation can be achieved.

- The second hypothesis is based on the velocity of the buoyant flow exiting the residue. A low value will allow large dilution of the gases within the reacting medium restricting the region where flammable conditions exist and preventing a proportion of the combustible gases to be further oxidized. The velocity of the buoyant flow is correlated to the reaction rate but it is also affected by the structure of the carbonaceous residue;

The influence of the concentration of oxidizer over the reaction rate affects the velocity of the buoyant flow of smouldering products. One postulates that the variations in gases emissions can be correlated to this buoyant parameter.

– An increase of the mass fraction of KNO_3 in the ternary powder from 40% to 50% is associated with a modification of the char structure. Analysis has shown that given the intensity of the kinetics of the smouldering process, physical properties of the carbonaceous residue differ. A low permeability and porosity describe the residue of the 40% KNO_3 ternary powder. As they could not exit, the smouldering products create a pressure rise resulting in a swelling of the char. On the other hand, the char structure of the 50% KNO_3 ternary powder is characterised by the coalescence of carbon particles which increases its porosity and permeability. The differences of char permeability modify the velocity of the buoyant flow by restricting the surface available for the release of gaseous products. As previously noticed, this affects the initiation and the strength of the flaming regime;

Finally, the burning of the two ternary powders consists in a coupling of two combustion processes: a smouldering combustion and a diffusion flaming dominated combustion. The concentration of oxidizer determines the predominant regime. Under a critical fraction of KNO_3 in the mixture, smouldering constitutes the main phenomenon and governs the initiation of a flaming regime. Above this critical concentration, the combustion becomes dominated by

the flaming regime. Reaction rates, gaseous emissions and char structures differ. This divergence can be explained by a “domino” process. The smouldering reaction rate is related to the proportion of KNO_3 in the mixture. The magnitude of the buoyant flow and the char structure result from the intensity of the smouldering reaction and define the conditions of flaming and consequently, the gaseous emissions. It appears clearly that the concentration of oxidizer is the critical parameter of the combustion behaviour of the studied compositions.

3.6.2. Influence of the reacting atmosphere

The critical parameter characterising the combustion behaviour of the ternary powder based on starch, lactose and KNO_3 mixtures is the internal oxidizer. Nevertheless, comparison of the experiments carried out under various reacting atmosphere for O_2 concentrations between 20.95% (ambient air) and 0% (inert atmosphere) stress that the reacting atmosphere supports the reaction taking place in the gas phase beyond a critical O_2 concentration estimated at 18%. Below this value, the diffusion flame regime is prevented. According to the concentration of oxidizer present in the ternary mixture, smouldering (40% KNO_3 ternary mixture) or premixed flaming (50% KNO_3 ternary mixture) become the main combustion processes. The reduction of the O_2 concentration in the reacting atmosphere appears to be a practical technique to decouple the combustion phenomena. The application of this method allows the estimation of the influence of the smouldering and flaming processes on the kinetics and the nature of the gaseous emissions generated.

By suppressing the diffusion flame, one can identify the nature of the gases when the secondary oxidation is inactive. They form the combustible mixture that undergoes oxidation in the diffusion flame. Beyond the critical O_2 concentration, the combustion products remain unchanged independently of the composition of the reacting atmosphere. They are engendered in the condensed phase (for the 40% KNO_3 and 50% KNO_3 ternary mixtures) and in the gaseous phase if premixed flaming occurs (for the 50% KNO_3 ternary mixture)to be further oxidize if a diffusion regime initiates.

A change in the composition of the reacting atmosphere does not affect the mass loss rate which remains unchanged for a given mixture. For the 40 % KNO_3 ternary mixture, the kinetics of the condensed phase controls the burning rate which remains unaffected by the kinetics of the gaseous phase. The heat feedback generated by the diffusion flame does not modify the

smouldering process. One assumes that the char layer is characterised by a low conductivity and acts as a thermal insulation layer. Furthermore, as the smouldering front propagates downward, the distance between the virgin material and the flame increases reducing the potential effect of an in-depth radiation. Regarding the 50% KNO_3 ternary mixture, the kinetics associated with both smouldering and premixed flame combustion determine the burning rate.

The smouldering (and premixed flaming) combustion generates the combustible gases that burn in the diffusion flame. The flaming mode sustains a secondary oxidation which provides a "cleaner" combustion. Smouldering promotes diffusion flaming. However, diffusion flaming does not support the smouldering mode taking place in the condensed phase. Independently of the composition of the supporting atmosphere, the combustion behaviour of the two ternary powders is governed by the smouldering process. A variation of the combustion kinetics in the condensed phase would modify the entire burning process. On the other hand, a modification of the diffusion flame regime (for example by varying the supporting atmosphere) only involves the kinetics of the gaseous phase but let unaffected the smouldering combustion process.

3.6.3. Final Remarks

The combustion behaviour of the two ternary powders based on lactose, starch (fuels) and KNO_3 oxidizer is characterised by two main processes: a smouldering combustion in the condensed phase and a diffusion flame combustion in the gaseous phase. The analysis has shown that the overall combustion process was controlled by the kinetics of the condensed phase. Varying the concentration of oxidizer in the mixture affects the reaction kinetics which stresses KNO_3 as the critical parameter of the combustion behaviour. The smouldering generated species consists in products oxidized by O_2 resulting from the decomposition of KNO_3. The quantity of oxidizer embedded in the material is too low to theoretically fully oxidize the fuel volatiles. As shown by the experiments carried under N_2 atmosphere, incomplete combustion products are released from the condensed phase and still constitute a combustible mixture. One can represent the whole system as a gas burner whose supply would be the smouldering combustion products. Varying the flow of gases affects the burning behaviour (i.e. the gaseous emissions and the type of flame). However, the flame does not influence the flow of combustible gases. Similar mechanism is observed for the combustion of

the ternary powders. In the present work, the flow of gases is adjusted by the concentration of oxidizer.

Safety issues regarding the manufacture, the use, transport, storage and disposal of an energetic material like a smoke powder based on the composition studied exist as proved by recent accidents. In terms of fire safety, the concern of a combustion reaction involving energetic materials such as the characterised ternary powders is real. Fighting the flame only would not prevent the undergoing of the reaction. Furthermore, experimental results have underlined that toxic emissions are enhanced when the smouldering process is the dominant one. Consequently, the main efforts should be assigned to the limitation of the reactions taking place in the condensed phase. The intensity of the smouldering behaviour is correlated to the KNO_3 concentration. Restricting or suppressing this phenomenon can then be obtained by controlling the contribution of the oxidizer. An evident method would be to stop its thermal decomposition by cooling the reacting medium. Nevertheless if the theory is easy, its application is much more intricate.

Analyses of the thermal evolution and the chemical emissions from the combustion of the two ternary powders have been carried out separately. However, the predominating impression is that in order to characterise the behaviour of the material undergoing combustion, an element linking the two aforementioned variables needs to be defined. Babrauskas [65] suggested that thermal and chemical aspects can be correlated from an energetic angle. Therefore, he illustrated that the heat release rate is a critical predictor of fire hazard. Consequently, the following chapters intend to investigate the energetic issue of the combustion reaction of the studied energetic material.

3.7. References

[1] Turns, S., R., An Introduction to Combustion, 1st Edition, Mc Graw Hill, New York, 1996;

[2] Law, C., K., Makino, A., Lu, T., F., On the Off-Stoichiometric Peaking of Adiabatic Flame Temperature, Combustion and Flame, 145, pp. 808 – 819 (2006);

[3] Bakhman, N., N., A Stoichiometric Coefficient Reflecting the Elemental Composition of Fuel and Oxidizer, Combustion, Explosion and Shock Waves, Vol. 4, 1, pp. 16 – 19 (1968);

[4] Babrauskas, V., Explosives, propellants, pyrotechnics and reactive substances, in: Ignition Handbook, Fire Science Publishers, Issaquah, 2003, pp. 444 – 496;

[5] Jain. S., R., Adiga, K., C., Pai Verneker, V., R., A New Approach to Thermochemical Calculations of Condensed Fuel-Oxidizer Mixtures, Combustion and Flames, 40, pp 71 – 79 (1981);

[6] Jain, S., R., Energetics of Propellants, Fuels and Explosives; A Chemical Valence Approach, Propellants, Explosives and Pyrotechnics, 12, pp 188 – 195 (1987);

[7] ASTM E2058-03, Standard Test Methods for Measurements of Synthetic Polymer Material Flammability Using a Fire Propagation Apparatus (FPA), West Conshohocken, PA: The American Society for Testing and Materials, 2001;

[8] Tewarson, A., Pion, R., F., Flammability of Plastics – I. Burning Intensity, Combustion and Flame, 26, pp. 85 – 103 (1976);

[9] Kovacich, R., P., Martin, N., A., Clift, M., G., Stocks, C., Gaskin, I., Hobby, J., Highly Accurate Measurement of Oxygen using a Paramagnetic Gas Sensor, Measurement Science and Technology, 17, pp.1579 – 1585 (2006);

[10] Holm, T., Aspects of the Mechanism of the Flame Ionization Detector, Journal of Chromatography A, 842, pp. 221 -227 (1999);

[11] Pitts, W., Application of Thermodynamics and Detailed Chemical Modelling to Understanding Combustion Product Generation in Enclosure Fires, Fire Safety Journal, 23, pp. 271 – 303 (1994);

[12] Blackwood, J., D., Bowden, F., P., The Initiation, Burning and Thermal Decomposition of Gunpowder, Proceedings of the Royal Society of London, Series A, Mathematical and Physical Sciences, 213, 1114 (1952), pp 285 – 306;

[13] Lelievre, J., Starch Gelatinization, Journal of Applied Polymer Science, 18, 1, pp 293 - 296 (1973);

[14] Fessas, D., Schiraldi, A., Starch Gelatinization Kinetics In Bread Dough, DSC Investigations on 'simulated' baking processes, Journal of Thermal Analysis and Calorimetry, 61, pp. 411 -423 (2000);

[15] Beyler, C., L., Ignition and Burning of a Layer of Incomplete Combustion Products, Combustion Science and Technology 39, pp. 287 – 303 (1984);

[16] Glassman, I., Combustion, 1st Edition, Academic Press, New York, 1977;

[17] Schefer, R., W., Kulatilaka, W., D., Patterson, B., D., Settersten, T., B., Visible Emission of Visible Hydrogen Flames, Combustion and Flame, 156, Iss. 6, pp. 1234 – 1241 (2009);

[18] Proust, C., Flame Propagation and Combustion in Some Dust-Air Mixtures, Journal of Loss Prevention in the Process of Industries, 19, pp. 89 – 100 (2006);

[19] Gottuk, D., T., Roby, R., J., Beyler, C., L., The Role of Temperature on Carbon Monoxide Production in Compartment Fires, Fire Safety Journal, 24, pp. 315 – 331 (1995);

[20] Gaydon, A., G., Wolfhard, H., G., Flames, Their Structure, Radiation and Temperature, 4th Edition, Chapman and Hall, London, 1979;

[21] NIST Chemistry WebBook, NIST Standard Reference Database Number 69, online resources;

[22] Freeman, E., S., The Kinetics of Thermal Decomposition of Potassium Nitrate and of the Reaction between Potassium Nitrite and Oxygen, Journal of the American Chemical Society, 79, pp. 838 – 842 (1957);

[23] Dosanjh, S., S., Pagni, P., J., Fernandez-Pello, A., C., Forced Cocurrent Smoldering Combustion, Combustion and Flame, 68, pp. 131 – 142 (1987);

[24] Putzeys, O., Bar-Ilan, A., Rein, G., Fernandez-Pello, A., C., Urban, D., L., The role of secondary char oxidation in the transition from smoldering to flaming, Proceedings of the Combustion Institute 31 (2), pp. 2669 – 2676, 2007;

[25] Torero, J. L., Fernandez – Pello, A. C., Forward Smolder of Polyurethane Foam in a Forced Air Flow, Combustion and Flames, 106, pp. 89 – 109 (1996);

[26] Rein, G., Smouldering Combustion Phenomena in Science and Technology, International Review of Chemical Engineering, 1, pp. 3 – 18 (2009);

[27] Drysdale, D., An Introduction to Fire Dynamics, 2nd Edition, Wiley, New York, 1998;

[28] Ohlemiller, T., J., Lucca, T., A., An Experimental Comparison of Forward and Reverse Smolder Propagation in Permeable Fuel Beds, Combustion and Flame, 54, pp. 131 – 147 (1983);

[29] Rogers, F., E., Ohlemiller, T., J., Studies of the Smoldering Combustion of Flexible Polyurethane Cushioning Materials Journal of Fire and Flammability, 9, pp. 5-13 (1978);

[30] Torero, J., L., PhD Thesis, Dept. Mech. Eng., University of California, Berkeley (1992);

[31] Kanury, A., M., Introduction to Combustion Phenomena, 1st Edition, Gordon and Breach, New York, 1975;

[32] Semenov, N., N., Chemical Kinetics and Chain Reactions, Oxford University Press, London, 1935;

[33] Glassman, I.,Yetter, R., Combustion, 4th Edition, Academic Press, London, 2008;

[34] Quintiere, J., G., Surface Flame Spread, in: SFPE Handbook of Fire Protection Engineering, 3rd Edition, The National Fire Protection Association Press, 2002, p. 2-248 – 2-250;

[35] Turns, S., R., An Introduction to Combustion – Concepts and Applications, 2nd Edition, McGraw Hill, London, 2000;

[36] Mowrer, F., W., Section 3 – Chapter 9: Enclosure Smoke Filling and Fire-Generated Environmental Conditions, in SFPE Handbook for Fire Protection Engineering, 4th Edition, National Fire Protection Association, Quincy (Massachusetts), 2008;

[37] Marlair, G., Turcotte. R., Qwok, Q., S., Branka, R., Toxicity Issues Pertaining to Burning Pyrotechnics, Proceedings of the 33rd International Pyrotechnic Seminar, 16 – 21 July, Fort Collins, USA, 2006, pp. 467 – 484;

[38] Brohez, S., Etude Des Feux de Substances Chimiques en Milieu Confiné, PhD Dissertation, Université Polytechnique de Mons, 2002;

[39] Turcotte, R., Fouchard, R., C., Turcotte, A.-M., Jones, D., E., G., Thermal Analysis of Black Powder, Journal of Thermal Analysis and Calorimetry, 73, pp 105 – 188. (2003);

[40] Von Malitz, I., Our Present Knowledge of the Chemistry of Black Powder, Journal of Pyrotechnics, 14, pp. 27 – 39 (2001);

[41] Urbanski, T., Chemistry and Technology of Explosives, Chapter 3, Pergamon Press., Oxford, 1967;

[42] Pitts, W., M., Bryner, N., P., Johnson, E., L., Production Mechanisms for Carbon Monoxide in Enclosure Fires, Combustion Institute/ Central and Eastern States Section, Combustion Fundamentals and Applications, Joint Technical Meeting, March 1993, New Orleans, LA, pp. 102 – 106, 1993;

[43] Di Blasi, C., Combustion and gasification rates of lignocellulosic chars, Progress in Energy and Combustion Science, 35, pp. 121 – 140 (2009);

[44] Hottel, H., C., Williams, G., C., kinetic studies in stirred reactors: Combustion of carbon monoxide and propane, Proceedings of the 10th International Symposium on Combustion, 10 (1), The Combustion Institute, pp. 111 – 121 (1965);

[45] Abam, D., P., S., Carbon Monoxide Oxidation in Laminar Diffusion Flames, Combustion and Flame, 68, pp. 95 – 107 (1987);

[46] Abam, D., P., S., Computation of the aerodynamic field of laminar diffusion flames, Proceedings of the Institution of Mechanical Engineers, London, 198 C, 12, pp. 175 – 187 (1984);

[47] Warnatz, J., Combustion Chemistry, Edited by Gardiner, W., C., Springer, New York, 1984, pp. 224 – 232;

[48] Tucker, D., M., Drysdale, D., D., Rasbash, D., L., The Extinction of Diffusion Flames Burning in Various Oxygen Concentrations by Inert Gases and Bromotrifluoromethane, Combustion and Flame, 41, pp. 293 – 300 (1981);

[49] Ohlemiller, T., J., Smouldering propagation through a permeable horizontal fuel layer, Combustion and Flame, 81, pp.341 – 353 (1990);

[50] Ohlemiller, T., J., Forced smoulder propagation and the transition to flaming in cellulosic insulation, Combustion and Flame, 81, pp. 354 – 365 (1990);

[51] Kansa, E., J., Perlee, H., E., Chaiken, R., F., Mathematical Model of Wood Pyrolysis Including Internal Forced Convection, Combustion and Flame, 29, pp. 311 - 324 (1977);

[52] Bar-Ziv, E., Kantorovich, I., I., Role of porous structure in char oxidation, Applied Thermal Engineering, 18, pp. 991 – 1003 (1998);

[53] Nield, D., Bejan, A., Convection in Porous Media, 3rd Edition, Springer, New York, 2006;

[54] Ohlemiller, T., J., Bellan, J., Rogers, F., E., A Model of Smoldering Combustion Applied to Flexible Polyurethane Foams, Combustion and Flame, 36, pp. 197-215 (1979);

[55] Staggs, J., E., J., Heat and mass transport in developing chars, Polymer Degradation and Stability, 82, pp. 297 – 307 (2003);

[56] Kantorovich, I., I., Bar-Ziv, E., Heat transfer within highly porous chars: a review, Fuel, 78, pp. 279 – 299 (1999);

[57] Ishihara, A., Brewster, M., Q., Sheridan, T., A., Krier, H., The Influence of Radiative Heat Feedback on Burning Rate in Aluminized Propellants, Combustion and Flame, 84, pp. 141 – 153 (1991);

[58] Horton, M., D., Youngberg, L., Z., Effect of radiant energy on the burning rate of a composite solid propellant, AIAA Journal, 8, pp. 1738 – 1741 (1970);

[59] Ibiricu, M., M., Williams, F., A., Influence of Externally Applied Thermal Radiation on the Burning Rates of Homogeneous Solid Propellants, Combustion and Flame, 24, pp. 185 – 198 (1975);

[60] Quintiere, J., G., Fundamentals of Fire Phenomena, Chapter 9: Burning Rate, 1st Edition, Wiley, London, 2006;

[61] Pitts, W., M., Reactivity of Product Gases Generated in Idealized Enclosure Fire Environments, Proceedings of the 24th International Symposium on Combustion, Sydney, Australia, 5 – 10 July 1992, pp. 1737 – 1746;

[62] Pitts, W., M., The Global Equivalence Ratio Concept and the Formation Mechanisms of Carbon monoxides in Enclosure Fires, Progress in Energy and Combustion Science, 21, pp. 197 – 237 (1995);

[63] Chelliah, H., K., Makino, A., Kato, I., Araki, N., Modeling of Graphite Oxidation in a Stagnation-Point Flow Flied Using Detailed Homogeneous and Semiglobal Heterogeneous Mechanisms with Comparisons to Experiments, Combustion and Flame, 104, pp. 469 – 480 (1996);

[64] Marlair, G., Turcotte. R., Qwok, Q., S., Branka, R., Toxicity Issues Pertaining to Burning Pyrotechnics, Proceedings of the 33rd International Pyrotechnic Seminar, 16 – 21 July, Fort Collins, USA, 2006, pp. 467 – 484;

[65] Babrauskas, V., Peacock, R., D., Heat Release Rate: The Single Most Important Variable in Fire Hazard, Fire Safety Journal, 18, pp. 255 – 272 (1992);

4. Principles of Heat Release Rate Estimation

4.1. Heat Release Rate: The Energetic Issue

The two previous chapters have enabled to define the main processes taking place during the combustion of two compositions of ternary powders based on lactose, starch and KNO_3 mixtures. The reaction kinetics and the nature of the species emissions have been investigated individually. At this point, the present study lacks of a parameter that could relate both physical and chemical mechanisms involved in the burning process. Babrauskas has proposed to correlate the thermal and chemical aspects [1] from an energetic angle. Consequently, he introduces the heat release rate (HRR) as a critical predictor of fire hazard.

4.1.1. Origin and Definition

In case of a fire hazard where people might be involved, the essential information that needs to be investigated is the time available before reaching untenable conditions. For several years, one of the aims of the fire community was to determine the parameter that could provide the best prediction on the rate at which an extreme fire environment is created. First, the toxicity pertaining to the combustion of materials was seen as the critical factor that allows understanding the severity of a fire [1]. A study conducted by NIST for the Fire Retardant Chemicals Association (FRCA) and reported by Babrauskas [1] showed that a fire performance could not be well predicted by CO yields. The same work underlined that ignition behaviour was not able to assess the fire evolution. Finally, it was found that the variable that correlated the best with the total emissions of toxic species was the heat release rate. Over the past thirty years, the characterisation of fire behaviour has become closely associated to the estimation of the heat release rate (HRR) [2]. It seems that the HRR has the convenience of carrying enough indicating information while other parameters requires to be combined (for instance, the upper layer temperature with the smoke density and the toxicity) to describe the fire behaviour. According to Tewarson [3], HRR is a relevant indicator for assessing the fire growth rate, fire size, flame height and spread. This explains the strong impulse to develop methods

that allow estimating the HRR. It has to be noticed that HRR is not an intrinsic property of the material and is influenced by external conditions such as ventilation. By definition, the HRR corresponds to the amount of energy release per unit of time and is expressed in kilowatt (kW). Finally, this variable can be seen as the thermal response of a material under conditions of combustion. As stated by Babrauskas, its magnitude provides some insight of the fire development. Temperature rates, burning rate, flame height, smoke density, rate of flame spread, velocity of fuel vapours or radiation from the flame characterise as much fire parameters as can be estimated from the knowledge of the HRR. These latter are some of the variables that are investigated through modelling. Thus, it is not surprising if, nowadays, accurate HRR estimations have become also essential for assessment and validity of developed fire models.

The HRR is one of the most important variables for characterising a fire since most variables associated to tenability can be linked to it [1]. Babrauskas alleged the latter statement while he reported an historical review of bench-scale fire tests. From the 1970's, several small scale apparatuses have been developed offering the possibility to estimate the HRR through different methods. One is a simple principle relying on the measure of the mass loss rate and a heat of combustion. The latter parameter consists in the amount of energy released by unit mass of fuel consumed assuming complete combustion. A second method is based on the measurement of the temperature rise within a control volume. The Ohio State University apparatus (OSU) [4] has been the first calorimeter designed for HRR indirect measurement. T he enthalpy change of the constant flow of air through the apparatus provides an estimation of the HRR. Despite a relatively simple principle, the method was suffering consequent systematic errors due to heat losses. Then, it remained used until the rise of species evolution based methodologies. The first standard method for measuring heat release rates in room fires dates from 1982 and since then, bench scale techniques have been developed for this purpose on the basis of an approach called, Oxygen Consumption Calorimetry (OC) [5] [6]. At the same time, an alternate HRR calculation formula, relying on the CO_2 and CO generation, was defined. Errors related to the system were supposed lower with these two methods than with other HRR estimation principles. The most common calorimeter, integrating the two latter principles, is the Cone Calorimeter[7] [8], which was designed to measure simultaneously the heat release rate, time of ignition, burning rate, smoke production, CO_2, CO and O_2 concentrations. The principles of the Cone Calorimeter have been extended to study flammability parameters for

polymers, standard “fire” fuels and many chemicals [9] by using the FM-Global FPA [10] that has already been presented in the previous part. The main advantage of the FPA over the Cone Calorimeter is that the combustion region is physically delimited by an infrared transparent quartz tube; thus, the incoming flow can be adjusted in order to simulate both under ventilated and well ventilated conditions (i.e. atmosphere poor or rich in O_2).

The gas analysing systems of the Cone and the FPA are appropriate for applying OC and the alternative Carbon Dioxide Generation (CDG) [3] calorimetries. Mass balance or thermal methods can also be processed. Some available HRR calculation principles will be introduced and assessed in section 4.2. Benefits and drawbacks of each technique will be analysed in order to discuss the preferences of the fire community according to the material and the experimental configuration.

4.1.2. Heat Release Rate: an energetic material issue

From the combustion tests performed on the 40% and 50% KNO_3 ternary mixtures at various levels of O_2 concentration in the reacting chamber, one notices again that identical mass losses have been measured for different flame dynamics. The mass loss is controlled by the reactions taking place in the condensed phase. Products evolving in the gaseous phase undergo different kinetics depending on the O_2 concentration of the reacting atmosphere. As a consequence, different chemical emissions are generated which implies various reaction pathways with distinct levels of energy involved. This unconventional behaviour raises questions. According to the described combustion behaviour of the two ternary powders, one can already predict that evaluating the HRR based on usual calorimetric methods such as a mass loss rate or an O_2 consumption principle will be likely to lead to incorrect results. A similar mass loss characterise different chemical kinetics and thus related energy releases. On the other end, one has to wonder the validity of applying a methodology based on the estimation of O_2 consumption when the material itself embedded a quantity of O_2 which participates in the combustion with a possible significant contribution. HRR is a critical variable and it is essential being able to calculate it with acceptable accuracy. One needs to investigate if the HRR can be evaluated using a usual protocol or if calorimetric methods have to be adapted for materials containing oxidizer. Furthermore, whatever the methodology used, the essential point is to be able to assess the most accurate range of error bars. Each methodology relies on stated

approximations assumptions. Most of them have been established for relatively conventional fuels such as methane or solids like PMMA. Their validity limits have not been clearly defined and need to be assessed for materials presenting a different overall combustion processes. This extensive study is carried out in the four next chapters.

4.2. Heat Release Measurement Methodology

Any burning material generates heat. Regarding energetic materials, it is likely that it comes along with smoke but also toxic gases and vapours [11]. Depending on the size of the fire (i.e. the amount of energy released), different scenarios may occur [12]. Thus, the knowledge of the heat release rate of a burning material is essential in order to characterise a fire hazard. Furthermore, the production of smoke particles and toxic gases can be directly linked to this parameter [1] [13]. Different techniques have been developed to evaluate the HRR. Four are presented in the following section. The first one is based on mass loss rate measurement. The second one is the thermal method that is implemented in the OSU apparatus. Finally, the two calorimetric principles, relying on the measurement of species evolution, OC and CDG, are described.

4.2.1. Mass loss rate approach

The HRR does not constitute an intrinsic property of the burning material unlike the heat of combustion, ΔH_c (kJ.g^{-1}). The latter quantity corresponds to the amount of energy, per unit of mass that releases a material when it undergoes complete combustion. In other terms, the heat of combustion is equal to the heat of reaction of a complete combustion, for respective conditions of pressure and temperature of 1 atmosphere (atm) and 298 K. Given a fuel $C_xH_yO_z$, one can write the complete combustion equation,

$$C_xH_yO_z + \eta_{O_2}(O_2 + 3.76\,N_2) \longrightarrow \eta_{CO_2}\,CO_2 + \eta_{H_2O}\,H_2O + 3.76\,\eta_{O_2}N_2 \quad (1)$$

The heat of combustion is then defined at 298 K and 1 atm by,

$$\Delta H_c = \eta_{CO_2}\left(\Delta H_f^{298}\right)_{CO_2} + \eta_{H_2O}\left(\Delta H_f^{298}\right)_{H_2O} - \left(\Delta H_f^{298}\right)_{C_xH_yO_z} \quad (2)$$

If the burning material has been identified and its heat of formation is available in the literature, a theoretical value of ΔH_c can be evaluated. Otherwise, the gross heat of

combustion can be experimentally measured by means of an oxygen bomb calorimeter. Procedure and use are explained in detail in various reports or standards [14] [15]. Concisely, the procedure involves the burning of a small mass of sample (about 1g) sealed in a closed vessel within a compressed O_2 atmosphere of about 30 atm. The vessel is settled in a water bath, instrumented with high precision thermometers. The water is covered by an insulating jacket to reduce heat losses to the environment. An electrical wire, located inside the vessel, induces ignition. The elevation of temperature in the water bath is monitored and represents the heat released accounting for the losses engendered by convective heat exchanges and for the combustion of the ignition wire. However, interesting value for fire applications is not necessary the gross heat of combustion but rather the net heat of combustion where it is assumed that the water remains in a vapour state. It is expressed as,

$$\Delta H_c = \Delta H_c^{gross} - (8.936\, Y_H + Y_W)\Delta h_v \quad (3)$$

Where, Y_H and Y_W are, respectively, the mass fraction of hydrogen in the material and its moisture content; Δh_v is the latent heat of vaporization of water, 2.442 kJ.g^{-1} at 25°C.

As mentioned previously, ΔH_c is an intrinsic material property unlike the HRR. ΔH_c represents the maximum amount of energy, per unit of mass, that can release the material. One can define the HRR on the basis of this parameter. The HRR corresponds to the energy released for a given mass of burning material per unit of time. According to the latter definition, if the mass loss rate is measured, the HRR can be formulated as [16],

$$\dot{q}_{mlr} = \chi\, \Delta H_C\, \dot{m}_{fuel} \quad (4)$$

Where $\dot{m}_{fuel}$ is the mass loss rate of the burning material (kg.s^{-1}) and χ represents the combustion efficiency ($\chi \leq 1$). When the combustion is complete, $\chi = 1$. However, as often in fire scenarios, a fraction of the vapours do not achieve full oxidation. In this case, combustion products such as CO, soot, unburnt hydrocarbons are produced. The heats of formation of incomplete combustion products are lower than the one of CO_2 and H_2O [16]. Consequently, the heat of incomplete combustion reaction ($\chi\, \Delta H_C$) can be significantly lower than ΔH_C. Tewarson reports a large number of values of combustion efficiency, χ, for gases, liquids and solids. Drysdale proposes another approach to estimate the term $\chi\, \Delta H_C$ [16]. Under well ventilated conditions, for most common gases and liquids, χ lies within the range

[0.7 – 1] while for solids, a wider range [0.4 – 0.9] is usually acknowledged ([3], Table 3-4.16) ([16], Table 5.12). Combustion of solids exhibits a lower efficiency because of the more complex chemistry of decomposition of the material. During the combustion, a large number of intermediate products are generated. The potential chemical pathways are increased and are correlated to the combustion process itself. Then, the overall burning regime might differ from the one encountered during the measurement of the heat of combustion because of different reaction conditions. Furthermore, materials that can char on heating will develop a flaming combustion in the gaseous phase coupled to smouldering on the condensed phase. The interaction between the two modes also varies according to the reaction conditions. Consequently, the levels of energy for the effective heat of combustion can diverge from the ones measured for the net heat of combustion. Considering a case of an incomplete combustion where the major gaseous contributors to the HRR are CO_2, H_2O and CO, if the ratio ξ_{CO/CO_2} defined as follow,

$$\xi_{CO/CO_2} = \frac{Y_{CO}}{Y_{CO_2}} \tag{5}$$

is known, one can consider the following reactions;

$$C_xH_yO_z + \left(x + \frac{y}{4} - \frac{z}{2}\right) O_2 \xrightarrow[\Delta H_c]{} x\,CO_2 + \frac{y}{2}\,H_2O \tag{6}$$

$$C_xH_yO_z + \left(\frac{x-z}{2} + \frac{y}{4}\right) O_2 \xrightarrow[\Delta H_{ic}]{} x\,CO + \frac{y}{2}\,H_2O \tag{7}$$

With ΔH_{ic} the heat of reaction for (7). An expression of $\chi\,\Delta H_C$ can be derived,

$$\chi\,\Delta H_C = \frac{\Delta H_c + \xi_{CO/CO_2}\,\Delta H_{ic}}{1 + \xi_{CO/CO_2}} \tag{8}$$

For conditions close to complete combustion, one can assume $\chi \approx 1$. When important amount of CO, unburnt HC are generated, one can wonder how much the combustion efficiency is affected. Table 4.1 shows the evolution of χ according to ξ_{CO/CO_2} in the case of PMMA burning and with the hypothesis where CO is the only incomplete combustion gas considered. The knowledge of the combustion efficiency allows estimating the heat of reaction, also mentioned in Table 4.1. If the oxidation of CO into CO_2 cannot be initiated, CO being an end product, the heat of the incomplete reaction represents only 43% of the energy that would be released for complete combustion. Although the latter decrease seems substantial, it has to be noticed that

this is not a realistic case as CO_2 formation is fully inhibited. A more probable situation, for $\xi_{CO/CO_2} = 1$ (i.e. same production of CO and CO_2), leads to a combustion efficiency of 0.72. It is interesting to calculate the magnitude of the uncertainty on the HRR estimation by use the mass loss rate approach where the ratio ξ_{CO/CO_2} would be ignored. In this case, χ would be taken as 1. The uncertainty of the method has been calculated and results have been reported in Table 4.1. The uncertainty related to the mass loss rate for the present work has been estimated standing within the range of ± 0.1 $g.s^{-1}$. When correctly calibrated, bomb calorimeters provide ΔH_c values with a precision of 0.05% [14]. For complete combustion, it was evaluated that the error can rise up to 17.9%, the main contribution originating from the mass loss rate measurements. One assumes that the precision on the HRR to remain acceptable should not exceed 30%. An error superior to the latter value is reached for $\xi_{CO/CO_2} > 0.5$ (or $\chi < 0.81$).

Table 4.1. Combustion efficiency as a function of the CO/CO_2 ratio and error induced on the HRR by assuming a heat of reaction equal to ΔH_C.for PMMA [17].

ξ_{CO/CO_2}	χ	$\chi\,\Delta H_C$ ($kJ.g^{-1}$)	Error (%)
0	1	24.88	17.9
0.2	0.91	22.52	21.9
0.5	0.81	20.16	31.0
0.8	0.75	18.59	38.3
1	0.72	17.81	42.0
3	0.57	14.27	59.8
5	0.53	13.09	65.9
∞	0.43	10.73	78.1

For conditions close to complete combustion, the uncertainty on the HRR estimation through a mass loss approach is less than 18%. For incomplete combustion, with CO as the main

incomplete species produced, the accuracy decreases if ξ_{CO/CO_2}.is unknown. Non-negligible amounts of CO, unburnt hydrocarbons and soot are generated. The reactions leading to the formation of incomplete combustion compounds release less energy than the ones resulting in the only production of CO_2 and H_2O. The use of equation (4) could lead to a significant overestimation of the HRR. The assumption of a combustion efficiency remaining equal to unity can be hold as a conservative approximation for estimating the HRR. This hypothesis could present a convenience in terms of performance design as the HRR will be overestimated. Nevertheless, this will result in an underestimation of the burning time which can break down the entire fire safety strategy and lead to disastrous consequences.

Furthermore, in the present calculation, it is assumed that ξ_{CO/CO_2} remains constant during the different stages of the fire. This hypothesis does not reflect the reality. Because the ratio ξ_{CO/CO_2} is not an intrinsic characteristic of the burning material but is dependent of configuration factors (such as the ventilation), the chemical composition of the fuel vapours and the combustion products varies during the evolution of the fire. Tewarson [3] and Janssens [6] show that for charring materials such as wood, the heat of combustion change according to the phase of the reaction. While the heat of combustion of volatiles is between 12 and 13 $kJ.g^{-1}$, it raises up to 30 $kJ.g^{-1}$ for the solid char residue. The net heat of combustion of dry wood is in the range of 16 to 18 $kJ.g^{-1}$. In the bomb calorimeter, most of the char is burnt and the value found for ΔH_c is a weighted average of the two types of combustion taking place, one in gaseous phase (flaming), the other one in the condensed phase (smouldering).

The mass loss principle has the potential to provide relevant outcomes but it is strictly dependent on the knowledge of the heat of combustion and the chemical decomposition of the material. The heat of combustion is unfortunately not always available.

4.2.2. Sensible enthalpy rise approach

4.2.2.1. Theoretical method

Another way to estimate the HRR is by conducting a gas phase energy balance between the heat released by the burning material and the rise of enthalpy (temperature) of the mass of air and combustion products within a control volume [18]. Considering an ideal adiabatic system,

as illustrated on Figure 4.1, the energy balance between the heat release by the fire and the supporting atmosphere can be expressed as,

$$Q = m_e \, C_p (T_e - T_o) \tag{9}$$

Where, Q is the total heat release; m_e is the mass of air and combustion products within the control volume; C_p represents the specific heat capacity of the gaseous mixture; T_e is the temperature in the control volume, assumed homogeneous and T_o is the initial temperature of the system.

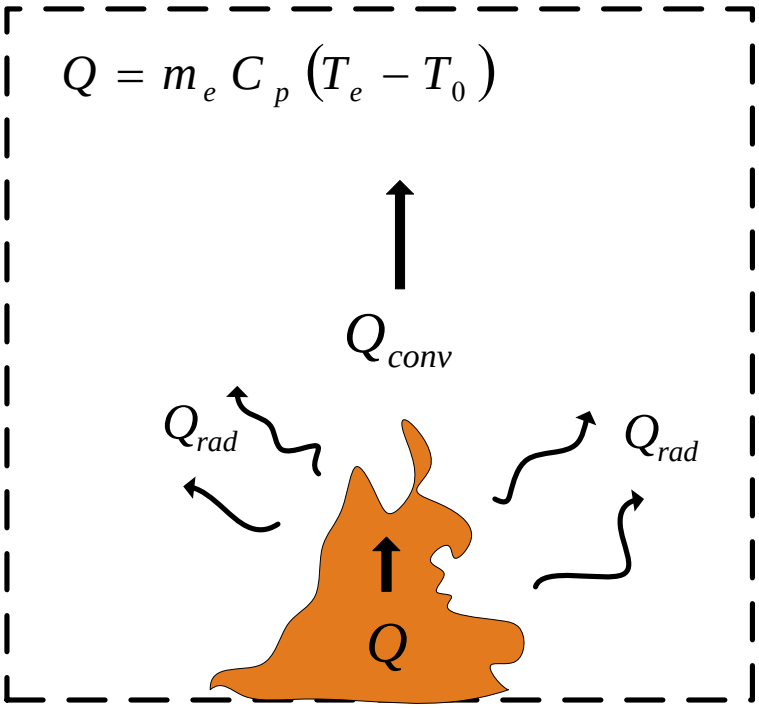

Figure 4.1. Gas phase energy balance within an adiabatic system.

By differentiation of equation (24), the HRR, $\dot{q}_{conv}$, can be determined,

$$\dot{q}_{conv} = \dot{m}_e \, C_p(T_e(t) - T_o) \tag{10}$$

Where $\dot{m}_e$ is the mass flow of air and combustion products passing through the control volume.

The original design of the OSU Release Rate Apparatus developed at the Ohio State University relies on Equation (10). The HRR is estimated from the elevation of temperature $(T_e - T_o)$ of the flow of air and combustion products ($\dot{m}_e = \dot{m}_a + \dot{m}_{fuel}$, with $\dot{m}_a$, the imposed flow of air passing through the OSU and $\dot{m}_{fuel}$, the fuel burning rate) through the apparatus induced by the energy released by the burning of the material. The present method is based on a simple change of enthalpy. It has to be noticed that equation (10) implies the restrictive assumption of an adiabatic system, which is not the case for the OSU apparatus. Consequently, a major issue impacting uncertainty of the method is the evaluation of the heat losses. For flames with high emissivity, such as the ones encountered in sooty fires, the amount of radiation absorbed by the walls of the device becomes significant enough to introduce important errors on the HRR estimation. Smith proposed an expression to account for the transient heat exchange between the air stream and the calorimeter apparatus which entails significant additional temperature measurements and several calibration factors [19]. During the combustion, a fraction of the HRR is absorbed by the apparatus. According to Smith, the heat losses from the flame in the OSU can be expressed as,

$$\dot{q}_{flame,loss} = \dot{q}_{wall\ absorption} + \dot{q}_{exchange\ wall/surrounding} \tag{11}$$

With,

$$\dot{q}_{wall\ absorption} = m \, C_{p,wall} \frac{dT_a}{dt} \tag{12}$$

And,

$$\dot{q}_{exchange\ wall/surrounding} = c \left(T_a - T_{a,\infty}\right) \tag{13}$$

Where, m is the mass of the metal wall (kg); $C_{p,wall}$ is the heat capacity of the metal wall (kJ.kg^{-1}.K^{-1}); c is the convective heat transfer coefficient of the apparatus (kW.K^{-1}) and T_a

represents the apparatus temperature (K), $T_{a,\infty}$ being the initial one (K). Finally, Smith gives the following expression to estimate the HRR,

$$\dot{q}_{OSU} = \dot{m}_e \, C_p(T_e(t) - T_o) + m \, C_{p,wall} \frac{dT_a}{dt} + c \left(T_a - T_{a,\infty}\right) \tag{14}$$

Equation (14) demonstrated good agreement with other HRR calculation methods once the apparatus was correctly calibrated and the correction for the time delay due to the instruments response time was applied [20]. One needs to that the calibration of the OSU consists of an intricate process which nevertheless allows accurate calculation of the HRR.

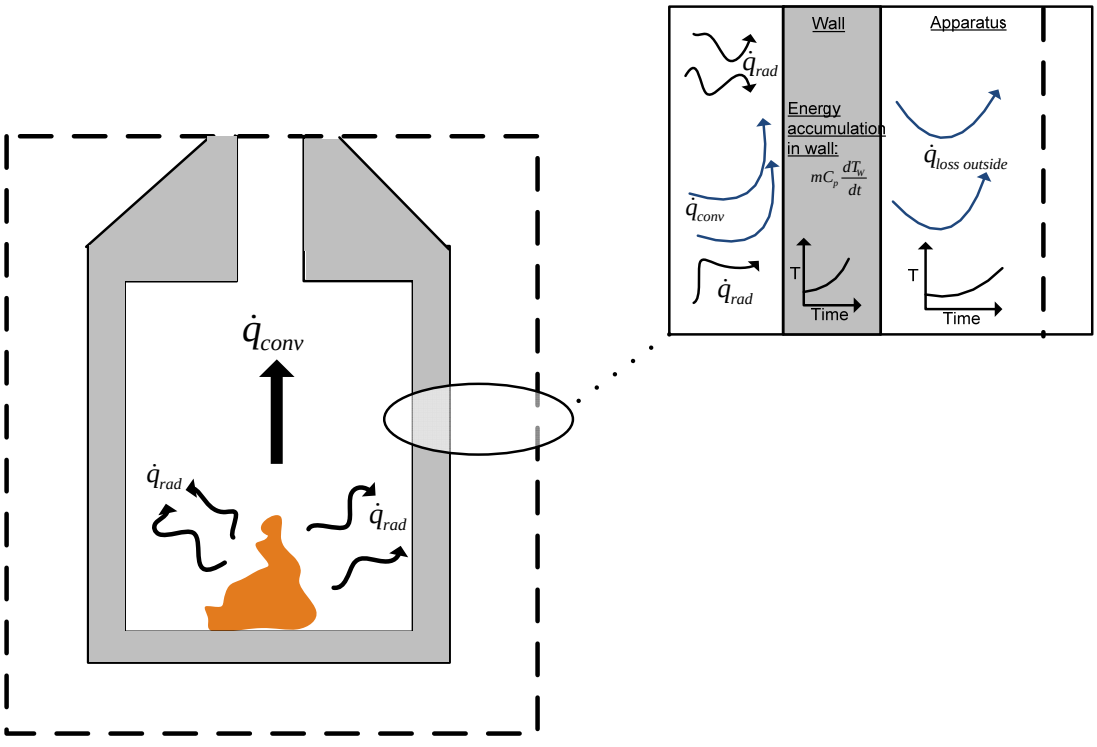

Figure 4.2. Scheme of the OSU describing the inherent heat losses.

4.2.2.2. Uncertainty analysis of the sensible enthalpy rise approach

Performance of the OSU Rate of Heat Release Apparatus has been extensively assessed in the past. Detailed studies are available in the literature [19 - [23]. They principally present comparison analyses between the results obtained by applying the enthalpy rise and the OC approaches when estimating the HRR. One of the main issues of such works is that when the two techniques are exploited on two distinct apparatuses (for example, the cone calorimeter with the OC method and the OSU with the sensible enthalpy rise approach), the differences in the calorimeters design result in different combustion behaviours of the tested material and so, different heat release. Nevertheless, the strategic aim of these comparison works was to prove the relevance of the two HRR approximation methods when both implemented on the same apparatus. In the end, the achievement of a convergence between the results usually raised the opportunity for the authors to promote one method over the other according to their own perspective [20] [21]. As a matter of fact, both approaches encounter pros and cons. The sensible enthalpy rise technique including the heat losses correction is intricate to implement correctly and requires fastidious calibrations. On the other hand, the OC calorimetry, which requires a simpler calibration protocol, relies on the use of an empirical energy constant whose validity can be questioned for combustion reactions involving complex materials.

Paradoxically, the determination of the uncertainty related to the enthalpy rise approach has received significantly less attention than the convergence studies with OC calorimetry whose relevance highly depends on the correctness of calculation assumptions (cf. Chapters 5 and 6). A brief error quantification analysis of the enthalpy rise method is proposed.

4.2.2.2.1. Uncertainty related to the convective HRR

First, one considers the original HRR approximation theory associated with the use of the OSU calorimeter. Equation (10) allows the estimation of the convective HRR. $\dot{m}_e$ is measured by means of an orifice plate. An approximated expression of $\dot{m}_e$is given by [24],

$$\dot{m}_e = C\sqrt{\frac{\Delta P}{T_e}} \tag{15}$$

Where, ΔP is the pressure drop across the orifice plate (Pa), T_e the gas temperature at the orifice plate location (K) and C is the orifice plate coefficient ($kg^{1/2}.m^{1/2}.K^{1/2}$). According to Janssens [24] and Enright [25], C can be assumed constant as long as ΔP and T_e vary within a narrow range during the test. However, for large changes in pressure and temperature, C has to be calculated by applying corrections accounting for the effects of the Reynolds number and the pressure at the downstream side of the orifice plate [26]. The relative uncertainty associated with the calculation of $\dot{q}_{conv}$ is about 7 % when performed by means of the OSU calorimeter (cf. Table 4.2).

Table 4.2. Absolute uncertainties of the parameters included in equation (15) and relative uncertainty of $\dot{q}_{conv}$ when using the OSU calorimeter.

Parameter	Absolute uncertainty
C	δC =0.0004 [ref Enright]
ΔP	$\delta(\Delta P)$ =20 Pa
T_e	δT_e =2 K
	Relative uncertainty
$\dot{q}_{conv}$	~ 7 %

Despite the OSU design allows achieving a good precision on the estimation of $\dot{q}_{conv}$, the heat losses to the walls, if not accounted, constitute a critical source of error. Holding the hypothesis that the losses are fuel independent, one can define a constant loss fraction, χ_r, such as [6],

$$\dot{q}_{flame,loss} \approx \chi_r \dot{q}_{OSU} \tag{16}$$

Combining equations (10) and (16), one expresses $\dot{q}_{OSU}$ a

$$\dot{q}_{OSU} \approx \frac{\dot{m}_e \, C_p (T_e(t) - T_o)}{(1 - \chi_r)} \tag{17}$$

The term χ_r can be estimated from a gas burner calibration of known HRR or from another compound if an accurate HRR approximation can be obtained using a different method (i.e. OC or CDG). Tewarson has estimated χ_r values for manifold materials (cf. Table 4.3 [13, Table 3 – 4. 16). He showed that materials that burn cleanly with little soot formation (non luminous flame) will lie in the range [0.1 – 0.2]. However, a large majority of plastics or aromatic hydrocarbons that burn with a sooty flame present a radiant fraction in the range [0.3 – 0.6]. The interval of χ_r values is large. This indicates that χ_r closely depends on the type of material.

Table 4.3. Loss fraction of heat for various materials [13].

Material	χ_r
Methane (diffusion flame)	0.14
Acetone	0.26
PMMA	0.31
Polyethylene	0.43
Wood	0.38

Given the magnitude of χ_r values compared to $\delta\dot{q}_{conv}$, the overall error is likely to be dominated by the uncertainty of the losses. However, one can attempt to estimate the overall uncertainty associated on the calculation when the convective HRR is only considered. From Tewarson's χ_r values, one can define a distribution characterised by a mean value $\bar{\chi}_r$, and a standard deviation $\delta\chi_r$,

$$\bar{\chi}_r = 0.41 \pm 0.27\ (95\%\ confidence\ ) \tag{18}$$

Finally, using the equation (17), with $\bar{\chi}_r$, the assumed constant loss fraction characterised by the uncertainty $\delta\chi_r$, allows a calculation of the overall error,

$$\%\ \frac{\delta\dot{q}_{OSU}}{\dot{q}_{OSU}} \approx 77\% \tag{19}$$

The uncertainty is too large to rely on an HRR approximation based on the enthalpy rise approach where the estimation of the heat losses would have been neglected. Consequently, implementing the heat losses correction for the radiant fraction is necessary. Furthermore, an estimation of the uncertainty associated with the expression (14) requires to be performed.

4.2.2.3. Uncertainty related to the total sensible enthalpy rise

The difficulty of the error calculation dwells in the evaluation of the uncertainty associated with the terms m, $C_{p,wall}$ and c. They are not directly measured during the experiment but evaluated prior to it through two calibrations procedures described by Smith [19] and Filipczak [20]. The best method to assess the uncertainty related to m, $C_{p,wall}$ and c would be to combine the uncertainties associated with the measurements required to assess these data and the uncertainties pertaining from the calibration protocol. The latter can be performed by creating a distribution of the m, $C_{p,wall}$ and c values, defining the averages $\overline{m}$, $\bar{C}_{p,wall}$ and $\bar{c}$ and their respective standard deviations as absolute errors, σ_m, $\sigma_{C_{p,wall}}$ and σ_c. However, this distribution analysis could not be performed in the present work due to a lack of experimental data.

The error analysis is only focused on the measurements involved in the calculation of m, $C_{p,wall}$ and c. The calibration assumptions have been considered with no contribution on the uncertainty evaluation.

According to works of Smith [19] and Filipczak [20], one can rewrite equation (14) by introducing the expressions used to assess m, $C_{p,wall}$ and c through the calibration protocol,

$$\dot{q}_{OSU} = \dot{q}_{conv} + m\,C_{p,wall}\frac{dT_w}{dt} + \frac{\dot{q}_{burner} - \dot{q}_{conv}}{\Delta T_{a,\infty}^{calib}}\left(T_a - T_{a,\infty}\right) + \frac{\dot{q}_{conv}\left(1 - \frac{1}{\Delta T_{a,\infty}^{calib}}\right) + \frac{\dot{q}_{burner}}{\Delta T_{a,\infty}^{calib}}}{\left(\frac{dT_a}{dt}\right)_{calib}}\frac{dT_a}{dt} \quad (20)$$

Where, $\dot{q}_{burner}$ is the constant HRR delivered by a methane gas burner (kW), $\Delta T_{a,\infty}^{calib}$ is the temperature change of the apparatus measured during the calibration process (K), $\left(\frac{dT_a}{dt}\right)_{calib}$ is

the temperature gradient in the apparatus at t → 0 during the calibration process where an imposed heat flux was set.

Regarding expression (20), $\dot{q}_{conv}$ and $\dot{q}_{burner}$ are independent variables, as well as from T_a. However, covariance terms need to be considered for $T_a, \Delta T_{a,\infty}^{calib}, \frac{dT_a}{dt}$ and $\left(\frac{dT_a}{dt}\right)_{calib}$. Finally, the uncertainty is calculated using the described expression:

Defining a function, $y = f(x_1, x_2, x_3 \dots, x_N)$, the uncertainty δy is given by,

$$\delta y = \sqrt{\sum_{i=1}^{N}\left(\frac{\partial y}{\partial x_i}\delta x_i\right)^2 + 2\sum_{i=1}^{N-1}\sum_{j=i+1}^{N} r(x_i, x_j)\frac{\partial y}{\partial x_i}\frac{\partial y}{\partial x_j}\delta x_i\,\delta x_j} \quad (21)$$

Where, $r(x_i, x_j)$ is the correlation coefficient of the couple of measurements (x_i, x_j) and has been assumed equal to 1 for all the dependent variables. The calculation is based on a 4.3 kW methane fire. Results are presented in Table 4.4.

Table 4.4. Uncertainty calculation of the total sensible enthalpy $\dot{q}_{OSU}$.

Parameters	Absolute uncertainty (*relative uncertainty*)
$\dot{q}_{burner} (= 4.3\ kW)$	$\delta\dot{q}_{burner} =$ 0.4 kW *(~9%)*
$\dot{q}_{conv}$ $(\sim 3.7\ kW)$	$\delta\dot{q}_{conv} =$ 0.3 kW *(~7%)*
T	$\delta T =$ 2 K
ΔT	$\delta\Delta T =$ 3 K
$\frac{dT_a}{dt}$	$\delta\frac{dT_a}{dt} =$ 0.05 K.s^{-1}
	Total relative uncertainty
	$\delta\dot{q}_{OSU} =$ ~ 18 %

According to the uncertainty analysis, the sensible enthalpy rise approach is estimated within a ± 18% range. This value only considers the error related to the measurements required to calculate $\dot{q}_{OSU}$. The calculation assumptions have not been considered. Nevertheless, if the intricate calibration protocol is adequate to provide pertinent and accurate estimations of the necessary parameters in equation (14) (m, $C_{p,wall}$ and c), the uncertainty analysis shows that the sensible enthalpy rise approach offers reliable HRR approximations.

The limitation of the mass loss approach and the complexity of estimating accurately the heat losses of the energy conservation methods encouraged researchers to develop a methodology based on species conservation. The potential use of any method to establish the HRR needs to be assessed on the basis of a comparison between the potential errors embedded in the methodology. These errors have been carefully estimated for the mass loss [6] and the energy conservation [19] [20] methods but not for the species conservation approach.

4.2.3. Species Evolution Approach: Theoretical principle

4.2.3.1. Origins

Although suggested in the 19th century [27], it has been acknowledged that the species evolution approach originates from Thornton's principle [28]. In 1917, Thornton established that for a large number of organic liquids and gases, the amount of energy released by a burning material for a complete combustion was proportional to the amount of O_2 consumed by the reaction. Given the reaction of complete combustion for a chemical $C_xH_yO_z$,

$$C_xH_yO_z + \nu_{O_2}(O_2 + 3.76\,N_2) \longrightarrow \nu_{CO_2}\,CO_2 + \nu_{H_2O}\,H_2O + 3.76\,\nu_{O_2}\,N_2 \quad (22)$$

Then, Thornton's principle can be expressed as,

$$\frac{\Delta H_c\, M_{C_xH_yO_z}}{\nu_{O_2}} = E_{O_2} \qquad \text{with } E_{O_2} \approx constant \quad (23)$$

Later in the 1970s, Tewarson developed a similar postulate based on the generation of CO_2 [13]. It is of interest to compare these observations with the HRR calculation based on the mass loss approach presented in section 4.2.1. Recalling equation (4) and assuming a complete combustion reaction (i.e. $\chi = 1$), HRR is proportional to the amount of fuel burnt, the

proportional coefficient being ΔH_c. According to the reaction of complete combustion for a chemical $C_x H_y O_z$ given in (22), one can formulate relations of the fuel burning rate as a function of the O_2 consumption or the CO_2 generation. Expressions are given by,

$$\dot{m}_{fuel} = \frac{\Delta \dot{m}_{O_2} M_{fuel}}{\nu_{O_2} M_{O_2}} \tag{24}$$

and

$$\dot{m}_{fuel} = \frac{\Delta \dot{m}_{CO_2} M_{fuel}}{\nu_{CO_2} M_{CO_2}} \tag{25}$$

Where,

$$\Delta \dot{m}_{O_2} = \dot{m}^0_{O_2} - \dot{m}_{O_2} \tag{26}$$

$$\Delta \dot{m}_{CO_2} = \dot{m}_{CO_2} - \dot{m}^0_{CO_2} \tag{27}$$

They, respectively, represent the O_2 consumption (26)) and the CO_2 generation (27), $\dot{m}^0_{O_2}$ ($\dot{m}^0_{CO_2}$) being the mass flow rate of O_2 (CO_2) from the entrained air and can be defined as the air flowing through the exhaust duct when no combustion occurs.

Equation (4) can be rewritten using expressions (24) and (25). If the HRR is estimated based on the consumption of O_2, the expression becomes,

$$\dot{q} = \Delta H_c \frac{\Delta \dot{m}_{O_2} M_{fuel}}{\nu_{O_2} M_{O_2}} = E_{O_2} \Delta \dot{m}_{O_2} \tag{28}$$

With $$E_{O_2} = \frac{\Delta H_C M_{fuel}}{\nu_{O_2} M_{O_2}} \tag{29}$$

If the HRR is estimated based on the production of CO_2 from the reaction, equation (4) evolves into,

$$\dot{q} = \Delta H_c \frac{\Delta \dot{m_{CO_2}} M_{fuel}}{\nu_{CO_2} M_{CO_2}} = E_{CO_2} \Delta \dot{m}_{CO_2} \tag{30}$$

With $$E_{CO_2} = \frac{\Delta H_C M_{fuel}}{\nu_{CO_2} M_{CO_2}} \tag{31}$$

A dimension analysis of coefficients E_{O_2} and E_{CO_2}shows that they characterise the amount of energy release per unit mass, respectively, of O_2 consumed and CO_2 generated. They are defined as energy coefficients. For a given fuel, one mole of O_2 consumed (or CO_2 produced) releases a certain amount of energy. One can notice that equation (29) corresponds to Thornton's principle expressed in (23). Equations (28) and (30) agree with Thornton and Tewarson statements if $\mathrm{E}_{\mathrm{O}_2}$ and E_{CO_2} remain relatively constant for any material. Both expressions form the basis of the calorimetric methodology and are respectively referred as Oxygen Consumption Calorimetry (OC) [5] and Carbon Dioxide Generation Calorimetry (CDG) [13].

Formulas (28) and (30) stress that the basic hypotheses to estimate HRR hinge on the knowledge of energy constants and the ability to measure the evolution of combustion gases concentration. The reason why these two techniques became widely used for HRR evaluation (especially the OC calorimetry) stem from the assumption that for a large number of organic solids, liquids and gaseous compounds, values found for E_{O_2} and E_{CO_2}appear to be approximately constant. Energy constants estimated by Huggett [29] and Tewarson [13] have been gathered in Table 4.5 and Table 4.6. Average values and standard deviations have been calculated. It came that,

$$\bar{E}_{O_2} = 13.09 \pm 0.64 \text{ kJ.g}^{-1} \text{ of } O_2 \quad (32)$$

$$\bar{E}_{CO_2} = 13.32 \pm 1.76 \text{ kJ.g}^{-1} \text{ of } CO_2 \quad (33)$$

The standard deviations of the sets of energy coefficients values evaluated by Huggett and Tewarson correspond to 5% of $\bar{E}_{O_2}$and 13% of $\bar{E}_{CO_2}$. Accounting for the only materials considered in Table 4.5 and Table 4.6, based on the standard deviations, it appears that the E_{O_2} and E_{CO_2}can be restricted within a relatively narrow range of values. Huggett and Tewarson underline that the process occurring during the combustion of these materials is the breaking of C-C, C-H and O=O bonds which require approximately the same amount of energy and the formation of C=O and O-H bonds which releases heat.

First consider, arbitrarily, that an estimation of HRR requires an uncertainty less than 30% to be considered accurate enough. One can estimate the maximum uncertainty acceptable on the species evolution terms ($\Delta\dot{m}_{O_2}$ and $\Delta\dot{m}_{CO_2}$). Simple error calculation indicates that, if

energy constants values are used, uncertainties on $\Delta\dot{m}_{O_2}$ and $\Delta\dot{m}_{CO_2}$ should not exceed, respectively, 29.5% and 27%. Several studies relative to the propagation of uncertainty for HRR estimation by means of OC and CDG calorimetry estimated that errors on $\Delta\dot{m}_{O_2}$ or $\Delta\dot{m}_{CO_2}$ were less than 20% [25] [30] [31]. Consequently, the assumption of energy constant, $\bar{E}_{O_2}$ and $\bar{E}_{CO_2}$, can be considered as valid, at least, within the range of species reported in Table 4.5 and Table 4.6. Longer discussion about the assumption of energy constants will be developed in the next chapter.

The main advantage of OC and CDG compared to a mass loss approach is that they allow calculating the HRR even without a detailed chemistry of the materials of interest. If the hypothesis of energy constants can be applied, the only basic requirements end up to be accurate evaluations of the O_2 consumption or the CO_2 production depending on the method used. They can be performed by collecting all gases through an exhaust duct once homogeneous mixing is achieved. Apparatuses such as the Cone Calorimeter, developed in NIST by Babrauskas [7] [8] or the FM-Global Fire Propagation Apparatus (FPA) [10] developed by Tewarson have been specially designed to allow these measurements. The gas collection system of both devices is relatively similar. A hood system topped the “reaction zone”. It has been dimensioned so that all the combustion gases are sucked up. From the hood, the system narrows to an exhaust duct to ensure gases mixing. Further down, volumetric flow rate is measured by a Pitot tube and gas sampling is operated. Gases pass through a soot filter and a cold trap. They are continuously distributed to a set of different analysers. The O2 concentration is estimated through a paramagnetic analyser while CO/CO_2 concentrations are determined using an infrared technology. Adding instrumentation for measuring CO, Total unburned Hydrocarbon (THC) and soot enable to improve the accuracy of the results [24]. As regards the THC measure, a Flame Ionization Detector (FID) device is used. A laser beam at λ = 632 nm is projected along the exhaust duct in order to evaluate the extinction and the smoke molar fraction. The main distinctions between the two calorimeters lie in the combustion enclosure. The heating and ventilation systems are significantly different. The radiation spectrum f a fire depends on its size. For a well ventilated fire, an important fraction of radiation is emitted at wavelengths characteristic of CO_2 and H_2O. For under ventilated combustion conditions, a sooty fire is likely to arise. Radiation can be approximated by a grey body radiation. The temperature for such radiation is around 1000°C. A conical electrical radiant heater has been implemented above the sample on the cone calorimeter. It presents

radiative characteristics close to the ones of a grey body and a high emissivity [7] [8] [32]. On the FPA, the resistance heater has been replaced by infrared tungsten filament tubular lamps implemented inside a compact reflector body and located around the sample in a position such that the heat flux impinges the surface of the material homogeneously [10]. Radiating temperature is about 2205°C. Wavelengths beyond 2 µm are absorbed by the quartz bulb envelope and the window of the reflector. The spectral energy peak is at 1.15 µm so in the near infrared. The spectral distribution at such temperatures can diverge from one operating at 1000°C. The degree of discrepancy depends on the material absorbance. This can potentially affect the sample ignition [32]. In order to avoid dependency on wavelengths of the material absorbance, Tewarson suggests covering the surface of the sample with a black paint or fine graphite powder [13]. The second major difference between the two apparatuses stems from the combustion area. The combustion zone of the FPA is restricted by the quartz tube. On the other hand, the latter has been designed such a way, that, once the control volume within the quart tube has been insulated from the outside environment, the composition of the reacting atmosphere can be varied by means of flow meters. For instance, the concentration of O_2 can be modified in order to be in low or high O_2 atmosphere. This feature was particularly interesting given the context of the present work from the energetic materials prospect. As they carry their own oxidizer, reducing the O_2 level within the reacting medium allowed investigating both contributions from oxidizer and supporting atmosphere. The FPA has been selected for the current study as presenting several significant advantages according to the peculiarity of energetic materials. However, the measurement procedure of the species evolution for both calorimeters is similar and will be introduced in the following.

4.2.3.2. Theoretical principles

The bases of OC and CDG calorimetry have been introduced. Both principles rely on the knowledge of energy constants and the ability to measure the consumption of O_2 in the case of OC and the generation of CO_2 regarding the CDG. Before presenting the calculation protocol of OC and CDG, it needs to be emphasized that both methods require the validity of several assumptions to be applied. These hypotheses are presented first.

4.2.3.2.1. Assumptions

OC and CDG methods constitute approximate HRR calculation procedures. They require series of assumptions that are presented in the continuation.

1. Energy coefficients for OC and CDG can be approximated by constants. For OC, Huggett estimated the constant to be [29],

   $\bar{E}_{O_2} = 13.1 \pm 0.7$ kJ.g^{-1} of O_2 (34)

   When applying CDG calorimetry, Tewarson suggests using a constant [13],

   $\bar{E}_{CO_2} = 13.3 \pm 1.5$ kJ.g^{-1} of CO_2 (35)

   These values are valid within a range defined by their standard deviation.

2. Gases behaviour is assumed to follow ideal gas law (i.e. for identical pressure and temperature, one mole of two different material occupy the same volume);

3. Gases accounted for the calculations consist of N_2, O_2, CO_2, H_2O, CO, unburnt HC. They represent 99% of the exhaust gases according to Janssens [33].Every other gas is considered to behave as inert and is assimilated to N_2;

4. N_2 and gases assimilated to N_2 do not take part in the combustion reaction;

5. Chemistry associated with the release of energy is assumed to be a one step chemical reaction such as,

   $$C_xH_yO_z + \nu_{O_2}O_2 + \nu_{N_2}N_2 \longrightarrow \nu_{CO_2}CO_2 + \nu_{CO}CO + \nu_{THC}THC + \nu_{H_2O}H_2O + \nu_{N_2}N_2 \quad (36)$$

6. The calorimeter is designed in a way that gases are perfectly mixed in the exhaust duct before being collected for concentration measurements;

7. The flow within the exhaust duct is laminar. No significant velocity discrepancies are encountered so an average flow rate can be estimated and considered as a characteristic parameter;

8. Combustion gases are measured on a dry basis. Water vapour has been removed from the gaseous mixture prior to concentration measurement. Species Concentrations are expressed as molar fraction:

$$X_i = \frac{\dot{n}_i}{\dot{n}_e} \quad (37)$$

Where, $\dot{n}_i$ and $\dot{n}_e$ are, respectively, the mole flow rate of the species i and the total mass flow rate of the exhaust gases (i.e. combustion gases + residual air).

9. Response times of the analysers are low enough to capture evolutions in the chemistry of the combustion reaction;

10. Water vapour is measured if an analyser is integrated to the measuring system. Otherwise, the water vapour formed during the combustion is neglected in the calculations;

If all these assumptions can be applied, OC and CDG calorimetry predict relevant and accurate estimation of the HRR. The methodology is described below.

4.2.3.2.2. Methodology

Recalling equations (28) and (30) and assuming the hypotheses defined previously (section 4.2.3.2.1) valid, the relevance of the HRR calculations highly depends on the precision of the concentration measurements flowing across the exhaust duct.

Calculation of species concentration evolutions

Consumption or generation rate of a species i corresponds to the variation in concentration of the aforementioned species as it flows through the control volume between the moment it enters and the moment it exists. Combustion reaction consumes O_2 from air and produce CO_2. Then, the O_2 (CO_2) consumption (generation) constitutes the difference in O_2 (CO_2) concentration between the entrained air and the exhaust gases mixture. Given the above definition, species evolution of a species i can be expressed as,

$$\Delta\dot{m}_i = \left|\dot{m}_\iota - \dot{m}_i^0\right| \quad (38)$$

Where $\dot{m}_i^0$ and $\dot{m}_\iota$ are, respectively, the mass flow rates of species i entering and exiting the control volume. Considering the control volume defined as the combustion enclosure of the calorimeter, the mass flow of air entrained (or supporting atmosphere) corresponds to the entering stream while the exhaust gases mass flow is illustrated by the exiting stream as

illustrated on Figure 4.3. Nevertheless, $\dot{m}_i$ and $\dot{m}_i^0$ cannot be measured directly. They are determined from species molar fractions using the following expression,

$$\dot{m}_i = \frac{X_i M_i}{M_e}\,\dot{m}_e \tag{39}$$

Where X_i is the molar fraction of species i; M_i is the molecular weight of i; M_e is molecular weight of the exhaust gases and can be expressed as,

$$M_e = \sum_j X_j\, M_j \qquad \text{(With } j\text{the different species present in the exhaust gases according to assumption 3)} \tag{40}$$

$\dot{m}_e$ is the mass flow rate of exhaust gases. An expression is given by,

$$\dot{m}_e = \rho_e\, \dot{V}_e \tag{41}$$

With ρ_e, the exhaust gases density, expressed as,

$$\rho_e = \frac{P_e M_e}{R T_e} \tag{42}$$

P_e and T_e being, respectively, the pressure (Pa) and the temperature (K) measured in the exhaust duct.

Conditioned to the validity of assumption 7, a measure of the volume flow rate, $\dot{V}_e$, can usually be evaluated using an averaging Pitot tube [10] located in the test section of the exhaust duct,

$$\dot{V}_e = K\, A \sqrt{\frac{2\Delta P}{\rho_e}} \tag{43}$$

Where ΔP is the pressure difference across the averaging Pitot tube; A is the cross section of the exhaust duct and $K$the flow profile coefficient relative to the averaging Pitot tube. From equations (41) and (43), it comes that,

$$\dot{m}_e = KA \sqrt{2\, \rho_e\, \Delta P} \tag{44}$$

Knowledge of $\dot{m}_e, M_e$ and X_i allows to calculate $\dot{m}_i$. The only remaining unknown variable from equation (38) is $\dot{m}_i^0$, corresponding to the mass flow rate of species i in the entrained air

(or supporting atmosphere). According to equation (39) and the definition of the variable, an expression arises,

$$\dot{m}_i^0 = \frac{X_i^0 M_i}{M_a} \dot{m}_a \tag{45}$$

With X_i^0 the molar fraction of species i in the entrained air, $M_a$the molecular weight of air and $\dot{m}_a$, the mass flow rate of entrained air. Two different procedures can be applied to estimate $\dot{m}_a$. Depending on the configuration of the experiment, one can be more reliable, accurate and/or convenient than the other. Both are introduced in the following.

Conservation of N_2 (Non production of N_2 during the reaction)

According to assumptions 3 and 4, N_2 is considered as inert. Based on this hypothesis, N_2 conservation is expected. This can be formulated as,

$$\dot{n}_{N_2}^o = \dot{n}_{N_2} \tag{46}$$

$$\Leftrightarrow X_{N_2}^0 \frac{\dot{m}_e}{M_e} = X_{N_2} \frac{\dot{m}_a}{M_a} \tag{47}$$

Consistent with assumption 3, one can express N_2 molar fraction as,

$$X_{N_2} = 1 - X_{O_2} - X_{CO_2} - X_{CO} - X_{THC} - X_{H_2O} \tag{48}$$

From equations (47) and (48), one can write a first expression for the mass flow rate of entrained air,

$$\dot{m}_a = \frac{\left(1 - X_{O_2} - X_{CO_2} - X_{CO} - X_{THC} - X_{H_2O}\right)}{\left(1 - X_{O_2}^0 - X_{CO_2}^0 - X_{H_2O}^0\right)} \frac{M_a}{M_e} \dot{m}_e \tag{49}$$

O_2 depletion and expansion factor

The second procedure that allows estimating $\dot{m}_a$ is based on the amount of O_2 depleted by the combustion. During the reaction, combustion gases will be produced and a part of O_2 from the air entrained will be consumed. Considering reaction equation (22), for each mole of fuel burnt, υ_{O_2} moles of O_2 are consumed while $\upsilon_{CO_2} + \upsilon_{H_2O}$ moles of combustion gases are

generated. There is a chemical expansion due to the reaction. Applying the conservation of mass, the relation between $\dot{m}_e$ and $\dot{m}_a$ can be written as],

$$\frac{\dot{m}_e}{M_e} = \frac{\dot{m}_a}{M_a} - \frac{\Delta\dot{m}_{O_2}}{M_{O_2}} + \beta\frac{\Delta\dot{m}_{O_2}}{M_{O_2}} \tag{50}$$

With $\beta = \frac{\sum \nu_{products}}{\nu_{O_2}}$, expression of the gaseous expansion (51)

The depletion factor ϕ, and the expansion factor, α are introduced. ϕ is the fraction of the entrained air that is fully depleted of its oxygen during the combustion process and is given by the following expression[5]:

$$\phi = \frac{\dot{m}^0_{O_2} - \dot{m}_{O_2}}{\dot{m}^0_{O_2}} = \frac{X^0_{O_2}\left(1 - X_{H_2O} - X_{CO_2} - X_{CO} - X_{THC}\right) - X_{O_2}\left(1 - X^0_{H_2O} - X^0_{CO_2}\right)}{X^0_{O_2}\left(1 - X_{O_2} - X_{H_2O} - X_{CO_2} - X_{CO} - X_{THC}\right)} \tag{52}$$

The expansion factor α, is defined as follow [5],

$$\alpha = 1 + X^0_{O_2}(\beta - 1) \tag{53}$$

Finally, expressions (52) and (53) allow rewriting equation (50) as follow,

$$\dot{m}_e = \dot{m}_a\frac{M_e}{M_a}\left(1 + \phi(\alpha - 1)\right) \tag{54}$$

The main difference between the expressions (49) and (54) stems from the coefficient α. Calculating α supposes the knowledge of the chemical reaction taking place. Parker [5] proposes an intricate expression of α depending on the depletion factor ϕ and the stoichiometric coefficient of the combustion reaction. On the other hand, when the composition of the burning material is not known, Janssens suggests using an average value $\bar{\alpha} = 1.105$ (which corresponds to methane). Expression (49) relies on assumptions 3 and 4. It has to be noticed that expression (52) of the O_2 depletion factor requires also the validity of the same assumptions to be applicable. In the end, the uncertainty related to the estimation of α would suggest to favour the procedure based on the N_2 conservation. An error calculation will be carried in Chapter 6 to assess the limitations of both formulas. However, one can comment that when ASTM [8] [10] or ISO [7] standards are followed, the exhaust mass flow

rate has to comply with a minimum of about 0.12 kg.s^{-1}. Usually, the maximum mass loss rates measured do not exceed few g.s^{-1}. Two orders of magnitude separate these two values ($\dot{m}_a \gg \dot{m}_{volatiles}$). To some extent, when high precision is not required and if standard recommendations are followed, the approximation $\dot{m}_e \approx \dot{m}_a$ can be done.

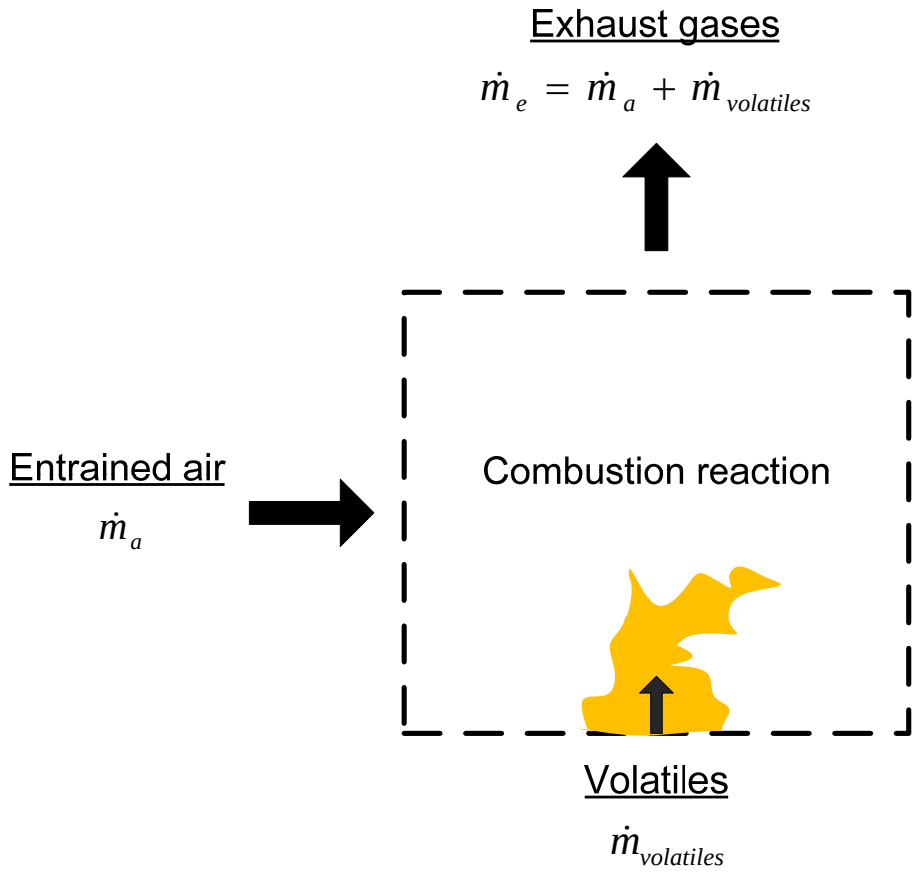

Figure 4.3. Combustion system and control volume for mass conservation.

Formulas (38) to (54) allow an expression to estimate species concentration evolutions,

$$\Delta\dot{m}_i = \left|\frac{X_i M_i}{M_e}\dot{m}_e - \frac{X_i^0 M_i}{M_a}\dot{m}_a\right| \tag{55}$$

Recalling assumption 8, combustion gases are measured on a dry basis; water vapour has been removed. Then, molar fractions are expressed as,

$$X_i = \left(1 - X_{H_2O}\right)X_i^A \tag{56}$$

Where X_i^A corresponds to the molar fraction measured by the analyser. Expression (56) implies the introduction of the water vapour molar fraction term in equation (55). The water vapour in the entrained air corresponds to its moisture content and is given by,

$$X_{H_2O}^0 = \frac{\%RH}{100}\frac{P_{sat}(T_{amb})}{P_{amb}} \tag{57}$$

During the combustion, water vapour is one of the major reaction products. X_{H_2O} can be measured by means of an infrared analyser. Janssens and Parker [5]], consider the contribution of the water vapour on the HRR estimations to be negligible. Parker estimates that for a relative humidity of 50% at 20°C in the air, the error induced by neglecting the ambient water vapour (i.e. $X_{O_2}^0 = X_{O_2}^{A^0}$) was less than 1%. Janssens suggests not considering the water vapour generated by the combustion reaction (i.e. $X_{H_2O} = X_{H_2O}^0$). Brohez [34] proposes to model the water vapour molar fraction based on a H_2O mass balance. Apart from H_2O, if the two other major combustion products are CO_2 and CO, then, the combustion can be modelled by the two reactions,

$$C_xH_yO_z + \left(\mathrm{x} + \frac{\mathrm{y}}{4} - \frac{\mathrm{z}}{2}\right)O_2 \longrightarrow \mathrm{x}\,CO_2 + \frac{\mathrm{y}}{2}\,H_2O \tag{58}$$

and

$$C_xH_yO_z + \left(\frac{\mathrm{x}}{2} + \frac{\mathrm{y}}{4} - \frac{\mathrm{z}}{2}\right)O_2 \longrightarrow \mathrm{x}\,CO + \frac{\mathrm{y}}{2}\,H_2O \tag{59}$$

From reaction equations (58) and (59), the H_2O mass balance can be derived,

$$X_{H_2O}\frac{\dot{m}_e}{M_e} = X_{H_2O}^0\frac{\dot{m}_a}{M_a} + \left(\frac{\Delta\dot{m}_{CO_2}}{M_{CO_2}} + \frac{\dot{m}_{CO}}{M_{CO}}\right)\frac{y}{2x} \tag{60}$$

The system formed by the expressions (49) and (60) can be solved for X_{H_2O}. Brohez obtained discrepancies lower than 10% for methane and heptane fires when comparing results of X_{H_2O} from analyser and from the model.

All the parameters required for the HRR estimations can be calculated. First, equations for complete combustion are introduced. Subsequently, corrections accounting for incomplete combustion are integrated into the calorimetric equations.

4.2.3.2.3. HRR Estimation assuming complete combustion

Based on the equations (28) and (30), and considering the parameters defined from the expressions (38) to (57), expressions of the HRR through OC and CDG for complete combustion can be derived [13]].

For OC, the equation obtained is,

$$\dot{q}_{OC} = E_{O_2}\phi X_{O_2}^{A}\left(1 - X_{H_2O}\right)\frac{M_{O_2}}{M_e}\frac{\dot{m}_e}{1+\phi(\alpha-1)} \tag{61}$$

And for CDG,

$$\dot{q}_{CDG} = \left(\frac{\dot{m}_e}{M_e}\left(1 - X_{H_2O}\right)E_{CO_2}\,X_{CO_2}^{A} \;-\; \frac{\dot{m}_a}{M_a}\left(1 - X_{H_2O}^{0}\right)E_{CO_2}\,X_{CO_2}^{A^0}\right) M_{CO_2} \tag{62}$$

4.2.3.2.4. Correction for incomplete combustion

Complete combustion is rarely achieved. Furthermore, using equations (61) and (62) for under-ventilated fire conditions leads to serious errors. In the case of OC, all the O_2 consumed is assumed to only contribute to CO_2 production. However, a fraction of the depleted O_2 participates in the less energetic CO formation. Thus, the HRR through OC is likely to be overestimated. Regarding CDG, if only CO_2 is taken into account in the calculation (as it is done for complete combustion), a proportion of the energy release through the generation of CO is ignored and consequently the HRR through CDG becomes underestimated. In order to account for the effects of incomplete combustion, Parker and Tewarson introduced CO corrections inside their respective equations [5] [13]. Furthermore, Brohez has included an additional term in equations (61) and (62) in order to account for the soot formation [35].

<u>OC calorimetry</u>

Regarding the OC calorimetry, if a significant amount of CO is produced, the HRR becomes overestimated. A fraction of O_2 has reacted to form CO instead of CO_2. Assuming that the oxidation reaction leading to the formation of CO_2 is a two step process, it can be described by,

1. $$C_xH_yO_z \;+\; \left(\frac{\mathrm{x}}{2}+\frac{\mathrm{y}}{4}-\frac{\mathrm{z}}{2}\right)O_2 \;\longrightarrow\; \mathrm{x}\,CO + \frac{\mathrm{y}}{2}\,H_2O \tag{63}$$

2. $$CO + \frac{1}{2}O_2 \longrightarrow CO_2 \qquad \left(E_{O_2\,(CO \to CO_2)} = 17.6\ \text{kJ.g}^{-1}\ \text{of}\ O_2\right) \tag{64}$$

The amount of O_2 that would have been required to achieve step 2 is expressed as,

$$\Delta\dot{m}_{O_2\,(CO \to CO_2)} = \frac{1}{2}\dot{m}_{CO}\frac{M_{O_2}}{M_{CO}} = \frac{1}{2}\dot{m}_{O_2}\frac{X_{CO}^A}{X_{O_2}^A} = \frac{1}{2}(1-\phi)\frac{X_{CO}^A}{X_{O_2}^A}X_{O_2}^0\dot{m}_a\frac{M_{O_2}}{M_a} \tag{65}$$

Then, the HRR would have been given by,

$$\dot{q}_{OC\ total} = E_{O_2}\left(\Delta\dot{m}_{O_2} + \Delta\dot{m}_{O_2\,(CO \to CO_2)}\right) \tag{66}$$

The energy associated with the reaction (64) has been included into the HRR calculation and need then to be removed. The excess of energy is given by the formula,

$$\dot{q}_{excess\ OC} = E_{O_2\,(CO \to CO_2)}\,\Delta\dot{m}_{O_2\,(CO \to CO_2)} = \frac{1}{2}(1-\phi)E_{O_2\,(CO \to CO_2)}\frac{X_{CO}^A}{X_{O_2}^A}X_{O_2}^0\dot{m}_a\frac{M_{O_2}}{M_a} \tag{67}$$

Finally, the HRR expression based on the OC calorimetry and accounting for the CO contribution is denoted as,

$$\dot{q}_{OC} = \left[E_{O_2}\phi - \left(E_{O_2\,(CO \to CO_2)} - E_{O_2}\right)\left(\frac{1-\phi}{2}\right)\frac{X_{CO}^A}{X_{O_2}^A}\right]X_{O_2}^{A^0}\left(1 - X_{H_2O}^0\right)\frac{M_{O_2}}{M_a}\frac{\dot{m}_a}{1+\phi(\alpha-1)} \tag{68}$$

<u>CDG calorimetry</u>

Tewarson [13] adds a CO contribution to the equation (62) to allow HRR calculation in incomplete combustion configuration,

$$\dot{q}_{CDG} = E_{CO_2}\Delta\dot{m}_{CO_2} + E_{CO}\,\dot{m}_{CO} \tag{69}$$

$$\dot{q}_{CDG} = \frac{\dot{m}_e}{M_e}\left(1 - X_{H_2O}\right)\left(E_{CO_2}\,X_{CO_2}^A\,M_{CO_2} + E_{CO}\,X_{CO}^A M_{CO}\right) - \frac{\dot{m}_a}{M_a}\left(1 - X_{H_2O}^0\right)E_{CO_2}\,X_{CO_2}^{A^0}\,M_{CO_2} \tag{70}$$

Tewarson evaluated the energy coefficient E_{CO} for a large range of materials. He determined an average value, $\bar{E}_{CO} = 11.1$ kJ.g^{-1} of CO with a standard deviation of ± 18%. Distribution of E_{CO}values is wider than for E_{O_2} and E_{CO_2}. The reliability of the HRR estimation from a combustion configuration where the material is unknown and largely under-ventilated becomes questionable.

4.3. Concluding Remarks

Over the past thirty years, different methods have been developed to calculate the HRR. A mass loss approach constitutes a simple indicator. It only requires the measurement of the burning rate and the knowledge of the heat of combustion of the material. The highest uncertainty with this method is related to this latter variable. Under well ventilated combustion, gases and liquids burn following the same chemical pathways than the ones associated with the energy flow ΔH_C. For solid materials, the physical and chemical mechanisms defining their thermal decomposition process can lead to several coupled combustion reactions (i.e. smouldering in the condensed phase and flaming in the gaseous phase). Consequently, if the reaction pathway taking place during the burning experiment differs from the one encountered during bomb calorimeter test, the effective heat of combustion is also likely to differ from ΔH_C. The accuracy of the mass loss approach is correlated to the ability to correctly estimate the effective heat of combustion. However, In the case of a room fire, assessing this value becomes complex.

Another possible method that has arisen on bench scale tests apparatuses is the enthalpy rise principle. The theoretical basis is relatively simple to apply. Nevertheless, for burning materials with high emissivity, the heat losses due to apparatus heat absorption have to be weighed. The heat compensation procedure defined by Smith [19] significantly improves the accuracy of the results but requires following a precise and intricate calibration protocol. In the end, it significantly rises the price of the apparatus which might partially explain why fire researchers favoured another calorimetric technique.

The restrictions and other relative difficulties of applying the mass loss and the enthalpy rise approaches promoted the rise of OC and CDG calorimetry in the early 80s. Based on the evolution in concentration of combustion species, both methods have shown their ability to predict HRR accurately for standard fuels, polymers or chemicals [35]. Their principal advantage stems from the hypothesis of energy constants applicable for a large range of chemical compounds. Several studies have conducted uncertainty analyses on OC and CDG [25] [30] [31]. They highlighted that in most of the situations, the overall error propagating through the calculations do not exceed 30%, except for very low HRR, where the variation in O_2 and CO_2 are too small to be correctly captured by the analysers. Authors of the analyses

showed that the main contributors to uncertainty propagation were the energy constants, the O_2 and CO_2 molar fractions and the exhaust flow rate. Apart from the molar fractions whose uncertainty only depends on the measurement, the correct use of energy constants and precise estimation of the exhaust flow rate rely on the validity of several assumptions (see section 4.2.3.2.1). For example, the error associated with the energy constants does not include physical conception. It only represents the standard deviation of a distribution of energy coefficients and should then be restricted to the elements comprised in it. The average values, $\overline{E}_{O_2}$, $\bar{E}_{CO_2}$ and $\bar{E}_{CO}$ defined by Huggett and Tewarson mainly originate from standard materials. Questions arise for atypical new materials like nano-composite polymers, energetic materials or complex chemical structure such as pine needles. The validity of $\bar{E}_{O_2}$, $\bar{E}_{CO_2}$ and $\bar{E}_{CO}$ has to be investigated. On the other hand, the limit of legitimacy of the other calculation assumptions (hypotheses 2 to 10) has not been fully considered yet. Combining the two principles, may present also noticeable interests. For defined test conditions, convergence of HRR methods can highlight the consistency of the calorimetric methodology. Inversely, divergence of the results would underline that the assumptions of at least one of the calculations is not valid. It is necessary to assess this last statement when burning elements presenting peculiarity such as energetic materials and evaluate the ability of calorimetric equations and calorimeters data to correctly estimate their HRR.

Table 4.5. Net heats of combustion and O_2 energy constants for various organic gases, liquids and solids from Huggett [29].

3	Formula	$\Delta H_C\ (kJ.g^{-1})$	$E_{O_2}\,(kJ.g^{-1}\,O_2)$
Methane (g)	CH_4	50.01	12.54
Ethane (g)	C_2H_6	47.48	12.75
n-Butane (g)	C_4H_{10}	45.72	12.78
n-Octane (l)	C_8H_{18}	44.42	12.69
Polyethylene (s)h	$(-C_2H_4-)_n$	43.28	12.65
Acetylene (g)	C_2H_2	48.22	15.69
Ethylene (g)	C_2H_4	47.16	13.78
Benzene (l)	C_6H_6	40.14	13.06
1-Butanol (I)	$C_4H_{10}O$	33.13	12.79
n-Butyraldehyde (I)	C_4H_8O	31.92	13.08
Butyric acid (I)	$C_4H_8O_2$	22.79	12.55
n-Butylamine (I)	$C_4H_{11}N$	37.96	12.85
1-Butanethiol (I)	$C_4H_{10}S$	32.77	12.32
Ethyl chloride (I)	C_2H_5Cl	19.01	12.78
Ethyl bromide (I)	C_2H_5Br	11.93	12.50
Polypropylene	$(-C_3H_6-)_n$	43.31	12.66
Polyisobutylene	$(-C_4H_8-)_n$	43.71	12.77
Polybutadiene	$(-C_4H_6-)_n$	42.75	13.14
Polystyrene	$(-C_8H_8-)_n$	39.85	12.97
Polyvinylchloride	$(-C_2H_3Cl-)_n$	16.43	12.84
Polyvinylidene chloride	$(-C_2H_2Cl_2-)_n$	8.99	13.61
Polyvinylidene fluoride	$(-C_2H_2F_2-)_n$	13.32	13.32
Polymethylmethacrylate	$(-C_5H_8O_2-)_n$	24.89	12.98
Polyacrylonitrite	$(-C_3H_3N-)_n$	30.80	13.61
Polyoxymethylene	$(-CH_2O-)_n$	15.46	14.50
Polyethyleneterephthalate	$(-C_{10}H_8O_4-)_n$	22.00	13.21
Polycarbonate	$(-C_{16}H_{14}O_3-)_n$	29.72	13.12
Cellulose triacetate	$(-C_{12}H_{16}O_4-)_n$	17.62	13.23
Nylon-6,6	$(-C_6H_{11}NO-)_n$	29.58	12.67
Isobutene polysulfone	$(-C_4H_8O_2S-)_n$	20.12	12.59
Cellulose	$(-C_6H_{10}O_5-)_n$	16.09	13.59
Cotton		15.55	13.61
Newsprint		18.40	13.40
Corrugated box		16.04	13.70
Leaves, hardwood		19.30	12.28
Wood, maple		17.76	12.51
Lignite		24.78	13.12
Coal, bituminous		35.17	13.51
	Average Value	29.77	13.09
	Standard Deviation	12.52	0.64

Table 4.6. Net ΔH_C and CDG energy constants for various organic gases, liquids and solids from Tewarson [13].

	Material	Formula	$\Delta H_C\ (kJ.g^{-1})$	$E_{CO_2}\ (kJ.g^{-1}\ CO_2)$	$E_{CO}\ (kJ.g^{-1}\ CO)$
Alkanes	Methane	CH_4	50.1	18.2	18.6
	Ethane	C_2H_6	47.1	16.2	15.4
	Propane	C_3H_8	46.0	15.3	14.0
	Butane	C_4H_{10}	45.4	15.1	13.7
Alkenes	Ethylene	C_2H_4	48	15.0	13.6
	Propylene	C_3H_6	46.4	14.6	12.9
	Butylene	C_4H_8	45.6	14.3	12.5
	Pentene	C_5H_{10}	45.2	14.3	12.5
Alkynes	Acetylene	C_2H_2	47.8	14.3	12.4
	Heptyne	C_7H_{12}	44.8	13.9	11.8
	Octyne	C_8H_{14}	44.7	14.0	11.9
Aromatic hydrocarbons	Benzene	C_6H_6	40.1	11.9	8.7
	Toluene	C_7H_8	39.7	12.1	9.0
	Styrene	C_8H_8	39.4	12.0	8.8
	Xylene	C_8H_{10}	39.4	12.4	9.5
	Propylbenzene	C_9H_{12}	39.4	12.5	9.6
Alcohols	Methyl alcohol	CH_4O	20.0	14.5	12.9
	Ethyl alcohol	C_2H_6O	27.7	14.5	12.7
	n-Propyl alcohol	C_3H_8O	31.8	14.5	12.7
	n-Butyl alcohol	$C_4H_{10}O$	34.4	14.5	12.8
Aldehydes	Formaldehyde	CH_2O	18.7	12.7	10.1
	Acetaldehyde	C_2H_4O	25.1	12.6	9.7
	Butyraldehyde	C_4H_8O	33.8	13.9	11.7
Ketones	Acetone	C_3H_6O	29.7	13.1	10.5
	Methylethyl ketone	C_4H_8O	32.7	13.4	11.0
	Cyclohexanone	$C_6H_{10}O$	35.9	13.3	11.0
	Methyl butyl ketone	$C_6H_{12}O$	35.2	13.3	11.0
Carbon-hydrogen atoms in the structure	Polyethylene	CH_2	43.6	13.9	11.8
	Polypropylene	CH	43.4	13.8	11.7
	Polybutadiene	$CH_{1.5}$	42.8	13.1	10.7
	Polystyrene	CH	39.2	12.2	9.2
Carbon-hydrogen-oxygen-nitrogen atoms in the structure	Polyester	$CH_{1.4}O_{0.22}$	32.5	12.5	9.6
	Epoxy	$CH_{1.3}O_{0.20}$	28.8	10.8	6.9
	Polycarbonate	$CH_{0.88}O_{0.19}$	29.7	10.7	6.9
	Polyethyleneterephthalate	$CH_{0.88}O_{0.40}$	22.0	9.6	5.1
	Red Oak	$CH_{1.7}O_{0.72}N_{0.001}$	17.1	10.2	6.0
	Douglas Fir	$CH_{1.7}O_{0.74}N_{0.002}$	16.4	9.5	5.0
	Nylon	$CH_{1.8}O_{0.17}N_{0.17}$	30.8	13.3	10.8
		Average	36.33	13.32	10.91
		Standard Deviation	9.51	1.76	2.76

4.4. References

[1] Babrauskas, V., Peacock, R., D., Heat Release Rate: The Single Most Important Variable in Fire Hazard, Fire Safety Journal, 18, pp. 255 – 272 (1992);

[2] Babrauskas, V., Heat Release Rates, in: SFPE Handbook for Fire Protection Engineering, 3rd Edition, Section 3, Chapter 1, The National Fire Protection Association Press, 2002, pp. 3-1 – 3-37;

[3] Tewarson, A., Heat Release Rate in Fires, Fire and Materials, 4 (4), pp. 185 – 191 (1980);

[4] ASTM E 906 - 83, Standard Test Method for Heat and Visible Smoke Release Rates for Materials and Products, American Society for Testing and Materials, Philadelphia, PA;

[5] Parker, W., J., Calculation of the Heat Release Rate by Oxygen Consumption for Various Applications, NBSIR 81-2427, National Bureau of Standards, Gaithersburg, MD (1982);

[6] Janssens, M., Calorimetry, in: SFPE Handbook of Fire Protection Engineering, 3rd Edition, Section 3, Chapter 4, The National Fire Protection Association Press, 2002, pp. 3-38 – 3-62;

[7] ISO 5660, "Fire Tests – Reaction to Fire – Part 1: Rate of Heat Release from Building Products (Cone Calorimeter)", International Standards Organisation, Geneva, 1993;

[8] ASTM 1354-905, "Standard Test Method for Heat and Visible Smoke Release Rates for Materials and Products Using an Oxygen Consumption Calorimeter", American Society for Testing Materials, Philadelphia, 1995;

[9] Brohez, S., Marlair, G., Delvosalle C., Fire calorimetry relying on the use of the Fire Propagation Apparatus, Part I: Early Learning from the Use in Europe, Fire and Materials. 30, pp. 131 – 149 (2006);

[10] ASTM E2058-03, "Standard Test Method for Measurement of Synthetic Polymer Material Flammability Using a Fire Propagation Apparatus", ASTM International, West Conshohocken, 2003;

[11] Marlair, G., Turcotte, R., Kwok, Q. S. M., Branka, R., "Toxicity issues pertaining to burning pyrotechnics", Thirty Third International Pyrotechnics Seminar, Fort Collin, USA, July 2006, pp. 467 – 483.;

[12] Redfern, J.P., "Rate of Heat Release Measurement", Journal of Thermal Analysis, 35, (1989) 1861 – 1877;

[13] Tewarson, A., Generation of Heat and Chemical Compounds in Fires, in: SFPE Handbook of Fire Protection Engineering, 3rd Edition, Section 3, Chapter 4, The National Fire Protection Association Press, 2002, pp. 3-82 – 3-161;

[14] Jessup, R., S., Precise Measurement of Heat of Combustion with a Bomb Calorimeter, National Bureau of Standards, Gaithersburg, MD, 1960;

[15] ASTM D2015, Standard Test Method for Gross Calorific Value of Coal and Coke by the Adiabatic Bomb Calorimeter, American Society for Testing and Materials, Philadelphia;

[16] Drysdale, D., An Introduction to Fire Dynamics, 2nd Edition, Chapter 1, Wiley, Chichester, pp. 1 – 30 (2002);

[17] Babrauskas, V., Related Quantities: (a) Heat of Combustion and Potential Heat, in: Heat Release in Fires, Chapter 8, Editors: Babrauskas, V., and Grayson, S., J., Elsevier Applied Science, New York, 1992, pp., 207 – 223;

[18] Smith, E., E., Measuring Rate of Heat, Smoke and Toxic Gas Release, Fire Technology, 8 (3), pp. 237 – 245 (1972);

[19] Smith, E., E., Heat Release Rate Calorimetry, Fire Technology, 32 (4), pp. 333 – 347 (1996);

[20] Filipczak, R., Crowley, S., Lyon, R., E., Heat Release Rate Measurements of Thin Samples in the OSU Apparatus and the Cone Calorimeter, Fire Safety Journal, 40, pp. 628 – 645 (2005);

[21] Babrauskas, V., Performance of the Ohio State University Rate of Heat Release Apparatus using Polymethylmethacrylate and Gaseous Fuels, Fire Safety Journal, 5, pp. 9 – 20 (1982);

[22] Kandola, B., K., Horrocks, A., R>, Padmore, K., Dalton, J., Owen, T., Comparison of cone and OSU calorimetric techniques to assess the flammability behaviour of fabric used for aircraft interior, Fire and Materials, 30, pp. 241 – 255 (2006);

[23] Moussan, F., Delfau, J.-L., Vovelle, C., Pham Van Cang, C., Bosseboeuf, G., Heat Release Rate and Effective Heat of Combustion Measurements: A Comparative Study of Thermal and Oxygen Consumption Techniques, Journal of Fire Sciences, 13, pp. 482 – 499 (1995);

[24] Janssens, M., Parker, W., J., Oxygen Consumption Calorimetry, in: Heat Release in Fires, Chapter 3, Editors: Babrauskas, V., and Grayson, S., J., Elsevier Applied Science, New York, 1992, pp., 31 – 59;

[25] Enright, P. A., Fleischmann, C., M., Uncertainty of Heat Release Rate Calculation of the ISO5660-1 Calorimeter Standard Test Method, Fire Technology, 35 (2), pp. 153 – 169 (1999);

[26] BS EN ISO 5167-4:2003, Measurements of Fluid Flow by Means of Pressure Differential Devices Inserted in Circular Cross-section Conduits Running Full, Part 4: Venturi tubes, British Standards, 2003;

[27] Claudel, J., Formules, Tables et Renseignements usuels - Aide mémoire des ingénieurs, des architectes, etc, Partie Pratique, 10ème édition révisée par Barré, L.-A., Tome 1, Paris, Vve Ch. Dunod, 1892;

[28] Thornton, W.M., The Relation of Oxygen to the Heat of Combustion of Organic Compounds, Philosophical Magazine Series 6, 33, pp. 196 – 203 (1917);

[29] Huggett, C. Estimation of Rate of Heat Release by means of Oxygen Consumption Calorimetry, Fire and Materials, 4 (2), pp. 61 – 65 (1980);

[30] Brohez, S., Uncertainty analysis of heat release rate measurement from oxygen consumption calorimetry, Fire and Materials, 29, pp. 383 – 394 (2005);

[31] Axelsson, J., Andersson, P., Lönnermark, A., Van Hees, P., Wetterlund, I., Uncertainties in measuring heat and smoke release rates in the room/corner test and the SBI, SP Swedish National Testing and Research Institute, NT technical report, 477, NORDTEST Project No. 1480-00, SP Report 2001:04;

[32] Babrauskas, V., The Cone Calorimeter, Chapter 4, Editors: Babrauskas, V., and Grayson, S., J., Elsevier Applied Science, New York, 1992, pp., 61 – 91;

[33] Janssens, M., L., Measuring Rate of Heat Release by Oxygen Consumption, Fire Technology, 27 (3), pp. 234 – 249 (1991);

[34] Brohez, S., Etude Des Feux de Substances Chimiques en Milieu Confiné, PhD Dissertation, Université Polytechnique de Mons, 2002 ;

[35] Brohez, S., Marlair, G., Delvosalle C., Fire calorimetry relying on the use of the Fire Propagation Apparatus, Part I: Early Learning from the Use in Europe, Fire and Materials, 30, pp. 131 – 149 (2006);

5. The Assumption of Energy Constants

5.1. Problematic

The aim of OC and CDG calorimetry is to provide accurate HRR estimations using a relatively simple methodology that can be applied with an apparatus such as the cone calorimeter or the FPA. There are several ways to calculate the HRR from the combustion of a material (see Chapter 3, section 3.2) but OC and CDG present the valuable advantage that knowledge about the chemistry of the material is not a basic principle. HRR results calculated through OC and CDG are approximate and the best precision is sought. Nevertheless, OC and CDG equations are affected by the propagation of uncertainties. Different sources of errors can be identified [3],

a. Uncertainties associated with the sample and its preparation;

b. Uncertainties associated with the test conditions;

c. Uncertainties associated with the measurements carried out during the experiments to investigate the material response;

d. Uncertainties associated with the validity of the assumptions considered for the calculation.

The two first causes of error can only be determined in some cases. A repeatability analysis gives an insight of the overall contribution of these two sources on the final results. Source c has been widely studied and procedures have been defined to estimate with some confidence, the expected limits of error [4]. Paradoxically, uncertainties related to the calculation assumptions have received less attention. It is crucial to comprehend their range of validity. The present chapter will discuss about the restrictions relative to the assumption of energy constants. Huggett [1] and Tewarson [2] indicate that energy constants can be used for the calculation independently of the nature of the material. They estimated them from extensive sets of materials. Energy constants and related standard deviation are reported on Table 5.1. The error associated with each energy value depends only on the width of distribution obtained by the authors for the set of materials they considered. The more compounds are integrated the more comprehensive becomes the validity of the energy constants assumption.

However, side issues arise by encompassing more materials. Accuracy of the $\bar{E}_i$ values is dependent on the number of compounds comprised in the distribution. From this statement, two different prospects can be highlighted. Either the assumption of energy constants is very conservative and adding more elements in the distribution does not significantly affect the average and the variance or some products can present such completely different behaviours that the average value varies and the variance is increased. Considering unusual materials, like nano-composite polymers or energetic materials, one has to investigate to which of the two latter hypotheses tends to be favoured. While the first hypothesis strengthens Huggett and Tewarson statements, the second one emphasizes that constraints are required in order to use their energy constants values.

Table 5.1. Energy constants and related standard deviation for OC and CDG.

Huggett (OC)	Tewarson (CDG)	
$\bar{E}_{O_2} = 13.1$ kJ.g^{-1} of O_2	$\bar{E}_{CO_2} = 13.3$ kJ.g^{-1} of CO_2	$\bar{E}_{CO} = 11.1$ kJ.g^{-1} of CO
(±5%)	(±11%)	(±18%)

In a first time, energy coefficients values from various sources of the literature are gathered. Analysis of the distributions obtained allows assessing the sensitivity of Huggett's and Tewarson's energy constants as well as the uncertainty associated with their values. Subsequently, methods to estimate actual energy coefficients based on assumed chemical reactions are presented. In order to assess their relevance and validity, reckoning the uniqueness of the HRR for a material under given burning conditions, OC and CDG calculations are used as a comparison criterion. Assuming that experimental configurations have been set in a way that uncertainties related to the measurements are minimized, according to the converging conclusions of uncertainty analyses [5] [6] [7], the major error contributor is devoted to the energy coefficients. HRR results underlining large discrepancies between OC and CDG would highlight weakness of the assumption of constants of energy for certain materials. In this case, all the benefits of OC and CDG fall down. Two main issues clearly emanate. A seek for accurate HRR cannot be achieved without actual energy coefficients. A divergence between OC and CDG implies error in the calculation that cannot be accurately evaluated based on acknowledged uncertainties related to the energy constants. If energy

coefficients cannot be evaluated, another method, based on the physics of the process, needs to be elaborated in order to be able to define error bars for the energy values. This would then allow assessing appropriate accuracy of the HRR estimations. The insight followed in the present study is to estimate the error related to the energy coefficients based on the chemical composition. Assuming that the heat release comes from the energy stored in the chemical bonds of a molecule, the possibility of a finding a relation between this two parameters is investigated. If chemical bonds can be associated with a range of energy that can potentially be released when they break, it becomes then possible to evaluate the error associated with the energy coefficients of a material.

5.2. Energy coefficients distribution

Huggett and Tewarson energy constants have been obtained by gathering energy coefficients values from a large number of chemical compounds [1] [2]. They obtained distributions for which the average values were then defined as energy constants $\bar{E}_{O_2}$(for OC), $\bar{E}_{CO_2}$ and $\bar{E}_{CO}$ (for CDG) and are reported in Table 5.1.

In order to analyse the sensitivity of their results according to the number of materials considered, $\bar{E}_i$ values have been collected from different sources of the literature [1] [2] [8] [9] [10]. Given the three chemical reactions used to model the combustion,

$$C_xH_yO_zN_a + \left(x + \frac{y}{4} - \frac{z}{2}\right) O_2 \longrightarrow x\,CO_2 + \frac{y}{2}\,H_2O + \frac{a}{2}N_2 \quad (1)$$

$$C_xH_yO_zN_a + \left(\frac{x}{2} + \frac{y}{4} - \frac{z}{2}\right) O_2 \longrightarrow x\,CO + \frac{y}{2}\,H_2O + \frac{a}{2}N_2 \quad (2)$$

$$CO + \frac{1}{2}O_2 \longrightarrow CO_2 \qquad (\Delta H_{CO} = 10.10\ \text{kJ.g}^{-1}\ \text{of CO}\ [11]) \quad (3)$$

Under the assumption that the combustion is complete (reaction (1)) and the material composition ($C_xH_yO_zN_a$) known, formulas for E_{O_2} and $E_{CO_2}$are derived and expressed as,

$$E_{O_2} = \frac{\Delta H_C\, M_{fuel}}{\left(\frac{x}{2} + \frac{y}{4} - \frac{z}{2}\right) M_{O_2}} \quad (4)$$

$$E_{CO_2} = \frac{\Delta H_C \, M_{fuel}}{x \, M_{CO_2}} \tag{5}$$

Where, ΔH_C and M_{fuel} represent, respectively, the heat of combustion and the molecular weight of the material with the composition $C_x H_y O_z N_a$.

The third coefficient E_{CO} is determined using reactions (2) and (3). E_{CO} corresponds to the amount of energy released by unit mass of CO during the reaction (2). The latter can be interpreted as reaction (1) where the stage symbolized by reaction (3) would have not been reached. Then the reaction associated to reaction (2) can be expressed as,

$$\Delta H_{react\,(2)} = \frac{\Delta H_c M_{fuel} - x \Delta H_{CO} M_{CO}}{M_{fuel}} \tag{6}$$

And E_{CO} is given by,

$$E_{CO} = \frac{\Delta H_{react\,(2)} \, M_{fuel}}{x \, M_{CO}} = \frac{\Delta H_c \, M_{fuel}}{x M_{CO}} - \Delta H_{CO} = E_{CO_2} \frac{M_{CO_2}}{M_{CO}} - \Delta H_{CO} \tag{7}$$

The use of these expressions relies on the assumption that a combustion reaction can be described with enough precision by a combination of reactions (1) and (2). Finally, calculation of energy coefficients relies then on the knowledge of the heat of combustion of the material and the stoichiometric coefficients associated to the combustion reaction. The introduced procedure has been widely used by authors to estimate E_{O_2}, E_{CO_2} and E_{CO} for materials. Couples of data (Material, $E_{i\,(i = O_2, CO_2, CO)}$) have been compiled from the the literature [1] [2] [9] [10]. They encompass organic liquids and gases ([1] (OC), [2] (OC and CDG), [9] (OC)), synthetic polymers ([1] (OC), [2] (OC and CDG), [9] (OC), [10] (OC)), synthetic chemicals ([2] (OC and CDG)), natural solid fuels ([1] (OC), [2] (OC and CDG), [9] (OC)). Considering this population of materials, the associated distributions of energy values have been plotted on Figure 5.1, Figure 5.2 and Figure 5.3. The order of the materials on the y axis is arbitrary. The aim is to evaluate the scattering of the energy coefficient values between the materials. Normal distributions have been used.

Average values and standard deviations are advised on Table 5.2.

Table 5.2. Average energy coefficients and standard deviation of the normal distribution associated.

Energy Coefficients	$\bar{E}_i$	Standard Deviation	Standard Deviation (%)
$\bar{E}_{O_2}$ (kJ.g^{-1} of O_2)	13.1	1.86	14
$\bar{E}_{CO_2}$ (kJ.g^{-1} of CO_2)	13.1	2.17	16.5
$\bar{E}_{CO}$ (kJ.g^{-1} of CO)	10.7	3.39	31.7

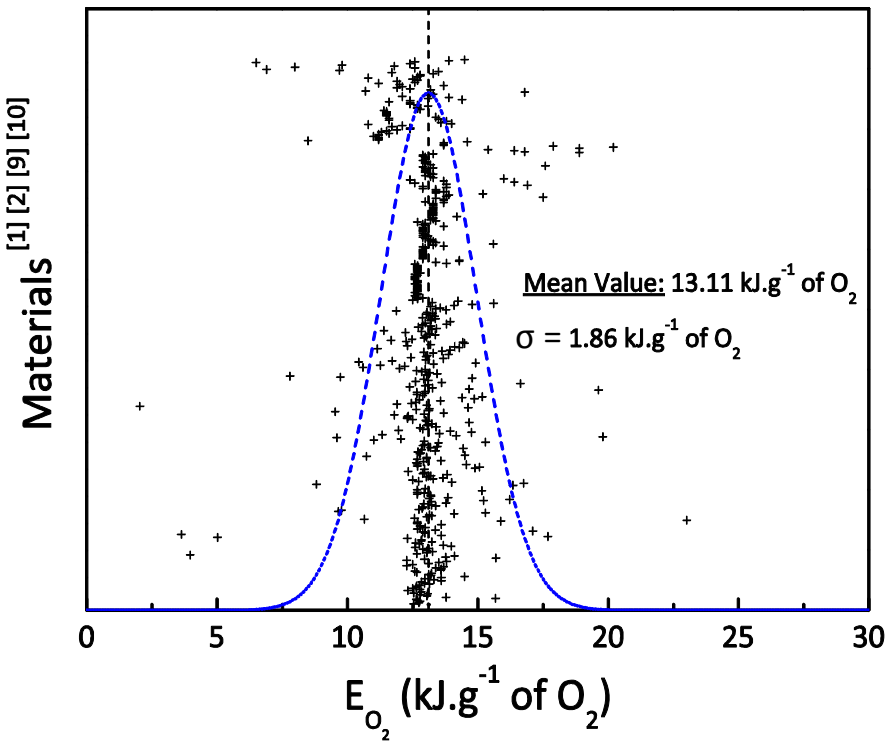

Figure 5.1. Distribution of OC energy coefficients associated with various materials from Huggett [1], Babrauskas [9], Walters et al [10], Janssens [8], Tewarson [2].

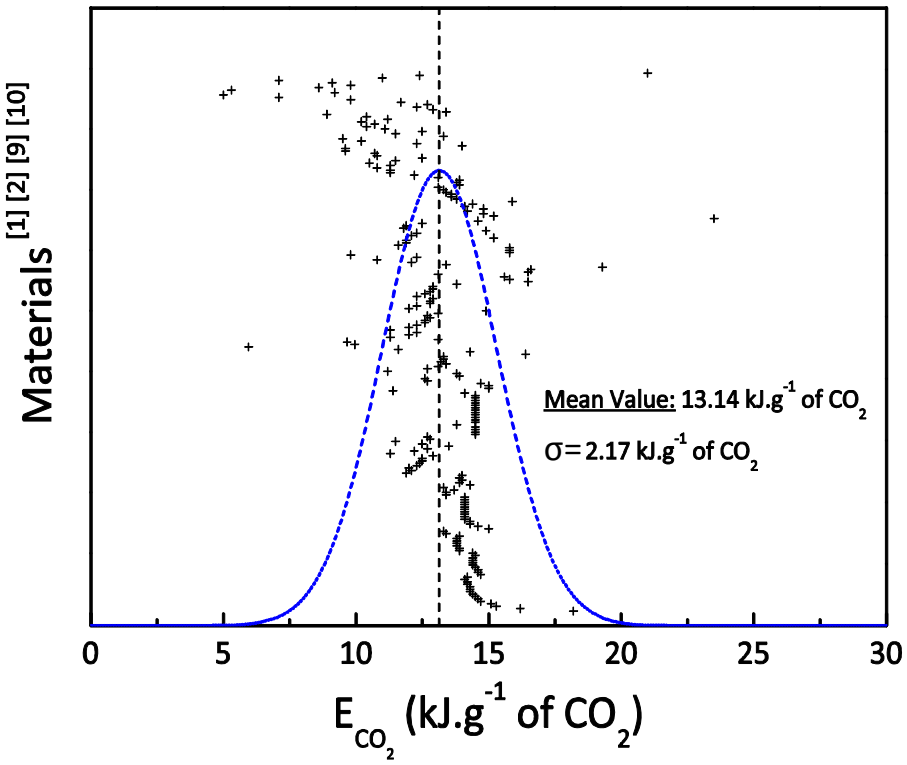

Figure 5.2. CDG energy coefficients $(E_{CO_2})$for various materials from Tewarson [2].

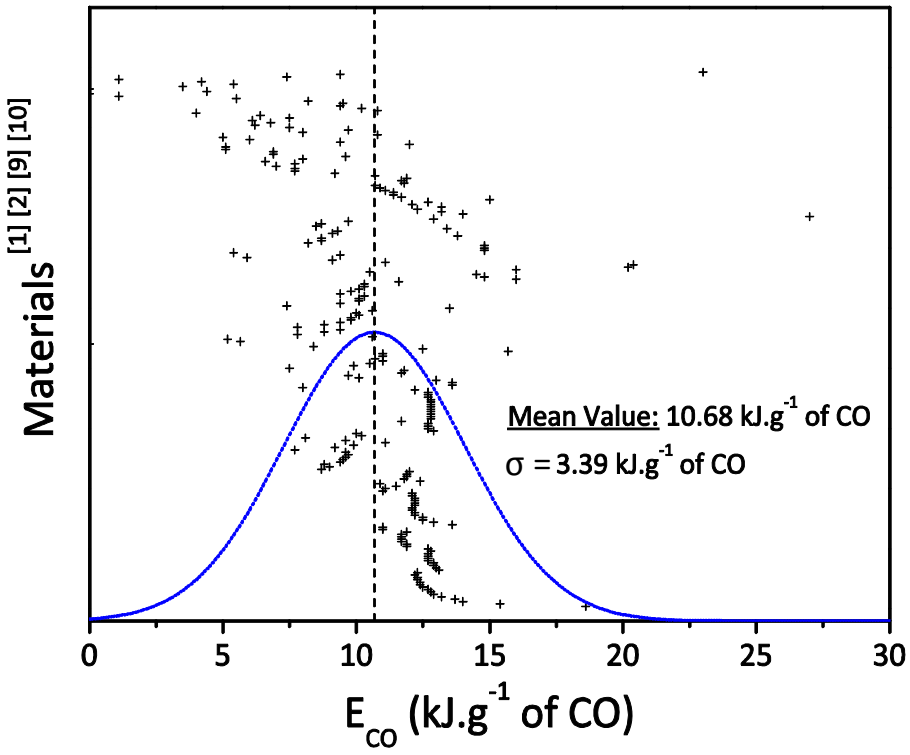

Figure 5.3. CDG energy coefficients $(E_{CO})$for various materials from Tewarson [2].

A comparison with the average values estimated by Huggett [1] and Tewarson [2] is done.. The same value as Huggett has been found for $\bar{E}_{O_2}$. Compared to Tewarson's energy constants, divergences on $\bar{E}_{CO_2}$ and $\bar{E}_{CO}$ are, respectively, less than 2 % and less than 5%. There are good agreements within the results. However, one notices that the standard deviations associated with the distributions are larger than the ones defined by Huggett and Tewarson especially for $\bar{E}_{O_2}$ and $\bar{E}_{CO}$. The standard deviation of $\bar{E}_{O_2}$ given in Table 5.2 is almost three times higher than the one calculated by Huggett. Similarly, the uncertainty related to $\bar{E}_{CO}$is more than 40 % higher than Tewarson estimate. One distinguishes materials whose energy coefficients lie outside the $[\bar{E}_i \pm 4\sigma]$ normal distributions range. They are listed in Table 5.3. No common trait clearly emerges from it. It comprises organic and inorganic gases, liquids and solids. Nevertheless, one notices that a majority appears to be synthesized compounds. Furthermore, given their compositions, some of these materials do not undergo the usual combustion reaction with major products being CO2, H2O and CO. Their unconventional chemistry might be one of the reasons to explain the difference noticed with their energy coefficients compared to the average values.

Table 5.3. Materials presenting E_{O_2} E_{CO_2} and/or E_{CO} values outside the $[\bar{E}_i \pm 4\sigma]$ range ($\bar{E}_i$ from Table 5.2).

Compound	Composition	Family	Energy coefficients
Teflon, Tedlar [2]	C-H-F base	Synthetic fluoropolymer (solid)	$E_{O_2(CO_2,CO)} \leq 5$ kJ.g^{-1} O_2 (CO_2, CO)
Carbon disulfide [2] [9]	CS_2	Volatile liquid	E_{O_2}= 5.03 kJ.g^{-1} O_2 E_{CO_2}= 23.5 kJ.g^{-1} CO_2 E_{CO}= 27 kJ.g^{-1} CO
Ammonium perchlorate [9]	NH_4ClO_4	Oxidizer (solid)	E_{O_2}= 3.97 kJ.g^{-1} O_2
Chlorotrifluoroethylene [9]	C_2F_3Cl	Chlorofluorocarbon (gas)	E_{O_2}= 3.64 kJ.g O_2
Diborane [9]	B_2H_6	Boron compound (gas)	E_{O_2}= 23.02 kJ.g O_2
Silicone [2]	C-H-O-Si base	Silicone polymers	$E_{CO_2} = 21$ kJ.g^{-1} CO_2 $E_{CO} = 23$ kJ.g^{-1} CO
Ethyl malonate (Ethyl oxalate) [2]	$C_7H_{12}O_4$ ($(CH_3)_2C_2O_4$)	Organic acids	$E_{CO} > 20$ kJ.g^{-1} CO

Noting that the materials considered remain, for most of them, relatively standard, Increasing their number for the evaluation of average values of energy coefficients (i.e. values defining energy constants) does not significantly alter the results. Nevertheless, discrepancies appear on the estimation of the errors associated with them. A dependency seems to arise according to the materials that have been taken into account. Consequently, question arises concerning the validity of the range of uncertainty that is related to the constants of energy defined by Huggett and Tewarson.

The calculation of the HRR through OC and CDG requires energy coefficients. According to the degree of characterisation of the material undergoing combustion, two scenarios arise:

1. If the composition of the burning material is known and if enough information on the combustion chemistry and the energy associated is available, energy coefficients can be estimated. The order of magnitude of the uncertainties related to the energy values could be calculated from their expression;

2. If the composition of the material is unknown and if the chemistry cannot be modelled. The calculation should rely on energy constants values. The HRR obtained is an approximate result. Consequently, more than the energy values, the ability to define error bars is fundamental. The high estimation needs to be conservative regarding the HRR peak while the low estimation should be conservative regarding the burning time.

5.3. Estimation of energy coefficients from the reaction chemistry

The main assumption on which are based the expressions (4) and (5) is that the chemistry follows a complete combustion (reaction (1)). The second hypothesis holds in the postulate that combustion reaction can be modelled by combining reactions (1) and (2) which allows assessing E_{CO}. Ventilation conditions during fire or burning behaviour of unconventional materials (for example nano-composites embedded in polymers, fire retardant or energetic materials) can cause the chemical process to significantly divert from complete combustion. The heat of combustion of such products can still be estimated through bomb calorimeter tests but energy involves in the combustion are often lower due to the generation of

incomplete products. However, the hypothesis of complete combustion can be avoided if the heat of the reaction as well as a chemistry model of the combustion can be defined.

Assuming that formations of CO_2, CO and H_2O constitute the main contributors of the HRR, one can model the combustion as a one step process,

$$C_xH_yO_z + \nu_{O_2}(O_2 + 3.76\,N_2) \longrightarrow \nu_{CO_2}\,CO_2 + \nu_{CO}\,CO + \nu_{H_2O}\,H_2O + 3.76\,\nu_{O_2}\,N_2 \quad (8)$$

The heat associated with reaction (8) can be derived from the knowledge of the fuel heat of formation and the reaction coefficients ν_{O_2}, ν_{CO_2}, ν_{CO} and ν_{H_2O}. The calculation of the heat of reaction is explained in Appendix A.

Expressions of the reaction coefficients ν_{O_2}, ν_{CO_2}, ν_{CO} and ν_{H_2O}.can be derived from calorimeter data, for each instant t

$$\nu_{O_2}(t) = \frac{\Delta\dot{m}_{O_2}}{\dot{m}_{C_xH_yO_z}}\frac{M_{C_xH_yO_z}}{M_{O_2}} = \frac{\left(X_{O_2}^{A^o}\left(1 - X_{H_2O}^0\right)\frac{\dot{m}_a}{M_a} - X_{O_2}^{A}\left(1 - X_{H_2O}\right)\frac{\dot{m}_e}{M_e}\right)M_{C_xH_yO_z}}{\dot{m}_{C_xH_yO_z}} \quad (9)$$

$$\nu_{CO_2}(t) = \frac{\Delta\dot{m}_{CO_2}}{\dot{m}_{C_xH_yO_z}}\frac{M_{C_xH_yO_z}}{M_{CO_2}} = \frac{\left(X_{CO_2}^{A}\left(1 - X_{H_2O}\right)\frac{\dot{m}_e}{M_e} - X_{CO_2}^{A^o}\left(1 - X_{H_2O}^0\right)\frac{\dot{m}_a}{M_a}\right)M_{C_xH_yO_z}}{\dot{m}_{C_xH_yO_z}} \quad (10)$$

$$\nu_{CO}(t) = \frac{\Delta\dot{m}_{CO}}{\dot{m}_{C_xH_yO_z}}\frac{M_{C_xH_yO_z}}{M_{CO}} = \frac{\left(X_{CO}^{A}\left(1 - X_{H_2O}\right)\frac{\dot{m}_e}{M_e} - X_{CO}^{A^o}\left(1 - X_{H_2O}^0\right)\frac{\dot{m}_a}{M_a}\right)M_{C_xH_yO_z}}{\dot{m}_{C_xH_yO_z}} \quad (11)$$

$$\nu_{H_2O}(t) = \frac{\Delta\dot{m}_{H_2O}}{\dot{m}_{C_xH_yO_z}}\frac{M_{C_xH_yO_z}}{M_{H_2O}} = \frac{\left(X_{H_2O}\frac{\dot{m}_e}{M_e} - X_{H_2O}^0\frac{\dot{m}_a}{M_a}\right)M_{C_xH_yO_z}}{\dot{m}_{C_xH_yO_z}} \quad (12)$$

Where, $\Delta\dot{m}_i$ is the generation (CDG) or consumption (OC) of species i; $\dot{m}_{C_xH_yO_z}$ and $M_{C_xH_yO_z}$ are, respectively, the mass loss rate and molecular weight of the material; $\dot{m}_a$ (M_a) and $\dot{m}_e$ (M_e) represent, respectively, the mass flow rate (molecular weight) of entrained air and exhaust gases.

According to expressions (4) and (5) for complete combustion, formulas for the energy coefficients based on the chemistry of the reaction can be evaluated at each interval t:

$$E_{O_2\,(ch)} = \frac{\Delta H_{reaction}\, M_{C_xH_yO_z}}{\nu_{O_2} M_{O_2}} \tag{13}$$

$$E_{CO_2\,(ch)} = \frac{\Delta H_{reaction}\, M_{C_xH_yO_z}}{\nu_{CO_2}\, M_{CO_2}} \tag{14}$$

In case of complete combustion, one can notice that expressions (4) and (5) are obtained. Using (13) and (14), the HRR can be retrieved applying the following relations,

$$\dot{q}_{OC} = E_{O_2\,(ch)}\, \Delta\dot{m}_{O_2} \tag{15}$$

$$\dot{q}_{CDG} = E_{CO_2\,(ch)}\, \Delta\dot{m}_{CO_2} \tag{16}$$

The use of equations (15) and (16) is of little interest considering that the reaction coefficients, ν_i, can only be defined from calorimeter data. Redundancies of terms appear in the formulas. They can easily be simplified to the more convenient form,

$$\dot{q} = \Delta H_{reaction}\, \dot{m}_{C_xH_yO_z} \tag{17}$$

where less parameters are introduced. Furthermore, with a restricted number of variables, the propagation of uncertainty is also reduced. An alternative would be to use a FTIR calibrated for quantitative measurements, in order to determine the concentrations of the combustion products released. Based on these emissions, a global chemistry of combustion could be defined and the heat associated with this process evaluated.

Nevertheless, equations (13) and (14) allow estimating physically the uncertainty related with the energy coefficients. It also allows verifying the assumption of energy constants. Given the value obtained and its uncertainty, one can ascertain the divergence from Huggett and Tewarson values for different burning conditions and then analyse how the energy coefficients scatter in the configurations of incomplete combustion. To draw any conclusions, a sense of the degree of uncertainties related to the expressions (13) and (14) is necessary.

The error that is evaluated corresponds to the maximum you can expect, under the conditions that the composition of the material and its heat of combustion are known. Considering $E_i = E_i(a, b, c \dots)$, uncertainty can be evaluated from the following expression,

$$\frac{\delta E_i}{E_i} = \sqrt{\sum_{a}^{Z} \left(\frac{\partial E_i}{\partial a}\frac{\delta a}{E_i}\right)^2} \tag{18}$$

Where, $a, b, c \dots$ represent the different variables associated with the calculation of E_i. Furthermore, E_i needs to be expressed in the most basic form in order to avoid combining the error from different parameters that shares variable. This leads to a massive formula that can be found in the Appendix A. The uncertainty analysis carried out on the two coefficients, $E_{O_2\,(ch)}$ and $E_{CO_2\,(ch)}$, underlines a maximum uncertainty that can rise up to 35%. The standard uncertainties associated with all the measured variables have been collected from manufacturers' data. When the burning conditions tend to a complete combustion process (i.e. $X_{CO} \longrightarrow 0$), equations (13) and (14) can then be approximated by the stoichiometric energy coefficients (4) and (5) with less than 5% uncertainty. Nevertheless, it needs to be emphasized that, in case of a fire, complete combustion configuration does not form the most likely scenario to occur.

One can estimate chemical energy coefficients by means of calorimeter data if the composition of the material and its heat of combustion are known. However, using these values to estimate the HRR would significantly enhance propagation of errors in the result, due to the present of shared parameters. A certain appeal of estimating chemical energy coefficients is that it allows the investigation of the divergence of these values from the ones defined by Huggett and Tewarson as constants. The maximum uncertainty associated with the coefficients has been assessed at about 35%. The ability to evaluate the errors associated with this calculation gives an insight of the range where the actual coefficients lie and if the energy constants of Tewarson and Huggett are included in. Close to complete combustion conditions, terms in the expressions of E_i becomes small and have a negligible contribution on the estimation. Energy coefficients tend to equations (4) and (5) where the uncertainty is limited to less than 5%.

As a conclusion, assuming that the heat of combustion and the compositions of a material are known, if enough information is available to define its chemistry, using a one step chemical reaction, energy coefficients can be calculated. Moreover, expressions can be defined to estimate the error related to these variables without considering the standard deviations assumed by Huggett and Tewarson that rely on the hypothesis that the burning material fall within the range of energies that they have defined.

However, this development cannot be applied if the product undergoing combustion has not been identified and characterised. In this situation, there is no procedure to be sure that the considered material releases energy in accordance with Huggett and Tewarson constants.

5.4. HRR comparisons and issues

The main asset of OC and CDG which favoured the spread of these calorimetric approaches over the others available is the possibility to estimate the HRR of a compound without composition information and energetic characteristics. This particularity originates from the assumption of energy constants. A lack of consideration concerning the validity of this hypothesis exists. Often, energy constants values are used without questioning the potential existence of restrictions in their applicability. This matter requires to be explored.

The uncertainty created by the assumption involving energy constants defined when evaluating the HRR of an unknown material is a fundamental concern. First, an analysis of the consistency of the calorimetric equations used to estimate the HRR with the acknowledged assumptions is conducted on two well studied materials. These are methane and PMMA. The HRR are calculated using average values ($\bar{E}_{O_2}, \bar{E}_{CO_2}$ and $\bar{E}_{CO}$), stoichiometric (E_{O_2}, E_{CO_2} and E_{CO}) and chemical values ($E_{O_2\,(ch)}$ and $E_{CO_2\,(ch)}$) as energy coefficients. HRR through mass loss and enthalpy rise approaches are also added. The results of these comparisons show the degree of convergence between the different principles. The distributions of levels of HRR also emphasize the divergence engendered by defining energy constants rather than using energy coefficients based on the stoichiometry or the chemistry of the reaction.

Afterwards, experiments have been performed for a set of more complex products. One assumes the reliability of Thornton's principle. Consequently, the application of OC calorimetry

with the energy constant of Huggett $\bar{E}_{O_2}$, provides an estimation of HRR taken as reference.. The energy coefficient associated to CDG, E_{CO_2}, is determined for each of the materials in order that the HRR result obtained through CDG correlates the OC one. E_{CO_2} fitted values are derived. According to their distribution around the average, one can conclude on the applicability of the energy constants assumption for the considered materials and highlight the potential importance of the chemistry.

5.4.1. HRR uniqueness assumption

For given tests conditions, the HRR estimated through different approaches (Mass Loss, OC, CDG, enthalpy rise...) needs to comply with the uniqueness principle. Any method used to determine the HRR from the combustion of a material, should theoretically provide the same result. In reality, each procedure propagates uncertainties associated with the parameters the calculation relies on. This creates discrepancies in the results. However, conditions exist for which errors related to the measurements are minimized. As mentioned previously, uncertainties related to the mass loss approach falls down to less than 20% when the combustion tends to be complete. Babrauskas reports that the error associated with ΔH_C is as low as 0.05 % [9]. Consequently, when burning occurs under well ventilated regimes, the system can be approximated as a complete combustion. Under this configuration, the major error when estimating the HRR using a mass loss approach originates from the mass measurements. The latter becomes limited if a steady burning is achieved. In a similar way, the errors related to OC and CDG are restricted. For a burning configuration close to complete combustion, the CO correction terms in the equations (Chapter 4, equations [68] and [70]) tend towards zero and so do the errors associated with them. Uncertainties associated with the calculations of species evolution (O_2 for OC and CO_2 for CDG) decrease below 20%. The error can be limited to less than 15% if a steady burning is attained. Finally, under the aforementioned conditions of a complete combustion and a steady burning, the major uncertainty becomes correlated to the energy coefficients. This configuration is clearly appropriate to assess the assumption of energy constants in the case of methane.

5.4.2. Methane

Methane gas was chosen as extensive information is available in the literature with regard to its combustion process. Combustion tests have been carried out using the FPA under air atmosphere. The flow of methane was set constant and so that complete combustion conditions were met. Figure 5.4 illustrates HRR curves resulting from different calculation approaches.

Mass flow (based on the mass loss approach developed in Chapter 4, section 4.2.1), enthalpy rise (appearing as Convective HRR) OC and CDG methods have been performed to estimate the HRR. OC and CDG have been applied using the energy constants respectively defined by Huggett and Tewarson and also using stoichiometric energy coefficient defined from equations (4) and (5). Methane flow rate is adjusted using a gas flow meter whose accuracy, given by the manufacturer, is ± 1 %. Only few ppm of CO are measured during the experiments while CO_2 exceeds 1000 ppm. One can assume complete combustion and then apply equation (4) from Chapter 3 (section 3.2.1) with $\chi = 1$. A simple uncertainty calculation reveals that the error related to the HRR values obtained is supposed to be less than 1%. According to the accuracy of the HRR value, the mass flow approach is taken as reference.

Figure 5.4 shows good correlation between OC and mass flow results. The HRR rise estimated from both methods exhibit a similar slope. The transient behaviour is well captured. The levels of HRR plateau evaluated by means of the different approaches as well as the divergence from the reference value (fixed as the average of the HRR plateau obtained from the mass flow calculation) are indicated in Table 5.4 .The HRR plateau (steady regime) is measured at 4.57 kW from the mass flow and ΔH_C technique. The HRR plateau attained through OC calculation using Huggett energy constant slightly overestimates the reference value. The HRR plateau issued from the use of stoichiometric coefficients (E_{O_2}=12.51 kJ.g^{-1}) reach the same level as the reference one. The difference between the OC methods using Huggett constant or a stoichiometric energy coefficient is easily interpreted by the value given to E_{O_2}. Huggett constant is about 5% higher than the stoichiometric coefficient. This discrepancy reflects the difference measured between the reference HRR and the one calculated through OC calorimetry using Huggett energy constant. The overestimation originates from the latter variable which, in the case of methane, is higher than the actual coefficient for complete

combustion. Afterwards, the HRR decrease suggests similar slope between the OC and the mass flow methods. Discrepancies are nevertheless observed at low HRR. The explanatory hypothesis holds in the correction applied to the O_2 analyser signal that failed to "clear" for low O_2 variation. Molar fraction measurements are altered by the time response of the different analysers. However, they can be represented as a first order system whose output signal and transfer function are known. The aim is then to reconstruct the input signal corresponding, in the present study to the real species concentration evolution. A correction can be applied by use of convolution and Laplace transforms [12] [13]. The signal processing procedure is developed in the next chapter.

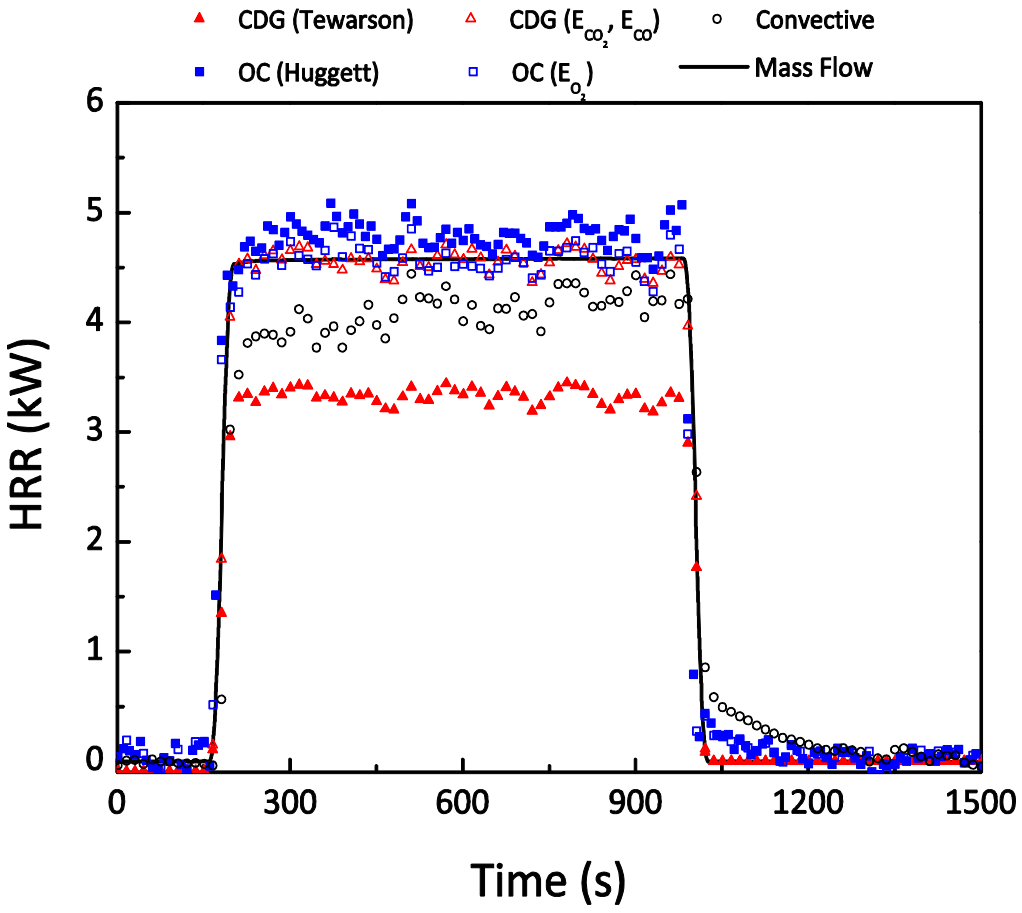

Figure 5.4. Methane HRR estimations using various techniques and assumptions. OC (Huggett) and CDG (Tewarson), respectively refer to OC and CDG principles using Huggett and Tewarson energy constants. OC (E_{O_2}) and CDG (E_{CO_2}, E_{CO}) represent OC and CDG principles used with stoichiometric energy coefficients.

CDG calorimetry captures accurately the HRR rise and decrease as shown on Figure 5.4. However, the calculation based on the use of Tewarson energy constant substantially under-predicts the HRR plateau. A divergence of 27 % is reported in Table 5.4. The CDG procedure relying on stoichiometric energy coefficients (E_{CO_2}=18.2 kJ.g^{-1} of CO_2, E_{CO}=18.6 kJ.g^{-1} of CO) exhibits a HRR plateau whose magnitude converges to the reference one. Consequently, one assumes that the underestimation highlighted originates from the use of Tewarson energy constants, $\bar{E}_{CO_2}$ and $\bar{E}_{CO}$. They are respectively 27 % and 40 % lower than E_{CO_2} and E_{CO}. Only few ppm of CO are produced from the combustion which can be assumed complete. The term related to the CO formation in the CDG equation has an infinitely small contribution on the HRR. The energy release can be directly correlated with the generation of CO_2. This confirms the origin of the HRR under-prediction.

The enthalpy rise approach (convective HRR) provides good characterisation of the transient periods (HRR rise and decrease rates). Nevertheless, the magnitude calculated for the HRR plateau is about 12 % lower than the reference one. Recalling the description of the method detailed in the previous chapter [Chapter 3, section 3.2.2], it suffers from heat losses issues. The apparatus absorbs a fraction of the heat emitted, mostly by radiation. Unlike the OSU calorimeter, no compensation system has been built on the FPA used to conduct the present experiments. Methane has a relatively low emissivity and the radiative losses are limited. The 12 % variation observed between the reference HRR plateau and the one estimated through enthalpy rise approach corresponds to the radiative HRR [2]. The actual expression of the HRR is given by Tewarson as,

$$\dot{q} = \dot{q}_{convective} + \dot{q}_{radiative} \quad (19)$$

Where $\dot{q}_{radiative}$ corresponds to the heat absorbed by the apparatus.

Finally, by considering the mass flow approach as the reference procedure, OC calorimetry yields to similar results. When used with Huggett energy constant, the HRR is only 5 % overestimated but the divergence is corrected by the application of the methane stoichiometric energy coefficient. This allows the conclusion that, in terms of OC calorimetry, the energy value is the main source of uncertainty for the present experimental conditions. However, if methane would have not been identified as the gas involved in the fire, the precision of the HRR outcomes would not be significantly affected. Figure 5.5 regroups the

HRR results from mass flow approach and OC calorimetry where the error range associated with the Huggett energy constant uncertainty (± 5 %) has been added. It shows that the HRR estimated at the low boundary ($\bar{E}_{O_2\ low}$= 12.45 kJ) encompasses the reference HRR. Consequently, the error range associated with Huggett energy constant is relevant for methane. Figure 5.6 stresses a similar procedure, CDG replacing OC calorimetry. The CO production being minimal, the error band associated with Tewarson energy constant $\bar{E}_{CO_2}$(± 11 %) is only considered. Figure 5.6 highlights that, despite considering the uncertainty range related to $\bar{E}_{CO_2}$, the CDG calorimetry by means of Tewarson energy values fails to estimate the HRR within a range of confidence. While the use of stoichiometric coefficient leads to accurate results, the assumption of validity of Tewarson energy has to be excluded in the case of methane gas fire. The applicability of CDG with methane relies on the knowledge of the gas chemistry and its heat of combustion.

For a steady burning of methane gas, assuming the mass flow approach as reference, OC and CDG calorimetries allow accurate approximations of the HRR. In the case of OC, the use of a stoichiometric energy coefficient improves the results accuracy although Huggett energy constant only slightly overestimates the HRR but remains included within the error range associated with $\bar{E}_{O_2}$. The CDG calorimetry provides precise HRR estimation when stoichiometric coefficients are used. However, Tewarson energy constants are not applicable with methane.

Table 5.4. Values of steady HRR calculated according to the different estimation techniques and divergence from the reference value.

Method	Mass Flow	OC (Huggett)	OC (E_{O_2})	CDG (Tewarson)	CDG (E_{CO_2}, E_{CO})	Convective
$\dot{q}_{steady}$ (kW)	4.57	4.78	4.57	3.33	4.56	4.00
$\Delta\dot{q}$ (%)	*Ref. Val.*	4.71	0.03	27.02	0.18	12.54

Ref. Val.: HRR estimated through the mass flow calculation is taken as reference.

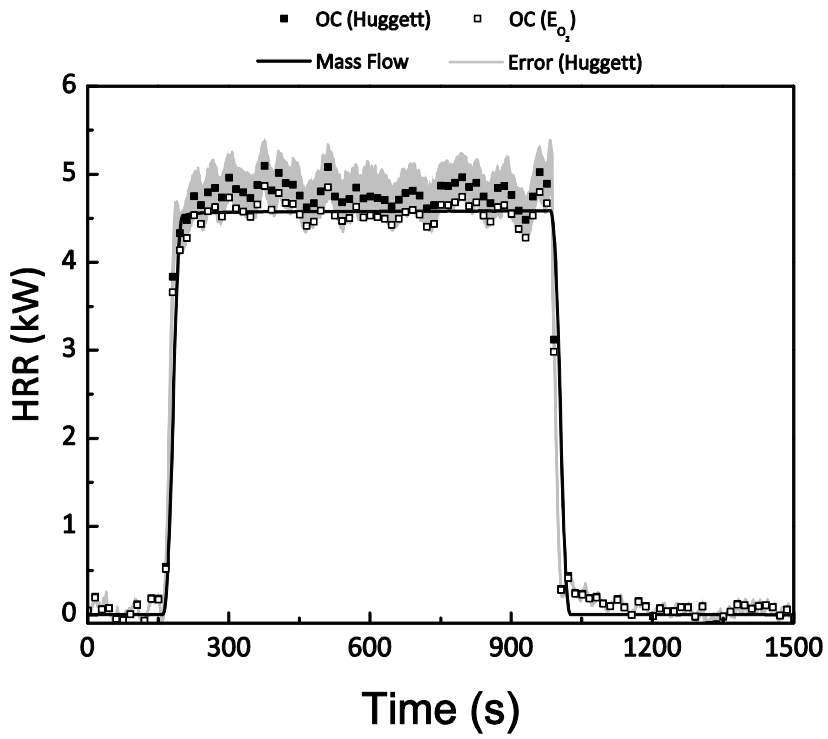

Figure 5.5. Comparison of HRR through mass loss approach and OC (Huggett's constants and stoichiometric energy coefficients) with error range for Methane.

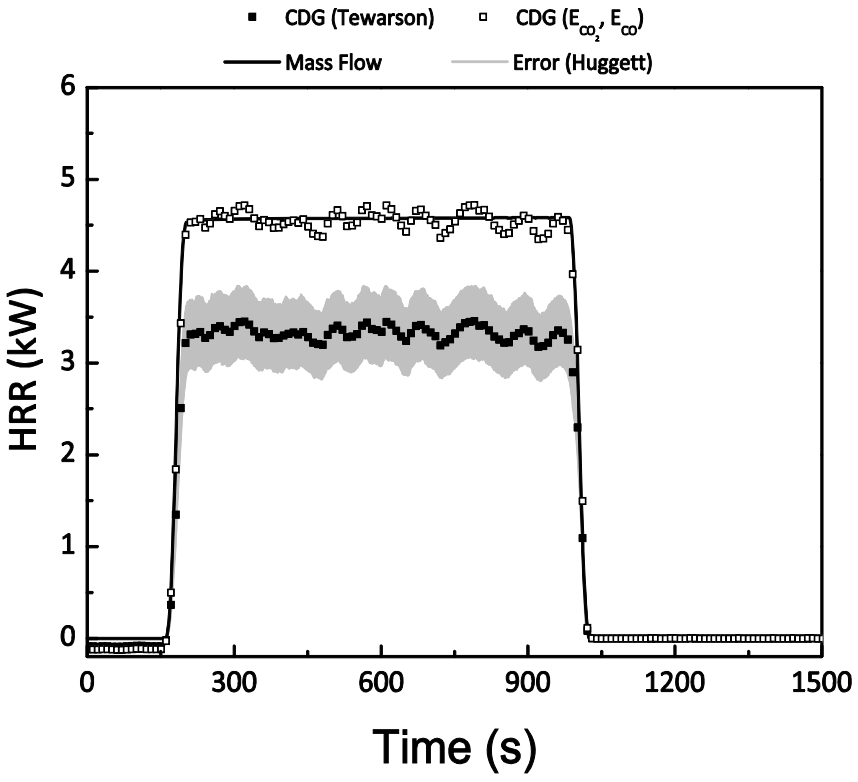

Figure 5.6. Comparison of HRR through mass loss approach and CDG (Tewarson's constants and stoichiometric energy coefficients) with error range for Methane.

5.4.3. PMMA

The second set of experiments are carried out with polymethylmethacrylate (PMMA, $(C_5H_8O_2)_n$). It is a synthetic solid polymer whose behaviour has been widely studied by the fire community. Its combustion process is more complex than the one of methane gas given its solid state. While methane burning was only controlled by mixing and kinetics, the burning of solids requires the decomposition of the solid phase into various volatiles prior to achieve combustion. On the other hand, while the flow of methane could be set constant, a steady pyrolysis rate is relatively difficult to obtain with a solid. If the solid is submitted to an external heating, a change in the surface shape (for instance, induced by swelling) modifies the heat transfer through it and then affects the decomposition rate. Also, the flame heats up the surface by convection and radiation and strongly influences the decomposition of the material. A similar experimental setup to the methane tests is complicated to create. On the other hand, the influence of the energy coefficients on the HRR estimation was previously investigated through a steady burning, while it appeared that the HRR rise and decrease were well captured by the different approaches. It is important to analyse into more details the response of the different HRR techniques to transient combustion modes. In order to minimize the uncertainties related to the measurements, ventilation conditions have been selected in order to achieve complete combustion. Only traces of CO are measured during the experiments. Terms related to the contribution of CO formation to the HRR are small enough not to influence the results and so do the associated errors. Like previously for methane, HRR calculated through a mass approach is adopted as reference. The uncertainty associated with ΔH_C is 0.05 % [9] and the assumption of complete combustion allows to apply ΔH_C and its related uncertainty. It comes that the main error resulting from this procedure originates from the mass loss measurement and was estimated for a maximum of ± 17%. From all the techniques used, this method offers the highest confidence and HRR comparison will be held on its basis.

Figure 5.7 depicts the HRR curves that have been calculated through different approaches: mass loss, OC and CDG based on energy constants, OC and CDG based on stoichiometric coefficients and enthalpy rise principles. Table 5.5 indicates the maximum HRR, total heat release and the standard deviation from the respective reference values calculated by means

of the different HRR estimations techniques. Both pieces of information are used to investigate about the accuracy that is able to offer each of the calculation methods.

Results deduced from OC calorimetry present good agreement with the reference HRR, whichever the assumption on the energy value is. In terms of HRR peak, OC combined with the use of Huggett energy constant exhibits better convergence with the reference HRR maximum than OC calorimetry based on the use of stoichiometric energy coefficient. Nevertheless, according to Table 5.5, the standard deviation between OC HRR peaks and the reference one does not exceed 6 %. With regard to total energy release, the divergence OC based on Huggett assumption or a stoichiometric energy coefficient (E_{O_2}=12.96 kJ.g^{-1} of O_2) and the reference value calculated from the mass loss approach is less than 2 %. Furthermore, the different phases of HRR increase and decrease depicted by means of OC calorimetry follow the HRR evolution described by the mass loss approach.

CDG results stress differences according to the energy values used. The method combined with the utilization stoichiometric energy coefficients (E_{CO_2}=11.50 kJ.g^{-1} of CO_2 and E_{CO}=8.00 kJ.g^{-1} of CO) present a HRR evolution similar to the reference curve. The latter statement is confirmed by the standard deviation data from Table 5.5 which do not exceed 2 %. Unlike the stoichiometric energy coefficients, Tewarson energy constants exhibit less convergence with the HRR reference results. Maximum HRR and total heat release are both overestimated between 15 and 17 %. However initial HRR increase and HRR decrease correlate well with the reference curve. Assuming the correctness of the mass loss HRR, this suggests that the chemistry describes correctly the HRR process but the energy level associated with the chemical reaction is too high. Tewarson energy constants characterise the combustion of PMMA with a lower precision than the stoichiometric energy coefficients. One can notice that the 15 % difference between $\bar{E}_{CO_2}$ and E_{CO_2} coincides with the discrepancies measured for the peak HRR and the total heat release when comparing the reference values with the CDG ones base on the use of Tewarson energy constants. This suggests that, considering a complete combustion configuration, the major potential source of error that can affect the HRR estimation from a CDG calculation stems from the energy coefficients. Another discrepancy arises with, CDG independently of the energy assumption. The divergence is observed during the HRR decrease and for low values. The HRR decreasing rate of the CDG methods becomes stronger than the ones related to the reference and OC principles. The source of divergence is

speculated to emanate from the correction applied to the CO_2 molar fraction signal. The process will be developed in more details in the next chapter but some notions of the occurring phenomenon are introduced here. The response of an analyser to a species concentration is not instantaneous and can require few seconds. Consequently, any analyser is characterized by a time constant or response time which represents the lag needed by the instrument to reach 90% of a steady state response from a constant input signal (for instance, a square signal)[12]. The shorter the response time, the better is the accuracy of the output signal. However, in case this characteristic time is too long to precisely capture the concentration evolution of a species or if the kinetics of a reaction is too rapid for allowing an accurate measurement, methods have been developed to reconstruct the input signal by processing the output response [13]. This can be achieved by determining the transfer function of the apparatus which depends on the response time and the derivative of the output signal. Some analysers respond differently whether the signal rises or decreases. In the present study, the CO/CO_2 analyser is characterized by two different response times, one associated with an ascending signal (i.e. an increase in species concentration), and the other defining the lowering. Both have been accurately measured. Nevertheless, the response time associated with a decreasing signal highlights a dependency on the magnitude of the signal. Furthermore, the precision on the derivative calculation relies on the sampling frequency of the output signal, 0.5 Hz. This low frequency introduces noise in the derivative. Small variations in the signal and its derivative cannot be well described which results in an important alteration of the signal at low level. In particular, a phenomenon of overshoot is caused by the correction. Unfortunately, none of the attempts to reduce the noise has succeeded.

The convective HRR remains significantly lower than the reference HRR. The difference corresponds to the heat absorbed by the calorimeter, mainly radiation emitted by the flame. The total heat release is overestimated by more than 50%. This is due to the 30 kW external heat flux applied at the sample surface to promote the decomposition of the material. The IR heaters have been heating the walls of the apparatus as well as the entrained air resulting in an elevation of the temperature inside the exhaust duct. Consequently, the convective HRR is altered by weaknesses relative to the calorimeter design.

Table 5.5. Values of HRR peak ($\dot{q}_{max}$) and total heat release (ΔQ) according to the different estimation techniques and divergences from the reference values.

Method	Mass Loss	OC (Huggett)	OC (E_{O_2})	CDG (Tewarson)	CDG (E_{CO_2}, E_{CO})	Convective
$\dot{q}_{max}$ (kW)	7.89	7.91	7.43	9.22	7.85	6.01
$\Delta\dot{q}_{max}$ (%)	*Ref. Val.*	0.34	5.72	16.86	0.49	23.80
Q (kJ)	1317	1340	1335	1519	1295	2029
ΔQ (%)	*Ref. Val.*	1.75	1.37	15.34	1.67	54.06

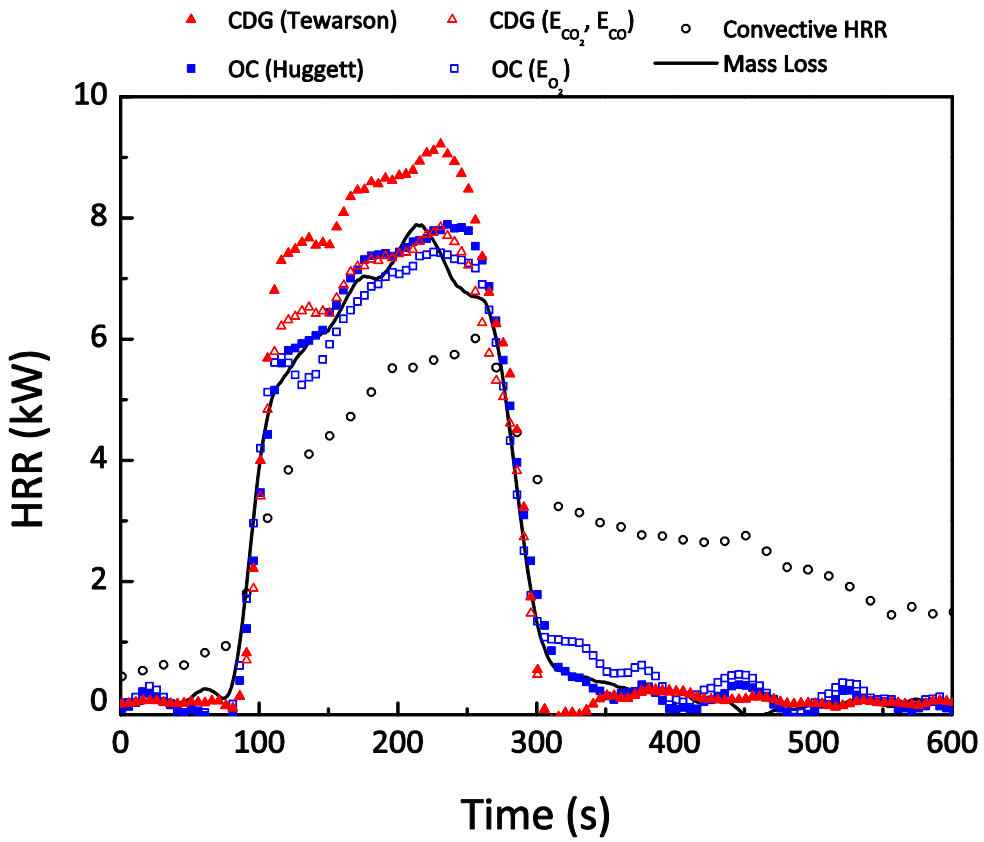

Figure 5.7. PMMA HRR estimations using various techniques and assumptions. OC (Huggett) and CDG (Tewarson), respectively refer to OC and CDG principles using Huggett and Tewarson energy constants. OC (E_{O_2}) and CDG (E_{CO_2}, E_{CO}) represent OC and CDG principles used with stoichiometric energy coefficients.

HRR estimated by means of mass loss approach, taken as a reference, and OC calorimetry highlight converging results. HRR calculation using OC combined with Huggett energy constant offers the lowest divergence with the reference variable. One can notice that, despite the

calculation of the stoichiometric energy coefficient for PMMA leads to E_{O_2} = 12.97 kJ.g^{-1} of O_2, Tewarson recommends using 13.1 kJ.g^{-1} of O_2 [2]. Similarly, CDG calorimetry based on stoichiometric energy coefficients allows accurate estimation of the HRR as depicted by the convergence of these results with the reference ones. Results derived from CDG calorimetry relying on the use of Tewarson energy constants develop larger discrepancies with the reference HRR as a consequence of too high energy values.

Figure 5.8 and Figure 5.9 propose, respectively, the reference HRR with the OC results and with the CDH results on a separate basis. On both graphs, the error range associated with the uncertainty related to Huggett and Tewarson energy constants has been added and appears as a grey area. The reference HRR is contained within the error range defined by Huggett for the OC calorimetry. The use of Huggett energy constants in the case of PMMA is totally relevant. Considering now the CDG calorimetry, HRR with the low bound of Tewarson uncertainty related to the $\bar{E}_{CO_2}$ constant exhibits a higher value, at each time, than the reference HRR. Apart from the overshoot period observed during the decrease of the HRR for low values, the CO_2 concentration evolution follows the dynamics of the mass loss which suggests that error related to the measurements are limited. Consequently, the main contributor susceptible to affect the results accuracy stands in the energy coefficient. Regarding the combustion of PMMA, confidence on the degree of accuracy of the HRR estimation obtained through CDG calorimetry coupled with the use of Tewarson energy constants cannot be achieved by simply considering their assumed error bound. Nevertheless, the divergence from the reference measured for the latter configuration does not exceed 17%, an acceptable precision.

Finally, for complete combustion conditions, a blind estimation of the HRR in the case of PMMA should not introduce an error significantly larger than 17% (with the hypothesis that the experimental configuration minimizes the uncertainty related to the measurements). OC calorimetry and CDG combined with stoichiometric energy coefficient generates accurate results in the present experimental configuration. Nevertheless, like for methane, the assumption that one can rely on the error range associated with Tewarson energy constants as a safety margin of the HRR level estimated is not valid.

So far, the results suggest that the accuracy of the results is usually improved by the use of stoichiometric energy coefficients. However, if these values are unknown, Huggett energy

constant and the uncertainty associated with the value have shown ability to define a range of confidence on the HRR level, unlike the CDG.

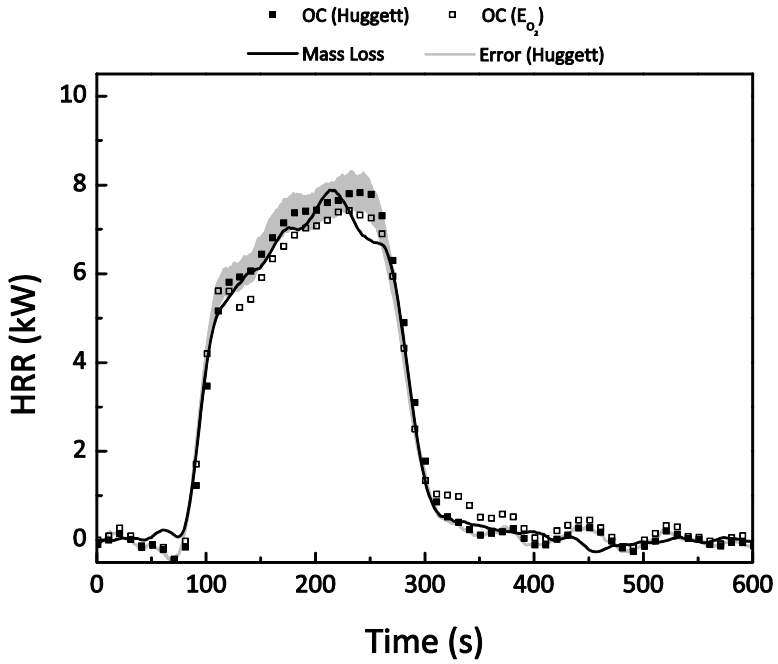

Figure 5.8. Comparison of HRR through mass loss approach and OC (Huggett's constants and stoichiometric energy coefficients) with error range for PMMA.

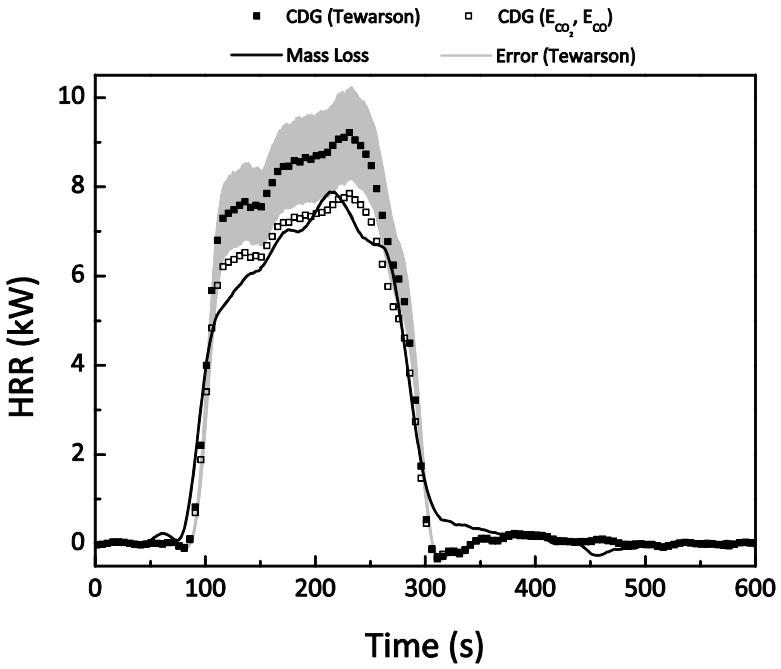

Figure 5.9. Comparison of HRR through mass loss approach and CDG (Tewarson's constants and stoichiometric energy coefficients) with error range for PMMA.

5.4.4. Complex and uncharacterised materials

If the present discussion is extended further, one can wonder if materials embedding a complex chemistry, such as fire retardants, nanocomposite polymers, energetic materials or simple pine needles, still comply with the assumption of energy constants. An attempt to answer to this question is conducted in two stages. For many materials, the combustion process remains not fully understood but a one step reaction can be defined. The heats of combustion might also have been estimated from bomb calorimeter tests. This is particularly true for materials presenting a complex chemistry. Accurate description of the thermal behaviour of materials whose decompositions are characterised by coupled physical and chemical mechanisms remains an aim to achieve. However, it is possible to gather some of these materials, to consider the distribution of their stoichiometric energy coefficient and compare its average and standard deviation to the values defined by Huggett and Tewarson. Subsequently, according to the conclusion previously raised, one will consider uncharacterised materials and try to assess the validity of the energy constants concept through blind HRR estimations under the hypothesis of the uniqueness of the HRR for a material under given combustion conditions.

For practical application, it is critical to perceive the limit of validity of the energy constants assumption and when knowledge of the material chemistry becomes fundamental. To assess this issue, a set of various materials has been considered. It encompasses the same compound PMMA ($(C_5H_8O_2)_n$, [2] [10]) as studied previously, polypropylene (PP, $(\text{-}CH_2\text{-}CH(CH_3)\text{-})_n$, [10]), polybutylene (PBT, $(C_{12}H_{12}O_4)_n$, [10]), Nylon (PA6, $(C_6H_{11}O)_n$, [2] [10]), pine needles (Pinus pinaster (PPi, $C_{4.22}H_{6.79}O_{2.595}$, [14]) and Pinus halepensis (PH, $C_{4.22}H_{6.79}O_{2.595}$, [14]) and the ternary powder based on a starch, lactose and potassium nitrate mixture previously characterised (40% KNO_3: $C_{3.23}H_{5.65}O_{4.30}N_{0.59}K_{0.59}$, 50% KNO_3: $C_{2.5}H_{4.36}O_{3.89}N_{0.69}K_{0.69}$). The heat of combustion of each of the materials was estimated by means of a bomb calorimeter or it was found in the literature [1] [2] [9] [10]. A single global complete combustion reaction is assumed for each of the materials which combined to their heat of combustion allows the estimation of stoichiometric energy coefficients, E_{O_2}, E_{CO_2} and E_{CO}. Unlike the two previous sections, the HRR curves will not be displayed as the comparison would become too intricate to be clear. Instead, it has been decided to stress the discussion on the distributions defined by the different values of stoichiometric energy coefficients associated with each material.

E_{O_2}, E_{CO_2} and E_{CO} are introduced, respectively in Figure 5.10, Figure 5.11 and Figure 5.12. Means and standard deviations from the distribution are also displayed on the aforementioned figures as well as on Table 5.6 and Table 5.7.

The stoichiometric energy coefficients for OC of the set of considered materials present a narrower distribution than the one illustrated on Figure 5.1 (σ=1.54 kJ.g^{-1} of O_2 for the present distribution and was 1.86 kJ.g^{-1} of O_2 for the distribution appearing on Figure 5.1). The mean value has been increased from 13.1 to 13.27 kJ.g^{-1} of O_2. The divergence from Huggett's value is less than 2 %. Considering the distribution, it arises that this slight transfer is mainly caused by the E_{O_2} values estimated for the ternary powders. As they carry an oxidizer (KNO_3), they require less O_2 from the reacting atmosphere to achieve complete combustion than if no O element was present in their structure. Consequently, the stoichiometric coefficient of the combustion reaction related to O_2 (the term $\left(\frac{x}{2}+\frac{y}{4}-\frac{z}{2}\right)$ in equation (4)) is reduced (z being higher) which results in enhancing E_{O_2}. While the calculated E_{O_2} coefficients remain close to the mean value of the distribution for five of the characterised materials (Pine needles, 40% KNO_3 ternary powder, PBT, PP and PMMA), two compounds highlight noticeable deviations. An explanation of the high E_{O_2} value exhibited by the 50% KNO_3 ternary powder has just been sketched. In the opposite direction, PA6 exposes a low OC stoichiometric energy coefficient compared to the other materials. One can attempt to underline a difference characterising this compound from the others. Its heat of combustion is of magnitude similar to PMMA or PBT that present higher E_{O_2}. However, the latter arise a higher O content (that can be estimated on the base of O/C ratio, cf. Table 5.8). In a matter of fact, PA6 will require more O_2 from the supporting atmosphere per unit mole of C in the fuel to achieve complete combustion. Considering the complete combustion equation, the stoichiometric coefficient, ψ_{O_2}, will be higher for PA6 than for PMMA or PBT (cf. Table 5.8). Recalling (4), as their heats of combustion are close, the higher ψ_{O_2} causes a lower E_{O_2}. This result suggests that it is not the complexity of the molecule that might tend deviating the stoichiometric energy coefficients from the acknowledged value defined by Huggett. On the other hand, the presence of O elements within the molecule appears being able to affect E_{O_2}.

Regarding the E_{CO_2} distribution on Figure 5.11 and the results from Table 5.7, values are more scattered than for the E_{O_2} distribution (σ=2.08 kJ.g^{-1} of CO_2). Also, the mean value of the

distribution is about 22% lower than the one defined by Tewarson. Apart from PP, none of the materials considered exhibits a stoichiometric energy coefficient higher than Tewarson energy constant. Pine needles, PA6, PBT and PMMA highlight E_{CO_2} values confined around the mean of the distribution. PP is characterised by a higher energy coefficient. Its heat of combustion is higher than the other materials. Furthermore, it encompasses the second smallest stoichiometric coefficient of the combustion reaction, ψ_{CO_2}. Combination of the two characteristics explains the higher E_{CO_2}. Unlike PP, the two ternary powders are featured with low E_{CO_2} value. This arises from their low heat of combustion. One can also notice that the heats of combustion related to PMMA, PBT, PA6 and the pine needles are comprised within a narrow range. Although, the structure of each material differs from one to another, the deviation within their E_{CO_2} values is limited to less than 0.3 kJ.g^{-1} of CO_2. This strengthens the hypothesis of a dependency on the chemical structure and the energy associated with. According to equations (4) and (5), the two major factors governing the magnitude of the stoichiometric energy coefficients are the heat of combustion, ΔH_c and the reaction stoichiometric coefficients, ψ_{O_2} and ψ_{CO_2}. A part of the energy release during the combustion originates from the material. It is credible to assume that the chemical structure of an element and the energy it contains are closely related.

Table 5.6. Mean and standard deviation of the E_{O_2} distribution and standard deviation from Huggett value.

OC	
E_{O_2} = 13.27 kJ.g^{-1} of O_2	(± 1.54 kJ.g^{-1} of O_2 ⇔ 11.6 % error band)
$\Delta_{[E_{O_2}, \bar{E}_{O_2[Huggett]}]}$ = 1.3 %	

Table 5.7. Means and standard deviations of the E_{CO_2} and E_{CO} distributions and standard deviations from Tewarson values.

CDG	
E_{CO_2}= 10.34 kJ.g^{-1} of CO_2	(± 2.08 kJ.g^{-1} of O_2 ⇔ 20.1 % error band)
$\Delta_{[E_{CO_2},\bar{E}_{CO_2\,[Tewarson]}]}$ = 22.3 %	
E_{CO}=6.1 kJ.g^{-1} of CO	(± 3.3 kJ.g^{-1} of O_2 ⇔ 53.3 % error band)
$\Delta_{[E_{CO},\bar{E}_{CO\,[Tewarson]}]}$ = 44.7 %	

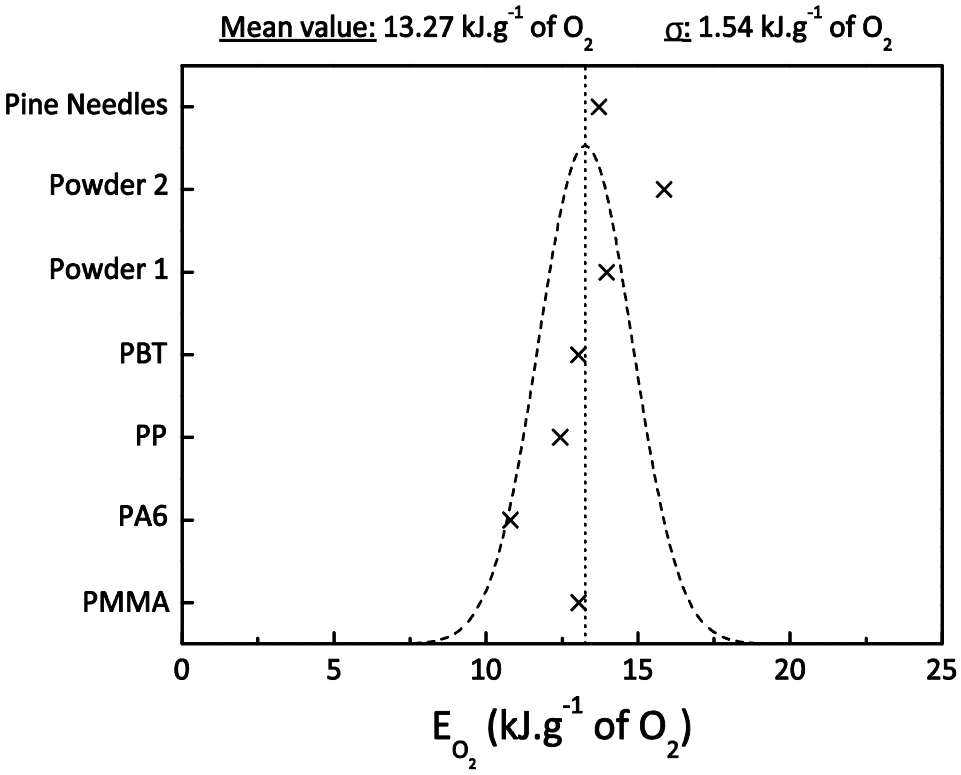

Figure 5.10. E_{O_2} stoichiometric energy coefficient distribution for a set of 7 different materials.

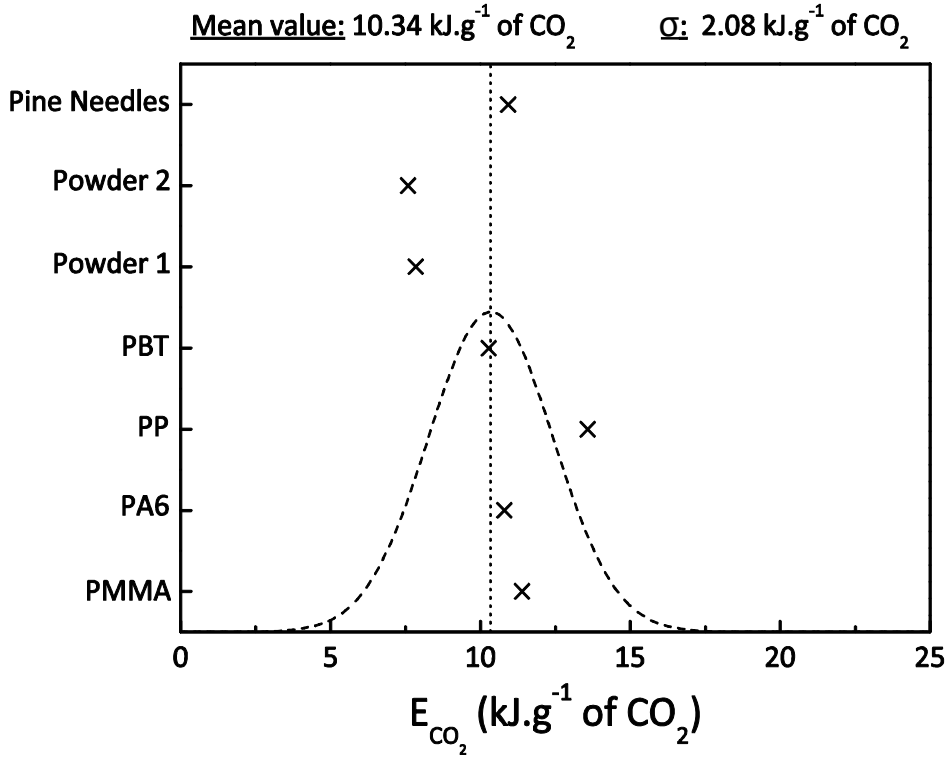

Figure 5.11. E_{CO_2} stoichiometric energy coefficient distribution for a set of 7 different materials.

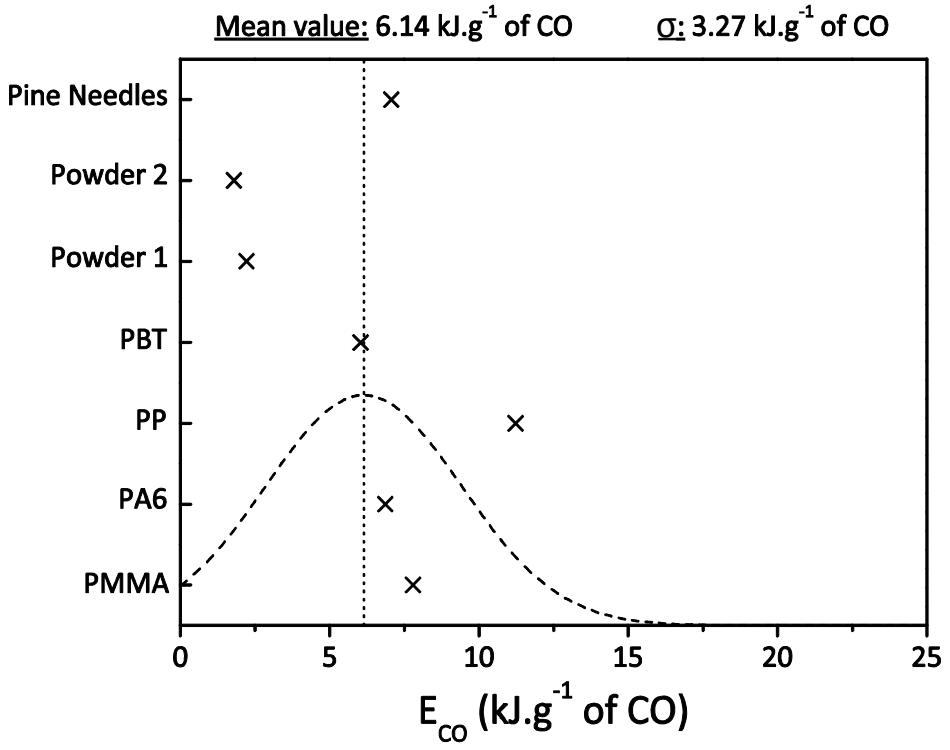

Figure 5.12. E_{CO} stoichiometric energy coefficient distribution for a set of 7 different materials.

Table 5.8. Information associated with the materials characteristics.

Material	C	H	O	N	M ($g.mol^{-1}$)	ΔH_C ($kJ.g^{-1}$)	E_{O_2} ($kJ.g^{-1} O_2$)	E_{CO_2} ($kJ.g^{-1} CO_2$)	E_{CO} ($kJ.g^{-1} CO$)	C/H	O/C	ψ_{CO_2}	ψ_{O_2}	$\frac{\psi_{O_2}}{\psi_{CO_2}}$
PMMA [2] [10]	5.00	8.00	2.00	0.00	100.00	24.88	12.96	11.31	7.67	0.63	0.40	5.00	6.00	1.20
PBT [10]	12.00	12.00	4.00	0.00	220.00	26.71	14.13	11.13	7.39	1.00	0.33	12.00	13.00	1.08
PA6 [2] [10]	6.00	11.00	1.00	0.00	99.00	28.80	10.80	10.80	6.87	0.55	0.17	6.00	8.25	1.38
PP [10]	3.00	6.00	0.00	0.00	42.00	43.23	12.61	13.76	11.52	0.50	0.00	3.00	4.50	1.50
Pine Needles [14]	4.22	6.79	2.60	0.00	98.95	20.50	13.72	10.92	7.07	0.62	0.61	4.22	4.62	1.09
Powder 1	3.23	5.65	4.30	0.59	149.5	7.46*	13.97	7.84	2.21	0.57	1.11	3.23	2.86	0.88
Powder 2	2.50	4.36	3.89	0.69	138.4	6.01*	15.86	7.58	1.80	0.57	1.22	2.50	2.07	0.83

*Bomb calorimeter measurement

Finally, the existence of energy constants should reflect a correlation between these two variables. From the previous distributions, regarding the materials considered, the assumption of an energy constant with an acceptable error associated with the OC calorimetry seems relevant. Energy coefficient distributions related to the CDG exhibit average values lower than the ones defined by Tewarson as well as larger uncertainties. Some of the tested materials comprise atypical chemistry. They probably cause the divergence observed but they might only constitute extreme cases. In order to verify the last statement, an approach based on the assumption of the uniqueness of the HRR has been developed. Theoretically, for a given material and under identical experimental conditions, OC and CDG should provide similar HRR estimations outcomes.

For a population of various and complex compounds, the validity of the assumption of energy constants (whether or not the values match Huggett and Tewarson ones) can be assessed by doing the hypothesis that OC calorimetry based on Huggett's energy constant applies (as appearing as the most robust of the two principles). The HRR associated with each sample of the population can then be estimated through OC calorimetry. According to the HRRuniqueness assumption, a calculation by means of CDG based on the same calorimetric data should lead to an identical result. One proposes to apply an inverse approach to each material of the population, by assuming $\dot{q}_{OC} \approx \dot{q}_{CDG}$ and then estimate E_{CO_2} and E_{CO}. E_{CO_2} and E_{CO} are determined by minimising the difference,

$$\Delta\dot{q} = |\dot{q}_{OC} - \dot{q}_{CDG}| \xrightarrow[[E_{CO_2}, E_{CO}]]{} 0 \tag{20}$$

The approach can be formulated as,

For a given $\nu \geq 0$ and small enough, there is a couple $\left(E_{CO_2/\,\Delta\dot{q}\to 0}, E_{CO/\,\Delta\dot{q}\to 0}\right)$, such as

$$\min\left(\Delta\dot{q}\left(E_{CO_2/\,\Delta\dot{q}\to 0}, E_{CO/\,\Delta\dot{q}\to 0}\right), \nu\right) = \Delta\dot{q}\left(E_{CO_2/\,\Delta\dot{q}\to 0}, E_{CO/\,\Delta\dot{q}\to 0}\right) \tag{21}$$

The considered population consists in the seven previous compounds whose stoichiometric energy coefficients were known. Furthermore, some of polymers have seen their chemical structure modified by adding fire retardants and/or nanocomposites elements to the parent matrix. These latter materials have not been previously characterized in terms of chemical emissions or heat of combustion. Their exact composition is unknown. OC and CDG appear as

the most eligible techniques to estimate the HRR. Assessed E_{CO_2} values are represented on Figure 5.13. Normal distribution, mean value and standard deviation are also included. First, one has to emphasize that their scattering does not stress the error associated with one method according to the other. One needs to recall that the applicability of OC calorimetry relying on the use of Huggett energy constant has been assumed. Previous results have shown that this hypothesis involves restrictions. The main information arising from the distribution featured on Figure 5.13 is that no energy constants, $\bar{E}_{O_2}$ and $\bar{E}_{CO_2}$, can be clearly defined so they would allow an acceptable estimation of the HRR by means of OC and CDG and that would comply with the uniqueness hypothesis. The $\bar{E}_{CO_2}$ obtained values are scattered. The average, despite being not too far from Tewarson estimate, is one other different value than the ones obtained previously (see Figure 5.2 and Figure 5.11) associated to a different standard deviation. No trend can be found from the different approaches used. One can assume that these coefficients are governed by the structure and the chemistry of the material. If a combustion reaction is often modelled as a simple one step equation leading to the formation of CO_2 and H_2O, this simplification applied to complex materials probably fails to characterise the actual material behaviour. More description of the reaction has to be added in order to better understand the mechanisms involved.

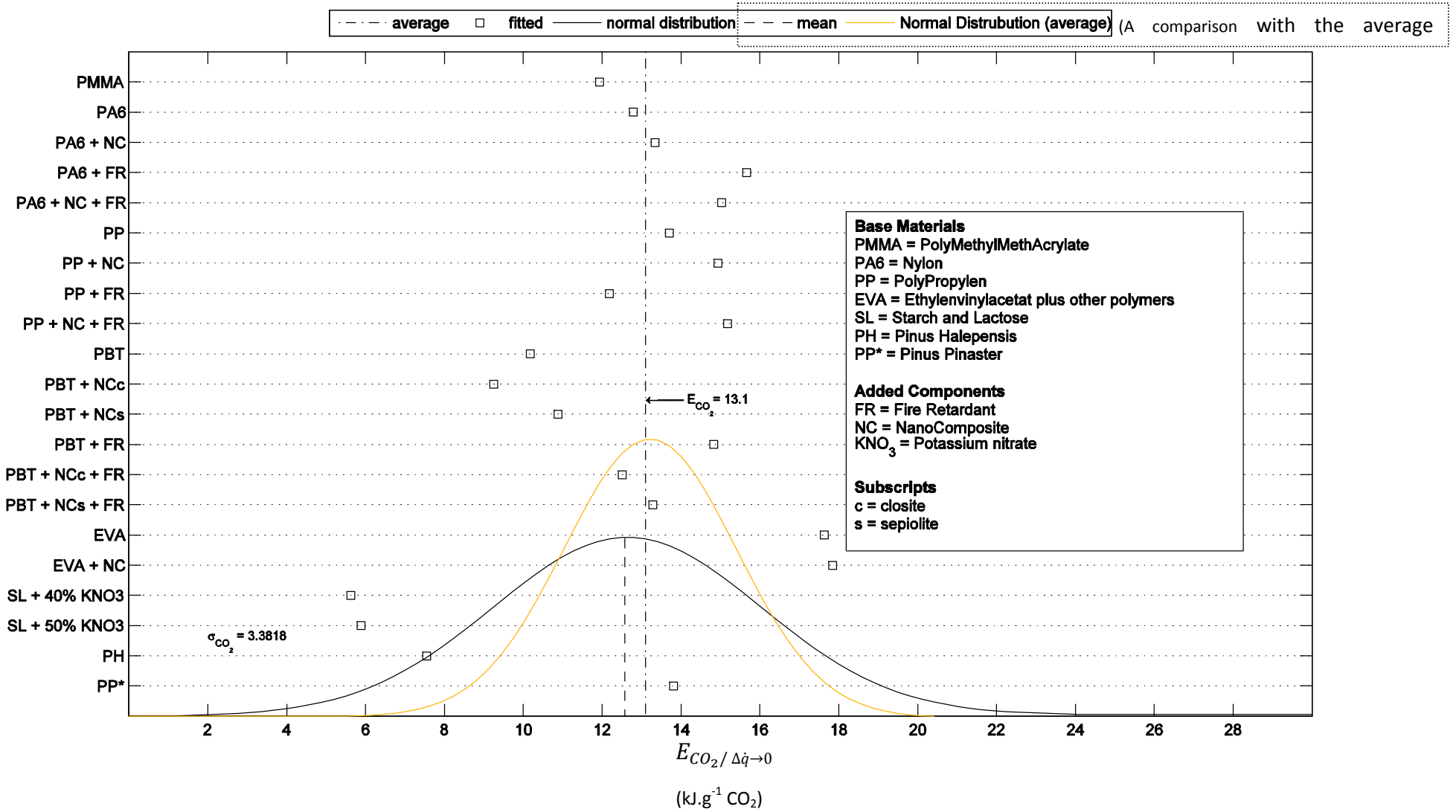

Figure 5.13. Estimated E_{CO_2} values based on an inverse approach assuming the correctness of $\dot{q}_{OC}$.

5.4.5. Limitations of the energy constants assumption

The hypothesis based on the use of Huggett and Tewarson values as energy coefficients applied, respectively, to OC and CDG methods has demonstrated its limitation when materials propose a complex chemistry. Nevertheless, the issue of not being able to define a value, that could describe a majority of compounds, has to be meditated from a coherent perspective. OC and CDG constitute approximate methods for assessing the HRR. They do not intend to produce a high precision value. Recalling the respective equations for OC and CDG [Chapter 3, section 3.2.3, expressions (61) and (63)], the wide number of parameters included in the expressions favours the propagation of uncertainties. Theoretically, regarding only the calculation, assuming the different simplifications of CO and CDG applicable [Chapter 4, section 4.2.3.2.1] and then neglecting uncertainties associated with the specimen being tested and the ones related to the experimental conditions, overall uncertainties of the methods can be lumped within two groups [3]: a first encompassing the different measurements and a second one describing a range of confidence attached to the energy values. This can be expressed as follow, assuming these two uncertainties independent,

$$\delta\dot{q}_{[OC,CDG]} = \sqrt{\left(\frac{\partial\dot{q}_{[OC,CDG]}}{\partial E_{[E_{O_2},E_{CO_2}]}}\delta E_{[E_{O_2},E_{CO_2}]}\right)^2 + \left(\frac{\partial\dot{q}_{[OC,CDG]}}{\partial\Delta\dot{m}_{[O_2,CO_2]}}\delta\Delta\dot{m}_{[O_2,CO_2]}\right)^2} \quad (22)$$

$$= \sqrt{\left(\Delta\dot{m}_{[O_2,CO_2]}\delta E_{[E_{O_2},E_{CO_2}]}\right)^2 + \left(E_{[E_{O_2},E_{CO_2}]}\delta\Delta\dot{m}_{[O_2,CO_2]}\right)^2}$$

Well characterised experimental configurations allow reducing the uncertainty related to the measurements below 15 %. Such accuracy was achieved for the previous methane experiments, carried out under complete combustion conditions and where a steady state was reached reducing the errors. Nevertheless, uncertainties associated with the species evolution rates ($\Delta\dot{m}_{O_2}$, $\Delta\dot{m}_{CO_2}$) have been evaluated to potentially rise up to 22 %. It comes from this result that, for most of the experimental configurations, the accuracy of OC and CDG are not intended to provide highly precise results with only few percents of uncertainty but rather an estimation of an HRR range. From this angle, the necessity of defining energy constants does not appear fundamental anymore. The critical characteristic that needs to be introduced into the OC and CDG principles is the ability to predict in a conservative way, the most accurate

HRR range comprising the actual energy level. This is essential in order to define the HRR magnitude of uncharacterised materials with an adequate confidence.

5.5. Attempt to estimate an energetic coefficient error range

Firstly, one needs to understand why no energy constants clearly emerge from the previous study. Recalling expressions (4) and (5), a general formula is given by,

$$E_i = \frac{\Delta H_C}{\psi_i}\frac{M_{material}}{M_i} \tag{23}$$

Where ψ_i is the stoichiometric coefficient of the reaction of complete combustion associated with the species i. Two governing parameters can be emphasized:

1. the term $\Delta H_C M_{material}$ corresponds to a heat of combustion per unit mole;
2. the stoichiometric coefficient ψ_i.

Although two materials are characterised by relatively similar heats of combustion like ethane and ethylene, they can exhibit different energy coefficients, as seen on Table 5.9. The divergence originates from different stoichiometric coefficients which are correlated to the material composition.

Table 5.9. Ethane and ethylene comparison.

Compound	$\Delta H_C M_{material}$ (kJ.mol^{-1})	ψ_{O_2}	E_{O_2} (kJ.g^{-1} of O_2)
Ethane (C_2H_6)	1423	$\frac{7}{2}$	12.71
Ethylene (C_2H_4)	1411	3	13.78

On the other hand, certain compounds can present a similar composition, such as monomers and polymers while their associated heats of combustion are significantly different (see Table 5.10). Finally, the two latter specific cases nevertheless confirm the previous statement: the energy coefficients are driven by two parameters: the heat of combustion and the stoichiometry of the complete combustion reaction.

Table 5.10. Polypropylene and propene comparison.

Compound	$\Delta H_C M_{material}$ (kJ.mol^{-1})	ψ_{O_2}	E_{O_2} (kJ.g^{-1} of O_2)
Polypropylene $(C_3H_6)_n$	1815.66	$\frac{9}{2}$	12.62
Propene (C_3H_6)	1923.18	$\frac{9}{2}$	13.38

The next step is to investigate the degree of independence of the two variables. Reaction stoichiometric coefficients rely on the composition of the material. For complete combustion, the potential maximum generation of reaction products is defined by the atoms embedded in the molecule. Regarding the heat of combustion, ΔH_c, any chemical reaction respects the conservation of energy. For a given chemical reaction, heat of formation of the initial material has to balance with the energy absorbed (endothermic reaction) or released (exothermic reaction) and the heats of formation of the reaction products. For a material $C_x H_y O_z$, one recall that ΔH_c can be expressed as,

$$\Delta H_c = \psi_{CO_2}\left(\Delta H_f^{298}\right)_{CO_2} + \psi_{H_2O}\left(\Delta H_f^{298}\right)_{H_2O} - \left(\Delta H_f^{298}\right)_{C_x H_y O_z} \quad (24)$$

With, $\left(\Delta H_f^{298}\right)_{H_2O}$ = -241.826 kJ.mol^{-1} and $\left(\Delta H_f^{298}\right)_{CO_2}$=-393.513 kJ.mol^{-1}.

Equation (24) highlights the dependency of the stoichiometry of the combustion reaction over ΔH_c. According to the previous equation, the E_i coefficients can be rewritten,

$$E_i = \frac{M_{material}}{M_i} \frac{\left[\psi_{CO_2}\left(\Delta H_f^{298}\right)_{CO_2} + \psi_{H_2O}\left(\Delta H_f^{298}\right)_{H_2O} - \left(\Delta H_f^{298}\right)_{C_x H_y O_z}\right]}{\psi_i} \quad (25)$$

ΔH_c can be redefined as a function of the combustion stoichiometry and the heat of formation of the considered material. These two parameters constitute intrinsic properties of the chemical compound; both are actually inherent to its chemical structure. While the stoichiometry of the combustion reaction is determined by the fundamental elements embedded in the material, the energy stored within the molecules depends on their structural arrangement. Few methods have been developed to allow the estimation of this enthalpy changes. Several techniques have been reviewed by Cohen and Benson [15]. They explain that three kinds of approaches have been investigated:

1. one can relate the enthalpies to global molecular properties;
2. one can define structural molecular subunits and assign them an energy contribution according to their location within the molecule;
3. Finally, one can also develop a similar approach to (2) except that the contribution is made regardless of the subunit location within the compound.

Very few procedures of type (1) have been developed as they only rely on complex thermodynamic relationship. An interesting approach of type (2) has been reviewed by Semenov [16]. The basic principle is to correlate the estimation enthalpy of a compound to the bond dissociation enthalpies (BDE) of the bonds being broken. The earliest method introduced by Voevodskii was only applicable to C-H bonds in hydrocarbons. Furthermore, it suffered from several restrictions. It is only limited to C-H bonds in hydrocarbons and an assumption is made so that the BDE value depends on the length of the C chain. For instance, in reality the secondary C-H bonds of propane and butane are of comparable strength, whereas Voevodskii's assumption leads to two different values. Given this problem, a critical lack of pertinence in the estimation arose. Pauling [17] was the first to propose energy constants for BDEs and atomic enthalpy in order to evaluate the heat of formation of a compound. For example, for ethane, $\left(\Delta H_f^{298}\right)_{C_2H_6}$ can be expressed as,

$$\left(\Delta H_f^{298}\right)_{C_2H_6} = 6\,E_{[C-H]} + E_{[C-C]} - 2\left(\Delta H_f^{298}\right)_C - 6\left(\Delta H_f^{298}\right)_H \quad (26)$$

$$= \text{-92.4 kJ.mol}^{-1}$$

The accepted value is -84 kJ.mol^{-1} [17], which corresponds to less than 10% discrepancy. However, similarly to Voevodskii's principle, the assumption of an energy constant associated to a chemical bond neglects the influence of the location of the bond in the structure which affects the energy stored within. A given bond is not always characterised by the same level of energy. It actually depends on the geometry of the structure since neighbouring elements interact on each other according to their nature and their distance. Finally, a third approach (3) was to define additivity models. The main purpose is to be able to divide a compound into smaller entities for which constants could be evaluated allowing the calculation of the thermochemical properties of the aforementioned compound. This approach has been justified by Benson and Buss who described the concept of chemical group additivities [19].

5.5.1. Chemical bonds contribution approaches

One of the intricacies related to the use of group additivities is that it requires the knowledge of thermochemical properties for an extensive number of groups which can become a deterrent to the application of such technique. Consequently, a simpler method based on chemical bonds additivity can be useful to estimate enthalpies of formation of compounds. Despite being less accurate than a group additivity procedure, an approach based on BDE would provide the feasibility to estimate the enthalpy of formation of various compounds within a finite error range of values. Recalling the uncertainty dilemma associated with the energy coefficients used for HRR estimation through OC and CDG, defining a bond additivity (BA) method could constitute a good approach for the assessment of reliable error bars. The investigation of the relevance of such a scheme is now carried out.

5.5.1.1. Bond dissociation energy approach

One can characterise the complete combustion of a material as a combination of breaking and forming chemical bonds to finally lead to the formation of CO_2 and H_2O molecules. A majority of materials considered by Huggett [1] and Tewarson [2] were mainly C_xH_y molecules. Consequently, $C-H$ and $C-C$ represent the main bonds composing these types of molecules.

Assuming a C_xH_y molecule, the energy release by the combustion can be seen as the energy release from the breaking of $C-H$ and $C-C$ bonds and the forming of $C=O$ and $O-H$ bonds. As an example, one considers a molecule of propane (C_3H_8). Table 5.11 gives the BDEs required to break the different bonds of the compound.

Table 5.11. Bond dissociation energies for propane [20].

Molecule	C	H	M	$\boldsymbol{CH_3}-C_2H_5$	$\boldsymbol{CH_3}-CH_2$	$CH_2-\boldsymbol{H}$	$CH-\boldsymbol{H}$	$C-\boldsymbol{H}$
			(g/mol)	(kJ/mol)	(kJ/mol)	(kJ/mol)	(kJ/mol)	(kJ/mol)
Propane	3	8	44	370.3	418.4	462.5	422.6	338.4

The reaction of complete combustion for propane is given by,

$$C_3H_8 + 5\,O_2 \longrightarrow 3CO_2 + 4H_2O \quad (27)$$

Given the complete combustion equation (27), beside the bond breakings occurring in C_3H_8 , 3 $O=O$(O_2) bonds need to be broken; 6 $C=O$ (CO_2) and 8 $O-H$ (H_2O) to be formed. The energy values for breaking $O=O$ and forming $C=O$ and $O-H$ bonds can be found in the literature (see Table 5.12 and Table 5.13) [20]. Writing the energy balance normalized by the number of O_2 consumed for complete combustion gives,

$$E_{O_2\ bonds} = \frac{E_{CH_3-C_2H_5} + E_{CH_3-CH_2-} + 2E_{CH_2-H} + 3E_{CH-H} + 3E_{C-H} + 5E_{O=O} - 6E_{C=O} - 8E_{H-O}}{32 \times 5} \quad (28)$$

$$\Longleftrightarrow E_{O_2\ bonds} = 12.8\ kJ.g^{-1}\ of\ O_2 \quad (29)$$

The E_{O_2} value obtained from the heat of combustion of propane gives 12.78 kJ.g^{-1} of O_2 [9]. Results derived through an energy balance based on a breaking/forming bonds principle appear relevant in this case. Nevertheless, as mentioned earlier and as shown in Table 5.11, the energy required for breaking a $C-H$ bond originated from a CH_2 or a CH group is different. Using this method to estimate with precision energy coefficients faces one major problem: two identical bonds do not necessarily require the same energy to be broken. Bond energies vary according to their location within the structure and the geometry of the molecule. The precision of this method relies on the knowledge of actual BDE values related to each bond connecting two elements of the considered compound. This would represent an extensive task to achieve but it has to be reminded that the present study does not aim to develop an approach allowing the highly precise estimation of energy coefficients for OC and CDG methods. Presently, the aspiration is to be able to define boundary values for the energy coefficients to approximate within a confident range the magnitude of an encountered HRR.

A database of BDE values can be created encompassing the variations of energy associated with a given bond. As accuracy is not a critical condition, average values can be defined. The uncertainty of the energy value can be deduced from the standard deviation of the bond fluctuations distribution. Bond energies have been first investigated for six different families of molecules: alkanes, alkenes, ethers, alcohols, carboxylic acids and aldehydes. For each family

of molecules, average BDE for $C-H$, $C-C$, $C=C$, $C-O$ and $O-H$ have been calculated as well as the associated standard deviations. Results are reported in Table 5.12. Overall mean values of the BDE distributions relative to each bond have also been calculated and the overall standard deviation accounting for the different families of molecule. Results are summarized in Table 5.12.

Table 5.12. Average bond energies and related standard deviations for different fuels.

	Bond Dissociation Energy (kJ/mo)l									
Family	$C-H$ (*Std Dev*)		$C-C$ (*Std Dev)*		$C-O$ (*Std Dev*)		$C=C$ (*Std Dev*)		$O-H$ (*Std Dev*)	
Alkanes	401.3	*±9*	395.8	*±11*	no	*no*	no	*no*	no	*no*
Alkenes	384.3	*±2.5*	397.5	*±29.6*	no	*no*	670.7	*±48*	no	*no*
Ethers	404.4	*±4.8*	418.4	*±0*	367.3	*±1.2*	no	*no*	no	*no*
Alcohol	391.7	*±3.9*	406.4	*±11.3*	418.2	*±30.7*	no	*no*	429.9	*0*
Carboxylic Acids	399	*±8*	391.3	*±16.1*	804.29		no	*no*	no	*no*
Aldehydes	347.8	*±30*	368.5	*±19.4*	460	*±15*	no	*no*	470	*±15*
(Max)	*(411.2)*		*(423.98)*		*(483.18)*		*(718.47)*		*(496.41)*	
Overall	388.9		395.6		414.49		670.7		449.95	
(Min)	*(348.2)*		*(358.37)*		*(356.12)*		*(623)*		*(424.71)*	

Standard deviations associated with each bond, for each molecular family, are less than 10%. The overall deviations estimated by accounting for the different molecular groups do not exceed 20%. Again, the accuracy is not a critical condition, as the main purpose is the evaluation of an error range relative to the energy coefficients. BDE related to the oxidizing agent (O_2) and complete combustion products (CO_2, H_2O) are given in Table 5.13.

Table 5.13. Bond Energies for O_2, CO_2 and H_2O.

Molecule	Chemical Bond	Energy (kJ/mol)	
O_2	O=O	497.4	
CO_2	O=C=O	532.2	Mean: 804.3
	C≡O (CO)	1076.4	
H_2O	H-O-H	497.1	Mean: 463.5
	O-H	429.9	

One can apply the BDE approach to the case of propane on the basis of average bond energy values to estimate an E_{O_2} range and compare the result with the previous calculation (29), estimation assumed to be accurate.

$$\bar{E}_{O_2\,BDE} = \frac{8\,\bar{E}_{C-H} + 2\,\bar{E}_{C-C} + 5\,E_{O=O} - 6\,E_{C=O} - 8\,E_{H-O}}{32\ \times 5} \tag{30}$$

$$\Longleftrightarrow \bar{E}_{O_2\,BDE} = 11.2\ kJ.g^{-1}\ of\ O_2 \tag{31}$$

This corresponds to a 12.4% divergence from the theoretical value $\left(E_{O_2} = 12.78\ kJ.g^{-1} of\ O_2, [9]\right)$. Accuracy is not the point of the method. The potential interest is the evaluation of an error range. According to Table 5.12, extreme attainable values of E_{O_2} according to the bonds present in the propane structure can be assessed:

$$\begin{cases} \bar{E}^{min}_{O_2\,BDE\,[C_3H_8]} = 9.94\ kJ.g^{-1}\ of\ O_2 & (32) \\ \bar{E}^{max}_{O_2\,BDE\,[C_3H_8]} = 13.25\ kJ.g^{-1}\ of\ O_2 & (33) \end{cases}$$

The theoretical energy coefficient for propane is comprised within the range. Another attempt was done to restrict the E_{O_2} value for PMMA within an acceptable range. In the case of PMMA, recalling $E_{O_2} = 12.97\ kJ.g^{-1} of\ O_2$, the range is given by,

$$\begin{cases} \bar{E}^{min}_{O_2\ BDE\ [C_5H_8O_2]} = 12.6\ kJ.g^{-1}\ of\ O_2 & (34) \\ \bar{E}^{max}_{O_2\ BDE\ [C_3H_8O_2]} = 18.8\ kJ.g^{-1}\ of\ O_2 & (35) \end{cases}$$

The energy range encompasses the theoretical E_{O_2} value for PMMA. The latter example emphasized the aforementioned characteristic of chemical bonds. The BDE varies according to the location of the bond within the molecule structure. The electronic interaction between two atoms is affected by the other surrounding fundamental elements enhancing attraction or repulsion effects. Consequently it influences the energy level of the bond over a potential scattered range. For low branched compounds, a method based on bonds additivity can be used to reduce the energy range.

5.5.1.2. Bond Additivity Approach

Benson and Buss [19] were the first to suggest the feasibility of an approach allowing the evaluation of molecular properties (such as heats of formation, molar heat capacity, entropy, etc...) based on the additive contribution from individual groups present in the molecule. This approximation can be extended by considering the chemical bonds instead of groups. By considering the database of chemical groups defined in [21] as well as their energy contribution to the heat of formation, one can derive the contribution from a chemical bond from the energy value of the different groups embedding it. One can create a system of equations where unknowns are the energy values associated with $C-H$, $C-C$, $C=C$, $C-O$, $-C(=O)-O$, $-C(=O)-C$ and $O-H$ bonds. This requires considering enough groups to be able to solve the system and adjust the bond energy values so to remain consistent with the group energies. For an example, considering three bonds, $X=Y$, $X-Z$ and $Z-R$ and the following group:

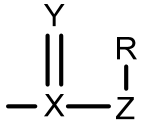

Figure 5.14. Virtual chemical group.

Given,

$$\Delta E = \left| E_{group} - E_{[X=Y]} - E_{[X-Z]} - E_{[Z-R]} \right| \quad (36)$$

Where, E_{group} represents the energy contribution from the group $-(X=Y)-Z-$R and $E_{[i]}$ is the energy associated with the bond i. Based on equation (36), one creates a system of ΔE where the unknowns are the energy contribution from the different bonds. In order to solve the system, one assesses $E_{[X=Y]}$, $E_{[X-Z]}$ and $E_{[Z-R]}$, so that $\Delta E \longrightarrow 0$ for each group where one of the bonds is comprised in. Energy contributions from the groups are collected from Benson and Buss database [19]. Relatively identical results as the ones estimated in [22] are determined. Values are reported in Table 5.14.

Table 5.14. Bond contributions to the heat of formation of compounds at 298 K, 1 atm.

Bond	$\bar{E}_{[Bond]}$ (kJ.mol^{-1})	$\bar{E}^{min}_{[Bond]}$ (kJ.mol^{-1})	$\bar{E}^{max}_{[Bond]}$ (kJ.mol^{-1})
C-H	-16.02	-7.66	-24.39
C-C	11.42	19.79	3.05
C-O	-50.21	-41.84	-58.58
O-H	-112.97	-104.60	-121.34
C=C	28.03	36.40	19.66
(C=O)-C	-60.25	-51.88	-68.62
(C=O)-O	-211.29	-202.92	-219.66
(C=O)-H	-58.16	-49.79	-66.53

Standard deviations on the bond energy values have been estimated based on a 64% confidence requirement. Nevertheless, this level of accuracy is not achieved when considering long chain molecules. Bond energy contributions allow the estimation of the heat of formation of a considered compound. Knowing the heat of formation of CO_2 and H_2O, one can assess the energy coefficients from equations (4), (5) and (6). As previously, one considers the two examples: propane and PMMA. Results are presented in Table 5.15.

Table 5.15. OC Energy coefficients and uncertainty range for propane and PMMA.

Compound	Formula	$E_{O_2\,theory}$ (kJ.g^{-1} of O_2)	$E_{O_2\,BA}{}^{*}$ (kJ.g^{-1} of O_2)	$E_{O_2\,BA}^{min}$ (kJ.g^{-1} of O_2)	$E_{O_2\,BA}^{max}$ (kJ.g^{-1} of O_2)
Propane	C_3H_8	12.78	12.75	12.22	13.27
PMMA	$(C_5H_8O_2)_n$	12.97	13.41	12.84	13.98

*BA: Bond Additivity approach

This Bond Additivity (BA) method reduces the range of energy values associated with a compound compared to the BDE approach. Nevertheless a limitation exists. Moreover, the energy coefficients estimated are quite accurate, with relative deviations from theoretical complete combustion values, respectively, of 0.25 % and 3.4 % for propane and PMMA. The BA energy values have been evaluated from the energy contributions of a restricted number of molecular groups. The latter technique becomes less reliable for long molecular chains. In order to assess the robustness of the BA principle with a more complex molecule, calculation has been carried out for lactose. Results from BDE and BA evaluations are presented below,

Table 5.16. OC Energy coefficients and uncertainty range through BDE and BA methods for lactose.

Lactose	$E_{O_2\,theory}$ (kJ.g^{-1} of O_2)	Method	$E_{O_2\,[Method]}$ (kJ.g^{-1} of O_2)	$E_{O_2\,[Method]}^{min}$ (kJ.g^{-1} of O_2)	$E_{O_2\,[Method]}^{max}$ (kJ.g^{-1} of O_2)
$(C_{12}H_{22}O_{11})_n$	14.69	BDE	13.37	8.4	18.3
		BA	14.69	13,71	15.67

Similar calculations have been carried out for E_{CO_2} and E_{CO} energy coefficients. Results are not presented to avoid redundancy, the conclusions being identical. The BDE method is every conservative and provides a large error range as it has been defined from an extensive assortment of BDE values. The BA method appears more accurate but less conservative than the BDE. However, the combination of both principles constitutes a relevant tool for assessing the degree of confidence that can be allowed in the HRR estimations through OC and CDG calorimetric techniques.

5.5.2. Defining error bars

The BDE and BA approaches presented in the previous section for evaluating the uncertainty range in energy coefficients associated with a given compound do not require the knowledge of its heat of combustion to be applied. They are appropriate for an uncharacterised material. However, one has to stress that the previous calculation were conducted knowing the chemical structure of the molecules. Given this configuration, the approach previously described is relevant to define error bars relative to the energy coefficients and should be used instead of the uncertainties defined by Huggett or Tewarson.

Nevertheless, in the situation that no information about the material are available, the structure of the considered compound being unknown, the estimation of an error range relative to the energy coefficients is considerably more intricate although still possible but less accurately. First, one needs to assess the composition of the sample material. In the following, it is assumed that the three main components that can be encountered in a molecule are C, H and O and constitute the only fundamental elements considered. Data collected from the calorimeter allow the calculation of the production of combustion species, the consumption of O_2 as well as the total mass loss of the compound. These measurements enable to approximate its chemical composition. Assuming the combustion chemistry can be modelled as the following single step reaction:

$$C_x H_y O_z + \nu_{O_2} O_2 \longrightarrow \nu_{CO_2} CO_2 + \nu_{CO} CO + \nu_{H_2O} H_2O \tag{37}$$

x, y, z composition parameters as well as stoichiometric coefficients, ψ_{CO_2}, ψ_{H_2O} and ψ_{O_2} can be approximated based on the procedure developed in Appendix B. An expression for the energy coefficients, in case of complete combustion, is given by,

$$E_i = \frac{\left|\psi_{CO_2}\left(\Delta H_f^{298}\right)_{CO_2} + \psi_{H_2O}\left(\Delta H_f^{298}\right)_{H_2O} - \left(\Delta H_f^{298}\right)_{compound}\right|}{M_i \psi_i} \tag{38}$$

One unknown remains, $\left(\Delta H_f^{298}\right)_{compound}$ that can be approximated through BDE and/or BA approaches. As the composition of the sample material is only approximated, it would be vain to attempt evaluating the energy coefficients. However, one can aim defining a confident

range of energy values. In order to simplify the calculation, the only bonds considered from the highest to the lowest contributor to $\left(\Delta H_f^{298}\right)_{compound}$, according to the BA ranking, are

$$O-H$$

$$C=O$$

$$C-O$$

$$C-H$$

$$C-C$$

$$C=C.$$

A low value is obtained for E_i (E_i^{low})by maximising $\left(\Delta H_f^{298}\right)_{compound}$. According to the approximated composition previously assessed, it is achieved by determining the highest number of the highest energetic bonds that could possibly embedded the molecule. Similarly, the high value of E_i (E_i^{high}) is deduced by minimising $\left(\Delta H_f^{298}\right)_{compound}$. The latter consists in favouring the low contribution bonds in the structure.

As an example, the previous experiment carried out with PMMA (section 5.4.3) is used. One assumes that the material was neither characterized nor identified. The approach defined in Appendix B is used to retrieve an approximation of the atomic composition of the molecule. One finds,

Table 5.17. Approximated composition of the unidentified compound.

C	H	O
4.95	8.13	2.03

The approximation gives a molecule composition close to PMMA. At this stage, either the characteristics of PMMA are recognised and the error range associated with the compound is used or the material remains unrevealed and E_i^{low} and E_i^{high} need to be determined. The combinations of bond leading to the highest and lowest $\left(\Delta H_f^{298}\right)_{compound}$have to be defined. Both configurations were built irrespectively of the C valence.

Table 5.18. Estimation of $E_{O_2}^{low}$.

Number of Bonds						$\left(\Delta H_f^{298}\right)_{high}$	$E_{O_2}^{low}$
$O-H$	$C=O$	$C-O$	$C-H$	$C-C$	$C=C.$	(kJ.mol^{-1})	(kJ.g^{-1} O_2)
2.03	0	2.03	6.1	3.95	0	-395.3	<u>12.68</u>

Table 5.19. Estimation of $E_{O_2}^{high}$.

Number of Bonds						$\left(\Delta H_f^{298}\right)_{low}$	$E_{O_2}^{high}$
$O-H$	$C=O$	$C-O$	$C-H$	$C-C$	$C=C.$	(kJ.mol^{-1})	(kJ.g^{-1} O_2)
0	2.03	0	8.13	3.95	0	-89.4	<u>14.85</u>

A similar approach can be applied to E_{CO_2} and E_{CO} energy coefficients. Recalling that the theoretical value of E_{O_2} for PMMA is 12.97 kJ.g^{-1} of O_2, the approach achieves, for the present case, a relevant restriction. The uncertainty associated with the calculation is not evaluated with regard to the extensive number of parameters and assumptions introduced. The validity of some hypotheses could be argued and particularly the choice of considered fundamental elements (only C, H and O) and bonds. The molecules considered are simple and only few bonds are accounted for short chains. Nevertheless, the purpose of the latter example was just to emphasize the ability, for certain and peculiar experimental configurations, to estimate error bars for the energy coefficients used through OC and CDG calorimetry without relying on the ones defined by Huggett and Tewarson whose limitations have been previously underlined. The applicability of such procedure, beside the considered bonds and fundamental elements assumptions, requires accurate measurements of species. A good calibration of a calorimeter is a necessary condition.

5.5.3. Interlude about Huggett's energy constant

There is another interest in the chemical bond approach. It can clearly describe the restricted validity of Huggett's assumption on energy constant. Considering the simplest molecule families where the major components are only C and H. The constituting groups identified are mainly $-CH_2-$ and $-CH_3$. In order to free the H atoms, $C-H$ bonds have to be broken. Moreover, the release of the C atoms corresponds to the breaking of $C-C$ bond. To oxidize the C and H atoms, O_2 molecules are necessary. For a $-CH_2-$ group, 1.5 O=O bond is needed as well as a sufficient supply of energy to achieve breaking. If the oxidation reaction takes place, 2 C=O bonds are formed to generate CO_2 and 2 O-H bonds to obtain H_2O (cf. Figure 5.15).

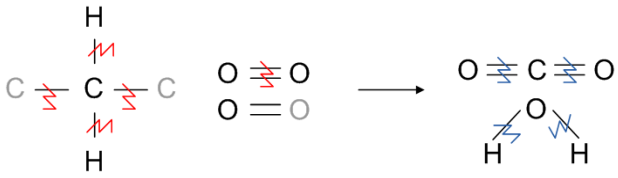

Figure 5.15. Oxidation of a $-CH_2-$ group by breaking and forming chemical bonds.

Using Table 5.12 and Table 5.13, the energy balance normalized to a unit mass of O_2 consumed for breaking and forming chemical bonds can be estimated for the $-CH_2-$ group. A similar calculation has been conducted for a $-CH_3$ group. Results are presented in Table 5.20.

The energy balances per unit mass of O_2 consumed for $-CH_2-$ and $-CH_3$ groups diverge only slightly from Huggett's constant. Moreover, the energy balance for many of C_xH_y can be defined as a combination of these two groups. In the case of alkanes, it would be given by,

$$E_{O_2\ C_xH_y} = \frac{(x-2)\,E_{O_2\,(-CH_2-)} + 2\,E_{O_2\,(-CH_3)}}{x} \tag{39}$$

Table 5.20. Estimation of $E_{O_2\ bonds}$ for CH_2 and CH_3 groups.

Group		Energy Balance(kJ/mol)	$E_{O_2\ bonds}$ (kJ.g^{-1} O_2)
-CH_2-	Alkanes	591.1	12.31
	Families average	618.52	12.89
CH_3-	Alkanes	726.9	12.98
	Families average	767.19	13.69

Considering equation (39), $E_{O_2\ C_xH_y}$ will vary between the two energy group values. The deviation between $E_{O_2\ (-CH_2-)}$ and $E_{O_2\ (-CH_3)}$ is about 6%. This allows to state that the energy value do not deviate from the range defined by Huggett. Finally, since the bond energies for C-H and C-C are relatively similar, adding a -CH_2- or CH_3- group will not consequently alter the E_{O_2} value. This explains why Huggett's constant, 13.1 kJ.g^{-1} of O_2, is relevant for C_xH_y molecules. One can notice that the energy values defined for alkanes are lower than Huggett's constant. Theoretical values of E_{O_2} that are found in the literature also highlight this lower tendency [1] [2] [9]. The reason stems in the bonds. For example the introduction of a double bond $C = C$ within a C_xH_y compound always increase the $E_{O_2\ C_xH_y}$ value compared to the molecule with the same number of C but only $C - C$ bonds. One remarks that the divergence in the heat of formation between such two molecules is often less than 1 %. It can be understood thanks to the observation that $C - C$ bonds are usually in majority in a molecular structure compared to $C = C$ bonds. Nevertheless the difference between their $E_{O_2\ C_xH_y}$ is of the order of 5 %. This comes from the fact that when $C = C$ replaces a $C - C$ bond, it also implies the loss of 2 H atoms. With less H, the amount of O_2 required to fully oxidize the compound is reduced which increases $E_{O_2\ C_xH_y}$.

Similarly, for molecules containing O atoms, the BDE associated with $C - C$ and $C - O$ bonds stands for both around 400 kJ.mol^{-1}. Similarly, $C - H$ bond and $C - OH$ groups present BDE of the same order of magnitude. Given that identical energy levels are involved, the introduction of such bonds within a molecule does not significantly alter its overall heat of formation. However, the insertion of O atoms within the molecular structure lowers the demand in

oxidizing agent from the reacting atmosphere. Consequently, this configuration will have a tendency to increase the energy coefficient E_{O_2}. The effect on E_{O_2} becomes stronger as the amount of O atoms within the molecule grows. It was found that for a ratio. As an example, E_{O_2} values for PMMA ($(C_5H_8O_2)_n$) and Polycarbonate ($(C_{16}H_{14}O_3)_n$)are respectively 12.98 and 13,12 kJ.g^{-1} O_2 while lactose ($(C_{12}H_{22}O_{11})_n$) and starch ($(C_6H_{10}O_5)_n$) exhibit, respectively, E_{O_2} values of 14.7 and 14.8 kJ.g^{-1} O_2.

Energy coefficients demonstrate a dependency on the molecular structure. According to the arrangement of the atoms inside the molecule, the energy associated with the chemical bonds can vary influencing the magnitude of the heat of formation of the compound and so the energy coefficient. Furthermore, the fundamental elements constituting the compound affect its value if they participate in the oxidation process.

5.6. Concluding Remarks

The validity of the hypothesis of energy constants is difficult to assess. One can assume that the energy coefficients distribution of series of materials present an asymptotic behaviour. The estimation of the boundaries (mean and standard deviation) would provide strong confidence in the error range of HRR estimation. Nevertheless, new materials arise nowadays, such as nano-composite embedded in polymers, fire retardants or energetic materials. They are characterised by complex chemical behaviours. There is no certitude that, given their intricate behaviour, they would not affect the means and standard deviations. Acknowledging conviction on the validity of the energy constants assumption for any material is an issue that needed to be investigated.

Uncertainties related to the Huggett and Tewarson's values only rely on the distributions without any scientific signification. Energy coefficient can be calculated based on the decomposition and combustion chemistry of the considered compound. This estimation requires the knowledge of an extensive number of parameters. Error analysis reveals that the uncertainty on the evaluation is susceptible to propagate up to 35 %. Despite it allows the estimation of actual values of energy, the protocol is complex and requires significant knowledge about the material (composition, heat of combustion). This calculation manifests an applicability to check that actual energy coefficients are comprised within the ranges defined by Huggett and Tewarson. However, for most of calorimeter test configurations, the

knowledge about the chemistry of the material is poor. This emphasizes the importance the assumption of universal energy constants. OC and CDG have not been designed for highly accurate HRR measurement. Both principles constitute approximated calculations. The ability of Huggett and Tewarson energy constants to approximate the HRR of a combustion reaction within a confident range has to be assessed. Based on the uniqueness principle of the HRR, combustion tests have been performed under conditions (complete combustion, steady state burning) allowing the reduction of the errors related to the measurements participating in the HRR calculation. Mass loss, OC, CDG and convective HRR approaches have been compared, the mass loss principle being taken as a reference. The OC calorimetry combined with Huggett energy constant offers accurate results for the combustion of methane and PMMA. At the same time, CDG associated with Tewarson energy constants fails to estimate an accurate HRR. Furthermore, the actual HRR lies beyond the postulated error range. These results tend to contradict the assumption of energy constants. When looking at the energy coefficients distribution for more complex materials, the assumption of $\bar{E}_{O_2}$ is still acceptable with regard to the standard deviation (±11.6 %) but the energy values observed for the CDG ($\bar{E}_{CO_2}, \bar{E}_{CO}$) are more scattered and significantly different from the ones defined by Tewarson. The last attempt to appraise the validity of the assumption of energy constants for complex materials of unknown composition is based on an invert method. Given the uniqueness of the HRR, the distribution of calculated $\bar{E}_{CO_2}$ clearly indicates that energy coefficients cannot be described by means of a constant value.

OC and CDG principles are designed to provide approximate estimations of the HRR. Consequently, as the determination of accurate energy coefficients highlights complex issues, efforts have to be directed towards the estimation of an error range associated with the energy values. Possible approaches based on the contribution of the chemical bonds to the heat released during a combustion reaction have been introduced. The two latter methods succeed in assessing relevant error bars to the energy coefficients of uncharacterised materials. The bond additivity approach refines this range but is restricted to certain types of molecules. A protocol has been applied in order to estimate error bars for a completely uncharacterised material whose composition is ignored. The method is tedious and requires the evaluation of the material composition from calorimeter data. Furthermore, the use of the method is restricted by several simplifying assumptions that have been postulated. The highest boundary is obtained by determining a virtual configuration presenting the lowest level of

energy that could be stored in the bonds. The lowest boundary corresponds to a virtual configuration where bonds with the highest energy contribution would be favoured. It is proved that, despite being intricate, for peculiar configurations, an approach based on bond additivity can specify a relevant indicator of an uncertainty range associated with energy coefficients. The aim that wants to be emphasized in the present work is not the approach used but the necessity of developing methodologies able to assess with confidence characteristic range of energy values for uncharacterised or even undefined materials.

There are materials for which OC and CDG principles cannot rely on the assumption of Huggett and Tewarson energy constants. Restrictions exist regarding the latter hypothesis but the boundary conditions where these limitations occur are difficult to clearly establish. The structure of the molecule and its constituting atoms influence the degree of energy that can restore the compound. Results obtained in the present analysis tend to stress a diverging behaviour for compounds of complex chemistry. It has been analysed that the presence of large amount of O compared to C and H within the compound structure is one of the situations where Huggett and Tewarson's assumptions can potentially fail to be valid.

It is essential to be aware of these restrictions related to the use of energy constants. An estimation of the degree of confidence can be achieved by a simple comparison between OC and CDG. The degree of divergence encountered in the calculation gives an insight of the confidence that can be expected in the results. This remains a useful indication but the advantage of using OC and CDG calculations instead of a simpler mass loss approach combined with a measured heat of combustion can be contested. Estimation of HRR through a mass loss approach does not provide higher precision than OC and CDG but gives an evaluation of the maximum HRR, which constitutes an important piece of information. The use of species evolution approach depends on the ability to determine error bars associated with the energy coefficients.

5.7. References

[1] Huggett, C. Estimation of Rate of Heat Release by means of Oxygen Consumption Calorimetry, Fire and Materials, 4 (2), pp. 61 – 65 (1980);

[2] Tewarson, A., Generation of Heat and Chemical Compounds in Fires, in: SFPE Handbook of Fire Protection Engineering, 3rd Edition, Section 3, Chapter 4, The National Fire Protection Association Press, 2002, pp. 3-82 – 3-161;

[3] Janssens, M., Uncertainty of Fire Test Results, (Interflam07) 11th International Interflam Conference, article not included in the Proceedings, September 3-5, 2007, London, England;

[4] Taylor, J., R. An Introduction to Error Analysis, University Sciences Books, 2nd Edition, 1997.

[5] Enright, P. A., Fleischmann, C., M., Uncertainty of Heat Release Rate Calculation of the ISO5660-1 Calorimeter Standard Test Method, Fire Technology, 35 (2), pp. 153 – 169 (1999);

[6] Brohez, S., Uncertainty analysis of heat release rate measurement from oxygen consumption calorimetry, Fire and Materials, 29, pp. 383 – 394 (2005);

[7] Axelsson, J., Andersson, P., Lönnermark, A., Van Hees, P., Wetterlund, I., Uncertainties in measuring heat and smoke release rates in the room/corner test and the SBI, SP Swedish National Testing and Research Institute, NT technical report, 477, NORDTEST Project No. 1480-00, SP Report 2001:04;

[8] Janssens, M., Parker, W., J., Oxygen Consumption Calorimetry, in: Heat Release in Fires, Chapter 3, Editors: Babrauskas, V., and Grayson, S., J., Elsevier Applied Science, New York, 1992, pp., 31 – 59;

[9] Babrauskas, V., Related Quantities: (a) Heat of Combustion and Potential Heat, in: Heat Release in Fires, Chapter 8, Editors: Babrauskas, V., and Grayson, S., J., Elsevier Applied Science, New York, 1992, pp., 207 – 223;

[10] Walters, R., N., Hackett, S., M., Lyon, R., E., Heats of Combustion of High-Temperature Polymers, Fire and Materials, 24 (5), pp. 245 – 252 (2000);

[11] Drysdale, D., An Introduction to Fire Dynamics, 2nd Edition, Chapter 1, Wiley, Chichester, pp. 1 – 30 (2002);

[12] Lyon, R., E., Abramowitz, A., Effect of Instrument Response Time on Heat Release Rate Measurements, Fire and Materials, 19, pp. 11 – 17 (1995);

[13] Point, R., Petit, J., L., Gravelle, P., C., Reconstruction of Thermokinetics from Calorimetric Data by means of Numerical Inverse Filters, Journal of Thermal Analysis, 17, pp. 383 – 393 (1979);

[14] Schemel, C., F., Simeoni, A., Biteau, H., Rivera, J., D., Torero, J., L., A Calorimetric Study of Wildland Fires, Experimental Thermal and Fluid Science, 32 (7), pp. 1381 – 1389 (2008);

[15] Cohen, N., Benson, S., W., Estimation of Heats of Formation of Organic Compounds by Additivity Methods, Chemical Reviews, 93 (7), pp. 2419 – 2438 (1993);

[16] Semenov, N., N., Some Problems in Chemical Kinetics and Reactivity, Boudart, M., Translator, Princeton University Press, Princeton, 1, pp. 49 – 56 (1958);

[17] Pauling, L., The Nature of The Chemical Bond, 2nd Edition, Chapter 3, Cornell University Press, Ithaca, 1940;

[18] NIST Chemistry WebBook, NIST Standard Reference Database number 69;

[19] Benson, S., W., Buss, J., H., J, Additivity Rules for the Estimation of Molecular Properties. Thermochemical Properties, Journal of Chemical Physics, 29 (3), pp. 546 – 572 (1958);

[20] Luo, Y.-R., Comprehensive Handbook of Chemical Bond Energies, CRC Press, London, 2007;

[21] Benson, S., W., Cruikshank, F., R., Golden, D., M., Haugen, G., R., O'Neal, H., E., Rodgers, A., S., Shaw, R., Walsh, R., Additivity Rules for the Estimation of Thermochemical Properties, Chemical Reviews, 69 (3), pp. 279 – 324 (1968);

[22] Benson, S., W., Thermochemical Kinetics, 2nd Edition, Chapter 2, Wiley, New York, 1976;

6. Sensitivity Analysis

6.1. Introduction

Extensive uncertainty analyses have been carried out to assess the dependence of OC and CDG principles to accurate measurements. Enright and Fleischmann [1] underlines that the accuracy of the OC principle is strongly correlated to the energy coefficient. They notice that the uncertainty on the calculation is reduced when the material composition and the heat of combustion are known. Furthermore, they also indicate that measurement of water vapour has also a positive effect on the level of accuracy of the HRR estimation. The other important parameters that the authors stressed, susceptible to noticeably propagate uncertainties in the calculation are the O_2 molar fraction, the Pitot tube coefficient and, for high HRR, the expansion factor α. The O_2 analyser is usually calibrated between 0 and 25% of O_2 while the O_2 depletion is often of the order of 1 %. Precision is restricted by the width of the considered measurement range. Uncertainty is increased as it is enhanced. Errors on the exhaust mass flow rate exhibit high dependency to the calibration of the Pitot tube, as well as the evolution of its state over time (deposit of soot coating, edge erosion). The uncertainty originated from the expansion factor α is minimized if the composition of the burning compound is known. Brohez [2] achieved a comprehensive analysis by characterising the influence of the major parameters susceptible to alter the HRR through OC calorimetry. Similarly to Enright and Fleischmann, he noticed that the energy coefficients were critical variables and the knowledge of actual values instead of constants allows a reduction of the potential error in the calculations. Furthermore, its original approach was to consider the propagation of uncertainties on HRR estimations through OC calorimetry according to the O_2 depletion that he described as a critical variable. He highlights that at very low O_2 depletion (open system), assuming the fuel composition unknown, the overall uncertainty associated with HRR measurements is highly due to the O_2 concentration uncertainty rather than the expansion factor. On the other hand, as the O_2 depletion increases, the contribution of the energy coefficient, the expansion factor α and the exhaust mass flow rate increases while the O_2 to the HRR global uncertainty becomes dominant. He also underlines that bench and large scale tests are usually characterised by low O_2 depletion (i.e. the mass flow rate of incoming air is orders

of magnitude larger than the O_2 consumption by the combustion reaction). Consequently, the uncertainty relative to the O_2 measurement turns to become important because, in this configuration, the O_2 depletion stands within the error range of the O_2 analyser. Brohez also considered the influence of the degree of completeness of the combustion. The use of energy constants instead of calculated energy coefficients enhances the error as the reaction falls into incomplete regime. Axelsson *et al.* [3] present similar conclusions to Brohez. They consider a wider set of contributors to the uncertainty but the O_2 concentration followed by the energy constant and the exhaust mass flow rate are stressed as the main sources of error to the calculation.

The previous studies have all focused on the measurement aspect (type (3) of the sources of uncertainty). The discussion conducted in the previous chapter highlighted another cause of potential error. Materials and test configurations can feature peculiarities breaching some of the different assumptions used to achieve the HRR calculation. The present study already stressed that Huggett and Tewarson energy constants usually combined to CO and CDG calculations entail restrictions in their use according to the structure, composition and chemistry of the considered compound. It has been clearly demonstrated that using the energy constants assumption for inappropriate materials is susceptible to introduce errors in the results that could not be assessed with confidence. The issue of material characteristics or test configurations that potentially infringe OC and CDG assumptions needs to be weighed up with the same consideration than measurement uncertainties and requires to be investigated. It appears complicated to associate uncertainties to the different assumptions. However, one can identify the sensitive parameters of OC and CDG. Subsequently, after ascertaining which of these factors depend on the calculation assumptions, their potential contribution to the overall HRR error can be evaluated by means of a sensitivity analysis. The considered parameters will be defined within ranges so that they breach the usual hypotheses required to apply OC and CDG. This procedure also allows the assessment of their robustness.

6.2. Experimental Procedure

The followed experimental protocol repeats the one previously described for combustion tests (see Chapter 3, section 3.3). The FM-Global FPA was the selected calorimeter for reasons that have already been highlighted. The sensitivity analysis is based on experimental data extracted

from combustion tests carried out on smoke the powders based on ternary mixtures of starch and lactose as fuel components and potassium nitrate as an oxidizer that have been characterised in chapters 2 and 3. Their composition characteristics are recalled in Table 6.1.

The use of these materials rather than more conventional ones presents some interest. Their chemistry manifests such peculiarities that one can question the validity of the assumptions that hold for the application of OC and CDG. One can for instance point out two potential issues associated with the energy constants and with the N_2 non production hypotheses.

Table 6.1. Composition in mass percentage of sample smoke powders.

Components	Powder 1	Powder 2
Starch	30%	25%
Lactose	30%	25%
KNO_3	40%	50%

According to the analysis conducted in the previous chapter, it appears that Huggett and Tewarson energy constants do not characterise properly the two ternary powders considered in the present work. The presence of an oxidizing agent (KNO_3) within the material reduces the consumption of O_2 originating from the supporting atmosphere. Considering the OC calorimetry, the action of the oxidizer affects the energy coefficient by heightening its magnitude compared to a reaction involving identical fuel compounds but where all the O_2 would come from the air. Consequently, Huggett constant is not appropriate for this type of materials. Regarding the CDG principle, both sample compounds have a low heat of combustion (i.e. ΔH_c =7.41 kJ.g^{-1} for the 40% KNO_3 ternary mixture; ΔH_c =6.01 kJ.g^{-1} for the 50% KNO_3 ternary mixture). Furthermore, the fuel components (starch and lactose) exhibit high C contents. Combination of these two characteristics suggests lower E_{CO_2} and E_{CO} values than the ones defined by Tewarson.

Furthermore, one of the products generated during the thermal decomposition of KNO_3 is N_2 [4]. The application OC and CDG principles require the evaluation of the mass flow rate of incoming air into the reaction zone. This measurement is obtained neglecting potential N_2

generation. However, the production of N_2 is expected as the powder decomposes. An important release of N_2 breaches the conservation hypothesis. According to the experimental configurations, the influence of a formation of N_2 on the error associated with the incoming air mass flow rate measurement has to be investigated. Afterwards, the estimation of an N_2 production range during the ternary powders combustion will allow verifying if the conservation assumption can still be applied.

Sensitive factors associated with OC and CDG calculation assumptions have to be identified in order to assess their robustness and applicability boundaries. Previous uncertainty analyses [1] [2] [3] have underlined that the highest contributors to the uncertainty propagation in the HRR estimations were the energy coefficients, the O_2 and CO_2 concentrations, the exhaust mass flow rate, the water vapour molar fraction as well as the expansion factor. The ability to estimate most of these parameters pertain to the validity of assumptions that were introduced in chapter 4 (section 4.2.3.2.1). A sensitivity analysis will allow the assessment of the degree of error introduced in the HRR calculations by applying unsuitable hypotheses.

6.3. Sensitivity Analysis

OC and CDG constitute approximated HRR calculation procedures. They rely on the combination of a wide range of measurements susceptible to propagate uncertainties. Moreover, applying these techniques also requires series of assumptions presented previously (see section 4.2.3.2.1). Table 6.2 reports the different parameters involved in OC and CDG regarding the assumptions they are related to. Considering the different calculation hypotheses, the breaking of one of them can induce deviations in some parameters from their true value and affect the HRR results. Because the information about the chemistry and the combustion of the sample material is sometimes limited, it can be intricate to verify that all assumptions can be applied in the considered configuration. An alternative unfortunately not sufficient to state on the validity of the results is to compare OC and CDG techniques for a set of data. According to the magnitude of the discrepancy between the two methods, one can possibly assess a certain number of parameters from which the divergence could originate. It requires evaluating the maximum error that can introduce the breaching of calculation hypotheses on the HRR estimation by affecting the integrity of the latter parameters.

Table 6.2. Parameters and associated assumptions involved in the HRR calculation through OC and CDG.

Parameters	Related assumptions *(Corresponding number in section 3.2.3.2.1)*	
$\bar{E}_{O_2}$, $\bar{E}_{CO_2}$, $\bar{E}_{CO}$	– Energy Constants exist and can be applied;	*(1)*
X_i^A	– Gases are perfectly mixed across the exhaust duct section; – Gases are measured on a dry basis; – The dynamics of the analysers used for the measurements are higher than that of the evolution of species concentrations;	*(6)* *(8)* *(9)*
$\dot{V}_e$	– Gases are perfectly mixed; – A laminar flow is achieved through the exhaust duct – The Pitot coefficient K has been estimated for the calorimeter	*(6)* *(7)*
M_e $\dot{m}_a$	– Exhaust gases only consist of N_2, O_2, CO_2, H_2O, CO, unburnt HC; – N_2 production is neglected;	*(3)* *(4) (5)*
X_{H_2O}	– The water vapour is measured if an devoted analyser is present; – Otherwise, $X_{H_2O} = X_{H_2O}^0$;	*(10)*
α	– Exhaust gases only consist of N_2, O_2, CO_2, H_2O, CO, unburnt HC; – The combustion reaction can be modelled as a one step reaction.	*(4)* *(5)*

Considering Table 6.2, for each highlighted calculation hypothesis, one identifies the different variables that depend on. In a second time, one evaluates a range of values that would characterise the latter parameters, taking into account the condition for which they do not

comply with their related assumptions. A sensitivity analysis allows the estimation of the engendered error on the HRR measurements.

6.3.1. Energy constants

The limitations associated with the validity of Huggett [5] and Tewarson [6] energy constants have been stressed in the previous chapter. It was shown that their use could not be generalized to any types of materials. Depending on the structure and the composition of a compound, its chemistry affects the behaviour when undergoing combustion. Energy coefficients and uncertainty associated can be estimated when composition, heat of combustion and information about the thermal decomposition of the material are known. However, these data are often unavailable. In this situation, the determination of energy coefficients adapted to the considered sample material becomes too complex and the focus has to be assigned to the ability of defining appropriate ranges of energy values. According to the level of knowledge about the compound, an error range can be determined with more or less confidence. The information of the structure and composition are valuable data that allow refining the accuracy of the interval (see Chapter 4, Section 4.5). An approach based on the energy contribution from chemical bonds provides relevant results. A more intricate problem arises when the sample material is totally uncharacterised and unknown. An attempt to retrieve the molecular composition of a material from calorimeter data is possible under the condition that the major elements of the molecule are identified through the measurement procedure. Energy error range can be assessed by defining the highest and lowest bonds configuration of the approximated molecule. However, the latter methodology relies on simplifications strongly correlated to the material composition. Consequently, situations exist where even the estimation of the energy coefficients error range is impossible. A sensitivity analysis based on the energy values highlights the predominance of these variables on the calculation and gives an insight of the degree of potential errors that can be introduced through an inappropriate assumption of energy constants.

Figure 6.1 to Figure 6.4 highlight the influence of the energy constants parameter on the HRR calculations by means of OC and CDG principles. The energy values have been varied between 5 and 25 $kJ.g^{-1}$ of O_2 (OC) or CO_2 (CDG). The studied range is assumed to be conservative for a majority of materials independently of their chemical complexity. The red cross appearing on

Figure 6.1.a and Figure 6.2.a and Figure 6.3.a and Figure 6.4.a represent the reference configuration (use of Huggett and Tewarson energy constants) respectively for OC and CDG. First, considering OC calorimetry, variation of the energy coefficient E_{O_2} over the range 5 to 25 kJ.g^{-1} of O_2 creates divergence rising up to 95% on the peak HRR and total energy release estimations. Figure 6.1.a and Figure 6.2.a exhibit a linear dependency of the OC expression to E_{O_2}. In the present configuration, the deviation induced by an increment of 1 kJ.g^{-1} of O_2 in E_{O_2} has been evaluated to 0.75 kW regarding the HRR peak and 13.25 kJ regarding the total heat release. Both values represent about 8 % of the HRR peak and total energy release that would be obtained for a calculation relying on the energy constants assumption. Regarding the CDG calorimetry, similar comments can be drawn. Figure 6.3.a and Figure 6.4.a stress a linear dependency of the CDG principle to the energy coefficient E_{CO_2}. Compared to the results obtained assuming the validity of energy constants, varying the energy coefficient E_{CO_2} between 5 and 25 kJ.g^{-1} of CO_2 generates discrepancy in the HRR peak and total heat release up to 86 %. Given the analysis configuration, the deviation engendered by a 1 kJ.g^{-1} of CO_2 increment in E_{CO_2} is equal to 1.45 kW regarding the HRR peak and 23.64 kJ considering the total heat release. Both values stand for about 7.5 % of the HRR peak and total energy release that would be obtained for a calculation relying on the energy constants assumption.

It was already established from the previous chapter that energy coefficients are critical parameters of OC and CDG principles. The sensitivity analysis applied for the experimental configuration of a 50g burning of ternary powder based on lactose, starch and KNO_3 shows that a divergence of few kJ.g^{-1} of O_2 or CO_2 between acknowledged constants and actual energy values potentially rises important over and underestimation of the HRR. In the current case, it has been underlined that an error of a unit increment in the energy coefficients introduces an error of the order of 8 % in the HRR estimation. It is then essential to ascertain if the general energy constants remain relevant with energetic materials.

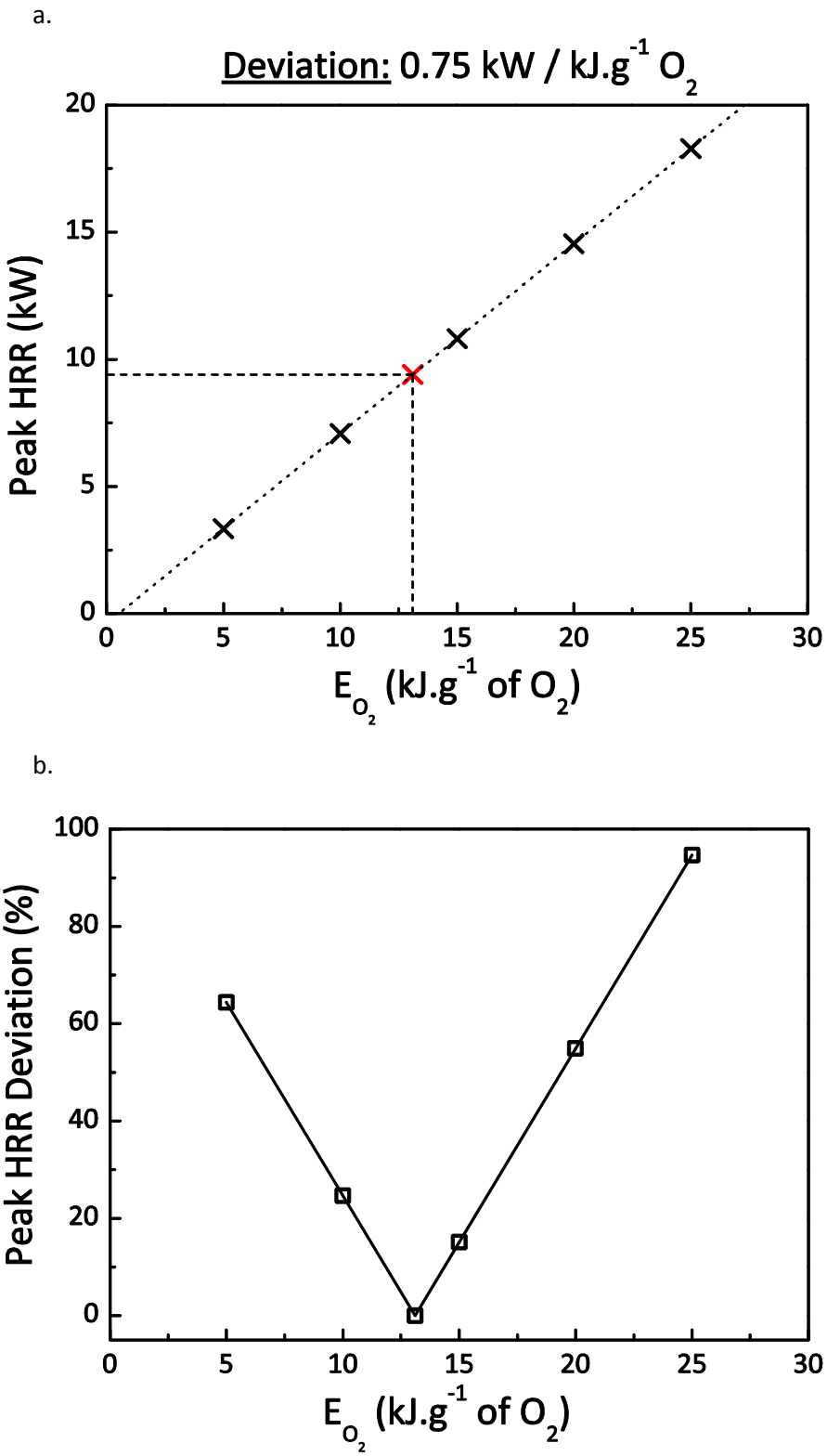

Figure 6.1. Sensitivity analysis of the peak HRR release based on OC calculation when varying the energy coefficient. Results are presented as absolute variation (Figure 6.1.a) and relative deviation (Figure 6.1.b) from calculation conducted with Huggett energy constant (13.1 kJ.g^{-1} of O_2).

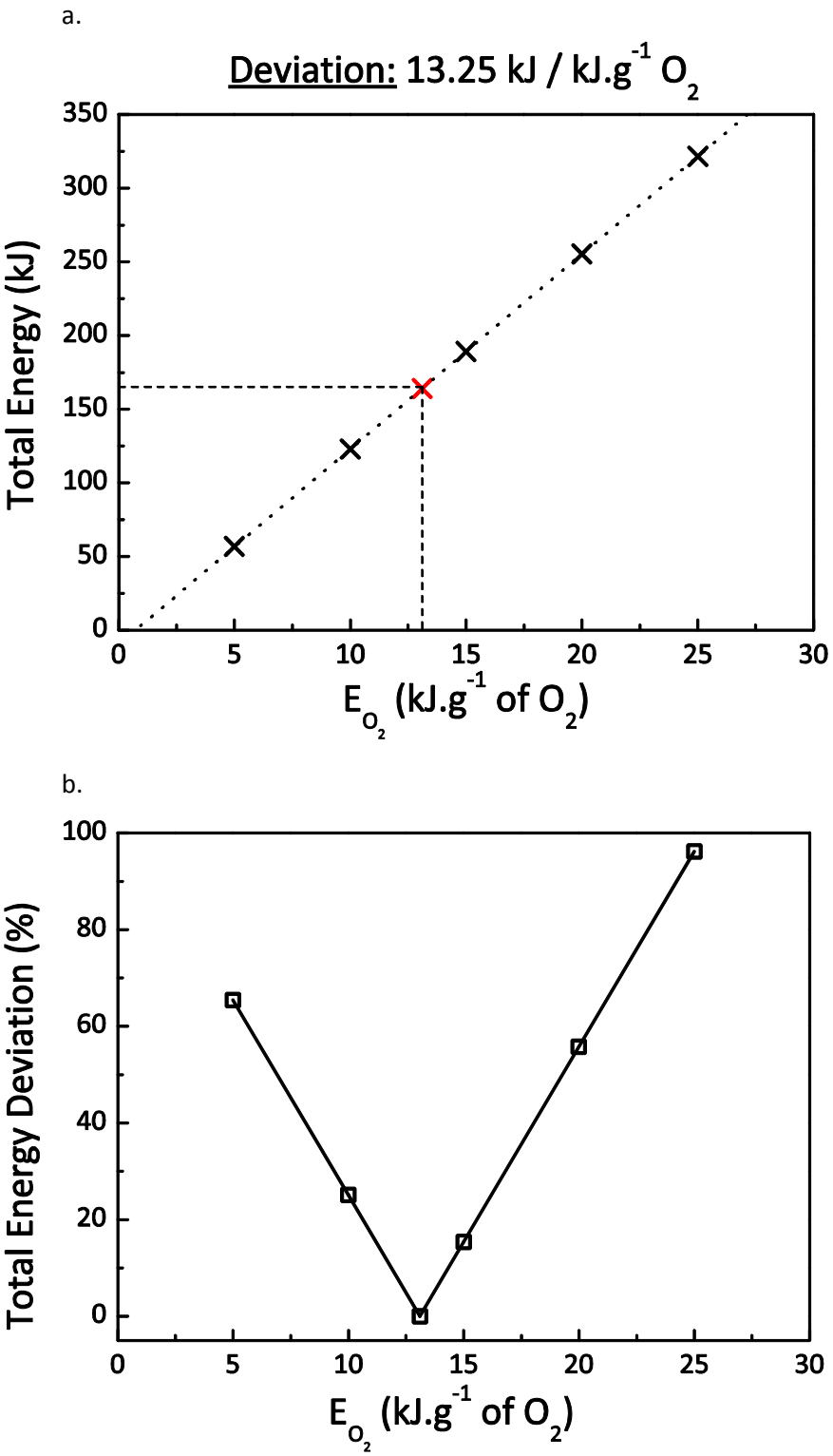

Figure 6.2. Sensitivity analysis of the total energy release based on OC calculation when varying the energy coefficient. Results are presented as absolute variation (Figure 6.2.a) and relative deviation (Figure 6.2.b) from calculation conducted with Huggett energy constant (13.1 kJ.g^{-1} of O_2).

a.

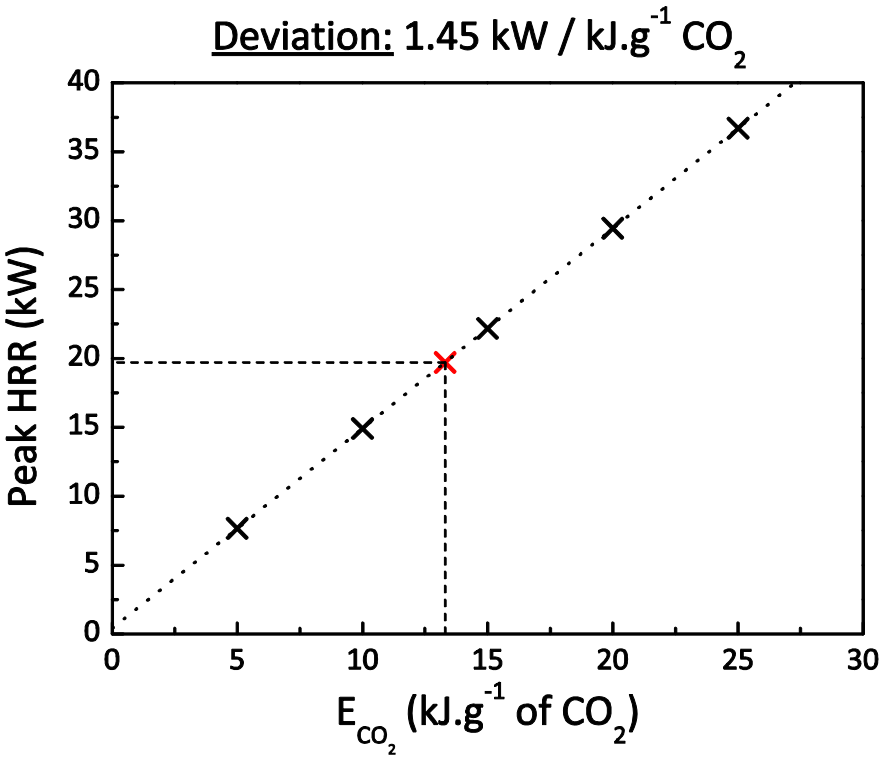

b.

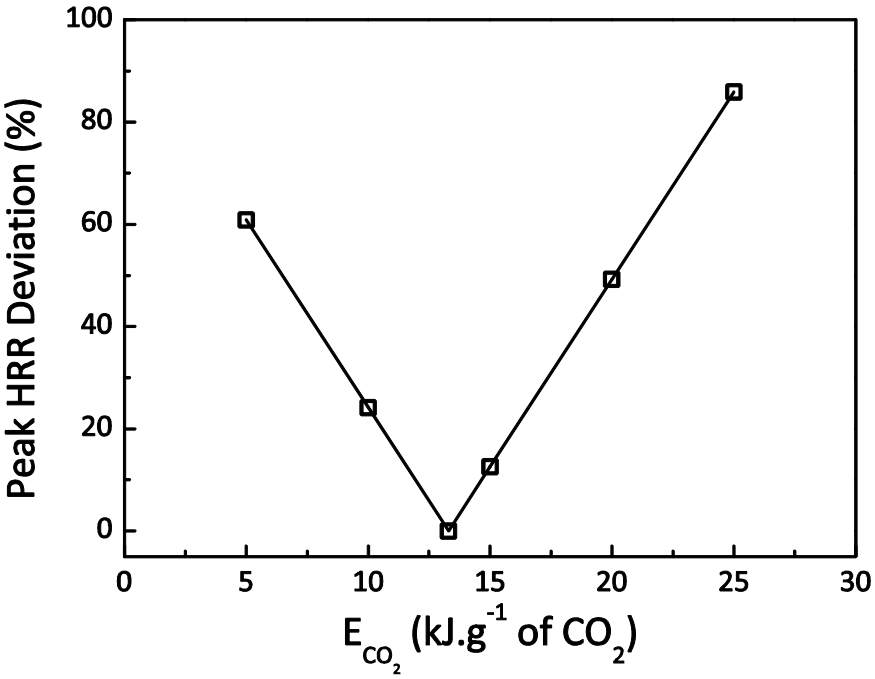

Figure 6.3. Sensitivity analysis of the peak HRR and total energy release based on CDG calculation when varying the energy coefficient. Results are presented as absolute variation (Figure 6.3.a) and relative deviation (Figure 6.3.b) from calculation conducted with Tewarson energy constant (13.3 $kJ.g^{-1}$ of CO_2).

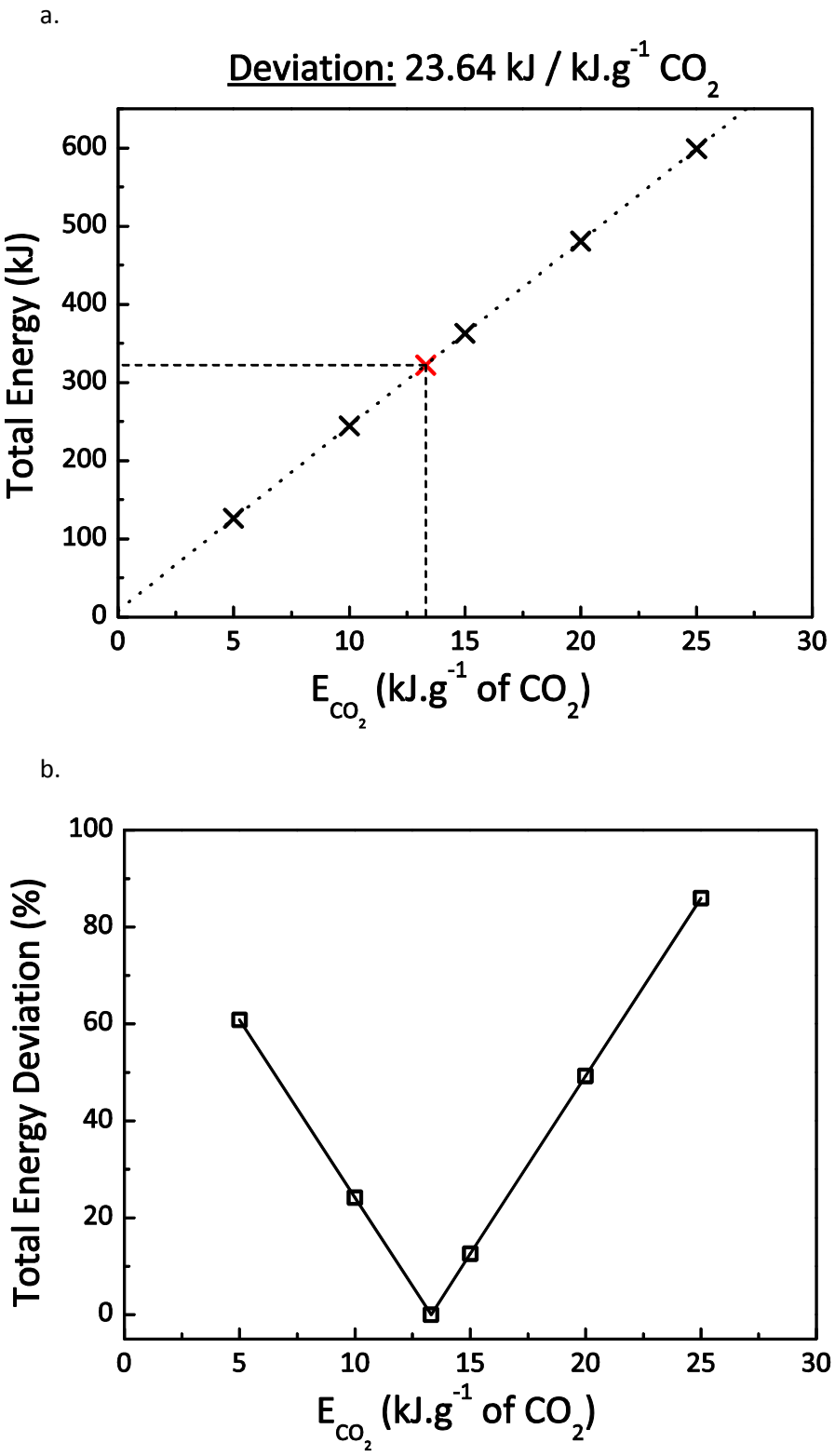

Figure 6.4. Sensitivity analysis of total energy release based on CDG calculation when varying the energy coefficient. Results are presented as absolute variation (Figure 6.4.a) and relative deviation (Figure 6.4.b) from calculation conducted with Tewarson energy constant (13.3 $kJ.g^{-1}$ of CO_2).

6.3.2. Response time of the measuring system

Beside the requirement of relevant energy coefficients, another critical parameters emerging from the OC and CDG expressions [Chapter 3, expressions (61) and (63)] are the molar fraction measurements. The basis of OC and CDG is to assess the consumption of O_2 (OC) or the production of combustion gases (CDG) to estimate the HRR instead of the evaluating the burning rate of fuel. Consequently, the approximation of species concentrations constrains reducing to a minimum the sources of imprecision. Two fundamental features have to be specially considered: the synchronisation of the measurements and the time response of the analysers system. Confidence in species concentration calculations relies on their appreciation.

6.3.2.1. Synchronised time measurements

Given the extensive number of variables integrated in OC and CDG principles, the inherent time delay associated with each measurement needs to be estimated. Data collection takes place in different locations. As an example, temperature measurement in the exhaust duct at an instant t does not correspond to a species molar fraction estimated at the same time. Each gaseous species is characterised by a transport time between the sampling point in the exhaust duct and the arriving in the measuring cell of the devoted analyser. Characteristic transport times have to be evaluated for each analyser. Synchronisation of the different variables needs to be achieved according to a defined reference. Given their fast response to the chemical reaction, exhaust duct temperature or mass loss are appropriate candidates Delay times do not remain constant over the apparatus lifetime. It is actually dependent to the efficiency of the sampling system that can evolve in time. Synchronisation data calibration should be performed regularly in order to avoid propagation of errors in the calculation. Figure 6.5 represents an estimation of HRR through OC calorimetry. One notices that the HRR rise is preceded by a negative inflexion. The HRR negative region (located inside the red ellipse on Figure 6.5) prior increase does not embody physical sense. The present inconsistency results from unsynchronised molar fraction measurements. The experimental configuration features shorter transport time for the CO/CO_2 analyser than for the O_2 one. The CO/CO_2 measures a CO_2 production few seconds before the O_2 analyser detects the species consumption. As a consequence, the O_2 depletion factor ϕ encounters negative values and so the HRR. The error is only apparent for this portion of curve but it propagates at each step time. The HRR peak is also affected by the asynchronous

phenomenon. The intensity of the error depends on the combustion kinetics as well as the levels of concentration encountered. An estimation of HRR based on unsynchronized data for a fast reaction with important gaseous emissions would provide the unphysical inflexion prior to increase and the peak HRR would be underestimated.

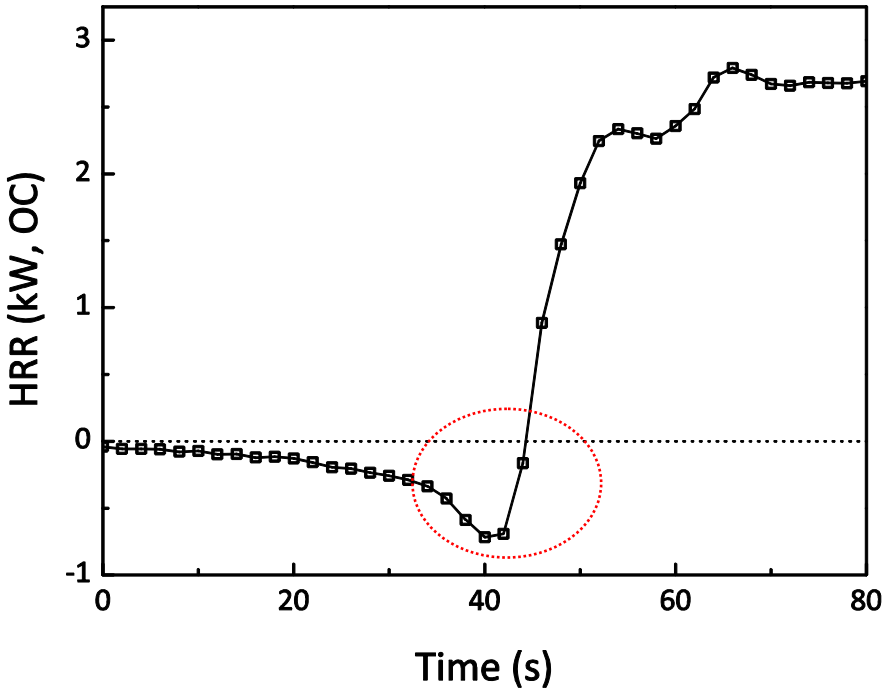

Figure 6.5. HRR estimation through OC calorimetry based on unsynchronised data.

6.3.2.2. Influence of analysers response times

The curve inflexion stressed on Figure 6.5 is also favoured by a well-known feature of experimental devices. The ability of measuring instruments to measure accurately species production and consumption is described by their response time also referred as time constant τ. Prior to develop the discussion further, in order to be consistent, one needs to clearly define the notion of response time and time constant in the present study. The response time is interpreted as the period required by a system to respond to a signal input up to a given percentage, usually 90%, of the final value, the time constant corresponding to a 63% response time [7]. Gas analysers rely on various principles. O_2 analysers usually make the most of the paramagnetic property of the material. CO and CO_2 analysers are based on the spectral emissions of these species over wavelengths within the infrared region. Concentrations through a THC analyser are often estimated by means of a Flame Ionization

Detector (FID). Gases flow through a flame and ions emitted are detected by means of electrodes. The proportion of reduced carbon atoms (ions) in the flame is then estimated. The accuracy of these different techniques has been widely demonstrated over the last decades. However, beyond the detection approach, the measuring unit consists in an electrical system with a temporal resolution. Although analysers are assumed to well quantify species evolution impulses, when the characteristic time of the reaction kinetics is of the order or even shorter than the instrument response time, output signals suffer from distortion due to lags of the converter and amplifier systems. Response times are normally mentioned by device manufacturers. Nevertheless, recalling that the efficiency of the measuring apparatus evolves over time, they have to be regularly controlled. Furthermore, intrinsic response times do not always characterise properly the system. One needs to consider the complete sampling line rather than the only apparatus. The reason of the latter is highlighted on Figure 6.6. The simplest signal that allows the estimation of the response time of a device is the output resulting from a step change in a species concentration. Figure 6.6 represents the response to a step change in CO_2 concentration. One can compare an ideal step response (i.e. response time τ_{90} where $\tau_{90} \rightarrow 0$), with the analyser's responses when CO_2 is injected through the calibration line and through the entire exhaust duct line. Regarding the latter, the grade gas flows through various filters intended to remove the soot from the combustion mixture and followed by drying columns designed to absorb water vapour. Finally the calibration gas is directed to the devoted analyser at a given operating range by means of a vacuum pump. While the calibration line is directly connected to the measuring instrument, the transport through the exhaust line encounters several "obstacles" capable of affecting its response time.

It comes from Figure 6.6 that the output signal when grade CO_2 gas enters the analyser through the calibration line represents the characteristic response of the device. The signal obtained when CO_2 flows through the entire exhaust duct line is impaired. Assumptions that have been developed to explain the origins of the noise rely on the porosity of the drying agents combined to the vacuum pump faculty to create a sufficient pressure drop within the drying columns. Another hypothesis refers to the ability of certain kinds of drying agents to fix the CO_2. Nevertheless, a change in the drying compound composition did not engender better analyser responses. Table 6.3 indicates the response time and time constant of the CO_2 analyser for the different considered configurations. The values related to the sole analyser (i.e. calibration line) comply with the manufacturer specifications. The 90 % response time stands

around 20 s but becomes tremendously extended when the grade gas is injected through the exhaust line. The time constant rises up to 37 s and the response time up to 136 s. The latter can be explained as being more sensitive to noise because located on a less steep part of the output signal [8]. The temporal resolution of the system is long. In the case of a steady state burning, this issue can be solved by prolonging the experiment until the final value was reached. In most of the combustion tests involving the HRR characterisation of a material, in order to comply with standards, the sample size is defined in such a way that transient phenomena are mainly encountered. Considering the CO_2 concentration step change illustrated on Figure 6.6, 20 s after the CO_2 flow was established in the exhaust duct line, the CO_2 analyser only detects 975 ppm when the grade mixture exhibit a CO_2 molar fraction of 2595 ppm that is a 62% divergence. By way of comparison, the detected CO_2 concentration 20 s after injection of the grade mixture through the calibration line gives 2284 ppm that is only 12% deviation.

In the situation of a combustion reaction with a fast kinetics and CO_2 emissions of a magnitude similar to the one of the grade gas, the output signal would suffer of important distortion. According to the previous observation, one can consider an underestimation of the actual CO_2 concentration superior to 50%. Identical investigations have been carried out on the O_2 molar fraction signal. Alteration of the step response is lower than for CO_2. Characteristic times are reported in Table 6.4. They comply with the manufacturer specifications. Nevertheless, the ability of the measuring system to accurately describe the evolution of species emissions for a fast reaction remains to be investigated.

Table 6.3. Estimation of response time and time constant for the IR CO_2 analyser.

Characteristic times	Manufacturer specifications (s)	Calibration line (s)	Exhaust duct line (s)
Time constant, τ_{63}		13	37
Response time, τ_{90}	< 20	21	136

Table 6.4. Estimation of response time and time constant for the paramagnetic O_2 analyser.

Characteristic times (s)	Manufacturer specifications (s)	Exhaust duct line (s)
Time constant, τ_{63}		12
Response time, τ_{90}	< 15	15

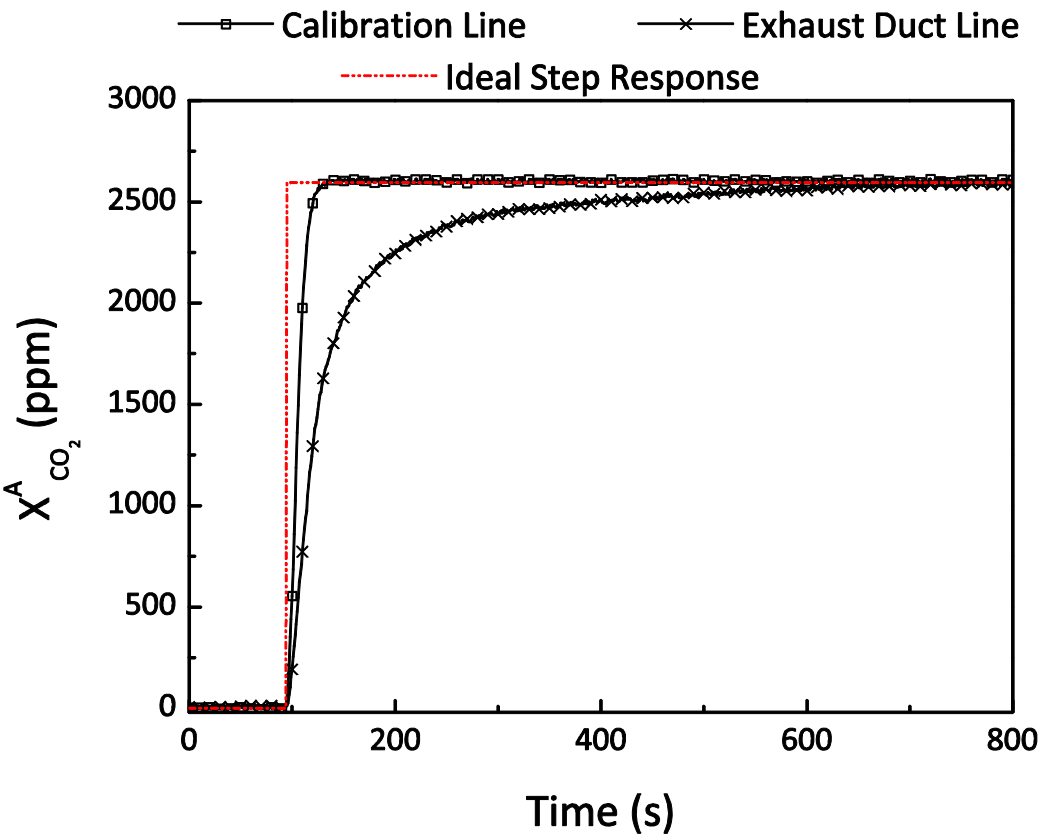

Figure 6.6. Comparison between an ideal step response and calibration line and exhaust duct line responses of a CO_2 analyser.

It comes from Table 6.3 and Table 6.4 that, the pertinence of measurements of CO_2 molar fractions during transient combustion reactions shorter than 37 s has to be assessed. Similarly, confidence in O_2 molar fraction data for reaction kinetics inferior to 15 s stands identical

doubts. In order to evaluate the degree of dependence of OC and CDG principles to O_2 and CO_2 concentration variables, a sensitivity analysis has been carried out.

6.3.2.3. Sensitivity of CDG to CO_2 measurement

Figure 6.6 illustrates the potential issue relative to CO_2 concentration measurements in the case of large emissions with a reaction dynamics faster than the response time of the analyser. The lag of the analyser dynamic behaviour can introduce important underestimation and overestimation of the actual CO_2 level during production rate changes. According to Figure 6.6, an underestimation higher than 50% from the actual species molar fraction is possible given a long response time. One needs to assess the influence of this phenomenon on HRR estimations. The contribution of the CO_2 molar fraction to the CDG expression can be stressed by means of a sensitivity analysis. The evolution of $X_{CO_2}^A$ during combustion reaction involving the 50% KNO_3 ternary powder under air atmosphere has been adopted as reference. $X_{CO_2}^A$ has been interpolated using a Gaussian approach. Amplitude of the fitted curve has been varied between 20 and 200 % of its original magnitude. Results are presented on Figure 6.7. From Figure 6.7.a and Figure 6.8.a, one notices that HRR estimation by means of CDG exhibits a linear dependency with regard to the CO_2 molar fraction measurement. Given the experimental configuration, a 1 % variation of $X_{CO_2}^A$ causes changes in HRR peak and total energy release of, respectively, 4.35 kW and 74.4 kJ. Figure 6.7.b and Figure 6.8.b present the divergences engendered, respectively, in HRR peak and total energy release in relation to a given percentage of change in the reference $X_{CO_2}^A$. One notices that variations are identical for both parameters and variations in $X_{CO_2}^A$. That suggests that, under the present combustion conditions (well-ventilated regime, low CO emissions), the HRR equation based on the CDG principle can be approximated by an expression where it is directly proportional to $X_{CO_2}^A$:

$$\dot{q}_{CDG} \propto X_{CO_2}^A \quad (1)$$

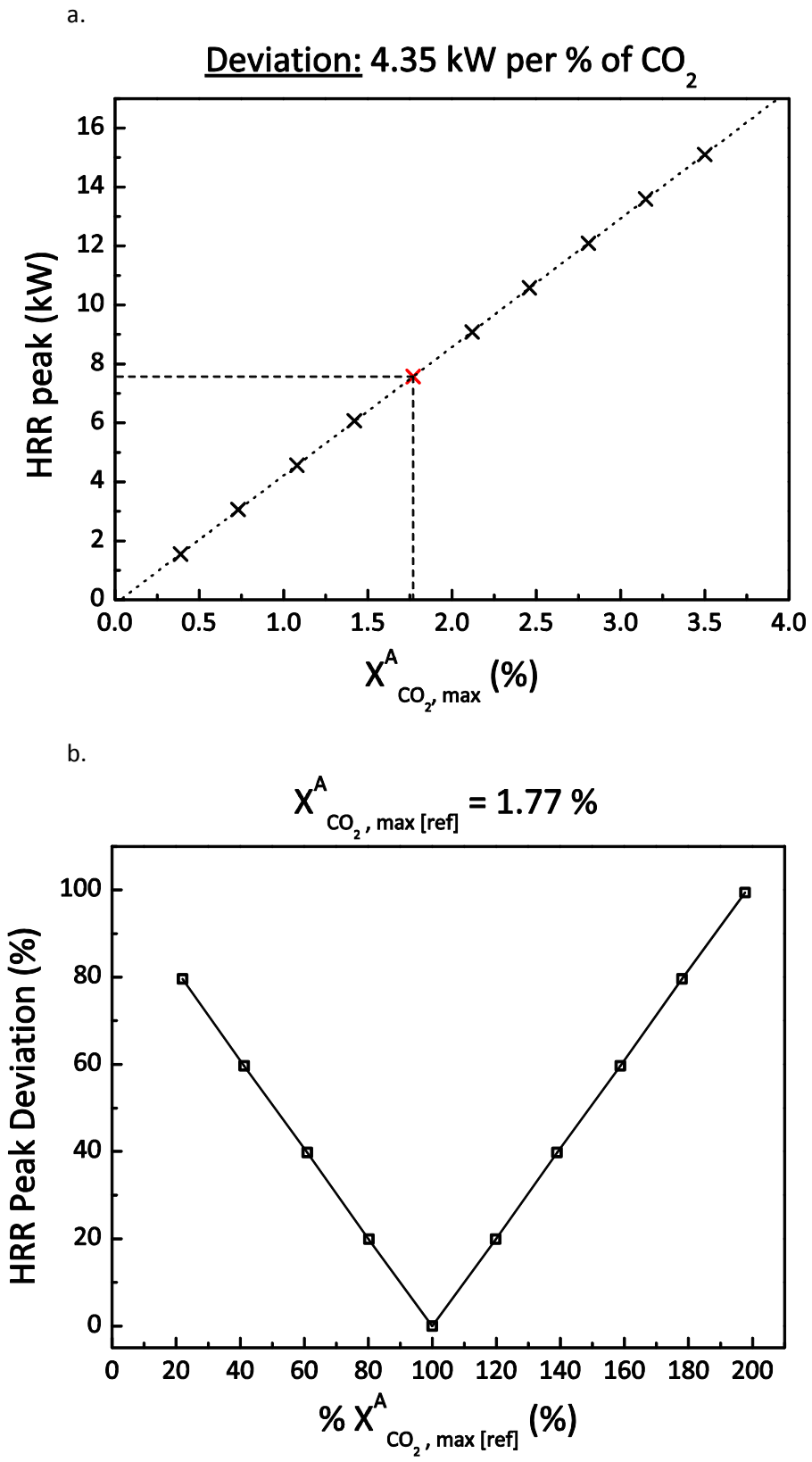

Figure 6.7. Sensitivity analysis of the peak HRR based on CDG calculation when varying the CO_2 molar fraction. Results are presented as absolute variation (Figure 6.7.a) and relative deviation (Figure 6.7.b).

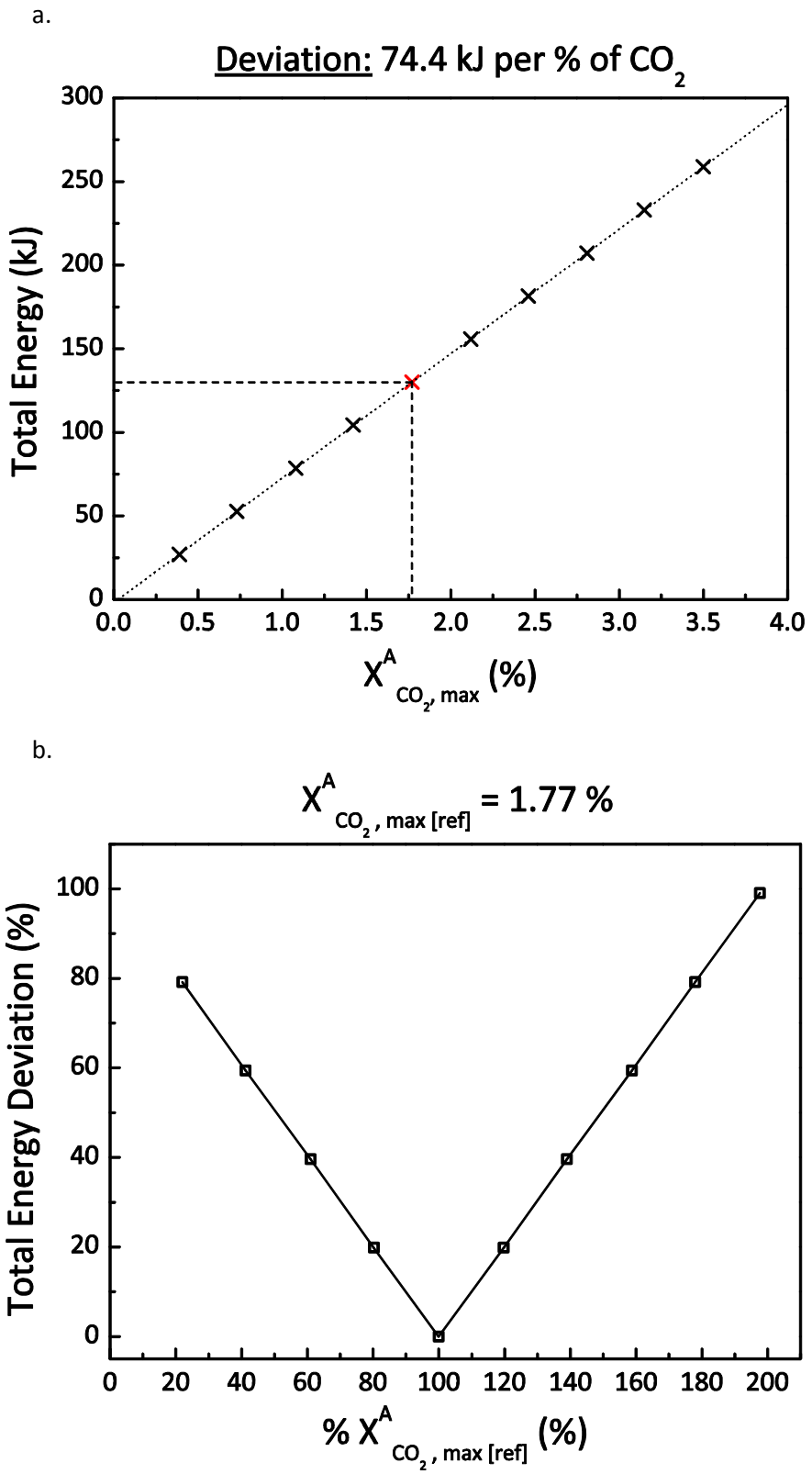

Figure 6.8. Sensitivity analysis of the total energy release based on CDG calculation when varying the CO_2 molar fraction. Results are presented as absolute variation (Figure 6.8.a) and relative deviation (Figure 6.8.b).

The latter statement is strengthened by Figure 6.9. It illustrates that a relative deviation from $X_{CO_2}^A$ is directly transferred to the HRR estimation based on CDG. For example, varying by 50 % the magnitude of $X_{CO_2}^A$ from a reference level generates a similar 50% divergence in the HRR result. This phenomenon is observed for a range of $X_{CO_2}^A$ fluctuating between 20 and 200 % from the original measurement,

$$\pm 1\%\ X_{CO_2}^A \xrightarrow[CDG]{} \pm 1\%\ \dot{q}_{CDG} \tag{2}$$

The linear behaviour of $\dot{q}_{CDG}$ is conserved when increasing $X_{CO_2}^A$ beyond the previous deviation range. Recalling the CDG equation,

$$\dot{q}_{CDG} = \frac{\dot{m}_e}{M_e}\left(1 - X_{H_2O}\right)\left(E_{CO_2}\, X_{CO_2}^A\, M_{CO_2} + E_{CO}\, X_{CO}^A M_{CO}\right) - \frac{\dot{m}_a}{M_a}\left(1 - X_{H_2O}^0\right) E_{CO_2}\, X_{CO_2}^{A^0}\, M_{CO_2} \tag{3}$$

As previously mentioned, the CO contribution is small enough to be neglected in the considered case. Furthermore, although the expression of mass of incoming air (supply + dilution air flow), $\dot{m}_a$, contains $X_{CO_2}^A$, the sensitivity analysis highlights that the last right term of equation (3) (representing an energy associated with the CO_2 from the air) has an insignificant contribution to $\dot{q}_{CDG}$. Finally, in the present analysis equation (3) can be approximated as,

$$\dot{q}_{CDG} \sim \frac{\dot{m}_e}{M_e}\left(1 - X_{H_2O}\right)\left(E_{CO_2}\, X_{CO_2}^A\, M_{CO_2}\right) \tag{4}$$

The sensitivity analysis clearly suggests that an over or under estimation of the CO_2 molar fraction introduces a variation of similar magnitude in the HRR estimation using the CDG method. Consequently, the issue related to the time response of the analysers is susceptible to engender large discrepancy in the HRR estimation. As illustrated on Figure 6.6, a long response time combined with a fast reaction dynamics can easily lead to a 50% underestimation of the CO_2 molar fraction. In this situation, the CDG principle would similarly underestimate the HRR up to 50 %.

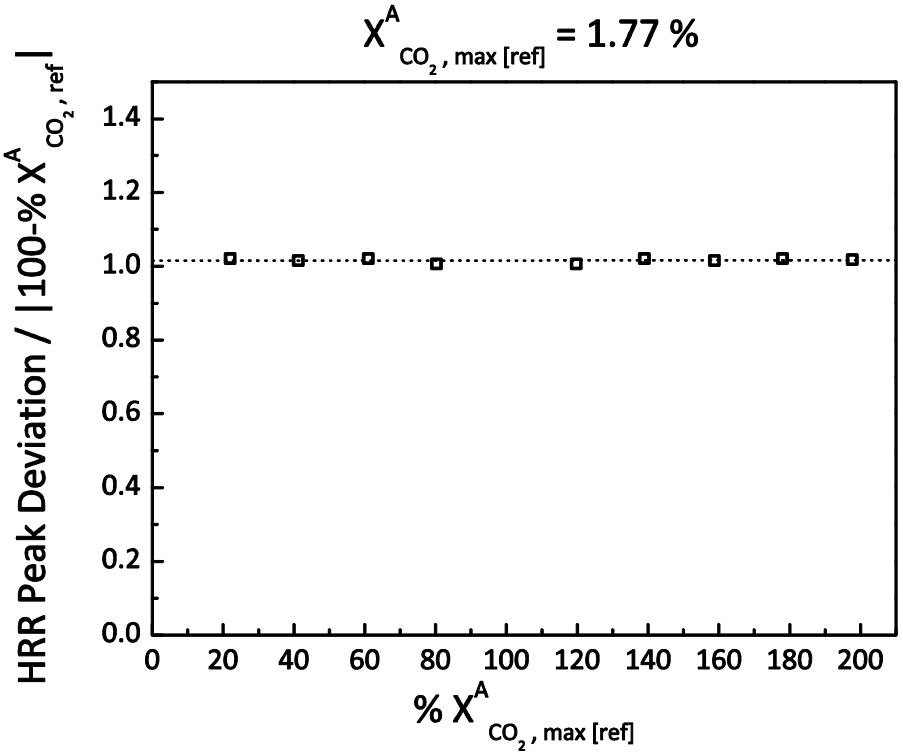

Figure 6.9. Ratio of the HRR peak deviation to the deviation from the reference CO_2 molar fraction $X^A_{CO_2,\ ref}$.

6.3.2.4. Sensitivity of OC to O_2 measurement

An identical analysis to the one carried out on the sensitivity of the CDG equation to the CO_2 molar fraction is conducted on the OC equation regarding the influence of the O_2 molar fraction. The response time issue can also affect O_2 analysers. Furthermore, as previously mentioned, the operating range of O_2 analysers is usually significantly wider than the one related to CO_2 analysers. O_2 analysers are usually calibrated between 0 and 20.95 % of O_2 while CO_2 calibration is generally run between 0 and 4 % maximum within the framework of bench scale tests. Uncertainties on concentration values are affected by inherent noise altering the quality of the signal. This phenomenon increases with the operating range [9].

In order to assess the potential effect of misestimating the O_2 molar fraction for the calculation of HRR based on OC principle, a similar approach than for CO_2 has been developed. A Gaussian approach has been used to interpolate the experimental $X^A_{O_2}$ curve taken as reference. The variation was applied such that the maximum O_2 depletion varied between 93 % and 104 % of the reference value (i.e. $X^A_{O_2\,\min[\mathrm{ref}]}$ = 19.57%) corresponding to a minimum O_2 molar fraction

decreasing from 20.5 % to 18%. The scenario on which is based the definition of the $X_{O_2}^A$ sensitivity range relies on the occurrence of a fast combustion reaction with different emission levels of combustion products generating an O_2 consumption. Results are featured on Figure 6.10.

Figure 6.10.a and Figure 6.11.a represent, respectively, the deviations engendered in HRR peak and total energy when modifying the magnitude of $X_{O_2}^A$. Linear approximations can be determined to characterise the variations associated with the two variables in relation with $X_{O_2}^A$. Considering the experimental configuration, a 1 % variation of $X_{O_2}^A$ generates shifts in HRR peak and total energy release of, respectively, 8 kW and 146 kJ. Compared to the results described in the sensitivity analysis carried out on the CO_2 measurement, the distortions observed on HRR peak and total energy release for a 1% fluctuation of the considered species molar fraction are about two times higher regarding O_2. A relative deviation of 1 % from the reference $X_{O_2}^A$ introduces about 18 % change in the HRR peak and 19.5 % in the total energy estimation (cf. Figure 6.10.b and Figure 6.11.b).

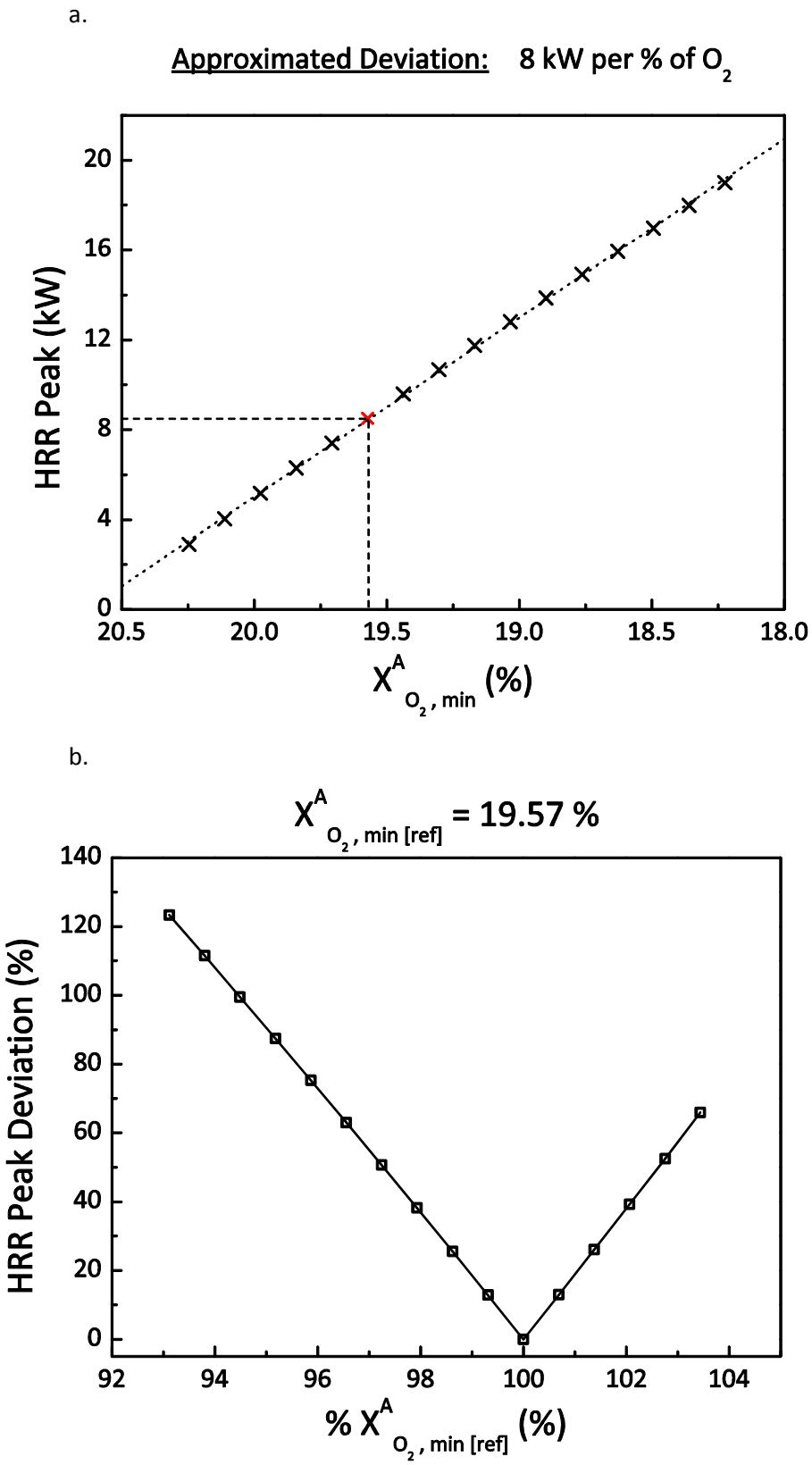

Figure 6.10. Sensitivity analysis of the peak HRR based on OC calculation when varying the O_2 molar fraction. Results are presented as absolute variation (Figure 6.10.a) and relative deviation (Figure 6.10.b).

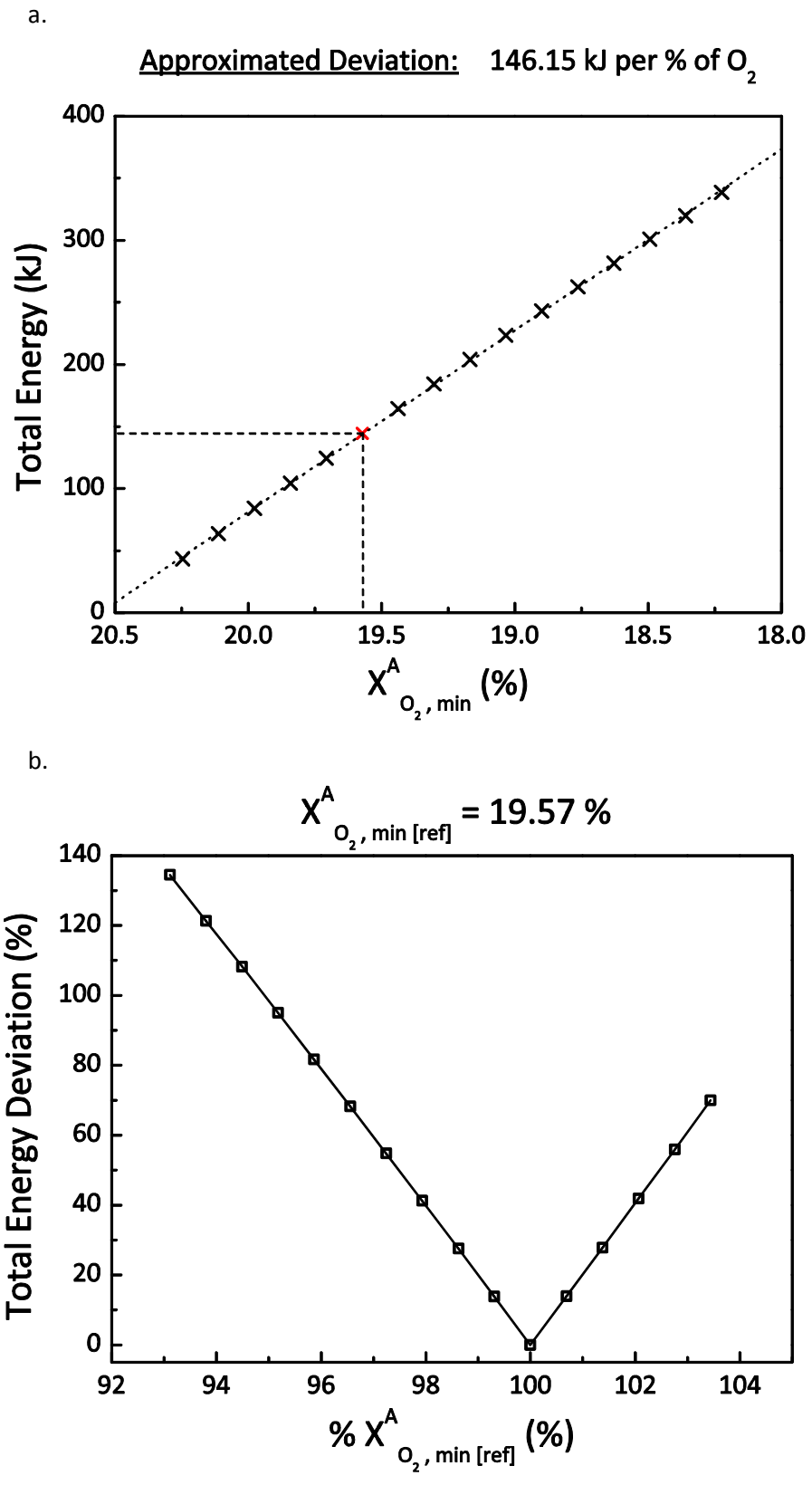

Figure 6.11. Sensitivity analysis of the total energy release based on OC calculation when varying the O_2 molar fraction. Results are presented as absolute variation (Figure 6.11.a) and relative deviation (Figure 6.11.b).

Recalling the OC equation,

$$\dot{q}_{OC} = \left[E_{O_2}\phi - \left(E_{O_2\,(CO \to CO_2)} - E_{O_2}\right)\left(\frac{1-\phi}{2}\right)\frac{X_{CO}^A}{X_{O_2}^A}\right] X_{O_2}^A\left(1 - X_{H_2O}\right)\frac{M_{O_2}}{M_e}\,\frac{\dot{m}_e}{1+\phi(\alpha-1)} \tag{5}$$

$X_{O_2}^A$ appears in equation (5) as the molar fraction term but is also present in the expression of the depletion factor ϕ. Figure 6.10 and Figure 6.11 describe a deviation behaviour regarding the HRR peak and the total energy release when the amplitude of $X_{O_2}^A$ is altered. The relative deviation of the two parameters can be approximated by a linear function, which suggests then,

$$\dot{q}_{OC} \propto X_{O_2}^A \tag{6}$$

The CO concentration is several orders of magnitude lower than $X_{O_2}^A$ so the energetic contribution of the term $\left(E_{O_2\,(CO \to CO_2)} - E_{O_2}\right)\left(\frac{1-\phi}{2}\right)\frac{X_{CO}^A}{X_{O_2}^A}$ can be neglected. For $X_{O_2}^A$ varying within a range [18 % - 20.95 %] the depletion factor ϕ fluctuates between 0 and 15% and finally the term $1+\phi(\alpha-1)$ can be approximated by,

$$1+\phi(\alpha-1) \sim 1 \tag{7}$$

Equation (5) can be rewritten,

$$\dot{q}_{OC} \sim E_{O_2}\phi\, X_{O_2}^A\left(1 - X_{H_2O}\right)\dot{m}_e\,\frac{M_{O_2}}{M_e} \tag{8}$$

The linear divergence observed depends on $\phi\, X_{O_2}^A$. Recalling the expression of the depletion factor, ϕ is given by,

$$\phi = \frac{X_{O_2}^0\left(1 - X_{H_2O} - X_{CO_2} - X_{CO} - X_{THC}\right) - X_{O_2}\left(1 - X_{H_2O}^0 - X_{CO_2}^0\right)}{X_{O_2}^0\left(1 - X_{O_2} - X_{H_2O} - X_{CO_2} - X_{CO} - X_{THC}\right)} \tag{9}$$

Then $\phi\, X_{O_2}^A$ can be expressed as follow,

$$\phi X_{O_2}^A = \frac{X_{O_2}^A\, X_{O_2}^{A^0}\left(1 - X_{CO_2}^A - X_{CO}^A - X_{THC}^A\right) - {X_{O_2}^A}^2\left(1 - X_{CO_2}^{A^0}\right)}{X_{O_2}^{A^0}\left(1 - X_{O_2}^A - X_{CO_2}^A - X_{CO}^A - X_{THC}^A\right)} \tag{10}$$

Assuming that the exhaust flow rate is significantly larger than the mass loss rate (i.e. $\dot{m}_e$ ($\sim$ 55 g.s^{-1}) $\gg$ $\dot{m}_{loss}$ ($\sim$ 2 g.s^{-1})), one can approximate equation (10) by,

$$\phi X_{O_2}^A \sim \frac{X_{O_2}^A X_{O_2}^{A^0} - {X_{O_2}^A}^2}{X_{O_2}^{A^0}\left(1 - X_{O_2}^A\right)} \tag{11}$$

Figure 6.12 illustrates the plot derived from expression (11). The latter constitutes a rational polynomial. Consequently, one notices that its overall behaviour stresses parabolic rather than linear characteristics. The linear behaviour can be assimilated to asymptotic variations for O_2 molar fractions close to $X_{O_2}^{A^0}$. Considering the function $f\left(X_{O_2}^A\right)$ such that,

$$f\left(X_{O_2}^A\right) = \phi X_{O_2}^A \tag{12}$$

In the vicinity of $X_{O_2}^{A^0}$, the linear deviation can be described by the following expression,

$$y = f'\left(X_{O_2}^{A^0}\right)\left(X_{O_2}^A - X_{O_2}^{A^0}\right) \tag{13}$$

A linear approach describes well the sensitivity of the OC method to $X_{O_2}^A$ for molar fraction close to $X_{O_2}^{A^0}$. Nevertheless in the case of combustion reactions associated with large O_2 depletion, $X_{O_2}^A$ can be significantly reduced. The divergence can then be interpolated using a higher order polynomial.

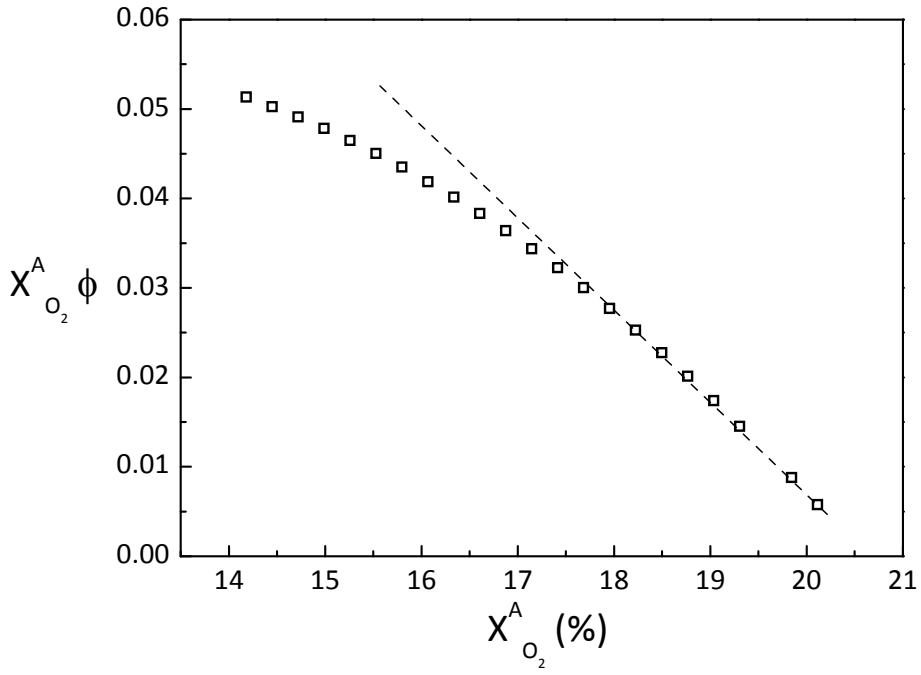

Figure 6.12. Evolution of $\phi X_{O_2}^A$ according to $X_{O_2}^A$ (based on data obtained from the combustion of 50 g of 50% KNO_3 ternary powder).

A sensitivity analysis based on a larger range of $X_{O_2}^A$ values has been carried out in order to assess the influence on the HRR estimation for lower levels of O2 concentration. Results are reported in **Error! Reference source not found.**.a and Figure 6.14.a indicate the divergences engendered, respectively, on the HRR peak and the total energy release by varying $X_{O_2}^A$ over the range 14 % to 20.5 %. One notices that for an about 5.5 % decrease in $X_{O_2}^A$, both parameters present results about 5 times higher than for the reference values (red crosses on the plots). Furthermore, the best fits describing the evolution of HRR peak and total energy deviations for the considered $X_{O_2}^A$ range are second order polynomials. The trend is coherent with the behaviour of $\phi X_{O_2}^A$ previously stressed. Although less accurate, both divergences can still be interpolated using a linear regression. According to **Error! Reference source not found.**.a and Figure 6.14.a, the slopes obtained are lower than the ones reported on Figure 6.10.a and Figure 6.11.a. This is due to the parabolic inflexion characterising the evolution of both curves. A relative deviation of 1 % from $X_{O_2,\min[\mathrm{ref}]}^A$ respectively initiates 16% and 18% changes in HRR peak and total energy release deviations.

One can consider that less accuracy is associated with the O_2 measurement than with the CO_2 one. This issue is explained by the larger operating range associated with the use of the O_2 analyser allowing a higher level of noise propagation through the signal. Similar conclusions than those observed for CO_2 can be expressed. If the O_2 analyser is characterised by a long response time, in the situation of a fast transient regime with large O_2 consumption (or combustion gases emissions), the output signal is likely to comprise important distortions. According to Figure 6.10, Figure 6.11 and Figure 6.13 and Figure 6.14, this can generate significant under and/or over estimations of the HRR based on OC calculation. Results related to discrepancies affecting HRR calculations through OC and CDG and initiated, respectively, from inherent O_2 and CO_2 molar fraction mismeasurements are summarized in Table 6.5.

Table 6.5. HRR deviations related to O_2 and CO_2 measurements.

HRR Principle	Sensitive Parameter	HRR peak deviation *(per unit % of sensitive parameter)*	Total energy release deviation *(per unit % of sensitive parameter)*
OC	$X_{O_2}^A$	91 %	99 %
CDG	$X_{CO_2}^A$	58 %	58 %

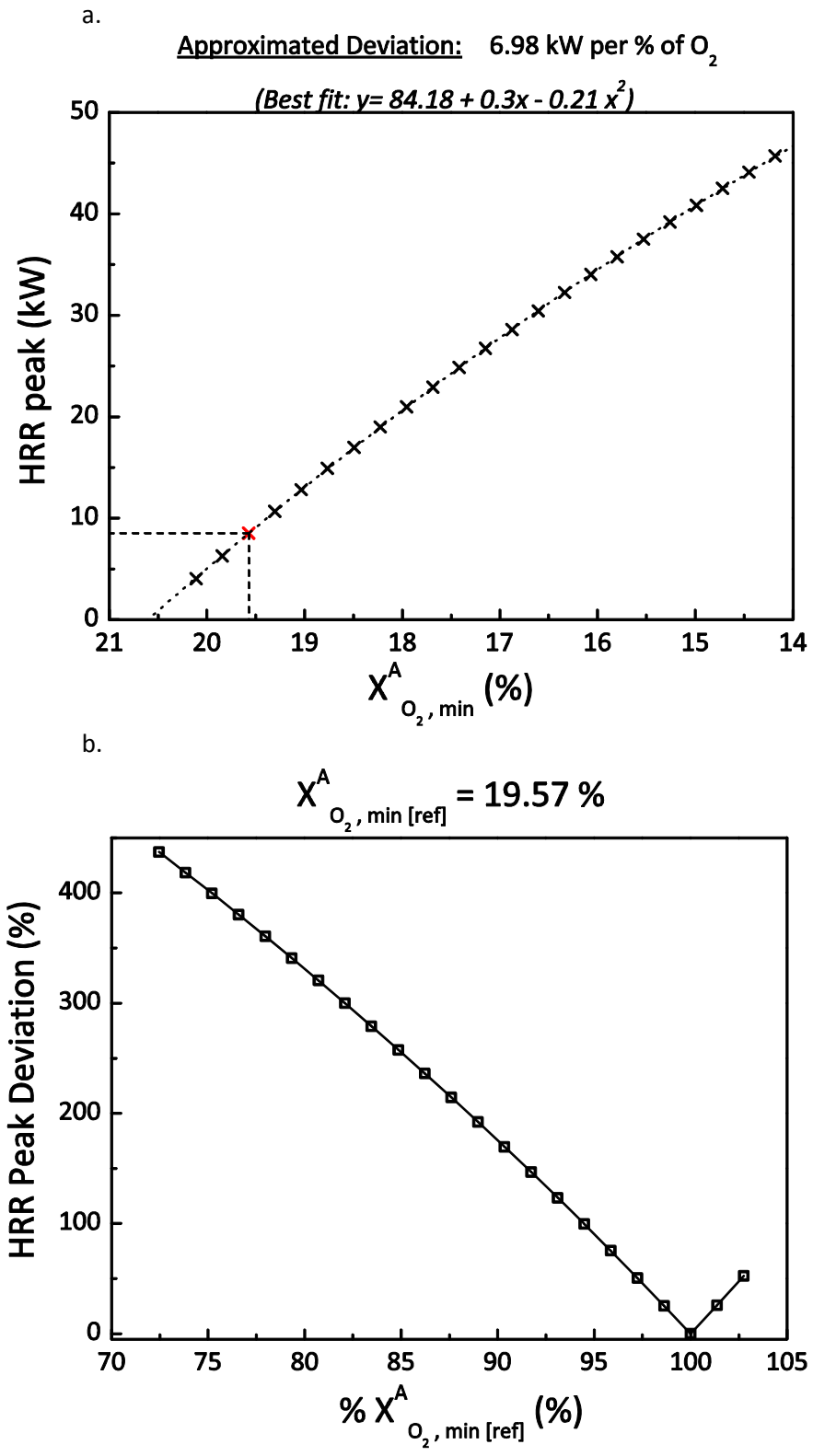

Figure 6.13. Sensitivity analysis of the peak HRR based on OC calculation when varying the O_2 molar fraction and considering large O_2 depletion. Results are presented as absolute variation (Figure 6.13.a) and relative deviation (Figure 6.13.b).

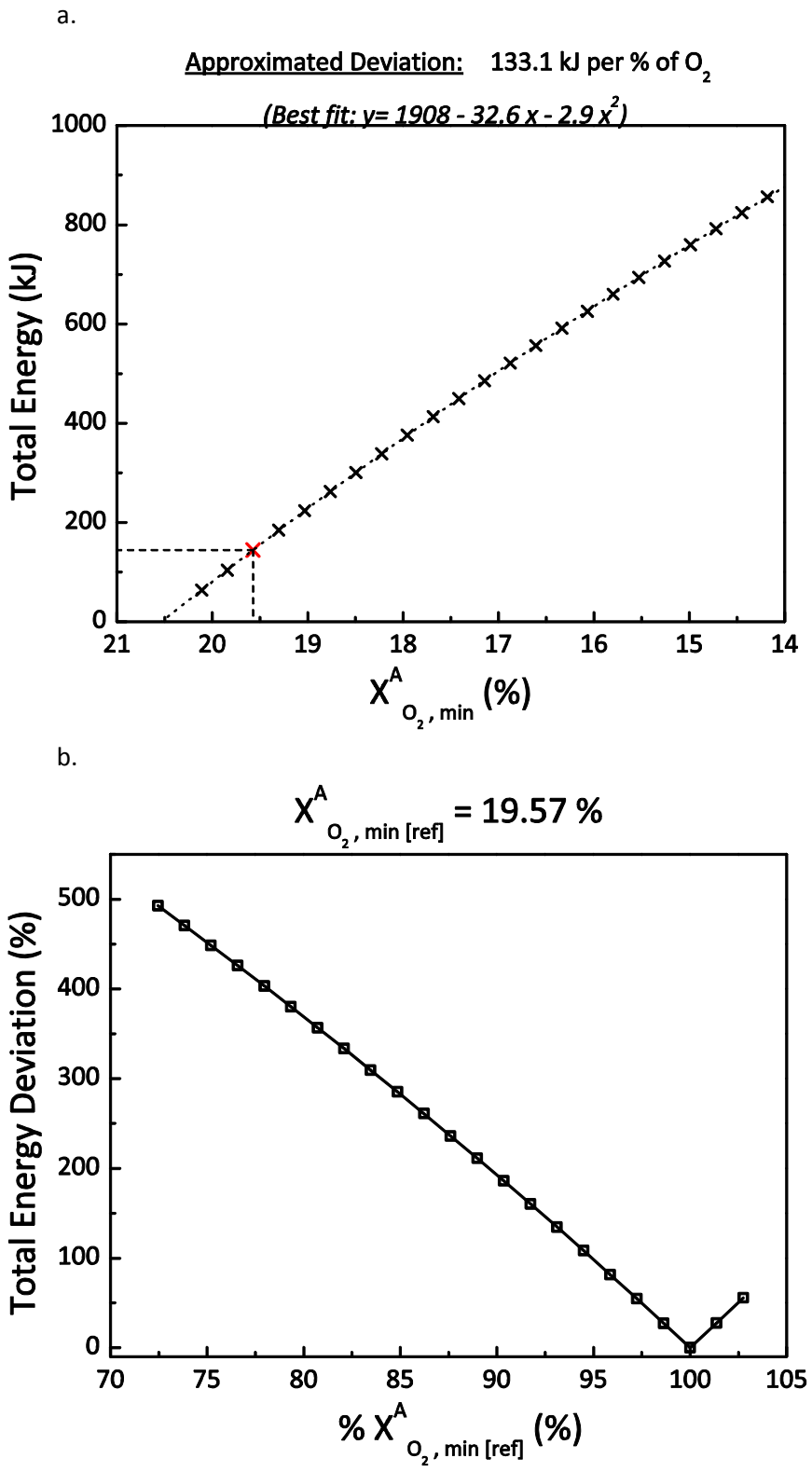

Figure 6.14. Sensitivity analysis of the peak HRR and total energy release based on OC calculation when varying the O_2 molar fraction and considering large O_2 depletion. Results are presented as absolute variation (Figure 6.14.a) and relative deviation (Figure 6.14.b).

According to Table 6.5, inaccurate species measurements would lead to high errors in the HRR estimations preventing from any confidence in the results. Furthermore, the response time of a device constitutes an inherent characteristic and cannot be decreased apart from modifying the dynamics of the system itself. The problematic of the response time of a system arises for any electrical instrument where fast accurate acquisitions are required. Domains such as signal processing (filters modelling), medicine (patients monitoring), chemistry (gases emissions from chemical reactions) encounter this potential issue [8] [10] [11]. Corrections have been proposed.

6.3.2.5. Signal Correction

Referring to Figure 6.6, it clearly shows that the signal is not only affected by the inherent characteristics of the analysers but also of the sampling and filtering system. The output signal exhibits similarity with the behaviour of a RC filter. Like capacitors, analysers can be described by a characteristic function or kernel function. According to Point et al [12] and Lyon and Farris [13], the transient behaviour of a measuring device can be approximated by exponential series. A characteristic function can be expressed as,

$$h(t) = \sum_{i=1}^{n} a_i \, e^{-\frac{t}{\tau_i}} \tag{14}$$

Where a_i represents the calibration constant of the i^{th} transfer element and τ_i its associated time constant. Considering the sampling system, if a function $h(t)$ exists so that it describe its transient behaviour and $h(t)$ is independent of any sample properties or thermal history, then, the measured output signal $s(t)$ is the convolution of $h(t)$ (source of distortions) and the input signal $e(t)$,

$$s(t) = (h * e\,)(t) = \int_0^t h\,(t-\vartheta)\; e(\vartheta)\; d\vartheta \tag{15}$$

By using the properties of the Laplace transforms, one can reconstruct the input signal according the output one using the following expression,

$$e(t) = s(t) + \tau\, \frac{ds(t)}{dt} \tag{16}$$

The different steps of the **Error! Reference source not found.**calculation are explained in Appendix D. Equation (16)**Error! Reference source not found.Error! Reference source not found.Error! Reference source not found.** requires the estimation of the time constant of the system (τ) and an approximation of the derivative of the output signal. For discrete data, assuming a sampling time Δt, equation (16) is formulated as follow,

$$e_i(t) = s_i(t) + \tau \left(\frac{s_{i+1}(t) - s_{i-1}(t)}{2\,\Delta t} \right) \tag{17}$$

Where i is the sampling point. Direct application of equation (17) to the CO_2 signal is characterized by an important overshoot before reaching the steady state value of the step impulse. It is a common phenomenon often encountered when using low pass filters. This is explained by the impulse response of a step function in the frequency domain. In the time domain, the impulse response is represented by a sinc function featuring oscillations. The step response being the integral of impulse response over time, overshoots and ringing artefacts are ineluctably generated. Regarding the present system, the overshoot stems from several sources:

1. The characteristic function of the system is an approximation and does not describe perfectly the apparatus behaviour. Consequently, the interpolations of rising and falling signals encounter similar issues. It has been noticed that expression **Error! Reference source not found.** used to model the step response presented discrepancies with the actual signal at low species concentration; Furthermore, expression (16) entirely relies on the assumption that the characteristic function of the system can be described by an affine combination of exponential;

2. The output signal propagates uncertainty that can be related to an embedded noise. Assuming δs as the error associated to the signal measurement, the calculation of the derivative in equation (17) is also affected by the propagation of errors. A simple estimation of the uncertainty associated with the derivative gives,

   $$\delta\left(\frac{ds}{dt}\right) = 2\,\delta s \tag{18}$$

   Large uncertainties on the signal measurement are susceptible to introduce important noise in the derivative calculation;

3. The calculation of the derivative relies on an approximated expression and depends on the sampling time;

Several adjustments can be applied. The exponential defining the characteristics function of the sampling system can be modified to a Gaussian function. Interpolation of the step response allows to better capture the initiation of the rise. The noise is partially filtered, for instance, by means of a Savitzky-Golay algorithm [16]. The overshoot is mainly engendered by the rising part of the discretized derivative which should not emerge if the exponential perfectly described the output signal. Finally, by introducing a damping factor in expression (17), one obtains,

$$e_i(t) = s_i(t) + K\tau \left(\frac{s_{i+1}(t) - s_{i-1}(t)}{2\,\Delta t} \right)_{S-Golay} \tag{19}$$

Where K is a damping coefficient. Equation (19) has been applied for CO_2 step responses performed at various steady state concentrations. According to the level of the steady state, damping coefficient values fluctuate between 0.3 and 0.5. When possible, a mass balance on the C elements released during flaming combustion is conducted in order to verify that the damping coefficient is not too high and gives an overestimation of the measurement. In other case, an average value of 0.4 was used. It allows correct reconstruction of most of the studied step signals, the overshoot being significantly reduced. Figure 6.15 shows the correction of a CO_2 molar fraction step impulse obtained following the aforementioned methodology. The reconstruction of a correct signal is achieved. Nevertheless, it has to be noticed that as the step impulse experiments are carried out, responses from the sampling system start to lengthen after few tests. One suggests that this phenomenon is related to a decline of efficiency of the drying agent. Predicting the evolution of the response time according to the efficiency level of the drying agent appears as an intricate problem and has not been investigated further. In order to prevent this behaviour from taking place, a limited time and number of experiments was prescribed to be sure that the drying agent does not influence the response time of the system.

The elaboration of a correction has been based on the analysis of a step response. The method has also been assessed for transient behaviour. Combustion reactions of different known fuels have been performed under well ventilated conditions. HRR were estimated through OC, CDG

and mass loss approaches. Energy coefficients were available in the literature. The assessment criterion relies on the comparison of the magnitudes and shapes of HRR curves obtained from the various calculation principles. To prevent any potential error propagation from the exhaust flow measurements, the OC/CDG ratio was also evaluated. The correction method is considered satisfactory if and only if discrepancy between the three HRR calculation techniques was less than 10% and the OC/CDG ratio lies between 0.9 and 1.1 during the combustion period. Criterion was achieved with methane, PMMA, heptane and acetone tests. As a consequence the correction method is assumed suitable for reactions presenting identical levels of gaseous emissions and reaction kinetics with no significantly shorter characteristic times.

Beside the evaluation of adequate energy coefficients, accurate measurements compose another basis of HRR estimation through OC and CDG. Sensitivity analysis on the O_2 and CO_2 molar fraction data demonstrates that both parameters are critical ones. Variations introduce significant divergence in the HRR calculations. Consequently, if accurate measurements cannot be achieved with a required confidence, the use of OC and CDG has to be proscribed. Nevertheless, issues related to the response time of the sampling system of a calorimeter can be remedied under the conditions that the characteristic function of the exhaust line as well as the derivative of the output signal are correctly approximated.

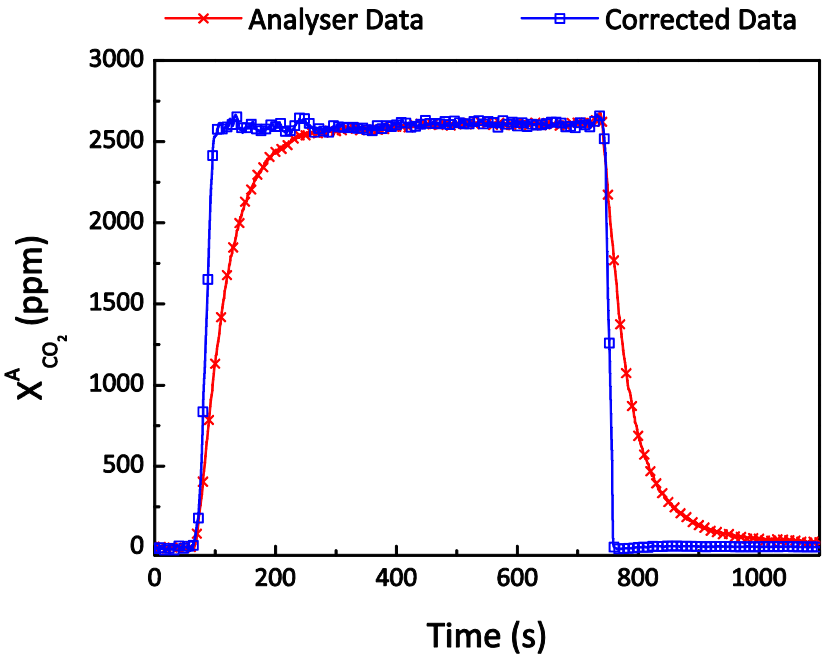

Figure 6.15. Experimental and corrected CO_2 molar fraction signal.

6.3.3. Exhaust flow

The exhaust flow rate has been pointed out as another potential source of important uncertainty by Brohez [2], Enright and Fleischmann [1] and Axelsson *et al.* [3]. The results they obtain coincide well. They estimated the contribution of the uncertainty on the exhaust mass flow rate to the overall error in the HRR calculation to be about 3 %. They highlighted that the major error arises from the estimation of the flow profile coefficient, K [Chapter 4, equation (43)]. Uncertainty calculation conducted in the present study on the exhaust mass flow rate exhibits that the potential error on the measurement can rise up to 10%. Difference with previous results is explained by the evaluation of larger relative errors for the duct cross section area and the pressure drop across the Pitot tube (ΔP). The main contributors to the error are the cross section area A, followed by the pressure drop ΔP and the flow profile coefficient K. By means of a sensitive analysis, one can estimate how variations initiated in the exhaust volume flow rate propagate to the HRR calculations and the magnitude of the divergences they can engender. Uncertainty calculation assumes corrects the different measuring devices to work correctly. The error is only related to intrinsic limitations of accuracy. The effect of a deficient instrument can be investigated through the sensitivity analysis. Regarding the exhaust flow rate, situations can be encountered where deficiency of the measuring system is generated by external causes. A wrong calibration of the flow profile coefficient, deformation of the exhaust duct due to heat expansion and/or obstruction of the Pitot tube holes by soot or other solid particles deposit will affect the measurement of the volume flow rate. The related effect on the HRR calculation is estimated varying this sensitive parameter from 50 % to 150 % of its reference value (167 $Nm^3.h^{-1}$). Results are presented on Figure 6.16. Divergences of the HRR peak and total energy release (Figure 6.16.a and Figure 6.16.b) from the reference calculation exhibit a linear trend. This is coherent with OC and CDG equations ($\dot{q}_{OC\ (CDG)} \propto \dot{V}_e$). Under the assumption of a reference exhaust flow of 167 /$Nm^3.h^{-1}$, absolute variations of HRR peak and total energy release have been respectively evaluated at 0.05 kW.Nm-^{3}.h and 0.91 kJ.Nm^{-3}.h.

Small errors in the volume flow rate estimation do not impact the accuracy of the HRR calculations. This analysis suggests that the inherent error on the volume flow rate measurement does not affect the precision of OC and CDG principles. On the other hand, failure of the system can be initiated by external phenomena as mentioned previously. If

misestimation of the actual flow rate becomes important, the discrepancy introduced in the HRR from the actual value increases beyond confidence levels. As an example, considering a reference HRR peak of 8 kW, one can conceive a 4 kW discrepancy as significant. A 80 Nm^3/h variation from the reference volume flow rate would engender such deviation. A 50% error on the flow profile coefficient, a 50% deformation of the duct cross section area or obstruction of 2/3 of the Pitot tube holes are susceptible to induce this magnitude of change on the volume flow rate measurement. Figure 6.17 represents the relative deviation of the HRR peak according to a given variation (also shown as a relative deviation) from the reference flow rate value. It highlights that a 1% change in volume flow rate is entirely transferred to the HRR estimation (i.e. 1% changed is also observed on the HRR). This is easily explained by the linearity of OC and CDG expressions regarding the flow rate variable.

The existence of errors in the volume flow rate measurement is sometimes intricate to identify. A relevant indicator is defined by the CDG/OC ratio. Under stoichiometric conditions, complete combustion can be assumed and OC and CDG expressions are linearly dependent on the exhaust volume flow rate variable. Consequently, the CDG/OC ratio is uncorrelated from the latter. Considering the case where the comparison of HRR curves would highlight discrepancies between OC, CDG and mass loss results, if the CDG/OC ratio remains constant around 1, this indicates that errors are embedded in the exhaust volume flow rate estimation. On the contrary, a ratio different to 1does notifies the existence of errors within other parameters of the OC and CDG equations. Figure 6.18 illustrates the developed argument. CDG/OC ratios have been calculated for heptanes pool fire tests and for ternary powder compositions (mixture: lactose, starch and KNO_3 at various proportions) at different exhaust volume flow rates. An expected ratio of 1 is found within the framework of the heptanes burnings. No critical error seems to propagate in the calculations. On the contrary, ratios regarding the ternary powders combustion experiments exhibit larger discrepancies. Furthermore, the average ratio is about 2.5. HRR estimations through OC and CDG were conducted based on the use of usual calorimetric assumptions in terms of energy coefficients, expansion factor, and water vapour molar fraction. Obviously, one or several calculation hypotheses are not relevant for the present materials.

a.

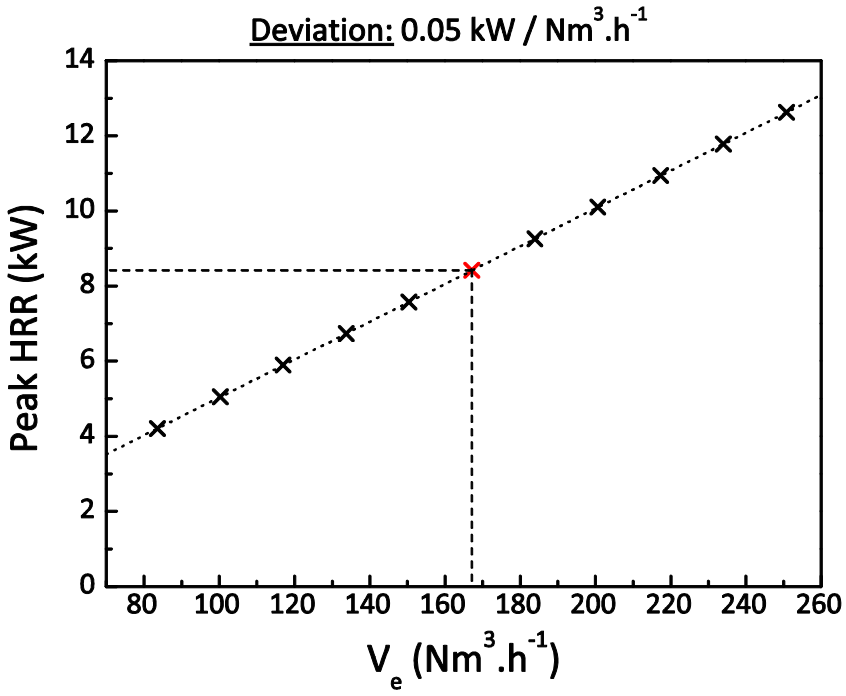

b.

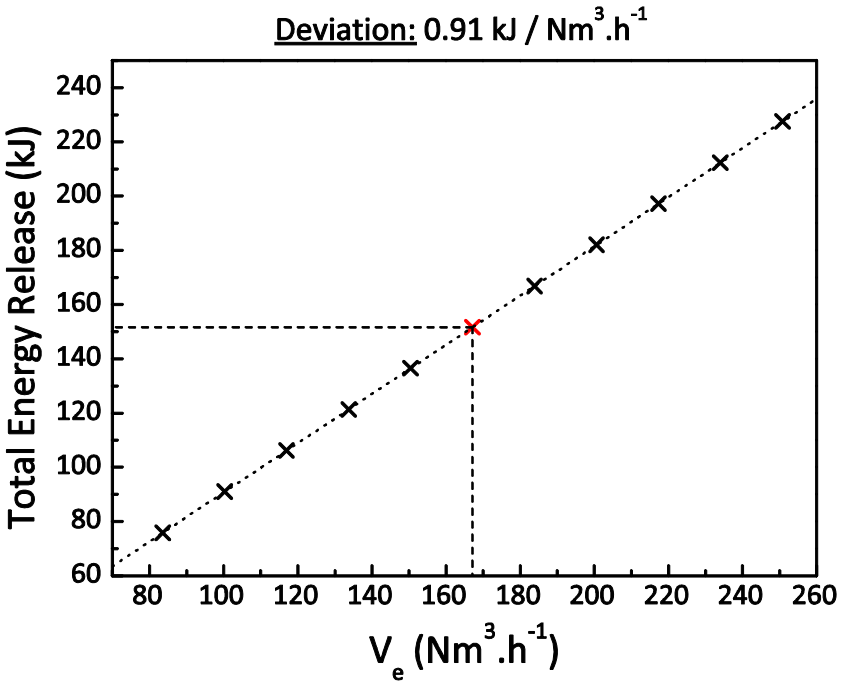

Figure 6.16. Sensitivity analysis of the peak HRR (a) and total energy release (b) based on OC calculation when varying the exhaust volume flow rate.

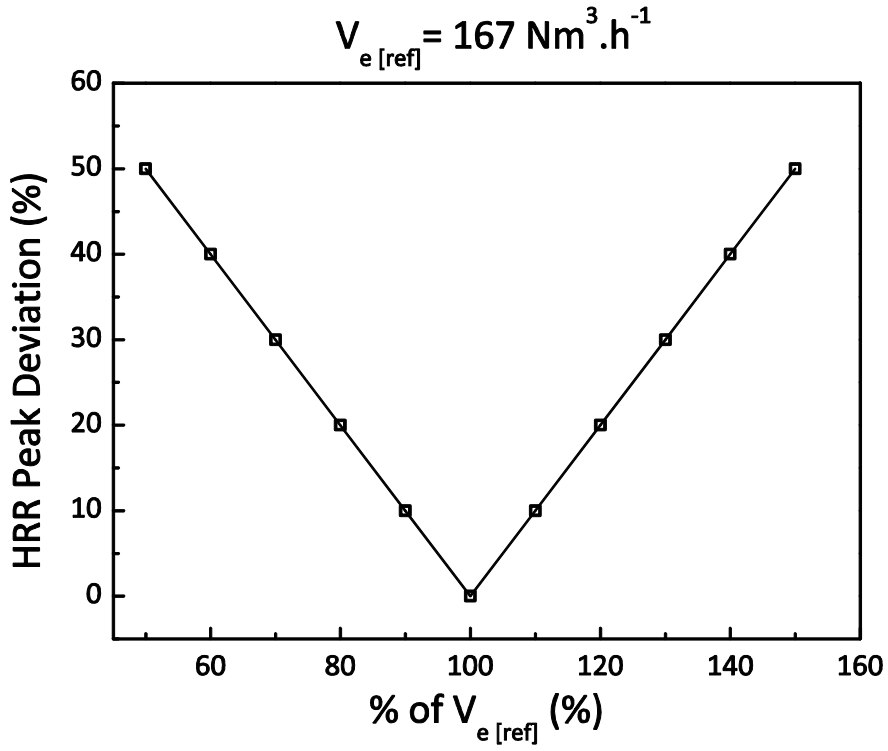

Figure 6.17. Sensitivity analysis of the peak HRR presented as a relative deviation on OC calculation when varying the exhaust volume.

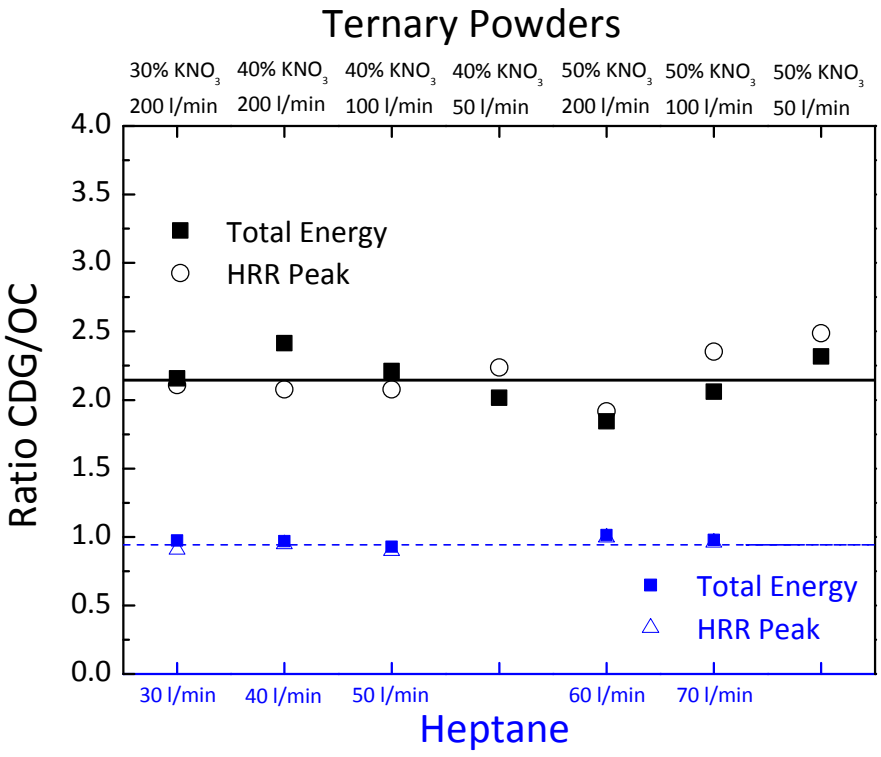

Figure 6.18. OC/CDG Ratio of heptane and ternary powders based on lactose, starch and KNO_3 mixtures (calculations conducted using Huggett and Tewarson energy constants).

To conclude on the exhaust flow rate, if an error initiates from this parameter, the divergence is entirely transferred to the HRR estimations due to the linear dependency of OC and CDG to the exhaust flow rate variable.

6.3.4. N_2 emissions

Theory of OC and CDG is based on the estimation of the energy release according to the consumption of oxidizing agent or the production of combustion products. Both principles follow species conservation and require then the knowledge of an important parameter: the amount of incoming air, defined as the flow generated by the supply and the entrained (or dilution) air). One can formulate a relation between the incoming and exhaust mass flow rates:

$$\dot{m}_e = \dot{m}_a - \Delta\dot{m}_{O_2} + \dot{m}_{fuel} \tag{20}$$

Where, $\dot{m}_e$ is the exhaust mass flow rate (kg.s^{-1}), $\dot{m}_a$, the mass of incoming air (kg.s^{-1}), $\Delta\dot{m}_{O_2}$, the O_2 consumption (kg.s^{-1}) and $\dot{m}_{fuel}$ the mass loss rate of burning material (kg.s^{-1}). $\Delta\dot{m}_{O_2}$ can be expressed according to molar fraction measurements, $\dot{m}_e$ and $\dot{m}_a$. Finally, it allows rewriting equation (20),

$$\dot{m}_a = \frac{\dot{m}_e\left(1 - \frac{X_{O_2}M_{O_2}}{M_e}\right) - \dot{m}_{fuel}}{1 - \frac{X^0_{O_2}M_{O_2}}{M_a}} \tag{21}$$

Equation (21) is relatively simple and easy to implement. One notices that if $\dot{m}_e \gg \dot{m}_{fuel}$, it can be simplified by $\dot{m}_a \approx \dot{m}_e$. The dilution of the combustion gases is large enough so that no significant variations occur. Nevertheless equation (21) requires the knowledge of the mass loss rate of the burning material which is not always available. Small scale apparatuses such as the cone calorimeter or the FPA incorporate mass loss measurements allowing the use of Equation (21). Nevertheless, large scale experiments do not always comprise a load cell while one of the purpose of the calorimetric principles to constitute a multi-scale methodology. As a consequence, alternative equations have been determined based on species molar fraction measurements and the exhaust mass flow rate (cf. Chapter 3) and independent of the term of fuel mass. The evaluation of the mass flow rate of incoming air relies on the validity of a fundamental assumption: the conservation of N_2. Considering the following combustion reaction,

$$C_xH_yO_zN_a + \nu_{O_2}O_2 + \nu_{N_2}N_2 \longrightarrow \nu_{CO_2}CO_2 + \nu_{CO}CO + \nu_{THC}THC + \nu_{H_2O}H_2O + \nu_N N_2 + \nu_{N_2O}N_2O + \nu_{NO}NO + + \nu_{NO_2}NO_2 \quad (22)$$

Usual simplifying hypotheses used for OC and CDG calculations consist in only considering N_2, O_2, CO_2, H_2O, CO and unburnt HC as exhaust gases. Regarding the chemical reaction (22), OC and CDG principles consider N_2O, NO and NO_2 as inert gases and assimilate them to N_2. A significant production of these gases is susceptible to introduce two approximations:

1. The production of N_2O, NO and NO_2 requires consumption of O_2 from the air or from the material. The energy associated with the generation of these compounds is different than the one associated with the oxidation reactions leading to CO_2, H_2O and CO;

2. N_2O, NO and NO_2 are considered as N_2. Furthermore, if the sample material contains N atoms, N_2 can be a product resulting from the material decomposition. If the generation of "N compounds" (i.e. N_2, N_2O, NO and NO_2) is important compared to the amount of N_2 present in the reacting atmosphere (usually the incoming air), the principle of N_2 conservation is breached by neglecting the material emissions.

The two previous approximations contribute to the propagation error in OC and CDG results. The energy issue by non considering N_2O, NO or NO_2 productions can be related to the sensitivity analysis carried out on the energy constants. One needs to assess the degree of divergence that introduces a disregard of the hypothesis of N_2 conservation in the HRR approximations. Assuming internal N_2 production, the equation of N_2 conservation is given by,

$$\dot{m}_{N_2}^0 = \dot{m}_{N_2\,[exhaust\ gases]} - \dot{m}_{N_2\,[reaction\ product]} \quad (23)$$

Where $\dot{m}_{N_2}^0$ and $\dot{m}_{N_2\,[exhaust\ gases]}$ represent, respectively, the N_2 mass flow rates from the incoming air, from the exhaust gases and $\dot{m}_{N_2\,[reaction\ product]}$ the N_2 production rate from the combustion reaction.

Estimation of the N_2 mass flow rate is required for the calculation of the term of incoming air regarding the CDG principal and of the depletion factor, ϕ, regarding the OC approach. Consequently, given the 2 methods estimate the mass flow rate of incoming air based on 2 different approaches, their dependency to a N_2 conservation breach is likely to engender

distinct effects on the HRR evaluations. It appears important to study separately the robustness of OC and CDG methods according to a production of N_2 from the burning compound. The sensitive parameter that is varied within the framework of the analysis is the percentage of N_2 mass flow rate produced compared to N_2 mass flow rate originating from the supply and entrained air.

6.3.4.1. CDG principle

In the situation of N_2 production during the combustion reaction and taking into account its conservation, an expression of the mass flow rate of incoming air is given by,

$$\dot{m}_a = \left(\frac{\frac{\dot{m}_e}{M_e}\left(1 - X_{H_2O}\right)\left(1 - X_{O_2}^A - X_{CO_2}^A - X_{CO}^A - X_{THC}^A\right) - \frac{\dot{m}_{N_2\,[reaction\ product]}}{M_{N_2}}}{\left(1 - X_{H_2O}^0\right)\left(1 - X_{O_2}^{A^0} - X_{CO_2}^{A^0}\right)} \right) M_a \tag{24}$$

Considering expression (24) and recalling the HRR equation based on the CDG principle [Chapter 4, expression (70)], it comes that a production of N_2 during the reaction can influence the HRR estimation for certain configurations. Assuming complete combustion conditions, the CDG equation can be approximated by the following expression,

$$\dot{q}_{CDG} \sim \dot{q}_{CDG\,[base]}\left(1 + f(N_2)\right) \tag{25}$$

With, $\dot{q}_{CDG\,[base]}$ the usual CDG equation (i.e. no production of N_2 during the combustion reaction). $f(N_2)$ is the term representing the variation introduced in the HRR estimation by the N_2 production and is given by,

$$f(N_2) = X_{CO_2}^{A^0} \frac{\dot{m}_{N_2\,[reaction\ product]}}{\Delta\dot{m}_{CO_2}\left(1 - X_{O_2}^{A^0} - X_{CO_2}^{A^0}\right)} \frac{M_{CO_2}}{M_{N_2}} \tag{26}$$

One can notice that the contribution of this term varies according to the magnitude of the energy release. One assesses separately the conditions of high HRR (i.e. high CO_2 emissions) and low HRR (i.e. low CO_2 emissions) as well as the magnitude of the exhaust mass flow rate.

6.3.4.1.1. High HRR

For a given exhaust mass flow rate, high HRR is associated with large CO_2 emissions. One can show that if $X^A_{CO_2} \gg X^{A^0}_{CO_2}$ and $\Delta\dot{m}_{CO_2} \geq \frac{\dot{m}_{N_2\,[reaction\ product]}}{100}$ (cf. Table 6.6) equation (25) can be approximated by,

$$\dot{q}_{CDG} \sim \dot{q}_{CDG\,[base]} \tag{27}$$

Except if a tremendous release of N_2 takes place during the combustion reaction (i.e. $\frac{\dot{m}_{N_2\,[reaction\ product]}}{\Delta\dot{m}_{CO_2}} > 1000$), the contribution of $f(N_2)$ to the HRR is not significant. Neglecting the term $f(N_2)$should not affect the accuracy of the results.

Table 6.6. Order of magnitude of $f(N_2)$ according to the ratio $\frac{\dot{m}_{N_2\,[reaction\ product]}}{\Delta\dot{m}_{CO_2}}$.

$\left[\frac{\dot{m}_{N_2\,[reaction\ product]}}{\Delta\dot{m}_{CO_2}}\right]$	0.01	0.1	1	10	100	1000
$[f(N_2)]$	10^{-5}	10^{-4}	10^{-3}	10^{-2}	10^{-1}	1

6.3.4.1.2. Low HRR

For low HRR (i.e. low production of CO_2), $\left[X^A_{CO_2}\right] \sim \left[X^{A^0}_{CO_2}\right]$ and if the N_2 production rate is substantially higher than the CO_2 generation rate, the ratio $\left[\frac{\dot{m}_{N_2\,[reaction\ product]}}{\Delta\dot{m}_{CO_2}}\right]$ can become large enough for the $f(N_2)$ contribution to be noticeable on the HRR estimation through the CDG principle.

6.3.4.1.3. Sensitivity Results

A sensitivity analysis was carried out to investigate the variations introduced on the HRR calculation by neglecting a N_2 production during the combustion reaction. The defined sensitive parameter was the ratio of the N_2 production rate compared to the N_2 mass flow rate from the incoming air. The variable considered is the total energy obtained by integration of

the HRR. Two HRR calculations have been conducted. In the first one, a modelled N_2 production was included in the combustion reaction and taken into account for evaluating the mass flow rate of incoming air. In the second, the N_2 production was also present in the reaction process but was neglected for the HRR calculation. Figure 6.19 shows the deviation between the two CDG calculations. Furthermore, the analysis was carried out for several CO_2 emission levels in order to consider different magnitude of HRR.

One can observe that up to 10% of the original CO_2 molar fraction, the deviation introduced by not considering N_2 emissions from the combustion remains lower than 12% for N_2 production up to 47% of the N_2 mass flow rate of incoming air (maximum values). This is homogeneous with the predictions deduced by approximating the CDG equations for high HRR. It also show that the amount of N_2 generated has to be relatively large for the deviation to become important. Following the FPA ASTM standard [17], given the prescribed exhaust flow (150 $l.s^{-1}$) and the maximum sample dimension, it is unlikely to meet conditions where a material would release a maximum generation rate of N_2 equivalent to up to 47% of the mass flow rate of N_2contained in the incoming air.

In case of very low HRR (low $X_{CO_2}^A$ values), the deviations tend to increase as it appears on Figure 6.19 (case: 4% of the CO_2 original molar fraction). The divergence rises up to 27% for a maximum production rate of N_2 equivalent to 47% of the N_2 mass flow rate from incoming air. Results agree with the interpretation developed in section 6.3.4.1.2. One can also notice that the deviation in total energy remains below 10% for production of N_2representing up to 15% of the N_2 mass flow rate of incoming air.

Similar calculations were conducted by varying the exhaust volume flow rate instead of the CO_2 molar fraction. When decreasing $\dot{m}_e$ by a factor of 10, deviations induced by neglecting N_2 emissions during the reaction stay below 6 %.

Regarding CDG principle, non respect of the N_2 conservation principle for the air income mass flow rate estimation does not introduce critical errors in the calculation as long as the production of N_2 remains small compared to the amount of N_2 present in the incoming air (< 50% in case of high HRR and < 15% for low HRR). For a given N_2 production rate, discrepancy is enhanced as the emissions of CO_2 are reduced.

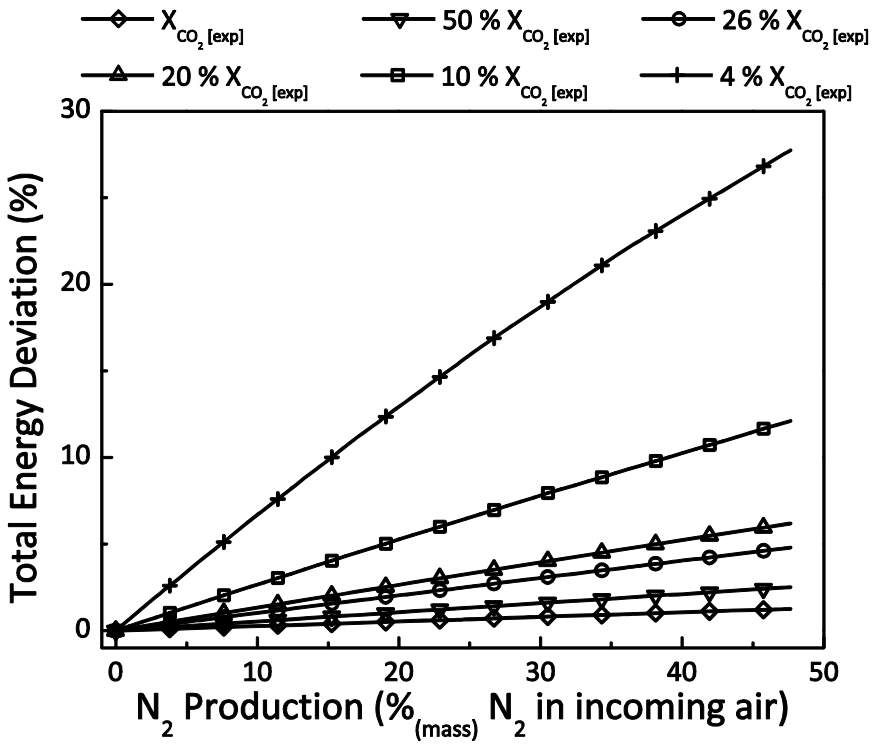

Figure 6.19. Sensitivity of the total energy according to the N_2 production and the magnitude of CO_2 molar fraction.

6.3.4.2. OC principle

Considering the OC principle, application of the N_2 conservation principle is necessary to evaluate the depletion factor ϕ. The expression of ϕ is given in Chapter 4 (expression (52)). Production of N_2 during the combustion reaction introduces an additional term in ϕ. Assuming that $\phi_{[base]}$ is the expression of the depletion factor when no generation of N_2 takes place, ϕ can be expressed as,

$$\phi = \phi_{[base]} - \frac{X_{O_2}^{A}\left(1 - X_{O_2}^{A^0} - X_{CO_2}^{A^0}\right)}{X_{O_2}^{A^0}\left(1 - X_{O_2}^{A} - X_{CO_2}^{A} - X_{CO}^{A} - X_{THC}^{A}\right)}\left(\frac{\dot{m}_{N_2\,[reaction\ product]}}{\dot{m}_{N_2}^{0}}\right) \tag{28}$$

Assuming conditions close to complete combustion and defining a constant B given by,

$$B = \frac{\left(1 - X_{O_2}^{A^0} - X_{CO_2}^{A^0}\right)}{X_{O_2}^{A^0}} \tag{29}$$

One can approximate expression (28),

$$\phi \sim \phi_{[base]} - \frac{B\, X_{O_2}^A}{\left(1 - X_{O_2}^A - X_{CO_2}^A\right)} \left(\frac{\dot{m}_{N_2\,[reaction\ product]}}{\dot{m}_{N_2}^0} \right) \tag{30}$$

Defining ϕ_{N_2} such as,

$$\phi_{N_2} = B \left(\frac{X_{O_2}^A}{1 - X_{O_2}^A - X_{CO_2}^A} \right) \left(\frac{\dot{m}_{N_2\,[reaction\ product]}}{\dot{m}_{N_2}^0} \right) \tag{31}$$

Finally, one can express (30) as,

$$\phi \sim \phi_{[base]} - \phi_{N_2} \tag{32}$$

If ϕ_{N_2} presents an order of magnitude similar to or higher than the one of $\phi_{[base]}$, significant discrepancies can alter the correctness of the ϕ value by neglecting N_2 emissions during the combustion. In order to assess the contribution of the term ϕ_{N_2} to the ϕ value, the ratio $\frac{\phi_{N_2}}{\phi_{[base]}}$ has been evaluated according to the degree of O_2 depletion encountered and for several ratios $r = \frac{\dot{m}_{N_2\,[reaction\ product]}}{\dot{m}_{N_2}^0}$. Figure 6.20 highlights the evolution of $\frac{\phi_{N_2}}{\phi_{[base]}}$ according to $X_{O_2[\min]}^A$.(i.e. highest O_2 depletion occurring during the experiment which coincides with the HRR peak) One notices that the ratio increases for low O_2 depletions (i.e. low HRR) while it is lower for strong ones (i.e. high HRR). For r=0.01, ϕ_{N_2} can represent up to 28 % of $\phi_{[base]}$. One can predict that the divergences introduced on the HRR estimations when violating the assumption of N_2 conservation are susceptible to be important for limited N_2 productions if low O_2 consumption occurs during the reaction. Such a phenomenon could be experienced during the combustion of energetic materials where an important part of the oxidizer originates from the material. Furthermore, one also underlines from Figure 6.20 that the weight of ϕ_{N_2} to ϕ becomes higher as the production of N_2 rises. Magnitudes of the N_2 production and the O_2 depletion affect ϕ and present then potential sources of discrepancy of HRR estimations.

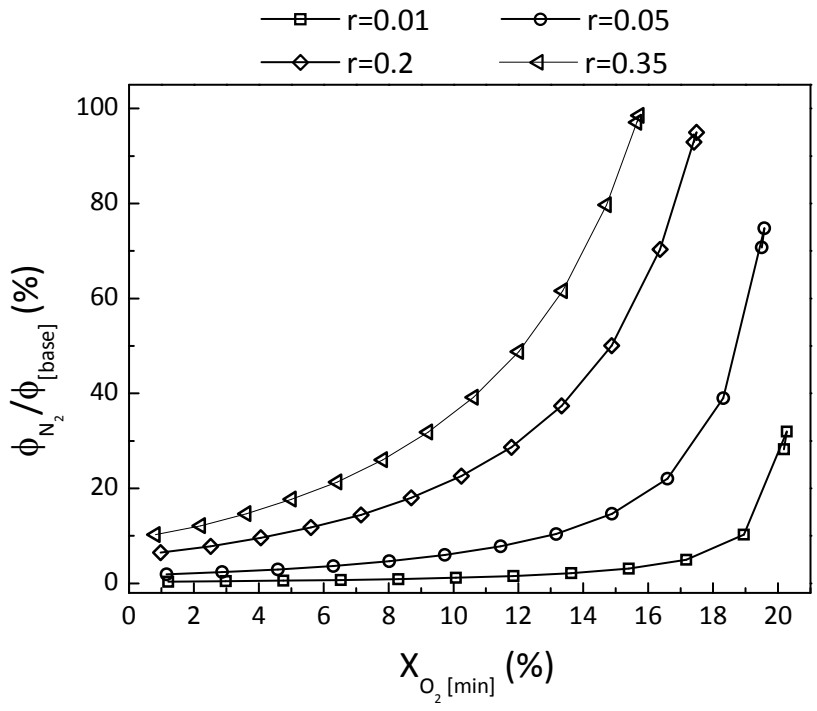

Figure 6.20. Ratio $\phi_{N_2}/\phi_{[base]}$ according to the O_2 molar fraction for various ratios $r = \frac{\dot{m}_{N_2\,[reaction\,product]}}{\dot{m}^0_{N_2}}$.

In order to verify the latter statement, a sensitivity calculation is carried out. By varying the production of N_2 during the combustion for mass flow rates up to 47% of the N_2 mass flow rate in the incoming air, the discrepancy introduced in the HRR peak by neglecting the N_2 production has been investigated. O_2 and CO_2 molar fractions were varied accounting for the N_2. The analysis has been conducted regarding 2 configurations: low and high HRR. For the low HRR, total emissions of combustion gases (CO_2, CO, THC) were kept identical with the productions achieved during the actual experiments carried out with 50% KNO_3 powder under air atmosphere. For the high HRR, the CO_2 production was increased. The O_2 depletion was estimated according to the combustion gases productions (CO2, CO, THC) and the N_2 generation. Results are illustrated on Figure 6.21. For low HRR, as long as the N_2 production remains low (<2% of the N_2 mass flow rate in incoming air) the error introduced remains under 10% and is acceptable according to the overall error associated with the OC calculation. For small scale experiments (i.e. cone calorimeter, FPA...), dilution of the combustion gases in the exhaust duct by the entrained flow is usually so important that $\dot{m}_e \gg \dot{m}_{fuel}$. If N_2 production takes place, one can expect $\dot{m}_{N_2\,[reaction\,product]} < 0.01\,\dot{m}^0_{N_2}$. However, for larger scale experiment of for modelling purposes, one observes from Figure 6.21, that the error

introduced in the HRR by non-considering $\dot{m}_{N_2\,[reaction\,product]}$ becomes serious. For a N_2 production equivalent to 10% of the N_2 mass flow rate in the incoming air, the HRR peak deviation engendered by non-respecting the principle of conservation of N_2 is about 100 % and increases fast. For high HRR, the deviation between the HRR peaks by accounting for the N_2 emission remains low ($< 5\%$). This phenomenon was already highlighted on Figure 6.20. It is due to the higher O_2 depletion, ϕ_{N_2} being function of $X_{O_2}^{A}$.

Dependency of the HRR estimation to the contribution of N_2 is higher when using OC than when using the CDG principle. When the N_2 conservation is questioned, the main interrogation has to rely on the ratio of the mass loss compared to the exhaust flow rate or dilution flow rate. If several orders of magnitudes of differences arise, a production of N_2 will not contribute significantly to the propagation of error in the OC calculation. Nevertheless, there is a potential for substantial error if the mass loss and the exhaust flow are of identical orders.

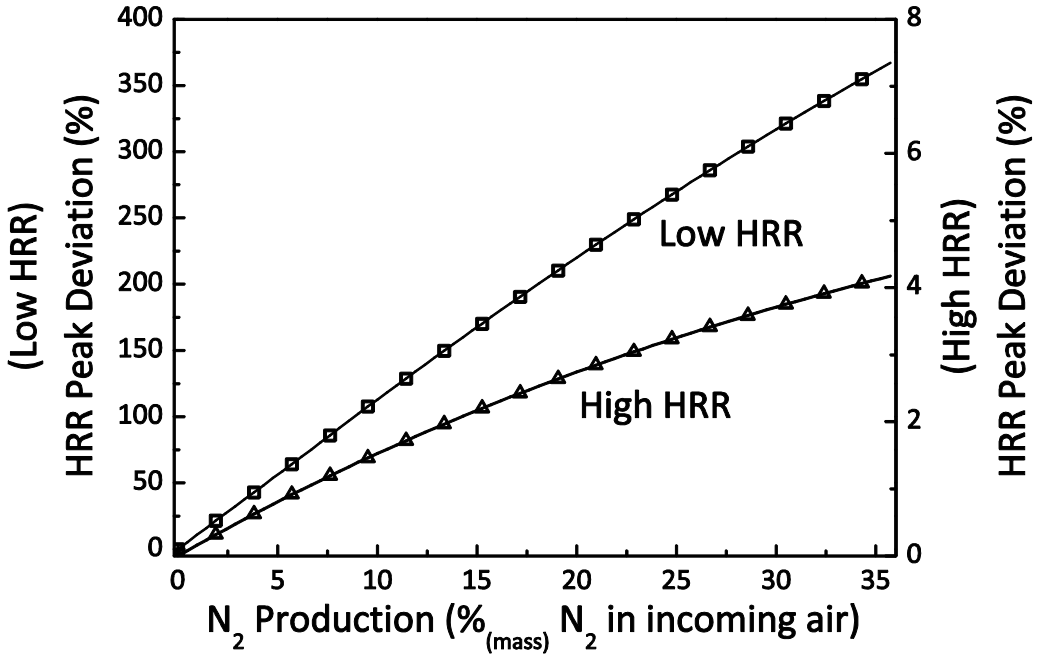

Figure 6.21. Sensitivity Analysis on the HRR Peak (OC) according to N_2 production presented as a percentage of N_2 mass flow rate in incoming air.

Sensitivity analysis conducted on the basis of neglecting a N_2 production occurring during the combustion reaction reveals that important alteration in the HRR results can arise under the condition that important productions of N_2 take place and if $\phi < 0.7$ (HRR peak Deviation > 10 %). According to the exhaust flow prescribed and the size and mass of the samples, the

eventuality of high N_2 emissions remains low. This prevents from important propagation of errors due to a non respect of the principle of N_2 conservation. Nevertheless, in the situation of large emissions of N_2, not accounting for this production deeply affects the relevance of the HRR results. Furthermore, error Furthermore, it has been shown that the OC principle is more sensitive to engender higher divergence at lower N_2 generation levels than the CDG approach. This is due to the higher values of molar fraction for O_2 than CO_2 (usually $X_{O_2}^A \gg X_{CO_2}^A$). A production of N_2 during combustion would affect a dominant term of the OC equation (the flow of O_2 from the incoming air). For CDG, the term on which a N_2 emission would hold (the flow of CO_2 from the entrained air) is usually minor except for low CO_2 production (i.e. low HRR). The two latter arguments explain why the OC calorimetry is more sensitive to a potential production of N_2 during the combustion reaction.

6.3.5. Water vapour concentration

Regarding OC and CDG equations, the water vapour molar fraction term appears for both approaches. When no water vapour analyser is present in the measuring system and when information about the combustion chemistry is too limited to allow modelling of the parameter, the calculation assumption is to neglect the water produced during the combustion. In order to estimate the error associated with such a hypothesis, one carries out a sensitivity analysis on the HRR estimations by varying X_{H_2O} over the range [1 % – 45 %] (as maximum values). Within the framework of calorimeter tests, given the prescribed exhaust mass flow rate and the sample size, the H_2O molar fraction usually remains of the order of few percents. Sensitivity analyses have been conducted on the HRR peak and total energy release calculated through OC and CDG methods. Results are presented for OC and CDG, respectively, on Figure 6.22 to Figure 6.25 as absolute magnitude variations (Figures .a) as well as relative deviations (Figures .b). They are relatively similar for both methods; one only notices that divergences affecting the HRR peak through OC are lower than through CDG. Regarding OC calorimetry, X_{H_2O} is used in the calculation of the expansion factor (α) and the molecular weight of exhaust gases (M_e). The divergence on the HRR peak (Total Energy) with the calculation carried using the experimental data never exceeds 17% (25%) when X_{H_2O} rises up to 45%. On the expected X_{H_2O} range [0.5 %– 10 %], discrepancy are less than 4 % which is not significant.

The divergence introduced in the calculation by varying X_{H_2O} shows a linear behaviour. Linear regression highlights that a change of 1 % in X_{H_2O} results in a 0.04 kW (0.06 kW in case of CDG) variation on the HRR peak and about 1.04 kJ (1.05 kJ in case of CDG) on the total energy. The latter values are quite low. Consequently, according to the uncertainty associated with the method, the hypothesis $X_{H_2O} \sim X_{H_2O}^0$ is relevant as long as X_{H_2O} remains below 10% and assuming $X_{H_2O}^0$ with an order of magnitude of about 1%.

a.

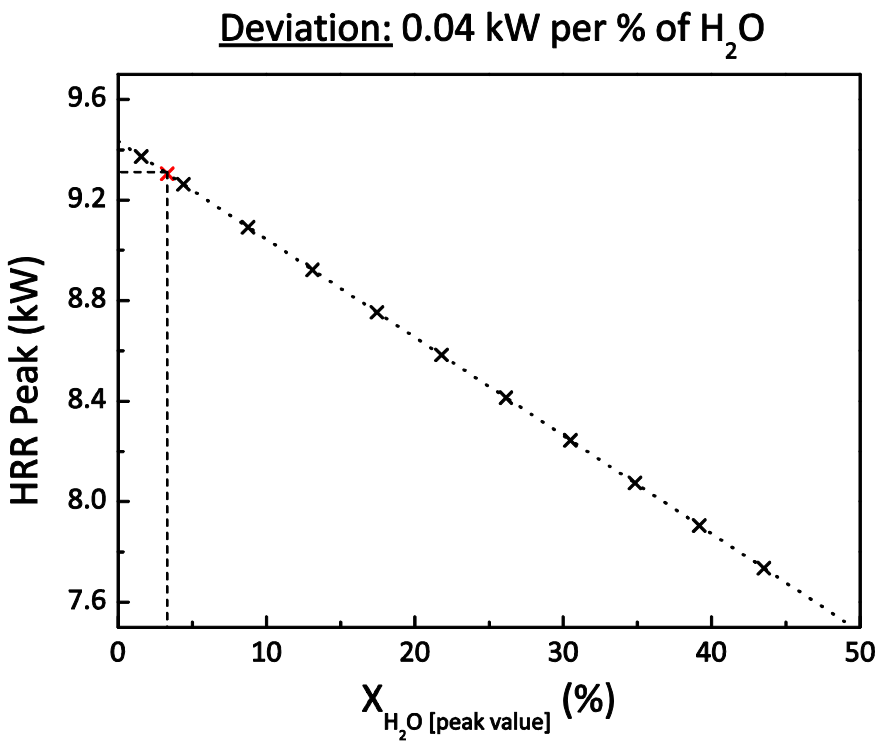

b.

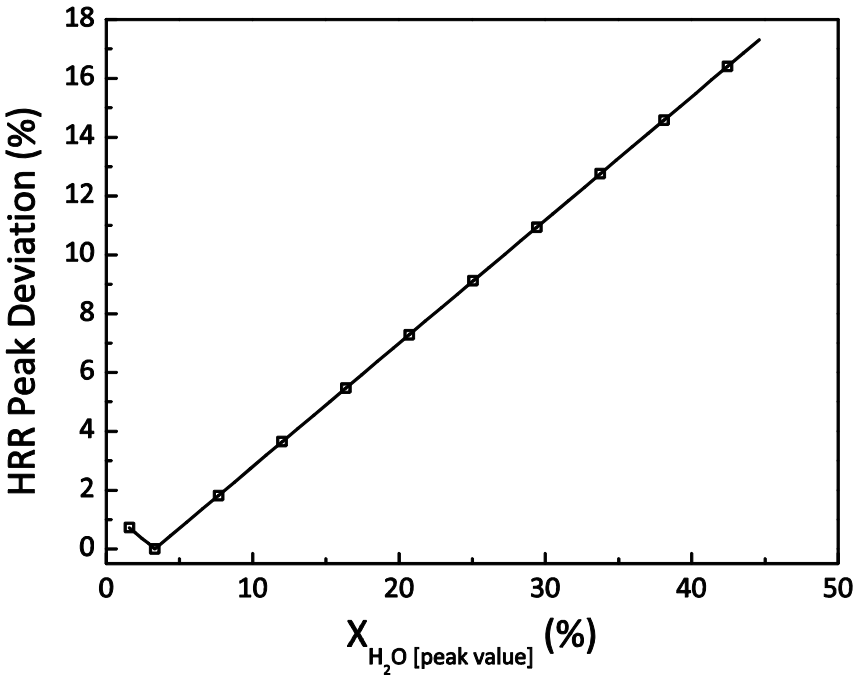

Figure 6.22. Sensitivity analysis of the peak HRR based on OC calculation when varying the water vapour molar fraction. Results are presented as absolute variation (a.) and relative deviation (b.).

a.

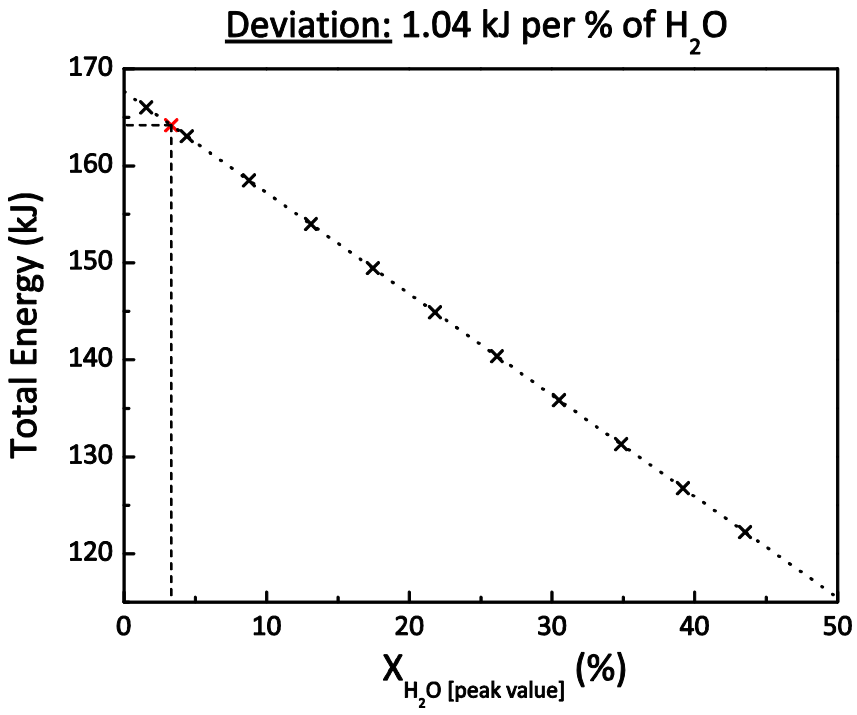

b.

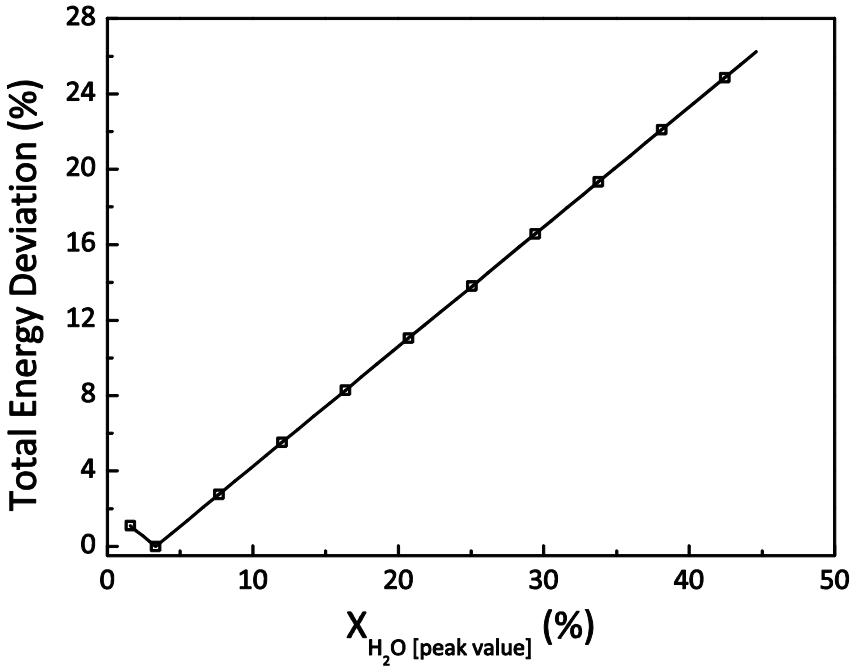

Figure 6.23. Sensitivity analysis of the total energy release based on OC calculation when varying the water vapour molar fraction. Results are presented as absolute variation (a.) and relative deviation (b.).

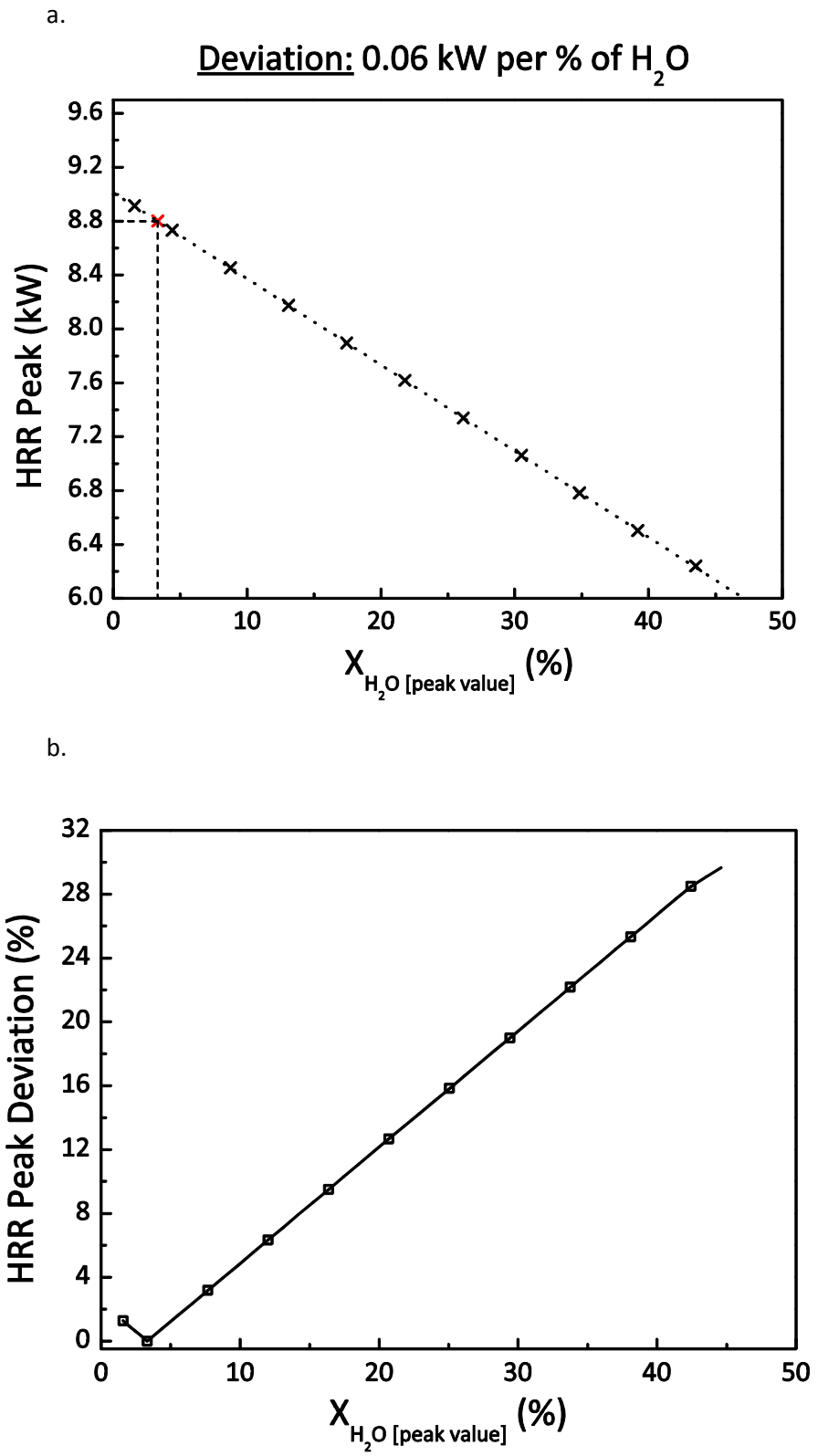

Figure 6.24. Sensitivity analysis of the peak HRR based on CDG calculation when varying the water vapour molar fraction. Results are presented as absolute variation (a.) and relative deviation (b.).

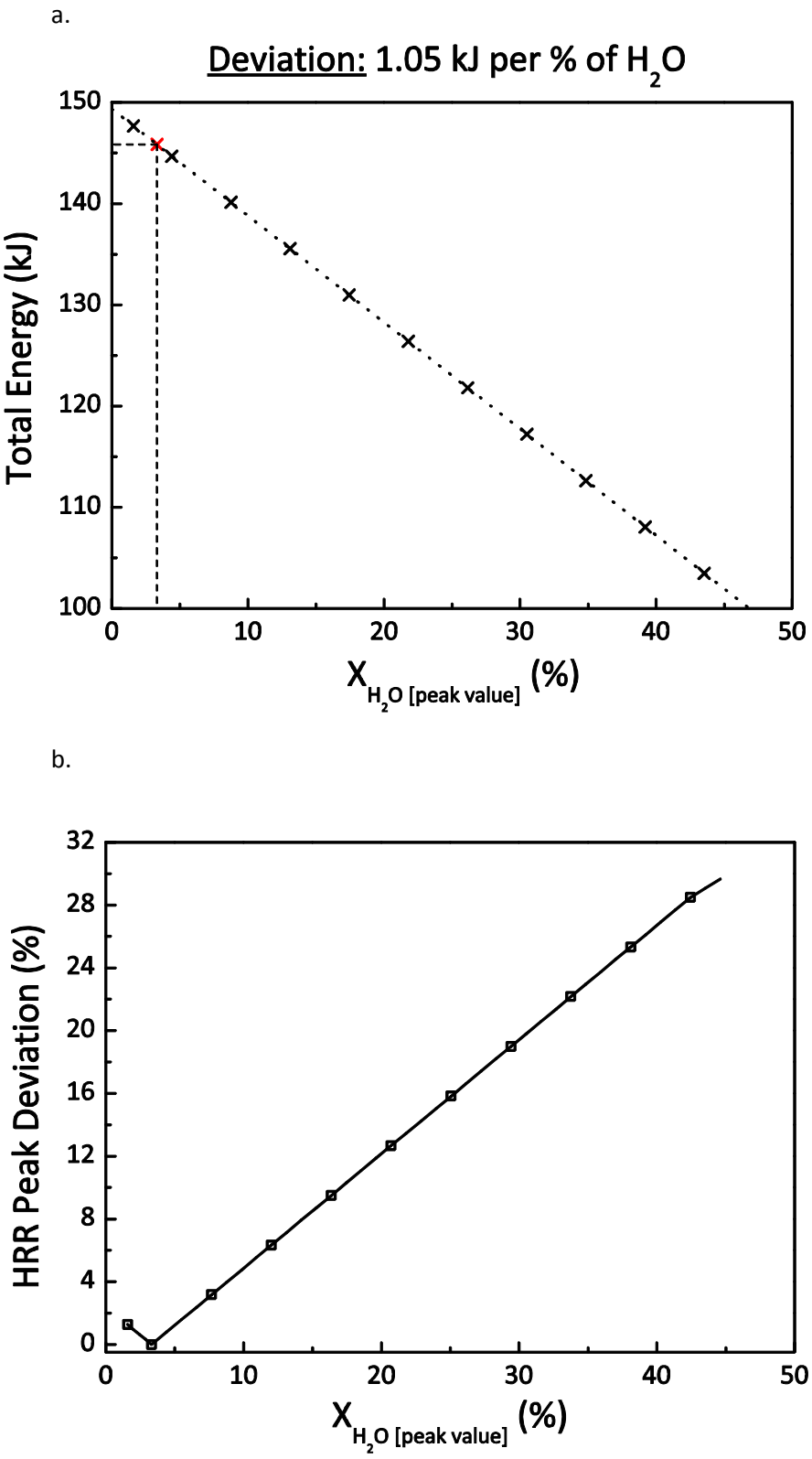

Figure 6.25. Sensitivity analysis of the total heat release based on CDG calculation when varying the water vapour molar fraction. Results are presented as absolute variation (a.) and relative deviation (b.).

6.3.6. Combustion reaction model and expansion factor

Modelling the combustion as a one step reaction is necessary to estimate the expansion factor, α, of OC calorimetry. Information about the composition has to be known. The expression of the expansion factor is given by,

$$\alpha = 1 + X_{O_2}^0(\beta - 1) \quad (33)$$

With $$\beta = \frac{\sum \nu_{products}}{\nu_{O_2}} \quad (34)$$

Janssens defines a [1 – 2] range of operation for β values [18]. $\beta = 1$ corresponds to the complete combustion of pure carbon in dry air while $\beta = 2$ describes the complete combustion of H_2. This coincides with a [1 – 1.21] range for α under the condition that combustion occurs under air atmosphere. He recommends an average value for α= 1.105 (corresponding to methane) when the material composition is unknown and a combustion reaction cannot be modelled. One considers the latter range to be restrictive to certain types of materials. For instance, after having defined a modelling based on a one step reaction describing the combustion of the 50% KNO_3 ternary powder mixture, a O_2 depletion factor, ϕ = 1.39 was found which is beyond the range specified by Janssens. Materials embedding an oxidizer in their composition decreases the amount of O_2 required in the reacting atmosphere to reach stoichiometric conditions. As a consequence, β increases and so does α. Furthermore, if experiments are carried under an enriched O_2 atmosphere, $X_{O_2}^0$ is enhanced and α rises. Based on these statements, one decided to extend the range of α values to [1 – 5] in order to account for energetic materials. Nevertheless, this range is conservative and one assumes that most of the materials lie in the range [1 – 2].

Sensitivity analysis of the OC equation considering the expansion factor α as sensitive parameters has been conducted. One focus on divergence introduced in the HRR peak and the total energy release as absolute results and relative deviation from the given reference (i.e. HRR estimation obtained using only experimental data). Results obtained are presented on Figure 6.26. The variation induced on the OC equation can be modelled by a 2nd order polynomial. The divergence increases with the expansion factor. One notices that the level of variation of the HRR peak and the total energy is respectively less than 2 kW and less than 30 kJ over the [1 – 5] range. They correspond to relative deviations lower than 20 % for the HRR

peak and lower than 15 % for the total energy. Over the [1 – 2] range of α values, the relative deviation induced by varying the expansion factor is about 5 % for the HRR peak and 4 % for the total energy release. Divergence on the HRR remains low; this tends to confirm the relevance of using an average α. Nevertheless, one needs to reconsider the experimental configuration. Data used to carry out the sensitivity analysis originate from the combustion of 50 % KNO_3 ternary powder. The heat of combustion of such compound has been estimated to 6.01 $kJ.g^{-1}$ which is relatively low. Consequently, given the mass of material encountering combustion, the HRR magnitude is also expected to be low. Brohez noticed that the uncertainty associated with the HRR estimation through OC becomes strongly coupled with the expansion factor α when the HRR attains high levels. A model has been developed allowing the variation of the species molar fractions (N_2, O2, H_2O, CO_2, CO and THC) and accounting for species conservation. Following a given chemistry, it allows to predict the HRR for different combustion gases concentrations. After defining high emissions of CO_2 and H_2O, the OC equation was used to estimate the HRR. α was varied over the range [1 – 5] to study the sensibility of the calculation for high HRR. Results are illustrated on Figure 6.27. Deviation on the HRR peak rises up to 70% while the one related to the total energy reaches a maximum of almost 58%. When considering the [1 – 2] α range, divergence related to the HRR peak rises up to 35% while the one associated with the total energy tends to about 25%. Results confirm Brohez statement. The potential contribution of the expansion factor to errors propagating in the HRR calculation increases with the magnitude of energy release. For low HRR, the use of an average value for α appears appropriate. However, for high HRR (i.e. HRR of several dozens of kW), the use of an inappropriate α values can tend to significantly alter the correctness of the HRR estimation, even over the [1 – 2] range. The latter result suggests that, for high HRR, the applicability of OC equation would require knowledge of the chemistry in order to be able to estimate the reaction expansion factor.

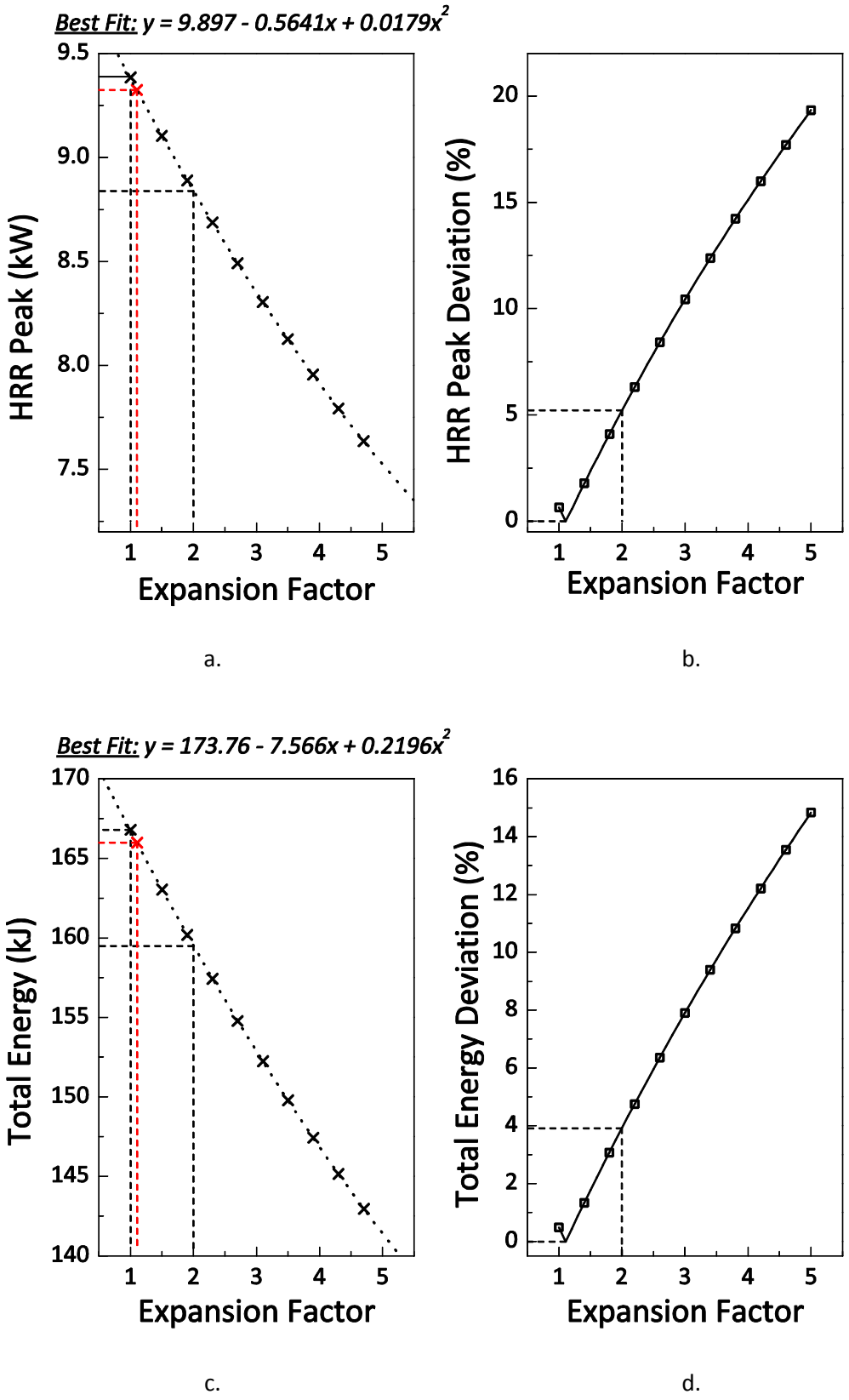

Figure 6.26. Sensitivity analysis of the peak HRR and total energy release based on OC calculation when varying the expansion factor α. Results are presented as absolute variation (a. and b.) and relative deviation (c. and d.).

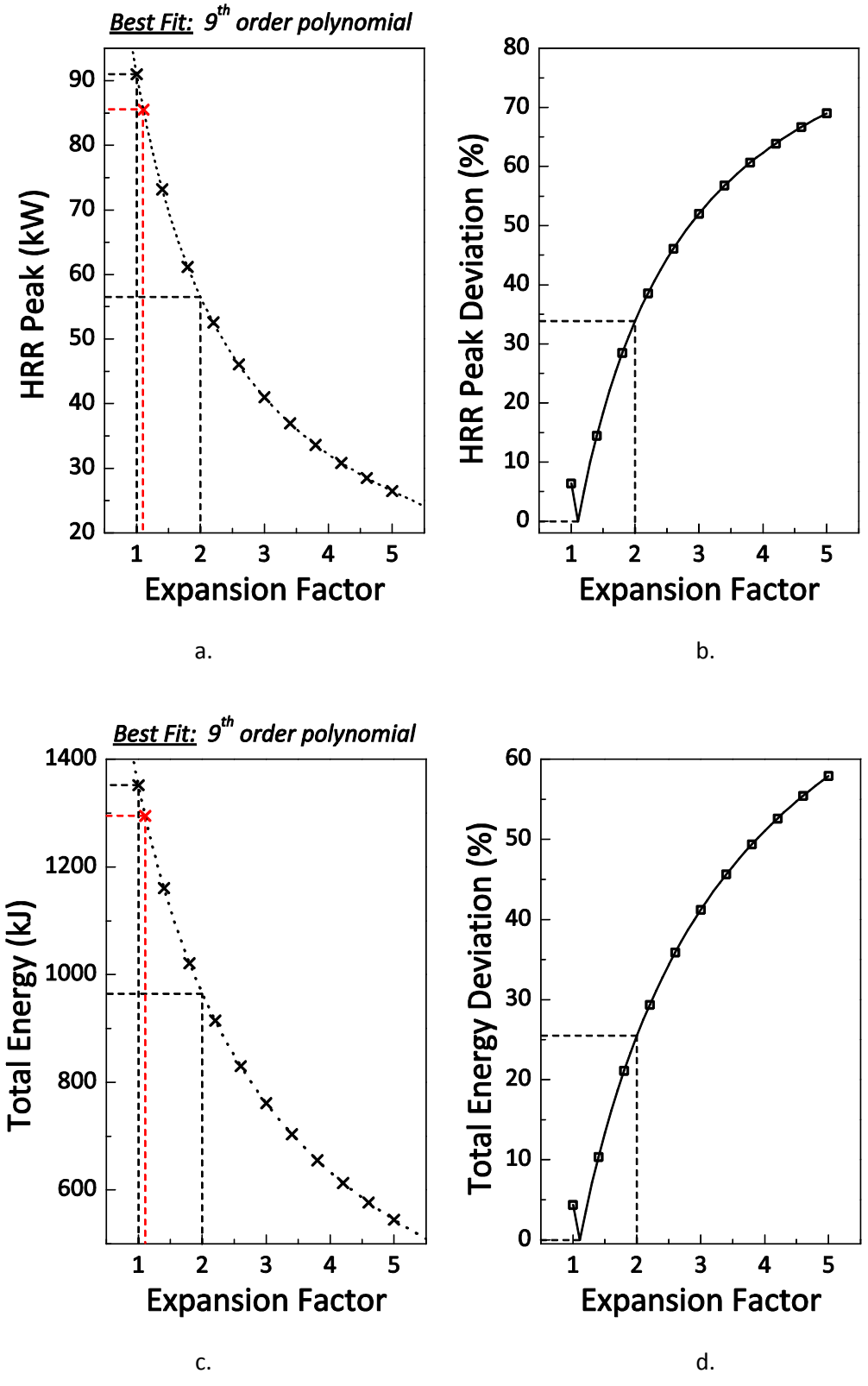

Figure 6.27. Sensitivity analysis of the peak HRR and total energy release based on OC calculation for high HRR when varying the expansion factor α. Results are presented as absolute variation (a. and b.) and relative deviation (c. and d.).

6.4. Concluding Remarks

A summary of the results from the different sensitivity analyses is indicated on Table 6.7.

Table 6.7. Sensitivity analysis results summary.

Method	Sensitive Parameter	Considered variation	Resulting HRR deviation
OC	E_{O_2} (kJ.g^{-1} O_2)	$\pm$1 kJ.g^{-1} O_2	$\sim$ 8 %
CDG	E_{CO_2} (kJ.g^{-1} CO_2)	$\pm$1 kJ.g^{-1} CO_2	$\sim$ 7.5 %
OC	$X_{O_2}^A$ (%)	$\pm$0.1%	$\sim$ 10 %
CDG	$X_{CO_2}^A$ (%)	$\pm$0.1%	$\sim$ 6 %
OC CDG	$\dot{V}_e$ (Nm^3.h^{-1})	$\pm$10% from prescribed $\dot{V}_e$	10 %
OC	N_2 conservation (%$_{mass}$ $N_{2\ [incoming\ air]}$)	$\frac{\dot{m}_{N_2\ [reaction\ product]}}{\dot{m}_{N_2}^0} = 0.2$	OC: – *Low HRR:* $\sim$ 200 % – *High HRR*: $< 3\%$
CDG			CDG: – *Low HRR:* $\sim$ 13 % – *High HRR:* $< 1\%$
OC CDG	X_{H_2O} (%)	$\pm$1%	$< 1\%$
OC	α	[1 – 2]	- $\phi \xrightarrow[Low\ HRR]{} 0$: $\sim$ 5 % - $\phi \xrightarrow[High\ HRR]{} 1$: $\sim$ 25 %

Conclusions are mainly similar to the ones obtained by Enright and Fleischmann [1], Brohez [2] and Axelsson *et al.* [3]. Considering the experimental conditions and the sample material, the HRR magnitude does not exceed the order of a dozen of kW. In this configuration, major sensitive parameters are the energy coefficients, the O_2 (OC) and CO_2 (CDG) molar fraction measurements and the exhaust volume flow rate. Nevertheless, certain situations are susceptible to significantly enhance the sensitivity of the calorimetric equations given variations of other parameters. Brohez highlighted that α was an important contributor to the propagation of errors in HRR calculations for high O_2 depletion. The sensitivity analysis carried in the present study stressed an identical outcome. Another fundamental assumption used for HRR estimation trough OC and CDG calorimetry is based on the conservation of N_2. One underlined that for low HRR, in the case where important quantities of N_2 are produced during the combustion reaction, the error on the calculation by non accounting for this N_2 generation can be significant. Nevertheless, large quantities of N_2 would have to be released and this production could be, if not identified, at least detected by a mass balance of the combustion products that would feature an important discrepancy when compared to the mass loss and O_2 consumed.

The sensitivity analysis allows defining suggestions for an appropriate use of OC and CDG methodologies. If the product is unknown, a comparison of OC and CDG calculations based on usual assumptions brings an insight of the relevance of using Huggett and Tewarson constants for the sample material. If the chemistry is known to be complex, constants are likely to be inappropriate. Furthermore, they can introduce large discrepancy form reality in the HRR estimation.

Cone calorimeters are rather designed for relatively long and steady state burning, although they have shown ability to describe transient behaviours. Nevertheless, in the case of fast combustion reactions (few dozens of seconds) with high amplitudes of gases emissions, the signal obtained from the measuring system might be distorted due to the too fast kinetics compared to the time constant of the instrumentation. The present study has underlined that large divergence can emerge between the actual combustion species concentrations and the measured ones. In case of fast reactions, the relevance of the concentrations measured has to be questioned using a mass balance but the latter assumes that the major gases emitted are identified and measured. Corrections can be applies to the molar fractions signal but it has to

be stressed that the method has to be modified according to the operating state of the analysing line (efficiency of the drierite and other filters) and the level of emissions.

The exhaust volume flow rate is measured using a Pitot tube. The design of the calorimeters has been developed such a way that the flow reaching the Pitot tube is well mixed and not too turbulent. However, it needs to be well calibrated because every percent of error in the volume flow is directly transferred to the estimation of the HRR.

The conservation of N_2 is an important hypothesis of the calculation as it allows the evaluation of the mass flow rate of incoming air. For small scale experiments, a production of N_2 from the burning material would not affect the accuracy of the results. Nevertheless for larger types of experiments where the amount of material becomes more important or in the case of modelling, the non-consideration of N_2 production allows the potential propagation of large errors in the OC and CDG calculations, especially in the OC one, more sensitive to this parameter. However, for large fire (i.e. high HRR), the divergence introduced by breaching the N_2 conservation assumptions becomes small enough to be neglected.

Similarly to the conservation of N_2 assumption, the hypothesis of an average expansion factor α is restricted by the type of material used. Taking energetic materials as an example, their reduced consumption of O_2 from the supporting atmosphere increases the value of α higher than the usual defined range. For high HRR, the error introduced by using the average value of α can become significant. To estimate α, the burning material needs to be known but one also needs to model the combustion reaction. Divergences in the HRR originating from α are related to the O_2 consumption. In order to assess the possibility of the material to contain an oxidizer or to embed important quantities of O, a mass balance of the O elements contained in CO_2, H_2O and CO produced from the combustion and the O_2 consumed should be performed.

6.5. References

[1] Enright, P. A., Fleischmann, C., M., Uncertainty of Heat Release Rate Calculation of the ISO5660-1 Calorimeter Standard Test Method, Fire Technology, 35 (2), pp. 153 – 169 (1999);

[2] Brohez, S., Uncertainty analysis of heat release rate measurement from oxygen consumption calorimetry, Fire and Materials, 29, pp. 383 – 394 (2005);

[3] Axelsson, J., Andersson, P., Lönnermark, A., Van Hees, P., Wetterlund, I., Uncertainties in measuring heat and smoke release rates in the room/corner test and the SBI, SP Swedish National Testing and Research Institute, NT technical report, 477, NORDTEST Project No. 1480-00, SP Report 2001:04;

[4] Freeman, E., S., The Kinetics of Thermal Decomposition of Potassium Nitrate nad of the Reaction between Potassium Nitrite and Oxygen, Journal of the American Chemical Society, 79, pp. 838 – 842 (1957);

[5] Huggett, C. Estimation of Rate of Heat Release by means of Oxygen Consumption Calorimetry, Fire and Materials, 4 (2), pp. 61 – 65 (1980);

[6] Tewarson, A., Generation of Heat and Chemical Compounds in Fires, in: SFPE Handbook of Fire Protection Engineering, 3rd Edition, Section 3, Chapter 4, The National Fire Protection Association Press, 2002, pp. 3-82 – 3-161;

[7] Messerschmidt, B., Van Hees, P., Influence of Delay Times and Response Times on Heat Release Measurements, Fire and Materials, 24, pp. 121 – 130 (2000);

[8] Brunner, J., X., Westenskow, D., R., How the Rise Time of Carbon Dioxide Analysers Influences the Accuracy of Carbon Dioxide Measurements, British Journal of Anaesthesia, 61, pp. 628 – 638 (1988);

[9] Agilent, Spectrum and Signal Analyzer Measurements and Noise, Application Note 1303, Agilent Technologies, 2009;

[10] Mittermayer, C., Steininger, A., On the Determination of Dynamic Erros for Rise Time Measurement with an Oscilloscope, IEEE Transactions on Instrumentation and Measurement, 48 (6), pp. 1103 – 1107 (1999);

[11] Graham, B., L., Buchanan, P., R., Withy, S., J., Harris, E., A., Data Acquisition from a Multiplex, Quadrupole Mass Spectrometer, Clinical Physics and Physiological Measurement, 6 (1), pp. 17 – 25 (1985);

[12] Point, R., Petit, J., L., Gravelle, P., C., Reconstruction of Thermokinetics from Calorimetric Data by means of Numerical Inverse Filters, Journal of Thermal Analysis, 17, pp. 383 – 393 (1979);

[13] Lyon, R., E., Farris, R., J., Analysis of Heat Flux Calorimeter Signals, Thermochimica Acta, 161, pp. 287 – 296 (1990);

[14] Lyon, R., E., Abramowitz, A., Effect of Instrument Response Time on Heat Release Rate Measurements, Fire and Materials, 19, pp. 11 – 17 (1995);

[15] Spiegel, M., R., Theory and Problems of Laplace Transforms, Schaum's Outline Series in Mathematics, McGraw Hill Publishing Company, New York, 1965;

[16] Staggs, J., E., J., Savitzky-Golay Smoothing and Numerical Differentiation of Cone Calorimeter Mass Data, Fire Safety Journal, 40, pp. 493 – 505 (2005);

[17] ASTM E2058-03, "Standard Test Method for Measurement of Synthetic Polymer Material Flammability Using a Fire Propagation Apparatus", ASTM International, West Conshohocken, 2003;

[18] Janssens, M., Parker, W., J., Oxygen Consumption Calorimetry, in: Heat Release in Fires, Chapter 3, Editors: Babrauskas, V., and Grayson, S., J., Elsevier Applied Science, New York, 1992, pp., 31 – 59;

[19] Brohez, S., Comments to the Paper Uncertainty of Heat Release Rate Calculation of the IS05660-1 Cone Calorimeter Standard Test Method, Fire Technology, 45, pp. 381 – 384 (2009);

7. Heat Release Rate Estimation for an Energetic Material

7.1. Introduction

The purpose of this chapter is to assess the possibility to estimate the HRR of an energetic material using OC and CDG principles. A part of the O_2 used for oxidizing the volatiles resulting from the fuels decomposition originates from the material. This lowers the demand in O_2 from the supporting atmosphere to achieve stoichiometric conditions. Consequently, one can wonder about the suitability of the OC method based on the measurement of O_2 depletion. Furthermore, these materials are known to be characterized by complex reaction chemistries. The relevance of using Huggett and Tewarson energy constants has to be investigated for such configurations. Another noticeable characteristic highlighted in the first part of the present work is the fast kinetics that often describes the combustion behaviour of energetic materials. Short transient phenomena are encountered.

In a first time, one analyses the efficiency of the measuring instrumentation to retrace the actual dynamics of the combustion reaction. If necessary, the application of a signal correction is performed. The validity of the concentration results obtained has to be considered before using these data to evaluate the HRR.

Subsequently, one applies the OC and CDG equations using the usual assumptions defined by Janssens and Tewarson [1] [2]. Beside the divergence between the two results, another comparison criterion is introduced by calculating the HRR with a mass loss approach. If the HRR derived from the three different techniques converge, one can conclude on the relevance of the assumptions concerning the sample material. However, if important discrepancies arise, information about the material chemistry are then necessary in order to reach acceptable results. One of the main traits describing the studied ternary powders holds in the decomposition of the oxidizer and the release of O_2. The capacity to correctly represent this stage is essential to understand the combustion behaviour of the sample material. The rate of diffusion of O_2 inside the combustible volatiles influences the combustion regime. An approach is developed based on the description of an actual overall reaction including the oxidizer

decomposition. If appropriate, this method should allow the estimation of critical parameters such as the energy coefficients. Consequently, one believes that the HRR can be estimated. Error bars will be calculated to evaluate the order of confidence that can be associated with the different approaches.

Finally, having stressed the ability of energetic materials to burn even under N_2 atmosphere, an attempt will be conducted to approximate the HRR of such a compound when burning under inert atmosphere.

7.2. Experimental Setup

7.2.1. Sample material

The sample material used is the previously presented ternary powder based on a lactose, starch and potassium nitrate mixture. The study focuses on the composition with the highest concentration of oxidizer: 50 % KNO_3 / 25 % starch / 25 % lactose, in mass. Each of the experiments analysed consisted in the combustion of 50 g of the ternary powder randomly distributed on a sample holder.

7.2.2. Experimental Apparatus

The calorimeter used to carry out the experimental analysis is the FM-Global FPA presented previously and whose equipment was detailed in Appendix C. A scheme of the apparatus is recalled on Figure 7.1. Data from paramagnetic O_2, infrared CO/CO2 and FID THC analysers are taken into account for the HRR study. The sample holder was located on a load cell providing mass loss data during the reaction. In order to control the reacting atmosphere, the sample material was restricted by a quartz tube. The incoming flow of air inside the tube was set at 200 $l.min^{-1}$ ($\dot{m}_a \gg \dot{m}_{fuel}$). The exhaust mass flow rate was regulated to remain around 160 $Nm^3.h^{-1}$.

Using the FPA to characterise an energetic material is an original attempt. Calorimeters are not primarily designed to examine the combustion behaviour of fast kinetics compounds. Usually, tests are conducted under well ventilated conditions where a configuration close to stoichiometry is attained. If steady states are not reached, transient phenomena evolve slowly

enough for the measuring system to capture the gases emissions dynamics. Energetic materials behaviour might approach very closely or even stand beyond the measuring boundaries of the instrumentation implemented in calorimeters. Nevertheless, given the relative "ease" associated with the application of calorimetric methods, it appears very tempting to assess the capacity of calorimeters such as the FPA combined with the use of species evolution approaches such as OC and CDG to estimate the HRR of energetic materials under conditions where the latter do not evolve towards deflagration or detonations regimes. Being able to predict the energy susceptible to be released from a compound which could accidentally encounter a combustion transition is essential in terms of risks management or for defining regulations associated with these types of materials.

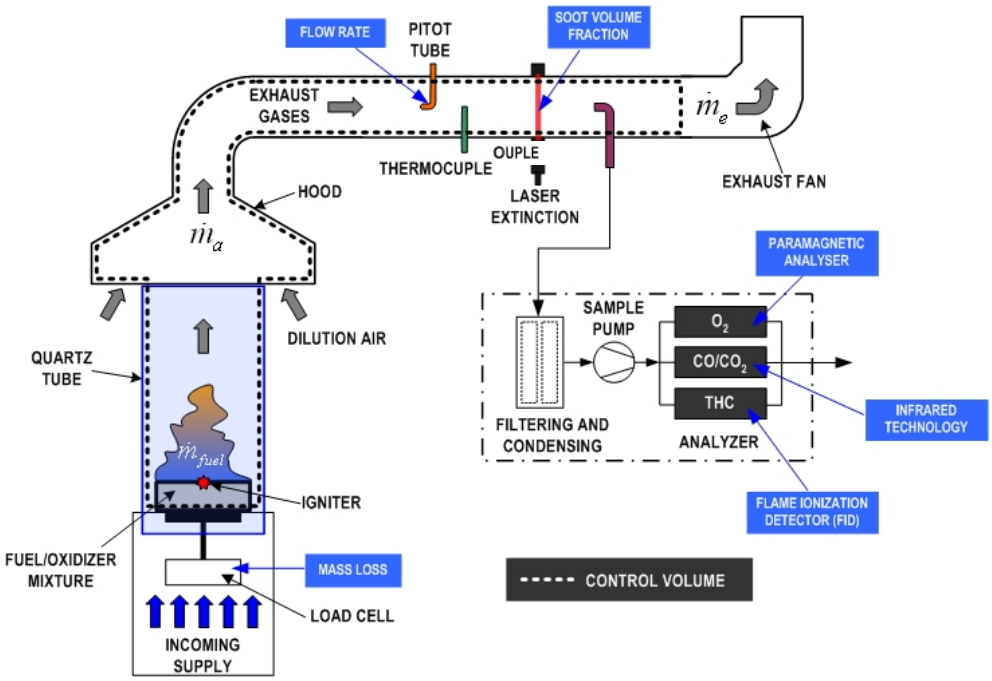

Figure 7.1. Schematic of the FM-Global Fire Propagation Apparatus [4].

7.3. Reaction dynamics

Prior applying OC and CDG equations to the set of data obtained from the combustion of 50 % KNO_3 ternary mixture, one needs to determine if the measuring system is able to capture the evolution of the material kinetics encountering combustion. Recalling previous results, the average reaction duration of a combustion reaction involving 50% KNO_3 ternary mixture is of

the order of 30 seconds. Regarding the response times of the different analysers (cf. Chapter 5, section 5.3.2.2, Tables 3 and 4), the reaction taking place are of an identical order. The correction presented in the previous Chapter (c.f. Chapter 5, section 5.3.2.5) was applied. Nevertheless, correctness of the procedure has to be verified. The simplest controlling method is to conduct a mass balance between the production of combustion gases, the O_2 consumption and the material mass loss. As mass conservation applies, the appropriateness of the correction model is verified if,

$$\left(\sum_{product} m_{product}\right) - m_{O_2[consumption]} = m_{loss\ material} \quad (1)$$

Where $\left(\sum_{product} m_{product}\right)$ represent the total mass of combustion products (g) measured through the analysers when the reaction occurs; $m_{O_2[consumption]}$ is the total O_2 consumption (g) that occurred during the reaction duration and $m_{loss\ material}$ is the mass loss (g) of the compound.

Assuming that CO_2, H_2O CO, THC and N_2 are the major gases produced, one calculates the total production associated with each aforementioned species over the temporal interval when the reaction took place. Similarly, the total O_2 consumption was also estimated as well as the production of soot and particles. Soot was measured using laser optical extinction diagnostics [5]. Estimation of the mass of particles agglomerated on the quartz tube has also been performed. Results are gathered in Table 7.1. One notices that equation (1) is well approximated. Mass conservation is verified and one can assume that the correction of the species concentration signal is applied correctly.

Table 7.1. Mass balance between the production of combustion gases, the O_2 consumption and the material mass loss for the combustion of 50g of 50% KNO_3 ternary mixture under air atmosphere (Species productions based a single experiment).

Species total production *Measurement technique*	CO_2 *Infrared Sensor*	26.62 g
	CO *Infrared sensor*	1.17 g
	THC *FID sensor*	0.14 g
	H_2O *IR sensor , FTIR*	16.92 g
	N_2 *Conservation principle*	~ 3 g
	Soot & residual particles on tube *Laser and trap*	~ 2 g
Species consumption	O_2 *Paramagnetic sensor*	14.25 g
$\left(\sum_{product} m_{product}\right) - m_{O_2[consumption]}$		35.59 g
$m_{loss\ material}$		36.34 g
Standard Deviation		*~2 %*

7.4. Application of OC and CDG using usual assumptions

One has established that the molar fraction measurements gained from the different analysers provide relevant data that can be used to estimate the HRR of the burning sample by means of OC and CDG methods. However, prior to start the calculation, one needs to assess the correctness in the present configuration of the different hypotheses that the procedure holds. In a first time, one postulates that usual assumptions of OC and CDG apply in case of reactions involving the sample material:

1. One assumes that Huggett and Tewarson energy constants and their associated uncertainties (c.f. Chapter 3, section 3.2.3.2.1) are appropriate for the material considered;
2. Gases behaviour is supposed to follow the ideal gas law;
3. The considered gases are: O_2, N_2, H_2O, CO_2, CO and THC;
4. N_2 and other assimilated gases are supposed inert;
5. The average expansion factor $\alpha = 1.105$ is assumed relevant for the sample material and the experimental configuration;
6. Species molar fraction measurements correctly capture the evolution of the reaction dynamics;
7. The water vapour generated by the combustion reaction is not considered in the calculation: $X_{H_2O} = X^0_{H_2O}$.

Given the aforementioned hypotheses, estimation of the HRR through OC and CDG can be performed for the 50 g samples of 50% KNO_3 ternary mixtures under air atmosphere. Two comparison criteria will be considered:

1. Convergence or divergence between OC and CDG HRR curves will underline the degree of coherence in the results. Consequently, ratios of HRR peaks and total energies obtained through both methods represents a good indicator of the confidence that can be associated with the results in terms of accuracy;

2. HRR results obtained by means of a mass loss rate approach will be also indicated. The order of magnitude of the potential discrepancies between this calculation and the OC and CDG procedures constitutes another pertinent criterion to assess the correctness of the calculation.

Results are presented on Figure 7.2. Calculations accounting for the error range associated with Huggett and Tewarson energy constants have also been performed. The OC/CDG relative deviations associated with the HRR peak and total energy are indicated on Table 7.2. HRR estimated from a mass loss rate approach is also provided. The heat of combustion of the 50% KNO_3 ternary mixture has been measured by means of a bomb calorimeter test (in air atmosphere),

$$\Delta H_{c\,[50\%\,KNO_3]} = 6.01\ kJ.g^{-1} \quad (2)$$

According to the thermal and chemical analysis of the 50% KNO_3 ternary mixture [see Chapter 2], it has been stressed that two types of combustion were occurring: a flaming combustion of the volatiles as well as combustion of the char. The energy associated with these two phenomena is likely to be different. Furthermore, when modifying the nature of the reacting atmosphere (i.e. lowering the O_2 concentration up to an inert atmosphere), one observes a transition in the flaming regime from a large diffusion flame to short premixed ones. The latter procedure emphasized the occurrence of chemical reactions in gaseous and solid phases. Similarly to previous, one assumes that the variations of energy associated with the reactions in the gaseous phase are different to the ones in the solid phase. Consequently, the heat of combustion measured, $\Delta H_{c\,[50\%\,KNO_3]}$, is a balance of the various phenomena initiated, given the proportion of each of them to the overall process. According to the combustion configuration, one or several regimes are susceptible to be favoured, affecting $\Delta H_{c\,[50\%\,KNO_3]}$. Nevertheless, $\Delta H_{c\,[50\%\,KNO_3]}$ represents a relevant indicator of the magnitude of energy release for experimental conditions close to the ones encountered during the bomb calorimeter measurement. For this reasons, HRR obtained through a mass loss rate approach is taken as reference value.

Large discrepancies arise from Figure 7.2. Considering the HRR peaks, OC and CDG present a divergence of 93% (and 88% of relative deviation between the total energy values). HRR from

CDG based on Tewarson constants rises up to 15.2 kW while HRR from OC with Huggett's energy value exhibits a maximum at 7.9 kW. Including the error associated with the energy constant values does not allow assessing a confident order of magnitude of the HRR. Estimation through a mass loss approach based on $\Delta H_{c\,[50\%\,KNO_3]}$ corrected for the CO production (this defining an effective heat of combustion) is also conducted. The energy coefficient $\Delta H_{eff\,[50\%\,KNO_3]}$ is given by [Chapter 3, section 3.2.1],

$$\Delta H_{eff\,[50\%\,KNO_3]} = \frac{\Delta H_{c\,[50\%\,KNO_3]} + \xi_{CO/CO_2}\ \Delta H_{ic\,[50\%\,KNO_3]}}{1 + \xi_{CO/CO_2}} \tag{3}$$

Despite that $\Delta H_{eff\,[50\%\,KNO_3]}$ might not exactly describe the energy evolution of the material encountering combustion, if no major chemical changes exist between the bomb calorimeter test and the actual reaction, one assumes that $\Delta H_{eff\,[50\%\,KNO_3]}$ is a relevant value to characterise the burning process. One believes that the HRR obtained from a mass loss rate approach constitutes an appropriate indicator of the degree of correctness of OC and CDG results and, as a consequence, is considered as reference. From Figure 7.2, one notices that $\dot{q}_{mlr}$ rises up to 9.4 kW. OC and CDG relative deviations from $\dot{q}_{mlr}$ are indicated on Table 7.3. The CDG result largely overestimates $\dot{q}_{mlr}$ while the OC result underestimates $\dot{q}_{mlr}$ by less than 20 %. The latter divergence can find an explanation from the composition of the sample material. The presence of KNO_3 as an oxidizer lowers the demand in O_2 from air to reach stoichiometric conditions. Considering Huggett energy constant, it is unlikely that the same constant was able to describe the energy associated with a molecule independently of its content of O. As an example, given two imaginary molecules, $C_xH_yO_z$ and $C_xH_yO_{4z}$. The second requires less O_2 from the air to encounter complete combustion. Consequently, one guesses that Huggett energy constant cannot be appropriate for both molecules. For an identical O_2 consumption, the second compound will be closer to stoichiometric conditions, given its internal O_2 "supply", than the first one and is then expected to release a higher level of energy. On the contrary, the use of Huggett constant would show identical energy release. The energy associated with the second molecule is underestimated. By considering the role of the oxidizer, one comprehends that for a same amount of energy released, less O_2 is consumed from the reacting atmosphere which increases the value of the energy generated by unit mass of O_2 beyond Huggett's one. Regarding the CDG, the overestimation compared to $\dot{q}_{mlr}$ can also originate from the oxidizer. The decomposition of the latter needs energy and

this reduces the heat of combustion. Furthermore, lactose and starch are relatively heavy molecules with an important content in C. According to the expression introduced previously for estimating E_{CO_2} (c.f. Chapter 3, section 3.2.3.1, expression (24)), one expects the value to be less than the one defined by Tewarson.

The acknowledged energy constants appear to be inappropriate when used to estimate the HRR from the combustion of the 50% KNO_3 ternary mixture. Different coefficients have to be defined. Furthermore, the validity of the other calculation hypotheses in the case of the combustion of the present sample material need also to be investigated in order to be sure to trace every source of discrepancy.

Table 7.2. HRR peak and total energy relative deviations between OC and CDG methods using, respectively, Huggett and Tewarson energy constants (combustion of 50% KNO_3 ternary mixture under air).

OC/CDG Relative Deviation (%)	
HRR Peak	93
Total Energy	88

Table 7.3. HRR peak and total energy relative deviations of OC and CDG results using Huggett and Tewarson energy constants (combustion of 50% KNO_3 ternary mixture under air) from a reckoned HRR reference.

		Relative Deviation (%)
OC (with Huggett energy constant)	HRR Peak	16
	Total Energy	17
CDG (with Tewarson energy constants)	HRR Peak	62
	Total Energy	56

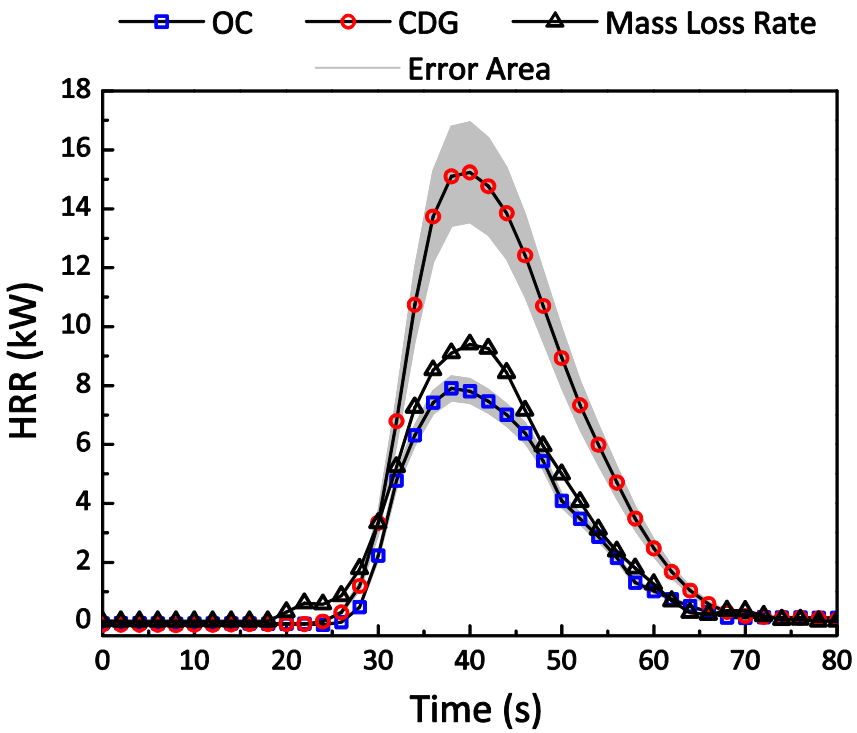

Figure 7.2. Comparison of HRR results from the combustion of 50 g of 50% KNO_3 ternary mixture under air atmosphere: methods used were the mass loss rate approach as well as OC and CDG with calculations based, respectively, on Huggett [3] and Tewarson [2] energy constants.

7.5. Application of OC and CDG assuming a material chemistry

Important discrepancies are observed on the HRR calculations through OC and CDG when Huggett and Tewarson energy constants are used. They appear to be unsuitable for the 50% KNO_3 ternary mixture. The assumption for explaining the divergences holds on the presence of the oxidizer in the material composition. Relevant energy coefficients need to be assessed. To achieve this aim, the decomposition chemistry of the material has to be considered, in particular the decomposition reaction associated with the oxidizer KNO_3.

7.5.1. Determination of suitable energy coefficients

A procedure has been developed to evaluate appropriate energy coefficients for OC and CDG methods in the event of a combustion involving the 50% KNO_3 ternary mixture. First, the thermal decomposition of the oxidizer is recalled. The energy associated with the latter

reaction is estimated. In a second time, a fictitious molecule describing an assumed single compound that takes part to the combustion and accounting for the oxidizer decomposition is defined. Energy coefficients are finally determined from the fictitious molecule and the heat of combustion related to the material.

7.5.1.1. KNO_3 thermal decomposition

The thermal decomposition of KNO_3 has already been investigated during the thermal and chemical analysis of the ternary powders (c.f. Chapter 2, section 2.3.1). The description developed by Freeman [6] is widely acknowledged. Consequently, one assumes that KNO_3 follows his reaction schematic within the powder ternary mixture. According to the residue analysis, it is suggested that KNO_3 mainly decomposes primarily into K_2O, N_2 and O_2 (the presence of K_2CO_3 in the residue has been interpreted as a reaction between K_2O and CO_2 formed in the solid phase). One suggests to model the decomposition as a single step reaction as follow,

$$2\,KNO_3 \longrightarrow K_2O + N_2 + \frac{5}{2}O_2 \qquad (4)$$

The energy associated with reaction (4) has been estimated based on heats of formation of the reactants and products [7] and was approximated by,

$$\Delta H_{KNO_3 \rightarrow K_2O} = 314 \pm 30 \text{ kJ.mol}^{-1} \ (\equiv 3.1 \pm 0.3 \text{ kJ.g}^{-1}) \qquad (5)$$

One notices that the reaction is endothermic. A part of the energy released from the oxidation of starch and lactose volatiles (exothermic reactions) is then used to generate O_2 from KNO_3 lowering the overall heat of reaction. This explains the low value of $\Delta H_{c\,[50\%\,KNO_3]}$.

7.5.1.2. Modelling of a fictitious molecule

Once the decomposition of the oxidizer has been assessed, one defines a fictitious molecule reflecting the burning compound. First, as the mass percentage of each component is known, one can express the mixture as a single molecule $C_xH_yO_zN_aK_a$ where x, y, z and a represent, respectively, the content in C, H, O, N and K according to the proportion (in mole percentage) of each component. One obtains the following molecule,

C	H	O	N	K
2.5	4.36	4.24	0.69	0.69

Considering the assumed KNO_3 decomposition, K_2O is produced but remains in the solid phase. One can define a fictitious mixture ,

$$C_{2.5}H_{4.36}O_{3.89}N_{0.69} + 0.345\ K_2O \tag{6}$$

A single step combustion reaction can then be modelled as,

$$(C_{2.5}H_{4.36}O_{3.89}N_{0.69} + 0.345\ K_2O) + 1.645\ O_2 \longrightarrow 2.5\ CO_2 + 2.18\ H_2O + 0.345\ (N_2 + K_2O) \tag{7}$$

The heat of combustion associated with this reaction is given by $\Delta H_{c\ [50\%\ KNO_3]}$. As mentioned previously, K_2O remains in the solid phase. An assumption is to account for K_2O as an inert compound and finally reduce the mixture to a fictitious molecule $C_{2.5}H_{4.36}O_{3.89}N_{0.69}$ associated with a heat of combustion defined as,

$$\Delta H_{C\ [fictitious\ molecule]} = \frac{\Delta H_{c\ [50\%\ KNO_3]}\ M_{[fictitious\ mixture]}}{M_{[fictitious\ molecule]}} \tag{8}$$

Combination of the fictitious molecule and its related heat of combustion are used to estimate the new energy coefficients suitable for the 50% KNO_3 ternary mixture.

7.5.1.3. Calculation of the energy coefficients

Based on the energy coefficients analysis developed in Chapter 4 (section 4.2, expressions (4), (5) and (7)), one formulates the expressions E_{O_2}, E_{CO_2} and E_{CO} relative to the 50% KNO_3 ternary mixture,

$$E_{O_2} = \frac{\Delta H_{C\ [fictitious\ molecule]}\ M_{[fictitious\ molecule]}}{1.645\ M_{O_2}} \tag{9}$$

$$E_{CO_2} = \frac{\Delta H_{C\ [fictitious\ molecule]}\ M_{[fictitious\ molecule]}}{2.5\ M_{CO_2}} \tag{10}$$

$$E_{CO} = E_{CO_2}\frac{M_{CO_2}}{M_{CO}} - \Delta H_{CO} \tag{11}$$

Values obtained are reported in Table 7.4. As expected, the newly evaluated E_{O_2} coefficient is higher than Huggett's value due to the action of the oxidizer. Similarly, one also notices that E_{CO_2} and E_{CO} are lower than Tewarson's energy constants. The mixture content in C atoms combined to a low heat of combustion explains this result.

Table 7.4. Energy coefficients associated with the OC and CDG methods and based on a fictitious molecule model of the 50% KNO_3 ternary mixture associated.

E_{O_2} (kJ.g^{-1} of O_2)	E_{CO_2} (kJ.g^{-1} of CO_2)	E_{CO} (kJ.g^{-1} of CO)
15.86	7.58	1.80

Energy coefficients supposed to be appropriate to the 50% KNO_3 ternary mixture have been calculated. Prior to conduct new HRR estimations based on OC and DG principles, one needs to verify that all the calculation assumptions are relevant.

7.5.2. Validity of the calculation assumptions

Analysis highlighted that two calculation assumptions remain to be assessed: the expansion factor value and the N_2 conservation hypothesis.

7.5.2.1. Expansion factor

HRR relative to the 50 % KNO_3 ternary mixture samples appear relatively low (~ 10kW). According to the conclusions of the previous sensitivity analysis (Chapter 5, section 5.3.6), the contribution of this variable to the uncertainty of the HRR evaluation is low (< 5 %). Nevertheless, as a fictitious molecule has been modelled, one can use its expression and the assumed combustion reaction (7) to estimate the expansion factor. An estimation of α gives,

$$\alpha \approx 1.39 \quad (12)$$

This value is higher than the average one defined by Janssens and Parker [1] and will be implemented in the OC and CDG equations relative to the 50 % KNO_3 ternary mixture.

7.5.2.2. N_2 conservation hypothesis

The decomposition of KNO_3 (chemical reaction (4)) highlights the generation of N_2. According to the sensitivity analysis carried out in the previous chapter, a large and non-considered production of N_2 is susceptible to introduce enough deviations in the HRR calculations to affect the correctness of the results if OC and CDG methods are used. Consequently, on needs to estimate the proportion of the N_2 production compared to the concentration of this molecule in the exhaust flow.

The maximum production of N_2 that can results from the decomposition of KNO_3 has been estimated with an order of magnitude of about 0.2 $g.s^{-1}$. In the same way, the flow rate of N_2 from the entrained air was evaluated to remain constantly beyond 41.6 $g.s^{-1}$ (exhaust flow rate: 160 $Nm^3.h^{-1}$). The ratio of these two measurements gives,

$$r_{N_2[\frac{production}{air}]} \approx 5.10^{-3} \quad (13)$$

The ratio is sufficiently low to avoid any influence from the N_2 production on the accuracy of the HRR estimations through OC and CDG procedures.

7.5.3. HRR Results

The applicability of the different calculations hypotheses necessary to provide relevant HRR results seems to be achieved. OC and CDG calculations are conducted on data obtained from the combustion of 50 g of a 50 % KNO_3 ternary mixture. The energy coefficients applied as well as the expansion factors are the one defined, respectively in sections 5.1.3 and 5.2.1 of the present chapter. The HRR curves are presented on Figure 7.3. The relative deviations between OC and CDG HRR peaks and total energies are indicated on Table 7.5. The relative deviations of OC and CDG results (HRR peak and total energy) compared to the reference HRR approximation (mass loss rate approach) are reported on Table 7.6.

It arises that the different HRR calculations converge. Relative deviations do not exceed 6 % on the different criteria of divergence analysed. Furthermore, OC and CDG give relatively similar results. One can be confident on the order of magnitude of the HRR measured. The technique based on the determination of a fictitious molecule developed from a simple model of the

material decomposition chemistry seems to be appropriate to correctly estimate the order of magnitude of the HRR by means of OC and CDG equations.

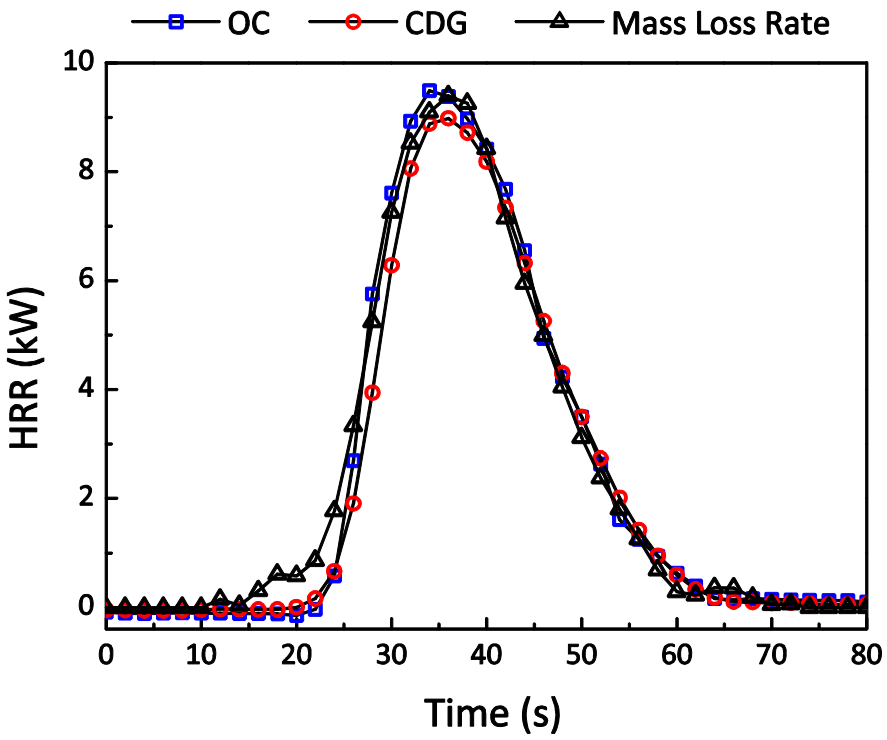

Figure 7.3. Comparison of HRR results from the combustion of 50 g of 50% KNO_3 ternary mixture under air atmosphere: methods used were the mass loss rate approach as well as OC and CDG with calculated energy coefficients assuming the material combustion chemistry.

Table 7.5. HRR peak and total energy relative deviations between OC and CDG methods using calculated energy coefficients (combustion of 50% KNO_3 ternary mixture under air).

OC/CDG Relative Deviation (%)	
HRR Peak	3
Total Energy	4

Table 7.6. HRR peak and total energy relative deviations of OC and CDG results (combustion of 50% KNO_3 ternary mixture under air) using calculated energy coefficients from a reckoned HRR reference.

		Relative Deviation (%)
OC (with Huggett energy constant)	HRR Peak	3
	Total Energy	1.7
CDG (with Tewarson energy constants)	HRR Peak	6
	Total Energy	6

The accuracy of the results is dependent on the pertinence of the heat of reaction used to assess the different energy coefficients. The convergence of the three approaches, OC, CDG and mass loss rate, tend to suggest the exactitude of the HRR obtained. Nevertheless, it appears fundamental to be able to assess the degree of confidence that can be associated with the results by defining error bars.

In order to estimate the low and high boundaries of the heat of combustion of starch and lactose, the Bond Additivity (BA) method was applied. One assumes the decomposition reaction (4) of the oxidizer KNO_3. The energy associated with is given by (5). An uncertainty range needs to be defined for this variable. The reaction is endothermic. The energy (5) is based on a configuration involving only KNO_3. In the ternary structure, KNO_3 is mixed with lactose and starch so the interaction between the molecules might vary the energy associated with the decomposition. One defines confident high and low bounds as ± 50 % of the energy value obtained in (5). Finally, given the molar percentage of each component in the mixture, considering the combustion reaction (7), the energy coefficients boundaries are given by,

$$E_{i\,[high\,(low)]} = \frac{\Delta H_{C\,[high\,(low)]} M_{[fictitious\,molecule]}}{\nu_i M_i} \qquad , i = O_2, CO_2 \qquad (14)$$

With

$$\Delta H_{C\,[high\,(low)]} = \sum_{fuel} \%_{fuel}\, \Delta H_{C\,[high\,(low)],fuel} + \%_{KNO_3}\, \Delta H_{KNO_3 \rightarrow K_2O\,[high\,(low)]} \qquad (15)$$

Determined error ranges for OC and CDG are indicated on Figure 7.4. Results allow the estimation of a level of confidence in the HRR estimations. According to the HRR calculated using newly assessed energy coefficients and the error bars associated with, one can specify a

maximum uncertainty of the order of 30 % respectively for OC and CDG. One believes that it is enough accuracy to provide a relevant insight of the magnitude of the fire taking place. However, one has to recall that information about the material chemistry was required to achieve the presented outcomes, the main one being the composition of the sample.

Enough knowledge about the chemistry of the material allows using OC and CDG methods for assessing correctly the HRR from a combustion reaction. To achieve accuracy, the composition of the material, the heat of combustion, and understanding of the chemical decomposition of the compound are necessary but potentially not always sufficient. Issues can be related to the appropriateness of the heats of combustion used. As mentioned previously, such parameters are usually measured from bomb calorimeter tests. The evolution of combustion chemistry of the material depends on the experimental setup. Several combustion behaviours (for instance, combustion of pyrolysis gases, combustion of char...) may overlap each other. Consequently the heat of combustion measured is a balance of the different phenomena taking place. As long as the combustion taking place in an apparatus such as the cone calorimeter or the FPA follow more or less the same combustion chemistry as the one encountered in the bomb calorimeter, using the measured heat of combustion is appropriate. Nevertheless, if the reacting configuration is such that chemical changes appear in the combustion behaviour of the material favouring one phenomenon over the other with a different chemistry than the one occurring during the bomb calorimeter tests, the relevance of using the measured heat of combustion becomes questionable. The solution would be to decouple the different combustion behaviours and to be able to assess the energetic contribution of each of them to the overall heat of reaction. This is out of the scope of the present work but should be considered as a next stage of research to explore. However, recalling that transitions in the flame regimes were observed when burning the 50 % KNO_3 ternary mixture under a critical O_2 concentration, one now investigates the degree of convergence of different HRR estimations methods (OC, CDG and mass loss rate principles) for combustion occurring under low O_2 and N_2 reacting atmospheres. Discrepancies in the results would highlight limitations of the calorimetric procedures. Furthermore, one of the sources of limitation could arise from the aforementioned point. One has observed that lowering the level of O_2 concentration in the reacting atmosphere below a critical value modifies the combustion behaviour. One needs to consider that these variations potentially affect the appropriateness of the measured heat of combustion.

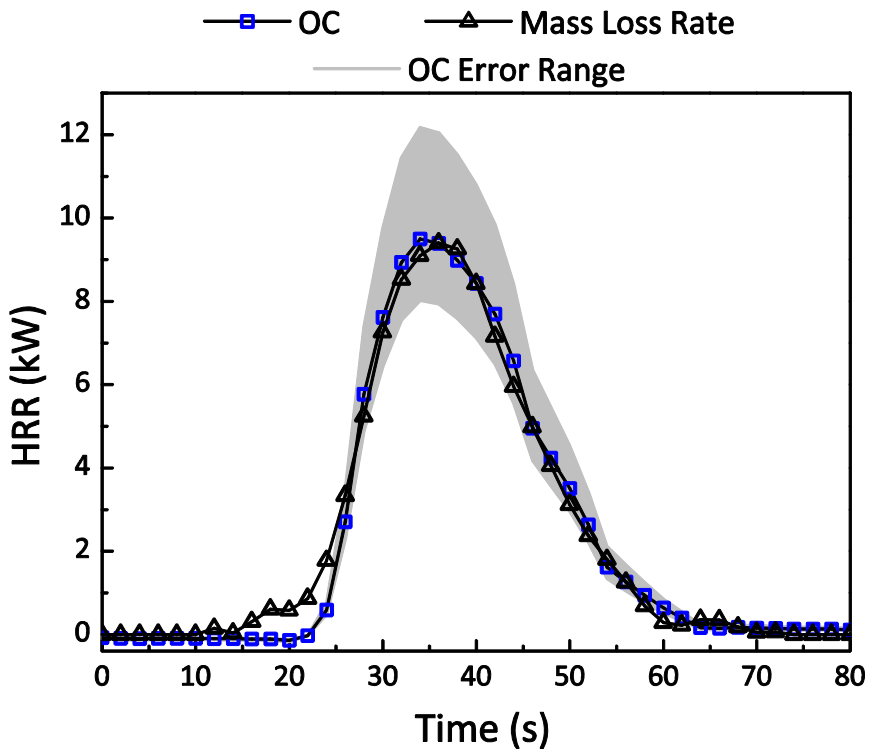

OC

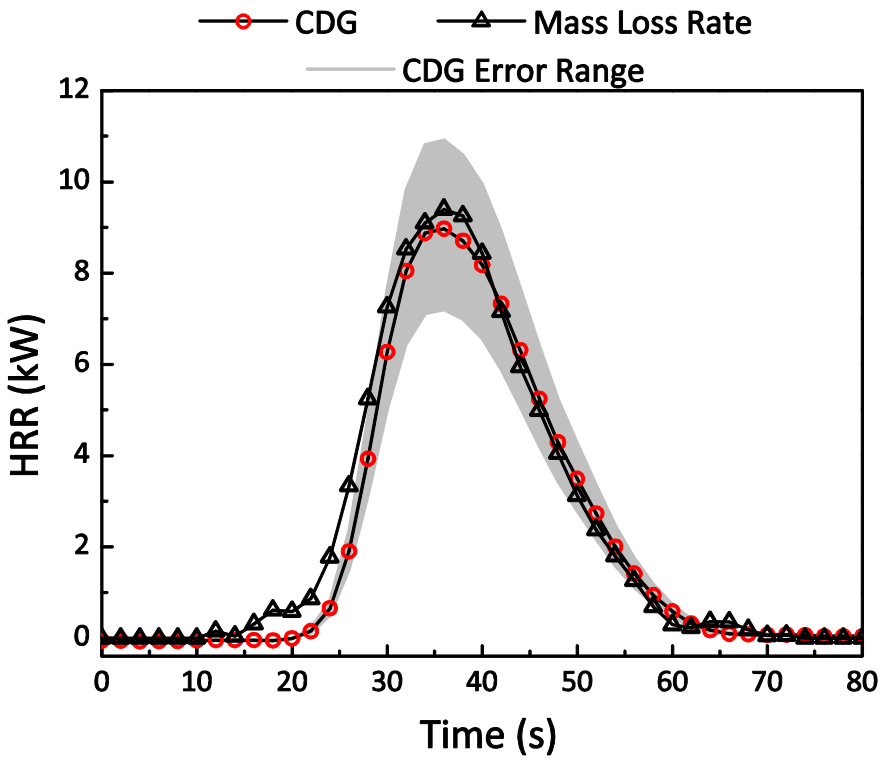

CDG

Figure 7.4. OC and CDG error ranges defined through a BA approach applied on the energy coefficients.

7.6. Application of calorimetric methodology for combustion under various atmospheres

Using the energy coefficients defined previously, HRR from the combustion of 50% KNO_3 ternary mixture under low O_2 concentration and inert atmospheres have been calculated using OC, CDG and the mass loss rate approaches. Results estimated from the data measured under 10 % O_2 and N_2 atmospheres are presented in the following.

7.6.1. Combustion test under 10 % O_2 atmosphere

Figure 7.5 illustrates the HRR results obtained from OC, CDG and mass loss rate calculations. The mass loss rate approach is combined with the heat of combustion $\Delta H_{c\,[50\%\,KNO_3]}$ (MLR Complete) and with an estimated heat of reaction including the CO formation (MLR Incomplete). For reasons that will be stressed later in the discussion, the HRR evaluation based on the OC method is not debated first.

The HRR estimation from the mass loss rate approach combined with $\Delta H_{c\,[50\%\,KNO_3]}$ rises up to 10 kW. The curve is relatively identical to the one obtained under air. It has already been noticed that the evolution of mass loss during the combustion reaction was independent of the composition of the reacting atmosphere. Nevertheless, considering Figure 7.6, the ratio of the CO and CO_2 molar fractions clearly stresses important generation of CO. The combustion is incomplete and one can expect the actual heat of reaction to be lower than $\Delta H_{c\,[50\%\,KNO_3]}$. The second curve derived from a mass loss approach, but involving a heat of reaction corrected for incomplete combustion, increases up to 7.4 kW. The correctness of this value relies on the appropriateness of $\Delta H_{c\,[50\%\,KNO_3]}$. to describe the actual energy generated by the combustion given the experimental configuration. Comparison with the CDG plot highlights discrepancies. Table 7.7 indicates the relative deviations related to the HRR peak and the total energy release between CDG and mass loss rate (including the incomplete combustion correction) results. The CDG underestimates the mass loss rate approach. Furthermore, the divergences encountered between the two methods are larger than when the reaction was carried out under air atmosphere. This tends to suggest that the heat of combustion used in the calculation does not characterise properly the reaction when conducted under low O_2 atmosphere.

Considering the OC curve, it has been previously underlined that under a critical O_2 concentration, the sample material was only relying on the oxidizer present in its composition to sustain the combustion. The critical O_2 concentration has been estimated around 18%. Consequently, experiments carried out under 10 % O_2 atmosphere should not exhibit O_2 depletion as no O_2 consumption occurs. However, it arises from Figure 7.5 that an O_2 depletion is measured. This result was obtained without correction of the O_2 and CO_2 molar fraction signals. Once the correction was applied, the OC calculation failed to predict the HRR as the O_2 depletion factor remained equal to zero. This example is presented to highlight the value of the signal correction for short duration combustion reactions with only transient regimes.

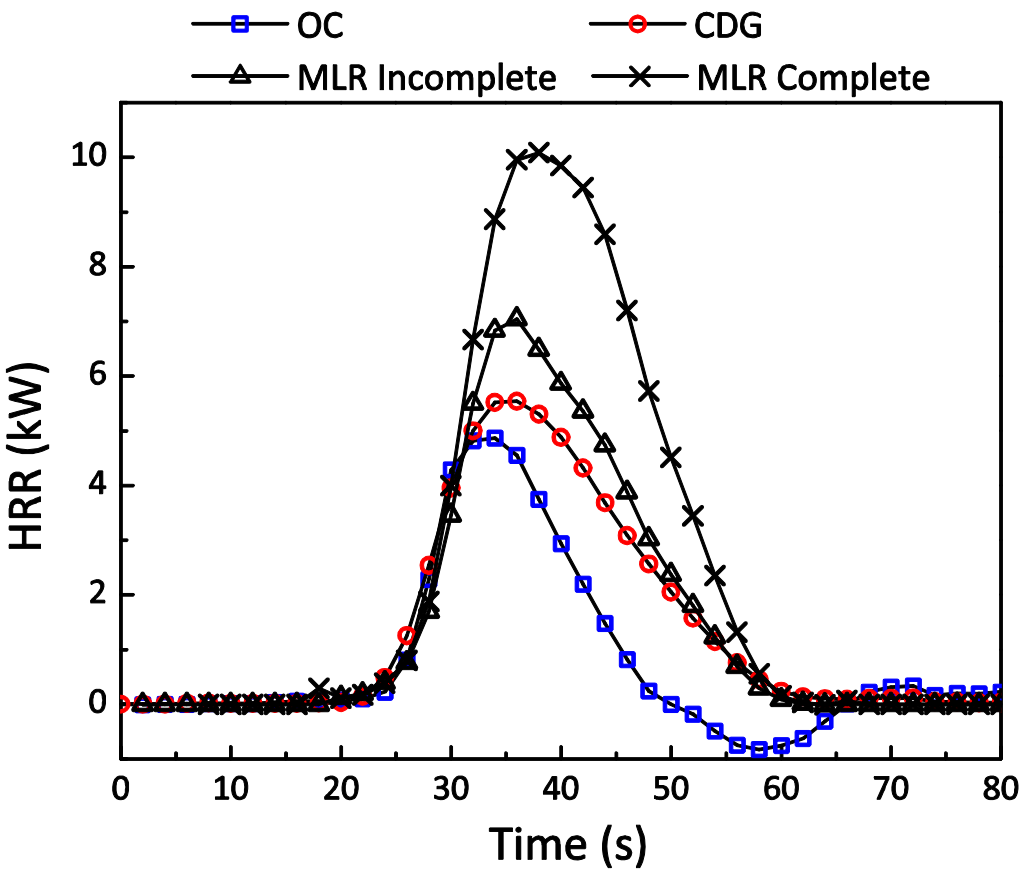

Figure 7.5. HRR results using OC, CDG and mass loss rate (complete and incomplete combustion assumptions) approaches from the combustion of 50 % KNO_3 ternary mixture under 10% O_2 atmosphere.

Table 7.7. HRR peak and total energy relative deviations between CDG and Mass loss rate (incomplete combustion correction) methods using calculated energy coefficients for the combustion of 50% KNO_3 ternary mixture under 10 % O_2 atmosphere.

	CDG/$MLR_{incomplete}$ Relative Deviation (%)
HRR Peak	21
Total Energy	12

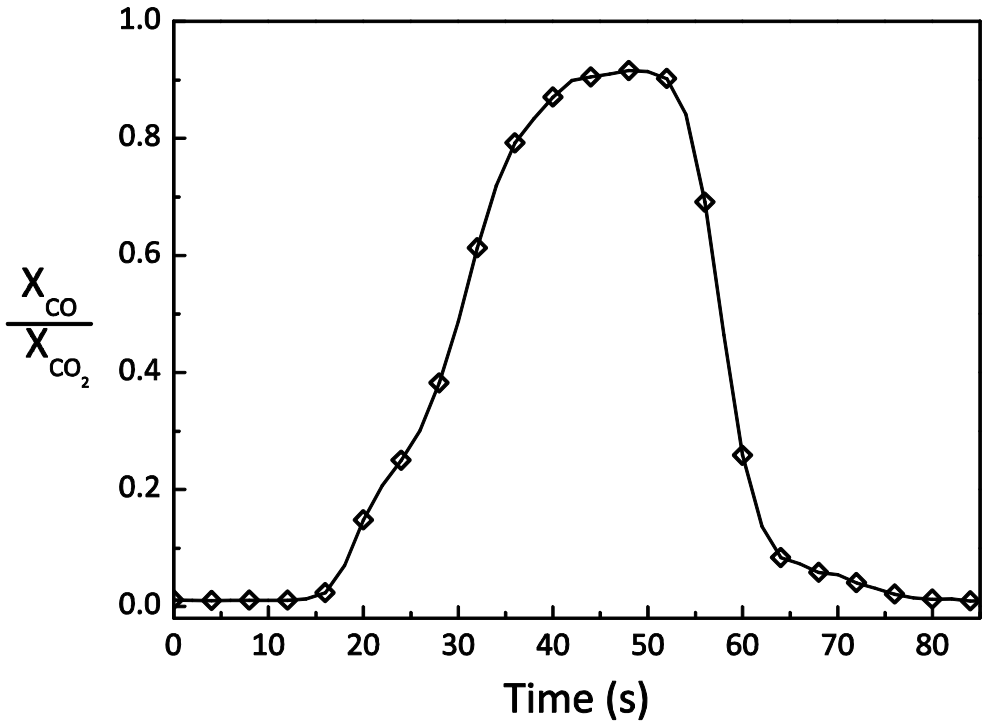

Figure 7.6. Ratio $\frac{X_{CO}}{X_{CO_2}}$ from the combustion of 50 % KNO_3 ternary mixture under 10 % O_2 atmosphere.

7.6.2. Combustion test under N_2 atmosphere

Combustion tests were conducted under N_2 atmosphere. Calculation procedures were similar to the ones applied for the 10 % O_2 atmosphere experiments. HRR results are shown on Figure 7.7. Obviously, OC calculation is unsuitable for reactions taking place under N_2 atmosphere and no plot is then presented. Observations from Figure 7.7 are similar to the ones stated from

Figure 7.6. As mentioned previously, under a critical O_2 concentration, the combustion chemistry of the 50% KNO_3 ternary mixture does not vary whatever the composition of the reacting atmosphere is. Relative deviations between the CDG and the mass loss rate principles are slightly higher (c.f. Table 7.8).

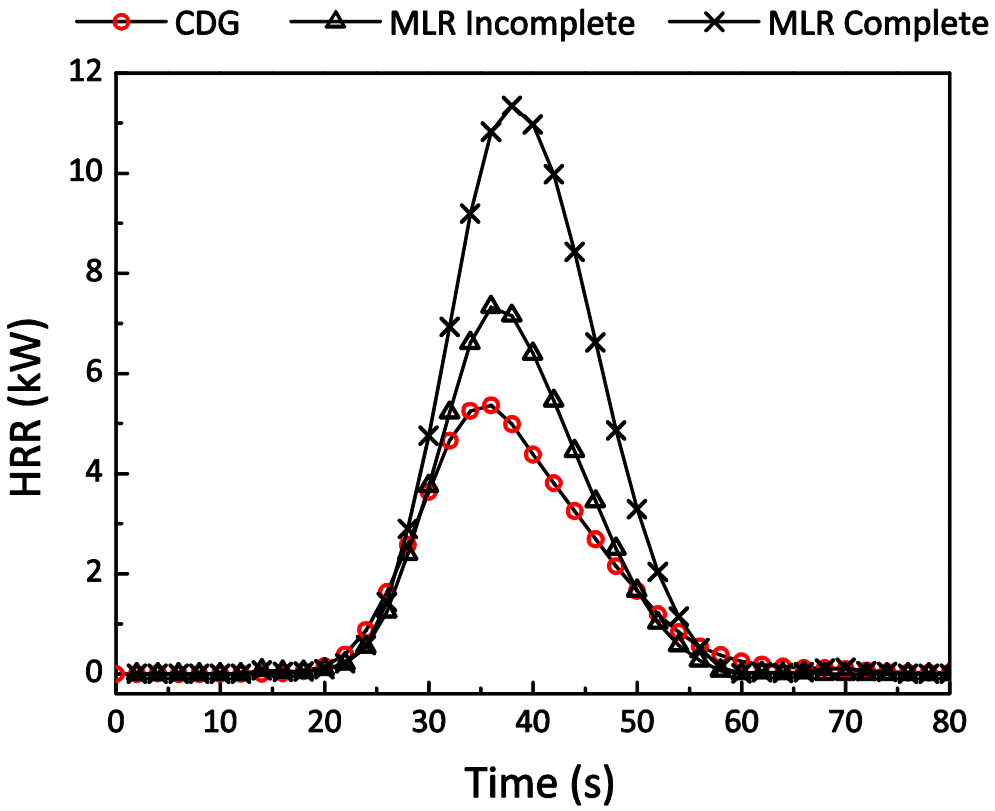

Figure 7.7. HRR results using OC, CDG and mass loss rate (complete and incomplete combustion assumptions) approaches from the combustion of 50 % KNO_3 ternary mixture under N_2 atmosphere.

Table 7.8. HRR peak and total energy relative deviations between CDG and Mass loss rate (incomplete combustion correction) methods using calculated energy coefficients for the combustion of 50% KNO_3 ternary mixture under N_2.

CDG/$MLR_{incomplete}$	Relative Deviation (%)
HRR Peak	27
Total Energy	15

7.6.3. Discussion

Convergence in the HRR estimations is achieved between OC, CDG and the mass loss rate approach when using the determined energy coefficients for combustion reaction under air involving the 50 % KNO_3 ternary mixture. However, discrepancies appear between the methods when the O_2 concentration in the reacting atmosphere is reduced below the established critical value. The peculiarity of the material to carry its own oxidizer allows combustion to occur even under inert atmosphere. Under the critical O_2 concentration, there is no consumption from the supporting atmosphere which prescribes the use of OC principle. Furthermore, relative deviation within a 20 % - 30 % range is observed between CDG and the mass loss rate principle corrected for incomplete combustion. One suggests that this divergence possibly arises from the measured heat of combustion of the mixture which could not correctly characterise the actual energy evolution from the chemical reactions taking place. As previously noticed, the measured heat of combustion is affected by the bomb calorimeter experimental configuration (reaction chamber filled with O_2 and pressure raised). The heat of combustion of the mixture is suitable as long as the chemical evolution of the material (thermal degradation) undergoing combustion follows a pathway nearly similar to the one of the bomb calorimeter experiment. According to the HRR results introduced in Figure 7.3, the aforementioned statement seems to apply for combustion reactions occurring under air. However, it becomes questionable for reactions under atmospheres with O_2 concentration lower than the critical value and characterising the flaming transition.

The experimental DSC curves of the KNO_3 ternary mixtures (c.f. Part I, Figures 7 and 8) features two main exotherms under air as well as N_2 atmospheres. The first exotherm ascends around 320°C - 330°C and was identified as the oxidation of the volatiles formed during the thermal decomposition of the material. The second exotherm arises around 390°C - 420°C and was interpreted as char oxidation and glowing combustion. Differences observed between the DSC curves describing the thermal evolution of the sample under air and under N_2 hold in the peaks temperature of the exotherms, their width and amplitude. Peaks under N_2 atmosphere are slightly shifted to lower temperatures. The amplitude of the first exotherms remain relatively identical whatever the reacting atmosphere is. The amplitude of the second exotherm associated with the char oxidation is significantly lower under N_2 than under air. Moreover, the width of the first exothermic peak is significantly narrower for the DSC carried out under N_2

than under air. The discrepancy between the two curves stresses the contribution of the O_2 from ambient air to the variation of enthalpy engendered by the oxidation processes. The release of energy associated with the overall thermal degradation can be expressed as,

$$\Delta H_{total} = \Delta H_{oxidizer} + \Delta H_{air} \quad (16)$$

Where $\Delta H_{oxidizer}$ represents the energy released by the oxidation reactions supported by the internal oxidizer supply and ΔH_{air}, the energy released by the oxidation processes sustained by O_2 from the ambient air. Similarly, considering this time a combustion reaction instead of a thermal degradation, one can express the heat of combustion of the KNO_3 ternary mixture as,

$$\Delta H_{c\,[50\%\,KNO_3]} = \Delta H_{r\,[oxidizer]} + \Delta H_{r\,[air]} \quad (17)$$

Where $\Delta H_{r\,[oxidizer]}$ corresponds to the heat of reaction of combustion processes (smouldering and flaming) sustained by the internal oxidizer KNO_3 and $\Delta H_{r\,[air]}$ is the heat of reaction of combustion reactions sustained by O_2 from the ambient air. Equation (17) is essential to understand the energetic mechanism associated with energetic materials. The estimation of $\Delta H_{r\,[oxidizer]}$ would allow assessing the contribution of the oxidizer to the total energy release from the combustion. One could define the influence of each oxidizing agent as a reaction partner. Furthermore, expression (17) highlights that a proper heat of reaction should be determined when the combustion phenomena are only sustained by the internal oxidizer. Recalling that oxidation of the volatiles and char oxidation are the two main exothermic processes taking place, $\Delta H_{c\,[50\%\,KNO_3]}$ and $\Delta H_{r\,[oxidizer]}$ can be formulated as,

$$\Delta H_{c\,[50\%\,KNO_3]} = \chi_{char}\Delta H_{char} + \chi_{volatiles}\Delta H_{volatiles} \quad (18)$$

$$\Delta H_{r\,[oxidizer]} = \chi_{char}\Delta H_{char\,[oxidizer]} + \chi_{volatiles}\Delta H_{volatiles\,[oxidizer]} \quad (19)$$

One clearly assumes,

$$\Delta H_{char} > \Delta H_{char\,[oxidizer]} \text{ and } \Delta H_{volatiles} > \Delta H_{volatiles\,[oxidizer]} \quad (20)$$

Doubts can be associated to the use of $\Delta H_{c\,[50\%\,KNO_3]}$ for CDG and mass loss rate calculations even if corrections are applied. Moreover, the probability that χ_{char} and $\chi_{volatiles}$ remain relatively constant during an experiment is arguable.Considering Figure I.8, the divergences observed on the DSC curves between the variations of enthalpy measured under air and N_2 indicate a different reaction kinetics. Correctness of the results cannot be assessed if the HRR

estimation is only based on these two methods. In addition, the appropriateness of the assumed kinetics has to be verified. One solution to estimate $\Delta H_{r\,[oxidizer]}$would be to perform a bomb calorimeter test filling the chamber with N_2 instead of O_2 and measured the heat of reaction. If the main combustion gases are identified and their concentration measured, one can model the reaction associated with the variation of enthalpy $\Delta H_{r\,[oxidizer]}$. Subsequently, one can follow the same procedure as developed previously to estimate new energy coefficients relative to the CDG principle. After conducting calculations relying on the newly defined variables, comparison of HRR results by means of CDG and mass loss rate approach would help assessing their relevance as well as the assumed kinetics for experimental conditions different to usual air atmosphere. Once achieving this step, one could express the HRR under air, $\dot{q}_{total}$, as,

$$\dot{q}_{total} = \dot{q}_{[oxidizer]} + \dot{q}_{[air]} \quad (21)$$

Where, $\dot{q}_{[oxidizer]}$ is the contribution to the overall HRR of the oxidation reactions sustained by the O_2 supplied by the internal oxidizer, and $\dot{q}_{[air]}$ represents the contribution of the oxidation processes supported by O_2 from the ambient air.

If $\Delta H_{r\,[oxidizer]}$ can be assessed, the energy contribution generated by the action of the oxidizer KNO_3 can be estimated ($\dot{q}_{[oxidizer]}$). By subtracting from the HRR results obtained for experiments carried out under air, one can estimate the degree of contribution of the oxidation reactions sustained by the O_2 from ambient air. Given this proportion to the overall HRR, one can evaluate the influence of the reacting atmosphere on the combustion behaviour of the material. Finally, this analysis could be of several interests. The decoupling of the energy release related to reactions sustained by the internal oxidizer from the one associated with oxidation reactions consuming O_2 from ambient air as oxidizing agent would be valuable to define a ranking of energetic materials based on $\dot{q}_{total}$ and $\dot{q}_{[oxidizer]}$ values. It could be used as a risk assessment tool. Also, it could allow stressing the materials from different families that present a similar energetic behaviour.

The characterisation of the reactional processes occurring during the combustion of energetic materials helps improving the description of their kinetics scheme which is essential from a modelling perspective. A pertinent model will have to consider separately the oxidation reactions using air and the ones relying on the supply from an internal oxidizer such as KNO_3.

The ability to decouple both processes through experiments would provide useful data to verify the relevance of the developed models.

The combustion of the sample material can be described by the following scheme,

1. Flaming combustion in the gaseous phase;
2. Smouldering combustion in the condensed phase;

The other objective that will have to be analysed is the magnitude of these two regimes. Conducted experiments on the KNO_3 ternary powders have stressed that flaming combustion comprised a diffusion flame regime sustained by O_2 from ambient air and according to the concentration of KNO_3 in the mixture, a premixed flame regime where the internal oxidizer constitutes the supply. Considering equation (21), $\dot{q}_{[air]}$ can be interpreted as the energy release through the diffusion flame and by the glowing combustion occurring at the surface of the sample and supported by O_2 from the ambient air. $\dot{q}_{[oxidizer]}$, from its part, corresponds to the energy release from a smouldering combustion taking place in the solid phase and from a premixed flaming combustion if the regime initiates (dependent on the concentration of oxidizer). The latter statements allow rewriting $\dot{q}_{[air]}$ and $\dot{q}_{[oxidizer]}$ as,

$$\dot{q}_{[air]} = \dot{q}_{flame\,[air]} + \dot{q}_{glowing\,[air]} \tag{22}$$

$$\dot{q}_{[oxidizer]} = \dot{q}_{smouldering\,[oxidizer]} + \dot{q}_{flame\,[oxidizer]} \tag{23}$$

The smouldering combustion under ambient atmosphere is sustained by both O_2 from the air (glowing combustion) and from the internal oxidizer. An attempt should be perform to ascertain the predominance of the smouldering induced by the internal oxidizer ($\dot{q}_{glowing\,[air]} \ll \dot{q}_{flame\,[air]}$). One should also establish the correctness of the assumption of a smouldering relying on oxidations reactions between the volatiles, the char and the oxidizer An approximation of HRR could be given by,

$$\dot{q}_{total} \sim \dot{q}_{smouldering\,[oxidizer]} + \dot{q}_{flame} \tag{24}$$

Where, $\dot{q}_{flame} = \dot{q}_{flame\,[oxidizer]} + \dot{q}_{flame\,[air]}$. (25)

It has been noticed during the experiments that the premixed flame only initiates for certain concentrations of oxidizer. If the latter is too low, no premixed flaming regime arises. A separation of the two combustion processes can be obtained by conducting the experiments under air (smouldering + flaming) and N_2 (smouldering). One could then formulate the HRR as,

$$\dot{q}_{total} \sim \dot{q}_{smouldering\,[oxidizer]} + \dot{q}_{flame\,[air]} \quad (26)$$

Smouldering is the limiting factor of energy release from the gaseous phase as it controls the flow of flammable volatiles. One assumes that most toxic products are generated in the condensed phase, the diffusion flame acting as a filter when it proceeds. FTIR analyses have highlighted formations of aldehydes and nitrous oxides were favoured when the reacting atmosphere was only composed of N_2. Consequently, detailed analysis of the smouldering should be performed in order to develop the comprehension of the chemical mechanisms taking place. As previously mentioned, one supposes that two reactions take place during the thermal degradation of the sample:

2.1. Oxidation of the volatiles;

2.2. Char oxidation.

The two exothermic peaks associated with these reactions clearly appeared on DSC curves. In order to better describe the smouldering phenomenon, the two oxidation reactions would need to be studied. From Figure 7.I.8, one can notice that the two oxidative processes overlap regardless of the reacting atmospheres. Decoupling the two phenomena would be highly valuable. Such procedure has already been conducted for lingo-cellulosic fuels [8] [9] using thermal and numerical separation of DSC results. Applying a technique inspired by the one described by Cancellieri [8] and Leroy [9], would allow the assessment of the energetic contribution of each process, $\Delta H_{char\,[oxidizer]}$ and $\Delta H_{volatiles\,[oxidizer]}$ to $\Delta H_{r\,[oxidizer]}$. In case of chemical change (i.e. favouring one process over the other) this would provide valuable information in order to define an error range associated with the heat of reaction. Even if the experimental conditions of DSC and TGA are far from the reality of a fire, such analysis is essential. However, one major problem arises. As shown on Figure 7.I.8, char and volatiles cannot be separated prior being oxidized as the internal oxidizer initiates the reactions. A method could be to consider the fuel and oxidizer compounds separately and then try to reconstruct the DSC curve.

Finally, to summarize, the heat of reaction $\Delta H_{r\,[oxidizer]}$ needs to be estimated to be able to calculate the HRR through CDG and mass loss rate approach. The chemical evolution of the material is different whether the reacting atmosphere is N_2 or ambient air. The knowledge of $\Delta H_{r\,[oxidizer]}$ allows the evaluation of $\dot{q}_{[oxidizer]}$, the contribution of the combustion reactions sustained by the internal oxidizer. Such parameter would be useful to compare energetic materials combustibility based on the level of energy they can release only based on the supply from an internal oxidizer. Furthermore, to better describe the physical and chemical mechanisms associated with the combustion of KNO_3 ternary powders, it would be useful to assess the HRR contribution of the smouldering and the one from the flaming regime. For some configuration where flaming is suppressed below the critical O_2 concentration, the decoupling could be approximated using equation (26). Such assumption would need to be verified before being applied. Attention should be devoted to improve the description of the smouldering process. Experimental results seem to point it out as the investigator of the emission of toxics. The development of a method allowing the separation of the phenomena of volatiles and char oxidations will be necessary.

The achievement of such characterisation would provide priceless information about the physical and chemical mechanisms taking place during the combustion reaction of an energetic material similar to the KNO_3 ternary powders used in the present study. They could be used to improve the accuracy of kinetics models as well as a validation tool.

7.7. Concluding Remarks

The potential of OC and CDG principles to estimate the HRR from the combustion of a 50% KNO_3 ternary mixture has been investigated. This attempt allowed the assessment of the limitations associated with these two methods. A protocol can be developed defining the restrictions that need to be considered to ascertain a correct use of OC and CDG. The validity of the each calculation hypotheses has to be evaluated, in particular the relevance of Huggett and Tewarson energy constants in the considered experimental conditions. An assessing criterion of the accuracy of the HRR results obtained is specified; it is simply based on the comparison of OC, CDG and mass loss rate approaches. Important divergences highlight that at least one of the calculation assumptions is breached. The sensitivity analysis has underlined that the highest error contributions relative to OC and CDG originate from the energy

constants, the species molar fraction measurements, the exhaust volume flow rate and the conservation of N_2. Corrections can be applied for the molar fraction measurements. Similarly, calibration of the Pitot tube that allows the estimation of the exhaust volume flow rate is simple and checking should be done regularly. Conservation of N_2 is only a critical issue if important generation of N_2 occurs compared to the amount of N_2 present in the exhaust flow. A mass balance can highlight such productions. Finally, the most critical parameters remain the energy coefficients. If Huggett and Tewarson constants appear unsuitable, appropriate values have to be evaluated. Regarding the sample material, it was shown that Huggett and Tewarson could not correctly describe the energy release by the combustion reaction. It is assumed the deviations of actual energy coefficients from Huggett and Tewarson constants originate from the action of the oxidizer. It has been emphasized that the determination of relevant energy values is closely related to the level of knowledge about the material chemistry. A procedure has been proposed in the case of the combustion of 50% KNO_3 ternary mixture. Three main pieces of information relative to the compound have been used:

1. The composition of the material;
2. The measured heat of combustion $\Delta H_{c\,[50\%\,KNO_3]}$;
3. A thermal decomposition model of the oxidizer.

Data about composition of the material and the assumed thermal decomposition scheme were processed to define a fictitious molecule representing the portion of the ternary mixture evolving in the gaseous phase and in the char. This was possible as the decomposition processes of the different components were assumed to occur simultaneously. Combining the fictitious molecule composition to the measured heat of combustion allows the calculation of energy coefficients taking into account the oxidizer mechanism. The fictitious molecule model approach offers accurate outcomes for combustion reaction taking place under air. Converging HRR results are achieved between OC, CDG and the mass loss rate methods corrected for incomplete combustion. Furthermore, error ranges applied to the energy values tends to confirm the credibility of the HRR estimations.

An important characteristic of energetic materials related to the presence of the oxidizer in the composition holds in their ability to burn under low O_2 or even N_2 reacting atmosphere. If a fire initiates, first it is likely to happen under air. Other scenarios are plausible but this one

constitutes an interesting example by its probability to occur. In case of a compartment fire, the supporting atmosphere evolves due to the emissions of combustion gases emissions. To some extent, the medium can become vitiated with only a very low level of O_2 remaining. One highlighted that under a critical O_2 concentration in the reacting atmosphere, materials such as the KNO_3 ternary mixtures would sustain combustion (flaming and smouldering) with the only O_2 supply from the decomposition of the internal oxidizer. As no O_2 consumption from the ambient air takes place, the OC method becomes unsuitable to estimate the HRR. Nevertheless, CDG and the mass loss rate approach can still be applied. HRR calculations are performed applying the energy coefficients defined for the fictitious molecule (CDG) and the measured heat of combustion corrected for incomplete combustion (mass loss rate principle). Unlike the convergence attained for experiments carried out under ambient air, discrepancies arise in the HRR outcomes when combustion reactions are conducted under low O_2 and N_2 atmospheres. Considering the different hypotheses necessary to perform the HRR calculations, the pertinence of using a measured heat of combustion emerges as a critical question. DSC and TGA results clearly underline differences in the heat release whether the supporting atmosphere is composed of air or N_2. Chemical emissions are different and chemical pathway might also significantly differ when changing the composition of the reacting atmosphere. One suggests that bomb calorimeter tests should be performed under N_2 rather than O_2 in order to estimate the actual heat of reaction under N_2. Analysis of the major gases would allow the reconstruction of an approximated chemical reaction equation. Using the fictitious molecule model and the measured heat of reaction to evaluate newly energy values would allow progressing on the question of the ability of CDG to accurately estimate the HRR from the combustion of a fuels/oxidizer compound under low O_2 atmosphere. A convergence between the mass loss rate approach combined with the heat of reaction under N_2 and the CDG calculation would provide valuable information on the combustion behaviour of energetic materials. The applicability of the method would allow the estimation of the energetic contribution offered by the internal oxidizer and the one originated from oxidation reactions sustained by the ambient air. One could define a novel ranking of energetic materials based on the magnitude of their “oxidizer” and “ambient air” energy releases. Furthermore, separation of the chemical processes would be useful to estimate, beside the oxidizing agent, which of the volatiles oxidation or the char oxidation is susceptible to release more energy. This would allow the improvement of the determination of the energy values used in the HRR

approximation approaches. For situations where experiments could not be carried out, the previous results would also be valuable for the development of kinetic models that would achieve a more accurate description of the physical and chemical mechanism taking place during the combustion of energetic materials.

Finally, the estimation of the HRR of an energetic material has to be considered according to an appropriate aim. The present chapter have shown that the HRR of an energetic material could be approximated under given conditions. Nevertheless, it was also emphasized that the accuracy in the results would be dependent on the actual knowledge of the chemical mechanisms of the compound as well as other properties such as its heat of combustion. The concluding message that is delivered is that two types of HRR estimations should be regarded. With limited information about a material, one cannot expect accuracy in the HRR result. In this situation, the use of error range is appropriate instead of a constant value which validity is arguable according to the material. Methods to assess energy coefficient error bars need to be defined. The use of a bond additivity approach has shown encouraging results but still requires to be improved. Moreover, the possibility to determine energy ranges for families of materials should be investigated. On the other hand, if information is available about the composition, the heat of reaction or combustion, the thermal decomposition processes taking place during the reaction, energy coefficients can be assessed. The relevance of the results will then depend on the correlation between the measured heat of reaction (or combustion) and the actual reaction taking place. In order to evaluate the confidence that can be granted in the outcomes, the convergence criterion can be used between the results obtained through the CDG and the mass loss rate approaches.

7.8. References

[1] Janssens, M., Parker, W., J., Oxygen Consumption Calorimetry, in: Heat Release in Fires, Chapter 3, Editors: Babrauskas, V., and Grayson, S., J., Elsevier Applied Science, New York, 1992, pp., 31 – 59;

[2] Tewarson, A., Generation of Heat and Chemical Compounds in Fires, in: SFPE Handbook of Fire Protection Engineering, 3rd Edition, Section 3, Chapter 4, The National Fire Protection Association Press, 2002, pp. 3-82 – 3-161;

[3] Huggett, C. Estimation of Rate of Heat Release by means of Oxygen Consumption Calorimetry, Fire and Materials, 4 (2), pp. 61 – 65 (1980);

[4] ASTM E2058-03, "Standard Test Method for Measurement of Synthetic Polymer Material Flammability Using a Fire Propagation Apparatus", ASTM International, West Conshohocken, 2003;

[5] Brohez, S., Marlair, G., Delvosalle C., Fire calorimetry relying on the use of the Fire Propagation Apparatus, Part I: Early Learning from the Use in Europe, Fire and Materials, 30, pp. 131 – 149 (2006);

[6] Freeman, E., S., The Kinetics of Thermal Decomposition of Potassium Nitrate and of the Reaction between Potassium Nitrite and Oxygen, Journal of the American Chemical Society, 79, pp. 838 – 842 (1957);

[7] Lide, D., R., CRC Handbook of Chemistry and Physics; 88th Edition; CRC Press: Taylor & Francis Group, NY, 2007-2008;

[8] Cancellieri, D., Leoni, E., Rossi, J., L., Kinetics of the Thermal Degradation of *Erica Arborea* by DSC: Hybrid Kinetic Method, Thermochimica Acta, 438, pp. 41 – 50 (2005);

[9] Leroy, V., Cancellieri, D., Leoni, E., Thermal Degradation of lingo-cellulosic Fuels: DSC and TGA Studies, Thermochimica Acta, 451, pp. 131 – 138 (2006);

8. Conclusions

Energetic materials encompass a wide range of chemical compounds such as explosives, propellants or pyrotechnics. Originally dedicated to military purposes, they become more and more used for industrial processes that require fast reaction times associated to large energy releases. The unifying characteristic of the different groups of energetic materials is within their composition, they are all based on a fuel/oxidizer mixture. Consequently, they do not require the presence of O_2 in the supporting atmosphere to undergo combustion, deflagration or detonation. As energetic materials decompose, the oxidizer releases O_2, directly mixes within the fuel volatiles. The diffusion time decreases and it enables the development of very fast reactions.

The other principal characteristic of these materials is the amount of energy they can liberate. Components generally comprise high energies of formation. The major drawback of such materials comes naturally when their stability is compromised. If the purpose of some of them is to deflagrate or detonate, one expects these phenomena to occur only for specific operating conditions. Nevertheless, conditions engendering instability can cause the initiation of unwanted reactions susceptible to lead to severe accidents. Severe events have been reported in the past, occurring during the manufacturing process as well as transport, storage and final disposal. The risks of deflagration and detonation associated with energetic materials have been largely studied. Nevertheless, the understanding of the physical and chemical mechanisms involved during the combustion reaction with no transition to a detonation regime remains limited.

The characterisation of the behaviour of energetic materials is essential to be able to predict the consequences of a fire involving these types of compounds. Models have to be developed allowing the description the of the reaction chemical kinetics. In order to achieve this objective, experimental results have to be provided. Two major features need to be considered: the gaseous emissions and the energy release. Furthermore, in terms of risk assessment, the knowledge relative to the toxicity originating from the combustion of energetic materials requires to be improved.

Regarding the chemical and thermal analysis, the first task was to assess the ability of usual tools such as DSC and TGA to reveal the thermal degradation of a selected sample material. In a second stage, from the obtained results one had to ascertain how much information could be extracted about the chemistry of the compound. It is fundamental to understand the kinetics of such product in particular to be able to predict the mechanism leading to the formation of toxic products. Concerning the energy release study, the main challenge was to conclude about the possibility of using simple HRR approximation methods to estimate the HRR of energetic materials.

8.1. Thermal and chemical analysis

Conclusions of this analysis have been already developed in detail. All experiments have been conducted on a ternary powder based on a starch, lactose and potassium nitrate mixture, the latter being the oxidizer. Qualitative description of the thermal decomposition of the sample was realised thanks to DSC, TGA and FTIR studies.

- Two main chemical processes have been highlighted: oxidation of the decomposing material in the gaseous phase and oxidation of the char (smouldering). They correspond to two combustion phenomena: flaming in the gaseous phase and smouldering in the solid phase. Reactions are sustained in both cases by the fuel decomposition products combining with the air and the oxidizer KNO_3. In flaming this occurs in the gas phase in a homogeneous manner, in the case of smouldering it corresponds to heterogeneous oxidation of the solid.

- Experimental results have stressed that the oxygen concentration affects the reaction kinetics of the compound. Furthermore, reaction rates are enhanced with the proportion of KNO_3. The flame height, the propagation rate of the smouldering front, the emissions of combustion and degradation gases, the formation of char are influenced by the fuel/oxidizer ratio.

- The propagation of the smouldering front appears as a limiting factor of the completeness of the combustion reaction. It governs the release of volatiles and oxidizing agents. According to the species concentrations and the diffusion, the strength of the reactions taking place in the solid phase varies. The structure of the

residual char has a coupled effect with the combustion reaction because decomposition induces changes in its porosity and permeability. Consequently, reactions in the gaseous phase are conditioned by the ones occurring in the solid phase. Low permeability induces swelling of the char structure which restricts the emissions of gaseous products from the smouldering combustion out of the compound. On the contrary, a high permeability allows combustible gases generated in the solid phase to diffuse through a wider surface and enhance the reactions in the gaseous phase. The flammability of the mixture is therefore correlated to the intensity of the smouldering combustion.

- The concentration in oxidizer in the mixture affects the strength of flaming and smouldering. The diffusion flaming combustion developing in the gaseous phase can be suppressed by decreasing the O_2 level in the surrounding medium below a critical value. This approach allows the decoupling of the reactions relying on the O_2 from the air and the O_2 originated from thermal decomposition of the oxidizer. Diffusion flaming appear to be supported by the ambient air while the smouldering seems to be sustained by the generation of oxidizer. The transition observed on the flaming regimes yields to significant variations in the gaseous emissions. The suppression of the diffusion flame limits the filtering of toxic compounds that are normally oxidized through the flame.

- FTIR analyses highlighted traces of aldehydes as well as emissions of nitrous oxides and carbon monoxide. Toxicity of such materials is high. A fire involving a large quantity of a powder similar to the one used for the present study could become the source of substantial release of toxic products. In particular, in the situation of an enclosure fire where the reacting atmosphere could be modified by the combustion emissions, the probability of toxic emissions increases. As previously mentioned, under low O_2 atmosphere, the smouldering combustion becomes the main process taking place. The low reaction temperatures associated with seem to favour the production of toxic products like aldehydes.

The realization that energetic materials can potentially emit toxics is one important step. Nevertheless, the ability to predict the level of concentrations is also an essential need and requires further knowledge. Kinetics models are necessary to better understand the physical

and chemical mechanisms arising during the combustion. The analysis carried out in the present study was mostly qualitative. The attempts to explain the different hypotheses put forward will have to be assessed. New experiments will have to be designed to refine the description of the material behaviour in more quantitative way and a kinetic scheme will have to be defined based on multi-step reaction mechanisms (c.f. Figure 8.1). In a first instance, thermal separation of the different chemical processes will be carried out on the DSC and TGA results. Subsequently, the decoupling of the reactions either sustained by the O_2 from the air or by the O_2 generated by the decomposition of the oxidizer has to be performed. It was stressed that modification of the reacting atmosphere allows suppressing the air contribution. If separation of the different chemical phenomena is achieved, one could attempt to apply methods such as isoconversional analysis in order to obtain their initial energies of activation.

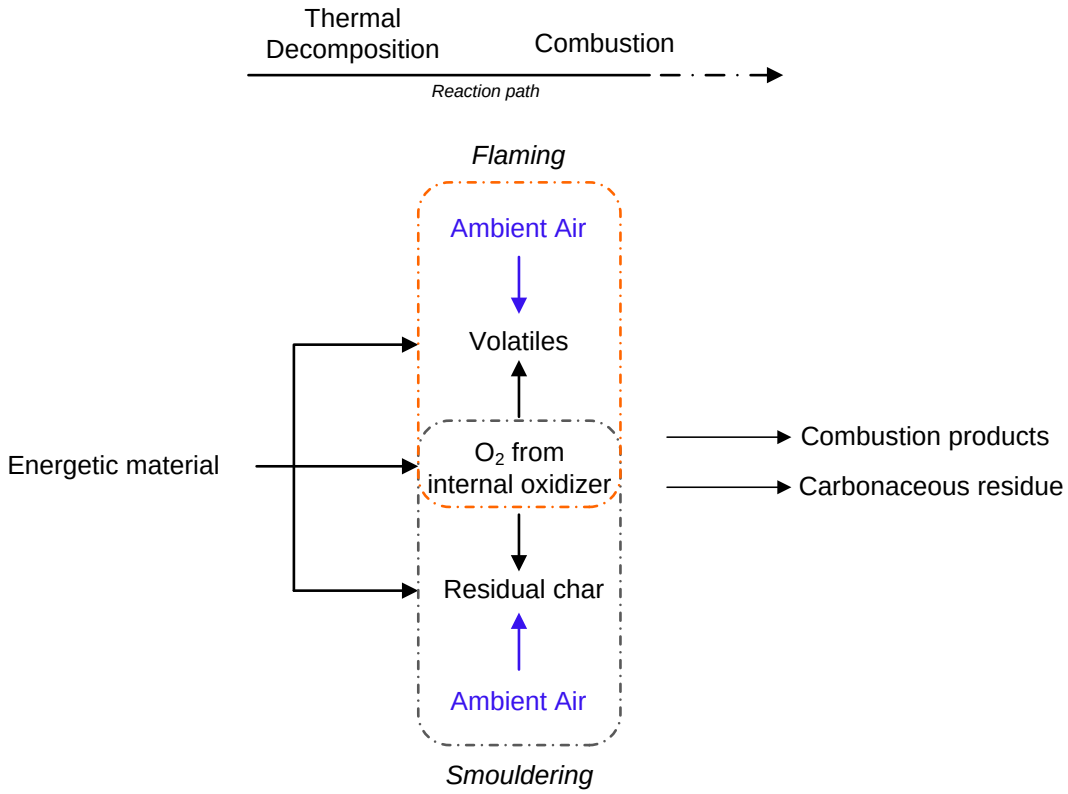

Figure 8.1. Schematic representation of the combustion reaction involving starch/lactose/KNO_3 mixture under air.

Nevertheless, the model will be appropriate for thermal decomposition of the sample material. Its applicability for describing the combustion will have to be assessed and adjustments will be necessary. A valuable parameter will be the estimation of the variation of enthalpy associated with flaming and smouldering combustion. A prerequisite will stand in the

ability to accurately approximate the HRR of the combustion reaction involving the energetic material. The estimation of the HRR has also other application. It is an important input of fire modelling codes. Furthermore, its knowledge often represents one of the pillars for defining standards and other safety regulations. The availability of methods to evaluate the HRR is a fundamental requirement of the fire community. Different methods have been developed over the last few decades. Their pertinence to approximate the HRR of energetic materials had to be assessed. In addition, the ability to assign an error to each calculation allowed appreciating the precision that can be expected from the different methods.

8.2. HRR analysis

As previously mentioned, important information is amalgamated within the HRR. In terms of risk assessment, the existence of calculation procedures to approximate the HRR is necessary to dimension appropriate safety barriers susceptible to limit a fire that would involve materials enclosing an oxidizer. Furthermore, to assess and prevent how such fires would propagate, understanding the reaction mechanisms is necessary and measurements of HRR represent valuable data as each chemical process associates an energetic contribution.

According to the available techniques of HRR approximations, the present study tried to answer several critical questions:

1. Is it possible to easily estimate the HRR from a combustion reaction involving an energetic material?
2. Can usual approaches still be applied using basic assumptions?
3. If not, can they be modified by taking into account their chemical characteristics?
4. Can the error associated with the HRR approximation be assessed?

Two different types of approaches have been highlighted in the present work. The first relies on the measurement of the mass loss while the second rests on the evolution of the concentration of species involved during the combustion.

A baseline technique is based on the mass loss rate measurement combined to the heat of combustion of the burning material. In case of complete combustion, the calculation is relatively simple to apply. At first glance, only two variables are required: the mass loss rate and a heat of combustion. In the case of incomplete reaction, corrections accounting for the

formation of CO can be introduced. The estimation of an appropriate heat of reaction requires the knowledge of few more variables. In terms of error, for a complete combustion the uncertainty associated with an HRR estimation by means of the mass loss approach has been assessed to lie within a ± 20 % range. The error to the mass loss rate depends on the accuracy of the load cell and the filtering of the output signal. One considers that the uncertainty relative to this parameter should be lower than 10%. The main issue relative to the mass loss rate approach is that one needs to know the heat of combustion associated with the burning material to perform the calculation. In addition, the knowledge of the heat of combustion does not ensure the correctness of the HRR estimation. Bomb calorimeter tests usually offer highly accurate measurement ofΔH_c (± 0.05%). Nevertheless, the pertinence of the heat of combustion relies on the assumption of a complete combustion occurring with a relative similar kinetics than the one encountered during the bomb calorimeter test. Using the uncertainty of ΔH_c for the calculation of the error associated with a HRR estimation through a mass loss rate approach is potentially misleading. The assumption of complete combustion is valid as long as the production of not fully oxidized species (CO, HC...) remains limited. If the emission of incomplete combustion gases tends to become important, the actual heat of reaction can significantly differ from the measured heat of combustion. Nevertheless, corrections can be applied taking into account the generation of CO. Consequently, the uncertainty related to the CO correction needs to be also accounted. An uncertainty analysis assuming large errors (~ 50 %) in the CO and CO_2 molar fraction measurements stresses a potential deviation of the order of 20 % on the evaluation of the heat of reaction. Furthermore, DSC curves of the KNO_3 ternary powders have highlighted the presence of two exotherms: a first characteristic of the oxidation of volatiles, the second of the oxidation of the char. Consequently, one can express the heat of combustion as,

$$\Delta H_{c\,[50\%\,KNO_3]} = \chi_{char}\Delta H_{char} + \chi_{volatiles}\Delta H_{volatiles} \quad (1)$$

It corresponds to an energetic balance between the heat of reaction associated with the oxidation of char and with the one corresponding to the oxidation of the volatiles accounting for the proportion of each of the processes. The estimation of $\Delta H_{c\,[50\%\,KNO_3]}$ is based on average χ_{char} and $\chi_{volatiles}$ values characteristic of the kinetics that occurred during the overall bomb calorimeter test. χ_{char} and $\chi_{volatiles}$ are not constant values and vary during a combustion reaction. For example, regarding the burning of pine needles, at ignition, the combustion mainly originates from the oxidation of volatiles ($\Delta H_{volatiles}$~12 – 13 kJ.g^{-1}) while

after extinction, glowing combustion remains active which characterises char oxidation (ΔH_{char}~30 kJ.g^{-1}). Taking into account the most extreme changes in the kinetics of the reaction, a confident variation range of ΔH_c would be to consider the [12 – 30 kJ.g^{-1}] interval, corresponding to a 150 % uncertainty. These variations can be neglected if $\Delta H_{volatiles} \approx \Delta H_{char}$ or if their energy contributions are small. At last, the heat of reaction varies during a combustion process and the approximation of a constant is valid as long as the reaction does not encounter significant chemical changes. The mass loss approach combined with the only heat of combustion can lead to errors in the HRR estimations. However, if the actual heat of reaction can be estimated, precise results can be expected. Their realisation will require the material chemistry to have been accurately characterised.

Two other techniques have largely spread over the fire community. They consist in measuring, for one, the evolution of the O_2 consumption (OC), for the other the CO_2/CO generation (CDG) during the reaction. The interest of these methods holds in the assumption that energy constants exist and can be used to conduct the HRR estimations. Consequently, no intrinsic information relative to the compound is necessary to evaluate the energy release. OC, in particular, has become the basic principle for HRR approximations. The data required to compute the OC equations is extracted from experiments carried out with apparatuses such as the cone calorimeter or the FPA. Compared to a mass loss rate technique, the number of variables becomes multiple and so the sources of uncertainties. Furthermore, it is legitimate to wonder how robust the assumption of energy constants is when one acknowledges that chemical compounds present a wide range of different compositions, structures or kinetics. By extension, noticing that the various HRR approximation procedures considered rely all on calculation assumptions, the question of limitations about their validity has to be investigated. In a matter of fact, whatever the approach used, the correctness of every hypothesis is a necessary condition that has to be verified in order to grant any confidence in the results obtained.

Regarding the mass loss rate approach, the analysis emphasized that the main hypothesis concerned the measured heat of combustion. For materials presenting chemical processes overlapping during the combustion, the reaction kinetics should not significantly differ from the one encounter during the bomb calorimeter test where the heat of combustion was measured. Considering OC and CDG principles, the first hypothesis that should be examined is

related to the dynamics of the reaction and the ability of the measuring system to accurately capture the chemical variations. It has been stressed in chapter 5 that if the reaction dynamics is faster than the dynamics of the measuring system, large distortions can be introduced in the output signals. For reaction durations of the order of few seconds, one can postulate that the analyser will not be able to capture the species evolutions if important quantities of gases are released. One can expect errors larger than 100 %. This prevents from attempting any HRR estimation. For such fast reactions, the use of apparatuses such as the cone calorimeter or the FPA should be excluded. Nevertheless, for reaction durations of the order of few tens of seconds, corrections can be applied but their suitability has to be ascertained. Furthermore, according to their precision, the resulting error originating from uncertainties on the species molar fraction measurements and affecting the HRR estimation should be restricted to less than 10 %.

Another potential cause of error that can be introduced by inaccurate measurements holds in the evaluation of the exhaust mass flow rate. OC and CDG equations are linearly dependent on this variable. Any error in the exhaust mass flow rate is transferred through OC or CDG equations increasing by the same order of magnitude their respective error. As a consequence, regular calibration of the Pitot tube needs to be conducted in order to limit such inaccuracy.

On the contrary, a sensitivity analysis has exhibited that neglecting the formation of water vapour during the combustion reaction does not alter the accuracy of the HRR calculation as long as the amount released is of the order of few percents. In the case of small scale experiments such as the ones performed by means of the FPA, the size of the sample and the magnitude of the dilution rate prevent from a generation of water vapour of the order of tens of percents.

Most of the OC and CDG calculation hypotheses can be assessed using the experimental data, nevertheless, few assumptions, more intricate to evaluate, remain. The assumption of N_2 conservation constitutes one of them. This hypothesis is necessary to estimate the incoming mass flow rate (supply flow + entrained air). Accurate estimation of the latter variable is essential in the case of low O_2 depletion or low HRR. A production of N_2 originated from the combustion of the material and not accounted in the conservation equation is susceptible to induce severe errors in the HRR estimations. For instance, a generation of N_2 during the combustion reaction equivalent to 20% of the N_2 brought through the incoming flow would

alter the HRR results obtained through OC up to 200 % (in case of low HRR) and up to 13 % through the CDG principle. Such breach in the assumption is complex to identify during the calculation process. However, it can be underlined by performing a mass balance between the mass loss of the material and the mass of combustion gases. Moreover, alike the validity of the water vapour hypothesis, the non respect of the N_2 assumption implies particular experimental conditions. For small scale experiments such as the ones carried out with the FPA or the cone calorimeter, the size of the sample and the standard dilution rate usually applied should avoid that a potential N_2 generation resulting from the combustion of a material became substantial enough compared to the mass flow rate of N_2 from the incoming flow rate (i.e. > 5 %). However, regarding room scale experiments and above, the N_2 hypothesis should be carefully examined prior to estimate HRR through OC and/or CDG principles.

A second problematic variable stands in the expansion factor α. It is usually assumes that α holds in the [1 – 1.21] range. One has demonstrated that this interval is not conservative anymore when considering energetic materials. One proposes to extend it to [1 – 2]. The exact calculation of α requires being able to model the combustion process. Information about the material (composition, thermal decomposition reactions...) is then necessary. Nevertheless, for low HRR, considering the experimental conditions and material used for the present study, the error induced by using the acknowledged 1.105 value would not introduce a deviation higher than 5% in case of low HRR calculated by means of the OC principle. On the contrary, for high HRR, the influence of α on the calculation is emphasized by a higher O_2 depletion factor. In this case, one has seen that the error could rise up to 25 %. The issue underlying an evaluation of α is that without knowledge of the material composition, the calculation relies on the acknowledged 1.105 without any certainty about the appropriateness of the latter value. In case of high HRR involving the combustion of an energetic material, it would be pertinent to prefer CDG and the mass loss rate approach or using a convergence criterion.

At last, a critical unknown remains concerning the range of validity of Huggett and Tewarson energy constants. No restrictions are clearly expressed about the use of energy constants for OC and CDG calculations. Furthermore, the uncertainties associated with each value only do not rely on physical or chemical interpretations. Uncertainty analyses have highlighted that the accuracy of the HRR estimation increases when calculated energy coefficients are applied. Nevertheless, their use brings the interrogation of the predominance of OC and CDG principles

over a mass loss rate approach simpler to conduct. In Chapter 5, the sensitivity analysis have stressed that an uncertainty of 1 kJ.g^{-1} of O_2 (CO_2) results in a deviation of 8% (7.5%) in the HRR estimation. Values obtained after the calculation of new energy coefficients suitable, under ambient air, for the KNO_3 ternary powders characterized during the various experiments reveal large discrepancies from the constants defined by Huggett and Tewarson. As an example, regarding the 50% KNO_3 ternary mixture, the new estimated E_{O_2} and E_{CO_2} values are respectively equal to 15.86 kJ.g^{-1} of O_2 and 7.58 kJ.g^{-1} of CO_2. The use of Huggett and Tewarson induces a 22% underestimation if the OC principle is applied and a 43% overestimation when applying the CDG calculation. Given these discrepancies, a different approach, not based on the usual energy constants, needs to be introduced in order to be able to correctly use the OC/CDG procedures.

For a known material composition and heat of combustion, the experimental scale and the test configuration represent the factors that will favour a method over another. In the present study, instead of opposing the different HRR approximation protocols, one proposes to present them as complementary. Due to the number of hypotheses each approach relies on, to base a calculation on only one result might be hazardous for atypical materials. The availability of different calculation approaches allows defining a convergence criterion by comparing the results obtained for each of them. One decided to follow this methodology for starch/lactose/potassium nitrate mixtures.

If the knowledge relative to the material is limited (i.e. no information about the composition, the structure and enthalpy values), the use of Huggett and Tewarson energy constants should hang on the conclusions arising from the study of the convergence criterion. Divergences in OC and CDG results based on calculations performed with Huggett and Tewarson energy constants have stressed the inappropriate character of the latter values in the case of combustion involving KNO_3 ternary powders. The limitation of the HRR methods originates, in the present case, in the inability to apply relevant energy values to the HRR approximation methods. However, a pursuit of precision for a completely uncharacterized material appears paradoxical. On the other hand, for unknown materials, one should only consider OC and CDG principles as HRR approximation tools and nothing more. Consequently, the aim of using exact values as energy constants is arguable. In a matter of fact, the ability of estimating a confidence HRR range can be appreciated as a sufficient approximation given the degree of

knowledge about the burning compound. Then, the motivation should not be devoted in determining energy constants but rather error bars confining the possible energy values. A possible approach is to formulate a methodology that would allow the determination of the maximum and minimum energy values that can be associated with a material with the least information about the latter. Methods proposed were based on chemical bonds analyses. Models have been developed relating an energy contribution to the heat of formation of a molecule with a chemical bond. Two techniques have been presented; the first based on bond dissociation energies (BDE) evaluation, the second relying on a Bond Additivity (BA) assumption. Given the considered examples, the latter method was efficient to refine the error range. To conduct the error range calculation, the composition of the material was the only necessary and sufficient condition. First results suggest that the basis of the methodology is correct. In the future, one should consider further development. Improvements can be introduced. The present study was limited to bonds between C, H and O atoms. Other elements should be introduced in order to characterize more than only CHO compounds. Furthermore, BA values could be affined for families of materials. Consequently, one could associate error range values with groups of compounds. Finally, applying the convergence criterion between OC and CDG principles could enhance the accuracy of the error range by considering as confident HRR range the HRR area where overlapping of the two calculation methods occurs. Such HRR approximation should be taken into account when the material composition is known or if it can be evaluated.

The degree of precision to describe a physical and chemical behaviour is often proportional to the level of information available about its constitutive mechanisms. Given the composition and the heat of combustion of the material and assuming the thermal decomposition reaction of KNO_3, one attempted to express suitable energy coefficients for OC and CDG taking into account the contribution of the internal oxidizer in supplying O_2 to the oxidation reactions. The method is based on the elaboration of a fictitious molecule that evolves into volatiles and char during the combustion. The associated heat of combustion is the one measured for the sample material through a bomb calorimeter test. Derivation of new energy coefficients is achieved by assuming a one step complete combustion reaction between the fictitious molecule and O_2 from ambient air. OC and CDG calculations were conducted based on these energy values. The mass loss rate calculation has been considered as a reference HRR. The convergence criterion was used to judge of the relevance of the developed approach. Application of OC, CDG and

mass loss rate principles in the case of experiments carried out under air atmosphere leads to identical results. Variations between the procedures remain limited. Conclusions of Chapter 6 underline the suitability of OC as well as CDG to assess the HRR from a combustion reaction involving an energetic material under the conditions where the reaction still consumes O_2 from the reacting atmosphere. The latter consideration is important.

While converging HRR calculations have been achieved for experiments carried out under air atmosphere, divergences were obtained when estimations through CDG and a mass loss rate principle were attempted for experiments where the O_2 concentration in the reacting medium was below the observed critical value. TGA and DSC curves have highlighted that the reaction kinetics for KNO_3 ternary mixtures differed whether the experiments were carried out under air or N_2. If the two chemical processes (i.e. oxidation of the volatiles and oxidation of the char) arise under both atmospheres, significant variations of enthalpy can nevertheless be stressed. Therefore, one suggests that the origins of the discrepancies observed between CDG and the mass loss rate approach for experiments carried out under the O_2 critical concentration hold in the use of a measured heat of combustion. In conclusion, for combustion reactions occurring under low O_2 or N_2 atmospheres, the specific heat of reaction needs to be measured in order to apply the mass loss rate principle in a more accurate way and to evaluate the appropriate CDG energy coefficients. The ability to use two different techniques to estimate the HRR will allow using the convergence criterion and help assessing the degree of pertinence of the results.

8.3. Future directions

From the present study, two directions to investigate have arisen,

1. The further development of a method based on a chemical bonds approach that allows the determination of a confident order of magnitude of the HRR associated with the combustion of a material;

2. The improvement of the description of the physical and chemical mechanisms taking place during the combustion of an energetic material.

The two prospects serve different purposes, according to the level of characterization of the considered sample material. The first perspective has already been discussed previously. When the level of knowledge about a compound is low, one should focus on restricting the HRR approximation to a confident interval allowing the determination of an order of magnitude of the result. The chemical bonds approach has to be improved. Other bonds will have to be added in order to describe more materials. The aim would be to define energy coefficient error bars relevant for a family of compounds. Moreover, according to the basis of the BA approach, a composition is associated with an energy range without concern of the molecular structure. A database could be created based on materials composition.

A more advanced characterization of the material allows investigating the second perspective. The understanding of the contribution of the oxidizer to the overall HRR is order to better understand the potential impact of a fire involving energetic materials. Two combustion processes are encountered during the reaction: smouldering and flaming. Smouldering is mainly sustained by the internal oxidizer while diffusion flaming is established by O_2 from ambient air. Finally, one can express the overall HRR as follow,

$$\dot{q}_{total} = \dot{q}_{smouldering} + \dot{q}_{flame} \quad (2)$$

If $\dot{q}_{smouldering\,[oxidizer]}$ can be precisely estimated using appropriate energy values, then it will be possible to deduce $\dot{q}_{flame}$ and estimate the magnitude of each of the processes compared to the final energy release. The highlighted issue holds in defining a relevant heat of reaction of the smouldering. One will have to consider a similar reaction to the one described by,

$$[C_xH_yO_zN_a + \ oxidizer\ ] \xrightarrow[\Delta H_{N_2}]{} (x-g-h)CO_2 + g\ CO + h\ CH_4 + \frac{y-4h}{2} H_2O + \frac{a}{2}\ N_2 + [Ox]_{residual} \quad (3)$$

One proposes to carry out bomb calorimeter tests under N_2 atmosphere and evaluate the heat release. The chemistry will have to be reconstructed and an experiment should be designed allowing the measurement of the major species emitted.

Once this next step is achieved, one could improve the understanding about the oxidation mechanisms for combustion reaction involving energetic materials. This will require a better description of the oxidizer contribution to the chemical processes. A technique will have to be defined for decoupling the overlapping chemical reactions. If such a goal can be attained, information will be useful to better assess combustibility and flammability of energetic materials. On the other they can provide essential data to introduce the behaviour of such material in modelling tools.

In the end, a precise evaluation of HRR is conditioned by the knowledge of the material chemistry. The question relative to the level of exactitude sought when applying a calculation method is relevant. Different reasons will raise different answers and requirements. According to the degree of information available, HRR approximations can be conducted to define orders of magnitude convenient for standards and regulations or values precise enough to improve the characterisation of chemical processes relative to the combustion of energetic materials which would allow ascertaining the correctness of kinetic models.

The accurate estimations of the HRR for energetic materials could offer valuable advancements regarding the fire risks associated with their use. In particular, one could describe the effect of a variation of the reacting atmosphere on the evolution of the energy release. Such results could be useful for defining ranking of energetic materials in terms of threats represented by hazardous combustions. Furthermore, a better description of the energetic mechanisms participating in the overall heat release from the combustion of energetic materials would contribute to refine the understanding and modelling of their reaction kinetics. As an example, this would allow enhancing the knowledge about the origins of the emission of toxic products pertaining to the burning of compounds like pyrotechnics.

Appendix A

B.1 Heat of formation

The heat of formation of a material can be deduced from the heat of combustion if the latter is known. Considering a compound $C_xH_yO_z$ and recalling the complete combustion reaction,

$$C_xH_yO_z + \left(x + \frac{y}{4} - \frac{z}{2}\right) O_2 \longrightarrow x\,CO_2 + \frac{y}{2}\,H_2O \qquad (\Delta H_c) \tag{1}$$

An expression of the heat of formation, ΔH_f, is given by,

$$\Delta H_{f,C_xH_yO_z} = x\Delta H_{CO_2} + \frac{y}{2}\,\Delta H_{H_2O} - \Delta H_c \tag{2}$$

A.2 Heat of reaction

Assuming that the combustion reaction can be modelled as the following one step process,

$$C_xH_yO_z + \nu_{O_2}(O_2 + 3.76\,N_2) \longrightarrow \nu_{CO_2}\,CO_2 + \nu_{CO}\,CO + \nu_{H_2O}\,H_2O + 3.76\,\nu_{O_2}\,N_2 \tag{3}$$

If the reaction coefficients ν_{O_2}, ν_{CO_2}, ν_{CO} and ν_{H_2O} can be estimated by means of calorimeter data, the heat of reaction (3) can be described with the following expression,

$$\Delta H_{reaction} = \sum_{products} \nu_{products}\,\Delta H_{f\ products} - \Delta H_{f,C_xH_yO_z} \tag{4}$$

Expression of the energy coefficients

An expression of the energy coefficients is given by,

$$E_i = \frac{\Delta H_{reaction}}{M_i\,\nu_i} \tag{5}$$

For a compound, $C_xH_yO_z$, $\Delta H_{reaction}$ is expressed as,

$$\Delta H_{reaction} = \left(\nu_{CO_2} - x\right)\Delta H_{f\ CO_2} + \left(\nu_{H_2O} - \frac{y}{2}\right)\Delta H_{f\ H_2O} + \nu_{CO}\,\Delta H_{f\ CO} + \Delta H_C \tag{6}$$

And the species reaction coefficients, ν_i, are formulated as,

$$\nu_i = \frac{\left(1 - X_{H_2O}\right)M_{fuel}}{\dot{m}_{fuel}}\left|X_i^A - \frac{X_i^{A^0}}{1 - X_{O_2}^{A^0} - X_{CO_2}^{A^0}}\left(1 - X_{O_2}^A - X_{CO_2}^A - X_{CO}^A - X_{THC}^A\right)\right| AK\sqrt{\frac{2\,\Delta P\,P_e}{RT_e\,M_e}} \tag{7}$$

With

$$\begin{aligned} M_e = {} & X_{H_2O}M_{H_2O} \\ & +\left(1 - X_{H_2O}\right)\left[\left(M_{O_2} - M_{N_2}\right)X_{O_2}^A + \left(M_{CO_2} - M_{N_2}\right)X_{CO_2}^A + \left(M_{CO} - M_{N_2}\right)X_{CO}^A + \left(M_{THC} - M_{N_2}\right)X_{THC}^A\right] \end{aligned} \tag{8}$$

In order to estimate the uncertainty related to the calculation of the energy coefficients, the analysis has to be performed on the most basic measurement inputs. This allows avoiding the combination uncertainties of mutually dependent parameters. Finally, E_i is expressed as,

$$E_i = \frac{A_1}{A_2} - A_3 \tag{9}$$

With

$$\begin{aligned} A_1 = {} & \Delta H_{f\ CO_2}\,X_{CO_2}^A + \Delta H_{f\ CO}\,X_{CO}^A + \Delta H_{f\ H_2O}\,\frac{X_{H_2O}}{1 - X_{H_2O}} \\ & - \frac{\left(1 - X_{O_2}^A - X_{CO_2}^A - X_{CO}^A - X_{THC}^A\right)}{1 - X_{O_2}^{A^0} - X_{CO_2}^{A^0}}\left(X_{CO_2}^{A^0}\,\Delta H_{f\ CO_2} + \frac{X_{H_2O}^0}{1 - X_{H_2O}^0}\Delta H_{f\ H_2O}\right) \end{aligned} \tag{10}$$

$$A_2 = M_i\left|X_i^A - \frac{X_i^{A^0}\left(1 - X_{O_2}^A - X_{CO_2}^A - X_{CO}^A - X_{THC}^A\right)}{1 - X_{O_2}^{A^0} - X_{CO_2}^{A^0}}\right| \tag{11}$$

$$A_3 = \frac{x\Delta H_{f\ CO_2} + \frac{y}{2}\Delta H_{f\ H_2O} - \Delta H_C}{\nu_i} \tag{12}$$

Appendix B

B.1 Approach for extracting the material composition from species measurements

The composition of an uncharacterized compound can potentially be approximated by means of calorimeter data from the species measurements and exhaust flow. The following approach relies on the assumption that the sample material composition is only composed of C, H and O fundamental elements and can then be described as a molecule $C_xH_yO_z$. Furthermore, one assumes that the combustion reaction can be modelled as a one step reaction, with the following form,

$$C_xH_yO_z + \nu_{O_2}O_2 \longrightarrow \nu_{CO_2}CO_2 + \nu_{CO}CO + \nu_{H_2O}H_2O \quad (13)$$

From the various species molar fractions and the exhaust flow rate measurement, one can calculate the total production of CO_2 (m_{CO_2}), CO (m_{CO}) and H_2O (m_{H_2O}), as well as the O_2 consumption (m_{O_2})). The total mass loss (m_{fuel}) can also be obtained by means of a weighing balance. If the $C_xH_yO_z$ is valid, the mass of C, H and O in the material can be determined, according to equation (13) by,

$$m_{[C]material} = 12\left(\frac{m_{CO_2}}{44} + \frac{m_{CO}}{28}\right) \quad (14)$$

$$m_{[H]material} = \frac{m_{H_2O}}{9} \quad (15)$$

$$m_{[O]material} = 16\left(\frac{m_{CO_2}}{22} + \frac{m_{CO}}{28} + \frac{m_{H_2O}}{18}\right) - m_{O_2} \quad (16)$$

Subsequently, one can defined the percentage of each element C, H and O in the material,

$$\%_{[C]mass} = \frac{m_{[C]material}}{m_{fuel}} \quad (17)$$

$$\%_{[H]mass} = \frac{m_{[H]material}}{m_{fuel}} \quad (18)$$

$$\%_{[O]mass} = \frac{m_{[O]material}}{m_{fuel}} \tag{19}$$

Recalling the $C_x H_y O_z$ molecule, it comes from equations (17) to (19),

$$\%_{[C]mass} = \frac{12x}{M_{fuel}} \tag{20}$$

$$\%_{[H]mass} = \frac{y}{M_{fuel}} \tag{21}$$

$$\%_{[O]mass} = \frac{16z}{M_{fuel}} \tag{22}$$

And

$$M_{fuel} = 12x + y + 16z \tag{23}$$

A system of 3 equations with 3 unknowns is introduced and can be solved. It allows assessing approximated values for x, y, z and M_{fuel}. Once the molecule relative to the material and the reaction has been ascertained, the complete combustion reaction can be expressed as well as the associated stoichiometric coefficients,

$$\psi_{CO_2} = x \tag{24}$$

$$\psi_{H_2O} = \frac{y}{2} \tag{25}$$

$$\psi_{O_2} = x + \frac{y}{4} - \frac{z}{2} \tag{26}$$

Appendix C

The FM Global Fire Propagation Apparatus

The Fire Propagation Apparatus (FPA) was developed by FM Global. This fire engineering tool is used to determine material flammability characteristics such as the time to ignition, the chemical and convective heat release rates, the mass loss rate and the effective heat of combustion.

The standard E 2058 defined every parts and protocols associated with the FPA. The main features of the FPA are: an infrared heating system [A], a load cell system [B], an ignition pilot flame[C], a gas analysis system [D] and an instrumented section combined with an exhaust system [E].

Three different protocols were created to standardize the use of this tool: Ignition test, Combustion Test and Fire Propagation Test.

The device provides a heat flux of up to 65 kW/m². The use of quartz tube enables to carry out experiments on controlled atmosphere with an oxygen concentration up to 40% to simulate the larger fires by increasing the flame radiation, or with an oxygen concentration lower than 20.9% to simulate the ventilation-controlled fires.

It should be noted that pure nitrogen is used to determine the heat of gasification of the sample.

C.1 Apparatus

The FPA is a very complex apparatus but it could be represented by five main features.

C.1.1. An infrared heating system [A]

The Infrared (IR) heating system consists of four IR heaters (6 lamps each). The four IR heaters are located symmetrically to the specimen. The lamps operate at a temperature of 2205°C and a system of cooling (water and air) helps to maintain a temperature sustainable for the lamps.

C.1.2. A load cell system [B]

The load cell system enables to measure the evolution of the masse of the specimen during all the experiments. This system has a range of 0 - 1000 g and should be calibrated before each experiment.

C.1.3. An ignition pilot flame[C]

The pilot flame is used to ignite the pyrolysis gas produced by the specimen. The flame, adjusted at a length of 10 mm, is obtained with an ethylene/air mixture (60/40) and it is placed at 10 mm above the horizontal specimen and 10 mm from the vertical specimen. It should be noted that a four holes ceramic device (situated in that horizontal supplied pipe of the pilot flame) is used to produce a stable flame and prevent flashback.

C.1.4. A gas analysis system [D]

The gas analysis system goals are to take samples, to filtrate them in order to eliminate the residue as soot particles and to treat them in order to determine their composition. The FPA integrates online gas analyzers for measuring the carbon dioxide and carbon monoxide, the oxygen and the hydrocarbons.

C.1.5. An instrumented section combined with an exhaust system [E]

The quartz tube leads the different combustion gases to intake funnel; gateway to a pipe within the instrumented section is located. This section is composed of a thermocouple, a Pitot probe, a pressure transducer and a smoke laser.

C.2 Flammability characterization tests

The apparatus was built to carry out 3 different kind of test: ignition test, combustion test and fire propagation test. The purposes of the different procedures described below correspond of the definition of the flammability characterization tests defined in the standard test method E2058. For the ignition test, the goal is to determine the time required from the application of

an externally applied heat flux to a horizontal test specimen until a sustainable flame appears on the specimen. Concerning the combustion test, the objective is to measure the chemical and convective heat release rates, the mass loss rate and to determine the Effective Heat of Combustion of a horizontal specimen. The technique used to measure the chemical heat release rate is the carbon dioxide generation whereas the convective one is measured thanks to a difference of temperature between the gas inside the duct before ignition and at each time after ignition. Finally the fire propagation test determines the chemical heat release rate of a vertical specimen during upward fire propagation and burning.

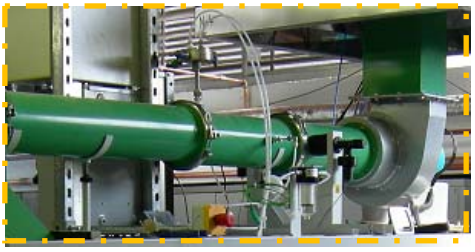

Figure 1. Structural scheme of the FM-Global FPA.

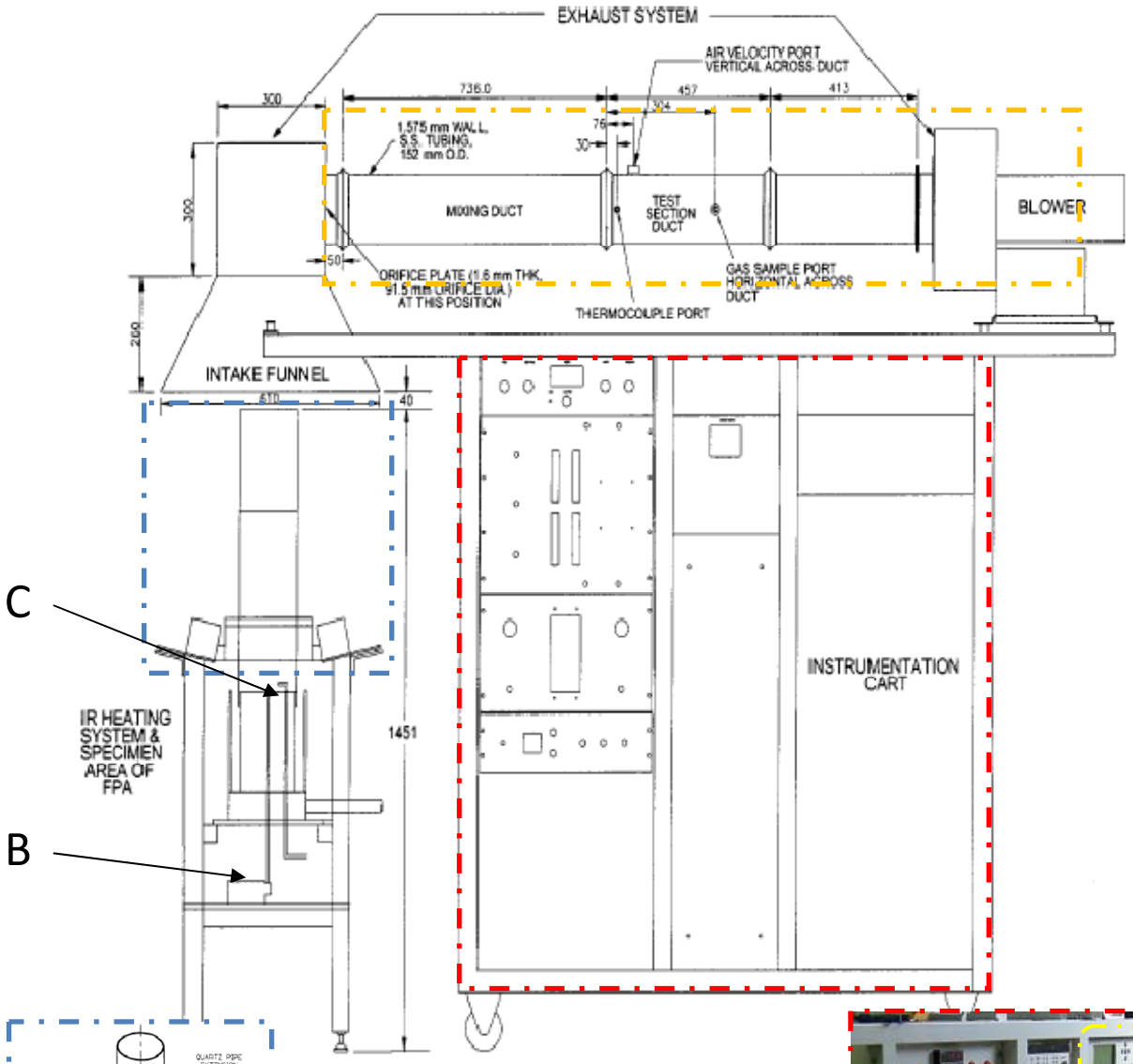

Appendix D.

Laminar flame speed

Russian scientists, Zeldovich, Frank-Kamenetskii and Semenov developed an expression for estimating the laminar flame speed by integrating in their development the conduction of heat and the diffusion of active radicals from the reaction zone to the pre-reaction zone. The following calculations are derived from the analyses carried out by Kanury [Chapter 3, Reference 30] and Glassman [Chapter 3, Reference 32]. The energy equation consists of a balance between conduction, convection and chemical reaction and is given by,

$$k\frac{d^2T}{dx^2} - \rho u C_p \frac{dT}{dx} - \Delta H\, \dot{\omega}_f''' = 0 \tag{27}$$

The conservation of species is presented as follow,

$$-D\rho\frac{d^2Y_f}{dx^2} + \rho u \frac{dY_f}{dx} + \dot{\omega}_f''' = 0 \tag{28}$$

Introducing the 2 changes of variable,

$$\tilde{T} = \frac{C_p(T - T_0)}{\Delta H} \tag{29}$$

And

$$\tilde{Y}_f = Y_f^0 - Y_f \tag{30}$$

Equations (27) and (28) can be rewritten,

$$\frac{k}{C_p}\frac{d^2\tilde{T}}{dx^2} - \rho u \frac{d\tilde{T}}{dx} - \dot{\omega}_f''' = 0 \tag{31}$$

$$D\rho\frac{d^2\tilde{Y}_f}{dx^2} - \rho u \frac{d\tilde{Y}_f}{dx} - \dot{\omega}_f''' = 0 \tag{32}$$

The boundary conditions for these equations are,

For $x \to -\infty$, $\tilde{Y}_f = 0$ and $\tilde{T} = 0$;

For $x \to +\infty$, $\tilde{Y}_f = Y_f^0$ and $\tilde{T} = \frac{C_p(T_f - T_0)}{\Delta H}$; (33)

With T_f, the flame temperature.

If the Lewis number is assumed unity, $Le = \frac{\alpha}{D} = 1$, equations (31) and (32) exhibit identical forms. If boundary conditions are the same, solving energy or species allows deducing the solution of the second equation. In his work, Zeldovich solves the energy conservation equation using several simplification assumptions.

An ignition temperature, T_i, is assigned. T_i is close to the flame temperature, T_f. Zeldovich assumes that for $T < T_i$, no chemical reaction occurs (i.e. $\dot{\omega}_f''' = 0$). The flame front is split in 2 regions: a pre-reaction zone and a reaction zone.

In the preheat zone, $T < T_i$, equation (27) becomes,

$$k\frac{d^2T}{dx^2} - \rho u C_p \frac{dT}{dx} = 0 \tag{34}$$

With the boundary conditions,

For $x = x(T_i), T = T_i$;

For $x \to -\infty$, $T = T_0$ and $\frac{dT}{dx} = 0$. (35)

Integrating equation (34) between T_0 and T_i,

$$\left.\frac{dT}{dx}\right|_{x_i} = \frac{\rho u C_p}{k}(T_i - T_0) \tag{36}$$

In the reaction zone, the convective term is neglected $(T_i \approx T_f)$, equation (34) can be rewritten,

$$\frac{dT}{dx}d\left(\frac{dT}{dx}\right) = \frac{\Delta H}{k}\,\dot{\omega}_f'''\,dT \tag{37}$$

Integrating between T_i and T_f,

$$\left.\frac{dT}{dx}\right|_{x_i} = \left(\frac{2\,\Delta H}{k}\int_{T_i}^{T_f}\dot{\omega}_f'''\;dT\right)^{\frac{1}{2}} \tag{38}$$

The temperature profile being continuous, equations (36) and (38) have to be equal and since $T_i \approx T_f$, $(T_i - T_0) \approx (T_f - T_0)$,

$$u_0 = \left(\frac{2\,k\,\Delta H}{\rho^2 {C_p}^2 (T_i - T_0)}\int_{T_i}^{T_f}\dot{\omega}_f'''\;dT\right)^{\frac{1}{2}} \tag{39}$$

The reaction rate depends on the temperature and can be expressed as,

$$\dot{\omega}_f''' = Z'(\rho^n Y_A^n)e^{-\frac{E}{RT}} \tag{40}$$

u_0 is defined as the flame speed.

Appendix E.

Analysers signal correction

According to Point et al [Chapter 6, Reference 12] and Lyon and Farris [Chapter 6, Reference 13], the transient behaviour of a measuring device can be approximated by exponential series. A characteristic function can be expressed as,

$$h(t) = \sum_{i=1}^{n} a_i \, e^{-\frac{t}{\tau_i}} \tag{41}$$

Where a_i represents the calibration constant of the i^{th} transfer element and τ_i its associated time constant. Considering the sampling system, if a function $h(t)$ exists so that it describe its transient behaviour and $h(t)$ is independent of any sample properties or thermal history, then, the measured output signal $s(t)$ is the convolution of $h(t)$ (source of distortions) and the input signal $e(t)$,

$$s(t) = (h * e\,)(t) = \int_0^t h\,(t-\vartheta)\; e(\vartheta)\; d\vartheta \tag{42}$$

Defining a step input as follow,

$$e(t) = \begin{cases} 0 & for\ t < 0 \\ A & for\ t > 0 \end{cases} \tag{43}$$

Then, equation (42) can be rewritten as,

$$s(t) = A \int_0^t \sum_{i=1}^{n} a_i \, e^{-\frac{t-\vartheta}{\tau_i}} \; d\vartheta = A \sum_{i=1}^{n} a_i \, \tau_i \left[1 - e^{-\frac{t}{\tau_i}}\right] \tag{44}$$

Boundary conditions are specified by,

$$t \; = 0 \qquad\qquad s(t) = 0 \tag{45}$$

$$t \longrightarrow \infty \qquad\qquad s(t) = A \tag{46}$$

This leads to the assumptions that,

$$\sum_{i=1}^{n} a_i \, \tau_i \, = 1 \tag{47}$$

Considering the Figure 6.4 in Chapter 6, one postulates that the exhaust line output signal can be adequately described by a 1st order characteristic function of the system,

$$h_1(t) = a_1 \, e^{-\frac{t}{\tau}} \tag{48}$$

And equation (44) becomes, for a rising output signal with $A = X^A_{CO_2\,[step]}$,

$$s_{rise}(t) = X^A_{CO_2\,[step]} \, a_1 \, \tau \, \left[1 - e^{-\frac{t}{\tau}}\right] \tag{49}$$

Complying with the boundary conditions requires $a_1 = \frac{1}{\tau}$.

Similarly, a falling signal is given by,

$$s_{fall}(t) = X^A_{CO_2\,[step]} \, e^{-\frac{t}{\tau}} \tag{50}$$

Knowing the characteristic function of the system and the output signal, one can attempt to reconstruct the input one. A simple method is defined based on the use of Laplace transforms [Chapter 6, References 12 to 14]. Applying the properties of the Laplace transforms [Chapter 6, Reference 15] for a rising signal,

$$S(p) = \mathcal{L}\big(s(t)\big) = \mathcal{L}\big((h * e\,)(t)\big) = H(p).E(p) \tag{51}$$

Where $\mathcal{L}$ represents the Laplace transform operator and $S(p)$, $H(p)$ and $E(p)$ are, respectively, the Laplace transforms of $s(t)$, $h(t)$ and $e(t)$. Equation (51) allows developing an expression for $E(p)$,

$$E(p) = \frac{S(p)}{H(p)} \tag{52}$$

With

$$H(p) = \frac{1}{1 + \tau \, p} \tag{53}$$

Equation (52) can be rewritten as,

$$E(p) = S(p) + \tau\, p\, S(p) \tag{54}$$

By using the inverse and derivative Laplace transforms theorems, one can express the input signal according the output one,

$$e(t) = s(t) + \tau\, \frac{ds(t)}{dt} \tag{55}$$

Response time lag correction can be applied to the output signal of the sampling system. However, the method requires estimation of the time constant of the system and an approximation of the derivative of the output signal. For discrete data, assuming a sampling time Δt, equation (55) is formulated as follow,

$$e_i(t) = s_i(t) + \tau \left(\frac{s_{i+1}(t) - s_{i-1}(t)}{2\,\Delta t}\right) \tag{56}$$

Where i is the sampling point.